Investigation on Transition Metal-Radical Complexes for Oxidative Cleavage of Aromatic C–C Bond, Aliphatic C–N Bond and Radical-to-Metal Electron Transfer Phenomena

A Dissertation Submitted in Partial Fulfilment of the
Requirement for the Degree of
Doctor of Philosophy
at
IIT Guwahati

by

Ganesh Chandra Paul
Roll No. 136122008

Department of Chemistry
Indian Institute of Technology Guwahati
Guwahati–781039, Assam
India

March 2018

To my loving parents

“It is the great beauty of our science, chemistry, that advancement in it, whether in a degree great or small, instead of exhausting the subjects of research, opens the doors to further and more abundant knowledge, overflowing with beauty and utility”

Michael Faraday

Indian Institute of Technology Guwahati

Department of Chemistry

Declaration

I do hereby declare that research work embodied in this thesis entitled "***Investigation on Transition Metal-Radical Complexes for Oxidative Cleavage of Aromatic C–C Bond, Aliphatic C–N Bond and Radical-to-Metal Electron Transfer Phenomena***" has been carried out by me under the supervision of Dr. Chandan Mukherjee, Department of Chemistry, Indian Institute of Technology Guwahati, Assam–781039, India. The research works have been carried out in the period of August, 2013 to February, 2018.

In keeping with the general practice of reporting scientific observations, due acknowledgements have been made wherever the work described is based on the finding of other investigators.

IIT Guwahati — Ganesh Chandra Paul

March, 2018 — Roll No. 136122008

Dr. Chandan Mukherjee
Associate Professor
Department of Chemistry
Indian Institute of Technology Guwahati
Guwahati, 781039, Assam, India

Phone no. +91-361-258-2327(O)
Fax no. +91-361-258-2349
Email: cmukherjee@iitg.ernet.in

CERTIFICATE

This is to certify that the research work presented in this thesis entitled "***Investigation on Transition Metal-Radical Complexes for Oxidative Cleavage of Aromatic C–C Bond, Aliphatic C–N Bond and Radical-to-Metal Electron Transfer Phenomena***" is an authentic record of the results obtained from the research work carried out by **Mr. Ganesh Chandra Paul** (**Roll No. 136122008**) under my supervision in Department of Chemistry, Indian Institute of Technology Guwahati, India. This work is original and has not been submitted elsewhere for a degree or award.

Place: IIT Guwahati
Date: 19/03/2018

Dr. Chandan Mukherjee
(Thesis Supervisor)

Acknowledgement

I would like to acknowledge many people who have contributed directly or indirectly help, support and encouragement during the course of my research work. I would like express my heartfelt thanks to all of them.

- First of all my deep sense of gratitude goes to my supervisor **Dr. Chandan Mukherjee** for his guidance during the course of my research. I have been enlightened by his wide knowledge and logical way of thinking. This thesis would not have been possible without his assistance. His encouragement has given me so much confidence. When I succeeded, he gave me great congratulation and encouragement. When I failed, he consoled, encouraged me. He is such a capable instructor and mentor that he can always help me to solve problems. His kindness, patience, positive direction lightened the way of my doctoral studies here. I especially thank him for spending numerous hours on my project, along with getting this thesis through its final stages.
- I am highly indebted to "**Indian Institute of Technology Guwahati**" for the doctoral fellowship.
- I would like to thank my doctoral committee members **Prof. Gopal Das** (IIT Guwahati), **Prof. Subhendu Sekhar Bag** (IIT Guwahati) and **Dr. Kingsuk Mahata** (IIT Guwahati) for their valuable suggestions during progress my research work.
- I acknowledge the invaluable assistance received from **Prof. Tapan Kanti Paine** sir and **Sridhar Banerjee** (**Department of Inorganic Chemistry, Indian Association for the Cultivation of Science, Kolkata**). My sincere thanks are to both of them for their help in other ways as well.
- I am highly grateful to **Dr. Prasanta Ghosh** sir and **Dr. Suvendu Maity** (**Department of Inorganic Chemistry, Ramakrishna Mission Residential College (Autonomous) Narendrapur, Kolkata)** for coulometry measurement.
- I would like to acknowledge **CIF (IIT Guwahati)**, **Department of Chemistry (IIT Guwahati)** and **SAIF (IIT Bombay)** for the instrument facilities.
- Thanks to, **Dr. Babulal Das**, **Mr. Aniruddha Gogoi**, **Mr. Imdadul Islam**, **Mr. Diganta Kumar Hira**, **Mr. John Sangma Dangou**, **Mrs. Abhilasha M. Baruah**, **Mr. Dr. Kulakamal Senapati** and **Mr. Kh Kesho Singh** for their support at instrumental laboratory during the research work.

- I express my sincere thanks to my lab mates namely, **Dr. Samir Ghorai**, **Dr. Manas Kumar Mondal**, **Dr. Bedika Phukan**, Late. **Ms. Richa Rakshit**, **Mr. Ujjal Ghosh**, **Ms. Mahmuda Khannam**, **Mr. Prasenjit Sarkar**, **Mr. Shashanka Shekhar Samanta** for their advice, well wishes, encouragement and constant support during the research period at IIT Guwahati.
- I am thankful to my friends, namely, **Mr. Buddhadeb Mondal**, **Mr. Raghunath Bag**, **Mr. Subhankar Panda**, **Mr. Sabyasachi Pramanik**, **Mr. Sayanta Sekhar Nag**, **Mr. Rana Dalapati**, **Mr. Rajat Subhra Giri**, **Mr. Sourav Pradhan** and **Mr. Arup Tarai** for providing a good, academic, friendly, peaceful and entertaining atmosphere outside from our lab.
- I am grateful to my parents (**Maa** and **Baba**) who have always supported all my decisions and have been a source of constant energy and inspiration to me. Thank you **Maa**, thank you **Baba** for being all the time with me and keeping so much faith on me. I would also like to thank my elder brothers **Asit Dada**, **Bimal Dada**, **Sona Dada**, **Kartik Dada** for always encouraging me. Thank you brothers for your encouragement. I want to thank two people, **Subrata** Sir and **Bidesh** (Dadababu), who have provided continuous encouragement and have been with me in my successes and failures.
- I would like to remember all of those who have guided or assisted me throughout the journey of my educational career and also throughout various aspects of my life.

Ganesh Chandra Paul

Thesis Title:

"***Investigation on Transition Metal-Radical Complexes for Oxidative Cleavage of Aromatic C–C Bond, Aliphatic C–N Bond and Radical-to-Metal Electron Transfer Phenomena***"

Date of Submission of Thesis:

22-03-2018

List of Publication:

1. "Dioxygen Reactivity of an Iron Complex of 2-Aminophenol-Appended Ligand: Crystallographic Evidence of the Aromatic Ring Cleavage Product of the 2-Aminophenol Unit", **Ganesh Chandra Paul**, Sridhar Banerjee and Chandan Mukherjee*, *Inorg. Chem.*, 2017, **56**, 729.
2. "Monoradical-containing four-coordinate Co(III) complexes: homolytic S–S and Se–Se bond cleavage and catalytic isocyanate to urea conversion under sunlight", **Ganesh Chandra Paul**, Samir Ghorai and Chandan Mukherjee*, *Chem. Commun.*, 2017, **53**, 8022.
3. "Geometry-Driven Iminosemiquinone Radical to Cu(II) Electron Transfer and Formation of an Elusive Five-Coordinate Cu(I) Complex: Synthesis, Characterization and Reactivity Study with KO_2" **Ganesh Chandra Paul**, Kanu Das, Suvendu Maity, Samiyara Begum, Hemant Kumar Srivastava and Chandan Mukherjee*, *Inorg. Chem.* **2018**, DOI: 10.1021/acs.inorgchem.8b01931.

List of Conferences/Symposiums

1. "***Frontier in Chemical Science, FICS–2016***" December 8–10, 2016, Department of Chemistry, Indian Institute of Technology Guwahati.
2. "***5th Symposium on Advanced Biological Inorganic Chemistry, SABIC–2017***" January 7–11, 2017, TIFR–IACS, Kolkata, India.
3. "***Chemconvene 2017***" July 25, 2017, Department of Chemistry, Indian Institute of Technology Guwahati.

4. "***Modern Trends in Inorganic Chemistry,* MTIC-XVII, 2017, Pune"** held at CSIR-NCL, Pune, IISER, Pune during 11–14th December, 2017.

Doctoral Committee:

Prof. Gopal Das (Chairman)
Prof. Subhendu Sekhar Bag (Member)
Dr. Kingsuk Mahata (Member)
Dr. Chandan Mukherjee (Supervisor)

Abstract

Chapter I

General Introduction

In biology, various enzymatic reactions are accompanied by metalloenzymes. In metalloenzymes, the active site(s) is(are) constituted by metal ion(s). While, most of the biological reactions are controlled solely by redox-active metal ions present at the active site; in some cases, redox-active metal ions are potentially assisted by redox-active organic cofactors. In the several metalloenzymes, namely; Aminophenol dioxygenase, Ribonucleotide Reductase IB, Galactose Oxidase, and Photosystem II, etc; the presence of phenol-based tyrosine radical has been found in the vicinity of the active site. The active participation of the radical in the enzymatic reactions has also been established. Hence, investigation on electronic- and geometrical-structure of active-site-like radical-coordinated transition metal complexes and thereafter, the use of those complexes as catalysts for various electron transfer phenomena, oxygenation activities, bond breaking and bond formation reactions have achieved considerable attention to chemists. In this context, three new aminophenol-based redox active ligands (**Scheme 1**) and their corresponding metal (Fe, Mn, Co, Cu) complexes were synthesized to understand the enzymatic activities and mechanistic pathways.

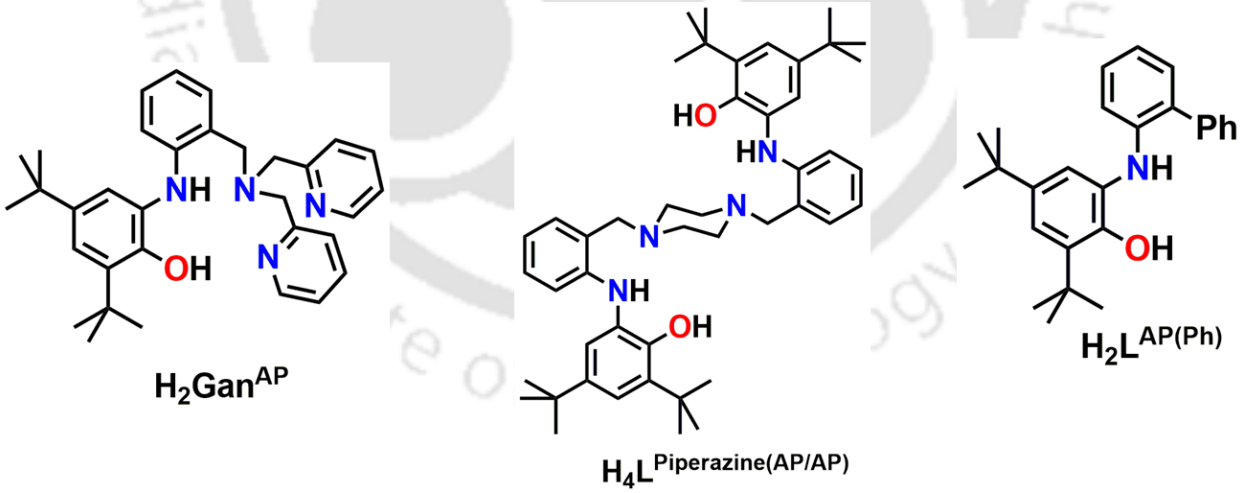

Scheme 1: *Schematic representation of the ligands.*

Chapter II

Synthesis and Characterization of Non-Innocent Ligand, [H_2Gan^{AP}] and its Corresponding Dinuclear μ_2-oxo-Bridge Fe(III) and Mn(III) Complexes

2-Aminophenol appended pentadentate ligand **H_2Gan^{AP}** was synthesized by mixing equimolar amounts of 2-[bis(2-pyridylmethyl)aminomethyl]aniline and 3,5-di-*tert*-butyl catechol in hexane in the presence of Et_3N under air. The ligand reacted with $Fe(ClO_4)_2 \cdot 6H_2O$ or $Fe(ClO_4)_3 \cdot 6H_2O$ in the presence of tetrabutylammonium perchlorate, and Et_3N under air and provided a μ_2-oxo-bridged dinuclear iron complex (**2A**). X-ray single crystal analysis of complex **2A** revealed the presence of a furan derivative, resulted from the oxidative aromatic C–C bond cleavage product of 2-aminophenol derivative, in the coordination sphere of each iron centre. Mechanistic investigation for the formation of complex **2A** established that in the absence of molecular oxygen no oxidation of the appended 2-amidophenolate unit took place. An iron(III)-amidophenolate complex(**2B**), formed initially, further reacted with molecular oxygen and caused oxidative aromatic C–C bond cleavage *via* a putative alkylperoxo species. The ligand, upon reaction with an equivalent amount of $Mn(ClO_4)_2 \cdot 6H_2O$ in the presence of Et_3N under air in MeOH, provided a mono(μ-oxo)-bridged binuclear Mn_2 complex(**2C**). X-ray crystal structure analysis of complex **2C** confirmed that the oxidation state of each Mn ion was +III and the 2-aminophenol unit of ligand **H_2Gan^{AP}** was in its one-electron oxidized iminosemiquinone form. ^{1}H-NMR measurement on complex **2C** confirmed that the complex acquired a diamagnetic ground state (S_t = 0) by experiencing antiferromagnetic couplings among the paramagnetic centers. The UV-vis/NIR spectrum of complex **2C** was consisted of ligand-to-metal charge transfer tramsitions in the visible region, while, ligand-to-ligand charge-transfer transitions were noticed in the near-infrared region due the presence of iminosemiquinone radical units. The cyclic voltammogram of the complex showed three one-electron oxidation waves and two one-electron reduction waves. DFT-based theoretical study indicated that the reduction and the first two oxidation processes corresponded to the ligand based reduction and oxidation phenomena. Thus, two Mn(III)-coordinated iminosemiquinone units underwent two successive reduction processes to generate two amidophenolate units, while, two iminoquinone units were formed upon two successive oxidation process of the coordinated iminosemiquinone units.

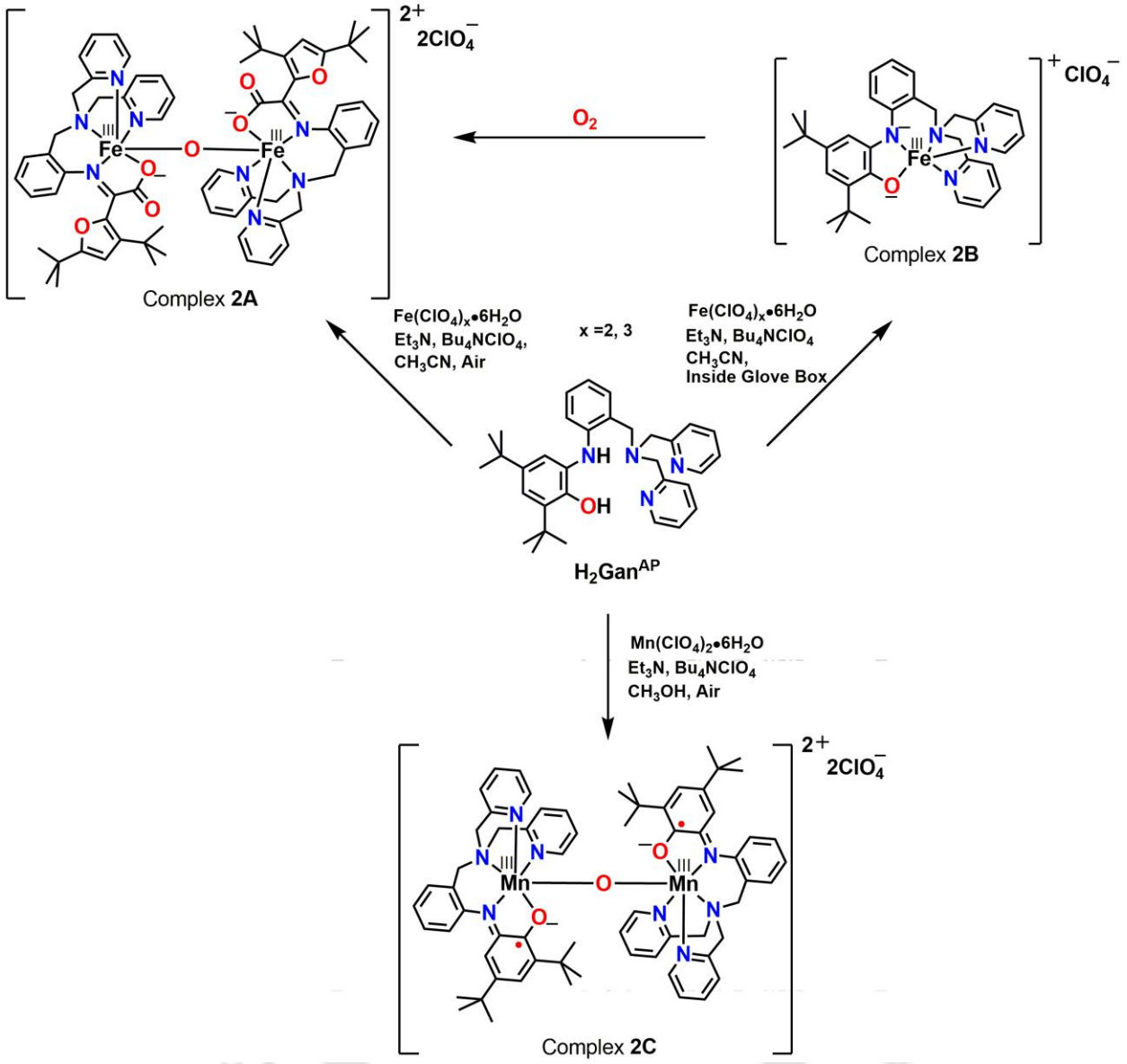

Scheme 2: *Synthesis of complex **2A**, **2B** and **2C** from ligand **H_2Gan^{AP}**.*

Chapter III

A New Piperazine-Based Non-Innocent Ligand, [$H_4L^{Piperazine(AP/AP)}$], and its Corresponding Radical-Containing Transition Metal Complexes: Synthesis and Characterization

A piperazine-based ligand **[$H_4L^{Piperazine(AP/AP)}$]** featuring two *o*-amidophenol non-innocent units was used to synthesize by reacting with 2,2'-(piperazine-1,4-diylbis(methylene))dianiline with 2 equivalents of 3,5-di-*tert*-butyl-catechol in air in the presence of Et_3N in hexane. X-ray single crystal analysis of the ligand **[$H_4L^{Piperazine(AP/AP)}$]** revealed that piperazine unit present in more stable chair form rather than that of boat form. Furthermore, a new octahedral Co(III) complex (**3A)** was synthesized by reacting with ligand **[$H_4L^{Piperazine(AP/AP)}$]** and $CoCl_2 \bullet 6H_2O$. Ligand **$H_4L^{Piperazine(AP/AP)}$** upon reacting with 2.0 equivalent amount of $CuCl_2 \bullet 2H_2O$ in CH_3CN in the presence of Et_3N under air provided a novel binuclear diradical-containing Cu(II) complex (**3B)**. Both the complexes were characterized by single crystal X-ray crystallographic measurement. Diamagnetic in nature (with S_t = 0 ground state) of the complexes (**3A** and **3B**) were as evident by ^{1}H-NMR spectroscopy. The ligand, upon reaction with an equivalent amount of $Cu(ClO_4)_2 \bullet 6H_2O$ in the presence of Et_3N under air in CH_3CN, provided a Cu(II) complex(**3C**). X-ray single crystal analysis of complex **3C** revealed that the bidentate substituted acridine frameworks occupied the coordination sites. The formation of acridine unit took place via C–N bond activation and thereafter homolytic C–H bond breaking and C–C bond formation through simultaneous electron transfer from iminosemiquinone [$(ISQ)^{\bullet 1-}$] to benzyl carbon adjacent to piperazine moiety.

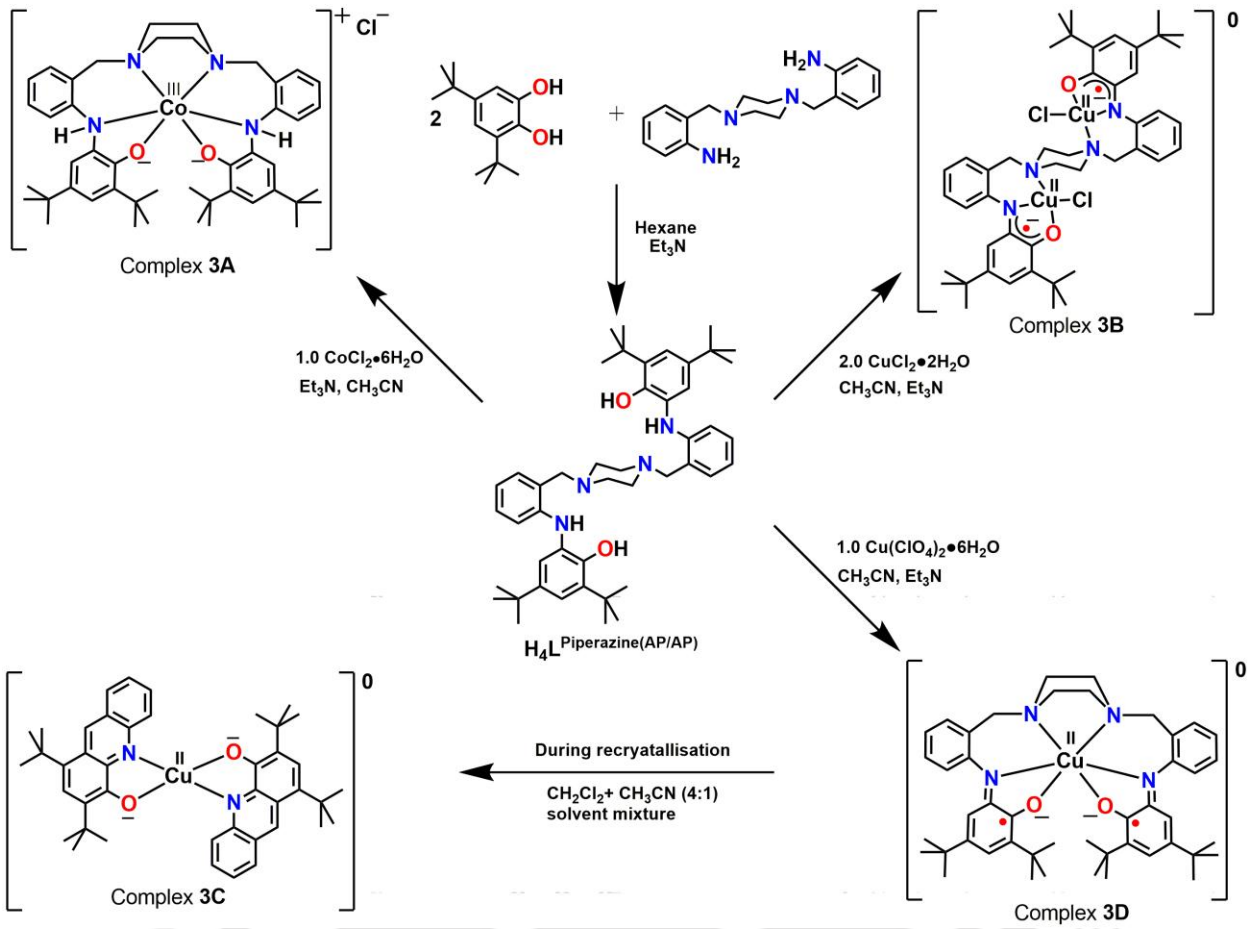

Scheme 3: *Synthesis of ligand* $H_4L^{Piperazine(AP/AP)}$ *and its corresponding complexes* ***3A***,***3B***,***3C*** *and* ***3D*** *from ligand* $H_4L^{Piperazine(AP/AP)}$.

Chapter IV

Synthesis of Monoradical-Containing Four Coordinate Co-Complexes: Homolytic S–S, Se–Se Bonds Cleavage and Catalytic Conversion of Isocyanate to Urea under Sunlight

The aminophenol-based ligand $\mathbf{H_2L^{AP(Ph)}}$, was synthesized during the reaction of 2-aminobiphenyl and 3,5-di-*tert*-butylcatechol in hexane in presence of Et_3N under air. In the ligand, one of the N-phenyl-ring *ortho*-positions of the parent $\mathbf{H_2L^{AP}}$ [N(2-hydroxy-3,5-di-*tert*-butyl phenyl) aniline] ligand was substituted by a bulky phenyl ring. The ligand reacted with 0.5 equivalent of $Co(ClO_4)_2 \cdot 6H_2O$ in the presence of Et_3N under air and provided a monoradical containing square planar Co(III) complex (**4A**). During recrystallsation from DCM:CH_3CN (4:1) solvent mixture, its provided a diradical containing square-pyramidal Co(III) complex(**4B**) where axial position occupied by –Cl atom while, complex **4B** was directly formed during the reaction of ligand $\mathbf{H_2L^{AP(Ph)}}$ with $CoCl_2 \cdot 6H_2O$ in the presence of Et_3N under air. Complex **4B** reduced diphenyl disulfide (Ph_2S_2) and diphenyl diselenide (Ph_2Se_2) by an electron and provided the corresponding five-coordinate, diradical-containing complexes (**4C** and **4D**) where the axial position was occupied by a –XPh group [X = S (**4C**) and Se (**4D**)]. All the complexes were characterized by X-ray crystallography except the complex **4A**. The electronic absorption spectra of all the complexes were dominated by IVCT, LLCT, LMCT charge-transfer transitions. When CH_2Cl_2 solution of complex **4C** was subjected to sunlight irradiation, complex **4A** was generated via homolytic Co–SPh bond cleavage which was confirmed by X-band EPR and UV-vis/NIR experiments. As five-coordinate, diradical-containing complexes could be converted to the corresponding four-coordinate, monoradical-containing complexes under the sunlight stimulus, and four-coordinate complexes have been found as one-electron transferring agent. We have investigated the catalytic ability of four-coordinate as well as five-coordinate complexes (**4A**, **4C** and **4E**) for the conversion of RNCO (R = phenyl and naphthyl) to the corresponding C–N coupled urea derivatives under sunlight.

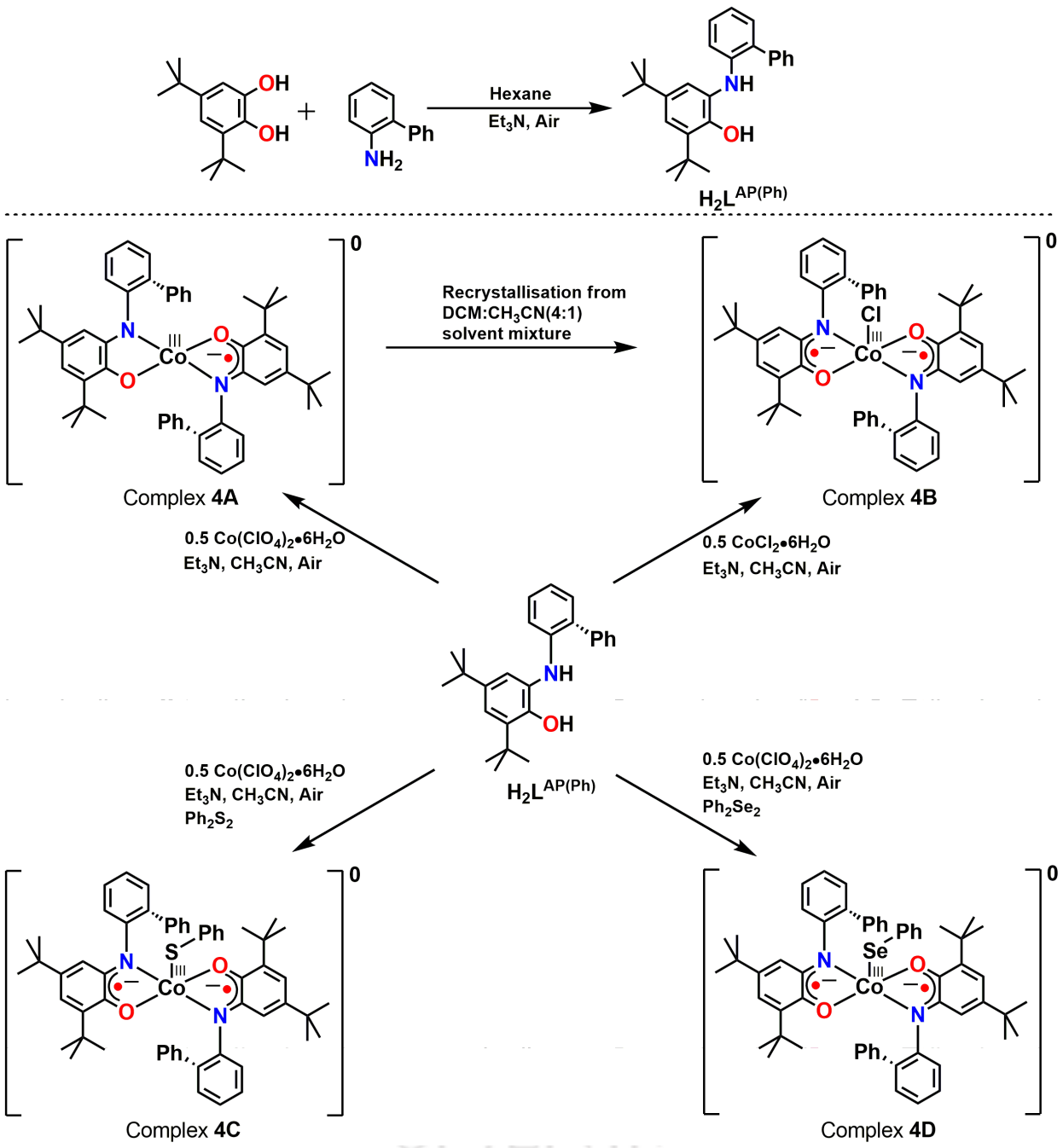

Scheme 4: *Synthesis of ligand* $H_2L^{AP(Ph)}$ *and its corresponding complexes* ***4A***,***4B***,***4C*** *and* ***4D*** *from ligand* $H_2L^{AP(Ph)}$.

Chapter V

Geometry Driven Iminosemiquinone Radical to Cu(II) Electron Transfer and Formation of an Elusive Five-Coordinate Cu(I) Complex: Synthesis, Characterization and Reactivity Study with KO_2

The bidentate non-innocent ligand $\mathbf{H_2L^{AP(Ph)}}$ contained a bulky phenyl substituent at the ortho-position to the aniline moiety. The ligand reacted with 0.5 equivalent of $CuCl_2 \cdot 2H_2O$ in the presence of Et_3N under air and provided a Cu(II)-bis(imonosemiquinone) complex (**5A**). The complex upon oxidation by stoichiometric amount of ferrocenium hexafluorophosphate ($FcPF_6$) yielded four-coordinate Cu(II)-(imonosemiquinone)(iminoquinone) complex (**5C**), while the oxidation by an equivalent amount $CuCl_2 \cdot 2H_2O$ produced five-coordinate Cu(I)-bis(iminoquinone)Cl complex (**5B**). Thus, a ligand-based oxidation followed by ligand-to-metal electron-transfer was realized for the latter oxidation process. Removal of axial Cl^- ion from complex **5B** rendered four-coordinate complex **5D**. No change in the oxidation state of either Cu(I) or iminoquinone moieties was realized on changing the coordination number from five to four. All the complexes were characterized by X-ray crystallography either at 293(2) or 100(2) K. Complexes **5B**, **5C**, and **5D** were diamagnetic with $S_t = 0$ ground state as evident by EPR and ^{1}H-NMR measurements. The UV-vis/NIR spectra of all the complexes were dominated by ILCT, LLCT, MLCT, LMCT charge-transfer transitions. Two oxidations and two reductions waves were noticed in the cyclic voltamogram (CV) of complex **5A**. Complex **5B** and complex **5C** underwent one oxidation and three reductions processes. Contrary to complex **5C**, which experienced ligand-based oxidation, in complex **5B** the oxidation was metal-centered [oxidation of Cu(I) to Cu(II)]. UV-vis/NIR spectral changes during the fixed-potential one-electron oxidation by coulomety and thereafter, X-band EPR analysis consolidated the metal-based oxidation in complex **5B.** Complex **5B** was air stable; however, it oxidized KO_2 to oxygen molecule. Complex **5A** was formed in due course as evident by UV-vis/NIR spectral changes and X-band EPR measurement.

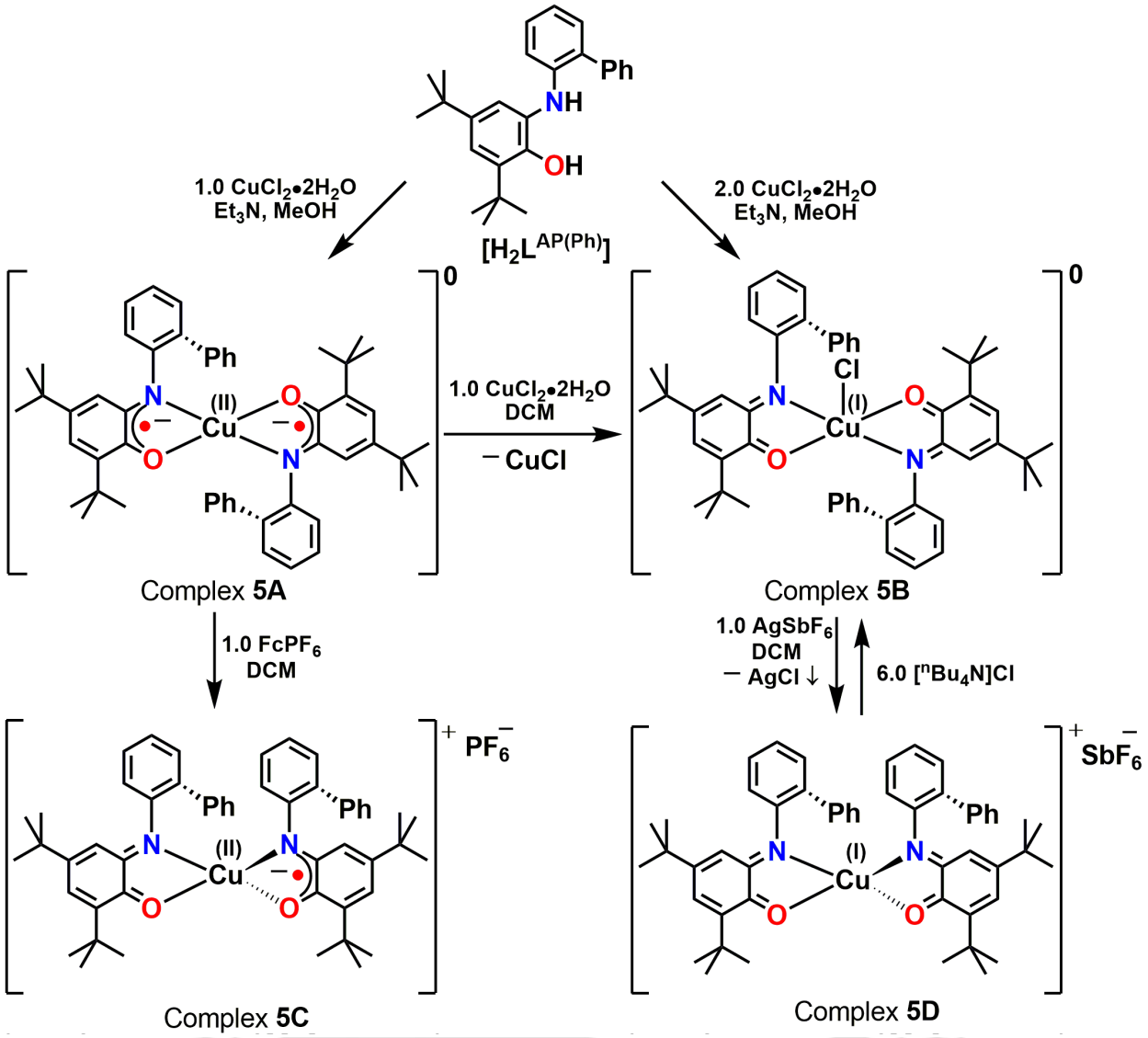

Scheme 5: *Synthesis of complexes **5A**,**5B**,**5C** and **5D** from ligand **$H_2L^{AP(Ph)}$**.*

CONTENTS

Chapter I

General Introduction, Motivation, and Objectives

Chapter II

Synthesis and Characterization of Non-Innocent Ligand, [H_2Gan^{AP}] and its Corresponding Dinuclear μ_2-oxo-Bridge Fe(III) and Mn(III) Complexes

Chapter III

A New Piperazine-Based Non-Innocent Ligand, [$H_4L^{Piperazine(AP/AP)}$], and its Corresponding Radical-Containing Transition Metal Complexes: Synthesis and Characterization

Chapter IV

Synthesis of Monoradical-Containing Four Coordinate Co-Complexes: Homolytic S–S, Se–Se Bonds Cleavage and Catalytic Conversion of Isocyanate to Urea under Sunlight

Chapter V

Geometry Driven Iminosemiquinone Radical to Cu(II) Electron Transfer and Formation of an Elusive Five-Coordinate Cu(I) Complex: Synthesis, Characterization and Reactivity Study with KO_2

ABBREVIATIONS

Technical terms:

av. : average
B : magnetic field
LMCT : ligand–to–metal charge transfer
MLCT : metal–to–ligand charge transfer
LLCT : ligand–to–ligand charge transfer
IET : intramolecular electron transfer
SET : single electron transfer
D : zero–field splitting
deg. : degree (°)
e^-: electron
E : total energy
Exp : experimental
Sim : simulated
H : Hamiltonian
J : coupling constant (cm_{-1}) /or Hz
hs : high spin
ls : low spin
I : nuclear spin
HOMO : highest occupied molecular orbital
LUMO : lowest unoccupied molecular orbital
m/z : mass per charge
RT : room temperature (30 ℃)
S : electron spin
s : singlet
d = doublet
t = triplet
q = quartet

Units:

Å : angstrom (10^{-10} m)
cm : centimetre
emu : electromagnetic unit
G : gauss
h : hour
K : Kelvin
M : molar
m / min. : minute
mm : millimeter
nm : nanometer (10^{-9} m)
s : second
T : tesla
μ_B : bohr magnetron
B : magnetic field
° : degree

Symbols:

λ : wavelength (nm)
ε : extinction coefficient ($M^{-1}cm^{-1}$)
μ_{eff} : magnetic moment (μ_B)
δ : Isomer shift
× : multiplication

Solvents and reagents:

TBAP : tetrabutylammonium perchlorate
Cat : catechol
SQ : semiquinone
ISQ : iminosemiquinone
IBQ : iminoquinone
CH_2Cl_2 : dichloromethane
Et_2O : diethylether
Et_3N : triethylamine
EtOAc : ethylacetate
$Et_4N^+Cl^-$: tetraethylammonium chloride
EtOH : ethanol
KBr : potassium bromide

$CHCl_3$: chloroform

MeOH : methanol

THF : tetrahydrofuran

CH_3CN : acetonitrile

Techniques:

EA : elemental analysis
EI : electron ionization
EPR : electron paramagnetic resonance
NMR : nuclear magnetic resonance
SQUID : superconducting quantum interface device

ESI : electrospray ionisation
IR : infrared
MS: mass spectrometry
UV-vis/NIR : ultraviolet-visible/near infrared

Latin expressions:

ca. : around
et al. : and co−workers
e.g. : for example
i.e. : namely

tert : tertiary
vs. : versus, against
via : through
vide infra : see below

Chapter I

General Introduction, Motivation and Objectives

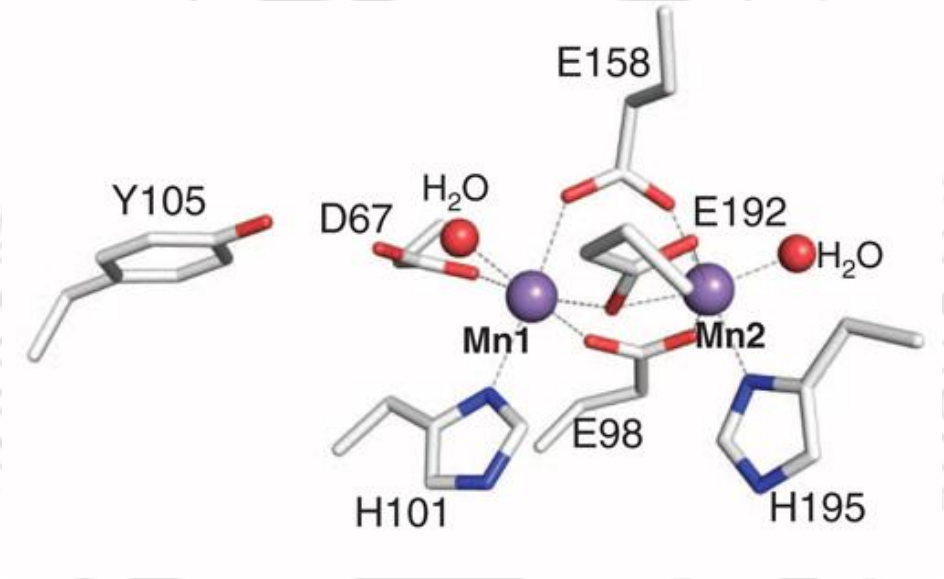

1.1 Introduction, Motivation, and Objectives

In biology, various enzymatic reactions are accompanied by metalloenzymes. In metalloenzymes, the active site(s) is(are) constituted by metal ion(s). While, most of the biological reactions are controlled solely by redox-active metal ions present at the active site; in some cases, redox-active metal ions are potentially assisted by redox-active organic cofactors.[1] In the several metalloenzymes, namely; Aminophenol dioxygenase,[2] Ribonucleotide Reductase 1B,[3] Galactose Oxidase,[4] and Photosystem II,[5] etc; the presence of phenol-based tyrosine radical has been found in the vicinity of the active site. The active participation of the radical in the enzymatic reactions has also been established. Hence, investigation on electronic- and geometrical-structure of active-site-like radical-coordinated transition metal complexes and thereafter, the use of those complexes as catalysts for various electron transfer phenomena, oxygenation activities, bond breaking and bond formation reactions have achieved considerable attention to chemists.

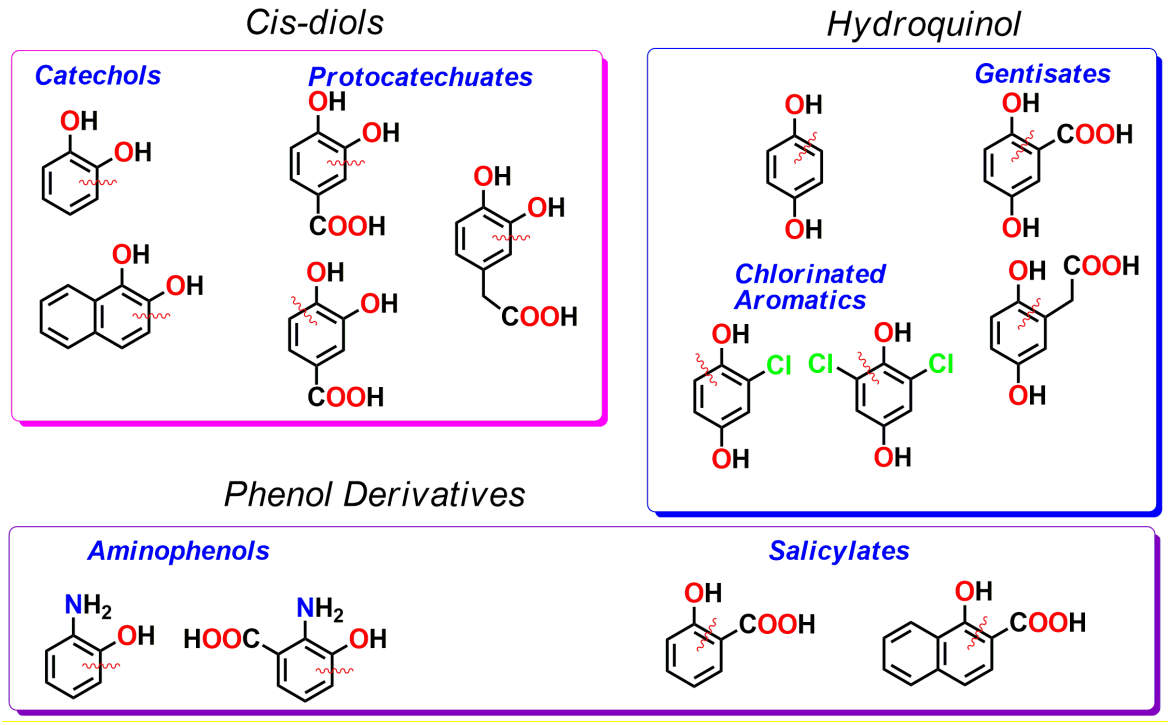

Figure 1.1: *Various aromatic substrates cleaved by non–heme iron dioxygenases.*

Bioremediation[6a-b] is a process where a number of important metalloenzymes are involved to breakdown and assimilate recalcitrant pollutants through metabolic pathways. Single as well as multi-ring containing hydrocarbons, which are a major class of pollutants, can easily liable to bioremediation. The aerobic degradation of these compounds is largely mediated by non-heme iron-containing dioxygenases (enzymes capable of incorporating both atoms of O_2 into substrate).[6c] For example, non-heme iron dioxygenases have been known for oxidative cleave of a wide variety of aromatic substrates, including catechol, protocatechuates,[7a] hydroquinones[7b-d], *o*-aminophenols,[7e-f] and salicylates[7g-i] (**Figure 1.1**).

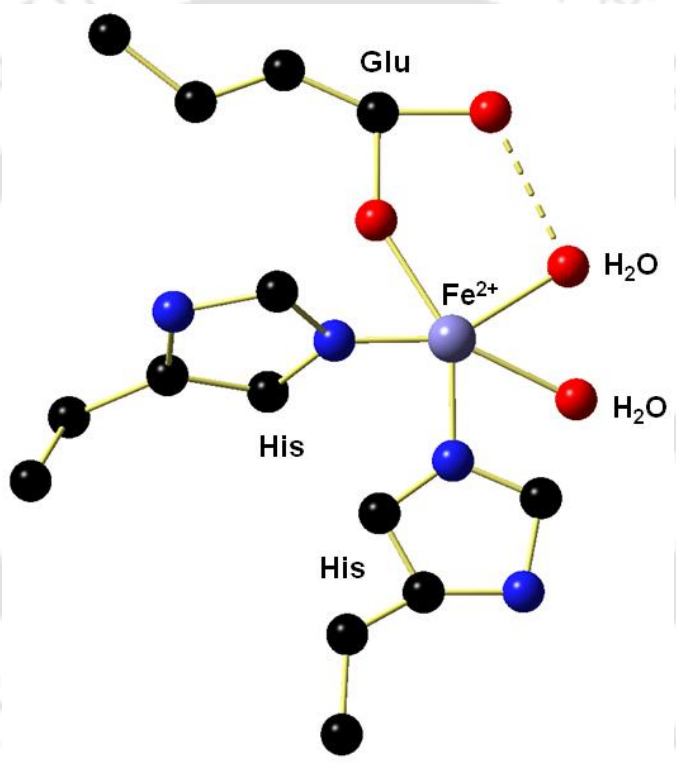

Figure 1.2: *Common active-site structure of non-heme Fe dioxygenases, featuring the 2-His-1-carboxylate facial triad of protein residues.*[8b]

Unlike the intradiol catechol dioxygenases, the ring-cleaving dioxygenases generally share a common active-site structure: a high-spin mononuclear iron(II) center that is bound to one aspartate (or glutamate) and two histidine residues in a facial triad fashion, along with two or three H_2O ligands (**Figure 1.2**).[8a-f] The "2-His-1-carboxylate (2H1C) facial triad" is the

dominant coordination motif found among non-heme mononuclear iron enzymes, which involve in O_2 activation. The 2H1C structure facilitates catalysis by permitting the iron center to bind both substrate and molecular O_2.

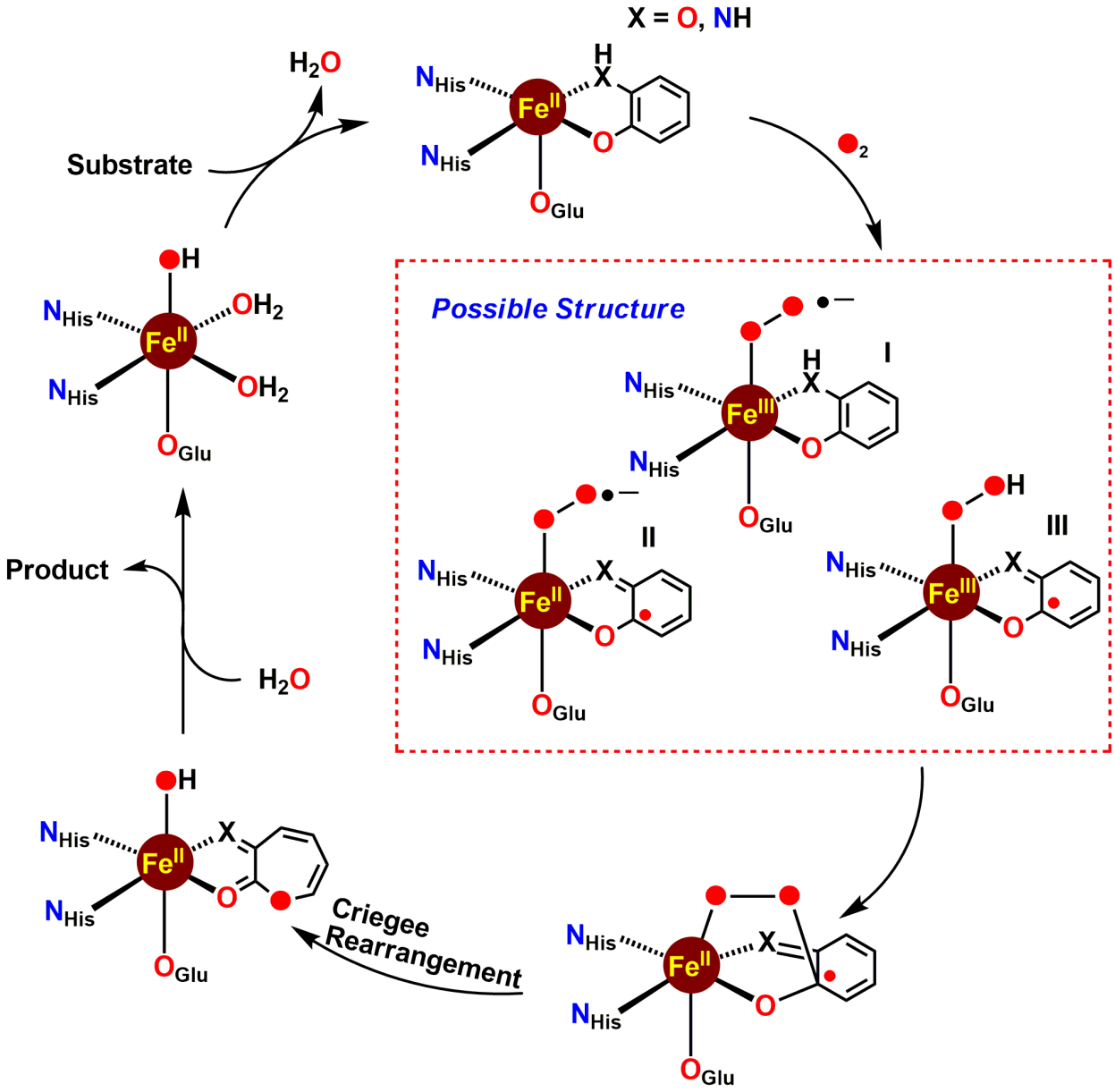

Figure 1.3: *Proposed mechanism for extradiol catechol dioxygenases and o-aminophenol dioxygenases.*

The catalytic mechanism (**Figure 1.3**) of the extradiol catechol dioxygenases has been studies extensively with experimental and computational methods. The first step involves

bidentate coordination of substrate to Fe with loss of a proton, accompanied by displacement of the coordinated H_2O ligands.[9a-b] The resulting five-coordinate Fe(II) center then binds O_2 in the vacant site adjacent to the bound substrate.[10a] Formation of a short-lived ferric-superoxo intermediate is thought to trigger the transfer of one electron from the substrate ligand to iron, resulting in a bound *o*-semiquinone radical.[8f] The existence of this putative intermediate would likely require deprotonation of the distal –OH group by a second sphere residue, although it is not clear whether these three events (O_2 coordination, electron transfer, and proton transfer) occur in a stepwise or concerted manner. The degree of semiquinone character on the substrate ligand in the O_2-bound form of the enzyme is also uncertain (*vide infra*); however, it is well-established that the next step of the catalytic cycle involves generation of an Fe(II)-alkylperoxo species, which undergoes a Criegee rearrangement and hydrolysis to eventually yield the ring-opened product. Interestingly, the general catalytic strategy employed by the ring-cleaving dioxygenases differs substantially from the O_2-activation mechanism employed by cytochrome P450s,[10b] methane monooxygenase,[10c] and *α*-ketoglutarate dependent dioxygenases.[10d] In these enzymes, O_2 is used to generate an iron(IV)-oxo intermediate that performs the demanding hydroxylation of an aliphatic substrate. In contrast, structural, mutagetic, and radical trap experiments and also computational studies have revealed that the ring cleaving dioxygenase mechanism does not involve high-valent Fe intermediates (**Figure1.3**).[10e-g]

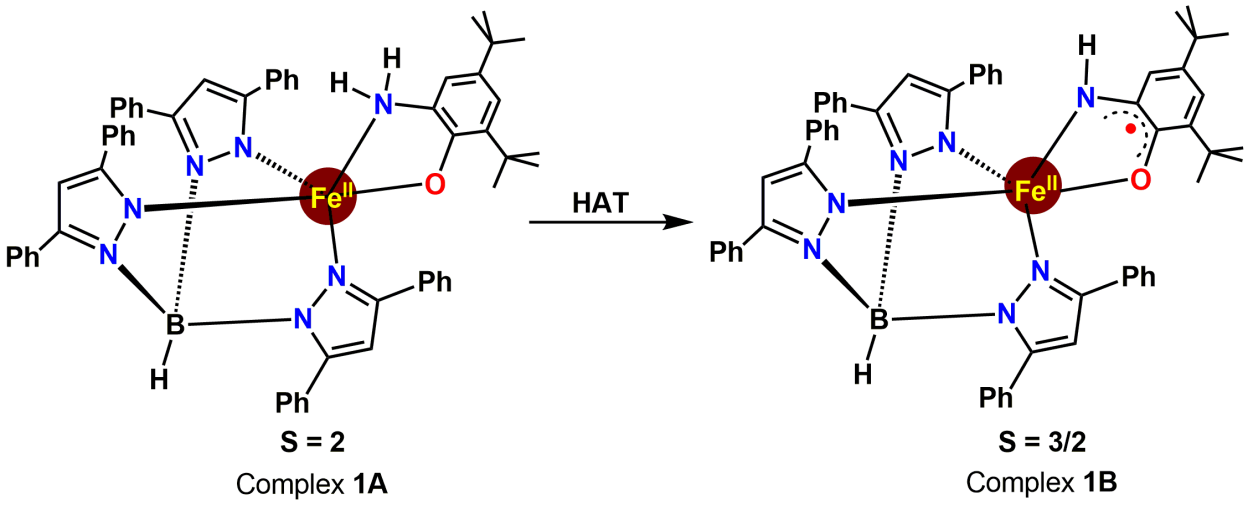

Scheme 1.1: *A synthetic model of the putative Fe(II)-iminobenzosemiquinonate intermediate in the catalytic cycle of o-Aminophenol Dioxygenases.*

The better understanding of reaction mechanism for the aromatic C-C bond cleavage processes by 2-aminophenol dioxygenase has achieved special attential. In this regard, Adam T. Fiedler and coworkers have investigated the oxidative ring cleavage of aromatic substrates by non-heme Fe complex.[11a] They describe the synthesis of the trigonal-bipyramdial complex (**1A**), the first synthetic example of an iron(II) center bound to an iminobenzosemiquinonate (ISQ) radical (**Scheme 1.1**). The unique electronic structure of the complex and its corresponding one-electron oxidized derivative (complex **1B**) with an S = 3/2 have been established on the basis of crystallographic, spectroscopic, and computational analysis. These findings further demonstrate the viability of Fe(II)-ISQ intermediates in the catalytic cycles of *o*-aminophenol dioxygenases.[11a]

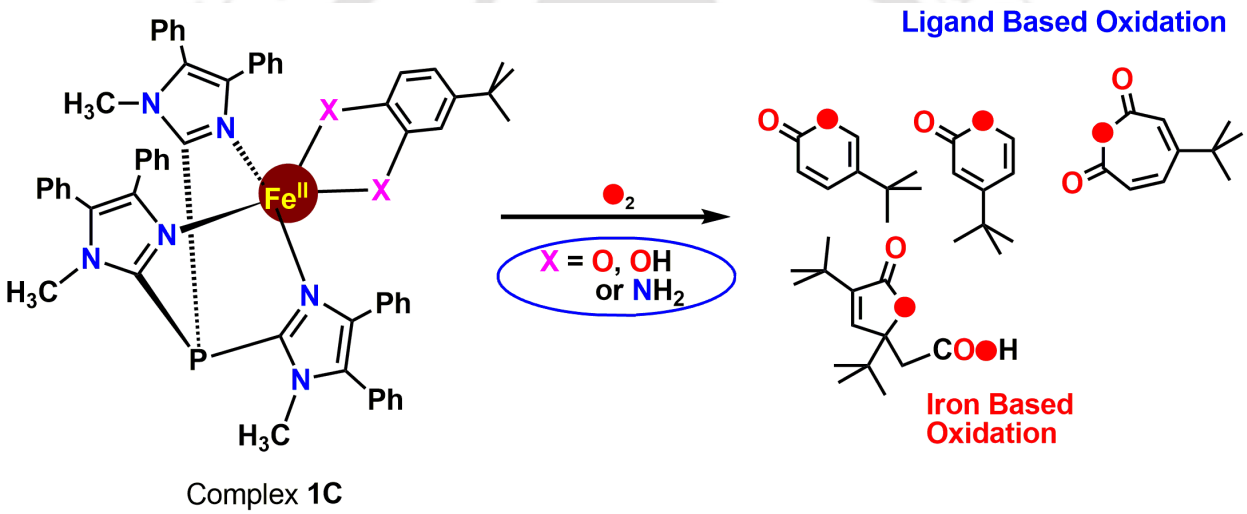

Complex **1C**

Scheme 1.2: *Dioxygen reactivity of biomimetic Fe(II)complex with non–innocent catecholate, o–aminophenolate and o–phenylenediamine ligands.*

In 2014, the same group has also reported spectroscopic, computational, O_2 reactivity, and reaction kinetics of three mononuclear Fe(II) complex (**Scheme 1.2**) containing "non-innocent" catecholate, *o*-aminophenolate, and *o*-phenylenediamine ligands. Depending on the nature of the non-innocent bidentate ligands, the O_2 reaction triggers either iron-based oxidation or ligand-based oxidation, or a combination of both processes (**Scheme 1.2**).[11b] Basically ligands are capable of donating protons as well as electrons, and the interplay between these two factors influences rates of reaction with O_2.

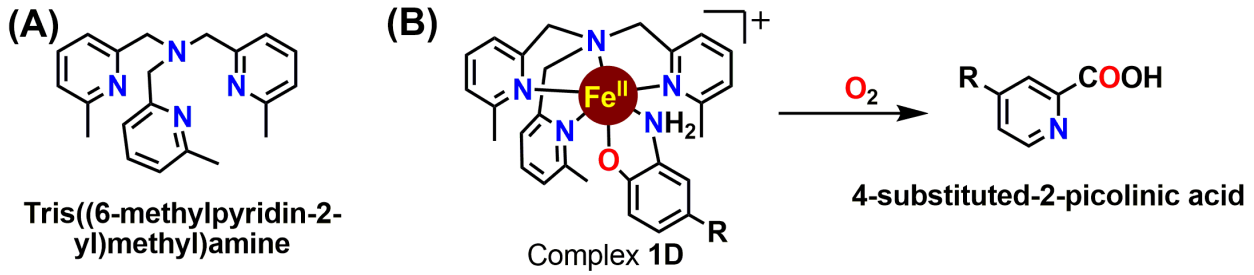

Scheme 1.3: ***(A)*** *Ligand tris(6-methyl-2-pyridylmethyl) amine, (B) Reaction of the iron(II)-aminophenolate complex with dioxygen.*

In 2013, T. K. Paine and coworkers have reported the dioxygen reactivity of six-coordinate iron(II)-2-aminophenolate complexes of an N_4 ligand using substituted 2-aminophenols. The complexes have been shown to react with dioxygen under ambient conditions to afford substituted 2-picolinic acids mimicking the function of 2-aminophenol dioxygenases (**Scheme 1.3**).[12a-b]

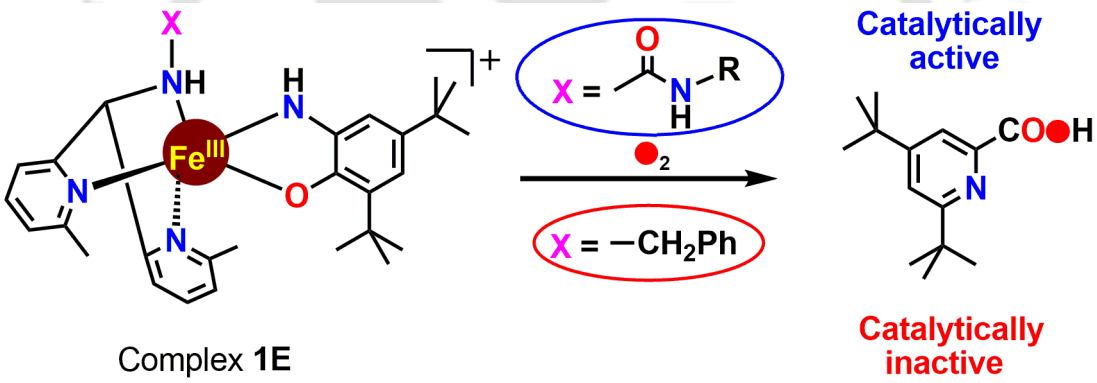

Scheme 1.4: *Reaction of the iron(III)-aminophenolate complex with dioxygen.*

Furthermore, in 2015 the same group have reported two Fe(III)-2-amidophenolate complexes of two different facial tridentate ligands; one ligand contains pendant urea moiety and the other with tethered benzyl moiety (**Scheme 1.4**). Both ligands react with dioxygen to cleave the aromatic ring of 2-amino-4,6-di-*tert*-butylphenol regiospecifically, resulting in the formation of 4,6-di-*tert*-butyl-2-picolinic acid. The complex supported by urea-bearing ligand shows catalytic C−C bond cleavage with multiple turnovers, whereas the complex without urea group shows no catalysis. The role of the urea group has been implicated to affect the catalytic reactivity (**Scheme 1.4**).[12c]

The drawback of the above stated model studies was the isolation of the final product by acidic work up. It is well know that during acidic work up hydrolysis occurs. Thus, a direct method was necessary to investigate the mechanistic path for the oxidative, aromatic C–C bond cleavage reaction of 2-aminophenol unit. In this context, ligand **H_2Gan^{AP}** has been investigated. The ligand itself contained a 2-aminophenol unit. Thus, the substrate needs not to be added externally.

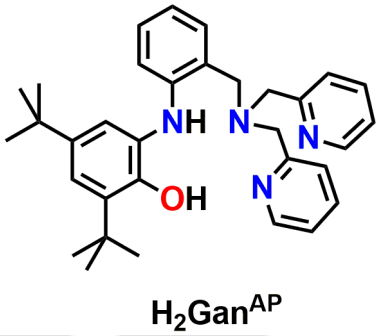

Figure 1.4: *Schematic representation of ligand* ***H_2Gan^{AP}***.

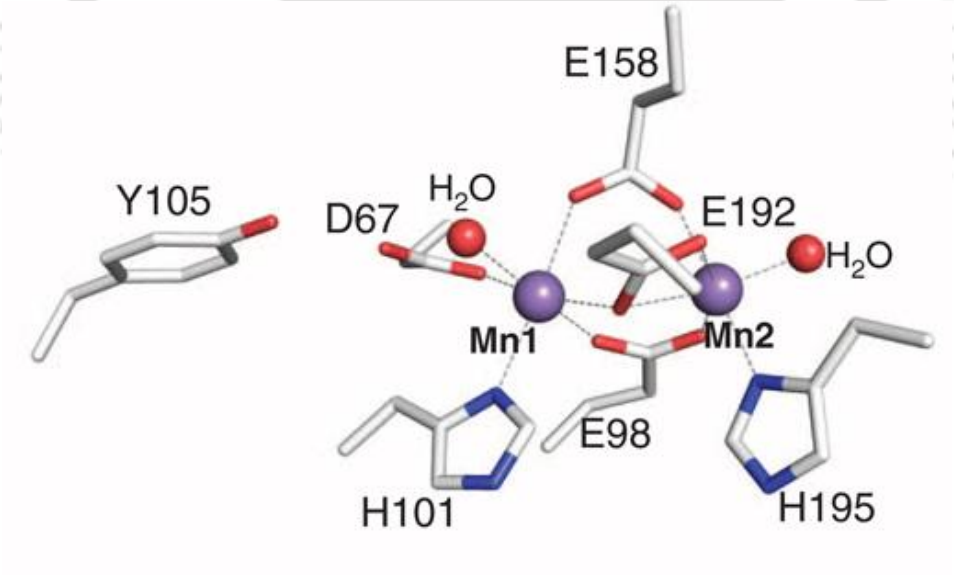

Figure 1.5: *Stereoview of the Mn^{II}_2-NrdF active site. Mn^{II} ions are shown as purple spheres, water molecules are shown as red spheres, and NrdF side chains are represented in stick format and colored by atom type.*[13i]

Ribonucleotide Reductase (RNRs) is an enzyme that catalyzes the formation of nucleotides to corresponding deoxynucleotides, required for DNA replication and repair for all organisms.[13a-f] In 1998, J. Stubbe and coworkers reported a manganese(III) containing RNRs having cofactor class Ib. The cofactor class-Ib comprises of a di-manganese cluster and a tyrosyl radical which is essential for the initiation of radical-dependent nucleotide reduction.[13g] It has been proposed that the formation of the active site proceeds *via* the initial reaction of a O_2 molecule and NrDF subunit, which is consequently transformed to superoxide radical form (**Scheme 1.5**).[13j-k] Thus generated superoxide species transforms Mn(II) to the higher oxidation state Mn(III) and Mn(IV). The Mn(IV) unit then oxidizes Tyr105 to the corresponding radical.

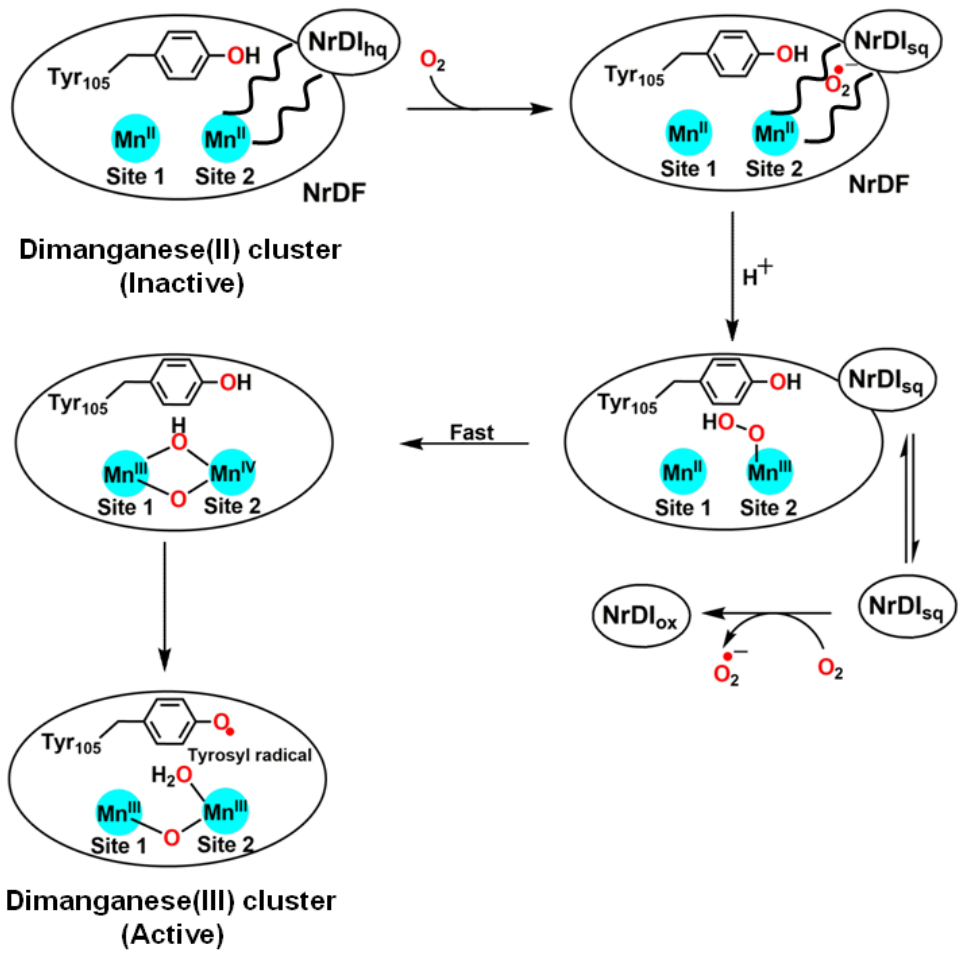

Scheme 1.5: *Generation of active tyrosyl radical in the active site of class–Ib Ribonucleotide Reductase(RNRs).*[13j]

Ligand **H_2Gan^{AP}** is pentadentate and also contained redox-active 2-aminophenol unit. Manganese complexes are generally six-coordinate. Thus, ligand **H_2Gan^{AP}** was employed for the possible synthesis of dinuclear oxo-briged Mn_2-radical complex to the structural and spectroscopic investigations.

Galactose Oxidase (GOase),[4] a mononuclear copper enzyme which uses a tyrosyl radical to facilitate the two-electron oxidation of primary alcohols to aldehydes with the subsequent reduction of dioxygen to peroxide. From single crystal X-ray crystallographic studies of GOase, it is pointed out that the active site structure of this metalloenzyme contains one copper atom, which is coordinated two tyrosine unit and two histidine units. The fifth coordination site is occupied by solvent molecule as water.[4e-f]

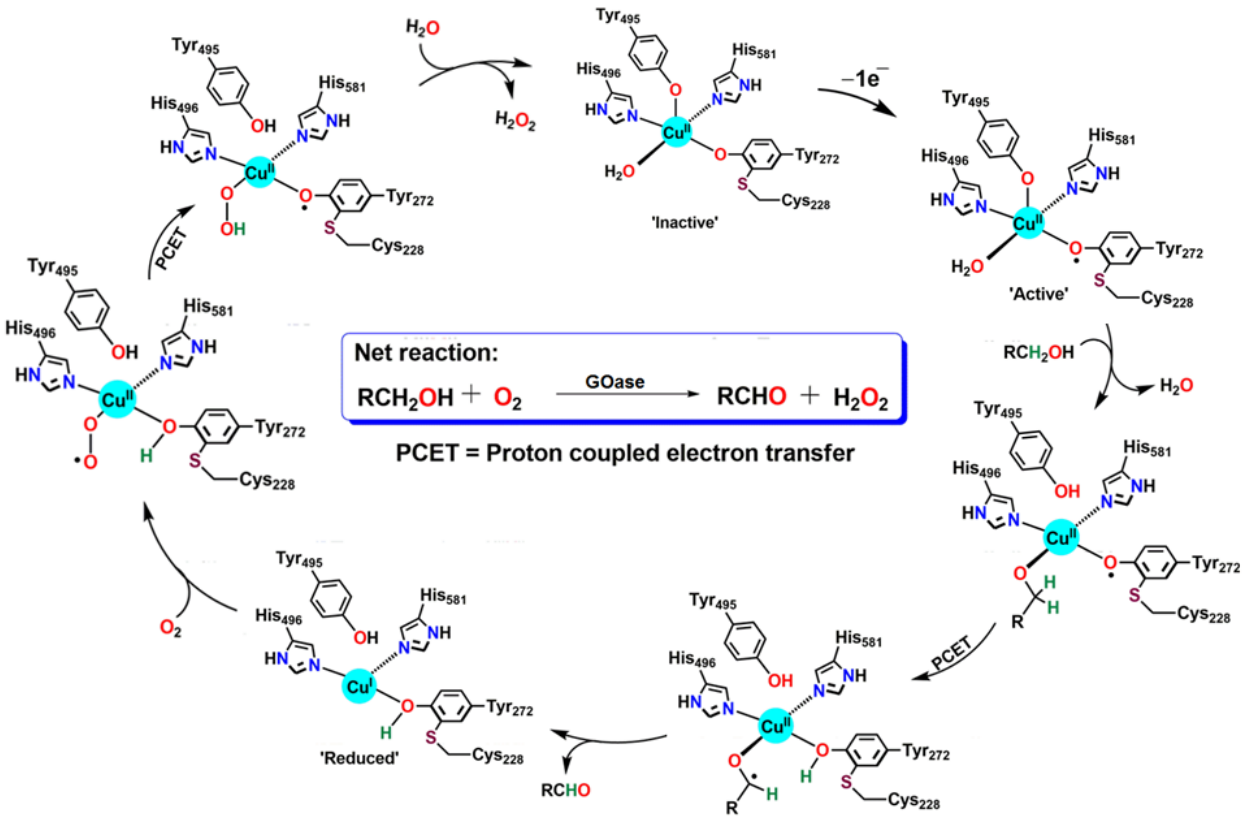

Scheme 1.8: *Proposed catalytic cycle of Galactose Oxidase(GOase).*[4e-f]

The active form of GOase consists of the Cu(II) ion, which is coordinated to Tyr272 radical. Both the redox active centers participate in the catalytic process (**Scheme 1.8**). Because of the simplicity of the active site, Cu(II)-radical-containing complexes have been successfully used as functional models for the oxidation of alcohols to the corresponding aldehydes.

Weighardt and coworkers extensively explore aminophenol based non-innocent ligand $\mathbf{H_2L^{AP}}$ [N(2-hydroxy-3,5-di-*tert*-butyl phenyl) aniline] as a basic constituent of several radical-containing transition metal complexes.[14a] Chaudhuri and coworkers reported that, different substituted ligands and their radical-containing metal complexes and their potential application on biomimetic model of GOase for transformation of alcohol to corresponding aldehyde (**Scheme 1.10**).[14b]

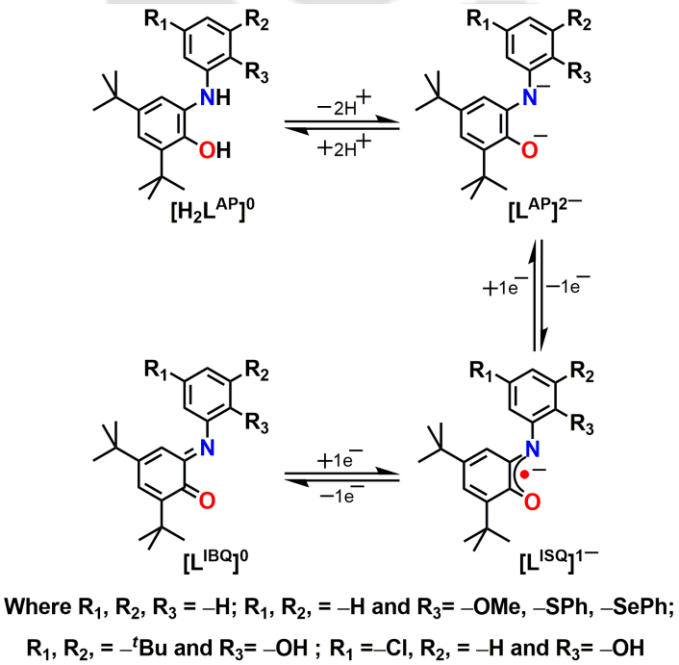

Scheme 1.9: *Probable oxidation states of different substituted* $\boldsymbol{H_2L^{AP}}$ *ligand.*

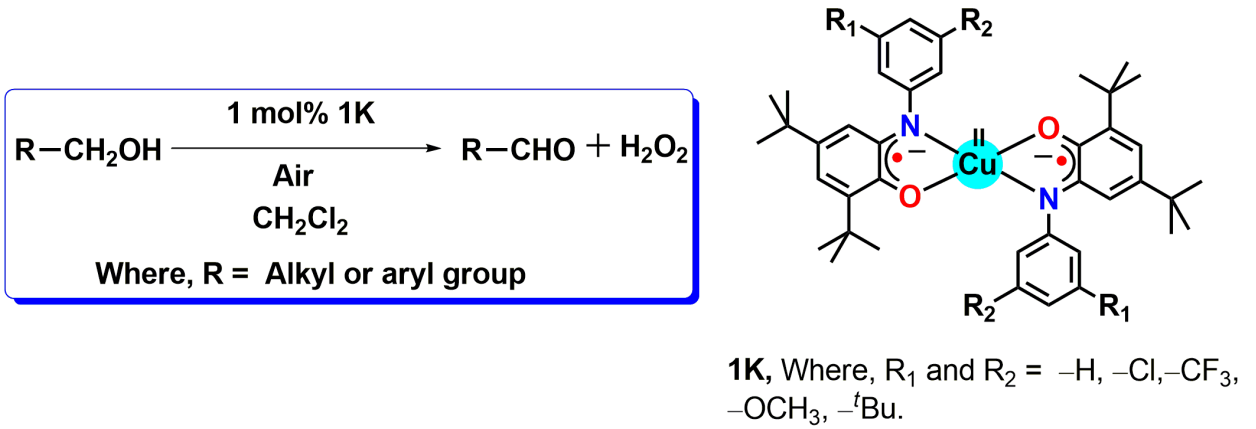

Scheme 1.10: *Mimicking model of Galactose Oxidase derived from aminophenol based ligand.*[14b]

To investigate on electronic structure and magnetic interactions between Cu(II) and a radical center, ligand $\mathbf{H_4L^{Piperazine(AP/AP)}}$ has been designed. In the ligand two redox-active 2-aminophenol units are bridged by a piperazine unit. The chair form of piperazine is more stable than that of boat form. Thus a binuclear four-coordinate Cu(II)-radical complex could be synthesized. The complex can be investigated as a catalyst for biomimetic aerial oxidation of alcohols to the corresponding aldehydes.

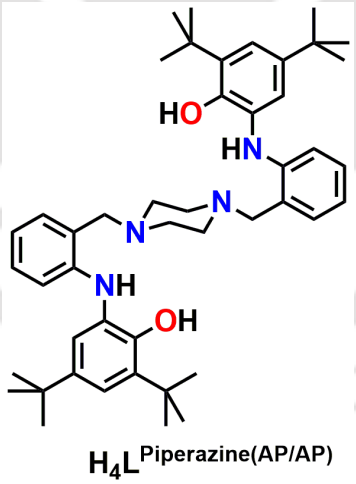

Figure 1.11: *Schematic representation of ligand* $\boldsymbol{H_4L^{Piperazine(AP/AP)}}$.

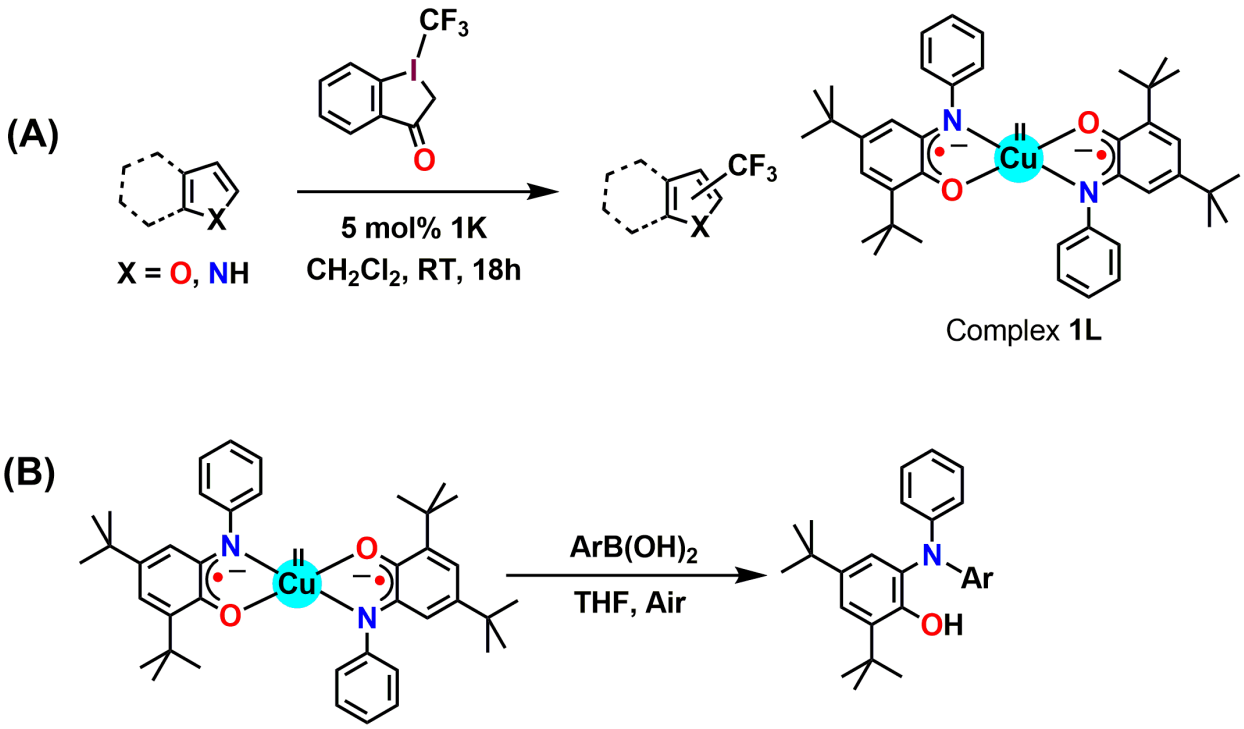

Scheme 1.12: *Utility of Cu(II)-bis(iminosemiquinone) complex; (A) –CF_3 group transfer reaction and (B) C–N bond forming reaction.*

In addition to alcohol oxidation, In 2016, Fensterbank and coworkers reported that utilising Cu(II)-bis(iminosemiquinone) complex **1L**, $CF_3^{\bullet}$ radical can be generated from a CF_3^{+} source.[15a] In the process, the one-electron reduction of CF_3^{+}-ion is assisted by the ligand centered single electron transfer (SET) of complex **1L**. Thus generated $CF_3^{\bullet}$ radical can be utilized in trifluoromethylation of heteroaromatics (**Scheme 1.12A**), trifluoromethylation of silyl enol ethers and hydrotrifluoromethylation of alkynes.[15a] The group has also reported that C–N bond forming reaction can also be performed under air (**Scheme 1.12B**)[15b] by using Cu(II)-bis(iminosemiquinone) complex (**1L**).

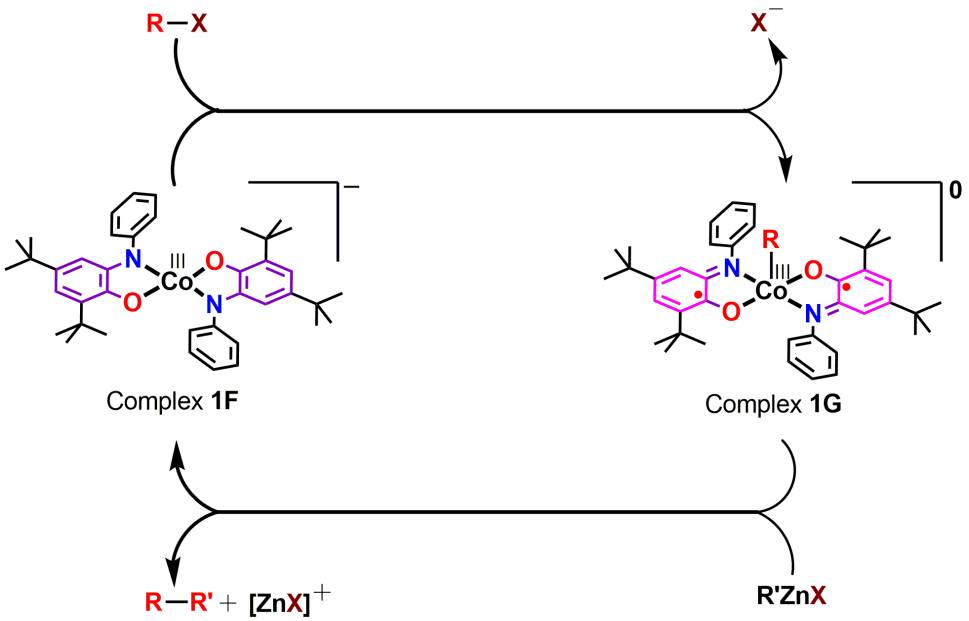

Scheme 1.13: *Negishi–like cross–coupling of alkyl halides with organozinc reagents by Co(III)bis(o-amidophenolato) complex.*

The radical moiety in the radical-coordinated metal complexes acts as electron reservoir. Easy oxidation as well as reduction of the radical unit has been successfully utilized in developing oxidation-reduction catalysts. In 2010, Soper and coworkers discovered that redox-active aminophenol-derived ligands can be used to bring about palladium-like organometallic oxidative addition and reductive elimination reactions at square planar later first row metal centers. In one application of this strategy, they showed that four coordinate cobalt(III) complexes with redox-active amidophenolate ligands are strong nucleophiles that react with alkyl halides, including primary alkyl chlorides, under gentle conditions to generate stable alkylcobalt(III) complexes. The electrophilic addition reactions are unusual because they formally oxidize the cobalt(III) fragment by two electrons, but there are no changes in cobalt oxidation state because the reactions proceed with single electron oxidation of each amidophenolate ligand. Subsequent treatment of the alkylcobalt(III) complexes with organozinc halides results in reductive coupling to form new C–C bonds, regenerating the four-coordinate cobalt(III) starting materials (**Scheme 1.13**).[16a]

Collectively, these reactions form an unusually well defined cycle for cobalt Negishi-like coupling of alkyl halides with organozinc halides. Importantly, this reaction scheme can be used for assembly of aliphatic alkyl-alkyl linkages without forming radical intermediates because, despite the thermodynamic bias for sequential one-electron transfer, the kinetically preferred reactions are concerted two-electron processes. Current efforts are optimizing the C–C reductive elimination reaction for development of highly active redox-active ligand complexes for cross coupling.

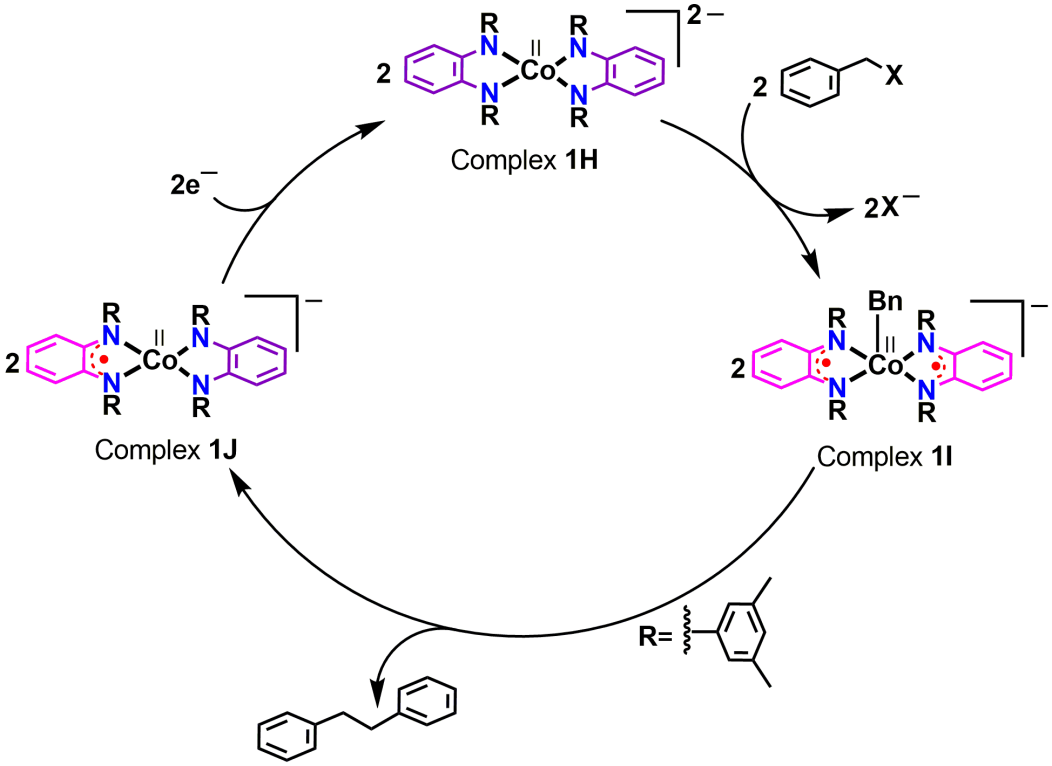

Scheme 1.14: *Electrocatalytic coupling of dibenzyl by Co(II)bis(o-phenylenediamine) complex.*

Recently, Sarkar and coworkars reported a four-coordinate cobalt complex **1H** capable of electrocatalytic C–C bond formation (**Scheme 1.14**).[16b] The ligand assisted oxidative addition of benzyl bromide to the metal ion provide a diradical-containing square pyramidal complex **1I**, where $-CH_2Ph$ (Bn) is axially coordinated to the metal ion. The formation of C−C coupled dibenzyl product results the complex **1J**, which upon one-electron reduction regenerates the active catalyst **1H**.

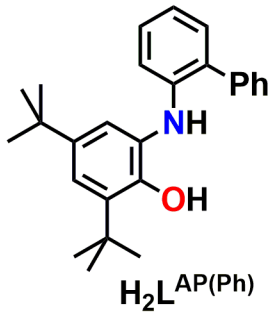

Figure 1.15: *Schematic representation of ligand* $H_2L^{AP(Ph)}$.

In order to investigate on C–C and C–N coupling reaction, ligand $\mathbf{H_2L^{AP(Ph)}}$ has been designed. In the ligand, one of the *ortho*-positions of the N-phenyl-ring of $\mathbf{H_2L^{AP}}$ [N(2-hydroxy-3,5-di-*tert*-butyl phenyl) aniline] ligand was substituted by a bulky phenyl ring. This bulky ring would block one of the two axial positions in four-coordinate complexes. Thus, one of the two axial positions will be available for the catalysis. Hence, more selectivity could be availed.

In short, the main objectives of this research work are: synthetic of radical-coordinated transition metal complexes; investigation on geometry and electronic structures of the complexes *via* X-ray crystallography, electrochemistry, spectroscopy and DFT-based computational method, and to examine the catalytic applications of the synthesized complexes.

References

1. 1. (*a*) I. G. Denisov, T. M. Makris, S. G. Sligar and I. Schlichting, *Chem. Rev.*, 2005, **105**, 2253; (*b*) S. Shaik, D. Kumar, S. P. de Visser, A. Altun and W. Thiel, *Chem. Rev.*, 2005, **105**, 2279; (*c*) J. T. Groves, *J. Inorg. Biochem.*, 2006, **100**, 434; (*d*) B. A. Jazdzewski and W. B. Tolman, *Coord. Chem. Rev.*, 2000, **200–202**, 633; (*e*) J. W. Whittaker, *Chem. Rev.*, 2003, **103**, 2347; (*f*) P. Verma, R. C. Pratt, T. Storr, E. C. Wasinger and T. D. P. Stack, *Proc. Natl. Acad. Sci. U. S. A.*, 2011, **108**, 18600; (*g*) R. C. Pratt, C. T. Lyons, E. C. Wasinger and T. D. P. Stack, *J. Am. Chem. Soc.*, 2012, **134**, 7367; (*h*) C. T. Lyons and T. D. P. Stack, *Coord. Chem. Rev.*, 2013, **257**, 528; (*i*) J. Stubbe and W. A. van der Donk, *Chem. Rev.*, 1998, **98**, 705.

2. (*a*) J. -F. Wu, C. -W. Sun, C. -Y. Jiang, Z. -P. Liu and S. -J. Liu, *Arch. Microbiol.*, 2005, **183**, 1; (*b*) S. Takenaka, S. Murakami, R. Shinke, K. Hatakeyama, H.Yukawa and K. Aoki, *J. Biol. Chem.*, 1997, **272**, 14727; (*c*) U. Lendenmann and J. C. Spain, *J. Bacteriol.*, 1996, **178**, 6227.

3. (*a*) B. M. Sjoberg, P. Reichard, A. Graslund and A. Ehrenberg, *J. Biol. Chem.*, 1978, **253**, 6863. (*b*) J. A. Cotruvo, T. A. Stich, R. D. Britt and J. Stubbe, *J. Am. Chem. Soc.* 2013, **135**, 4027; (*c*) A. K. Boal, J. A. Cotruvo Jr., J. Stubbe and A. C. Rosenzweig, *Science* 2010, **329**, 1526.

4. (*a*) N. Ito, S. E. V. Phillips, C. Stevens, Z. B. Ogel, M. J. N. McPherson, K. D. S. Yadav, P. F. Knowles, *Nature*, 1991, **350**, 87; (*b*) Whittaker, M. M.; Whittaker, J. W. *Biol. Chem.*, 1990, **265**, 9610; (*c*) J. Stubbe, W. A. van der Donk, *Chem. Rev.*, 1998, **98**, 705; (*d*) N. Ito, S. E. V. Phillips, K. D. S. Yadav and P. F. Knowles, *J. Mol. Biol.*, 1994, **238**, 794; (*e*) Y. Wang and T. D. P. Stack, *J. Am. Chem. Soc.*, 1996, **118**, 13097; (*f*) Y. Wang, J. L. DuBois, B. Hedman, K.O. Hodgson and T. D. P. Stack, *Science*, 1998, **279**, 537.

5. (*a*) J. Yano and V. Yachandra, *Chem. Rev.*, 2014, **114**, 4175; (*b*) K. J. Young, B. J. Brennan, R. Tagore and G. W. Brudvig, *Acc. Chem. Res.*, **2015**, *48*, 567; (*c*) M. Suga, F. Akita, K. Hirata, G. Ueno, H. Murakami, Y. Nakajima, T. Shimizu, K. Yamashita, M. Yamamoto, H. Ago and J.-R. Shen, *Nature*, 2015, **517**, 99; (*d*) S. Mukhopadhyay, S. K. Mandal, S. Bhaduri and W. H. Armstrong, *Chem. Rev.*, 2004, **104**, 3981; (*e*) J. P. McEvoy and G. W. Brudvig, *Chem. Rev.*, 2006, **106**, 4455.

6. (*a*) K. H. Baker and D. S. Herson, In *Bioremediation*; McGraw-Hill, Inc.: New York, 1994, p 9–60; (*b*) R. E. Parales and J. D. Haddock, *Curr. Opin. Biotechnol.*, 2004, **15**, 374; (*c*) D. T. Gibson and R. E. Parales, *Curr. Opin. Biotechnol.* 2000, **11**, 236.

7. (*a*) J. D. Lipscomb and A. M. Orville, *Met. Ions Biol. Syst.*, 1992, **28**, 243; (*b*) M. R. Harpel and J. D. Lipscomb, *J. Biol. Chem.*, 1990, **265**, 22187; (*c*) T. E. Machonkin, P. L. Holland, K. N. Smith, J. S. Liberman, A. Dinescu, T. R. Cundari and S. S. Rocks, *J. Biol. Inorg. Chem.*, 2010, **15**, 291;(*d*) E. J. A. Veldhuizen, F. H. Vaillancourt, C. J. Whiting, M. M. Y. Hsiao, G. Gingras, Y.F. Xiao, R. M. Tanguay, J. Boukouvalas and L. D. Eltis, *Biochem. J.*, 2005, **386**, 305; (*e*) U. Lendenmann and J. C. Spain, *J. Bacteriol.*,1996, **178**, 6227; (*f*) X. Li, M. Guo, J. Fan, W. Tang, D. Wang, H. Ge, H. Rong, M. Teng, L. Niu, Q. Liu and Q. Hao, *Protein Sci.*,2006, **15**, 761; (*g*) I. Matera, M. Ferraroni, S. Buerger, A. Scozzafava, A. Stolz, F. Briganti, *J. Mol. Biol.*, 2008, **380**, 856; (*h*) J. P. Hintner, T. Remtsma and A. Stolz, *J. Biol. Chem.*, 2004, **279**, 37250; (*i*) J. P. Hintner, C. Lechner, U. Riegert, A. E. Kuhm, T. Storm, T. Reemtsma and A. Stolz, *J. Bacteriol.*, 2001, **183**, 6936.

8. (*a*) B. Kauppi, K. Lee, E. Carredano, R. E. Parales, D. T. Gibson, H. Eklund and S. Ramaswamy, *Structure*, 1998, **6**, 571; (*b*) F. H. Vaillancourt, J. T. Bolin and L. D. Eltis, *Crit. Rev. Biochem. Mol. Biol.*, 2006, **41**, 241; (*c*) S. Han, L. D. Eltis, K. N. Timmis, S. W. Muchmore and J. T. Bolin, *Science*, 1995, **270**, 976; (*d*) F. H. Vaillancourt, C. J. Barbosa, T. G. Spiro, J. T. Bolin, M. W. Blades, R. F. B. Turner and L. D. Eltis, *J. Am. Chem. Soc.*, 2002, **124**, 2485; (*e*) A. Karlsson, J. V. Parales, R. E. Parales, D. T. Gibson, H. Eklund and S. Ramaswamy, *Science*, 2003, **299**, 1039; (*f*) E. G. Kovaleva and J. D. Lipscomb, *Science*, 2007, **316**, 453.

9. (*a*) F. H. Vaillancourt, C. J. Barbosa, T. G. Spiro, J. T. Bolin, M. W. Blades, R. F. B. Turner and L. D. Eltis, *J. Am. Chem. Soc.*, 2002, **124**, 2485; (*b*) J. D. Lipscomb, *Curr. Opin. Chem. Biol.*, 2008, **18**, 644; (*c*) N. Sato, Y. Uragami, T. Nishizaki, Y. Takahashi, G. Sazaki, K. Sugimoto, T. Nonaka, E. Masai, M. Fukuda and T. Senda, *J. Mol. Biol.*, 2002, **321**, 621.

10. (*a*) N. Sato, Y. Uragami, T. Nishizaki, Y. Takahashi, G. Sazaki, K. Sugimoto, T. Nonaka, E. Masai, M. Fukuda and T. Senda, *J. Mol. Biol.*, 2002, **321**, 621; (*b*) I. Schlichting, J. Berendzen, K. Chu, A. M. Stock, S. A. Maves, D. E. Benson, R. M. Sweet, D. Ringe, G. A. Petsko and S. G. Sligar, *Science*, 2000, **287**, 1615; (*c*) C. E. Tinberg and S. J. Lippard, *Acc. Chem. Res.*, 2011, **44**, 280; (*d*) C. Krebs, D. Galonić Fujimori, C. T. Walsh and J. M Bollinger, *Acc. Chem. Res.*, 2007,

40, 484; (*e*) Y. Zhang, K. L. Colabroy, T. P. Begley, S. E. Ealick, *Biochemistry*, 2005, **44**, 7632; (*f*) E. G. Kovaleva, M. B. Neibergall, S. Chakrabarty and J. D. Lipscomb, *Acc. Chem. Res.*, 2007, **40**, 475; (*g*) T. D. H. Bugg and S. Ramaswamy, *Curr. Opin. Chem. Biol.*, 2008, **12**, 134.

11. (*a*) M. M. Bittner, S. V. Lindeman and A. T. Fiedler, *J. Am. Chem. Soc.*, 2012, **134**, 5460; (*b*) M. M. Bittner, S. V. Lindeman, C. V. Popescu and A. T. Fiedler, *Inorg. Chem.*, 2014, **53**, 4047; (*c*) M. M. Bittner, D. Kraus, S. V. Lindeman, C. V. Popescu and A. T. Fiedler, *Chem. –Eur. J.*, 2013, **19**, 9686.

12. (*a*) B. Chkraborty and T. K. Paine, *Angew. Chem., Int. Ed.*, 2013, **52**, 920; (b) B. Chakraborty, S. Bhunya, A. Paul and T. K. Paine, *Inorg. Chem.*, 2014, **53**, 4899; (c) S. Chatterjee and T. K. Paine, *Inorg. Chem.*, 2015, **54**, 1720.

13. (*a*) A. Ehrenberg and P. Reichard, *J. Biol. Chem.*, 1972, **247**, 3485; (*b*) A. Gräslund and A. Ehrenberg, *Appl. Magn. Reson.*, 2007, **31**, 447; (*c*) M. A. S. Perez, P. A. Fernandes and M. J. Ramos, *J. Chem. Theory Comput.*, 2010, **6**, 2770; (*d*) T. P. Dang, A. J. Sobczak, A. M. Mebel, C. Chatgilialoglu and S. F. Wnuk, *Tetrahedron*, 2012, **68**, 5655; (*e*) E. C. Minnihan, D. G. Nocera and J. Stubbe, *Acc. Chem. Res.*, 2013, **46**, 2524; (*f*) J. Stubbe, D. G. Nocera, C. S. Yee and M. C. Y. Chang, *Chem. Rev.*, 2003, **103**, 2167; (*g*) J. Stubbe and P. Riggs–Gelasco, *Trends Biochem. Sci.*, 1998, **23**, 438; (*h*) M. D. Sintchak, G. Arjara, B. A. Kellogg, J. Stubbe and C. L. Drennan, *Nat. Struct. Biol.*, 2002, **9**, 293; (*i*) J. A. Cotruvo and J. Stubbe, *Biochemistry*, 2010, **49**, 1297; (*j*) Y. Zhang and J. Stubbe, *Biochemistry*, 2011, **50**, 5615; (*k*) J. A. Cotruvo, T. A. Stich, R. D. Britt and J. Stubbe, *J. Am. Chem. Soc.*, 2013, **135**, 4027.

14. (*a*) P. Chaudhuri, C. N. Verani, E. Bill, E. Bothe, T. Weyhermüller and K. Wieghardt, *J. Am. Chem. Soc.*, 2001, **123**, 2213; (*b*) C. Mukherjee, U. Pieper, E. Bothe, V. Bachler, E. Bill, T. Weyhermüller and P. Chaudhuri, *Inorg. Chem.*, 2008, **47**, 2740; (*c*) S. Mukherjee, T. Weyhermüller, E. Bothe, K. Wieghardt and P. Chaudhuri, *Dalton Trans.*, 2004, 3842.

15. (*a*) J. Jacquet, S. Blanchard, E. Derat, M. Murr and L. Fensterbank, *Chem. Sci.*, 2016, **7**, 2030; (*b*) J. Jacquet, P. Chaumont, G. Gontard, M. Orio, H. Vezin, S. Blanchard, M. Murr, and L. Fensterbank, *Angew. Chem., Int. Ed.*, 2016, **55**, 10712.

16. (*a*) A. L. Smith, K. I. Hardcastle and J. D. Soper, *J. Am. Chem. Soc.* 2010, **132**, 14358; (*b*) M. van der Meer, Y. Rechkemmer, I. Peremykin, S. Hohloch, J. van Slageren and B. Sarkar, *Chem. Commun.*, 2014, **50**, 11104.

Chapter II

Synthesis and Characterization of Non-Innocent Ligand, [H_2Gan^{AP}] and its Corresponding Dinuclear μ_2-oxo-Bridge Fe(III) and Mn(III) Complexes

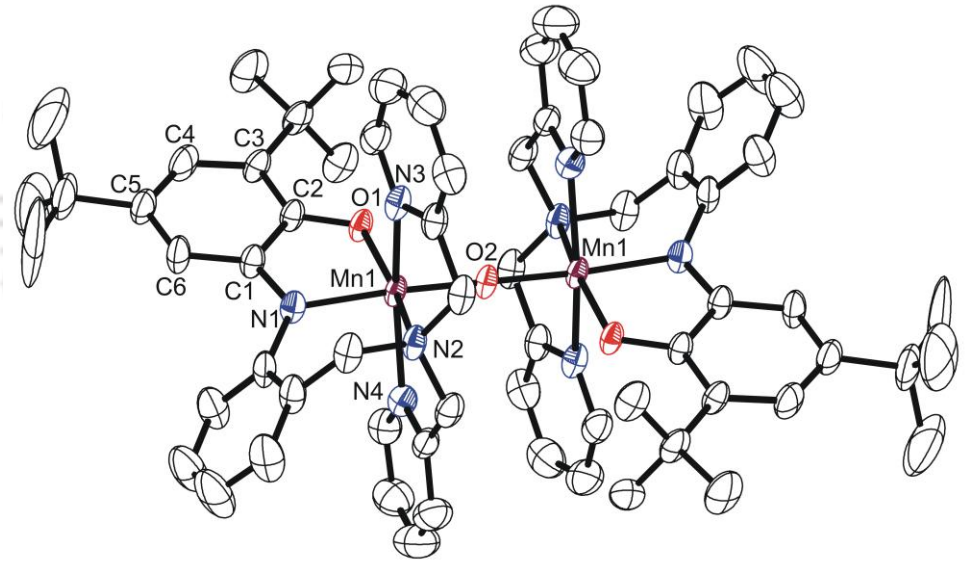

*Some results have been published in

***Inorg*. *Chem*.**, 2017, **56**, 729–736.

2.1 Introduction

2-Aminophenol-1,6-dioxygenase (APD)[1] belongs to dioxygenases family and catalyses the biodegradation of 2-aminophenol derivatives *via* oxidative extradiol-type aromatic C–C bond cleavage at the meta-position (C1–C6) under aerobic atmosphere. In the reaction, fission of a dioxygen bond and incorporation of both the oxygen atoms into aliphatic product 2-aminomuconic acid semialdehyde takes place.[2] The product then undergoes non-enzymatic condensation spontaneously and finally forms 2-picolinic acid (**Scheme 2.1**).

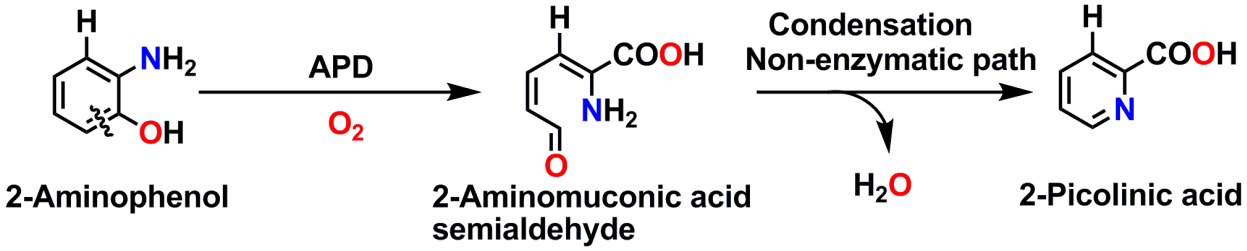

Scheme 2.1: *APD catalyzed C–C bond cleavage of 2-aminophenol.*

In 2013, Li *et al*[3] have reported the crystal structures of APD from *Comamonas sp.* strain CNB-1 as the apoenzyme, the holoenzyme and as complexes with the lactone intermediate (4Z,6Z)-3-iminooxepin-2(3H)-one, the product 2-aminomuconic-6-semialdehyde and with the suicide inhibitor 4-nitrocatechol. The active site of APD contains a mononuclear nonheme iron centre. The iron is in +II oxidation state[3] and the "His13-His62-Glu251 facial triad" occupies the coordination sites.[3] During the oxidation catalysis, both N and O atoms from the substrate 2-aminophenol derivative and an oxygen atom from a dioxygen molecule bind to the iron centre form the other face. Thus, a six-coordinate intermediate forms. The catalytic path for C–C bond cleavage of 2-aminophenol *via* the incorporation of two oxygen atoms is being proposed to follow the mechanism similar to that of extradiol cleavage by catechol dioxygenases.[4]

In general, it has been observed that redox-active 2-aminophenol or its derivatives upon coordination to iron center do not undergo aromatic C–C bond cleavage in the presence of dioxygen.[5] Rather, it exists mainly in its one-electron oxidized 2-iminobenzosemiquinonato π-radical state in the coordination complexes.[5] Thus, biomimetic model complexes for APD are very rare.[6] In the model complexes, either tridentate or tetradentate ligand scaffolds along with

substrate 2-aminophenol derivatives are being employed to form the corresponding five-coordinate and six-coordinate complexes under inert atmosphere. Dioxygen reactivity of those complexes is then studied for the mechanistic understanding of APD.[6] In all the reports, the aminophenol-derived cleavage products are isolated *via* acidic work up of the reaction solutions. In the procedure, the possibility of unexpected condensation and/or ring opening of the actual oxidative C–C cleavage species *via* hydrolysis cannot be revoked. Thus, a direct method for identification of the C–C bond cleavage product was necessary. In this context, we have incorporated a 3,5-di-*tert*-butyl-2-aminophenol unit at the *ortho*-position of a tripodal N,N-bis(pyridine-2-ylmethyl)benzylamine ligand scaffold (**Scheme 2.2**). Thus the designed ligand, designated here as $\mathbf{H_2Gan^{AP}}$, contains both substrate 2-aminophenol and tripodal N_3 iron coordination site. The ligand would provide a mononuclear five-coordinate iron complex that could allow its reaction toward dioxygen. Thus complex finally could provide the two oxygen atoms-incorporated C–C cleavage product of 3,5-di-*tert*-butyl-2-aminophenol unit. X-ray crystallographic analysis of the final complex would then provide crystallographic identification of the aromatic oxidative C–C cleavage product.

Manganese ions are omnipresent in living systems and catalyze a wide range of biological transformations, which include: water-splitting to oxygen molecule in photosynthesis (PS II);[7] the reduction of nucleotides to their corresponding deoxynucleotides for DNA replication and repair of all organisms (Ribonucleotide Reductase);[8] dismutation of toxic superoxide to hydrogen peroxide and oxygen molecule (Mn-Superoxide Dismutase);[9] decomposition of hydrogen peroxide to water and oxygen molecule (Catalase);[10] etc. In all the enzymatic activities, the manganese ions shuttle between various oxidation states. In addition to the involvement of manganese ions of different oxidation states, the participation and the pivotal role of a tyrosine radical in PS II are equivocally establishes. Recently, Stubbe and co-workers[8b] have concluded the presence of a mono(μ-oxo)-bridged Mn_2^{III}-tyrosine radical unit as the active site in the cofactor of Class Ib Ribonucleotide Reductase. Hence, the synthesis, as well as structural and spectroscopic characterization of mono(μ-oxo)-bridged, radical-containing binuclear Mn(III) complexes have attained a special interest.

Bis(μ-oxo)-bridged binuclear Mn-complex are well documented.[11a-f] Mono(μ-oxo)-bridged binuclear Mn(III) complexes and radical-conatining Mn(III) complexes are scarce. While, to the best of our knowledge, mono(μ-oxo)-bridged binuclear Mn(III) complex coordinated to π-radical anions is yet to be reported. Herein, we have initiated the plausible synthesis of a mono(oxo)-bridged, radical-containing binuclear Mn(III) complex.

2.2 Synthesis and Characterization of Five-coordinate Pyridine based Aminophenol Appended Non-innocent Ligand H_2Gan^{AP}

A schematic representation for the synthesis of ligand **H_2Gan^{AP}** is shown in **Scheme 2.2**.

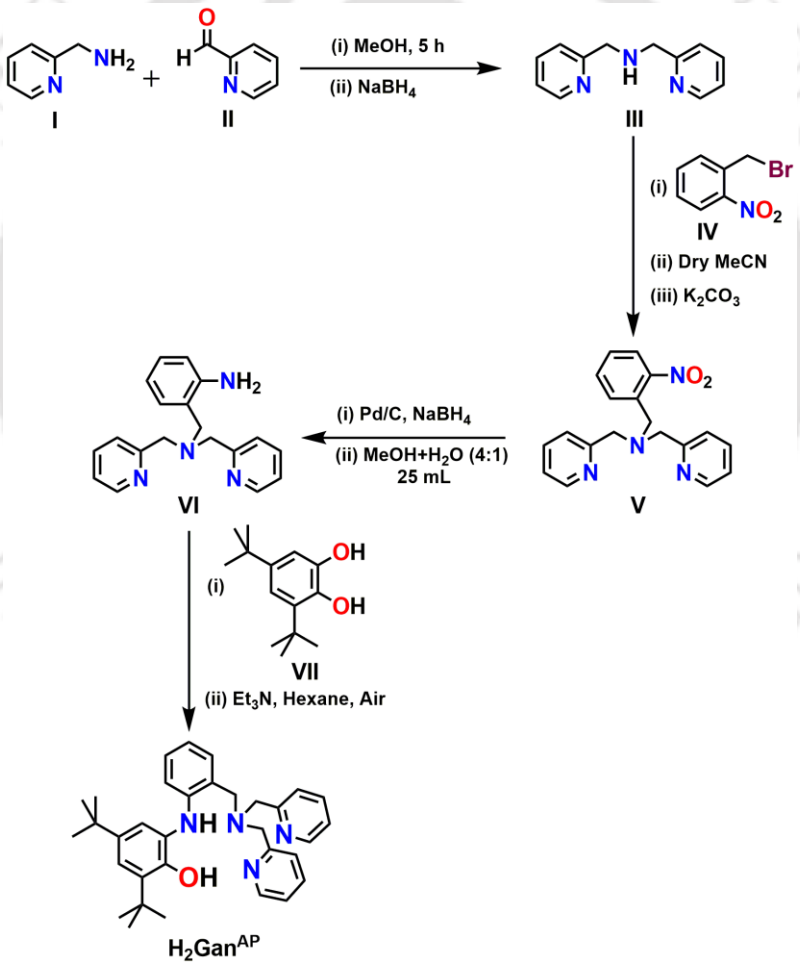

Scheme 2.2: *Synthetic route for the preparation of* ***H_2Gan^{AP}***.

A reaction between 1:1 2-picolyl amine (**I**) with pyridinecarboxaldehyde (**II**) in CH_3OH followed by $NaBH_4$ reduction gave bis(2-pyridylmethyl)amine (**III**).[11g] 2-[bis(2-pyridylmethyl)aminomethyl]-nitrobenzene (**V**) was formed by reaction between bis(2-pyridylmethyl)amine (**III**) with 2-nitrobenzyl bromide (**IV**) in dry CH_3CN in the presence of K_2CO_3, which upon reduction by Pd/C in the presence of $NaBH_4$ provided 2-[bis(2-pyridylmethyl)aminomethyl)]aniline (**VI**).[11h-i] The ligand **H_2Gan^{AP}** was was obtain in 50% yield (**Scheme 2.2**) by reacting equimolar amounts of 2-[bis(2-pyridylmethyl)aminomethyl]aniline (**VI**) and 3,5-di-*tert*-butyl catechol (**VII**) in hexane in the presence of Et_3N under air. The ligand was characterized by using FT-IR spectroscopy, NMR spectroscopy and mass spectrometry techniques.

Initially, in the presence of Et_3N and air, 3, 5-di-*tert*-butyl catechol (**VII**) gets oxidized to 3, 5-di-*tert*-butyl benzoquinone (**BQ**). 2-[bis(2-pyridylmethyl)aminomethyl]aniline(**VI**) then reacted with the generated 3,5-di-*tert*-butyl benzoquinone (**BQ**) and provided the compound (**Gan^{IBQ}**), which will get reduced by an equivalent amount of 3,5-di-*tert*-butyl catechol(**VII**) and consequently, provided the ligand **H_2Gan^{AP}** (**Scheme 2.3**).[11j]

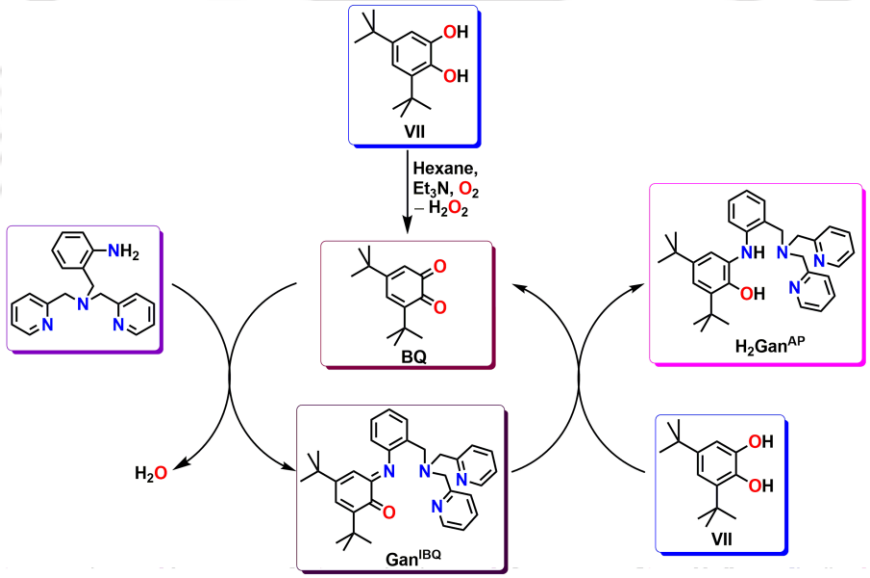

Scheme 2.3: *Probable mechanism for the formation of* ***H_2Gan^{AP}*** *from 3,5-di-tert-butyl catechol.*

The 2-aminophenol unit of the synthesized ligand **H_2Gan^{AP}** might behave as non-innocent and thus might exist in different oxidation states in the presence of metal ions (preferably transition metal) and molecular oxygen. The possible oxidation states of **H_2Gan^{AP}** are shown in **Scheme 2.4**.

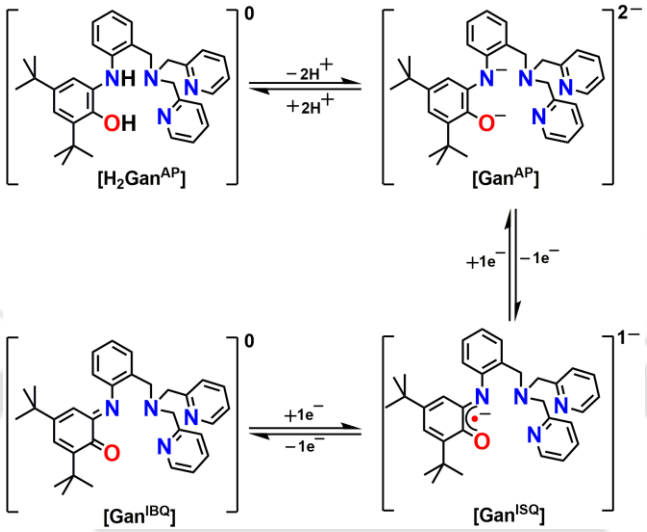

Scheme 2.4: *Possible oxidation states of* ***H_2Gan^{AP}***.

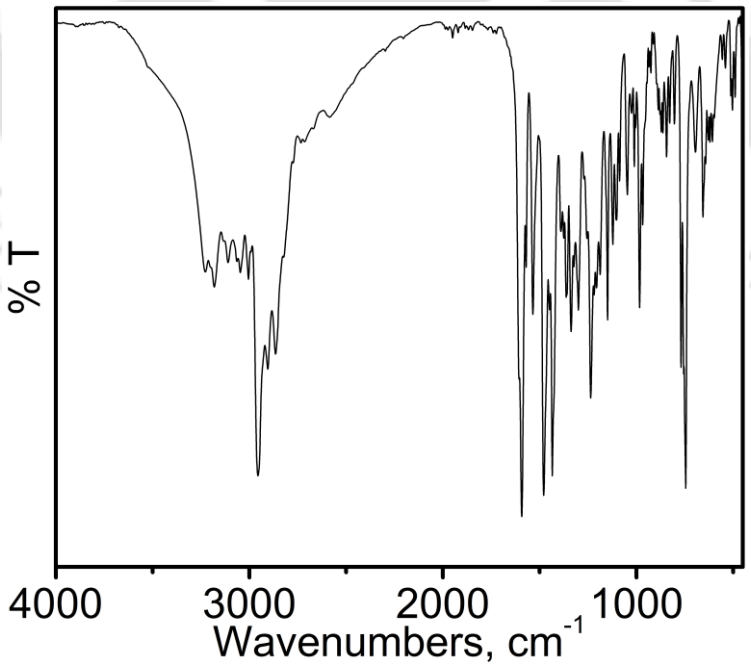

Figure 2.1: *FT-IR spectrum of ligand* ***H_2Gan^{AP}***.

In FT-IR spectrum of the ligand **H_2Gan^{AP}** (**Figure 2.1**)showed two sharp bands at 3227 cm^{-1} and 3181 cm^{-1} due to ν(O–H), and ν(N–H) stretching, respectively.[12a-b] A weak band appeared at 3047 cm^{-1} for the stretching of aryl ν(C−H). The asymmetric, symmetric and overtone bands of ν(C–H) stretching for *tert*-butyl groups appeared at 2955, 2904, 2864 cm^{-1}, respectively. [12a-d] In addition to this, the bending ν(C–H) stretching frequency for the $–CH_3$ groups, which belonged to *tert*-butyl groups, appeared at 1479 and 1362 cm^{-1}.[12a] The stretching bands at 1569, and 1434 cm^{-1} were attributed to the ν(C=C) stretches for phenyl system. [12a] The phenolic ν(C–O) stretching band appeared at 1318 cm^{-1} and ν(C–N) stretching band appeared at1218 cm^{-1}.[12a]

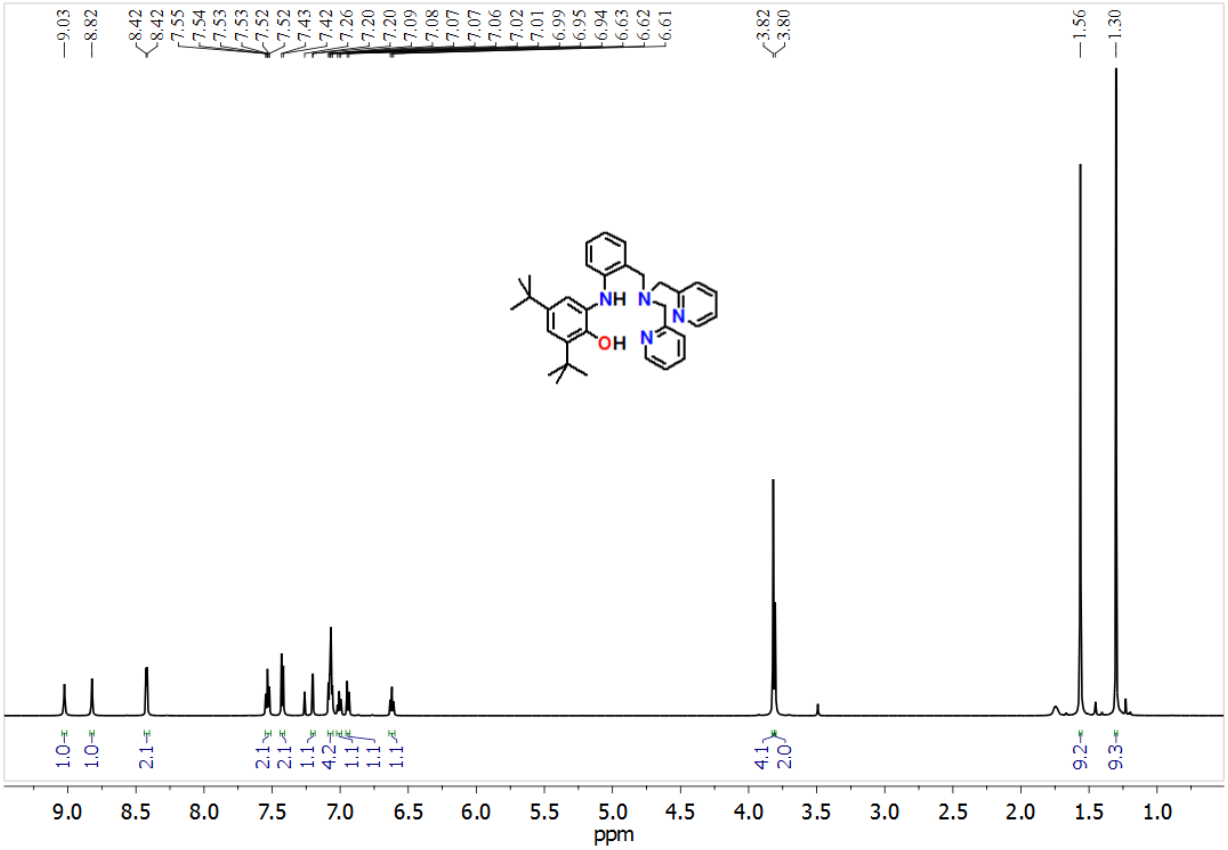

Figure 2.2: *^{1}H-NMR spectrum of **H_2Gan^{AP}** in $CDCl_3$.*

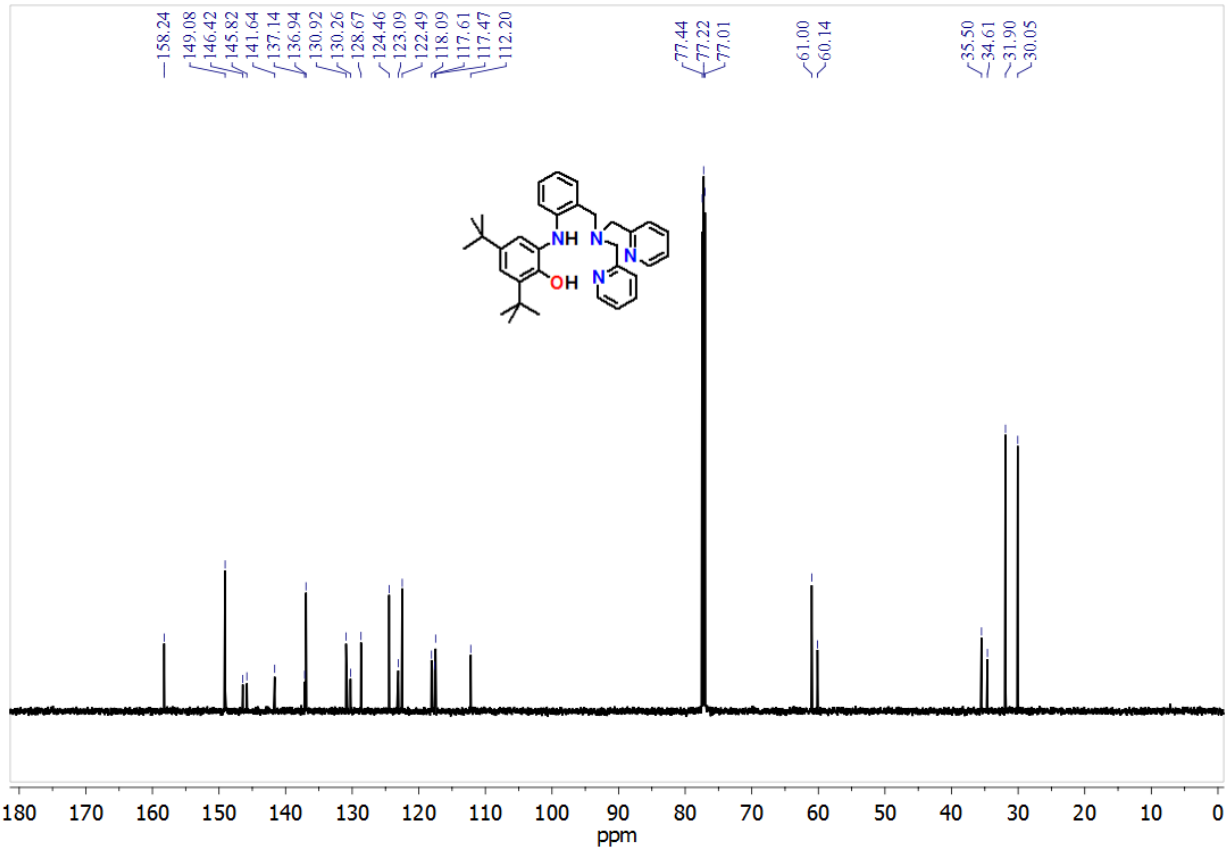

Figure 2.3: *^{13}C-NMR spectrum of* ***H_2Gan^{AP}*** *in $CDCl_3$.*

^{1}H-NMR spectrum for the ligand **H_2Gan^{AP}** displayed in (**Figure 2.2**). Two singlet resonance signals at δ =1.30 ppm and δ = 1.56 ppm were appeared due to two *tert*-butyl moiety containing hydrogen atoms. Fourteen aromatic protons appeared in the region of δ = 6.61–8.42 ppm. Two singlet peaks appeared at δ = 9.03 and δ = 8.82 ppm were because of N–H and O–H protons, respectively. ^{13}C-NMR spectrum (**Figure 2.3**) for the ligand **H_2Gan^{AP}** showed the 23 distinct characteristic peaks for 23 different kinds of carbon atoms.

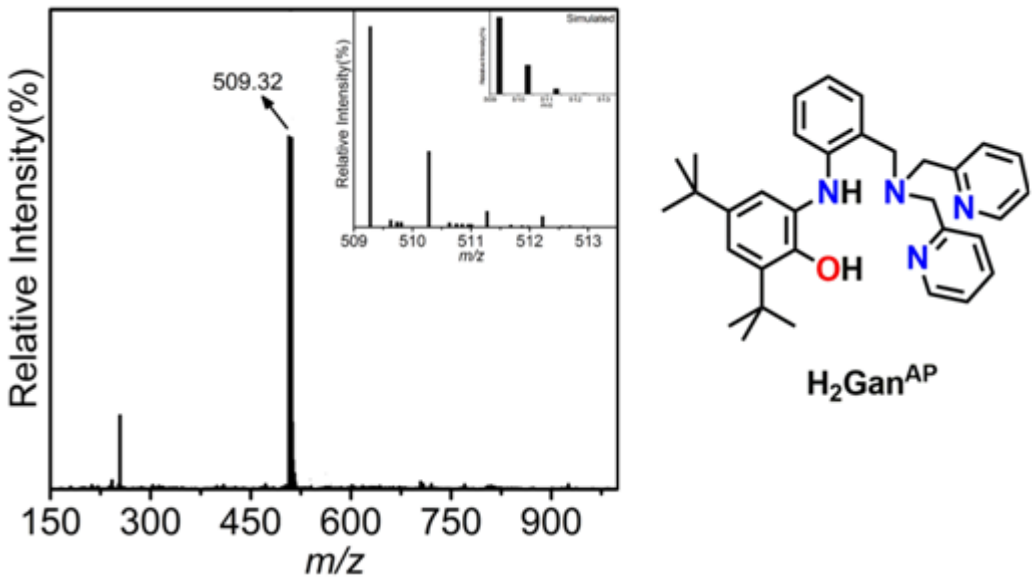

Figure 2.4: *ESI–mass spectra of ligand* ***H₂Gan*** ^{AP}*; experimental and simulated isotope distribution pattern (inset) for* $[C_{33}H_{40}N_4O+H]^+$.

Electrospray ionization mass spectrum (ESI-MS) of ligand **H₂Gan** ^{AP} in acetonitrile solution in positive mode showed a 100% molecular ion peak at *m/z* = 509.32 that corresponded to the $[M + H]^+$ (M = molecular mass). Isotope distribution pattern of the observed mass peaks confirmed the composition as $[C_{33}H_{40}N_4O +H]^+$ for **H₂Gan** ^{AP} (**Figure 2.4**).

2.3 Dioxygen Reactivity of an Iron Complex of 2-Aminophenol-Appended Ligand: Crystallographic Evidence of the Aromatic Ring Cleavage Product of the 2-Aminophenol Unit

Complex **2A** was synthesized in 54% yield by reacting equimolar amounts of ligand $\mathbf{H_2Gan^{AP}}$ and $Fe(ClO_4)_2 \bullet 6H_2O$ in CH_3CN (**Scheme 2.5**). X-ray quality single crystal of complex **2A** was obtained by slow evaporation of the reaction mixture.

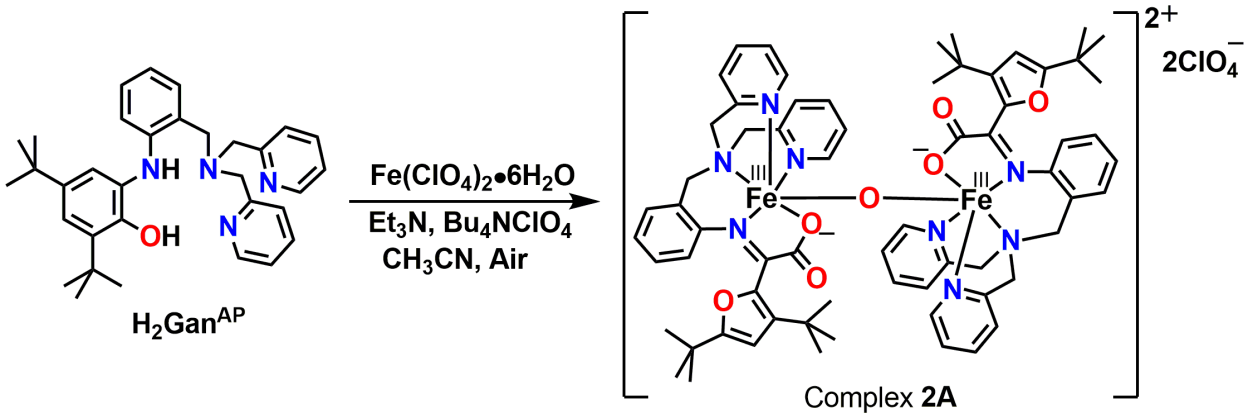

Scheme 2.5: *Synthetic route for the preparation of complex **2A**.*

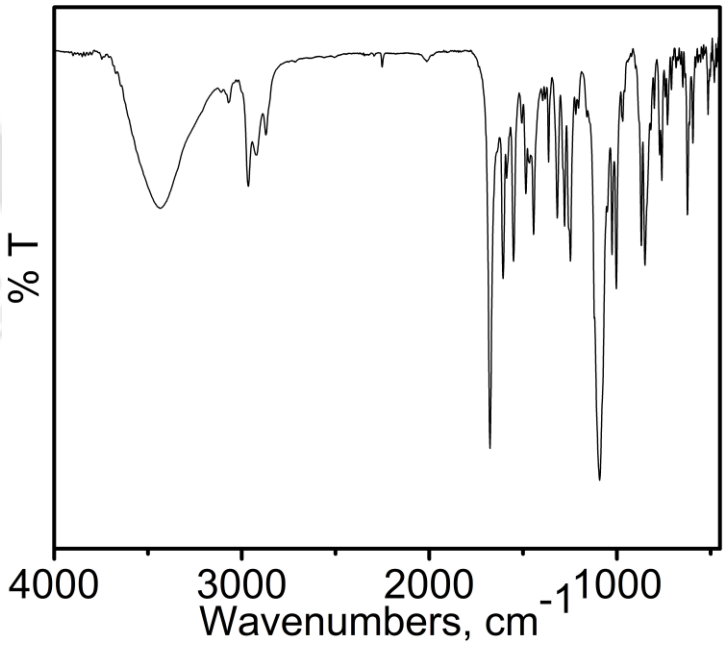

Figure 2.6: *FT-IR spectrum of complex **2A**.*

FT-IR spectrum of the complex **2A** (**Figure 2.6**) showed strong band at 1676 cm^{-1} due to the presence of ν(C=O) unit of the carboxylate group. The relatively weak band at 2251 cm^{-1} which is characteristic for ν(C≡N) suggested the presence of acetonitrile in complex **2A**. The strong band at 1092 cm^{-1} was attributed to the presence of perchlorate (ClO_4^-) anion. No characteristic stretching bands for ν(O–H) and ν(N–H) functional groups were found, which indicated the deprotonation of the groups occurred upon metal complex formation. The ν(C–H) stretching frequencies for the *tert*-butyl groups were found in 2956–2862 cm^{-1} region.[12a-d]

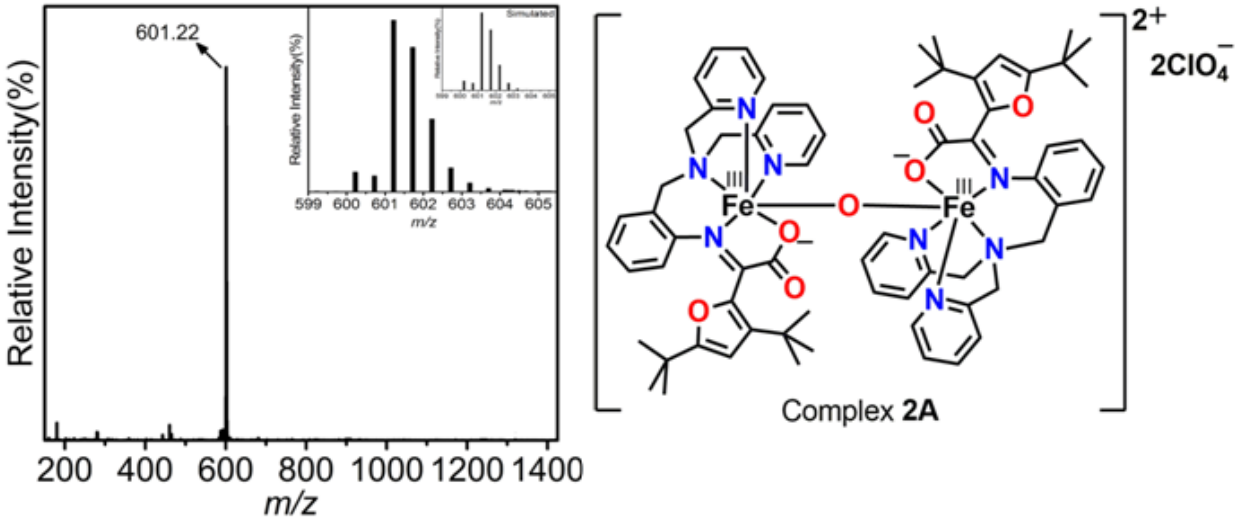

Figure 2.7: *ESI(positive mode)–Mass spectra of complex* ***2A*** *(m/z = $C_{66}H_{74}Fe_2N_8O_7$ where Z = 2); experimental and simulated isotope distribution pattern (inset).*

In the electrospray ionization mass spectrum (ESI-MS) of complex **2A** in CH_3CN a 100% molecular ion peak at *m/z* = 98.94 appeared in the negative mode, while, in the positive mode, a 100% molecular ion peak at *m/z* = 601.22 was observed (**Figure 2.7**). The peak at *m/z* = 98.94 confirmed the presence of perchlorate anion [$(ClO_4)^{1-}$] in the complex. Isotope distribution pattern indicated $[C_{66}H_{74}Fe_2N_8O_7]^{2+}$ composition for the observed positive mode peak at *m/z* = 601.22 and confirmed the formation of complex **2A**.

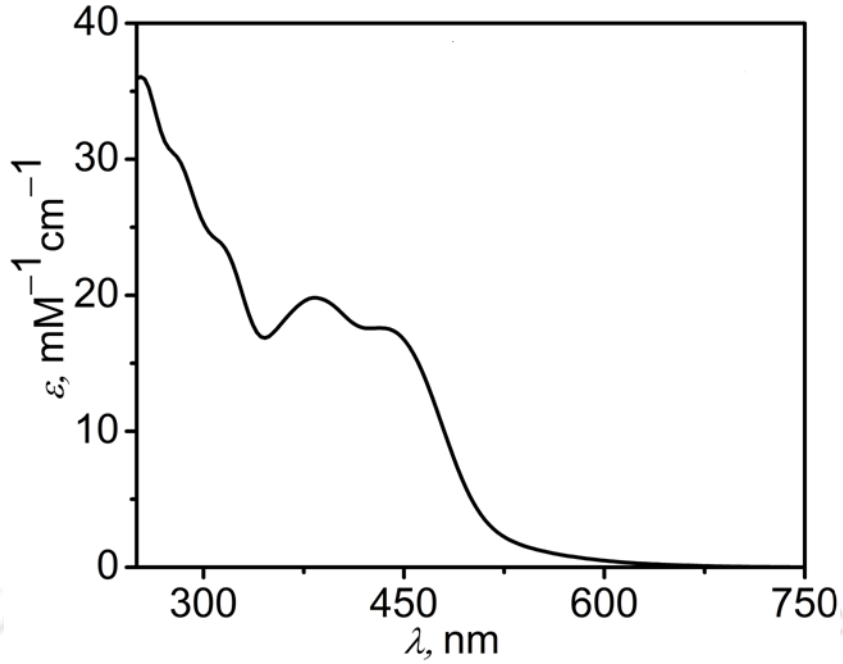

Figure 2.8: *UV-vis spectrum of complex **2A** in CH_2Cl_2 at 25 ℃.*

The UV-vis spectrum of complex **2A** was predominated by charge transfer transitions (**Figure 2.8**). The band at 440 nm (ε = 17450 $M^{-1}cm^{-1}$) was attributed to *oxo*-to-Fe(III) charge transfer (LMCT), while 383 nm (ε = 19800 $M^{-1}cm^{-1}$) was assigned as π–π* transition of the imine (C=N) moiety.

Table 2.2: *Electronic absorption data of complex **2A**.*

Complex	**λ_{max}, nm (ε, $M^{-1}cm^{-1}$)**
2A	440(17450), 383(19800), 315(23575), 280(30000)

Single crystal X-ray diffraction measurement for complex **2A** was performed at 296(2) K. It crystallized in the monoclinic space group *P* 21/c (No. 14). The molecular structure with atom labeling scheme is presented in **Figure 2.9**. Selected bond distances and bond angles are given in **Table 2.3**.

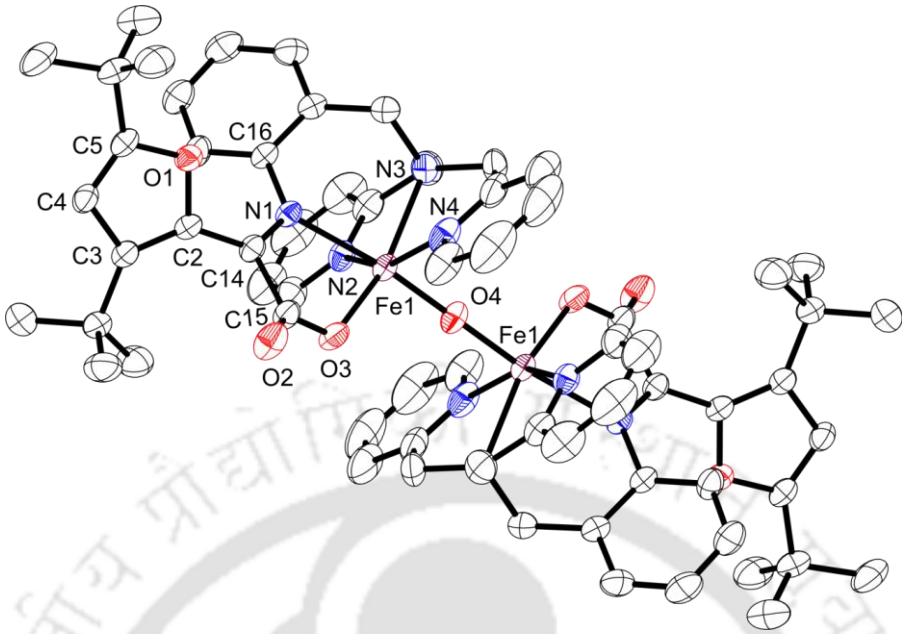

Figure 2.9: *ORTEP diagram of dinuclear dicationic oxo-bridged coordination unit of complex **2A**; Thermal ellipsoids were drown at 40% probability level. Solvent molecule (CH_3CN), anion (perchlorates) and H-atoms are omitted for clarity.*

Complex **2A** was comprised of a dicationic dinuclear oxo-bridged iron coordination unit and two perchlorate anions. In the cationic unit, both the iron centres were six-coordinate and related to each other by means of an inversion centre that was located on the bridging μ_2–O4 atom. Thus, one half of the molecule was reflected by the other half. The coordination sites of the Fe1 centre were occupied by two pyridine-N atoms (N2, and N4), one amide-N atom (N2), one imine-N atom (N1), one carboxylate-O atom (O3), and the bridging-O atom (O4). The Fe1–N1 = 2.229(2), Fe1–N2 = 2.140(2), Fe1–N3 = 2.183(2), Fe1–N4 = 2.154(2), and Fe1–O3 = 1.9739(19) Å bond distances were in accord with the previously reported high-spin Fe(III)–N and Fe(III)–O bond distances.[13] The N1–Fe1–O4 = 171.54(6), N2–Fe1–N4 = 154.45(10), and N3–Fe1–O3 = 159.54(8)° bond angles indicated that Fe1 centre acquired distorted octahedral geometry. In complex **2A**, neither 2-amidophenolate unit nor its one-electron oxidized iminobenzosemiquinone unit was found in the coordinated ligand backbone in complex **2A**. Instead of that, a newly formed *meta*-C–C-cleaved and an oxygen molecule added, a newly formed cyclic C_4O unit[14] was present in the ligand backbone. The N1–C14 =

1.291(3) Å bond distance indicated a double bond (imine) character of the unit. The O1–C2 = 1.386(3), C2–C3 = 1.367(4), C3–C4 = 1.435(3), C4–C5 = 1.341(4), and O1–C5 = 1.366(3) Å bond distances clarified the furan form of the C_4O unit. The longer O3–C15 = 1.296(3) Å bond distance compared to O2–C15 = 1.214(3) Å, confirmed the localization of the carboxylate^{1-} charge on O3 atom. Thus, it was evident from the molecular structure analysis of complex **2A** that desired dioxygen incorporation and simultaneous C–C bond cleavage at the *meta*- position of the aromatic 2-aminophenol moiety took place during the complex formation.

Table 2.3: *Selected bond distances (Å) and bond angles (°) for complex **2A**.*

Fe1–O3	1.9739(19)	C15–O2	1.214(3)
Fe1–O4	1.7789(3)	C14–N1	1.291(3)
Fe1–N1	2.229(2)	C16–N1	1.437(3)
Fe1–N2	2.140(2)	C16–C21	1.393(4)
Fe1–N3	2.183(2)	C21–C22	1.503(4)
Fe1–N4	2.154(2)	C22–N3	1.501(3)
O1–C2	1.386(3)	C23–N3	1.487(4)
C5–O1	1.366(3)	C23–C24	1.492(5)
C2–C3	1.367(4)	C24–N4	1.345(4)
C3–C4	1.435(3)	C28–N3	1.488(4)
C4–C5	1.341(4)	C28–C30	1.497(4)
C14–C15	1.530(4)	C30–N2	1.333(4)
Fe1–O4–Fe1^{i}	180.00(2)	C5–O1–C2	107.0(2)
O4–Fe1–N1	171.54(6)	C4–C5–O1	109.4(2)
O3–Fe1–N1	76.13(7)	C2–C3–C4	104.6(2)
N2–Fe1–N1	81.25(8)	C2–C3–C6	131.2(2)
N4–Fe1–N1	97.00(8)	C4–C3–C6	124.1(2)
N3–Fe1–N1	87.42(8)	C4–C5–C10	134.5(3)
O4–Fe1–N2	92.63(6)	O4–Fe1–O3	100.83(5)
O3–Fe1–N2	110.62(9)	O1–C5–C10	116.0(2)
N2–Fe1–N3	78.12(9)	O1–C2–C14	112.3(2)
N4–Fe1–N3	76.33(10)	C3–C2–C14	137.1(2)
O3–Fe1–N3	159.54(8)	N1–C14–C2	126.3(2)
O4–Fe1–N3	97.08(6)	N1–C14–C15	112.9(2)
N2–Fe1–N4	154.45(10)	C2–C14–C15	120.5(2)
O3–Fe1–N4	93.46(10)	O2–C15–O3	125.7(2)
O4–Fe1–N4	91.04(6)	O2–C15–C14	120.0(2)
C15–O3–Fe1	117.80(17)	O3–C15–C14	114.3(2)

2.4 Mechanistic Investigation for the Formation of Complex 2A

In order to investigate for the formation of complex **2A** along with the C–C bond cleavage, and dioxygen activation and addition processes, reaction was performed under inert nitrogen atmosphere (**Scheme 2.6**).

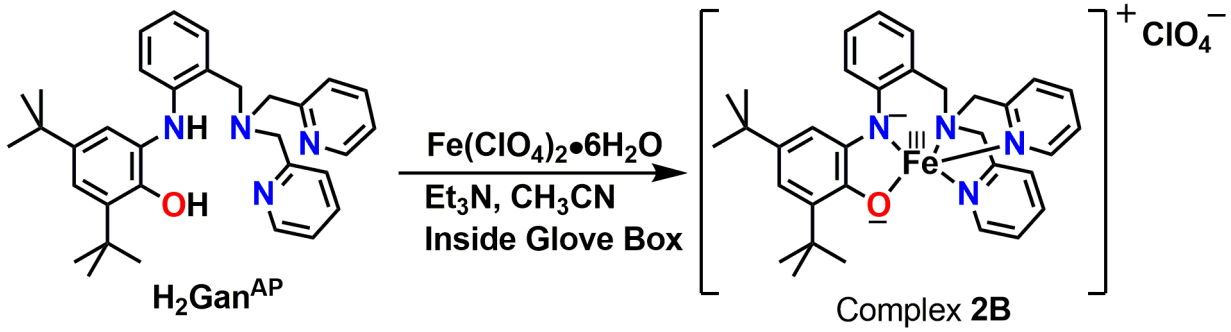

Scheme 2.6: *Synthetic route for the preparation of complex **2B**.*

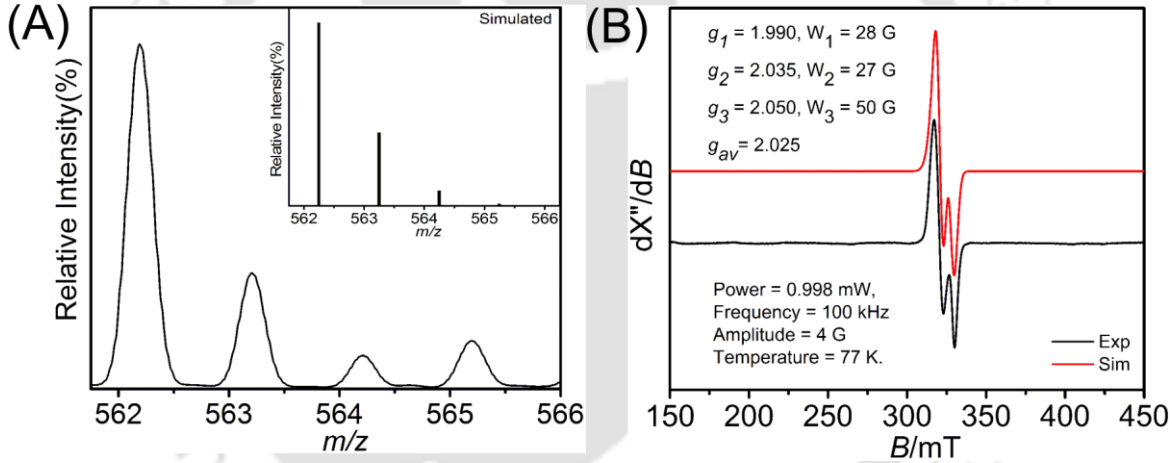

Figure 2.10: *(A) Mass spectra of complex **2B**. (B) Experimental and simulated X–band EPR spectrum of complex **2B** measured at 77 K.*

Electrospray ionization mass spectrum (ESI-MS) (positive mode) of isolated solid (complex **2B**) showed a 100 % mass peak at *m/z* = 562.23 ESI mass spectrum. Investigation on isotope distribution pattern revealed that the peak corresponded to composition $[C_{33}H_{38}N_4O_1Fe_1]$, which implied the formation of $[\mathbf{Gan^{AP}Fe^{III}}]^+$ species (**Figure 2.10A**).

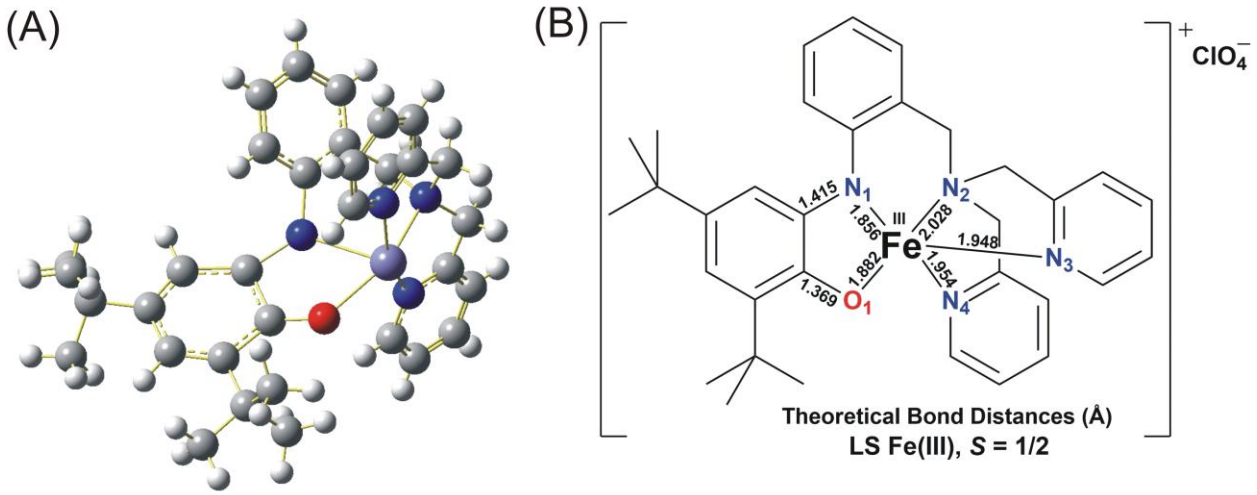

Figure 2.11: *(A) Optimized structure of the complex **2B** obtained from the DFT calculation with an S = 1/2 spin-state. (B) Selected bond distances of complex **2B** obtained from the DFT calculation*

Density functional theory (DFT) calculations were performed to optimize the geometry of **2B** by considering both high-spin (S = 5/2) and low-spin (S = 1/2) configurations of the central Fe(III) ion (**Figure 2.11**). Indeed, complex **2B** with low-spin Fe(III) state was found to be 9.11 kcal/mol more stable compared to high-spin Fe(III) state. Furthermore, X-band EPR spectrum (**Figure 2.10B**) of the species showed a rhombic signal that appeared for an S = 1/2 system. Simulation to the experimentally obtained spectrum provided the following parameter: g_1 = 1.990, g_2 = 2.035, g_3 = 2.050; g_{av} = 2.025; (W_1, W_2, W_3) = (28, 27, 50) G. From the spectrum nature and the g_{av} value it was evident that the paramagnetism of species [**Gan^{AP}Fe^{III}**]$^+$ appeared due to the presence of an unpaired electron on the iron centre.[15] Thus, the iron atom present in the species was low-spin Fe(III) in character and the 2-amidophenolate unit was in its close–shell (S = 0) configuration.

2.5 Reactivity Study of the Species $[Gan^{AP}Fe^{III}]^+$ with O_2

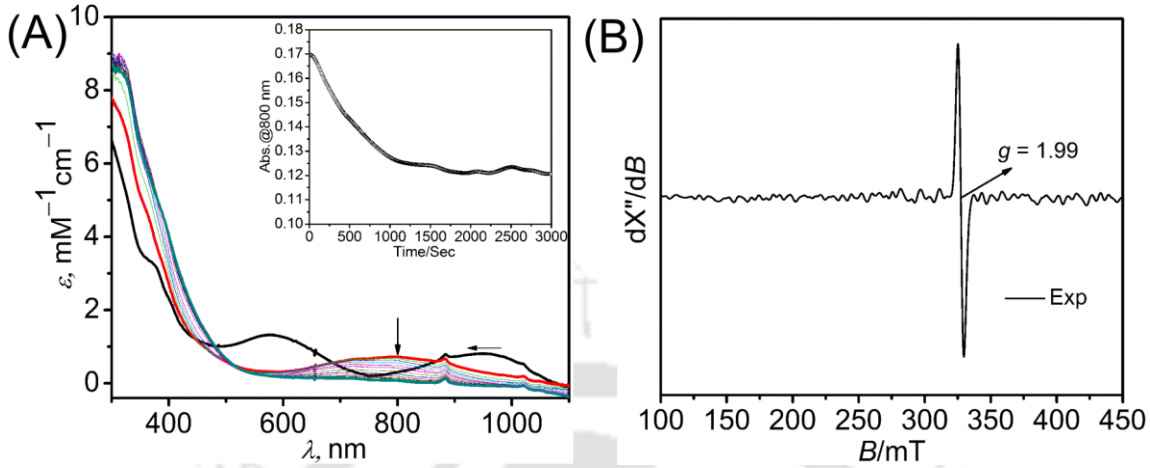

Figure 2.12: *(A) UV-vis/NIR spectral changes upon purging of molecular oxygen in the CH_3CN solution of complex **2B**. (B) X–band EPR spectrum of the initially formed species that shows absorption at 800 nm.*

The UV-vis/NIR spectrum of the species $[\mathbf{Gan^{AP}Fe^{III}}]^+$ in CH_3CN showed two broad absorption bands at 578 nm (ε = 1350 $M^{-1}cm^{-1}$) and 950 nm (ε = 800 $M^{-1}cm^{-1}$). Both the bands appeared due to 2-amidophenolate-to-Fe(III) charge transfers (LMCTs).[6b] When oxygen molecule was allowed to react with $[Gan^{AP}Fe^{III}]^+$ species, instantaneously, the spectral feature changed and a new absorption manifold centered at around 800 nm (ε = 900 $M^{-1}cm^{-1}$) appeared (**Figure 2.12A**).[16] The band decreased in intensity with time and finally shifted to lower wavelength (690 nm; ε = 150 $M^{-1}cm^{-1}$). This corresponded to the formation of complex **2A** as evident by ESI-MS analysis of the final solution (**Figure 2.13A**). X-band EPR spectrum of the initially formed species showed an isotropic signal with g = 1.99. This supported the formation of an iminobenzosemiquinone(ISQ)-coordinated low-spin Fe(II) species [Fe(II)-ISQ] {S_{ISQ} = 1/2; *ls* Fe(II) = 0} from the corresponding 2-amidophenolate-coordinated low-spin Fe(III) species $[\mathbf{Gan^{AP}Fe^{III}}]^+$ in the presence of molecular oxygen. Hence, it was presumed that the formation of an Fe(II)-ISQ species from $[\mathbf{Gan^{AP}Fe^{III}}]^+$ was molecular oxygen driven equilibrium shift. Thus formed Fe(II)-iminobenzosemiquinone species reacted with molecular oxygen and an Fe(III)-alkylperoxo complex (**B**) was possibly generated (*vide infra*). Finally, complex

2A was formed through Criegee rearrangement of (**B**) and oxidation of 2,5-dihydrofuran derivative (**C**) to furan derivative.

In order to reinforce the incorporation of a molecular oxygen to the *meta*-C–C cleaved product of 2-amidophenolae unit, $[\mathbf{Gan^{AP}Fe^{III}}]^{+}$ was allowed to react with $^{18}O_2$ in CH_3CN. The ESI-MS analysis of the finally formed product confirmed the incorporation of four ^{18}O atoms in complex **2A** (**Figure 2.13B**). Therefore, fifth oxygen atom, that is, the bridging oxygen atom, in complex **2A** was proposed to come from water molecule instead of aerial dioxygen.

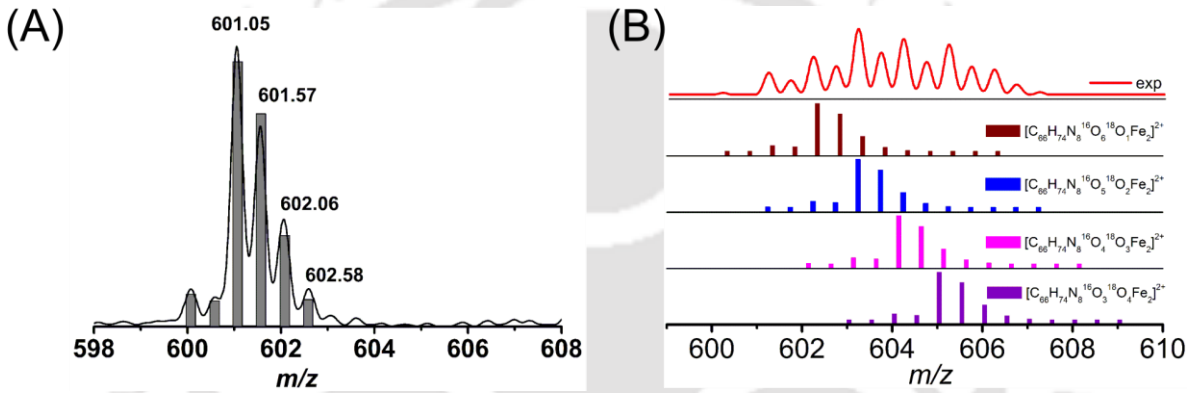

Figure 2.13: *(A) ESI-MS (positive mode) spectrum of the final species that formed by purging of molecular oxygen to CH_3CN solution of complex **2B**. (B) Experimental and simulated mass spectra (ESI, positive mode) of the final species upon reacting complex **2B** with $^{18}O_2$.*

To consolidate the proposal, the formation of complex **2A** was performed in the presence of H_2O^{18} in CH_3CN, and the positive mode ESI mass spectrum of the solution was recorded (**Figure 2.14A**). Interestingly, in addition to the expected molecular ion peak at 602.58 $\{[C_{66}H_{74}Fe_2N_8O_6{}^{18}O_1]^{2+}\}$, two more molecular ion peaks at 603.59 and 604.60 were observed. The respective compositions of the peaks were $[C_{66}H_{74}Fe_2N_8O_5{}^{18}O_2]^{2+}$ and $[C_{66}H_{74}Fe_2N_8O_4{}^{18}O_3]^{2+}$, as confirmed by isotope distribution pattern examinations. Thus, mass spectrum analysis indicated that in addition to the bridging oxygen atom, two more water molecules can participate in the formation of complex **2A**. This result implied (i) the generation of a Fe-hydroxyl species as an intermediate in the progress of complex **2A** formation and the

hydroxyl group can be replaced by a water molecule, and (ii) participation of the hydroxyl group in the formation the furan derivative.

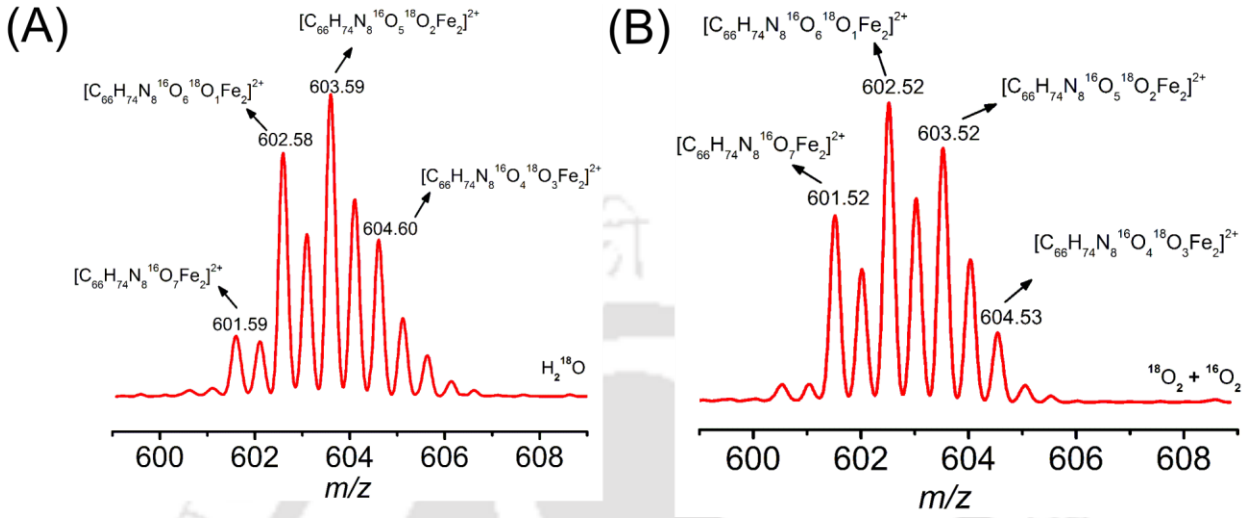

Figure 2.14: *(A) ESI-MS (positive mode) spectrum of the final species that formed by purging of molecular oxygen to CH_3CN solution of complex **2B** in the presence of H_2O^{18}. (B) Experimental mass spectra (ESI, positive mode) of the final species upon reacting complex **2B** with ~1:1 $^{16}O_2/^{18}O_2$ gas mixture.*

To examine the incorporation of both oxygen atoms of molecular oxygen to form the furan derivative in complex **2A**, a ~1:1 $^{18}O_2/^{16}O_2$ gas mixture was employed in the course of formation of complex **2A** in CH_3CN. The positive-mode ESI-MS spectrum of the solution showed molecular ion peaks at 601.52, 602.52, 603.52, and 604.53 (**Figure 2.14B**). The peak at 604.53 corresponded to composition $[C_{66}H_{74}Fe_2N_8O_4{}^{18}O_3]^{2+}$, which indicated the incorporation of three ^{18}O atoms in complex **2A**. Thus, it can be argued that both oxygen atoms from an oxygen molecule participated in furan derivative formation. Since the tetra O-18 species was observed in the labeling experiment with $^{18}O_2$ (**Figure 2.13B**), the peak was not observed in mixed $^{16}O_2/^{18}O_2$ experiment possibly due to low percentage incorporation and subsequent replacement of an Fe-coordinated $[HO^{18}]^-$ group by a $[H_2O^{16}]^0$ molecule at intermediate (**C**) stage (**Figure 2.15**).

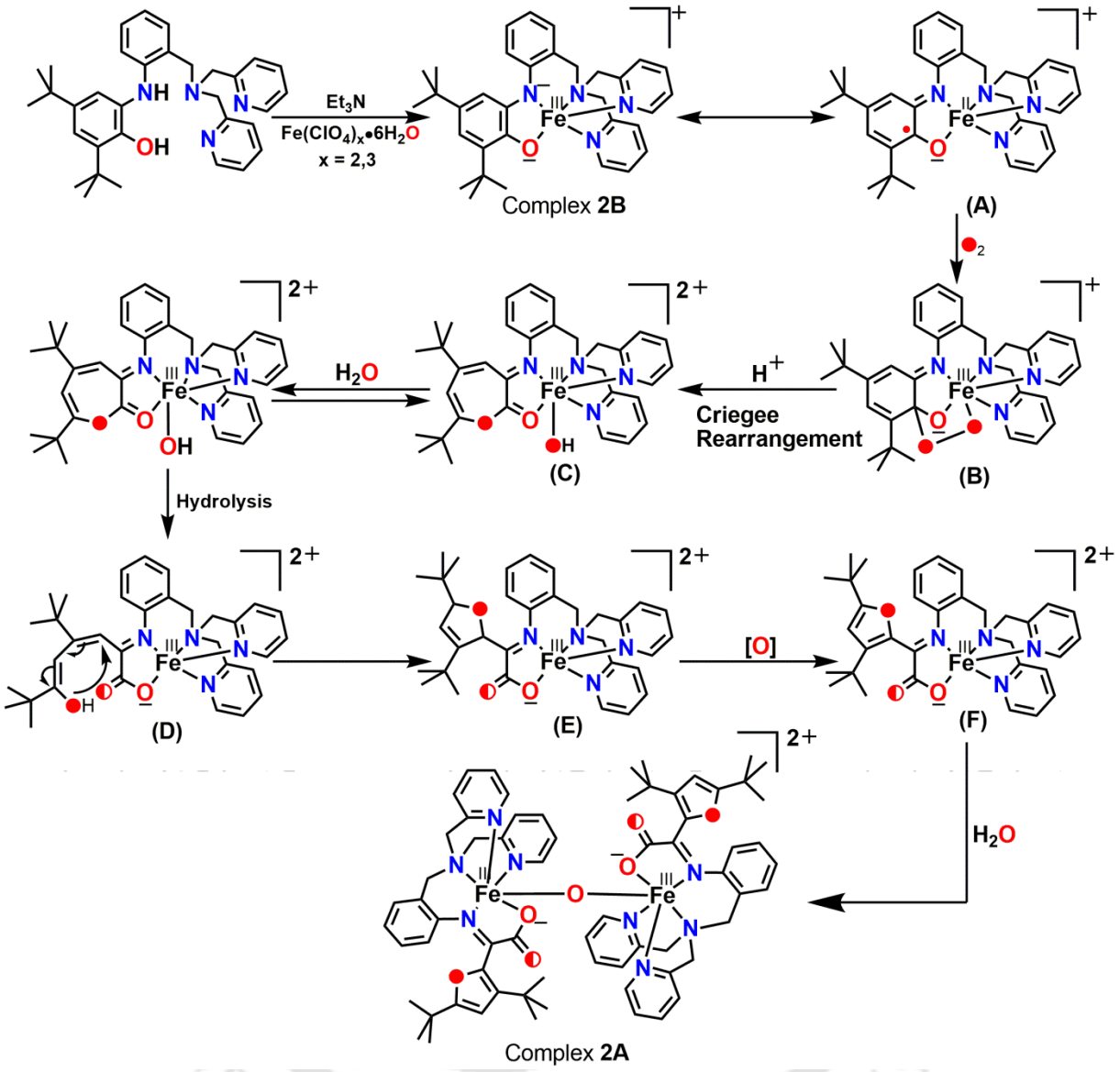

Figure 2.15: *Proposed mechanism for the oxidative meta C–C bond cleavage of 2-aminophenol derivative.*

A mechanistic proposal (**Figure 2.15**) for the formation of complex **2A** by aromatic C−C bond cleavage and incorporation of an oxygen molecule was drawn by summarizing the foregoing experimental results. UV-vis/NIR spectrum along with EPR spectrum revealed that ligand $\mathbf{H_2Gan^{AP}}$ upon reacting with Fe(II) perchlorate hydrate and a trace amount of molecular oxygen or iron(III) perchlorate hydrate in the presence of Et_3N and tetrabutylammonium perchlorate provided a five-coordinate $[\mathbf{Gan^{AP}Fe^{III}}]^+$ species. Akin to previous reports,[6] it is also

postulated that the species remained in equilibrium with its valence tautomeric [**Gan^{ISQ}Fe^{II}**]$^{+}$ species, which then reacted with molecular oxygen to generate an Fe(III)-alkylperoxo complex (**B**; **Figure 2.15**). Herein, ESI-MS analysis for the formation of complex **2A** by employing $^{18}O_2$ molecule consolidated the participation of molecular oxygen. The species (**B)** underwent Criegee rearrangement, and species (**C**) was formed. In the species, the Fe(III)-coordinated hydroxyl group can be replaced by a water molecule as evident by H_2O^{18} experiment. Furthermore, incorporation of three ^{18}O atoms during the reaction consolidated the participation of the hydroxyl group in the formation of the furan derivative. Cyclization of the product from hydrolysis (**D**) resulted in 2,5-dihydrofuran derivative (**E**). Species (**E**) then underwent oxidation to (**F**). Herein, the driving force could be the aromatization via radical pathway, and the process might be facilitated by the presence of Fe-salt and in situ generated superoxide or peroxide species.[17] Finally, two units of (**F**) combined with a water molecule, as evidenced by H_2O^{18} experiment, and complex **2A** was formed (**Figure 2.15**). To note, the reactivity observed may in fact be more complicated than the mechanistic scheme proposed.

2.6 An Mono(μ-Oxo)-Bridged Binuclear Mn(III,III) Complex Coordinated to Two Iminosemiquinone π-Radical Anions: Synthesis, Structure, and Redox Properties

A schematic representation for the synthesis of a dinuclear oxo-bridged manganese complex **2C** was shown in **Scheme 2.6**. Complex **2C** was synthesized in 42% yield by reacting an equimolar amount of the ligand $\mathbf{H_2Gan^{AP}}$ and $Mn(ClO_4)_2 \bullet 6H_2O$ in methanol.

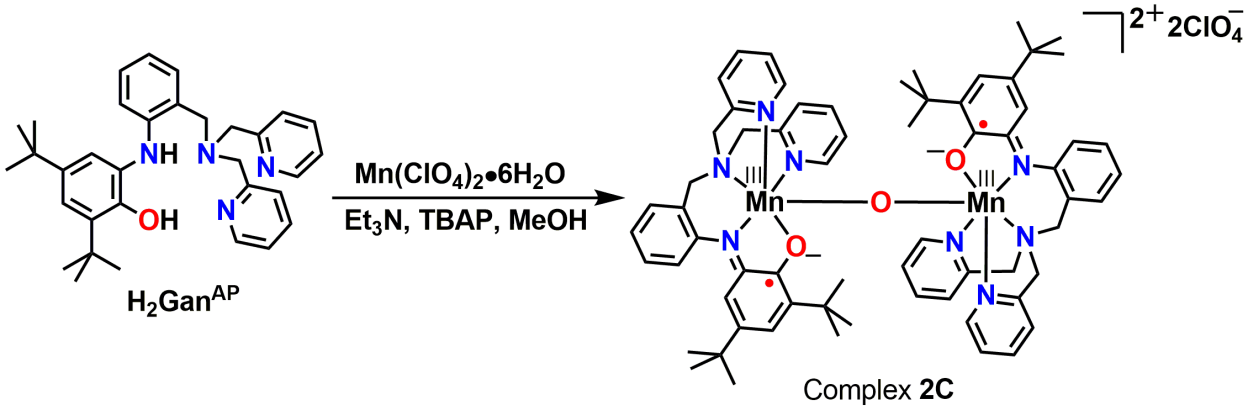

Scheme 2.6: *Synthesis route of dinuclear oxo-bridged manganese complex **2C**.*

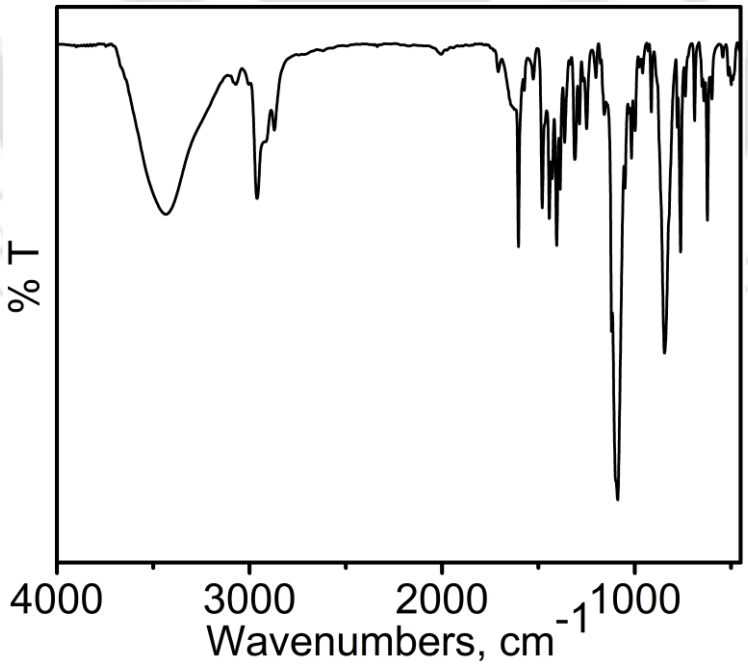

Figure 2.16: *FT-IR spectrum of complex **2C**.*

In the FT-IR spectrum of the complex **2C** (**Figure 2.16**) showed strong band at 1603 cm^{-1} due to the presence of imine ν(C=N) unit. The strong band at 1090 cm^{-1} was attributed to the presence of perchlorate (ClO_4^-) anion. No characteristic stretching bands for ν(O–H) and ν(N–H) functional groups were found, which indicated the deprotonation of the groups occurred upon metal complex formation. The ν(C–H) stretching frequencies for the *tert*-butyl groups were found in 2965–2870 cm^{-1} region.[12a-d]

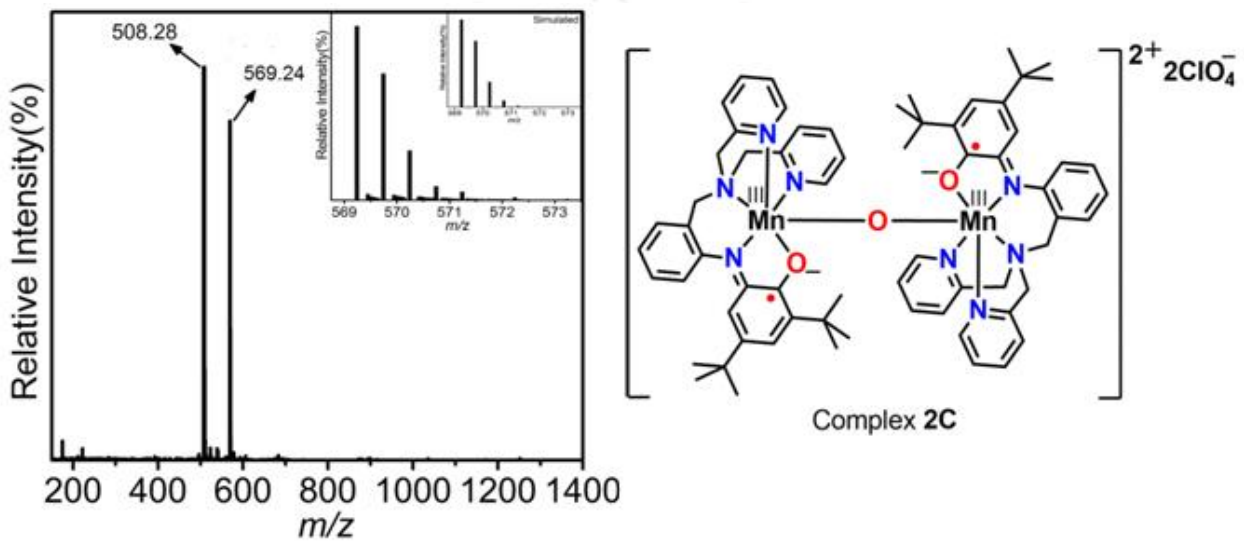

Figure 2.17: *ESI(+ve mode)-Mass spectra of complex **2C** (m/z = $C_{66}H_{76}N_8O_3Mn_2$ where Z = 2); experimental and simulated isotope distribution pattern (inset).*

In the electrospray ionization mass spectrum (ESI-MS) of complex **2C** was recorded in both positive and negative modes in CH_3OH. A 100% molecular ion peak at *m/z* = 569.24 was observed in the positive mode mass spectrum. The isotope distributation patterns of the observed mass corresponded to a dicationic species of $C_{66}H_{76}Mn_2N_8O_3$ composition (**Figure 2.17**) and thus confirmed the formation of the expected mono(μ-oxo)-bridged binuclear complex core. In the ESI-MS negative mode mass spectrum, a 100% peak at at *m/z* = 98.94 confirmed the presence of perchlorate ion [$(ClO_4)^{1-}$] as the counter anion in the complex.

To determine the molecular structure, X-ray single crystal diffraction measurement on complex **2C** was performed at 293(2) K. X-ray quality single crystals of complex **2C** were obtained by the slow evaporation of a 3:1 CH_2Cl_2:CH_3OH solution of the complex. Complex **2C** crystallized in the monoclinic space group 'P_{21}/n'. A single molecule consisted of a dication unit {[$Mn^{III}_2OL^{ISQ}_2]^{2+}$} and two perchlorate{[$ClO_4]^{1-}$} anions. ORTEP diagram of the dication unit with atom numbering scheme is presented in **Figure 2.18**. Selected bond distances and bond angles are given in **Table 2.4**.

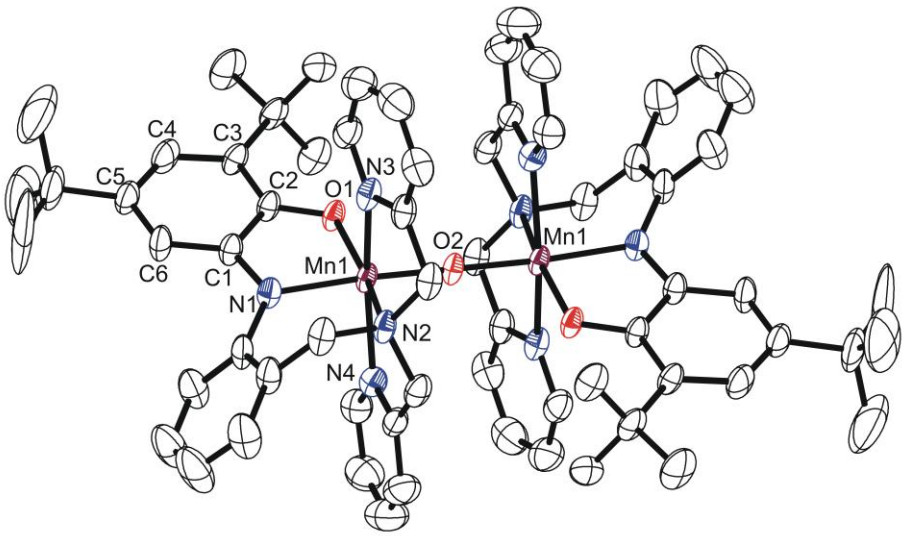

Figure 2.18: *ORTEP diagram of dinuclear dicationic oxo-bridged coordination unit of complex **2C**; Thermal ellipsoids were drown at 40% probability level. Anion (perchlorates) and H-atoms are omitted for clarity.*

In the dicationic unit, both the Mn centers were six-oordinated (distorted octahedral, **Table 2.4**) and connected by the bridging linear Mn1–O2–$Mn1^i$ unit (∠Mn1–O2–$Mn1^i$ =180.0°). The inversion center being on O2 atom reflected one octahedral core to another. Therefore, both the mononuclear cores were identical. The Mn1–O1 = 1.962(3) Å, Mn1–N2 = 2.190(4) Å, Mn1–N3 = 2.289(5) Å, Mn1–N4 = 2.170(5) Å, Mn1–N1 = 1.982(4) Å, Mn1–O2 = 1.7709(6) Å bond distances suggested that the central Mn atom was in +III oxidation state and DFT based calculation suggested that both the Mn were in low-spin electronic configuration. In the octahedral cores the equatorial plane was constituted by O1, N4, N2 and N3 atoms, while the axial positions were occupied by N1 and O2 atoms. Hence, a *John-Teller* contraction (Z-in) was realized in the complex along the N1–O2 axis.

In each octahedral core, the C–C bond distances of the 3,5-di-*tert*-butyl groups-containing C_6 ring were not consistant with 1.39 ± 0.01 Å bond distance that is expected for a n aromatic phenyl (C_6) ring. Three long C–C bonds [C1–C2 = 1.441(7) Å, C2–C3 = 1.415(7) Å, and C6–C1 = 1.425(6) Å] followed by an alternate short short-long-short C–C bond sequence [C3–C4 = 1.409(7) Å, C4–C5 = 1.452(8) Å, and C5–C6 = 1.346(7) Å] were noticed. Thus, a quinoid-type distortion was warranted. It is well documented that one-electron, as well as two-electron oxidized forms of 2-amidophenolato unit exhibit such distortion.[5b,18a-b] In the two electron oxidised iminoiminobenzoquonone($[IBQ]^0$) form, the C–N and C–O bonds are double bond, while, the bonds are in between of single bond (C–O = 1.36; and C–N = 1.42 Å) and double bond (C=O = 1.22; C=N = 1.30 Å) in case of one electron oxidized iminosemiquinone ($[ISQ]^{\bullet-}$) form. The C1–N1 = 1.351(6) Å and C2–O1 = 1.317(5) Å bond distances were commensurate with the iminosemiquinone form for the 2-amidophenolate ring. Hence, each monocation, octahedral core was composed of a paramagnetic Mn(III) ion, which was coordinated to a paramagnetic iminosemiquinone π-radical anion.

Table 2.4: *Selected bond distances (Å) and bond angles (°) for complex* ***2C.***

Mn1–O1	1.962(3)	N1–C1	1.351(6)
Mn1–O2	1.7709(6)	C1–C2	1.441(7)
Mn1–N1	1.982(4)	C2–C3	1.415(7)
Mn1–N2	2.190(4)	C3–C4	1.409(7)
Mn1–N3	2.289(5)	C4–C5	1.452(8)
Mn1–N4	2.170(5)	C5–C6	1.346(7)
O1–C2	1.317(5)	C6–C1	1.425(6)
Mn1–O2–Mn1^i	180.000(1)	N1–Mn1–N2	90.71(15)
O2–Mn1–O1	97.68(9)	N4–Mn1–N2	78.25(17)
O2–Mn1–N1	173.39(13)	O2–Mn1–N3	92.12(10)
O1–Mn1–N1	80.37(15)	O1–Mn1–N3	90.80(15)
O2–Mn1–N4	89.03(11)	N1–Mn1–N3	94.21(16)
O1–Mn1–N4	116.44(16)	N4–Mn1–N3	152.33(17)
O1–Mn1–N4	116.44(16)	N2–Mn1–N3	74.09(16)
N1–Mn1–N4	86.23(16)	C2–O1–Mn1	115.3(3)
O2–Mn1–N2	92.84(10)	C1–N1–Mn1	114.3(3)
O1–Mn1–N2	161.92(15)	C15–N1–Mn1	122.7(3)

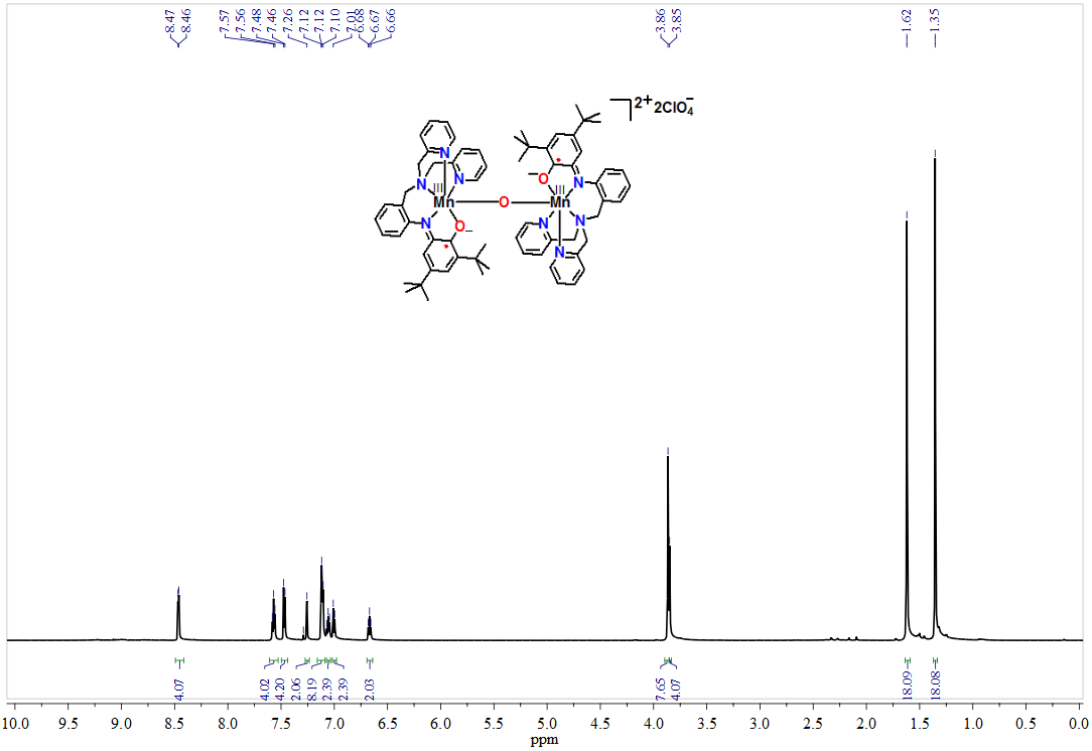

Figure 2.19: *^{1}H–NMR spectrum of complex **2C** in $CDCl_3$.*

The complex **2C** was diamagnetic with strong antiferromagnetic coupling amongst the paramagnetic centers as evident by ^{1}H-NMR spectrum (**Figure 2.19**) measurement at room temperature (25 °C). A low-spin Mn(III) ion [$3d^2$, $S_{Mn(III)} = 2/2$] contains four-unpaired electrons. It is well documented that the single π-symmetric unpaired electron of $[ISQ]^{\bullet-}$ couples strongly with the π-symmetric t_{2g} orbitals of Mn(III)/Mn(IV) ions in antiferromagnetic fashion.[18c-d] Thus, in complex **2C**, each octahedral core was expected to result in an S_{core} = 3/2 spin state. An antiferromagnetic coupling between the two μ-oxo-bridged octahedral cores thus provided a diamagnetic ground state in complex **2C**.

The UV-vis/NIR spectrum of complex **2C** was recorded in CH_2Cl_2 solution at room temperature and depicted in **Figure 2.20**. The complex **2C** exhibited several strong absorption bands, which ensured their charge-transfer characteristic. Herein, the *d-d* transition band for the Mn(III) ion could not be observed due to others strong absorption bands in the 450-550 nm region.

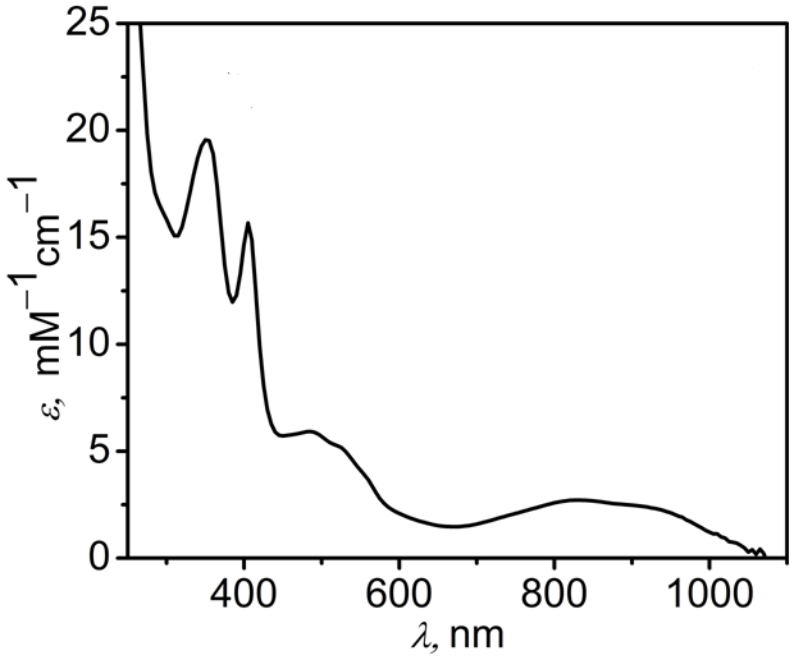

Figure 2.20: *UV-Vis/NIR spectrum of complex **2C** in CH_2Cl_2 at 25 ℃.*

Oxo-bridge dinuclear Mn(III) complexes with N(pyridine), N(amine), O(oxo), and O(phenolate) coordination sites do not exhibit absorption bands above 600 nm. Therefore, the charge-transfer bands at 915 nm (ε = 2450 $M^{-1}cm^{-1}$) and 830 nm (ε = 2800 $M^{-1}cm^{-1}$) appeared due to the presence of the iminosemiquinone unit in the complex.[17a-b] The broad absorption manifold appeared in between 600 to 445 nm region was due to closely located ligand(pyridine)-to-metal[Mn(III)], oxo-to-metal[Mn(III)], and ligand(phenolate)-to-metal[Mn(III)] charge-transfer transition (LMCT) bands.[19a-b] The intraligand π–π* transition (ILCTs) of the iminosemiquinone moiety occurred at 404 nm (ε = 15100 $M^{-1}cm^{-1}$) and at 352 nm (ε = 19050 $M^{-1}cm^{-1}$).[19c-g]

Table 2.5: *Electronic absorption data of complex **2C**.*

Complex	**λ_{max}, nm (ε, $M^{-1}cm^{-1}$)**
2C	915(2450), 830(2800), 524(5200), 484(5900), 404(15100), 352(19050)

The electrochemical behaviour of complex **2C** was investigated by cyclic voltametry measurements. Cyclic voltammograms (CVs) of the complex were being recorded in CH_2Cl_2 solutions containing 0.10 M $[(^nBu)_4N]ClO_4$ as supporting electrolyte at a glassy carbon working electrode, a platinum wire counter electrode, and a Ag/AgCl reference electrode. The experiments were performed at different scan rates. Ferrocene (Fc) was used as an internal standard and added to the solution at the end of the measurements. The potentials are referenced versus the ferrocenium/ferrocene (Fc^+/Fc) couple.

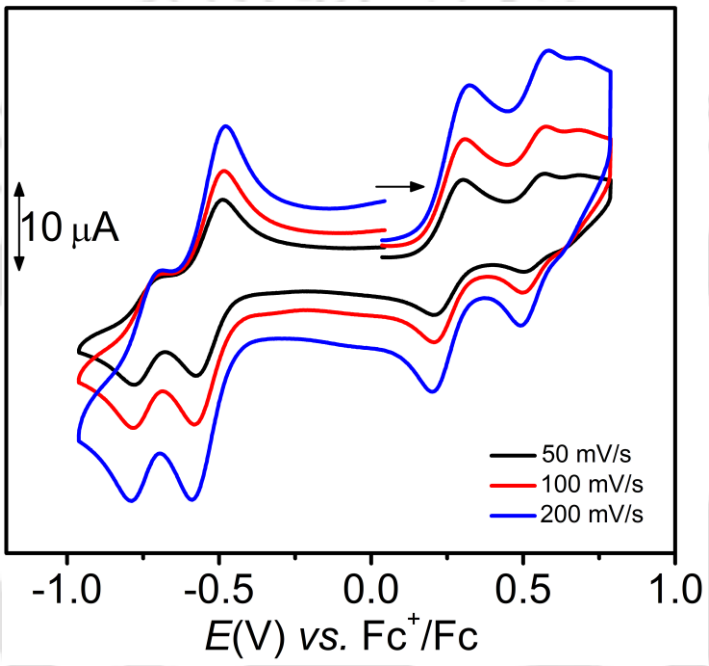

Figure 2.21: *Cyclic voltammogram of complex **2C** measured at 50, 100, and 200 mV.*

The cyclic voltammogram (CV) of complex **2C** exhibited three successive one-electron oxidation waves at $E_{1/2}^{Ox}$ = + 253 mV, + 531 mV, and + 650 mV and two successive one-electron reduction waves at $E_{1/2}^{Red}$ = – 534 mV, – 739 mV. The peak positions remained unaltered with the variation of scan rate (**Figure 2.21**). This consolidated the reversibility of the processes. The potential difference between two reduction process and the first and second oxidation process were 205 mV and 273 mV, respectively. Hence, very low electronic communication between the redox centers was warranted and the localization of charge in $\mathbf{2C}^{1+}$ and $\mathbf{2C}^{3+}$ species was indicated.

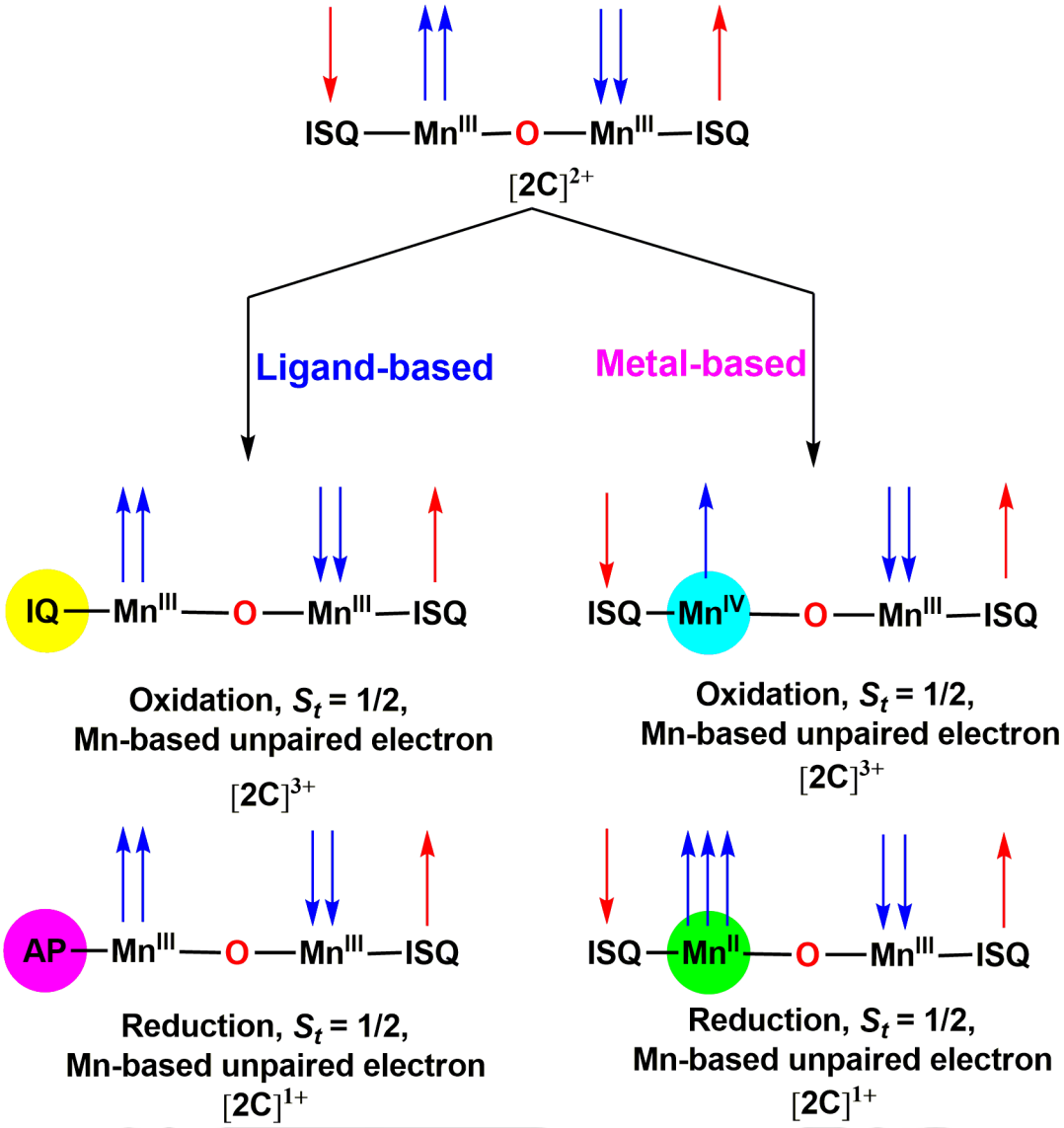

Figure 2.22: *The possible electronic structure of the species that might be generated by ligand-based and metal based oxidation and reduction processes.*

The symmetric dinuclear, μ-oxo-bridged complex **2C** was comprised of two iminosemiquinone π-radical anions and two Mn(III) ions, which can undergo redox activity feasibly. Each mononuclear unit in complex **2C**, that was antiferromagnetically coupled to other mononuclear unit to provider an $S_t = 0$ ground state, was of 3/2 spin state, where the locus of the three unpaired electrons were at Mn(III) ion. Thus, one-electron oxidation or one-electron reduction of complex **2C**, irrespective to metal-based or ligand-based process (**Figure 2.22**), would provide an $S_t = 1/2$ ground state with the

unpaired electron located at a Mn center. The crystallographic characterisation of the species was not successful. Therefore, to discern the locus of the redox sites, DFT-based calculation were performed (**Figure 2.23-2.27**). It has been found that the reductions were ligand based and the first two oxidations were metal based. The overall electrochemical behaviour of complex **2C** is summarized in **Scheme 2.7**.

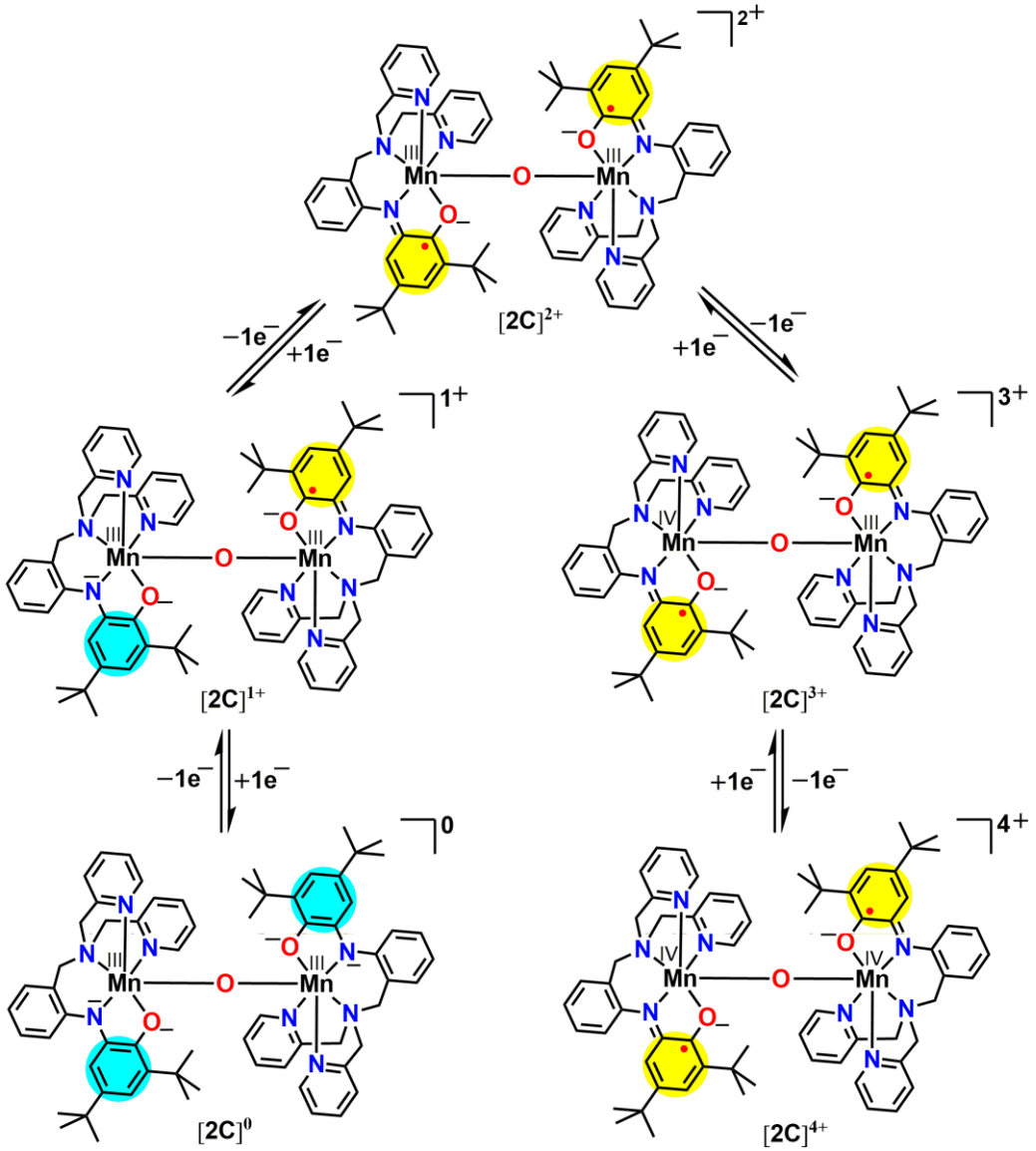

Scheme 2.7: *Species formed by two one-electron oxidation and two one-electron reduction processes.*

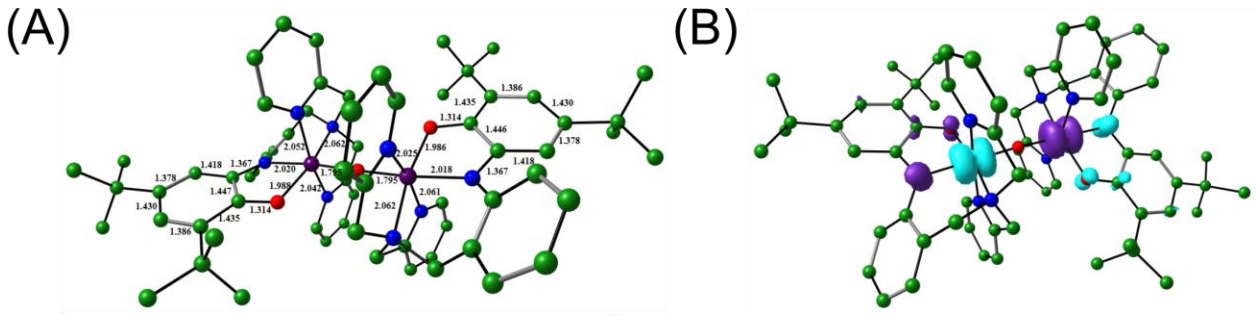

Figure 2.23: *(A) DFT Optimized bond distances parameter of complex [**2C**]$^{2+}$ (B) Spin density plot of complex [**2C**]$^{2+}$.*

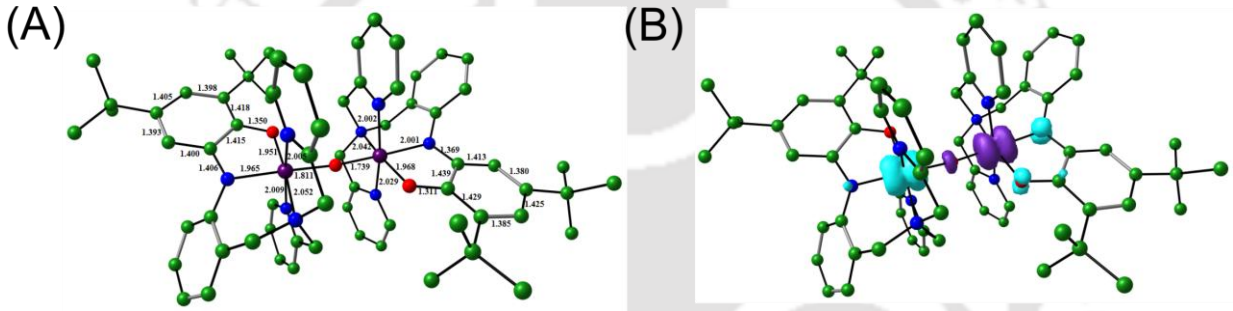

Figure 2.24: *(A) DFT Optimized bond distances parameter of complex [**2C**]$^{1+}$ (B) Spin density plot of complex [**2C**]$^{1+}$.*

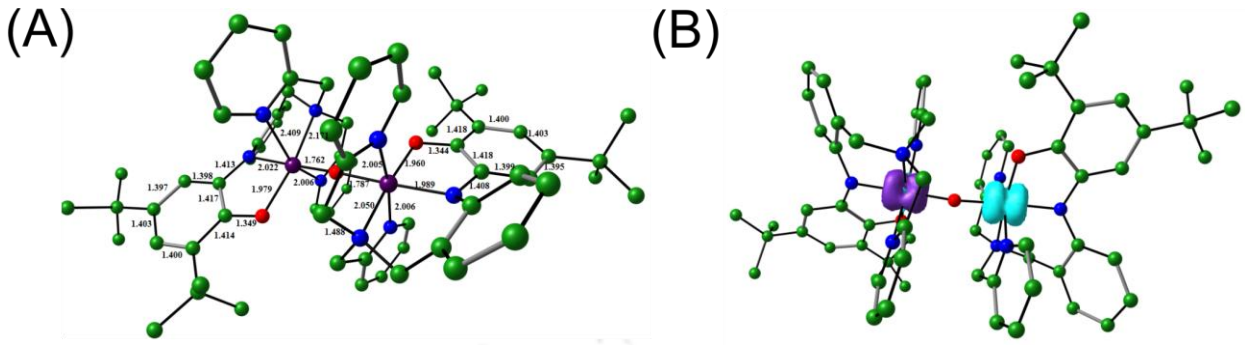

Figure 2.25: *(A) DFT Optimized bond distances parameter of complex [**2C**]^{0} (B) Spin density plot of complex [**2C**]^{0}.*

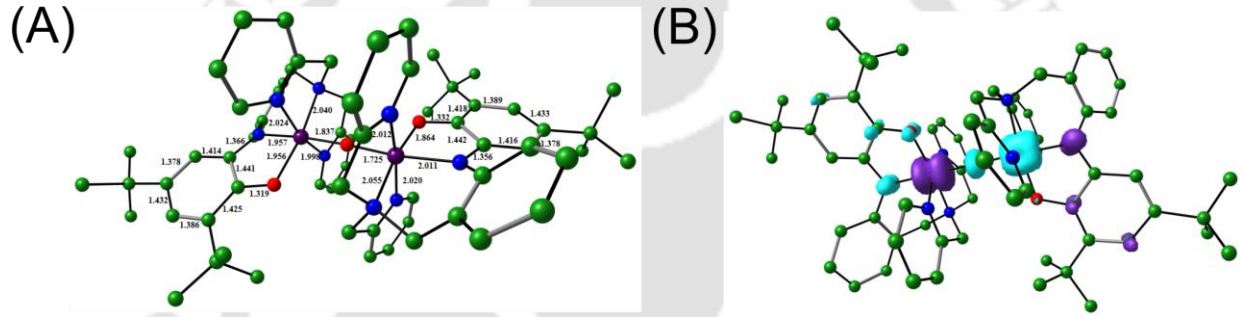

Figure 2.26: *(A) DFT Optimized bond distances parameter of complex [**2C**]$^{3+}$ (B) Spin density plot of complex [**2C**]$^{3+}$.*

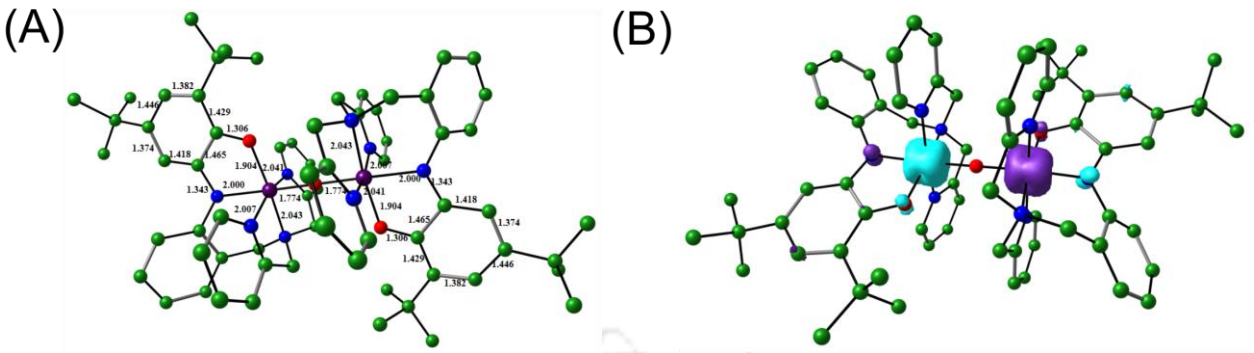

Figure 2.27: *(A) DFT Optimized bond distances parameter of complex [**2C**]$^{4+}$ (B) Spin density plot of complex [**2C**]$^{4+}$.*

2.7 Conclusions

To conclude, we have demonstrated the successful synthesis of 3,5-di-*tert*-butyl-2-aminophenol-appended **H_2Gan^{AP}** ligand. The ligand upon reacting with $Fe(ClO_4)_2 \bullet 6H_2O$ in the presence of air, Et_3N and tetrabutylammonium perchlorate provides complex **2A**. Noteworthy, complex **2A** can also be synthesized by using Fe(III) percholorale hydrate as the iron salt. X-ray structural analysis of complex **2A** reveals the presence of a furan derivation in the ligand backbone. Thus, the oxidative *meta*-C–C bond scission of 2-aminophenol derivative emulate the function of APD. Noteworthy, the complex **2C** provides crystallographic characterization of the cleavage product of 2-aminophenol derivative. Mechanistic investigation for the scission demonstrates the formation of [**Gan^{AP}Fe^{III}**]$^+$ species under anaerobic condition. The species undergoes valence tautomerization and provides [**Gan^{ISQ}Fe^{II}**]$^+$ species in the presence of molecular oxygen at the initial stage. The [**Gan^{ISQ}Fe^{II}**]$^+$ species in due course reacts with a dioxygen molecule and provides complex **2A**. Hence, herein, it has also been demonstrated that the reaction with dioxygen is initiated by the five-coordinate iminobenzosemiquinone-containing Fe(II) species. The incorporation of aerial dioxygen to the *meta*-C–C cleavage product is consolidated by mass spectrometric analysis of the final product that is generated by reacting [**Gan^{AP}Fe^{III}**]$^+$ species with $^{18}O_2$. Finally, the formation of Fe-

hydroxy group-coordinated species **C** and the incorporation of the bridging oxygen atom from a water molecule are consolidated by introducing H_2O^{18} during the complex formation reaction.

On the other hand a mono(μ-oxo)-bridged binuclear Mn_2 complex **2C** was successfully synthesized. X-ray structural analysis showed that complex **2C** consisted of two Mn(III) ions, which were in distorted octahedral coordination geometry, and one iminosemiquinone radical anion in the each coordination sphere. Noteworthy, the complex **2C** is the first report on a mono(μ-oxo)-bridged binuclear Mn(III) complex with coordinated-π-radical anions. The complex **2C** acquired singlet ground state due to strong antiferromagnetic interactions amongst the four paramagnetic centers. ^{1}H-NMR spectrum analysis supported the fact. The CV of the complex **2C** in CH_2Cl_2 solution showed two one-electron reduction waves and three one-electron oxidation waves. DFT-based geometry optimization on oxidized ([**2C**]$^{3+}$, [**2C**]$^{4+}$) and reduced ([**2C**]$^{1+}$, [**2C**]^{0}) species implied the stepwise oxidations and reductions of the two coordinated π-radical anions to the corresponding iminoquinone and amidophenolate forms, respectively.

References

1. (*a*) J. -F. Wu, C. -W. Sun, C. -Y. Jiang, Z. -P. Liu and S. -J. Liu, *Arch. Microbiol.*, 2005, **183,** 1; (*b*) S. Takenaka, S. Murakami, R. Shinke, K. Hatakeyama, H. Yukawa and K. Aoki, *J. Biol. Chem.*, 1997, **272**, 14727; (c) U. Lendenmann and J. C. Spain, *J. Bacteriol.*, 1996, **178**, 6227.

2. (*a*) Z. He and J. C. Spain, *J. Ind. Microbiol. Biotechnol.*, 2000, **25**, 25; (*b*) C. C. Somerville, S. F. Nishino and J. C. Spain, *J. Bacteriol.*, 1995, **177**, 3837; (*c*) Y. Zhang, K. L. Colabroy, T. P. Begley and S. E. Ealick, *Biochemistry*, 2005, **44**, 7632; (*d*) X. W. Li, M. Guo, J. Fan, W. Y. Tang, D. Q. Wang, H. H. Ge, H. Rong, M. K. Teng, L. W. Niu, Q. Liu and Q. Hao, *Protein Sci.*, 2006, **15**, 761.

3. (*a*) D. -F. Li, J. -Y. Zhang, Y. -J. Hou, L. Liu, Y. Hu, S. -J. Liu, D. -C. Wang and W. Liu, *Acta Crystallogr., Sect. D.*, 2013, **69**, 32.

4. (*a*) T. D. H. Bugg, and G. Lin, *Chem. Commun.*, 2001, **11**, 941; (*b*) T. D. H. Bugg, *Tetrahedron*, 2003, **59**, 7075; (*c*) M. Costas, M. P. Mehn, M. P. Jensen and L. Que Jr., *Chem. Rev.*, 2004, **104**, 939; (*d*) F. H. Vaillancourt, J. T. Bolin and L. D. Eltis, *Crit. Rev. Biochem. Mol.*, 2006, **41**, 241; (*e*) J. D. Lipscomb, *Curr. Opin. Struct. Biol.*, 2008, **18**, 644; (*f*) P. E. M. Siegbahn and F. Haeffner, *J. Am. Chem. Soc.*, 2004, **126**, 8919; (*g*) E. G. Kovaleva and J. D. Lipscomb, *Science*, 2007, **316**, 453.

5. (*a*) A. I. Poddel'sky, V. K. Cherkasov and G. A. Abakumov, *Coord. Chem. Rev.*, 2009, **253**, 291; (*b*) H. Chun, E. Bill, E. Bothe, T. Weyhermüller and K. Wieghardt, *Inorg. Chem.*, 2002, **41**, 5091; (*c*) H. Chun, T. Weyhermüller, E. Bill and K. Wieghardt, *Angew. Chem., Int. Ed.*, 2001, **40**, 2489; (*d*) H. Chun, E. Bill, T. Weyhermüller and K. Wieghardt, *Inorg. Chem.*, 2003, 42, 5612; (*e*) M. M. Bittner, D. Kraus, S. V. Lindeman, C. V. Popescu and A. T. Fiedler, *Chem.– Eur. J.*, 2013, 19, 9686; (*f*) A. Rajput, A. K. Sharma, S. K. Barman, D. Koley, M. Steinert and R. Mukherjee, *Inorg. Chem.*, 2014, **53**, 36.

6. (*a*) B. Chakraborty, S. Bhunya, A. Paul and T. K. Paine, *Inorg. Chem.*, 2014, **53**, 4899; (*b*) B. Chakraborty and T. K. Paine, *Angew. Chem., Int. Ed.*, 2013, **52**, 920; (*c*) S. Chatterjee and T. K. Paine, *Inorg. Chem.*, 2015, **54**, 1720; (*d*) T. R. Lakshman, S. Chaterjee, B. Chakraborty and T. K. Paine, *Dalton Trans.*, 2016, **45**, 8835.

7. (*a*) J. Yano and V. Yachandra, *Chem. Rev*. 2014, **114**, 4175; (*b*) K. J. Young, B. J. Brennan, R. Tagore and G. W. Brudvig, *Acc. Chem. Res.* 2015, **48**, 567; (c) M. Suga, F. Akita, K. Hirata, G. Ueno, H. Murakami, Y. Nakajima, T. Shimizu, K. Yamashita, M. Yamamoto, H. Ago and J. -R. Shen, *Nature* 2015, **517**, 99; (d) S. Mukhopadhyay, S. K. Mandal, S. Bhaduri and W. H. Armstrong, *Chem. Rev.* 2004, **104**, 3981; (e) J. P. McEvoy, G. W. Brudvig, *Chem. Rev.* 2006, **106**, 4455.

8. (*a*) J. A. Cotruvo, T. A. Stich, R. D. Britt and J. Stubbe, *J. Am. Chem. Soc.*, 2013, **135**, 4027; (*b*) A. K. Boal, J. A. Cotruvo Jr., J. Stubbe and A. C. Rosenzweig, *Science*, 2010, **329**, 1526.

9. (*a*) Y. Sheng, I. A. Abreu, D. E. Cabelli, M. J. Maroney, A. F. Miller, M. Teixeira, J. V. Valentine, *Chem. Rev.*, 2014, **114**, 3854; (*b*) A. -F. Miller and T. Wang, *Biochemistry*, 2017, **56**, 3787; (*c*) C. K. Vance and A.-F. Miller, *J. Am. Chem. Soc.*, 1998, **120**, 461.

10. (*a*) A. J. Wu, J. E. Penner-Hahn and V. L. Pecoraro, *Chem. Rev.*, 2004, **104**, 903; (*b*) M. U. Triller, W.-Y. Hsieh, V. L. Pecoraro, A. Rompel and B. Krebs, *Inorg. Chem.*, 2002, **41**, 5544; (*c*) V. V. Barynin, P. D. Hempstead, A. A. Vagin, S. V. Antonyuk, W. R. Melik-Adamyan, V. S. Lamzin, P. M. Harrison and P. J. Artymiuk, *J. Inorg. Biochem.*, 1997, **67**, 196; (d) G. S. Allgood and J. J. Perry, *J. Bacteriol.* 1986, **168**, 563.

11. (*a*) C. -M. Lee, W.-Y. Wu, M.-H. Chiang, D. S. Bohle and G. -H. Lee, *Inorg. Chem.*, 2017, **56**, 10559; (*b*) S. Blasco, J. Cano, M. P. Clares, S. García-Granda, A. Doménech, H. R. Jiménez, B. A. Verdejo, F. Lloret and E. García-España, *Inorg. Chem.* 2012, **51**, 11698; (*c*) O. Horner, E. Anxolabéhère-Mallart, M.-F. Charlot, L. Tchertanov, J. Guilhem, T. A. Mattioli, A. Boussac and J.-J. Girerd, *Inorg. Chem.*, 1999, **38**, 1222; (*d*) K. Ghosh, A. A. Eroy-Reveles, M. M. Olmstead, P. K. Mascharak,. *Inorg. Chem.*, 2005, **44**, 8469; (*e*) M. K. Coggins, S. Toledo, E. Shaffer, W. Kaminsky, J. Shearer, J. A. Kovacs, *Inorg. Chem.*, 2012, **51**, 6633; (*f*) C. Baffert, M.-N. Collomb, A. Deronzier, J. Pécaut, J. Limburg, R. H. Crabtree and G. W. Brudvig, *Inorg. Chem.*, 2002, **41**, 1404; (*g*) M. A. R. Raycroft, C. I. Maxwell, R. A. A. Oldham, A. S. Andrea, A. A. Neverov and R. S. Brown, *Inorg. Chem.*, 2012, **51**, 10325; (*h*) S. C. Burdette, C. J. Frederickson, W. Bu and S. J. Lippard, *J. Am. Chem. Soc.*, 2003, **125**, 1778; (*i*) Y. Miyazato, T. Wada, J. T.

Muckerman, E. Fujita and K. Tanaka, *Angew. Chem. Int., Ed.* 2007, **46**, 5728; (*j*) P. Chaudhuri and K. Wieghardt, *Prog. Inorg. Chem.*, 2001, **50**, 151.

12. (*a*) G. R. Pandhare, V. M. Shinde and Y. H. Deshpande, *Rasayan J. Chem.*, 2008, **1**, 337; (*b*) J. Coates, *Interpretation of Infrared Spectra: A Practical Approach*, John Wiley & Sons Ltd, Chichester, 2000; (*c*) D. L. Pavia, G. M. Lampman, G. S. Kriz and J. R. Vyvyan, *Introduction to Spectroscopy*, 4th edition, 31; (*d*) P. K. Kipkemboi, P. C. Kiprono and J. J. Sanga, *Bull. Chem. Soc. Ethiop.*, 2003, **17**, 211; (*e*) G. Hastings and V. Sivakumar, *Biochemistry*, 2001, **40**, 3681; (*f*) J. Breton, J. Burie, C. Berthomieu, G. Berger and E. Nabedryk, *Biochemistry*, 1994, **33**, 4953; (*g*) H. Suzuki, M. A. Nagasaka, M. Sugiura and T. Noguchi, *Biochemistry*, 2005, **44**, 11323.

13. (*a*) H. G. Jang, D. D. Cox and L. Que Jr., *J. Am. Chem. Soc.*, 1991, **113**, 9200; (*b*) Y. Zang, J. Kim, Y. Dong, E. C. Wilkinson, E. H. Appelman, L. Que, Jr., *J. Am. Chem. Soc.*, 1997, **119**, 4197; (*c*) G. Roelfes, M. Lubben, K. Chen, R. Y. N. Ho, A. Meetsma, S. Genseberger, R. M. Hermant, R. Hage, S. K. Mandal, V. G. Young Jr., Y. Zang, H. Kooijman, A. L. Spek, L., Que Jr. and B. L. Feringa, *Inorg. Chem.*, 1999, **38**, 1929.

14. (*a*) S. K. Zingales, M. Z. Wallace and C. W. Padgett, *Acta Cryst.*, 2015, **E71**, o707; (*b*) C. Martínez de León, H. Tlahuext and J. -M. Gre´vy, *Acta Cryst.*, 2015, **E71**, o922.

15. (*a*) H. Chun, C. N. Verani, P. Chaudhuri, E. Bothe, E. Bill, T. Weyhermüller and K. Wieghardt, *Inorg. Chem.*, 2001, **40**, 4157; (*b*) K. S. Min, T. Weyhermüller and K. Wieghardt, *Dalton Trans.*, 2003, 1126; (*c*) S. Mukherjee, T. Weyhermüller, K. Wieghardt and P. Chaudhuri, *Dalton Trans.*, 2003, 3483; (*d*) P. Halder, S. Paria and T. K. Paine, *Chem.–Eur. J.*, 2012, **18**, 11778.

16. (*a*) M. M. Bittner, S. V. Lindeman and A. T. Fiedler, *J. Am. Chem. Soc.*, 2012, **134**, 5460; (*b*) M. M. Bittner, S. V. Lindeman, C. V. Popescu and A. T. Fiedler, *Inorg. Chem.*, 2014, **53**, 4047.

17. (*a*) W. -J. Yoo and C. -J. Li, in C-H Activation, Vol. 292 (Eds.: J.-Q. Yu, Z. Shi), Springer, Berlin, 2010; (*b*) C. -J. Li, *Acc. Chem. Res.*, 2009, **42**, 335; (*c*) D. Liu, C. Liu, H. Li and A. Lei, *Angew. Chem., Int. Ed.*, 2013, **52**, 4453.

18. (*a*) X. Sun, H. Chun, K. Hildenbrand, E. Bothe, T. Weyhermüller, F. Neese and K. Wieghardt, *Inorg. Chem.*, 2002, **41**, 4295; (*b*) K. S. Min, T. Weyhermüller, E. Bothe and K. Wieghardt, *Inorg. Chem.*, 2004, **43**, 2922; (*c*) H. Chun, P. Chaudhuri, T. Weyhermüller and K. Wieghardt, *Inorg. Chem.*, 2002, **41**, 790; (*d*) S. Mukherjee, T. Weyhermüller, E. Bothe, K. Wieghardt and P. Chaudhuri, *Dalton Trans.*, 2004, 3842.

19. (*a*) H. Biava, C. Palopoli, C. Duhayon, J. P. Tuchagues and S. Signorella, *Inorg. Chem.*, 2009, **48**, 3205; (*b*) D. Mondal, S. Kundu, M. C. Majee, A. Rana, A. Endo and M. Chaudhury, *Inorg. Chem.*, 2017, **56**, 9448; (*c*) A. Anjos, A. J. Bortoluzzi, M. S. B. Caro, R. A. Peralta, G. R. Friedermann, A. S. Mangrich and A. Neves, *J. Braz. Chem. Soc.*, 2006, **17**, 1540; (*d*) A. Neves, S. M. D. Erthal, I. Vencato, A. S. Ceccato, Y. P. Mascarenhas, O. R. Nascimento, M. Horner and A. A. Batista, *Inorg. Chem.*, 1992, **31**, 4749; (*e*) M. G. Patch, K. P. Simolo and C. J. Carrano, *Inorg. Chem.*, 1982, **21**, 2972; (*f*) X. Li and V. L. Pecoraro, *Inorg. Chem.*, 1989, **28**, 3403; (*g*) K. Bertoncello, G. D. Fallon and K. Murray, *Inorg. Chim. Acta*, 1990, **174**, 57.

Chapter III

A New Piperazine-Based Non-Innocent Ligand, [$H_4L^{Piperazine(AP/AP)}$], and its Corresponding Radical-Containing Transition Metal Complexes: Synthesis and Characterization

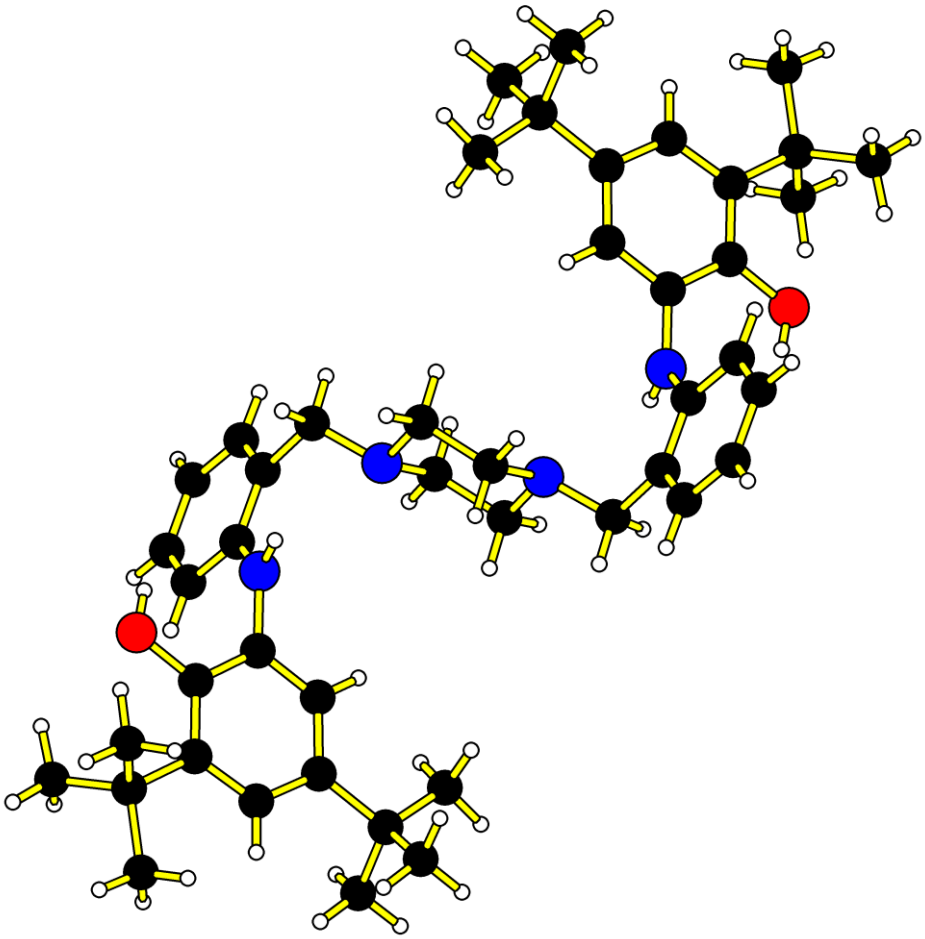

*Some results have been communicated in
Inorg. Chim. Acta.

3.1 Introduction

A growing interest in the area of metal-radical complexes is caused by: biomimetic activity[1a]; redox isomerism;[1b] and the development of new catalytic systems.[1c] In addition, poly *o*-semiquinone complexes exhibit various magnetic properties and thus, can be used as potential building blocks for single molecule-based magnetic devices.[2a-c] The specific features of transition metal complexes with paramagnetic metal ion-coordinated to redox-active ligands are known in the literatures.[1c] While, less attention has been given to the development of radical-containing metal-complexes with metal ions of diamagnetic electronic configurations. Noteworthy, the systems are suitable for the understanding of magnetic exchange coupling between organic radicals, which are not complicated by interactions with a paramagnetic transition metal ion. Investigation on the magnetic coupling between *o*-semiquinone ligands in diamagnetic metal complexes along with their structures would help in revealing magneto structural features, which, in turn, will offer an opportunity to design metal complexes with desired magnetic properties.

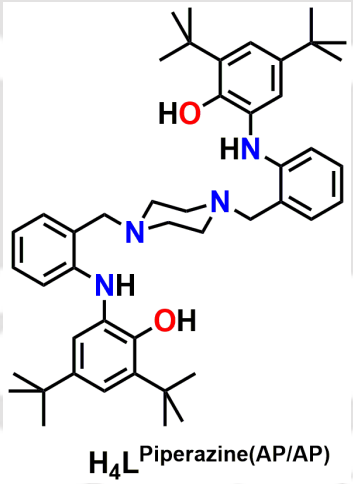

Figure 3.1: *Schematic presentation of ligand* $H_4L^{Piperazine(AP/AP)}$.

To investigate on electronic structure and magnetic interactions between transition metal complexes and the metal-coordinated radical centers, ligand $\mathbf{H_4L^{Piperazine(AP/AP)}}$ has been designed. In the ligand, a piperazine unit bridged two redox-active 2-aminophenol units. The chair form of piperazine is more stable than that of boat form. Thus, binuclear metal-radical complexes with boat form of the piperazine unit could be synthesized and the formed-complex

could be further investigated for the understanding of magnetic coupling amongst the unpaired spins. In addition, the probability of mononuclear complex formation with the boat form of the backbone piperazine could be investigated.

3.2 Synthesis and Characterization of Ligand [$H_4L^{Piperazine(AP/AP)}$]

A schematic representation for the synthesis of ligand $\mathbf{H_4L^{Piperazine(AP/AP)}}$ is shown in **Scheme 3.1.**

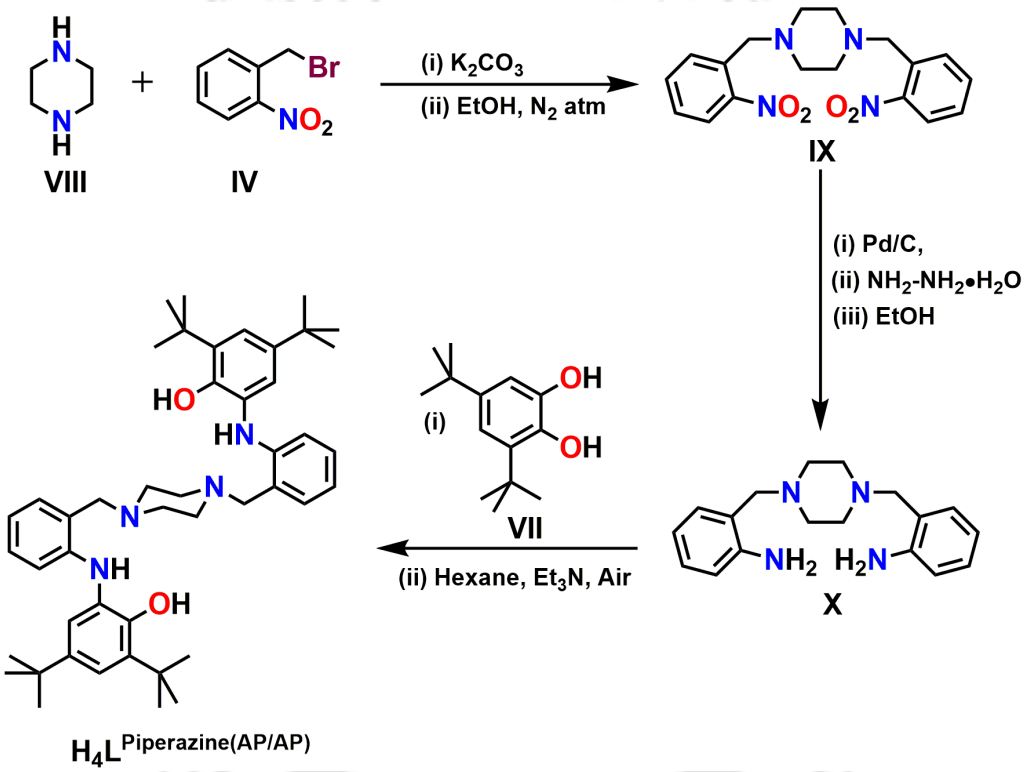

Scheme 3.1: *Synthetic route of ligand* $\boldsymbol{H_4L^{Piperazine(AP/AP)}}$.

A reaction between piperazine (**VIII**) and 2-nitrobenzylbromide (**IV**) (1:2) in the presence of K_2CO_3, provided 1,4-bis(2-nitrobenzyl) piperazine (**IX**), which upon reduction by Pd/C in the presence of $NH_2–NH_2•H_2O$ provided 2,2'-[piperazine-1,4-diylbis(methylene)] dianiline (**X**). The ligand $\mathbf{H_4L^{Piperazine(AP/AP)}}$ was obtained as a amorphous solid by reacting one equivalent of 2,2'-[piperazine-1,4-diylbis(methylene)] dianiline (**X**) with 2 equivalents of 3,5-di-*tert*-butyl-catechol (**VII**) in the presence of Et_3N in hexane with 49% yield. The ligand was characterized by using FT-IR spectroscopy, NMR spectroscopy, mass spectrometry and single crystal X-ray crystallographic techniques.

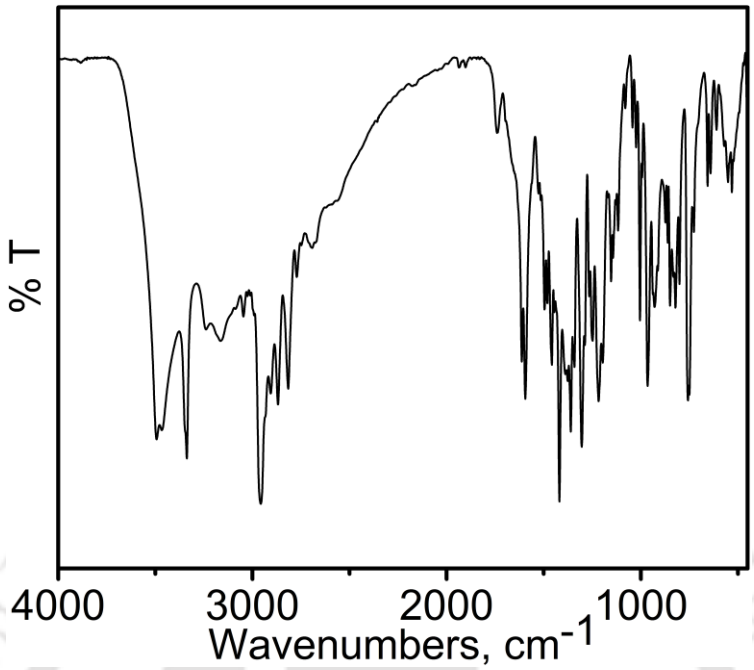

Figure 3.2: *FT-IR spectrum of* ***H$_4$L$^{Piperazine(AP/AP)}$***.

In infrared spectrum of ligand **H$_4$L$^{Piperazine(AP/AP)}$** (**Figure 3.2**), two sharp bands at 3494 and 3338 cm^{-1} corresponded to ν(O–H) and ν(N–H) stretching bands, respectively.[3a-b] The asymmetric, overtone and symmetric bands of ν(C–H) stretches for the *tert*-butyl groups were appeared at 2955, 2905 and 2868 cm^{-1} respectively. [3a-d] The bending ν(C–H) stretches for *tert*-butyl groups appeared at 1419 and 1360 cm^{-1}.[3a] The infrared stretching bands at ~1587, 1504 and 1483 cm^{-1} ascribed as ν(C=C) stretches of the aromatic rings.[3a] The phenolic ν(C–O) and the ν(C–N) stretching bands appeared at 1304 and 1218 cm^{-1}, respectively, for the *ter*-butyl groups-containing 2-aminophenol unit.[3a]

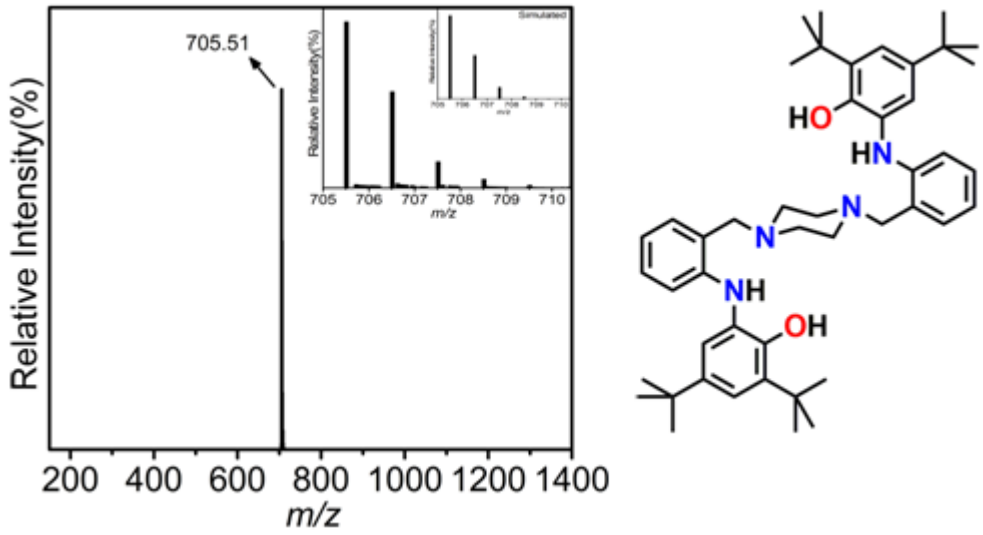

Figure 3.3: *ESI–mass spectrum (+ve mode) of* $\boldsymbol{H_4L^{Piperazine(AP/AP)}}$ *with experimental and simulated (inset) isotope distribution pattern.*

Electrospray ionization mass spectrum (ESI-MS) of a solution containing ligand $\mathbf{H_4L^{Piperazine(AP/AP)}}$ in CH_3CN provided a 100% molecular ion peak at *m/z* = 705.51 (**Figure 3.3**). Simulated isotope distribution pattern (inset) confirmed the composition as $[C_{46}H_{64}N_4O_2+H]^+$.

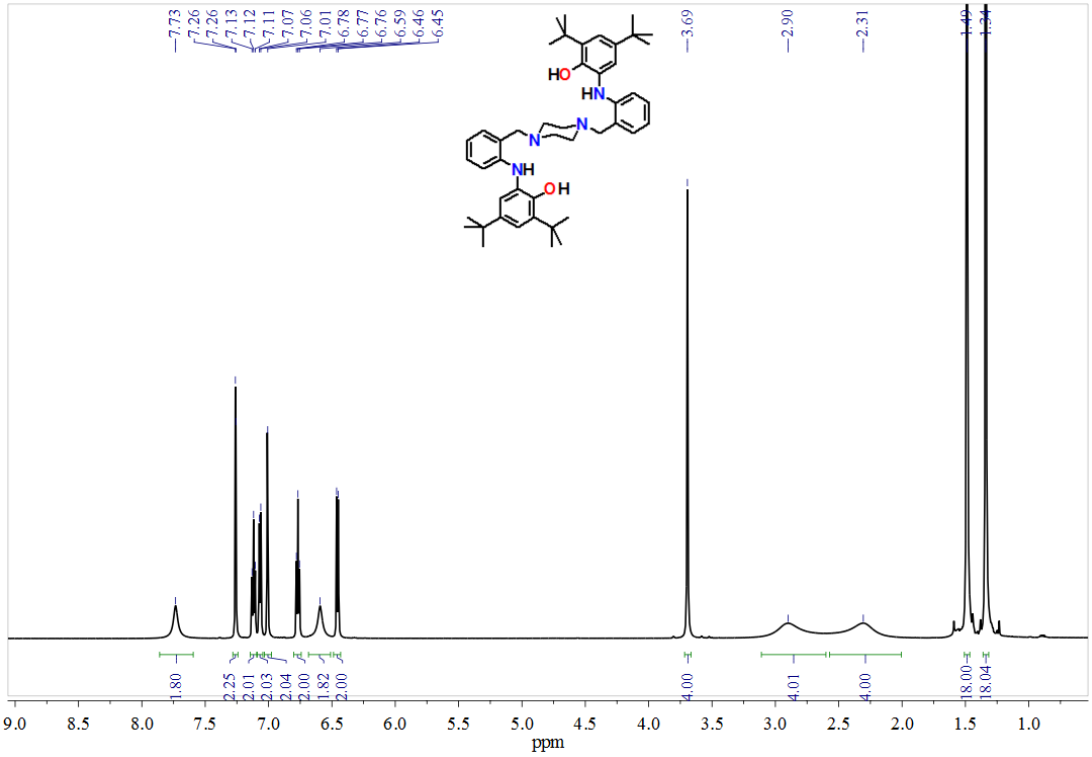

Figure 3.4: *^{1}H-NMR spectrum of* $\boldsymbol{H_4L^{Piperazine(AP/AP)}}$ in $CDCl_3$.

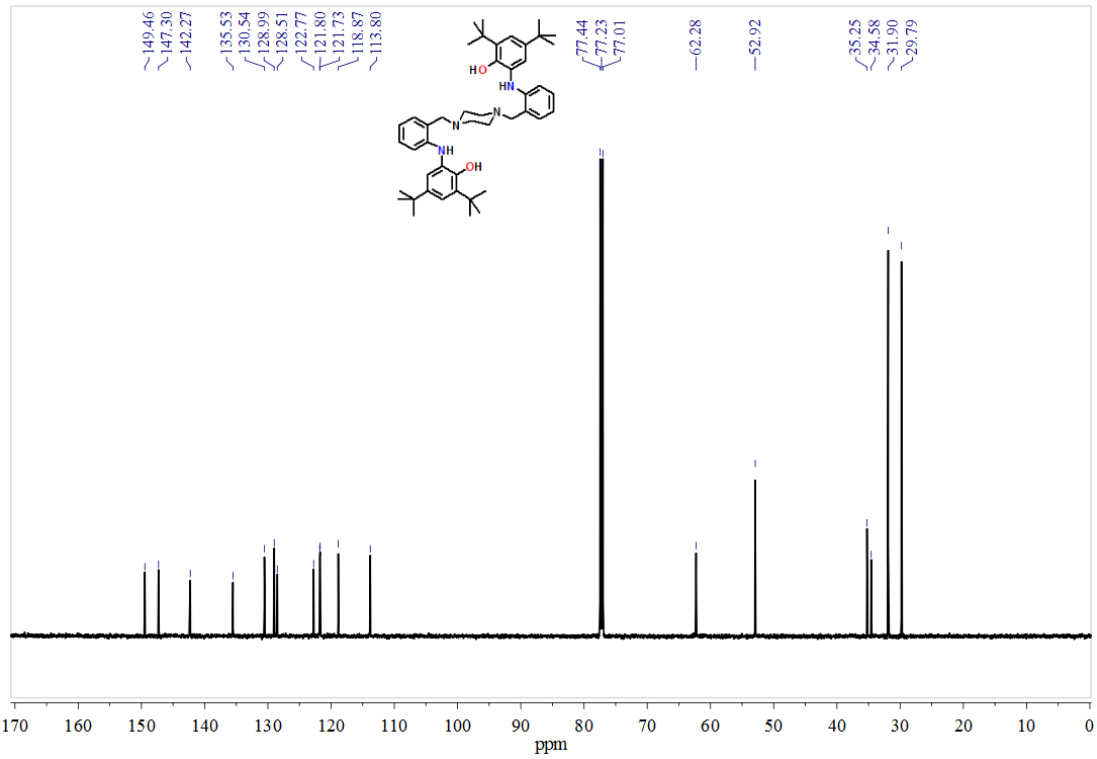

Figure 3.5: *^{13}C-NMR spectrum of* ***$H_4L^{Piperazine(AP/AP)}$*** in $CDCl_3$.

In ^{1}H-NMR spectrum of **$H_4L^{Piperazine(AP/AP)}$** (**Figure 3.4**), two singlet resonance signals at δ = 1.34 and δ = 1.49 ppm were appeared for each peak corresponded to the 18 hydrogen atoms attached to *tert*-butyl groups. One singlet peak at δ = 3.69 was attributed for four bezylic protons and two broad peaks at δ = 2.31 and δ = 2.90 were corresponded to each of four aliphatic protons in piperazine moiety. Two singlet peaks at δ = 6.59 and δ = 7.73 ppm were corresponded to N–H and O–H protons, respectively. Apart from this, signals for 12 aromatic protons were appeared in the range of 6.50–7.30 ppm.

In ^{13}C-NMR spectrum of **$H_4L^{Piperazine(AP/AP)}$** (**Figure 3.5**), the resonance signals for four aliphatic carbon were appeared in between of δ = 29 to 36 ppm and two peaks at δ = 52.92 and δ = 62.28 corresponded to two benzylic carbon and four aliphatic carbon present in piperazine moiety. All the aromatic carbon appeared at a region of 115 to 150 ppm.

Single crystal structure of $\mathbf{H_4L^{Piperazine(AP/AP)}}$ suitable for X-ray diffraction measurement was obtained by the slow evaporation of a $CHCl_3$/MeOH (3:1) solution of $\mathbf{H_4L^{Piperazine(AP/AP)}}$. $\mathbf{H_4L^{Piperazine(AP/AP)}}$ crystallized in the monoclinic space group 'I 2/c'. Molecular structure of $\mathbf{H_4L^{Piperazine(AP/AP)}}$ with atom labeling scheme was depicted in **Figure 3.6**. Selected bond distances and bond angles are given in **Table 3.1**.

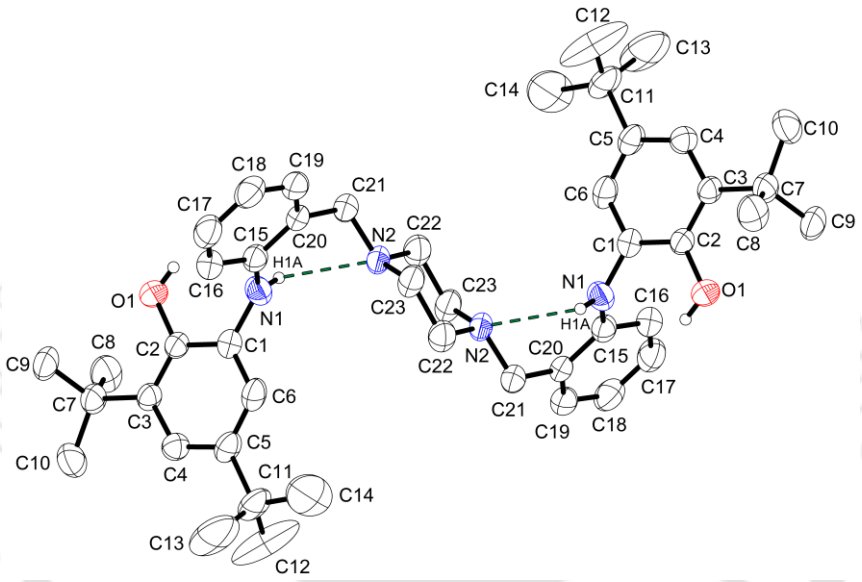

Figure 3.6: *ORTEP diagram of* $\boldsymbol{H_4L^{Piperazine(AP/AP)}}$ *shown at 40% thermal ellipsoid probability. H-atoms, except the H atoms of –NH and N present in H-bonding, were omitted for the clarity.*

In the molecular structure of $\mathbf{H_4L^{Piperazine(AP/AP)}}$, two N(2-methylphenyl)-3,5,-di-*tert*-butyl-2-aminophenol moieties were connected *via* a bridging piperazine ring, which was in chair conformation. Both the moieties were at the equatorial positions and a crystallographic inversion center was present in the middle of the piperazine ring. All aryl C–C bond distances were found to be within the range of 1.370–1.405(5) Å. This suggested the fully reduced phenyl form of the aryl units. The C2–O1 = 1.378(4) and C1–N1 = 1.420(5) Å bond distances were also of single bond values and thus, supported the aminophenol form of the aryl unit.

Table 3.1: *Selected bond distances (Å) for* $\boldsymbol{H_4L^{Piperazine(AP/AP)}}$.

C1–N1	1.420(5)	C7–C9	1.533(6)
C2–O1	1.378(4)	C7–C10	1.532(5)
C1–C2	1.397(5)	C5–C11	1.540(6)
C2–C3	1.395(5)	C11–C12	1.471(7)
C3–C4	1.389(5)	C11–C13	1.508(7)
C4–C5	1.405(5)	C11–C14	1.512(8)

C5–C6	1.388(5)	C15–C16	1.400(5)
C6– C1	1.385(5)	C16–C17	1.370(6)
N1–C15	1.389(5)	C17–C18	1.373(6)
C21–N2	1.469(5)	C18–C19	1.396(6)
C22–N2	1.457(5)	C19–C20	1.371(6)
C23–N2	1.463(5)	C20–C15	1.396(5)
C3–C7	1.537(5)	C20–C21	1.524(5)
C7–C8	1.560(5)	C22–C23	1.511(5)

The aminophenol-based ligand $\mathbf{H_4L^{Piperazine(AP/AP)}}$ is potentially redox active in character and its probable oxidation states are shown in **Scheme 3.2**.

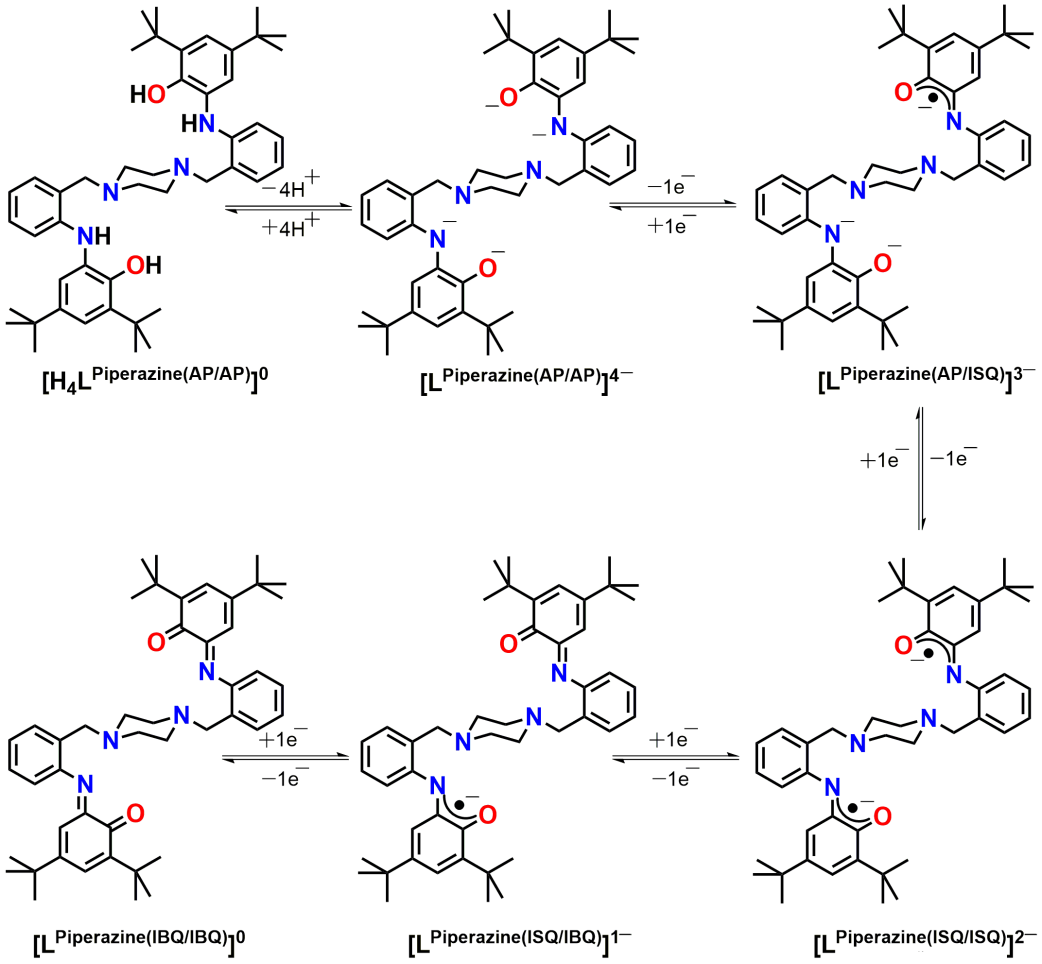

Scheme 3.2: *Possible oxidation states of* $\boldsymbol{H_4L^{Piperazine(AP/AP)}}$.

3.3 Synthesis and Characterization of an Octahedral Co(III) Complex(3A) of $H_4L^{Piperazine(AP/AP)}$

Ligand $\mathbf{H_4L^{Piperazine(AP/AP)}}$ upon reacting with an equivalent amount of $CoCl_2 \bullet 6H_2O$ in CH_3CN in presence of Et_3N under aerial atmosphere provided a octahedral mononuclear cobalt(III) complex (**3A**) in 46% yield (**Scheme 3.3**).

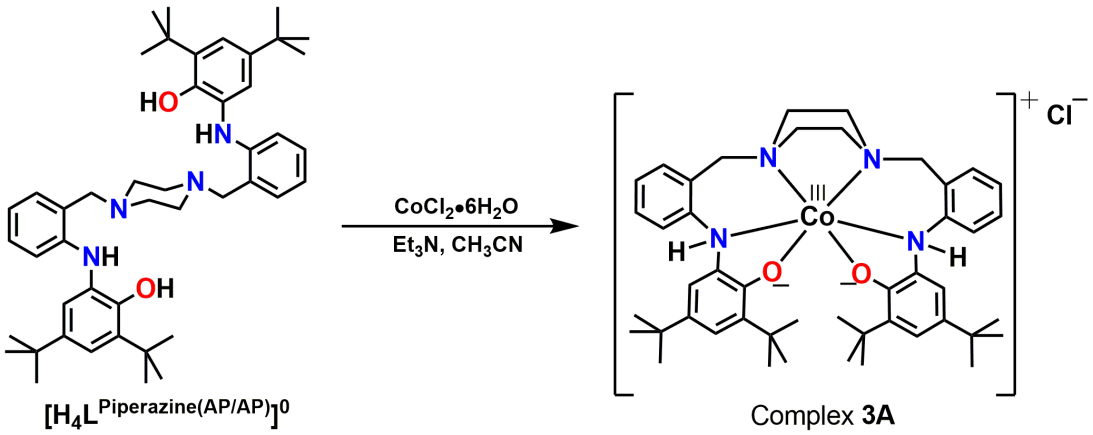

Scheme 3.3: *Synthetic route of complex **3A** from ligand $H_4L^{Piperazine(AP/AP)}$.*

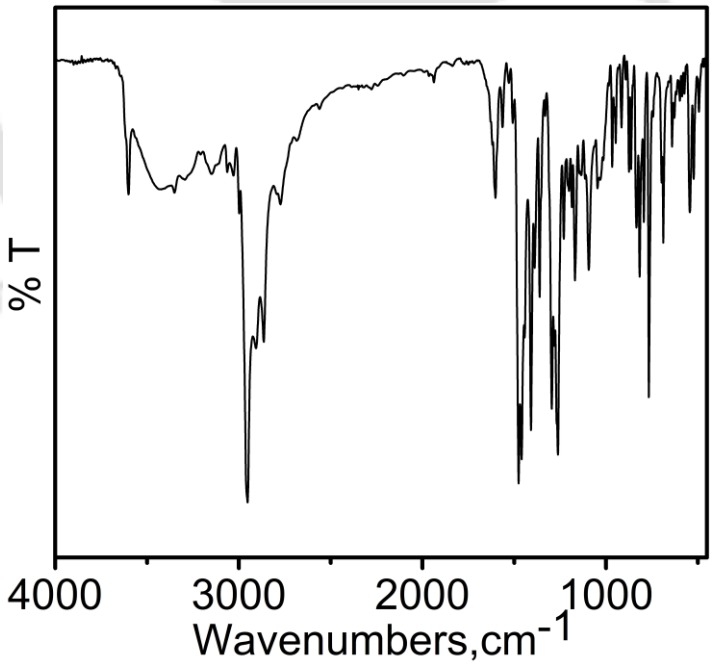

Figure 3.7: *FT-IR spectrum of complex **3A**.*

The infrared spectrum of complex **3A** (**Figure 3.7**) was recorded on KBr pallet. In infrared spectrum of complex **3A**, the band at 3600 cm^{-1} corresponded to ν(O–H) stretching of the unbound H_2O molecule present in the crystal.[3a] The band at 3350 cm^{-1} appeared due to ν(N–H) stretching. The asymmetric, overtone and symmetric bands of ν(C–H) stretches for the *tert*-butyl groups were appeared at 2952, 2906 and 2864 cm^{-1}, respectively. [3a-d] The band at 1601 cm^{-1} was attributed to ν(N–H) bending.

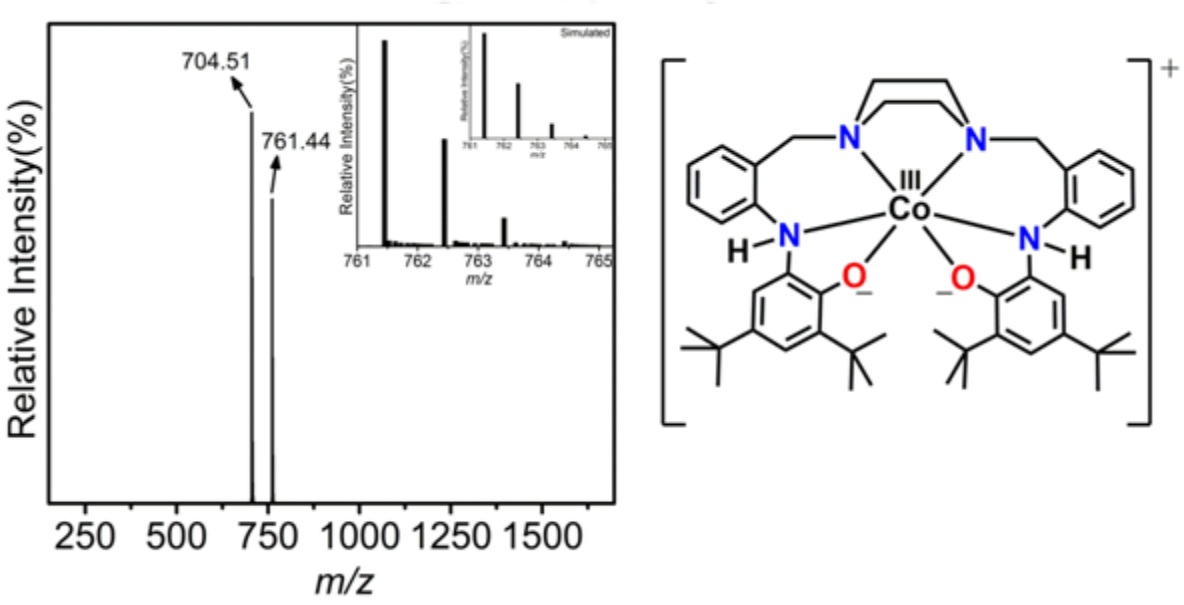

Figure 3.8: *ESI–mass spectrum (+ve mode) of complex **3A** with experimental and simulated (inset) isotope distribution pattern.*

Electrospray ionization mass spectrum (ESI-MS) of a solution of complex **3A** in CH_3OH provided a 100% molecular ion peak at *m*/*z* = 761.44 (**Figure 3.8**) in positive mode. Simulated isotope distribution pattern (inset) confirmed the composition as $[C_{46}H_{62}CoN_4O_2]^+$.

Crystals suitable for single crystal X-ray diffraction analysis of complex **3A** were obtained by slow evaporation of a $CH_3OH/CHCl_3$ (3:1) solvent mixture of the complex. Complex **3A** was crystalized in the monoclinic space group '*C* 2/*c*'. ORTEP diagram of the complex has been shown in **Figure 3.9** and selected bond distances and bond angles are given in **Table 3.2**.

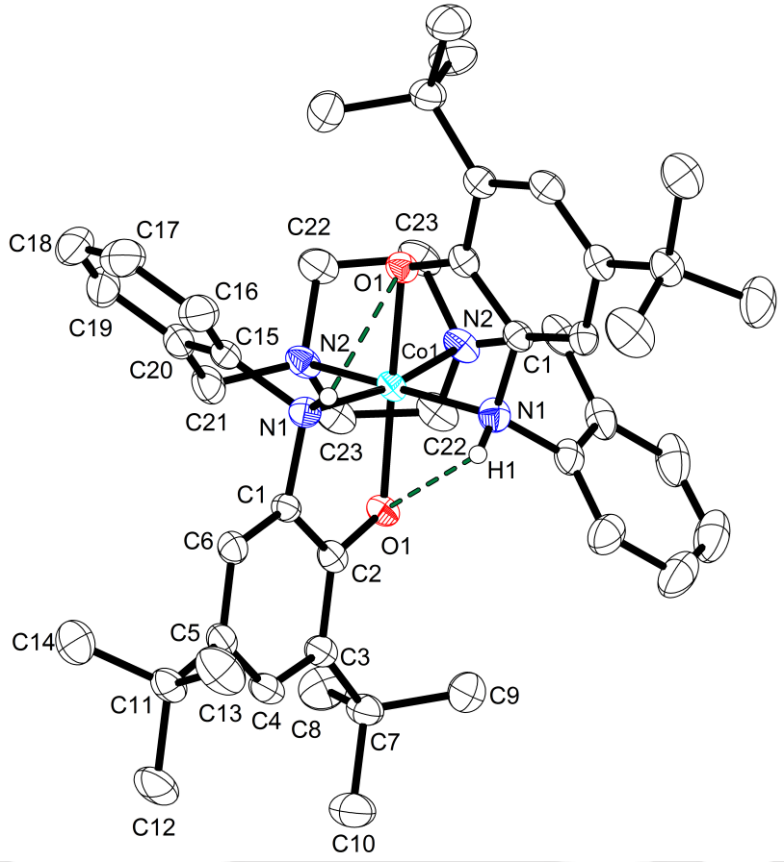

Figure 3.9: *ORTEP presentation of complex **3A**; thermal ellipsoids were drawn at 40% probability level. H-atoms, except the H atoms of –NH and O present in H-bonding, were omitted for clarity.*

In complex **3A**, the monocationic core was six-coordinate, where the basal plane was constituted by four nitrogen atoms; two N atoms (N2 and $N2^{i}$) were of the piperazine unit and the rest two (N1 and $N1^{i}$) belonged to two 2-aminophenolate units [**Figure 3.9**]. The axial positions were occupied by two phenolate O atoms, O1 and $O1^{i}$. The O1−Co−$O1^{i}$ = 171.98(9), N1−Co1− $N2^{i}$ = 169.07(8), and N1−Co1−N2 = 96.55(8)° bond angles indicated that Co1 center acquired a distorted octahedral geometry. The Co1−N1 = 1.9469(19), Co1−N2 =1.9780(18) and Co1−O1 = 1.9121(15) Å bond distances were in accord with the previously reported low-spin Co(III)−N and Co(III)−O bond distances.[4a]The C1–N1=1.453(3) Å bond was almost same in distances as found for the bond in ligand $\mathbf{H_4L^{Piperazine(AP/AP)}}$. Therefore, it was obvious that the bond was single bond and the N1 atom was in –NH form. The C2–O1=1.332(3) Å bond was slightly shorter than the –OH bond distance found in ligand $\mathbf{H_4L^{Piperazine(AP/AP)}}$. Nevertheless, the bond was much longer than C–O bond distance (C–O =1.30 Å) reported for

Co(III)–iminosemiquinone systems.[4d] In fact, the C2–O1 bond was commensurate well with phenolate C–O bond.[4e] Interestingly, both the amine-H atoms participated in intramolecular H-bonding with two phenolate O atoms. The H-bonds could be the driving force for stabilization of binegative $[\mathbf{H_2L^{Piperazine(AP/AP)}}]^{2-}$ form of the ligand. The coordination sphere was thus monopositive and the neutrality of the complex was maintained by the presence of a chloride ion as the counter anion.

Table 3.2: *Selected bond distances (Å) and bond angles (°) for complex **3A**.*

Co1–O1	1.9121(15)	C2–C3	1.422(3)
Co1–O1^{i}	1.9121(15)	C3–C4	1.393(3)
Co1–N1	1.9469(19)	C4–C5	1.400(3)
Co1–N1^{i}	1.9469(19)	C5–C6	1.390(3)
Co1–N2	1.9780(18)	C6–C1	1.382(3)
Co1–N2^{i}	1.9780(18)	C15–C16	1.381(3)
C1–N1	1.453(3)	C16–C17	1.398(4)
C2–O1	1.332(3)	C17–C18	1.379(5)
C15–N1	1.460(3)	C18–C19	1.371(5)
C21–N2	1.488(3)	C19–C20	1.392(4)
C22–N2	1.486(3)	C20–C15	1.393(4)
C23–N2	1.502(3)	C20–C21	1.502(4)
C1–C2	1.403(3)	C22–C23	1.531(4)
O1–Co1–O1^{i}	171.98(9)	O1–Co1–N1^{i}	88.52(7)
N1–Co1–N1^{i}	93.50(12)	C2–O1–Co1	112.59(13)
N2–Co1–N2^{i}	73.79(11)	C22–N2–Co1	103.46(13)
O1–Co1–N2	98.54(7)	C21–N2–Co1	115.18(14)
O1–Co1–N2^{i}	87.91(7)	C23–N2–Co1	105.54(14)
N1– Co1–N2	96.55(8)	C1–N1–Co1	108.74(14)
N1– Co1–N2^{i}	169.07(8)	C15–N1–Co1	114.28(14)
O1–Co1–N1	85.99(7)		

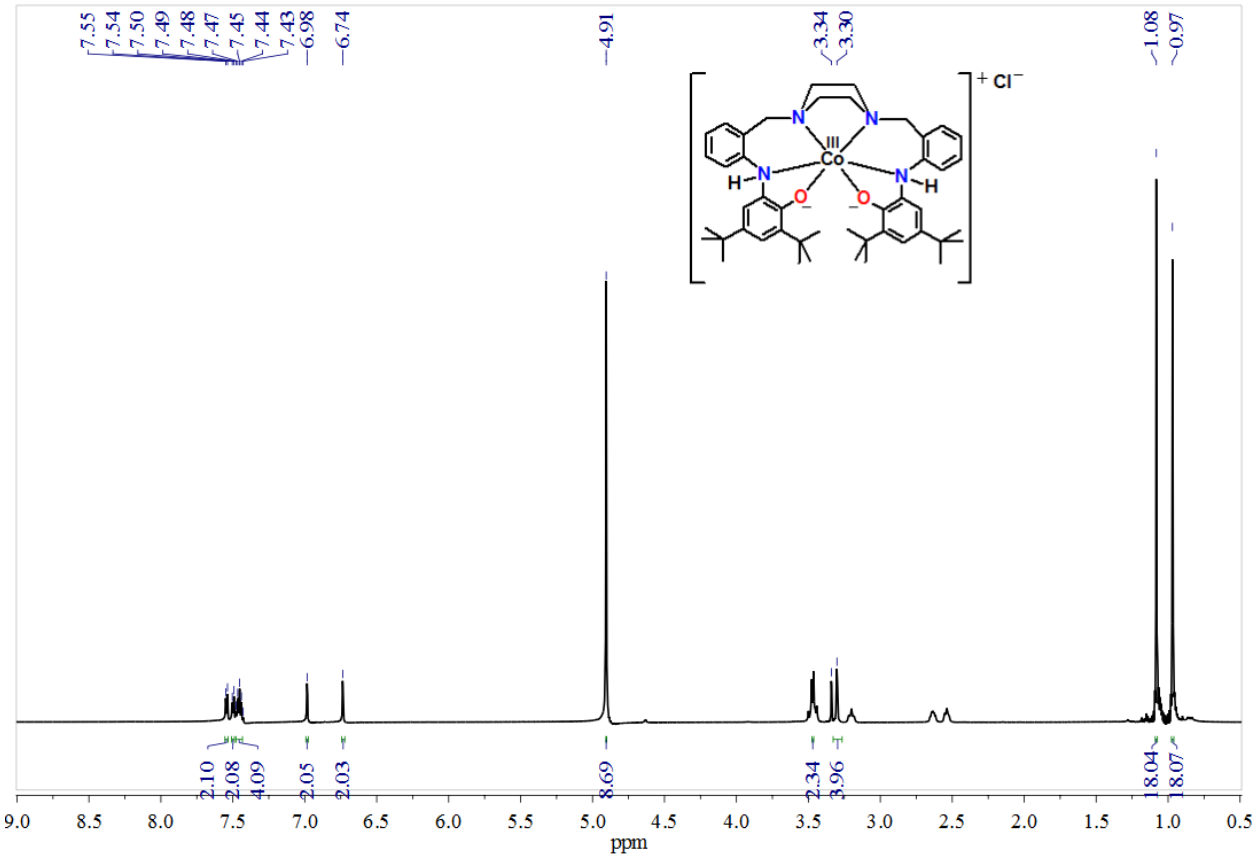

Figure 3.10: *^{1}H-NMR spectrum of complex **3A** in CD_3OD.*

Complex **3A**, was diamagnetic in nature with $S_t = 0$ ground state which was confirmed by ^{1}H-NMR spectroscopy (**Figure 3.10**). Thus, an antiferromagnetic coupling between the two iminosemiquinone-radicals was realized in the complex. Herein, the interaction propagated via the filled t_{2g} orbitals of Co(III) ion. The resonance signals at δ = 0.97 ppm and δ = 1.08 ppm were appeared for each of eighteen hydrogen atoms attached to two *tert*-butyl groups, whereas the resonance signal at δ = 3.30 ppm was attributed for four bezylic protons and a peak at δ = 4.91 ppm corresponded to the eight aliphatic protons present in piperazine moiety. On the other hand, resonance signals for twelve aryl protons were appeared in a range of 6.74-7.55 ppm.

The electronic absorption spectrum of complex **3A** was recorded in HPLC grade CH_3OH at room temperature and depicted in **Figure 3.11**. The electronic absorption bands along with corresponding absorption coefficient values were summarized in **Table 3.3**.

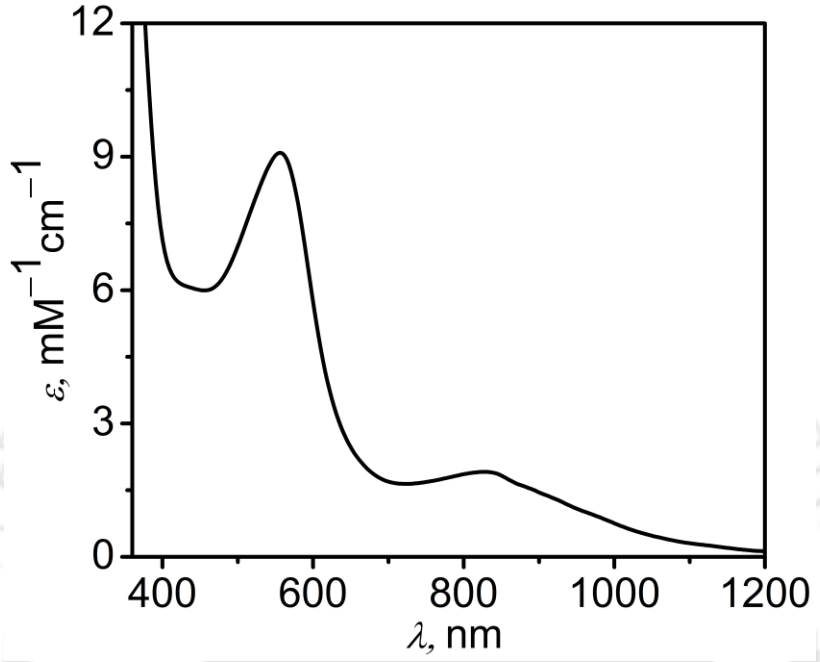

Figure 3.11: *UV-vis/NIR spectrum of complex **3A** in CH_3OH at 25 ℃.*

Complex **3A** showed two characteristic absorption band at λ_{max} = 830 nm and λ_{max} = 555 nm respectively. Both the absorption band were attributed to charge transfer transition (CT).[4b-c]

Table 3.3: *Electronic absorption data of complex **3A***.

Complex	**λ_{max}, nm (ε, $M^{-1}cm^{-1}$)**
3A	830(1900),555(9100)

3.4 Synthesis and Characterization of a Dinuclear Cu(II) Complex(3B) of $H_4L^{Piperazine(AP/AP)}$

Ligand $\mathbf{H_4L^{Piperazine(AP/AP)}}$ upon reacting with 2.0 equivalent amounts of $CuCl_2 \cdot 2H_2O$ in CH_3CN in the presence of Et_3N under aerial atmosphere in 2 hours provided complex **3B** in 42 % yield (**Scheme 3.4**).

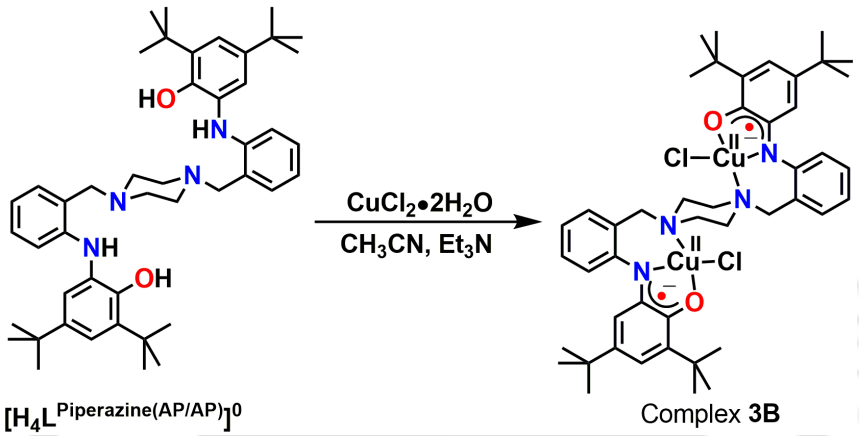

Scheme 3.4: *Synthetic route of complex **3B** from ligand $H_4L^{Piperazine(AP/AP)}$.*

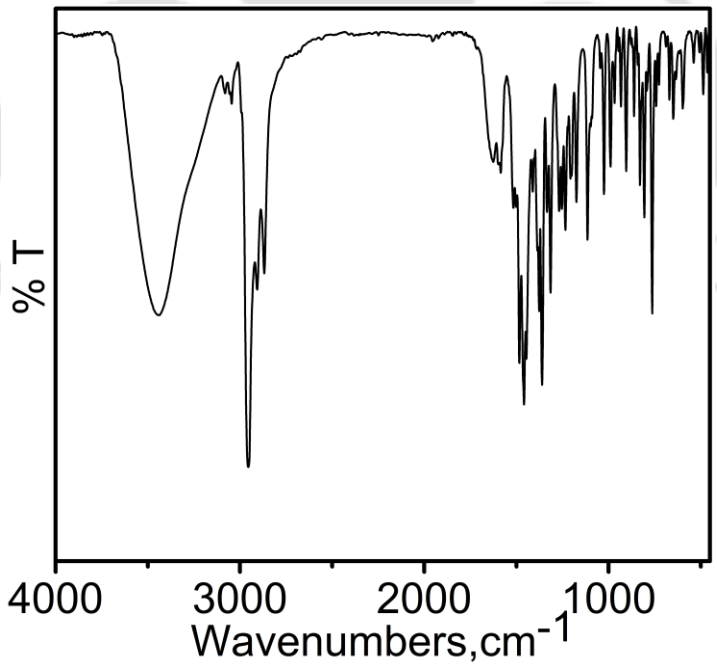

Figure 3.12: *FT-IR spectrum of complex **3B**.*

The infrared spectrum of complex **3B** (**Figure 3.12**) was recorded on a KBr pallet. The infrared spectrum of complex **2B** endorsed the basic coordination of the ligand with the metal ion. The disappearance of bands at 3494 cm^{-1} for ν(O–H) and 3338 cm^{-1} for ν(N–H) clarified the copper coordination with the N–H and O–H deprotonated aminophenol. A weak band corresponding to aryl ν(C−H) stretching observed at around 3055 cm^{-1}.[3a] The asymmetric, overtone and symmetric ν(C–H) bands were appeared at 2954, 2906, and 2868cm^{-1}, respectively.[3a-d] Two peaks at around 1572 cm^{-1} and 1470 cm^{-1} were due to ν(C=N) and ν(C⋯O) stretching, respectively.[3f-g] Those bands implied that the existence of aminophenolate moieties as its one-electron oxidized iminosemiquinone [$(ISQ)^{\bullet 1-}$] form.

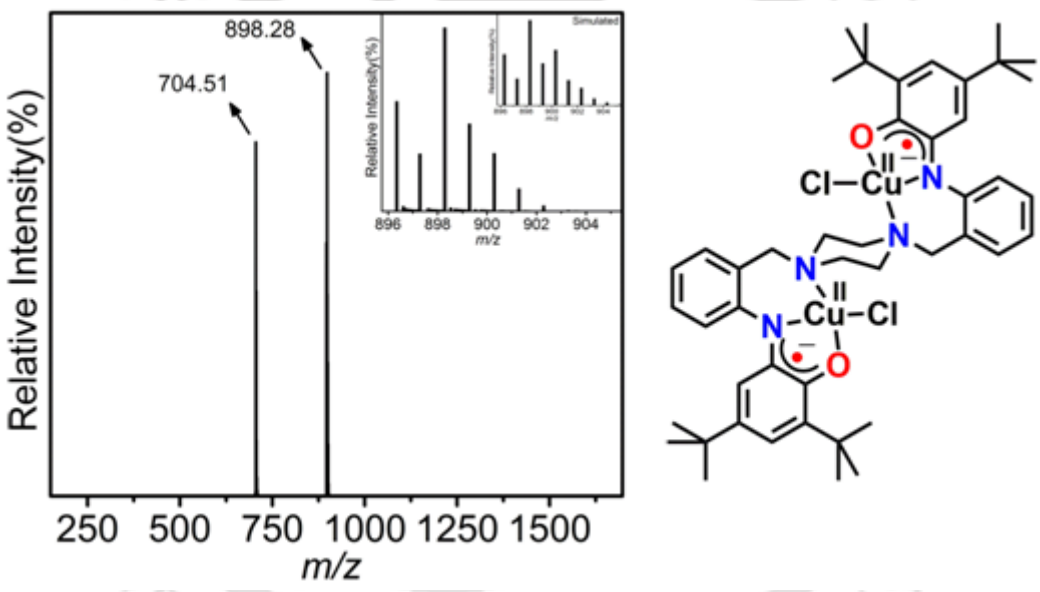

Figure 3.13: *ESI–mass spectrum (+ve mode) of complex **3B** with experimental and simulated (inset) isotope distribution pattern.*

Electrospray ionization mass spectrum (ESI-MS) of a solution of complex **3B** in CH_3OH provided a 100% molecular ion peak at *m*/*z* = 828.35 (**Figure 3.13**) in positive mode. Simulated isotope distribution pattern (inset) confirmed the composition as $[C_{46}H_{60}Cu_2N_4O_2–2Cl]^+$.

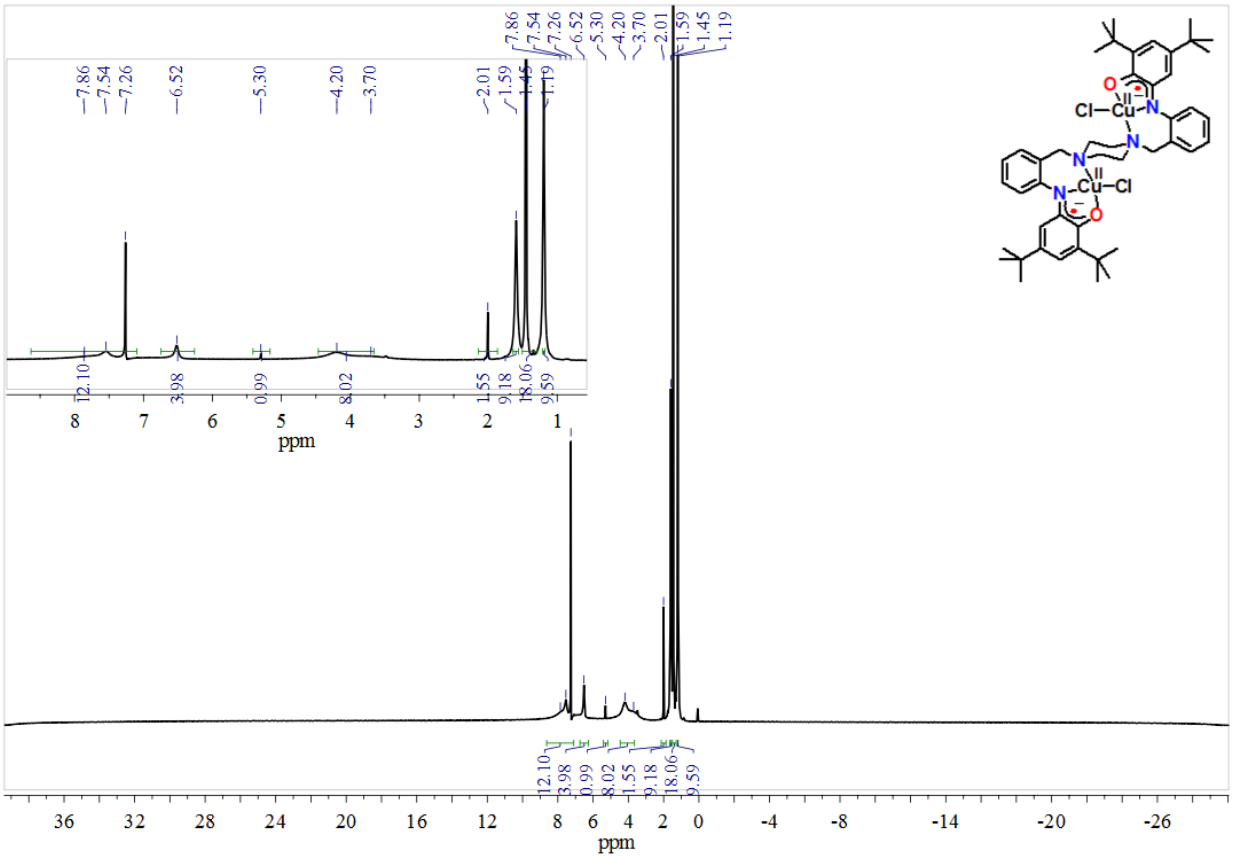

Figure 3.14: *^{1}H-NMR spectrum of complex **3B** in $CDCl_3$.*

Complex **3B** was diamagnetic in nature which was confirmed by ^{1}H-NMR spectrum (**Figure 3.14**) analysis. The resonance signals at δ = 1.19 ppm, δ = 1.45 and δ = 1.59 ppm were appeared for each of thirty-six hydrogen atoms attached to four *tert*-butyl groups, whereas the resonance signal at δ = 2.10 ppm was attributed for two bezylic protons and a peak at δ = 4.20 corresponded to the eight aliphatic protons present in piperazine meaty. The resonance signals for twelve aryl protons were appeared in a range of 7.26-7.86 ppm.

The four-coordinate Cu(II) unit in the complex acquired a distorted square planar geometry (*vide infra*). Thus, the unpaired electron of Cu(II) ion was at $d_x^2-_y^2$ orbital. Because of the distorted-geometry, the orbital was not in orthogonal orientation with the radical-containing p_z orbital of the Cu(II)-coordinated iminosemiquinone unit. Hence, antiferromagnetic interaction prevailed between the two paramagnetic centers which rendered a diamagnetic ground state in complex **3B**.

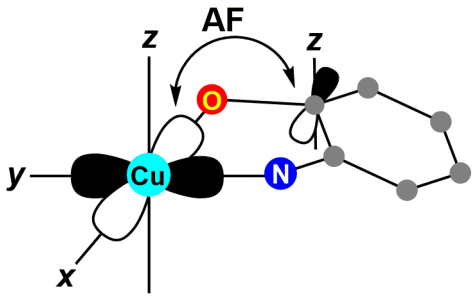

AF = Antiferromagnetic coupling

Non–orthogonal arrangement

Figure 3.15: *Anti ferromagnetic interaction between Cu(II) dx^2-y^2 and π-radical p_z orbitals arrangement via non-orthogonal arrangement.*

Crystals suitable for single crystal X–ray diffraction analysis of complex **3B** were grown by slow evaporation of a CH_2Cl_2/CH_3CN (3:1) solvent mixture of the complex. The complex was crystalized in the triclinic space group '*P–1*'. ORTEP diagram of complex **3B** has been shown in **Figure 3.15** and selected bond distances and bond angles are given in **Table 3.4**.

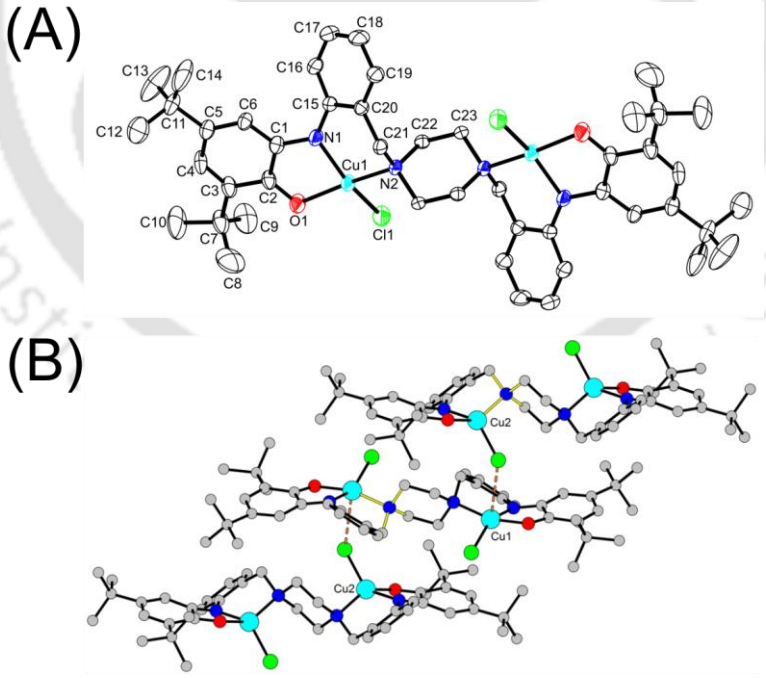

Figure 3.15: *(A) ORTEP presentation of an one asymmetric unit of complex **3B**; thermal ellipsoids were drawn at 40% probability level. (B) Intermolecular interaction present between Cu1 with Cl2 in complex **3B**. H–atoms were omitted for the clarity.*

In complex **3B**, each asymmetric unit comprised of two independent molecules, which were conformational isomers. In one isomer the piperazine N atoms (N2) coordinated to Cu1 atoms from the equatorial positions, while in the other isomer the coordination was from the axial position to Cu2 atoms. Although both molecules were binucler with two four-coordinate (N2OCl) copper units, the geometry around the copper atoms was not same in the two conformational isomers. The τ_4 was of 0.32 for Cu1, while, the value was almost double, 0.57, for Cu2. A scrutiny of the crystal structure revealed that Cl2, which was attached to Cu2, participated in a moderate interaction (3.216 Å) with Cu1 atom (**Figure 3.15B**). This interaction lifted Cu2 atom form the coordination plane in a greater extent compared to Cu1. The impact of the interaction was further realized in the coordination bonds. The Cu1–O1 and Cu1–N1 bond distances were 1.940(3) Å and 1.963(4) Å**,** whereas, the Cu2–O2 and Cu2–N3 bond distances were 1.982(3) Å and 1.959(4) Å, respectively. Nevertheless, the bond distances were in accord with previously reported Cu(II) physical oxidation state.[5a-f]

A systematic change in the C–N, C–O, and aromatic C–C bond distances of 2-aminopenol derivation has been noticed previously and being established as the potential tool in determining the innocent and non-innocent character of the coordinated ligands. In fact, physical oxidation state can be assigned by structural analysis. In a closed–shell 2–amidophenolate form, C–N = 1.37 Å, C–O = 1.35 Å bonds represent single bond character, and the aromaticity of the phenyl ring remains intact.[5g,h] The aromatic C–C bonds is of 1.39±0.01 Å distance. In one–electron oxidized iminosemiquinone state and two–electron oxidized iminoquinone state, the aromaticity of the ring is being destroyed. A quinoid–type distortion; three long bonds followed by an alternate long–short–long bond sequence; is noticed. In iminosemiquinone radical state C–N and C–O bond are 1.35 Å and 1.28 Å, respectively, while the respective bonds are double bond (C–N = 1.30 Å, C–O = 1.22 Å) in iminoquinone state.[5i,j] In complex **2**, C1–N1 = 1.354(6) Å, C2–O1 = 1.275(6) Å, bond distances along with quinoid-type distortion (**Table 3.4**) indicated that 3,5–di–*tert*–buyl–2–iminosemiquinone state of both the coordinated-units of the ligand.

Table 3.4: *Selected bond distances (Å) and bond angles (°) for complex **3B**.*

Cu1–O1	1.940(3)	C2–O1	1.275(6)
Cu1–N1	1.963(4)	C1–C2	1.440(6)
Cu1–N2	2.043(3)	C2–C3	1.440(6)
Cu1–Cl1	2.2222(15)	C3–C4	1.357(7)
C1–N1	1.354(6)	C4–C5	1.431(7)

C5–C6	1.363(6)	C21–N2	1.497(6)
C6–C1	1.416(7)	C22–N2	1.486(5)
N1–C15	1.389(5)	C23–N2	1.496(5)
O1–Cu1–N1	82.77(15)	C1–N1–Cu1	111.8(3)
O1–Cu1–N2	163.07(17)	C2–O1–Cu1	113.2(3)
N1–Cu1–N2	94.57(15)	C21–N2–Cu1	108.1(3)
O1–Cu1–Cl1	93.28(12)	C22–N2–Cu1	108.5(3)
N1–Cu1–Cl1	150.72(13)	C23–N2–Cu1	110.4(3)
N2–Cu1–Cl1	96.96(12)		

The electronic absorption spectrum of complex **3B** was recorded in HPLC grade CH_2Cl_2 at room temperature and depicted in **Figure 3.16**. The electronic absorption bands along with corresponding absorption coefficient values were summarized in **Table 3.5**.

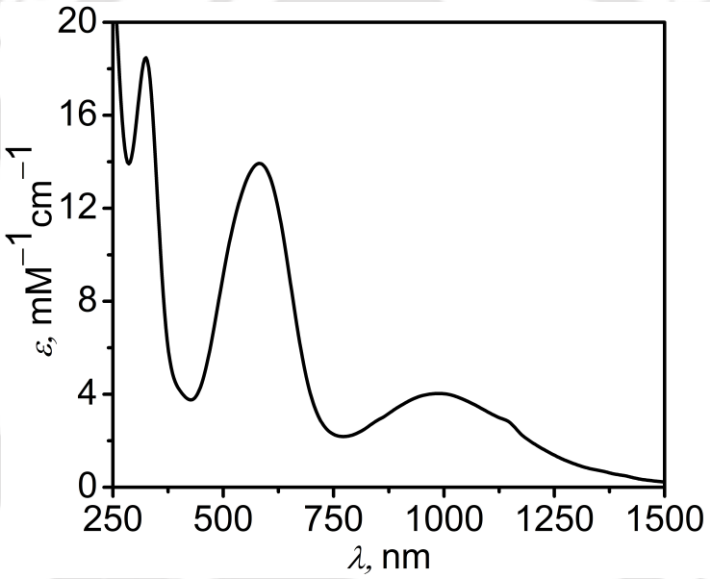

Figure 3.16: *UV-vis/NIR spectrum of complex **3B** in CH_2Cl_2 at 25 ℃.*

Complex **3B** showed two characteristic absorption band at λ_{max} = 990 nm and λ_{max} = 580 nm respectively. Both the absorption band were attributed due to charge transfer transition (CT).[6a-c] Band at λ_{max} = 990 nm due to intra ligand-to-ligand charge transfer (ILCT) and λ_{max} = 580 was due to ligand-to-metal charge transfer transition.[6d]

Table 3.5: *Electronic absorption data of complex **3B**.*

Complex	**λ_{max}, nm (ε, $M^{-1}cm^{-1}$)**
3B	990(4050), 580(13900), 324(18450)

3.5 Synthesis and Characterization of a Cu(II) Complex (3C) of $H_4L^{Piperazine(AP/AP)}$

When ligand $\mathbf{H_4L^{Piperazine(AP/AP)}}$ was treated with an equimolar amount of $Cu(ClO_4)_2 \cdot 6H_2O$ in acetonitrile in the presence of Et_3N under aerial atmosphere provided a green solid. After 7 days, during recrystallization from CH_2Cl_2:CH_3CN (4:1) solvent mixture, provided complex **3C** in 32 % yield (**Scheme 3.5**).

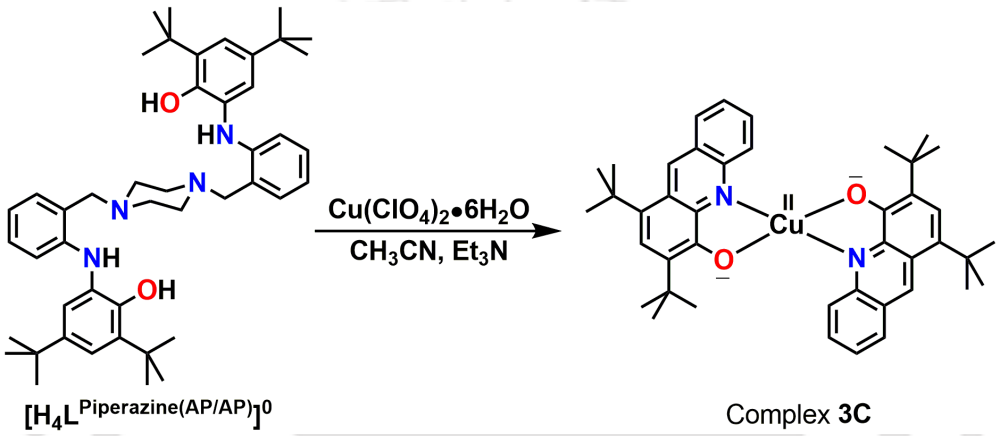

Scheme 3.5: *Synthetic route of complex **3C** from ligand $H_4L^{Piperazine(AP/AP)}$.*

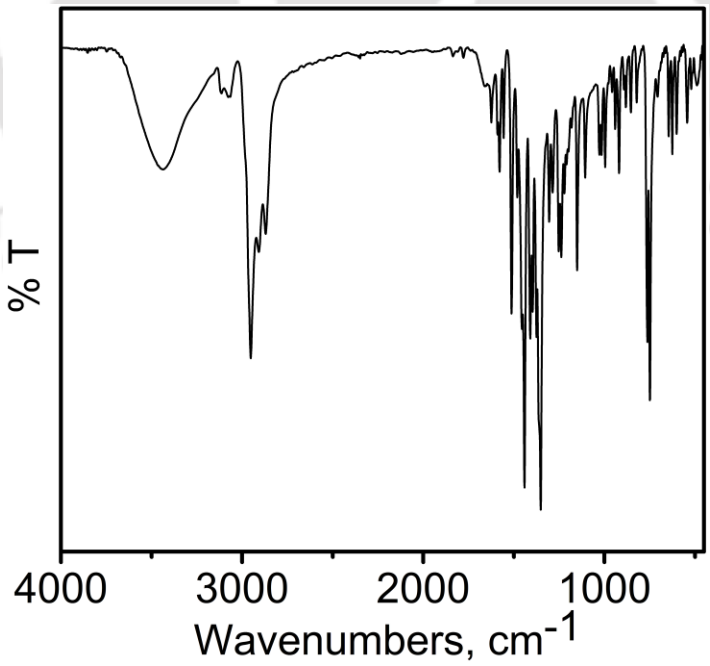

Figure 3.17: *FT-IR spectrum of complex **3C**.*

The infrared spectrum of complex **3C** (**Figure 3.17**) was recorded on a KBr pallet. The disappearance of bands at 3460 cm^{-1} for ν(O–H) and 3359 cm^{-1} for ν(N–H) clarified the copper coordination with the N–H and O–H deprotonated aminophenol. A weak band corresponding to aryl ν(C−H) stretching observed at around 3070 cm^{-1}.[3a] The asymmetric, overtone and symmetric ν(C–H) bands appeared at 2952, 2870 and 2910 cm^{-1}respectively.[3a-d] Two peaks at around 1578 cm^{-1} was due to ν(C=N) stretching.[3f-h]

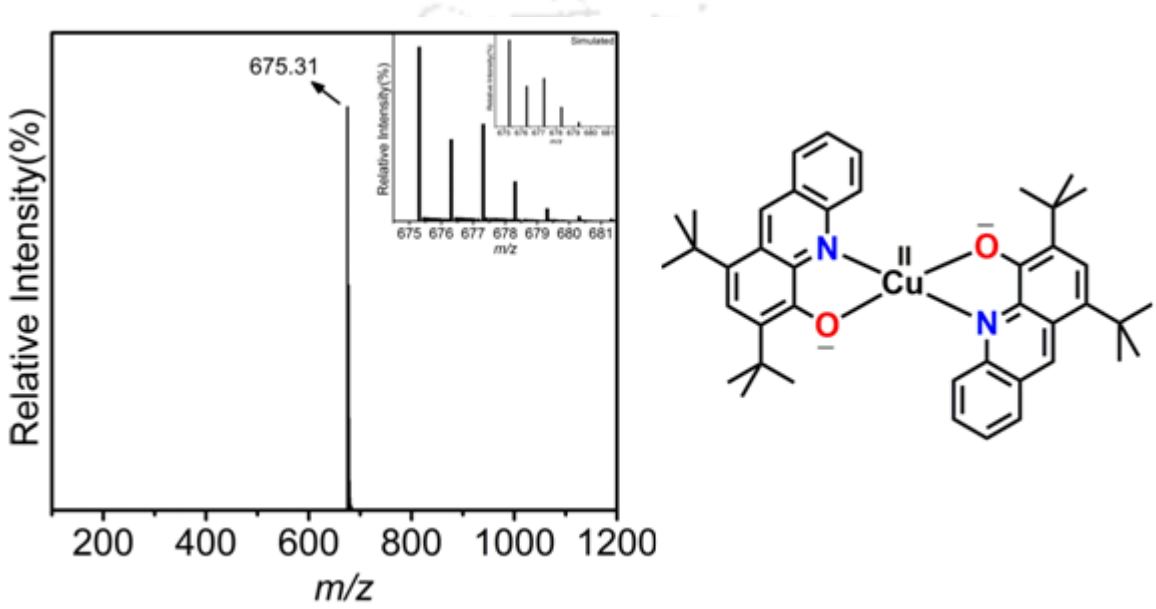

Figure 3.18: *ESI-mass spectrum (+ve mode) of complex **3C** with experimental and simulated (inset) isotope distribution pattern.*

Electrospray ionization mass spectrum (ESI-MS) of a CH_3OH solution of complex **3C** provided a 100% molecular ion peak at *m*/*z* = 675.31 (**Figure 3.18**) in positive mode. Simulated isotope distribution pattern (inset) confirmed the composition as $[C_{46}H_{48}CuN_4O_2]^+$ for the complex.

To determine the molecular structure, X-ray single crystal diffraction measurement on complex **3C** was performed at 293(2) K. X-ray quality single crystals of complex **3C** were obtained by the slow evaporation of a 3:1 CH_2Cl_2:CH_3CN solution of the complex. Complex **3C** crystallized in the monoclinic space group '*P*–1'. ORTEP diagram of the **3C** with atom numbering scheme is presented in **Figure 3.19**. Selected bond distances and bond angles are given in **Table 3.6**.

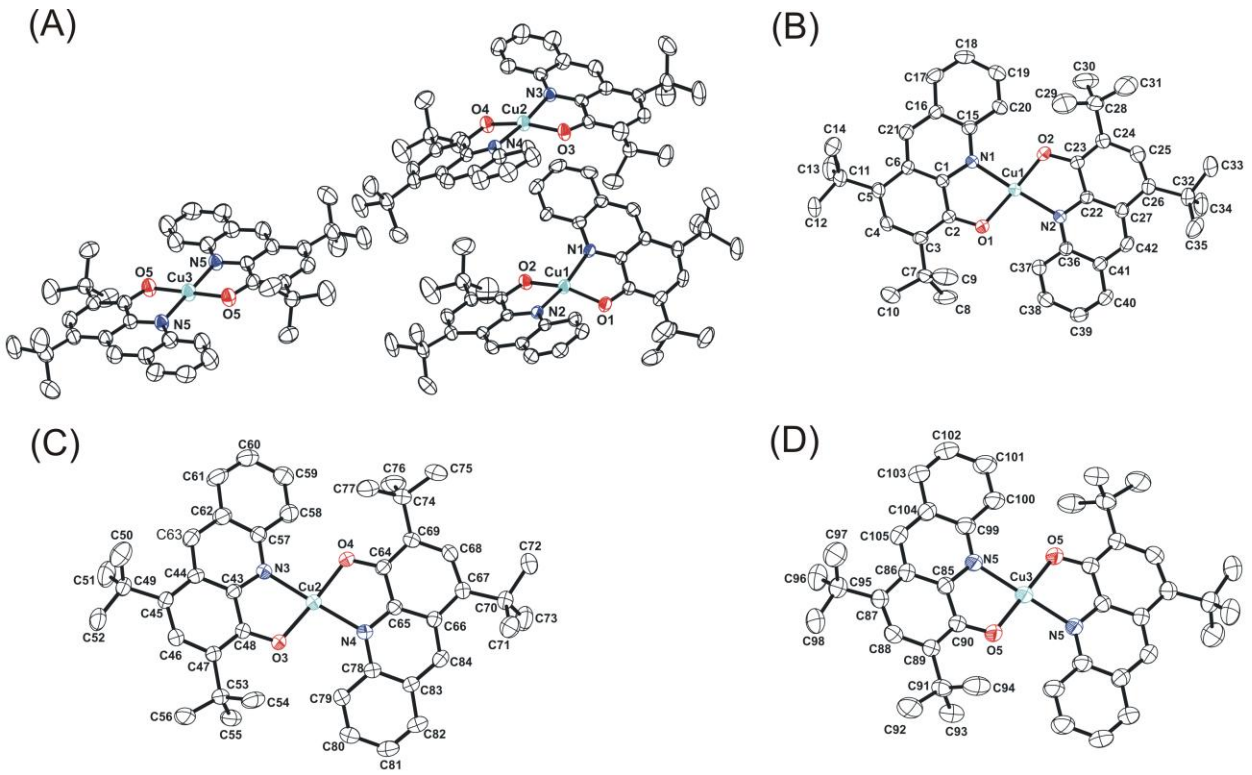

Figure 3.19: *(A) ORTEP presentation of complex **3C**; thermal ellipsoids were drawn at 40% probability level. H–atoms were omitted for clarity. (B) ORTEP plot of unit **1**. (C) ORTEP plot of unit **2**. (D) ORTEP plot of unit **3**.*

Complex **3C** was composed of three asymmetric units present in a unit cell and out of two units (unit **1** and **2**), geometry around the central Cu1 or Cu2 center was distorted square planar, while in unit **3** the geometry was square planar. In unit **1** and unit **2**, both the central atoms (Cu1 and Cu2) were four coordinate (τ_4 = 0.30, 0.16). The two N and two O atoms from the two bidentate acridine frameworks occupied the coordination sites. Same coordination sites were present in the case of unit **3**, where central Cu3 atom acquired square planar (τ_4 = 0.0) geometry. The bond distances of Cu1–O1 and Cu1–O2 were 1.892(3) Å and 1.883(3) Å for unit **1**, while in unit **2** the bond distances of Cu2–O3 and Cu2–O4 were 1.886(3) Å and 1.884(3) Å, respectively. In unit **1**, the bond distances of Cu1–N1 and Cu1–N2 were 2.010(4) Å and 2.006(4) Å, where as in unit **2** the bond distances of Cu2–N3 and Cu2–N4 were 2.037(4) Å and 2.043(4) Å, respectively. In the unit **3**, the bond distances of Cu3–O5 and Cu3–N5 were 1.889(3) Å and 2.099(4) Å, respectively. The observed bond distances were in accord with the previously reported Cu(II) complexes of NO coordination sites. Thus, herein, the oxidation state of the central copper ion has been assigned as +II.

In unit **3**, the both side acridine-ligating units experienced interligand π–π (3.279 Å) stacking interaction (**Figure 3.20**) with the other two asymmetric molecules of complex **3C**. The interactions were postulated as the induction force for imposing a planar geometry in unit **3**.

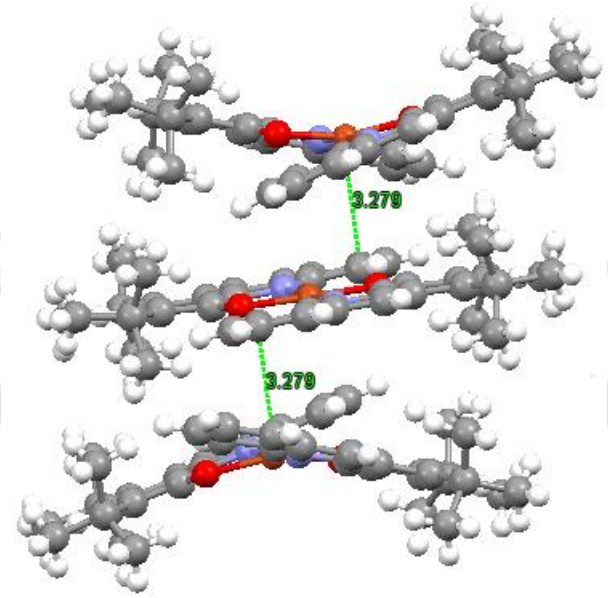

Figure 3.20: *Representation of π–π interactions present in complex **3C** between the acridine unit (in unit **3**) and the acridine (in unit **1** and unit **2**) in a coordinated ligand in complex **3C**.*

Table 3.6: *Selected bond distances (Å) and bond angles (°) for complex **3C**.*

Cu1–O1	1.892(3)	C26–C27	1.444(6)
Cu1–O2	1.883(3)	C27–C22	1.418(6)
Cu1–N1	2.010(4)	C36–C37	1.410(6)
Cu1–N2	2.006(4)	C37–C38	1.354(6)
Cu2–O3	1.886(3)	C38–C39	1.404(7)
Cu2–O4	1.884(3)	C39–C40	1.337(6)
Cu2–N3	2.037(4)	C40–C41	1.428(6)
Cu2–N4	2.043(4)	C41–C42	1.379(6)
Cu3–O5	1.889(3)	C42–C27	1.398(6)
Cu3–N5	2.099(4)	C43–C44	1.426(6)
N1–C1	1.350(5)	C44–C45	1.432(6)
N1–C15	1.365(5)	C45–C46	1.381(6)
O1–C2	1.324(5)	C46–C47	1.418(6)
N2–C22	1.350(5)	C47–C48	1.385(6)
N2–C36	1.359(5)	C48–C43	1.452(6)
O2–C23	1.314(5)	C57–C58	1.415(6)
N3–C43	1.352(5)	C58–C59	1.366(7)
N3–C57	1.366(5)	C59–C60	1.400(7)

O3–C48	1.318(5)	C60–C61	1.336(7)
N4–C65	1.357(5)	C61–C62	1.429(7)
N4–C78	1.362(5)	C62–C63	1.406(6)
O4–C64	1.310(5)	C62–C57	1.410(6)
N5–C85	1.365(6)	C63–C44	1.388(6)
N5–C99	1.351(6)	C64–C65	1.449(6)
O5–C90	1.325(6)	C65–C66	1.438(6)
C1–C2	1.453(6)	C66–C67	1.442(6)
C2–C3	1.383(6)	C67–C68	1.370(6)
C3–C4	1.402(6)	C68–C69	1.411(6)
C4–C5	1.377(6)	C69–C64	1.390(6)
C5–C6	1.442(6)	C78–C79	1.428(6)
C6–C1	1.422(6)	C79–C80	1.361(6)
C15–C16	1.420(6)	C80–C81	1.405(7)
C16–C17	1.422(6)	C81–C82	1.337(7)
C17–C18	1.354(7)	C82–C83	1.427(6)
C18–C19	1.403(7)	C83–C84	1.377(6)
C19–C20	1.350(6)	C83–C78	1.421(6)
C20–C15	1.411(6)	C84–C66	1.400(6)
C16–C21	1.383(6)	C85–C86	1.440(7)
C21–C6	1.412(6)	C86–C87	1.443(6)
C22–C23	1.455(6)	C87–C88	1.373(7)
C23–C24	1.372(6)	C88–C89	1.410(7)
C24–C25	1.415(7)	C89–C90	1.402(6)
C25–C26	1.363(6)	C90–C85	1.429(6)
C99–C100	1.407(7)	C103–C104	1.403(7)
C100–C101	1.353(7)	C104–C99	1.442(7)
C101–C102	1.432(8)	C104–C105	1.385(7)
C102–C103	1.335(7)	C105–C86	1.385(7)
O1–Cu1–O2	154.55(15)	C2–O1–Cu1	114.2(3)
N1–Cu1–N2	161.85(14)	C23–O2–Cu1	115.1(3)
O1–Cu1–N1	83.42(13)	C1–N1–Cu1	111.1(3)
O1–Cu1–N2	101.05(13)	C15–N1–Cu1	129.6(3)
O2–Cu1–N2	83.33(13)	C22–N2–Cu1	111.0(3)
O2–Cu1–N1	100.26(13)	C36–N2–Cu1	129.5(3)
O3–Cu2–O4	163.09(15)	C48–O3–Cu2	115.0(3)
N3–Cu2–N4	173.48(14)	C64–O4–Cu2	115.3(3)
O3–Cu2–N3	82.66(13)	C65–N4–Cu2	110.1(3)
O3–Cu2–N4	100.51(13)	C78–N4–Cu2	131.1(3)
O4–Cu2–N3	95.88(13)	C43–N3–Cu2	109.9(3)
O4–Cu2–N4	82.75(13)	C57–N3–Cu2	130.6(3)
O5–Cu3–O5^{i}	180.000(1)	C90–O5–Cu3	116.2(3)
N5–Cu3–N5^{i}	180.000(1)	C99–N5–Cu3	130.7(3)
O5–Cu3–N5	98.18(15)	C85–N5–Cu3	109.4(3)
O5–Cu3–N5^{i}	81.82(15)		

The electronic absorption spectrum of complex **3C** was recorded in CH_2Cl_2 at room temperature and depicted in **Figure 3.21**. The electronic absorption bands along with corresponding absorption coefficient values are summarized in **Table 3.7**.

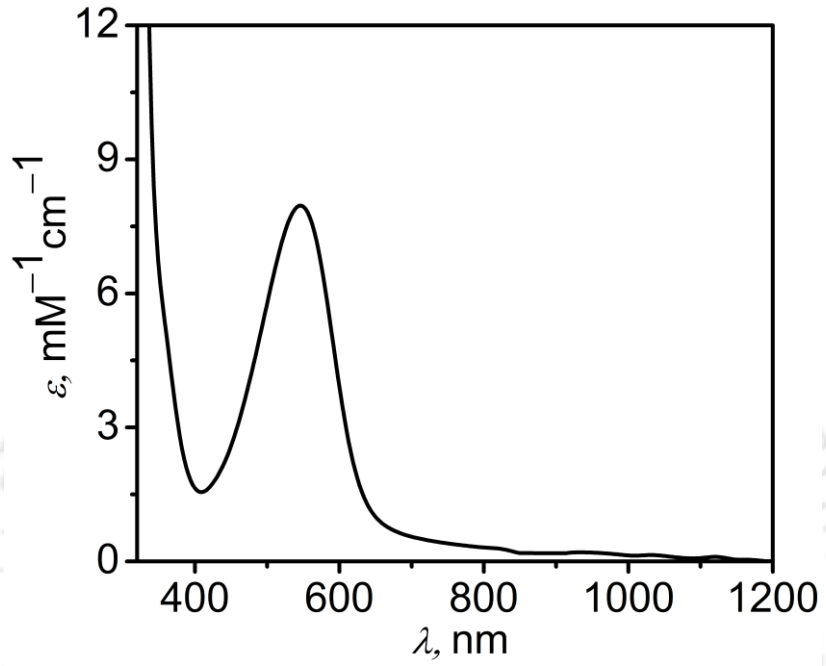

Figure 3.21: *UV-vis/NIR spectrum of complex **2C** in CH_2Cl_2 at 25 ℃.*

Complex **3C**, exhibit an intense absorption at λ_{max} = 545 nm (ε = 7950 M^{-1} cm^{-1}), which was attributed to a ligand-to-metal CT transition.[7a,b] The *d–d* transition in complex **3C** was observed at 668 nm (ε = 750 M^{-1} cm^{-1}).[7c,d] No charge transfer bands in the NIR region implied the absence of iminosemiquinone radical unit in the coordination sphere in complex **3C**.

Table 3.7: *Electronic absorption data of complex **3C**.*

Complex	**λ_{max}, nm (ε, $M^{-1}cm^{-1}$)**
3C	545(7950), 668(750)

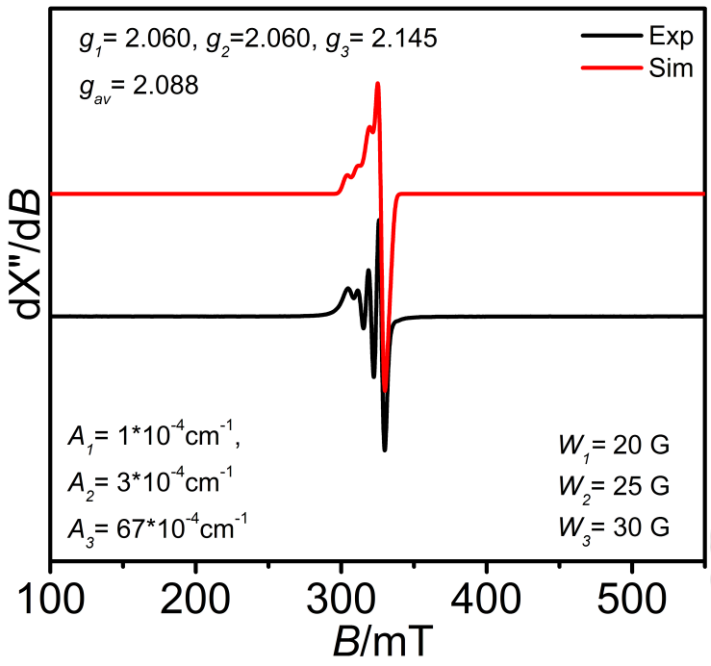

Figure 3.22: *Experimental and simulated X-band EPR spectra of complex **3C**. Experiment was performed at RT.*

In order to reinforce the electronic state of the central Cu ion complex **3C**, X-band EPR measurement was performed. An anisotropic signal appeared (**Figure 3.22**) with Cu(II) (^{Cu}I = 3/2)-based hyperfine coupling along the Z axis. Simulation to the experimental results provided the following parameters: g_1 = 2.060; g_2 = 2.060; g_3 = 2.145, g_{av} = 2.088, $^{Cu}(A_1, A_2, A_3)$ = (1, 3, 67) × 10^{-4} cm^{-1}. Using the relation g_{av} = 1/3($g_{\parallel}$ + 2$g_{\perp}$), it was found that $g_{\parallel}$ = 2.145 and $g_{\perp}$ = 2.060 for complex **3C**. The $g_{\parallel} > g_{\perp}$ indicated that the unpaired electron resided on the d_{x2-y2} magnetic orbital of Cu(II) in complex **3C**.[8a,b]

3.6 Probable Pathway to the Formation of Complex 3C from Ligand $H_4L^{Piperazine(AP/AP)}$

In order to investigate for the formation of complex **3C**, same reaction was performed (Scheme 3.5) by using an equimolar amount of ligand $\mathbf{H_4L^{Piperazine(AP/AP)}}$ and $Cu(ClO_4)_2 \cdot 6H_2O$ in acetonitrile in the presence of Et_3N under aerial atmosphere. During the reaction, the initially formed green solid precipitate was isolated and characterized by several spectroscopic/spectrometric techniques (**Figure 3.23**). Unfortunately, all attempts to grow single crystals of green solid (**I**) was unsuccessful. However, ESI-MS(+ve mode) analysis of green solid (**I**) in CH_3CN showed a 100% molecular ion peak at *m/z* = 763.41 (**Figure 3.23D**), which corresponded to 1:1 ligand:Cu complex. Experimental and simulated isotope distribution pattern confirmed the composition as $[C_{46}H_{60}CuN_4O_2]^+$.

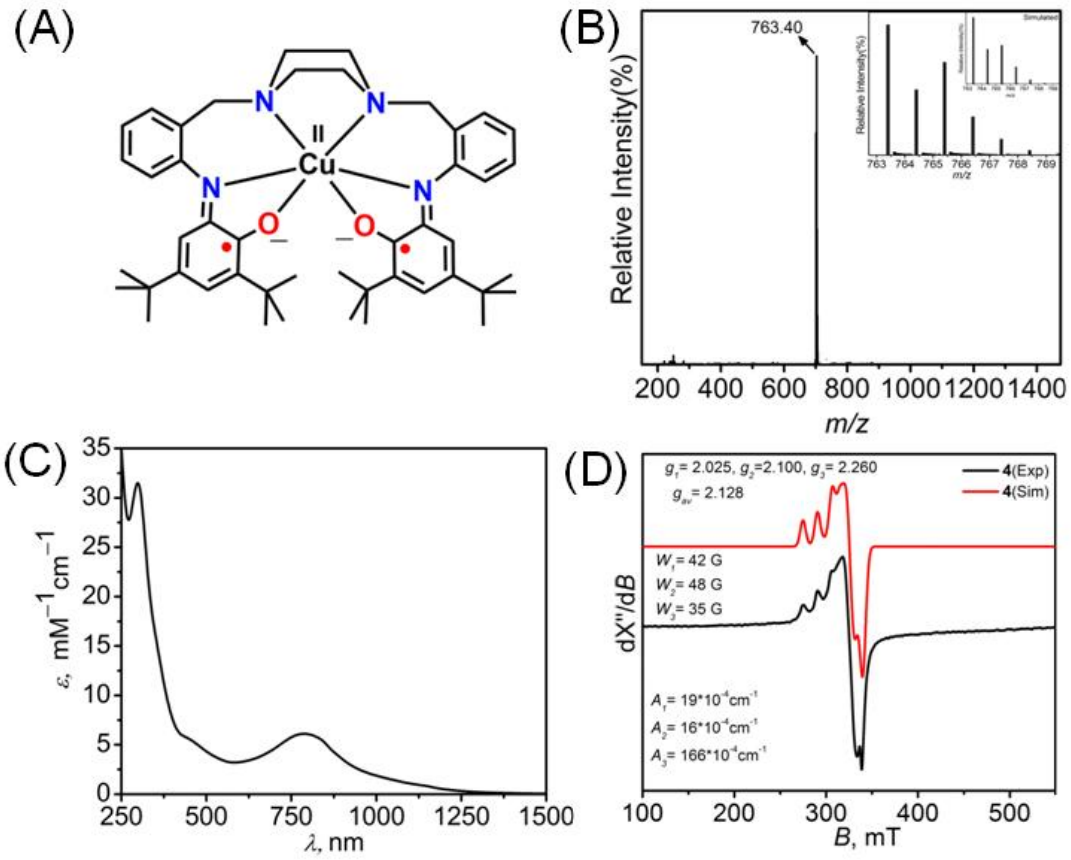

Figure 3.23: ***(A)*** *Proposed structure of intermediate* ***[XI]****,* ***(B)*** *ESI-MS spectrum of* ***[XI]****,* ***(C)*** *UV-vis/NIR spectrum of [****XI****] and (****D****) X-band EPR spectrum of intermediate [****XI****].Conditions: Microwave frequency(GHz), 9.446; modulation frequency (kHz), 100; modulation amplitude (G), 50.0; and microwave power (mW), 0.995.*

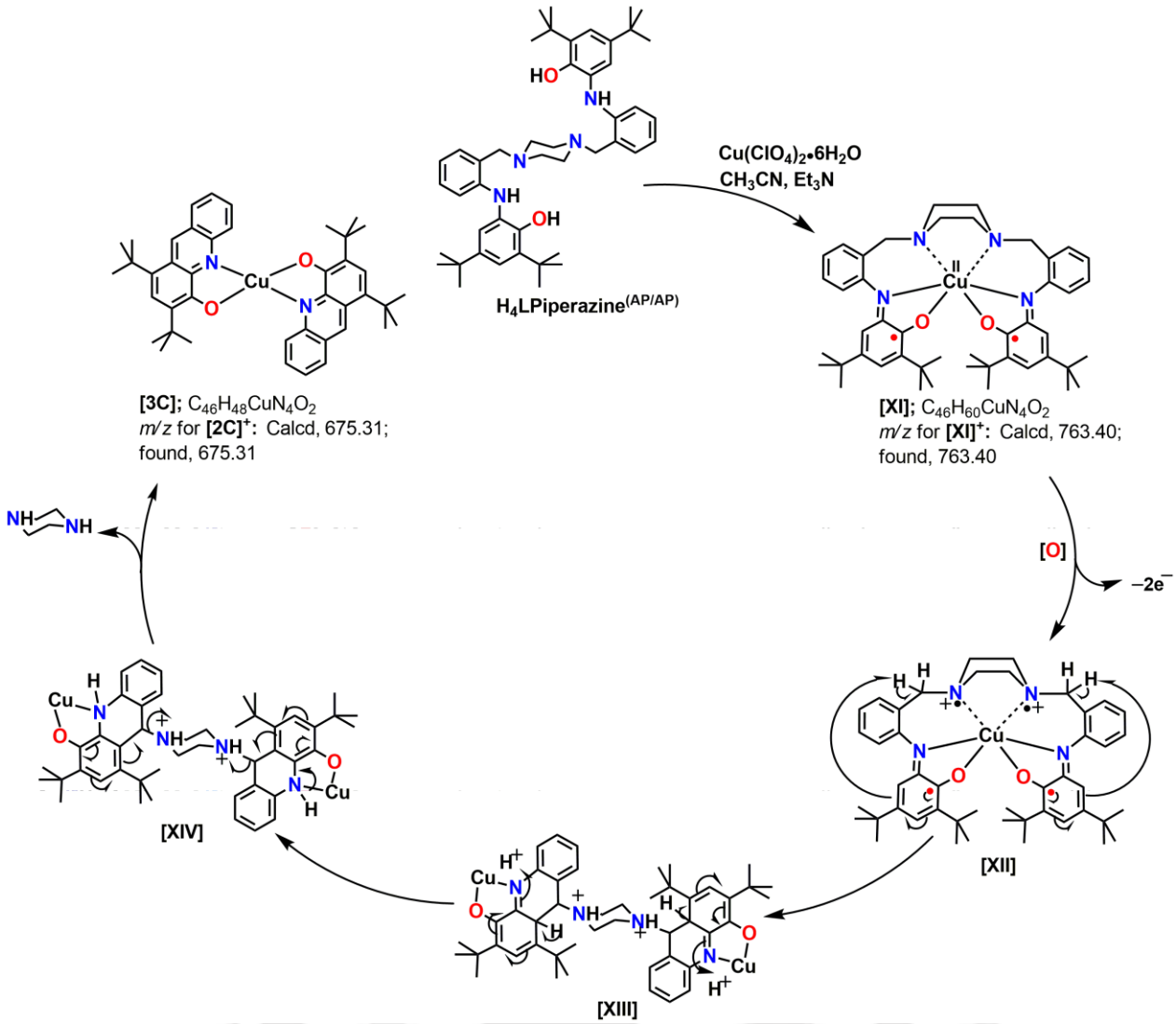

Scheme 3.6: *Proposed mechanism of the formation of complex* ***3C*** *from* $H_4L^{Piperazine(AP/AP)}$.

In UV-vis/NIR spectrum of intermediate **[XI]** was dominated by charge-transfer phenomena. The band at about 975 nm and 790 nm corroborated LLCT and LMCT charge transfer transitions as previously observed in Cu(II)-bis(iminosemiquinone) complexes.[9a-d] Thus, the proposed electronic structure of intermediate **[XI]** was justified.

During recrystallization of green solid **[XI]** from CH_2Cl_2:CH_3CN (4:1) solvent mixture, intermediate **[XII]** was formed. Formation of intermediate **[XIII]** occurred via the C–N bond activation and thereafter homolytic C–H bond breaking and C–C bond formation through simultaneous electron transfer took places from iminosemiquinone [$(ISQ)^{\bullet 1-}$] to benzyl carbon adjacent to piperazine moity. Furthermore, there was an aromatization followed by the release of

piperazine unit that provided the complex **3C** via intermediate **[XIV]**. The details proposed mechanism is shown in **Scheme 3.6**.

3.7 Conclusions

To conclude, we have successfully synthesized a new hexadentate non-innocent ligand with piperazine backbone and named as $\mathbf{H_4L^{Piperazine(AP/AP)}}$. The ligand $\mathbf{H_4L^{Piperazine(AP/AP)}}$ upon reacting with $CoCl_2 \bullet 6H_2O$ in the presence of air, and Et_3N provides a diamagnetic Co(III) octahedral complex **3A**, which was characterize by different spectroscopic techniques. The strong antiferromagnetic coupling between the two radical units *via* the diamagnetic Co(III) ion was been realized in the complex.

The piperazine backbone acquired a different configuration depending on the metal salts used for the formation of the corresponding copper complex. A diamagnetic dinuclear Cu(II)-radical complex **3B** has also been synthesized by employing $CuCl_2 \bullet 2H_2O$ salt. In the presence of $Cu(ClO_4)_2 \bullet 6H_2O$ salt mononuclear complex **3C** was formed *via* the ligand-based C-N bond breaking and C-C bond formation phenomena. Herein, the intermediate [**XI**], which was formed during the formation of complex **3C**, has also been assigned by the help of various spectroscopic techniques.

References

1. (*a*) W. Kaim, B. Schwederski, *Coord. Chem. Rev.*, 2010, **254**, 1580; (*b*) T. Tezgerevska, K. G. Alley and C. Boskovic, *Coord. Chem. Rev.*, 2014, **268**, 23; (*c*) D. L. J. Broere, R. Plessius and J. I. van der Vlugt, *Chem. Soc. Rev.*, 2015,**44**, 6886.

2. (*a*) V. I. Ovcharenko and R. Z. Sagdeev, *Russ. Chem. Rev.*, 1999, **68**, 345; (*b*) B. D. Koivisto and R. G. Hicks, *Coord. Chem. Rev.*, 2005, **249**, 2612; (*c*) I. Ratera and J. Veciana, *Chem. Soc. Rev.*, 2012, **41**, 303.

3. (*a*) G. R. Pandhare, V. M. Shinde and Y. H. Deshpande, *Rasayan J. Chem.*, 2008, **1**, 337; (*b*) J. Coates, *Interpretation of Infrared Spectra: A Practical Approach*, John Wiley & Sons Ltd, Chichester, 2000; (*c*) D. L. Pavia, G. M. Lampman, G. S. Kriz and J. R. Vyvyan, *Introduction to Spectroscopy*, 4th edition, 31; (*d*) P. K. Kipkemboi, P. C. Kiprono and J. J. Sanga, *Bull. Chem. Soc. Ethiop.*, 2003, **17**, 211; (*e*) G. Hastings and V. Sivakumar, *Biochemistry*, 2001, **40**, 3681; (*f*) J. Breton, J. Burie, C. Berthomieu, G. Berger and E. Nabedryk, *Biochemistry*, 1994, **33**, 4953; (*g*) H. Suzuki, M. A. Nagasaka, M. Sugiura and T. Noguchi, *Biochemistry*, 2005, **44**, 11323.

4. (*a*) H. Keypour, M. Mahmoudabadi, A. Shooshtari, M. Bayat, M. Ghassemzadeh, L. Hosseinzadeh, F. Mohsenzadeh and K. Harms, *Polyhedran*, 2017, **129**, 189; (*b*) A. I. Poddel'sky, V. K. Cherkasov, G. K. Fukin, M. P. Bubnov, L. G. Abakumova and G. A. Abakumov, *Inor. Chim. Acta.*, 2004, **357**, 3632; (*c*) E. Bill, E. Bothe, P. Chaudhuri, K. Chlopek, D. Herebian, S. Kokatam, K. Ray, T. Weyhermüller, F. Neese and K. Wieghardt, *Chem. Eur. J.*, 2005, **11**, 204; (*d*) C. N. Verani, S. Gallert, E. Bill, T. Weyhermüller, K. Wieghardt and P. Chaudhuri, *Chem. Commun.*, 1999, 1747; (*e*) H. Chun, C. N. Verani, P. Chaudhuri, E. Bothe, E. Bill, T. Weyhermüller and K. Wieghardt, *Inorg. Chem.*, 2001, **40**, 4157.

5. (*a*) P. Chaudhuri and K. Wieghardt, *Prog. Inorg. Chem.*, 2001, **50**, 151; (*b*) Jr. L. Que and W. B. Tolman, *Nature*, 2008, **455**, 333; (*c*) G. A. Abakumov, V. K. Cherkasov, V. I. Nevodchikov, V. A. Kuropatov, G. T. Yee and C. G. Pierpont, *Inorg. Chem.*, 2001, **40**, 2434; (*d*) S. Ye, B. Sarkar, F. Lissner, T. Schleid, J. van Slageren, J. Fiedler and W. Kaim, *Angew. Chem., Int. Ed.*, 2005, **44**, 2103; (*e*) C. Benelli, A. Dei, D. Gatteschi and L. Pardi, *Inorg. Chem.*, 1990, **29**, 3409; (*f*) C. G. Pierpont, *Coord. Chem. Rev.*, 2001, **216-217**, 99; (*g*) P. Sarkar, M. K. Mondal, A. Sarmah, S. Maity and C. Mukherjee, *Inorg. Chem.*, 2017, **56**, 8068; (*h*) X. Sun, H. Chun, K. Hildenbrand, E. Bothe, T. Weyhermüller, F. Neese and K. Wieghardt, *Inorg. Chem.*, 2002, **41**,

4295; (*i*) H. Chun, E. Bill, E. Bothe, T. Weyhermüller, F. Neese and K. Wieghardt, *Inorg. Chem.*, 2002, **41**, 5091; (*j*) H. Chun, P. Chaudhuri, T. Weyhermüller and K. Wieghardt, *Inorg. Chem.*, 2002, **41**, 790.

6. (*a*) C. Mukherjee, U. Pieper, E. Bothe, V. Bachler, E. Bill, T. Weyhermüller, P. Chaudhuri, *Inorg. Chem.*, 2008, **47**, 8943; (*b*) P. Chaudhuri, C. N. Verani, E. Bill, E. Bothe, T. Weyhermüller, K. Wieghardt, *J. Am. Chem. Soc.*, 2001, **123**, 2213; (*c*) S. Ye, B. Sarkar, F. Lissner, T. Schleid, J. van Slageren, J. Fiedler, W. Kaim, *Angew. Chem., Int. Ed.*, 2005, **44**, 2103; (*d*) S. Ghorai and C. Mukherjee, *Chem. - Asian J.*, 2014, **9**, 3518; (*e*) P. Verma, J. Weir, L. Mirica and T. D. P. Stack, *Inorg. Chem.*, 2011, **50**, 9816; (*f*) M. Franks, A. Gadzhieva, L. Ghandhi, D. Murrell, A. J. Blake, E. S. Davies, W. Lewis, F. Moro, J. McMaster and M. Schröder, *Inorg.Chem.*, 2013, **52**, 660.

7. (*a*) R. C. Pratt and T. D. P. Stack, *J. Am. Chem. Soc.*, 2003, **125**, 8716; (*b*) S. Di Bella, I. Fragala, I. Ledoux and T. J. Marks, *J. Am. Chem. Soc.*,1995, **117**, 9481; S. Di Bella, I. Fragala, T. J. Marks and M. A. Ratner, *J. Am. Chem. Soc.*, 1995, **117**, 9481. (*c*) C. Mukherjee, U. Pieper, E. Bothe, V. Bachler, E. Bill, T. Weyhermüller and P. Chaudhuri, *Inorg. Chem.*, 2008, **47**, 8943; (*d*) F. Thomas, O. Jarjayes, C. Duboc, C. Philouze, E. Saint-Aman and J.-L. Pierre, *Dalton Trans.* 2004, 2662.

8. (*a*) B. J. Hathaway and A. A. G. Tomlinson, *Coord. Chem. Rev.*, 1970, **5**, 1; (*b*) T. G. Brown and B. M. Hoffman, *Mol. Phys.*, 1980, **39**, 1073.

9. (*a*) C. Mukherjee, U. Pieper, E. Bothe, V. Bachler, E. Bill, T. Weyhermüller and P. Chaudhuri, *Inorg. Chem.*, 2008, **47**, 8943; (*b*) R. Rakshit, S. Ghorai, S. Biswas and C. Mukherjee, *Inorg. Chem.*, 2014, **53**, 3333; (*c*) A. I. Poddel'sky, V. K. Cherkasov and G. A. Abakumov, *Coord. Chem. Rev.*, 2009, **253**, 291; (*d*) S. Ye, B. Sarkar, F. Lissner, T. Schleid, J. van Slageren, J. Fiedler and W. Kaim, *Angew. Chem., Int. Ed.*, 2005, **44**, 2103; (*e*) C. Mukherjee, T. Weyhermüller, E. Bothe and P. Chaudhuri, *Inorg. Chem.*, 2008, **47**, 11620.

Chapter IV

Monoradical-containing Four-coordinate Co(III) Complexes: Homolytic S–S, Se–Se Bonds Cleavage and Catalytic Isocyanate to Urea Conversion under Sunlight

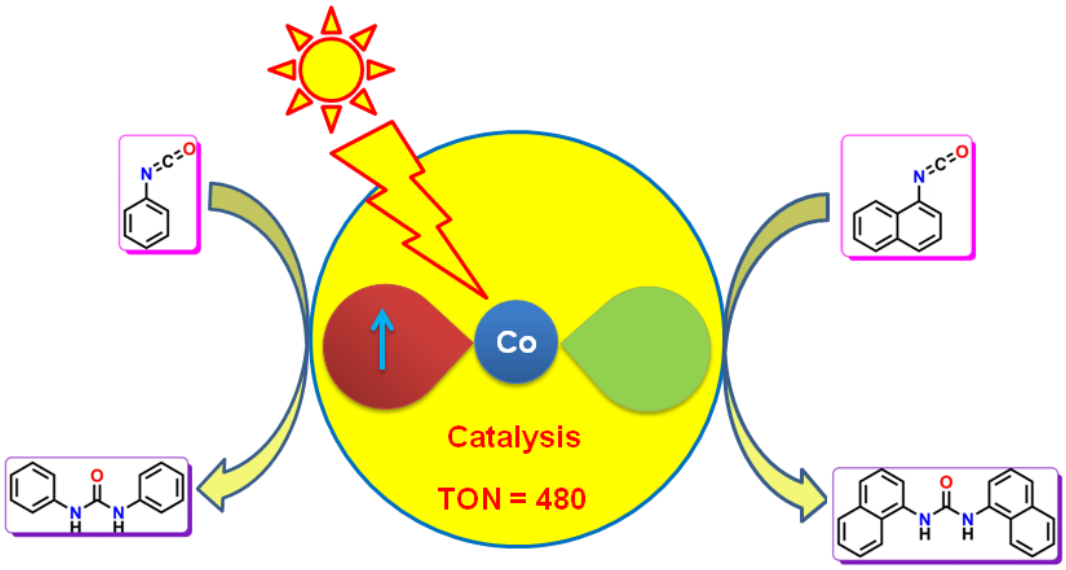

*Some results have been published in

***Chem**. **Commun.**, 2017, **53**, 8022–8025.

4.1 Introduction

Over the years, metal-coordinated redox active organic ligands, known as non-innocent ligands, are under continuous investigation as electron acceptor and/or electron donor for catalytic oxidation and reduction reactions.[1,2] For instances: Chaudhuri, Wieghardt, and coworkers have studied Cu(II)-bis(iminosemiquinone) complexes extensively as functional models of Galactose Oxidase for the two-electron oxidation of primary alcohols to their corresponding aldehydes[1h]; a four-coordinate Co(III)-bis(amidophenolate) complex has been successfully employed as a catalyst for C–C bond formation reactions by Soper and coworkers.[1a] Recently, Sarkar and coworkers have described an electrocatalytic C–C bond formation reaction employing electrochemically *in situ* generated a four-coordinate Co(II)-bis(1,2-diamide) complex as the catalyst and benzylbromide as the substrate.[1e] In 2015, van der Vlugt, de Bruin, and coworkers have utilized the redox active nature of a coordinated-2-amidophenoate derivative in a four-coordinate Pd(II) complex for the one-electron homolytic S–S bond cleavage of diphenyl disulfide.[1i] Recently, it has been demonstrated that H_2 gas can be generated employing Cu(II)-bis(iminoquinone) complex and $NaBH_4$ in dry acetonitrile.[1g]

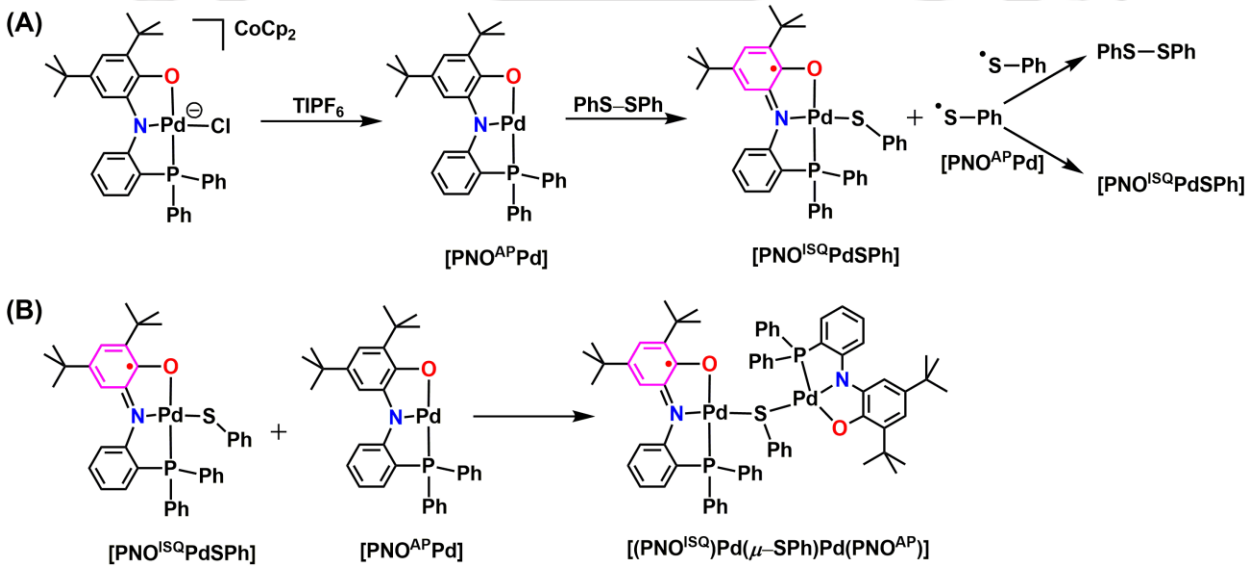

Scheme 4.1: *(**A**) Synthetic route for disulfide bond activation by four-coordinate Pd(II) complex.(**B**) Proposed mechanism for the S–S bond activation and formation of dinuclear [(PNO^{ISQ})Pd(μ-SPh)Pd(PNO^{AP})] complex with mixed valency in the two PNO scaffolds.*

To continue our study on the development of ligand-radical-containing transition metal complexes for diatomic (homo and/or hetero) bond scission/formation reactions, we have investigated on few Co(III) complexes based on the non-innocent ligand $\mathbf{H_2L^{AP(Ph)}}$ shown in **Scheme 4.2**. The ligand scaffolds were primarily based on bidentate 2-anilino-3,5-di-*tert*-butylphenol ($\mathbf{H_2L^{AP}}$) backbone with phenyl substituents at the *ortho*-position of the aniline part. We envisaged that the presence of an *ortho*-substituent would exert steric crowding and consequently, the possibility of four-coordinate cobalt complex formation over six-coordinate would be favorable. Noteworthy, cobalt complexes with unsaturated-coordination environment are essential for the substrate activation and catalysis.

4.2 Synthesis and Characterization of Ligand $H_2L^{AP(Ph)}$

In this regards, a phenyl substituted (*o*-position to aniline moiety) ligand $\mathbf{H_2L^{AP(Ph)}}$ was synthesized by reacting with equimolar amounts of 2-aminobiphenyl (**XV**) and 3,5-di-*tert*-butylcatechol (**VII**) in hexane in presence of Et_3N under air provided ligand $\mathbf{H_2L^{AP(Ph)}}$ (**Scheme 4.2**).

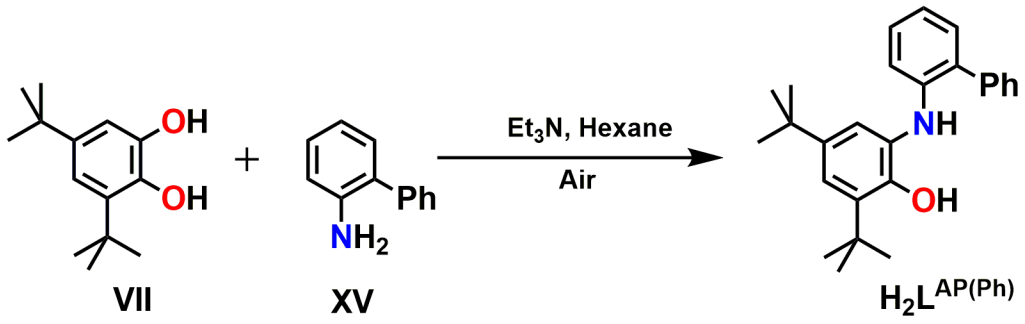

Scheme 4.2: *Synthetic route for the preparation of* $\boldsymbol{H_2L^{AP(Ph)}}$.

The synthesized ligand $\mathbf{H_2L^{AP(Ph)}}$ could behave as non-innocent and therefore, it might exist in different oxidation states in the presence of metal ions (preferably transition metal) and molecular oxygen. The possible oxidation states of $\mathbf{H_2L^{AP(Ph)}}$ are shown below in **Scheme 4.3**.

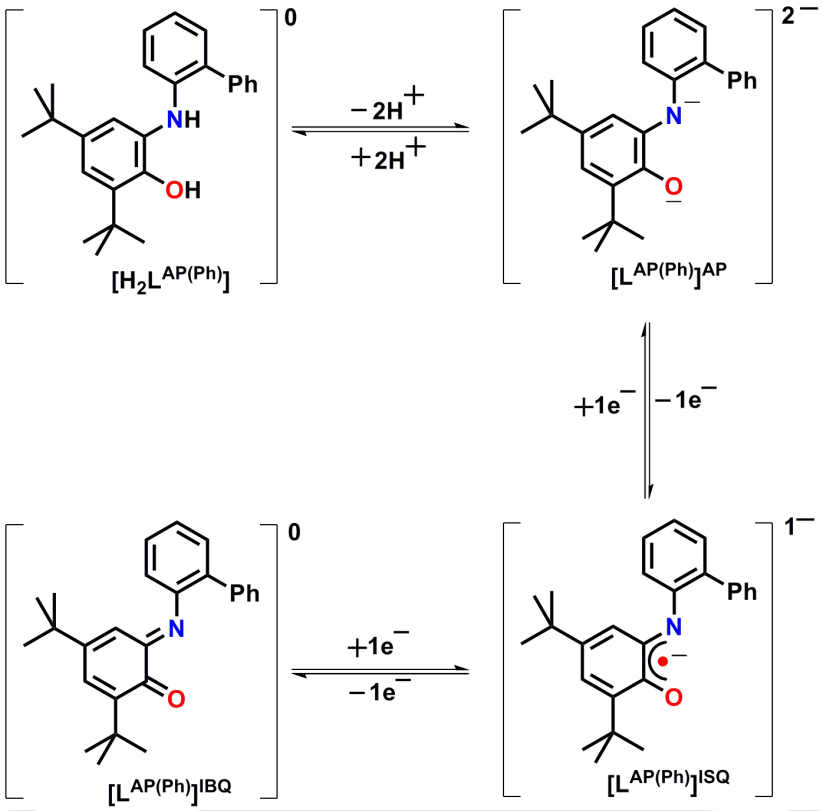

Scheme 4.3: *Possible oxidation states of* $H_2L^{AP(Ph)}$.

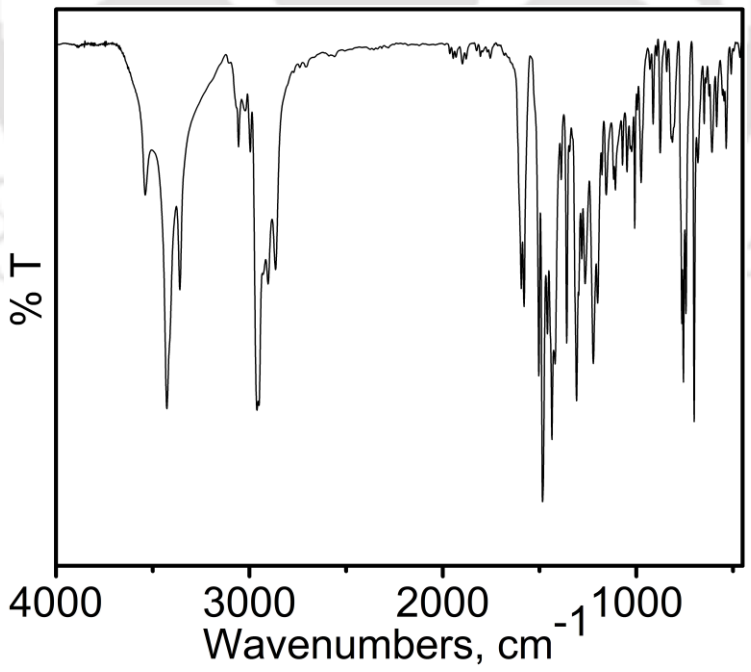

Figure 4.1: *FT-IR spectrum of* $H_2L^{AP(Ph)}$.

Ligand $\mathbf{H_2L^{AP(Ph)}}$ was characterized by FT-IR spectroscopy, NMR spectroscopy and mass spectrometry techniques. FT-IR spectrum of the ligand $\mathbf{H_2L^{AP(Ph)}}$ (**Figure 4.1**) showed two sharp bands at 3427 cm^{-1} and 3360 cm^{-1} due to ν(O–H), and ν(N–H) stretching, respectively.[3a-b] A weak band appeared at 3056 $cm^{-1}$for the stretching of aryl ν(C−H). The asymmetric, symmetric and overtone bands of ν(C–H) stretching for *tert*-butyl groups appeared at 2995, 2903, 2865 cm^{-1}, respectively.[3a-d] In addition to this, the bending ν(C–H) stretching frequency for the $–CH_3$ groups, which belonged to *tert*-butyl groups, appeared at 1484 and 1359 cm^{-1}.[3a] The stretching bands at 1580, and 1436 cm^{-1} were attributed to the ν(C=C) stretches for phenyl system.[3a] The phenolic ν(C–O) stretching band appeared at 1308 cm^{-1} and ν(C–N) stretching band appeared at1222 cm^{-1}.[3a]

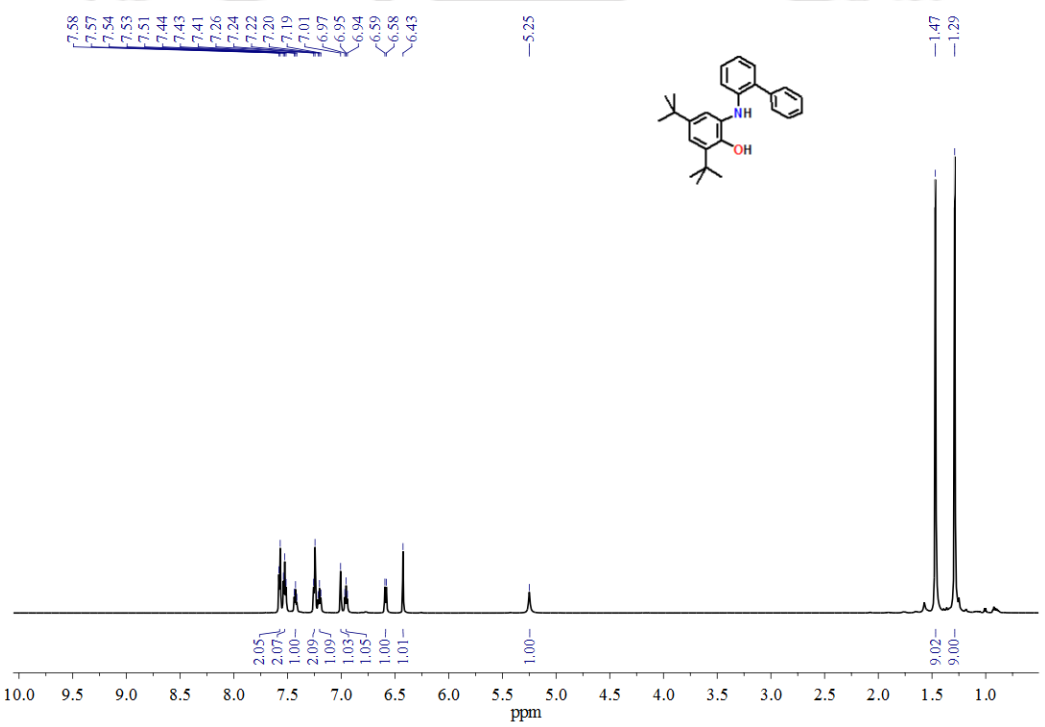

Figure 4.2: *^{1}H-NMR spectrum of $\mathbf{H_2L^{AP(Ph)}}$ in $CDCl_3$.*

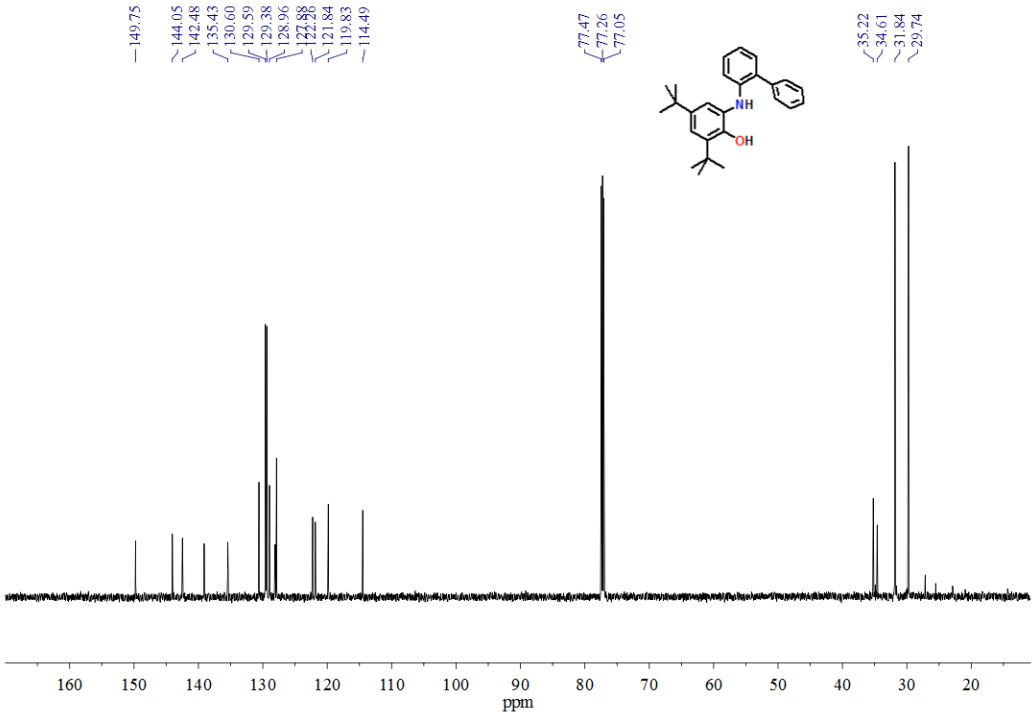

Figure 4.3: *^{13}C-NMR spectrum of $H_2L^{AP(Ph)}$ in $CDCl_3$.*

^{1}H-NMR spectrum for the ligand $\mathbf{H_2L^{AP(Ph)}}$ displayed in (**Figure 4.2**). Two singlet resonance signals at δ =1.29 ppm and δ = 1.47 ppm were appeared due to two *tert*-butyl moiety containing hydrogen atoms. Ten aromatic protons appeared in the region of δ = 6.94–7.58 ppm. Two singlet peaks appeared at δ = 6.58 and δ = 6.43 ppm were because of N–H and O–H protons, respectively. ^{13}C-NMR spectrum (**Figure 4.3**) for the ligand $\mathbf{H_2L^{AP(Ph)}}$ showed the seventeen distinct characteristic peaks for 17 different kinds of carbon atoms.

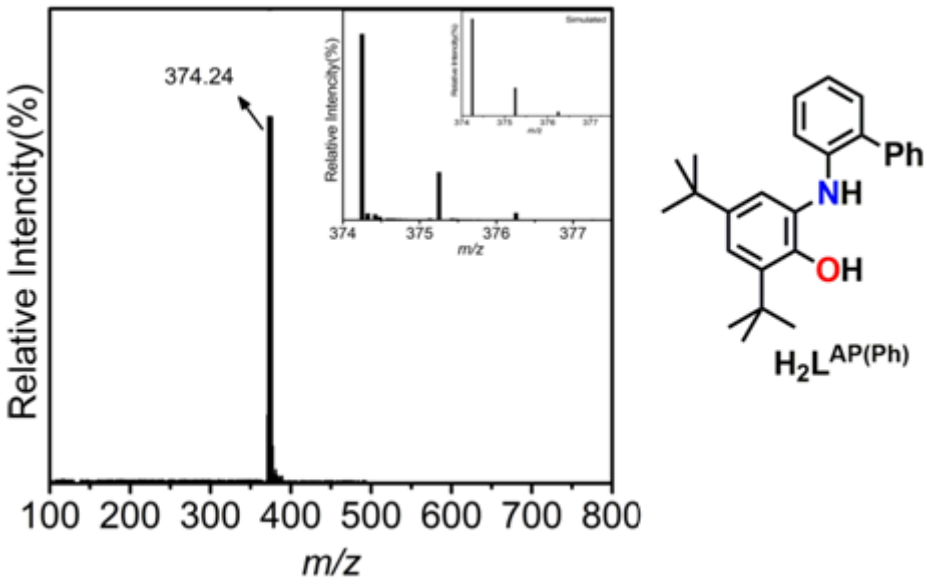

Figure 4.4: *Experimental and simulated mass spectra for* ***H$_2$L$^{AP(Ph)}$*** *[$C_{26}H_{31}NO+H]^+$ have been shown.*

Electrospray ionization mass spectrum (ESI-MS) of ligand **H$_2$L$^{AP(Ph)}$** in acetonitrile solution in positive mode showed a 100% molecular ion peak at *m/z* = 374.24 that corresponded to the $[M + H]^+$ (M = molecular mass). Isotope distribution pattern of the observed mass peaks confirmed the composition as $[C_{26}H_{31}NO + H]^+$ for **H$_2$L$^{AP(Ph)}$** (**Figure 4.4**).

4.3 Synthesis and Characterization of Co(III) Complexes (4A and 4B) of Ligand $H_2L^{AP(Ph)}$

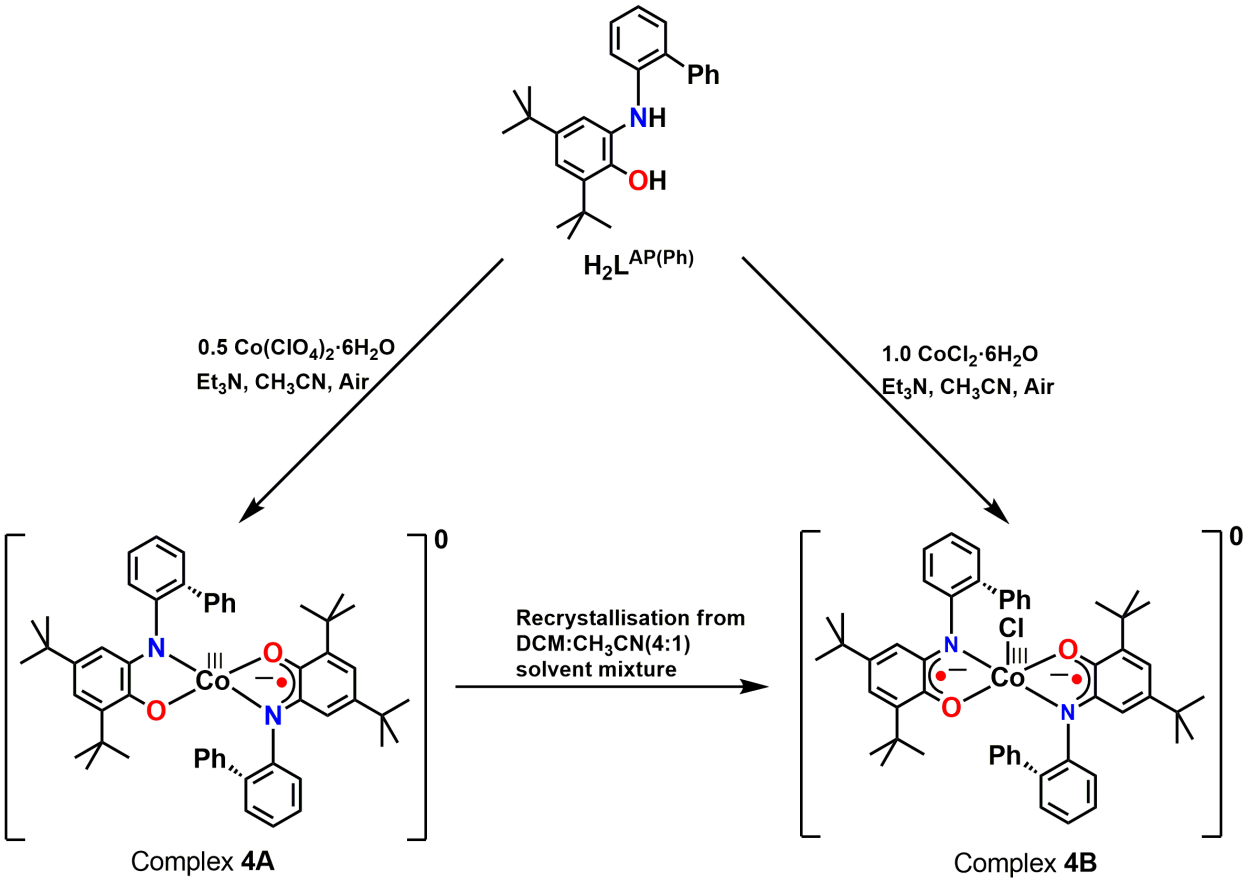

Scheme 4.4: *Synthetic route for the preparation of complex **4A** and complex **4B**.*

When ligand $\mathbf{H_2L^{AP(Ph)}}$ was treated with 0.5 equivalent of $Co(ClO_4)_2 \bullet 6H_2O$ in acetonitrile in the presence of triethylamine under air provided corresponding square planar cobalt complex **4A** with 52% yield. Due to solubility problem it was very difficult to get the crystal structure of complex **4A**. Interestingly, when complex **4A** was recrystallize by using dichloromethane and acetonitrile solvent mixture it provided complex **4B** by abstracting chlorine species from dichloromethane solvent (**Scheme 4.4**). Noteworthy, complex **4B** can also be synthesized using 1.0 equivalent of $CoCl_2 \bullet 6H_2O$ to ligand $\mathbf{H_2L^{AP(Ph)}}$ in acetonitrile in the presence of triethylamine with in 64% yield.

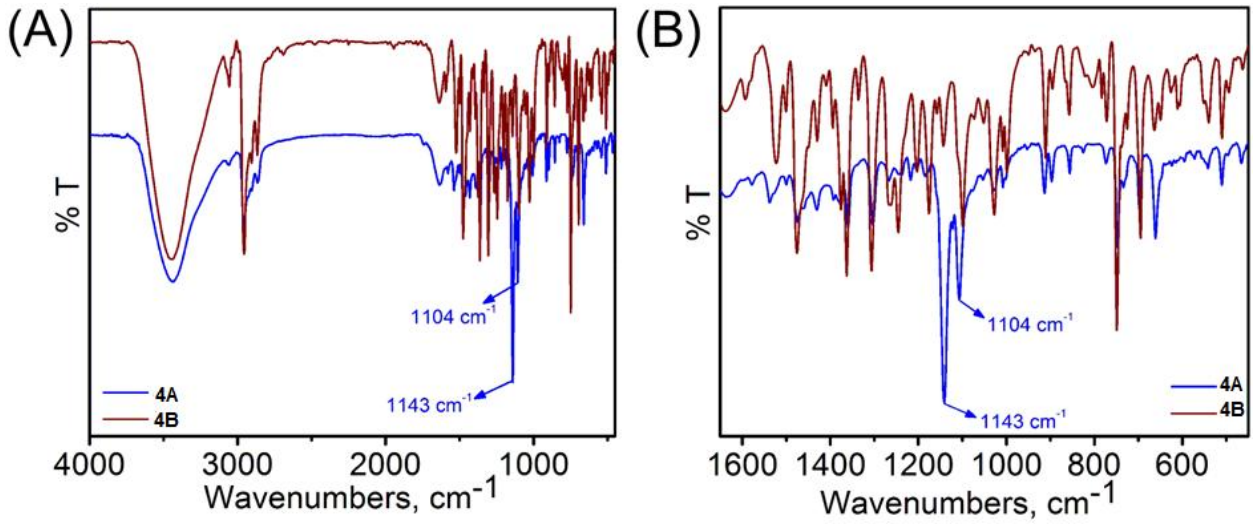

Figure 4.5: ***(A)*** *FT-IR spectral difference between square planar Co(III) complex* ***4A*** *vs square pyramidal Co(III) complex* ***4B (B)*** *Spectral difference is shown in 1650–450 cm^{-1} range.*

In the FT-IR spectra of the complexes (**4A** and **4B**), the absence of 3427 cm^{-1} ν(O–H), and 3360 cm^{-1} ν(N–H) stretching bands indicated the ligation of the ligand to the metal ion *via* deprotonated N and O atoms. In addition the presence of ν(C–H) stretching band of the *tert*–butyl groups in 2955–2863 cm^{-1} region emphasized the coordination of the ligand to the metal ion.[3a-d] The bands at 1474, 1359 cm^{-1} for **4A** and 1474, 1364 cm^{-1} for **4B**, were appeared due to the bending ν(C–H) stretch.[3a] The ν(C–O) vibrational mode for **4A**, and **4B** appeared at ~1301, 1258 cm^{-1} and 1302, 1259 cm^{-1}, respectively. Two intense sharp bands at 1143, 1104 cm^{-1} for **4A** was observed and attributed to phenyl skeleton ν(C–C) stretch in a one–electron oxidized (radical–center) delocalized system. In the FT-IR spectrum of **4B**, the band at 1363 cm^{-1} was appeared for ν(C⋯O) stretch.[3h] Interestingly, the bands at ~1143 and ~1104 cm^{-1} were absent in complex **4B** (**Figure 4.5**).

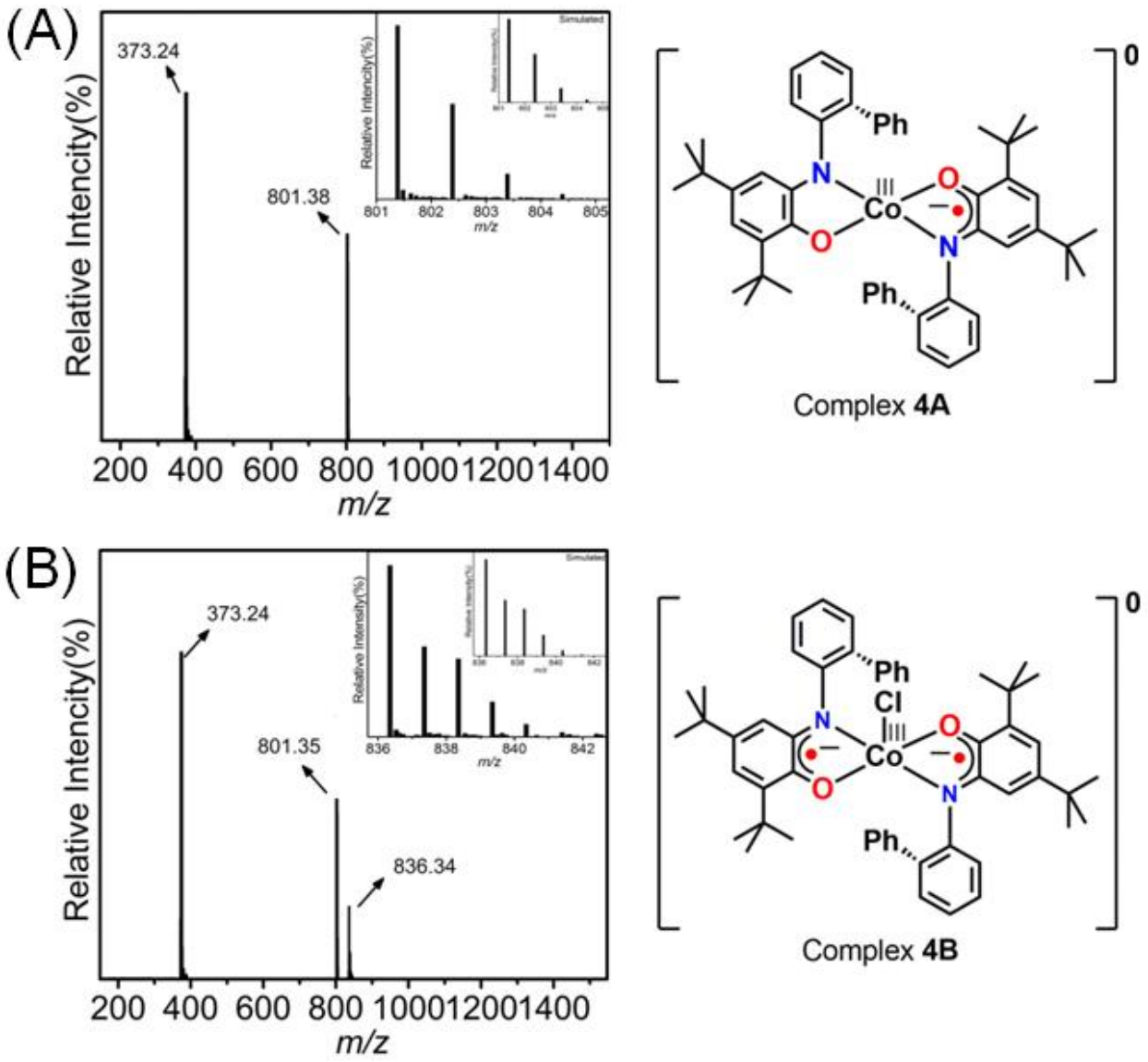

Figure 4.6: *ESI-mass spectra of (A) for **4A**, (B) for **4B**; experimental and simulated isotope distribution pattern (inset).*

Electrospray ionization mass spectra (ESI-MS) were measured in acetonitrile in positive mode. A 100% molecular ion peak at *m/z* = 801.38 appeared for the complex **4A** (corresponded to $[M]^+$); M = molecular mass (**Figure 4.6A**). On the other hand, a 100% molecular ion peak at *m/z* = 836.34 was found for the complex **4B** (corresponded to $[M]^+$) (**Figure 4.6B**). Isotope distribution pattern examinations of the observed mass peaks revealed the composition of **$C_{52}H_{58}CoN_2O_2$**, for **4A**; **$C_{52}H_{58}ClCoN_2O_2$**, for **4B**.

Crystals suitable for single crystal X-ray diffraction analysis of complex **4B** were grown by slow evaporation of a CH_2Cl_2/CH_3CN (3:1) solvent mixture of the complex. The complex was crystalized in the triclinic space group '*P–1*'. ORTEP diagram of complex **4B** has been shown in **Figure 4.7** and selected bond distances and bond angles are given in **Table 4.1**.

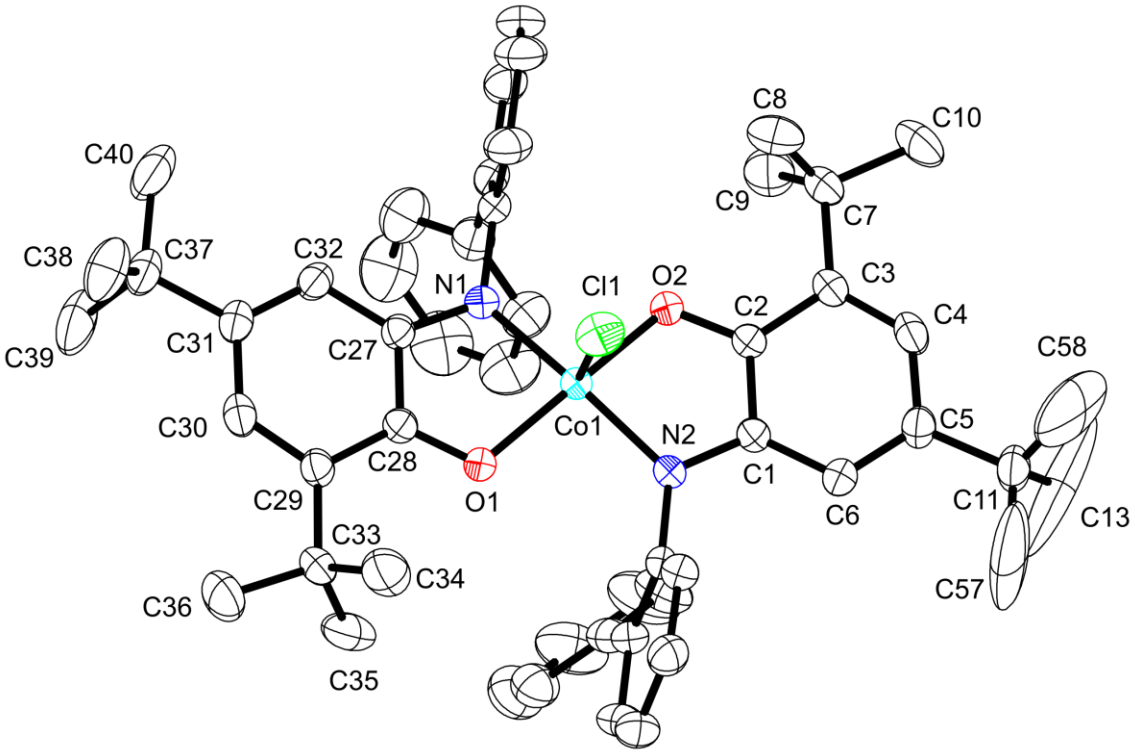

Figure 4.7: *ORTEP diagram of complex **4B**. Thermal ellipsoid was drawn with 40% probability. Hydrogen atoms were omitted for clarity.*

In the molecular structure of **4B**, two deprotonated ligands were connected with Co1 atom at the basal plane, while, a chloride ion attached with Co1 atom at the apical position. The five-coordinated metal ion was occupied in a distorted square pyramidal geometry. The Co1–O1, Co1–O2, Co1–N1, Co1–N2, and Co1–Cl1 bond distances were 1.8553(18), 1.8694(19), 1.873(2), 1.865(2), and 2.2661(9) Å, respectively. These bond distances were good in agreement with the +III oxidation state of central Co atom.[4a-c] The *tert*-butyl groups-containing phenyl rings showed an alternate short and long C–C bond distances. *i.e.* the C1–C2, C2–C3, C3–C4, C4–C5, C5–C6, and C6–C1 bond distances were 1.434(4), 1.425(4), 1.370(4), 1.430(4), 1.368(4), and 1.417(4) Å, respectively. Furthermore, C1–N1 = 1.341(3) Å, and C2–O1 = 1.300(3) Å bond

distances,[5,6] were neither their respective single bond character (C–N = 1.40 Å; C–O = 1.35 Å),[5*d*,6c,7] nor their respective double in character (C=N = 1.30 Å; C=O = 1.24 Å).[6d-e,7d] Similar type bond distances were also found in another coordinating ligand (**Table 4.1**). This clearly indicated the π-radical coordination nature of the ligands. Therefore, **4B** was a neutral diradical-containing square pyramidal Co(III) complex.

Table 4.1: *Selected bond distances (Å) and angels (°) for complex **4B**.*

Co1– N1	1.873(2)	C3– C4	1.370(4)
Co1– N2	1.865(2)	C4– C5	1.430(4)
Co1– O1	1.8553(18)	C5– C6	1.368(4)
Co1– O2	1.8694(19)	C6– C1	1.417(4)
Co1– Cl1	2.2661(9)	N1– C15	1.442(3)
N1– C1	1.341(3)	C27– C28	1.443(4)
O1– C2	1.300(3)	C28– C29	1.433(4)
N2– C27	1.337(3)	C29– C30	1.368(4)
O2– C28	1.291(3)	C30– C31	1.446(4)
C1– C2	1.434(4)	C31– C32	1.358(4)
C2– C3	1.425(4)	C32– C27	1.416(4)
N1– Co1– N2	167.33(10)	O2– Co1– Cl1	97.78(7)
O1– Co1– N2	93.64(9)	N1–Co1–Cl1	95.32(7)
N2– Co1– O2	83.70(9)	C28– O2–Co1	113.67(17)
O1– Co1–N1	83.94(9)	C2– O1–Co1	112.84(17)
O1– Co1– O2	168.71(9)	C1– N1– Co1	112.62(18)
O2– Co1–N1	96.25(9)	C15– N1–Co1	124.89(17)
O1– Co1–Cl1	93.43(7)	C27– N2–Co1	114.09(18)
N2– Co1–Cl1	97.23(7)	C41– N2– Co1	124.95(18)

The electronic absorption spectra of complex **4A** and **4B** were recorded in HPLC grade CH_2Cl_2 at room temperature and depicted in **Figure 4.8**. The electronic absorption bands along with corresponding absorption coefficient values were summarized in **Table 4.2**.

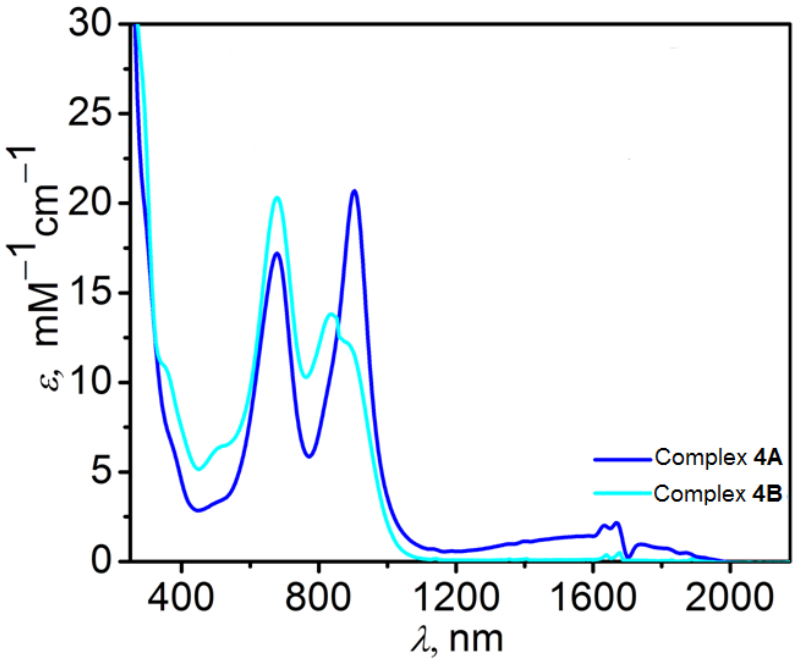

Figure 4.8: *UV-vis/NIR spectrum of complexes **4A** and **4B** in CH_2Cl_2 at 25 ℃.*

Complex **4A** showed three characteristic absorption band at λ_{max} = 1600 nm; λ_{max} = 903 nm and λ_{max} = 678 nm respectively. Extinction coefficient to the corresponding observed bands were summarized in **Table 4.2**. The absorption band at 1600 nm was attributed due to ligand-to-ligand intervalence charge transfer transition (LLIVCT),[8] on the other hand the band at 903 nm and 678 nm were appeared due to the ligand-to-metal charge transfer transition (LMCT).[8h,9a] Interestingly, for complex **4B** no band was observed above 1100 nm region. Complex **4B** showed a broad absorption band at λ_{max} = ~865 nm and a moderately sharp absorption band at λ_{max} = 675 nm. All these two absorption bands were appeared due to the charge transfer. The absorption bands at ~865 nm and 675 nm were considered as ligand-to-metal charge transfers transition (LMCT).[8e, g, 9a-b]

Table 4.2: *UV-vis/NIR spectral data for **4A**, and **4B**.*

Complex	λ_{max}, nm (ε, $M^{-1}cm^{-1}$)
4A	1600(1200), 903(20700), 678(17200)
4B	~865(13800), 675(20350)

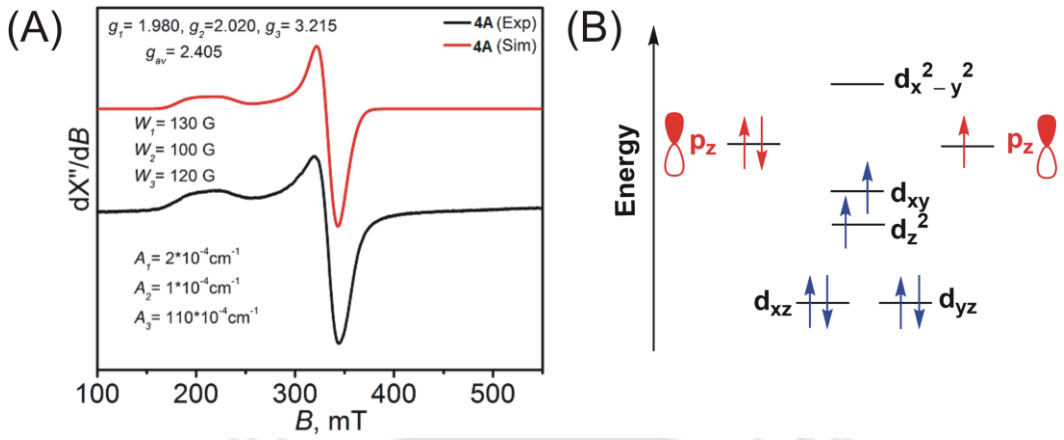

Figure 4.9: *(A) Experimental and simulated X-band EPR spectra of **4A** in CH_2Cl_2 solution. Conditions: temperature = 25 °C, microwave frequency (GHz) = 9.442, modulation frequency (kHz) = 100, modulation amplitude (G) = 50.0 and microwave power (mW) = 0.995.(B) d-orbital splitting of low spin Co^{3+} ion in square planar geometry, and ligand p_z orbital.*

In monoradical-containing four-coordinate square planar Co(III) complex **4A**, the metal center possesses two unpaired electrons, which resided at d_z^2 and d_{xy} magnetic orbitals [S_{Co} = 1.0]. An antiferromagnetic coupling between the Co(III) d_z^2 magnetic orbital, and ligand-based p_z orbital led to an S_{total} = 1/2 ground state and paramagnetism in the complexes, where the unpaired electron resided at the d_{xy} magnetic orbital. Hence, cobalt (III)-centered X-band EPR spectra for **4A** was observed. Experimental as well as simulated EPR spectra for **4A** complex was shown in **Figure 4.9**. X-band EPR signals of complex **4A** was anisotropic in nature. Simulation to the experimental spectra provided the following parameters: g_1 = 1.980; g_2 = 2.020; g_3 = 3.215; $^{Co}(A_1, A_2, A_3) = (2, 1, 110) \times 10^{-4}$ cm^{-1} for complex **4A**. The average g value for the complex **4A** was 2.405, and supported metal-centered unpaired electron.[4b,9a]

4.4 Homolytic (S–S) and (Se–Se) Bonds Activation and Synthesis and Characterization of Co(III) Complexes (4C and 4D) with $H_2L^{AP(Ph)}$ Ligand

Treatment of $Co(ClO_4)_2 \bullet 6H_2O$ (0.5 equivalent) to $\mathbf{H_2L^{AP(Ph)}}$ ligand and diphenyl disulphide (Ph_2S_2)/ diphenyl diselenide (Ph_2Se_2) in acetonitrile in the presence of triethylamine under air produced corresponding square pyramidal cobalt complexes **4C**, and **4D**, which were recrystallized from a ether-acetonitrile solvent mixture (**Scheme 4.5**).

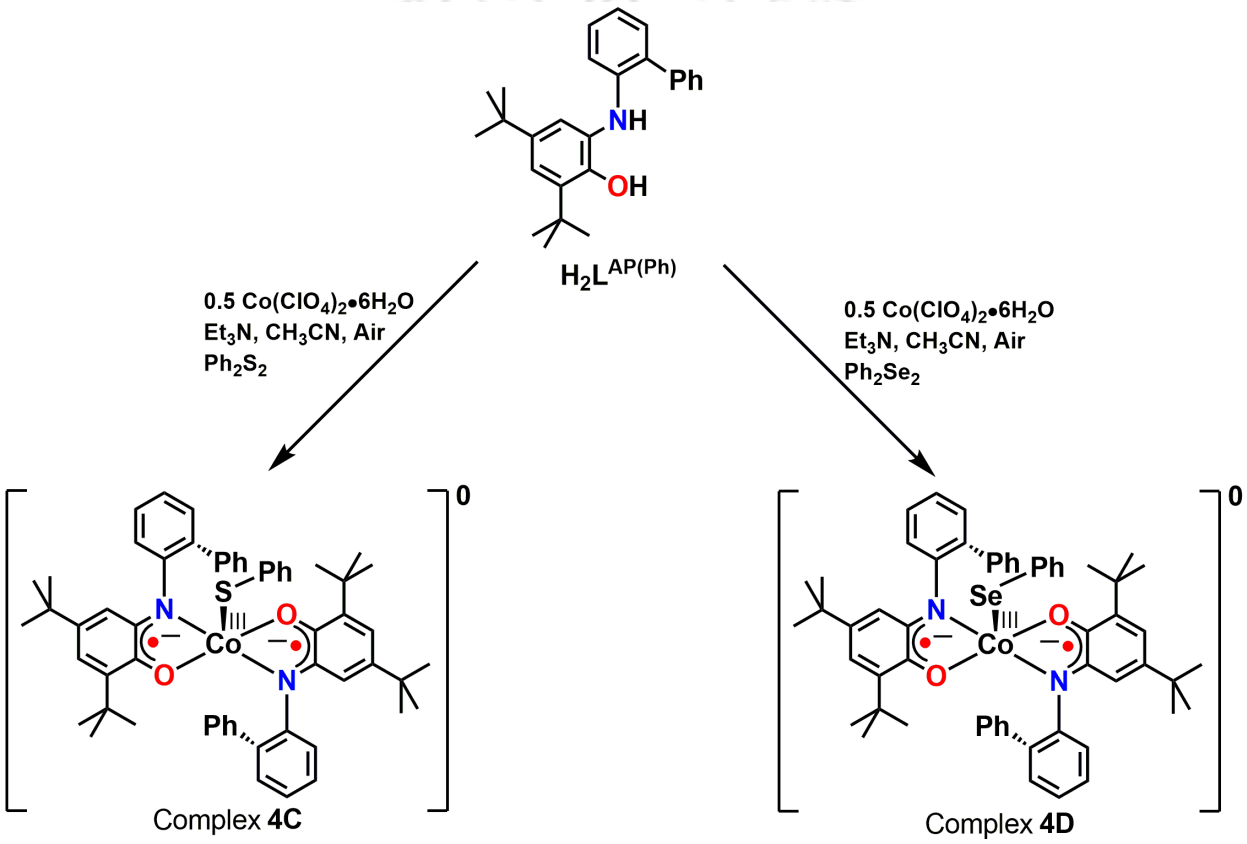

Scheme 4.5: *Synthetic route for the preparation of complex **4C** and complex **4D**.*

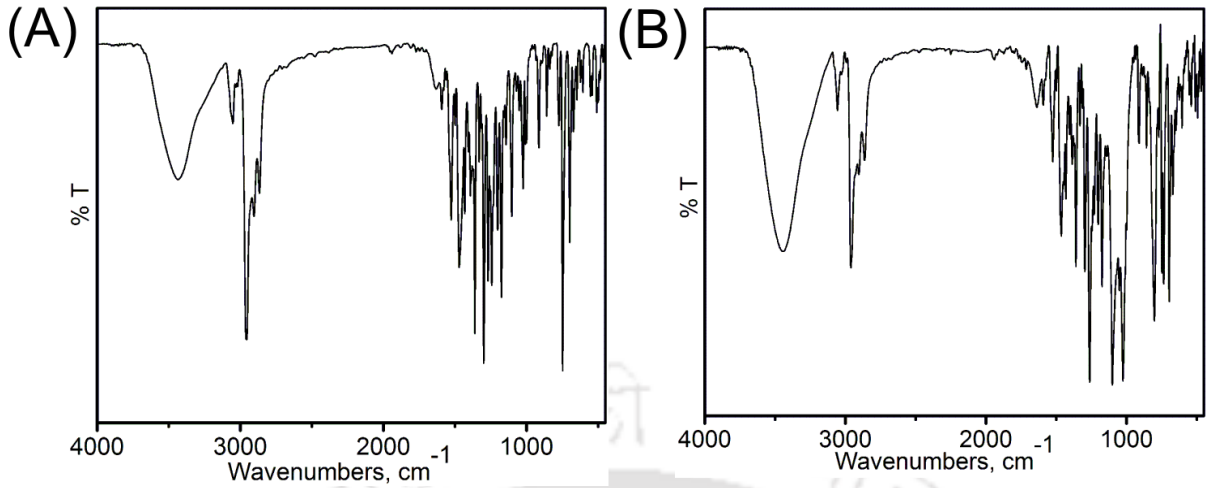

Figure 4.10: *FT-IR spectra of (**A**) complex **4C** and (**B**) complex **4D**.*

In the FT-IR spectra of the complexes (**4C** and **4D**), the absence of 3427 cm^{-1} ν(O–H), and 3360 cm^{-1} ν(N–H) stretching bands confirmed the coordination of the ligand to the metal ion *via* deprotonated N and O atoms. The coordination of the ligand to the metal ion was further consolidated by the presence of ν(C–H) stretching bands of the *tert*-butyl groups at 2961–2862 cm^{-1}.[3a-d] The bands at 1472, 1361 cm^{-1} for **4C** and 1463, 1359 cm^{-1} for **4D**, were appeared due to the bending ν(C–H) stretch.[3a] The ν(C⋯O) vibrational mode for **4C**, and **4D** appeared at ~1298, 1268 cm^{-1} and 1296, 1261 cm^{-1}, respectively (**Figure 4.10**).

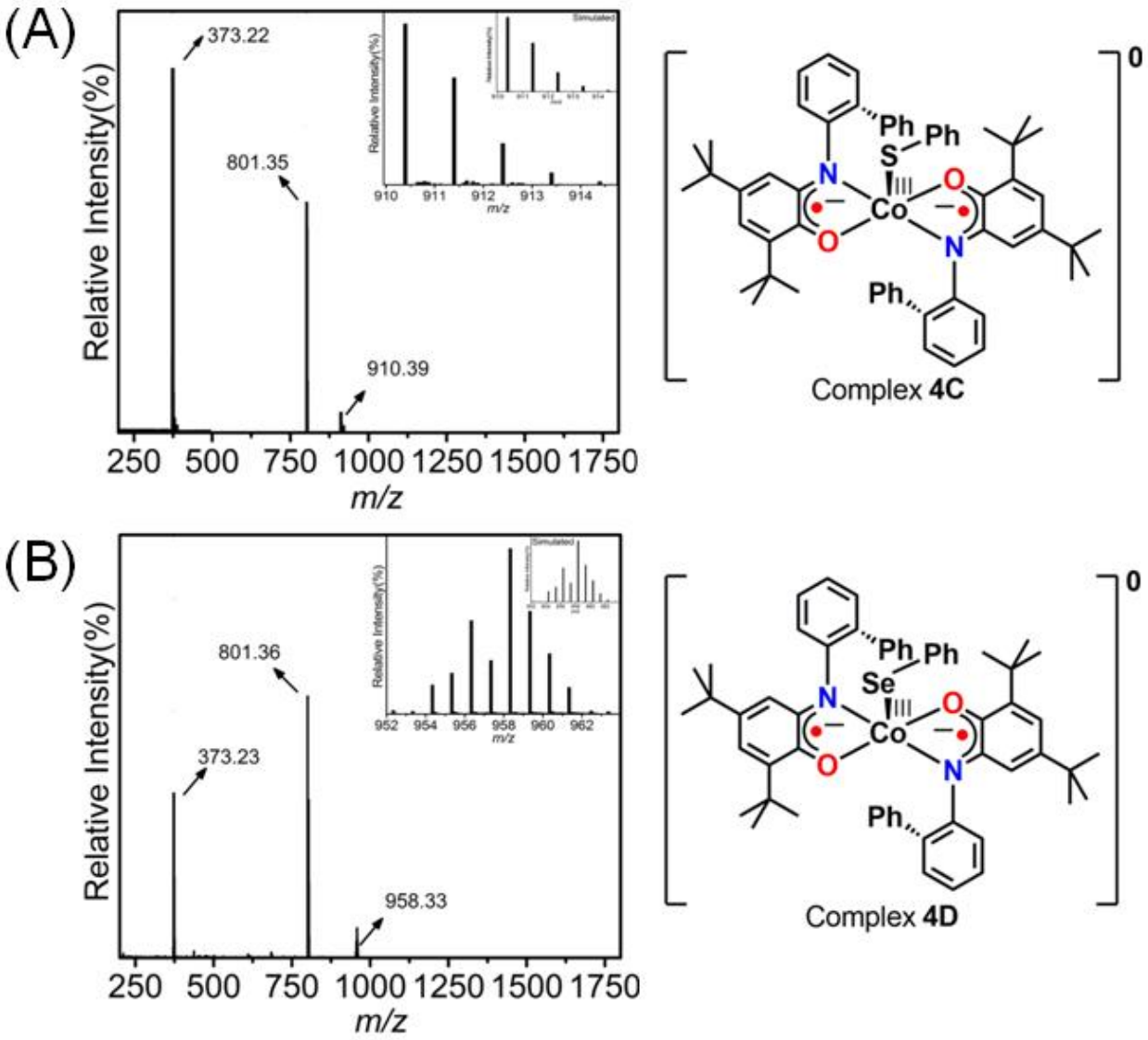

Figure 4.11: *ESI-mass spectra of (**A**) for **4C**, (**B**) for **4D**; experimental and simulated isotope distribution pattern (inset).*

Electro spray ionization mass spectra (ESI-MS) were measured in acetonitrile in positive mode. A 100% molecular ion peak at *m/z* = 910.39 appeared for the complex **4C** (corresponded to $[M]^+$); M = molecular mass (**Figure 4.11A**). On the other hand a 100% molecular ion peak at *m/z* = 958.33 was found for the complex **4D** (corresponded to $[M]^+$) (**Figure 4.11B**). Isotope distribution pattern examinations of the observed mass peaks revealed the composition of $\mathbf{C_{58}H_{63}CoN_2O_2S}$, for **4C**; $\mathbf{C_{58}H_{63}CoN_2O_2Se}$, for **4D**.

The molecular structure of complex **4C** and **4D** were clearly established by X-ray diffraction analysis. ORTEP diagram of complex **4C** and **4D** has been shown in **Figure 4.12**. The selected bond distances and angles are given in **Table 4.3** and **Table 4.4**.

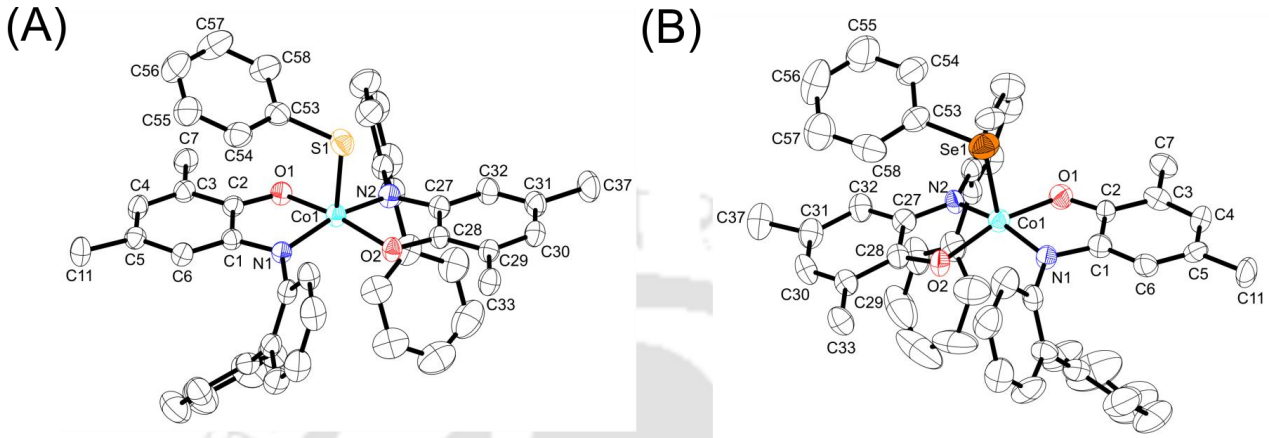

Figure 4.12: *ORTEP diagram of complex (**A**) complex **4C** and (**B**) complex **4D**. Thermal ellipsoids were drawn at 50% probability level. The H atoms and methyl groups of the tert-butyl groups were omitted for clarity.*

Complexes **4C** and **4D** are structurally similar and molecules consist of a cobalt atom chelated by two ligands and one –XPh group (X = S for **4C**, and X = Se for **4D**). The geometry around the cobalt center was almost square pyramidal (τ_5 = 0.08 [**4C**] and 0.0 [**4C**]) [4f] with two nitrogen atoms and two oxygen atoms from the ligands in the basal plane and –XPh group (X=S for **6**, and X=Se for **7**) present at the apical site. The two oxygen donor atoms of the two ligands were oriented in transposition (the same as the two nitrogen donors from the two ligands). Crystallographically both the coordinating ligands were distinguishable. The Co–O (1.858 to 1.881 Å) and Co–N (1.845 to 1.871 Å) bond distances (**Table 4.3** and **Table 4.4**) in the complexes corresponded to the previously reported square pyramidal cobalt complexes having a +III oxidation state.[4a-g] Thus, herein, the oxidation state of the central cobalt atom has been assigned as +III. The entire C–C bond lengths of the *tert*-butyl groups containing C_6 phenyl rings were not within 1.39±0.01 Å; rather, an alternating short-long-short C–C bond lengths were observed, *i.e.* a quinoid-type distortion (**Table 4.3** and **Table 4.4**). Furthermore, the average CPh–OPh (1.307(3) [**4C**] and 1.298(8) [**4D**] Å) and CPh–NPh (1.351(4) [**4C**] and 1.362(9) [**4D**] Å) bond distances were in between their single bond and double bond values, which emphasized

that the one-electron oxidized iminosemiquinone form[4,5a-f] of the coordinated ligands was present in the complexes. Hence, X-ray single crystal analysis suggested that, the five-coordinate complexes (**4C** and **4D**) were diradical-containing. Notably, better quality crystal data would have been more convincing; however, diffraction measurements even at 100 K could not improve the structural quality due to the nature of the crystals.

Table 4.3: *Selected bond distances (Å) and angels (°) for complex **4C**.*

Co1–N1	1.857(2)	C3–C4	1.367(4)
Co1–N2	1.850(3)	C4–C5	1.433(4)
Co1–O1	1.856(2)	C5–C6	1.362(4)
Co1–O2	1.871(2)	C6–C1	1.412(4)
Co1–S1	2.282(1)	N1–C15	1.440(4)
N1–C1	1.352(4)	C27–C28	1.430(4)
O1–C2	1.307(4)	C28–C29	1.422(4)
N2–C27	1.351(4)	C29–C30	1.381(4)
O2–C28	1.306(3)	C30–C31	1.421(5)
C1–C2	1.429(4)	C31–C32	1.358(5)
C2–C3	1.424(4)	C32–C27	1.409(4)
N1–Co1–N2	162.91(10)	O2–Co1–S1	90.95(7)
O1–Co1–N2	93.06(10)	N1–Co1–S1	99.15(8)
N2–Co1–O2	84.24(10)	C28–O2–Co1	113.18(16)
O1–Co1–N1	84.02(9)	C2–O1–Co1	114.20(17)
O1–Co1–O2	168.20(8)	C1–N1–Co1	113.71(18)
O2–Co1–N1	95.19(9)	C15– N1–Co1	127.33(18)
O1–Co1–S1	100.80(7)	C27– N2–Co1	114.01(19)
N2–Co1–S1	97.94(8)	C41– N2– Co1	127.45(19)

Table 4.4: *Selected bond distances (Å) and angels (°) for complex **4D**.*

Co1–N1	1.845(5)	C3–C4	1.380(11)
Co1–N2	1.856(5)	C4–C5	1.438(11)
Co1–O1	1.856(5)	C5–C6	1.355(11)
Co1–O2	1.881(5)	C6–C1	1.425(10)
Co1–Se1	2.4007(12)	N1–C15	1.425(10)
N1–C1	1.380(9)	C27–C28	1.426(10)
O1–C2	1.307(8)	C28–C29	1.461(10)
N2–C27	1.343(9)	C29–C30	1.357(10)
O2–C28	1.289(8)	C30–C31	1.416(11)
C1–C2	1.422(9)	C31–C32	1.412(11)
C2–C3	1.412(11)	C32–C27	1.415(10)

N1–Co1–N2	162.51(25)	O2–Co1–Se1	98.21(15)
O1–Co1–N2	93.63(24)	N1–Co1–Se1	96.93(17)
N2–Co1–O2	83.82(21)	C28–O2–Co1	113.61(43)
O1–Co1–N1	84.00(24)	C2–O1–Co1	115.03(47)
O1–Co1–O2	162.45(23)	C1–N1–Co1	114.29(45)
O2–Co1–N1	93.21(22)	C15– N1–Co1	126.02(45)
O1–Co1–Se1	99.33(16)	C27– N2–Co1	114.08(46)
N2–Co1–Se1	100.55(17)	C41– N2– Co1	124.50(44)

Electronic absorption spectra of complexes (**4C** and **4D**) were recorded in dichloromethane solvent at ambient temperature and depicted in **Figure 4.13**. The electronic absorption bands along with corresponding absorption coefficient values were summarized in **Table 4.5**.

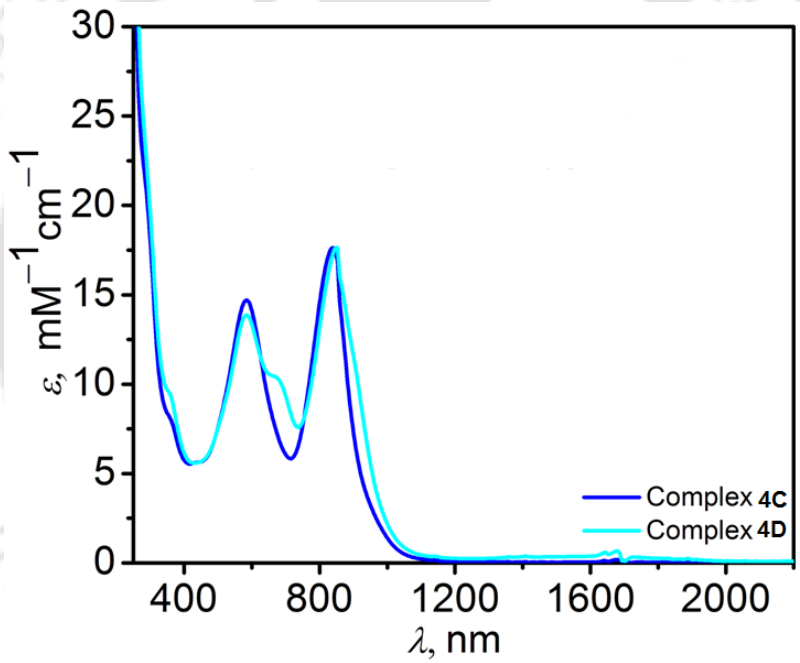

Figure 4.13: *UV-vis/NIR spectrum of complexes **4C** and **4D** in CH_2Cl_2 at 25 ℃.*

Complex **4C** showed two absorption bands at λ_{max} = 834 nm and λ_{max} = 583 nm, respectively. Both the absorption bands were attributed to ligand-to-metal charge transfer transition (LMCT).[4b,9a] On the other hand, complex **4D** showed a broad absorption band at λ_{max} = 843 nm and a moderately sharp absorption band at λ_{max} = 678 nm. All these two absorption

bands were appeared due to the charge transfer transition. The absorption bands at 843 nm and 583 nm were considered as ligand-to-metal charge transfer transitions (LMCT).[4b, 9a]

Table 4.5: *UV-vis/NIR spectral data for complexes **4C** and **4D**.*

Complex	λ_{max}, nm (ε, $M^{-1}cm^{-1}$)
4C	834(17700), 583(14750)
4D	843(17650), 678(10250), 583(13850)

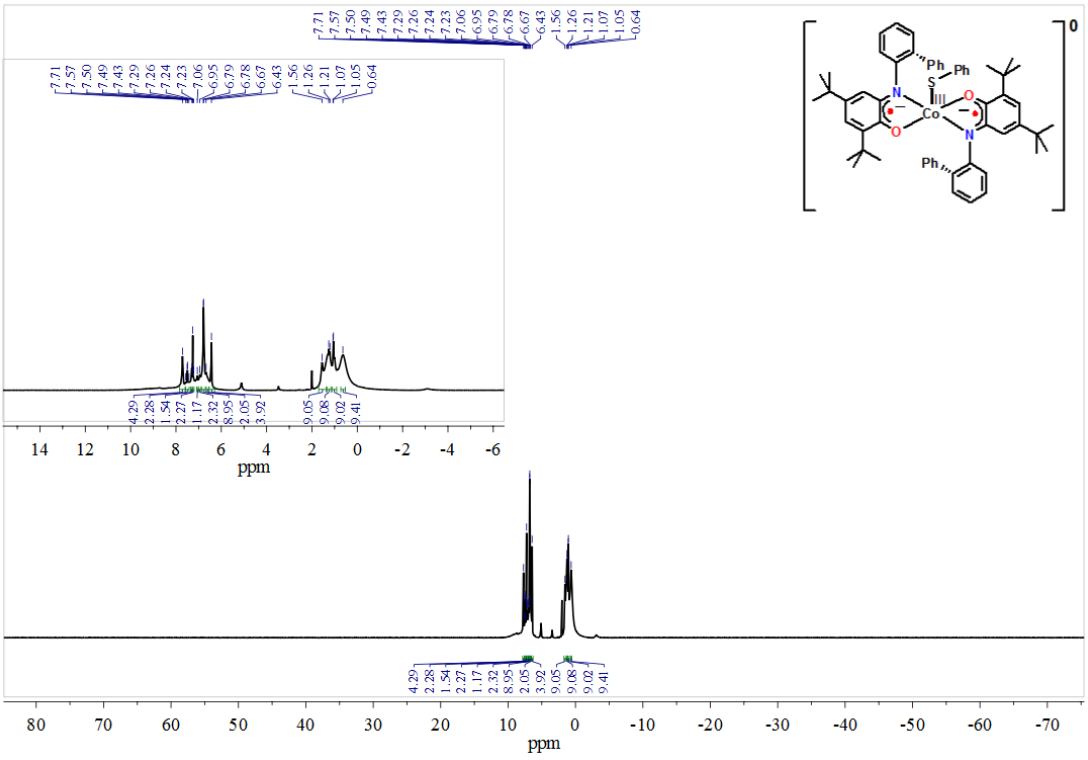

Figure 4.14: *^{1}H-NMR spectrum of complex **4C** in $CDCl_3$.*

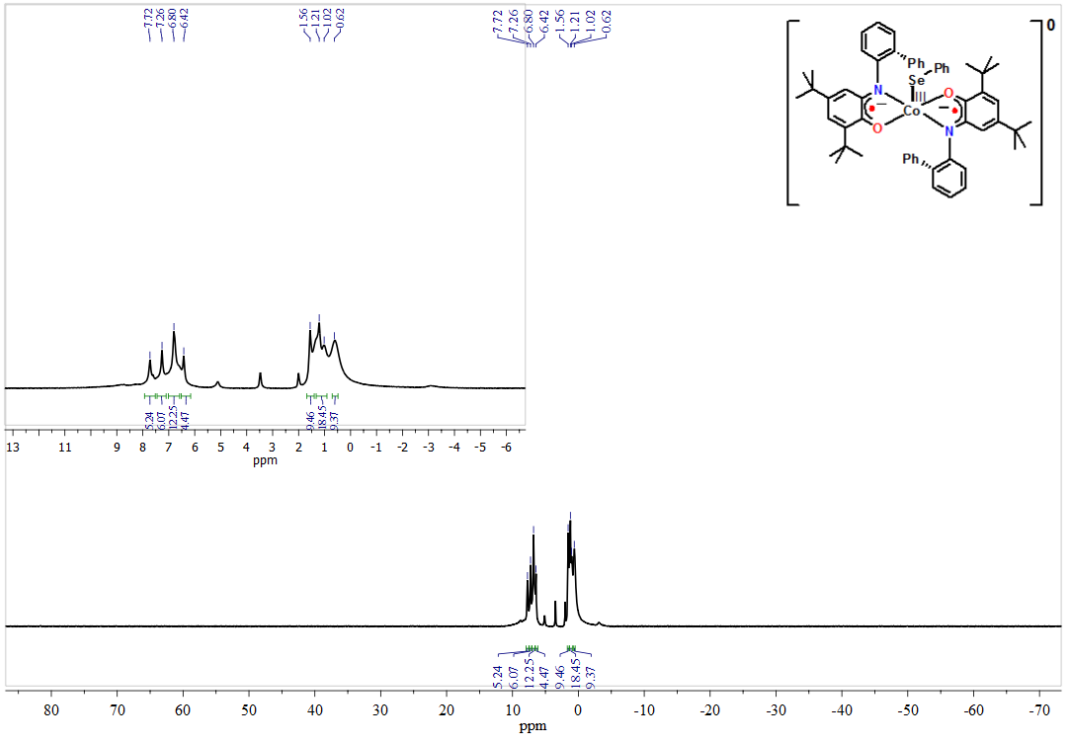

Figure 4.15: *^{1}H-NMR spectrum of complex **4D** in $CDCl_3$.*

The five-coordinate diradical-containing square pyramidal Co(III) (low-spin, S_{Co} = 0) complexes (**4C** and **4D**) were diamagnetic owing to a strong antiferromagnetic coupling between the two ligand-centered p-radicals (S_R = 1/2). The diamagnetic character of the complexes was further supported by ^{1}H-NMR analysis (**Figure 4.14** and **Figure 4.15**).

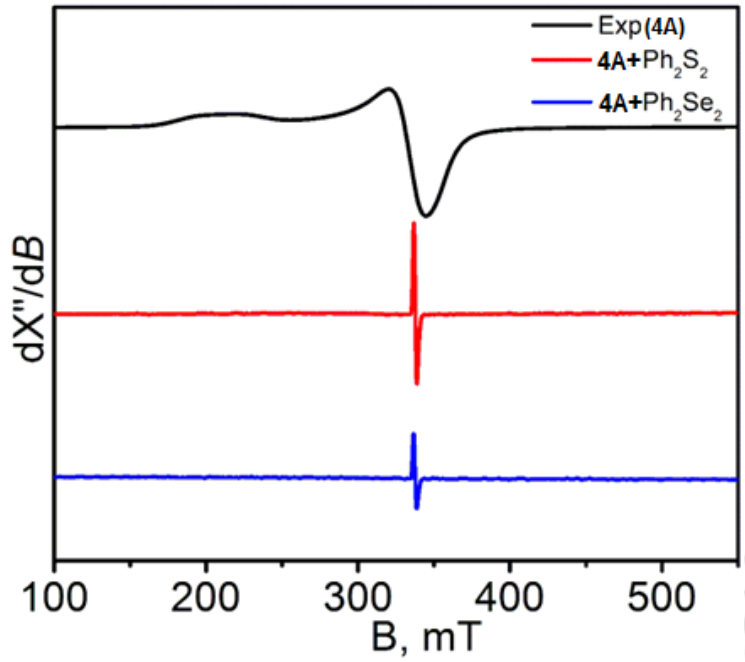

Figure 4.16: *Change in X-band EPR spectrum of **4A** with Ph_2S_2 and Ph_2Se_2 in CH_2Cl_2 solution. Condition: temperature = 25 ℃; microwave frequency (GHz) = 9.447[**4A**], 9.441[**4A**+Ph_2S_2], 9.436[**4A**+Ph_2Se_2]; modulation frequency (kHz) = 100[**4A**], 100[**4A**+Ph_2S_2], 100[**4A**+Ph_2Se_2]; modulation amplitude (G) = 10.0[**4A**], 70.0[**4A**+Ph_2S_2], 70.0[**4A**+Ph_2Se_2]; and microwave power (mW) = 0.995[**4A**], 0.998[**4A**+Ph_2S_2], 0.995[**4A**+Ph_2Se_2].*

The activation of diphenyl disulfide and diphenyl diselenide by complex **4A** was investigated. In this context, the complex **4A** was allowed to react with 10-fold excess of diphenyl disulfide or diphenyl diselenide. The pattern of X-band EPR spectrum of the complex immediately changed and a radical-based isotropic EPR signal at g = 2.001 appeared (**Figure 4.16**). The observation implied the formation of the corresponding five-coordinated diamagnetic cobalt(III) complexes and phenyl thiyl or phenyl selenyl radical.

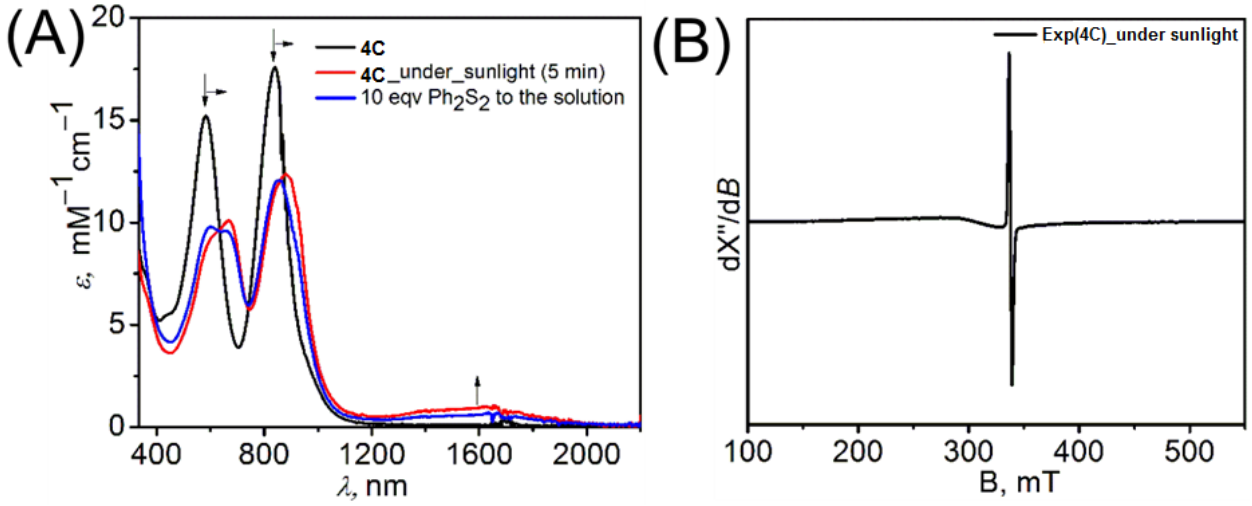

Figure 4.17: *(A) Change in UV-vis/NIR spectrum of **4C** upon exposure to sunlight. Peak shifting towards lower wavelength on addition of Ph_2S_2 into the sunlight-exposed solution emphasized the conversion of four coordinate to five-coordinate complex. (B) Appearance of Co-centered X-band EPR spectrum implied the formation of four-coordinate complex **4A** in CH_2Cl_2 solution. Condition: temperature = 25 ℃; microwave frequency (GHz) = 9.443; modulation frequency (kHz) = 100; modulation amplitude (G) = 100; and microwave power (mW) = 0.998.*

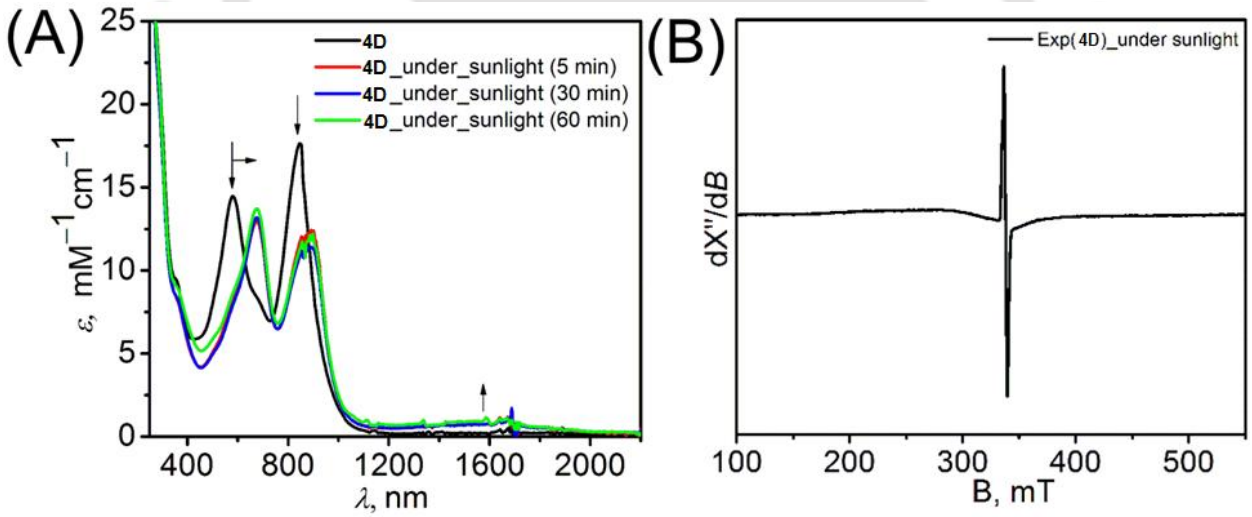

Figure 4.18: *(A) Change in UV-vis/NIR spectrum of **4D** upon exposure to sunlight. (B) Appearance of Co-centered X-band EPR spectrum implied the formation of four-coordinate complex **4A** in CH_2Cl_2 solution. Condition: temperature = 25 ℃; microwave frequency (GHz) = 9.445; modulation frequency (kHz) = 100; modulation amplitude (G) = 100; and microwave power (mW) = 0.995.*

When CH_2Cl_2 solution of complex **4C** was subjected to sunlight irradiation, the 1600 nm band started to appear, with concomitant shifting of the ~570 nm band to 660 nm (**Figure 4.17A**). These phenomena indicated homolytic Co–SPh bond cleavage and the consequent generation of **4A**. A similar phenomenon have also been observed for **4D** (**Figure 4.18A**), where **4A** was generated by the cleavage of the Co–SePh bond. The appearance of a Co-centered X-band EPR signal (**Figure 4.17B** and **Figure 4.18B**) in the processes further supported the formation of **4A**.

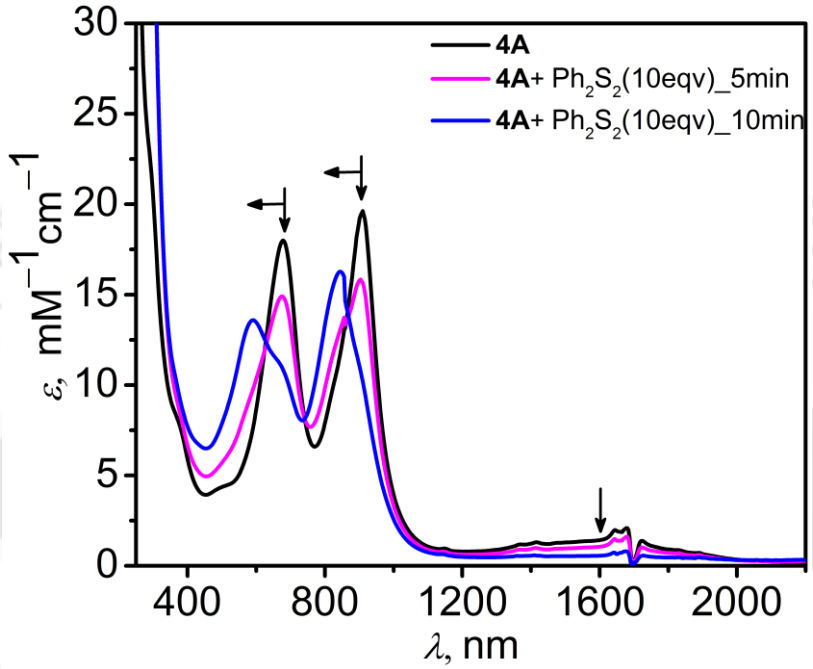

Figure 4.19: *Change in UV-vis/NIR spectrum of* ***4A*** *upon addition of* Ph_2S_2.

In the addition of excess of Ph_2S_2 to a CH_2Cl_2 solution of complex **4A**, the 1600 nm band gradually decreases, with concomitant shifting of the ~660 nm band to 570 nm (**Figure 4.19**). These phenomena indicated formation of Co–SPh bond cleavage and the consequent generation of **4C**.

As the five-coordinate, diradical-containing complexes could be converted to the corresponding four-coordinate, monoradical-containing complexes under sunlight stimulus, and *vice-versa* the four-coordinate complexes have already been found to be one-electron transferring agents.

4.5 Conversion of Isocyanate to Urea under Sunlight by Using Complexes (4A, 4C and 4E) as Catalyst

General method for the catalysis: A pressure tube was initially evacuated and then filled with argon. The process was repeated thrice. After that catalyst (**4A**/**4C**/**4E**) and dry dichloromethane (5.0 mL) were added. The solution was stirred for a few minutes and then to the catalyst solution isocyanate substrate was added by a syringe. The septum was then replaced by a Teflon screw cap under the argon flow. The reaction solution was then stirred under sunlight for 6 h, during which product was separated as white solid. The solid was collected by filtration and washed with dichloromethane.

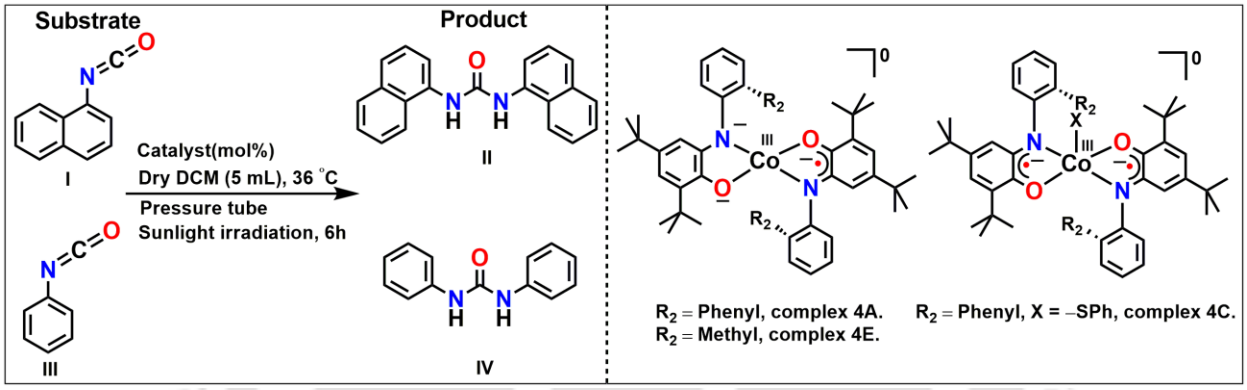

Scheme 4.5: *Reaction scheme for the catalysis.*

Table 4.6: *Catalysis at variable condition.*

Entry	Substrate	Product	Cat. Used (mol %)			Yield (%)		
			4C	**4A**	**4E**	**4C**	**4A**	**4E**
1	**III**	**IV**	2.5	2.5	2.5	72	78	76
2	**III**	NR	0	0	0	0	0	0
3	**I**	**II**	2.5	2.5	2.5	80	86	82
4	**I**	NR	0	0	0	0	0	0
5	**III**+Ph_2S_2[b]	**IV**	2.5	2.5	–	68	75	–
6	**III**	**IV**	–	1.0	–	–	72	–
7	**III**	**IV**	–	0.1	–	–	48	–
Absence of sunlight								
8	**III**	**IV**	2.5	2.5	2.5	10	12	15
9	**III**+Ph_2S_2[b]	**IV**	2.5	2.5	–	9	12	–
10	**I**	**II**	2.5	2.5	2.5	10	11	10

[a]*NR stands for no reaction. The temperature of the reaction bath was 36 °C. All reactions were carried out for 6 hours in a closed tube* [b]*1 :1 mixture.*

In ordered to investigated the catalytic ability of the four-coordinate as well as the five-coordinate complexes (**4A**, **4C** and **4E**) for the conversion of RNCO (R = phenyl and naphthyl) to the corresponding C–N coupled urea derivatives. Notably, 1,3-diaryl urea derivatives have agricultural and medicinal uses.[10] **Schame 4.6** contains the reaction details. In the catalytic reactions, a maximum TON of 480 was achieved by employing 0.1 mol% of complex **4A**. The bulkiness of the substrates and *ortho*-substituents did not have a pronounced effect on the product yield. This emphasized that the substrates approached the Co(III) centre along the axial position. The requirement for both the catalysts as well as sunlight was further established by performing blank reactions (**Table 4.6**). To note, the bulkiness of the substrates and *ortho*-substituents did not pronouncedly affect the product yield. This emphasized that substrates approached the Co(III) centre along the axial position. The essentiality of both the catalysts as well as sunlight was further established by performing blank reactions (**Table 4.6**). No products formation in the absence of catalyst refuted the conversion RNCO compounds to the corresponding amines and photo-driven [2+2] cycloaddition reaction (**Table 4.6**, entries 2 and 4). The low TON (4-6) in the absence of sunlight (**Table 4.6**, entries 8 and 10) supported the possibility that during the catalysis a substrate-bound five-coordinate intermediate was formed (**Figure 4.20**) and a photo stimulus was then essential for the regeneration of four-coordinate

catalysts by the cleavage of Co-substrate bond in the intermediate. The formation of 1,1,2,2,-tetrachloroethane was being established by GC and GC-MS (**Figure 4.21**) analyses during the catalysis of **III** to **IV** in the presence of catalyst **4A**. The compound was formed by the C–C coupling of two CH_2Cl_2 molecules and thus, implied the abstraction of hydrogen atom from the solvent molecule during the formation of urea derivatives. Depending on the above stated results a mechanistic proposal for the C–N coupling between two isocyanate molecules for the formation of urea derivative is given in **Figure 4.20**.

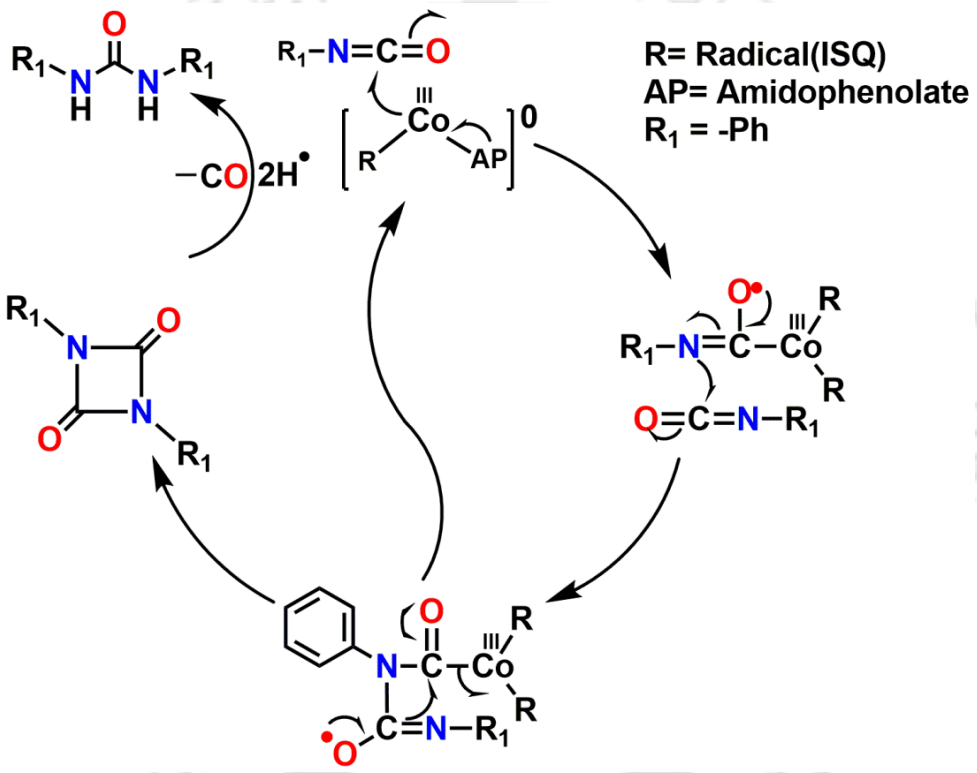

Figure 4.20: *Proposed mechanism for the formation of urea derivative from an isocyanate compound.*

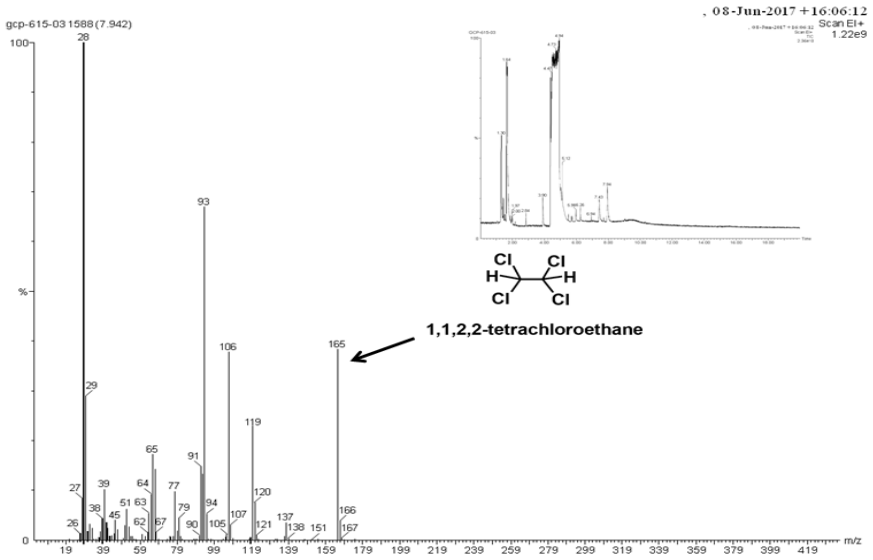

Figure 4.21: *GC-MS spectrum during the catalysis reaction, (inset) chromatogram of the reaction mixture.*

4.5 Conclusions

To Conclude, four-coordinate, monoradical-containing Co(III) complexes have been successfully synthesized and employed for the S–S/Se–Se bond activation and scission by an electron transfer to the bonds. The solo example known in literature for the ligand induced S–S bond cleavage reaction is based on air sensitive Pd(II)-amidophenolate complex. Thus, less explored phenomena has been studied employing air stable Co(III) complexes. The resulted diradical-containing square pyramidal Co(III) complexes with axial –XPh (X = S and Se) ligands experienced homolytic Co–XPh bond cleavage under the influence of sunlight and produced the corresponding four–coordinate, monoradical Co(III) complexes. Both four- and five-coordinate Co(III) complexes catalysed the conversion of aromatic isocyanates to the corresponding urea derivatives. Thus, the first examples for the synthesis of urea from the solo use of isocyanate compounds have been reported.

References

1. (*a*) A. L. Smith, K. I. Hardcastle, and J. D. Soper, *J. Am. Chem. Soc.*, 2010, **132**, 14358; (*b*) V. Lyaskovskyy and B. de Bruin, *ACS Catal*., 2012, **2**, 270; (*c*) W. I. Dzik, J. I. van der Vlugt, J. N. H. Reek and B. de Bruin, *Angew. Chem., Int. Ed.*, 2011, **50**, 3356; (*d*) O. R. Luca and R. H. Crabtree, *Chem. Soc. Rev.*, 2013, **42**, 1440; (*e*) M. van der Meer, Y. Rechkemmer, I. Peremykin, S. Hohloch, J. van Slageren and B. Sarkar, *Chem. Commun.*, 2014, **50**, 11104; (*f*) P. Chaudhuri, K. Wieghardt, T. Weyhermüller, T. K. Paine, S. Mukherjee and C. Mukherjee, *Biol. Chem.*, 2005, **386**, 1023; (*g*) M. K. Mondal and C. Mukherjee, *Dalton Trans.*, 2016, **45**, 13532; (*h*) P. Chaudhuri, K. Wieghardt, T. Weyhermüller, T. K. Paine, S. Mukherjee and C. Mukherjee, *Biol. Chem.*, 2005, **386**, 1023; (*i*) D. L. J. Broere, L. L. Metz, B. de Bruin, J. N. H. Reek, M. A. Siegler and J. I. van der Vlugt, *Angew. Chem., Int. Ed.*, 2015, **54**, 1516; (*j*) D. L. J. Broere, R. Plessius and J. I. van der Vlugt, *Coord. Soc. Rev.*, 2015, **44**, 6886.

2. (*a*) F. Diederich and P. J. Stang, Metal-Catalyzed Cross-Coupling Reactions, Wiley-VCH, Weinheim, 1998.

3. (*a*) G. R. Pandhare, V. M. Shinde and Y. H. Deshpande, *Rasayan J. Chem.*, 2008, **1**, 337; (*b*) J. Coates, *Interpretation of Infrared Spectra: A Practical Approach*, John Wiley & Sons Ltd, Chichester, 2000; (*c*) D. L. Pavia, G. M. Lampman, G. S. Kriz and J. R. Vyvyan, *Introduction to Spectroscopy*, 4th edition, 31; (*d*) P. K. Kipkemboi, P. C. Kiprono and J. J. Sanga, *Bull. Chem. Soc. Ethiop.*, 2003, **17**, 211; (*e*) G. Hastings and V. Sivakumar, *Biochemistry*, 2001, **40**, 3681; (*f*) J. Breton, J. Burie, C. Berthomieu, G. Berger and E. Nabedryk, *Biochemistry*, 1994, **33**, 4953; (*g*) H. Suzuki, M. A. Nagasaka, M. Sugiura and T. Noguchi, *Biochemistry*, 2005, **44**, 11323; (*h*) A. V. Piskunov, A. V. Lado, G. A. Abakumov, V. K. Cherkasov, O. V. Kuznetsova, G. K. Fukin, and E. V. Baranov, *Russ.Chem.Bull., Int.Ed.*, 2007, 56, 2007.

4. (*a*) C. N. Verani, S. Gallert, E. Bill, T. Weyhermüller, K. Wieghardt and P. Chaudhuri, *Chem. Commun.*, 1999, 1747; (*b*) E. Bill, E. Bothe, P. Chaudhuri, K. Chlopek, D. Herebian, S. Kokatam, K. Ray, T. Weyhermüller, F. Neese and K. Wieghardt, *Chem. -Eur. J.*, 2005, **11**, 204; (*c*) R. K. Sherwood, C. L. Kent, B. O. Patrickb and W. S. McNeil, *Chem. Commun.*, 2010, **46**, 2456; (*d*) D. Herebian, P. Ghosh, H. Chun, E. Bothe, T. Weyhermüller and K. Wieghardt, *Eur. J.*

Inorg. Chem., 2002, 1957; (*e*) S. R. Garaeva, A. A. Medzhidov, O. Beukgunger, A. Aydin, B. Yalcin and M. G. Abbasov, *Russ. J. Coord. Chem*., 2012, **38**, 140; (*f*) A. W. Addison, T. N. Rao, J. Reedijk, J.van. Rijn and G. C. Verschoor, *J. Chem. Soc., Dalton Trans.*, 1984, 1349–1356

5. (*a*) D. L. J. Broere, B. de Bruin, J. N. H. Reek, M. Lutz, S. Dechert and J. I. van der Vlugt, *J. Am. Chem. Soc.*, 2014, **136**, 11574; (*b*) C. Mukherjee, T. Weyhermüller, K. Wieghardt and P. Chaudhuri, *Dalton Trans.*, 2006, 2169; (*c*) M. E. Cass, Greene, D. L. Greene, R. M. Buchanan and C. G. Pierpont, *J. Am. Chem. Soc.*, 1983, **105**, 2680; (*d*) To review: S. N. Brown, *Inorg. Chem.*, 2012, **51**, 1251; (*e*) H. Chun, P. Chaudhuri, T. Weyhermüller and K. Wieghardt, *Inorg. Chem.*, 2002, **41**, 790; (*f*) C. Mukherjee. T. Weyhermüller, E. Bother and P. Chaudhuri, *Inorg. Chem.*, 2008, **47**, 11620; (*g*) A. Rajput, A. K. Sharma, S. K. Barman, D. Koley, M. Steinert and R. Mukherjee, *Inorg. Chem.*, 2014, **53**, 36; (*h*) A. L. Smith, L. A. Clapp, K. I. Hardcastle and J. D. Soper, *Polyhedron*, 2010, **29**, 164; (*i*) S. Ghorai and C. Mukherjee, *Chem. Commun.*, 2012, **48**, 10180; (*j*) S. Ghorai and C. Mukherjee, *Dalton Trans.*, 2014, **43**, 394; (*k*) R. Rakshit, S. Ghorai, S. Biswas and C. Mukherjee, *Inorg. Chem.*, 2014, **53**, 3333; (*l*) M. K. Mondal, A. K. Biswas, B. Ganguly and C. Mukherjee, *Dalton Trans.*, 2015, **44**, 9375.

6. (*a*) A. M. Morris, C. G. Pierpont and R. G. Finke, *Inorg. Chem.*, 2009, **48**, 3496; (*b*) S. Mukherjee, T. Weyhermüller, E. Bothe, K. Wieghardt and P. Chaudhuri, *Dalton Trans.*, 2004 , 3842; (*c*) A. I. Poddel'sky, V. K. Cherkasov and G. A. Abakumov, *Coord. Chem. Rev.*, 2009, **253**, 291. (*d*) C. Mukherjee, T. Weyhermüller, E. Bothe and P. Chaudhuri, *Inorg. Chem.*, 2008, **47**, 2740; (*e*) K. S. Min, T. Weyhermüller and K. Wieghardt, *Dalton Trans.*, 2003, 1126.

7. (*a*) K. C. Gross and P. G. Seybold, *Int. J. Quantum Chem.*, 2000, **80**, 1107; (*b*) A. I. Poddel'sky, Y. A. Kurskii, A. V. Piskunov, N. V. Somov, V. K. Cherkasov and G. A. Abakumov, *Appl. Organometal. Chem.*, 2011, **25**, 180; (*c*) A. V. Piskunov, I. V. Ershova, G. K. Fukin and A. S. Shavyrin, *Inorg. Chem. Commun.*, 2013, **38**, 127; (*d*) N. Deibel, D. Schweinfurth, S. Hohloch, M. Delor, I. V. Sazanovich, M. Towrie, J. A.Weinstein and B. Sarkar, *Inorg. Chem.*, 2014, **53**, 1021.

8. (*a*) T. Kurahashi and H. Fujii, *J. Am. Chem. Soc.*, 2011, **133**, 8307; (*b*) A. Rajput, A. K. Sharma, S. K. Barman, D. Koley, M. Steinert and R. Mukherjee, *Inorg. Chem.*, 2014, **53**, 36; (*c*) W. Kaim, *Inorg. Chem.*, 2011, **50**, 9752; (*d*) C. G. Pierpont, *Inorg. Chem.*, 2011, **50**, 9766; (*e*) M. M. Khusniyarov, K. Harms, O. Burghaus, J. Sundermeyer, B. Sarkar, W. Kaim, J. van

Slageren, C. Duboc and J. Fiedler, *Dalton Trans.*, 2008, 1355; (*f*) T. Storr, E. C. Wasinger, R. C. Pratt and T. D. P. Stack, *Angew. Chem., Int. Ed.*, 2007, **46**, 5198; (*g*) S. Kokatam, T. Weyherm ller, . Bothe, P. Chaudhuri and K. Wieghardt, *Inorg. Chem.*, 2005, **44**, 3709.

9. (*a*) A. I. Poddel'sky, V. K. Cherkasov, G. K. Fukin, M. P. Bubnov, L. G. Abakumova and G. A. Abakumov, *Inor. Chim. Acta.*, 2004, **357**, 3632; (*b*) C. N. Verani, S. Gallert, E. Bill, T. Weyhermüller, K. Wieghardt and P. Chaudhuri, *Chem. Commun.*, 1999, 1747.

10. (*a*) M. C. Mok, S. G. Kim, D. J. Armstrong and D. W. S. Mok, *Proc. Natl. Acad. Sci. U. S. A.*, 1979, **76**, 3880–3884; (*b*) P. Sikka, J. K. Sahu, A. K. Mishra and S. R. Hashim, *J. Med. Chem.*, 2015, **5**, 479–483.

.

Chapter V

Geometry Driven Iminosemiquinone Radical to Cu(II) Electron Transfer and Formation of an Elusive Five-Coordinate Cu(I) Complex: Synthesis, Characterization and Reactivity Study with KO_2

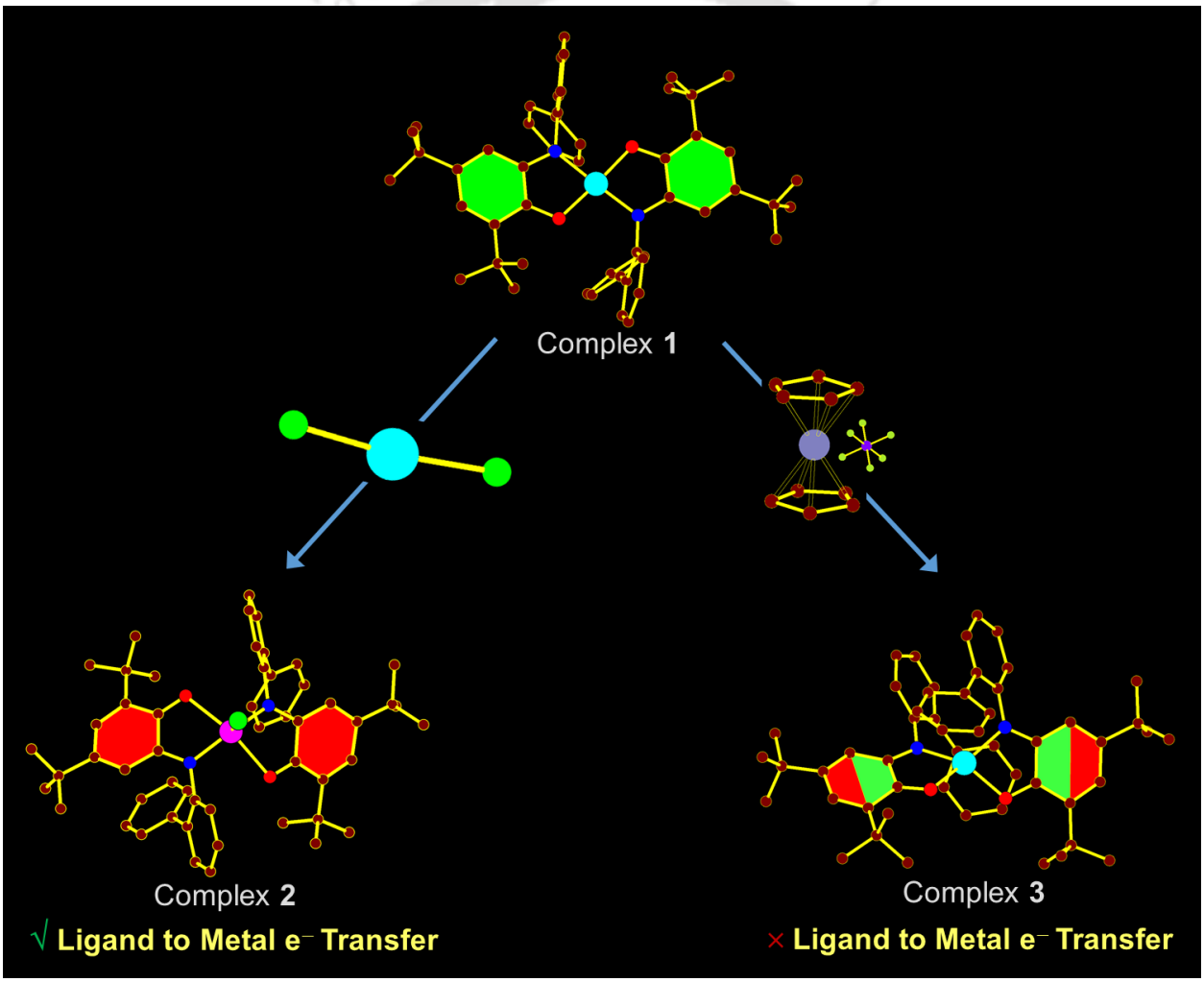

*Some results have been published in

Inorg. Chem., **DOI:** 10.1021/acs.inorgchem.8b01931

5.1 Introduction

Radical-containing copper complexes have emerged as the research interest over recent years because of the involvements of copper-radical species in various biological processes.[1] For instances: tyrosine radical-containing mononuclear Cu(II) ion serves as the active site in fungal metalloenzyme Galactose Oxidase[2] (GOase, **Scheme 5.1**) that catalyzes aerial oxidation of primary alcohols to their corresponding aldehydes with concomitant reduction of molecular oxygen to hydrogen peroxide; a similar active site and the similar reaction mechanism as that of GOase have also been found for Glyoxal Oxidase[3] (GALase), which catalyzes aerial oxidation of aldehydes to the corresponding acids; the biogenesis of topaquinone cofactor and the oxidative half reaction of copper-containing Amine Oxidases (AOase) have also been proposed to proceed *via* a Cu(I)-semiquinone intermediate;[4] the disproportionation of metastable toxic superoxide ($O_2^{\bullet-}$) to oxygen and hydrogen peroxide molecules by Cu,Zn-Superoxide Dismutase[5] (Cu,Zn-SOD, **Scheme 5.1**) occurs at the copper center. All the oxidations (electron transfer) and oxygenation (insertion of an oxygen atom) processes are governed by: (I) the geometry of the copper center; and (II) interactions between the redox-active copper (ranging between +I and +II) and the radical centers (phenolate/phenxyl, catecholate/semiquinone/quinine, O_2^0/ $O_2^{\bullet-}$/O_2^{2-}).[6] Thus, the understanding of metal-ligand interactions in the geometry-dependent electron transfer processes is one of the imperative objectives.

In this context, geometry, electronic structure and biomimetic reactivity of Cu(II)-bis(radical) and Cu(II)-bis(quinone) complexes have been extensively studied. For examples: Cu(II)-bis(radical) complexes have been successfully employed to mimic the function of GOase;[7] Cu(II)-bis(quinone) complexes have been utilize as catalysts for $-CF_3$ transferring reactions,[8a-b] C–N coupling reactions, [8c] H_2 gas production from $NaBH_4$ in dry acetonitrile.[8d] While, Cu(II)-bis(radical) and Cu(II)-bis(quinone) complexes are familiar in the literature, Cu(II)-monoradical system with two coordinating non-innocent ligands of two different oxidation states remains elusive and demands special attention.

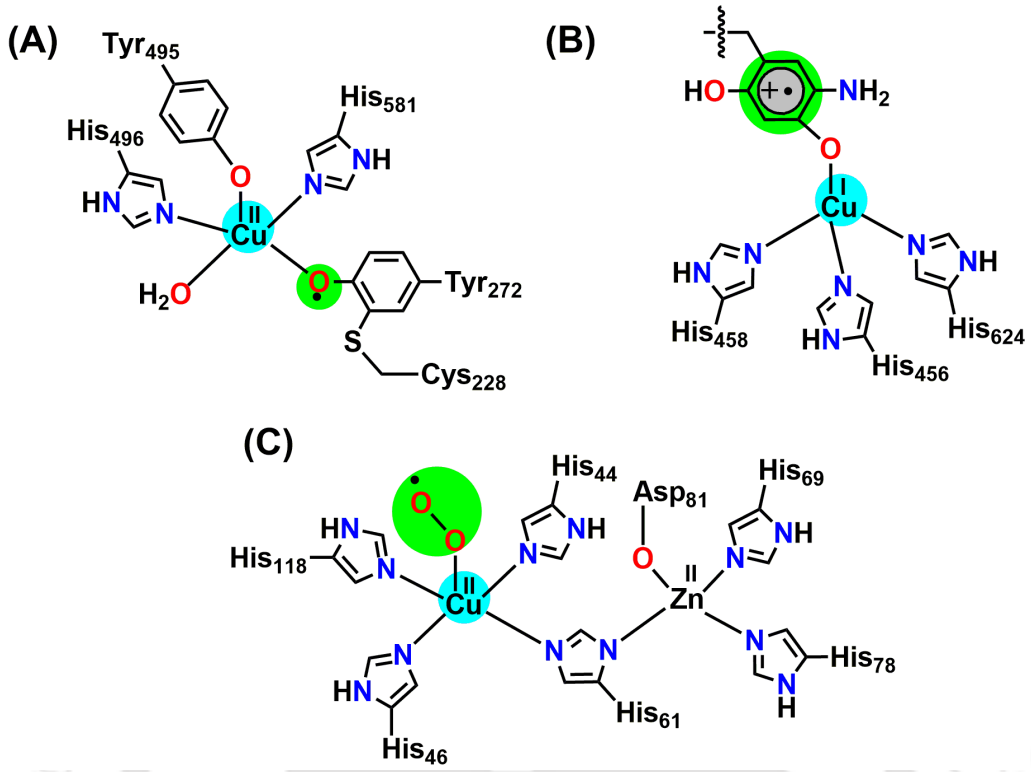

Scheme 5.1: *Copper-radical species, which are proposed to participate in (A) GOase, (B) AOase, and (C) Cu,Zn-SOD enzymatic reactions.*

2-Aminophenol derivatives have been well documented as being stabilized mainly in its one-electron oxidized iminosemiquinone ($ISQ^{\bullet-}$) radical form in the corresponding Cu(II) complexes.[7] Recently, our group develop a new method where a bis(iminoquinone)-coordinated Cu(II) complex can directly be synthesized in one-pot employing $CuCl_2$ as the oxidant.[8d] Mechanistic investigation suggests that two chlorine atoms of two individual $CuCl_2$ molecules bind at the axial positions to the Cu(II) center of the initially formed Cu(II)-bis(iminosemiquinone) complex, and subsequent two electrons transfer from two coordinated-iminosemiquinone units to the axially bound two $CuCl_2$ molecules renders a six-coordinate Cu(II)-bis(iminoquinone) complex where the axial positions are occupied by two chloride atoms.

In this study, the aforementioned oxidation method has been examined on Cu(II)-bis(iminosemiquinone) complex $[Cu(L^{ISQ(Ph)})_2]^0$ (**5A**) of ligand $\mathbf{H_2L^{AP(Ph)}}$ for the *in situ* synthesis of the corresponding five-coordinate, chloride-bound Cu(II)-(iminosemiquinone)(iminoquinone) complex. In complex **5A**, two phenyl rings, which are attached at the *ortho*- position to the

aniline moiety, are situated *cis*- to each other. Thus the steric hindrance created by the phenyl rings will favour the approach of only one $CuCl_2$ molecule along the axial position to the Cu(II) center and hence, one electron oxidation will lead to the expected complex. Interestingly, instead of the expected complex formation, a five-coordinate chloride-bound Cu(I)-bis(iminoquinone) complex $[Cu^{I}(L^{IBQ(Ph)})_2Cl]^0$ (**5B**) was generated *via* ligand[iminosemiquinone]-to-metal[Cu(II)] electron transfer during the oxidation process. To enlighten the geometry dependence on the electron transfer process, one-electron oxidation of **5A** has been performed employing ferrocenium hexafluorophosphase ($FcPF_6$) as the oxidant. Thus formed four-coordinate Cu(II)-complex $[Cu^{II}(L^{ISQ(Ph)})(L^{IBQ(Ph)})]PF_6$ (**5C**) refrained from such electron transfer phenomenon. Furthermore, four-coordinate $[Cu^{I}(L^{IBQ(Ph)})_2]SbF_6$ (**5D**) complex was synthesized from complex **5B** to extent the investigation on the geometry-dependent metal-to-ligand electron transfer process. Finally, the reactivity of the complexes with KO_2 was studied and reported, herein.

5.2 Synthesis and Characterization of Ligand $H_2L^{AP(Ph)}$

A schematic representation for the synthesis of ligand $\mathbf{H_2L^{AP(Ph)}}$ is shown in **Scheme 5.2**.

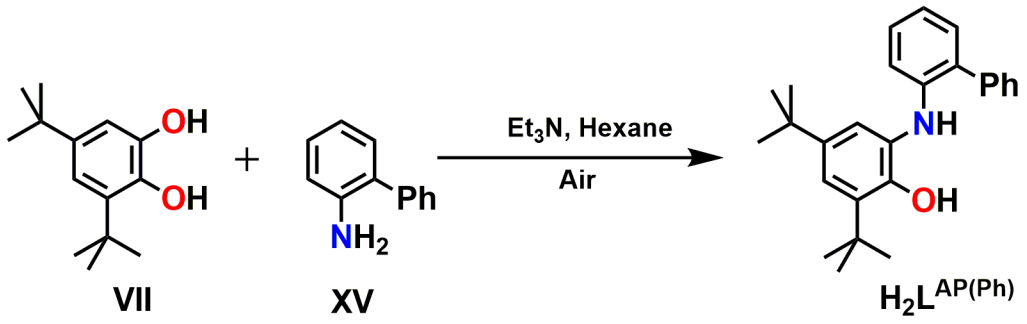

Scheme 5.2: *Synthetic route for the preparation of* $\boldsymbol{H_2L^{AP(Ph)}}$.

A reaction between equimolar amounts of 2-aminobiphenyl (**XV**) and 3,5-di-*tert*-butylcatechol (**VII**) in hexane in presence of Et_3N under air provided ligand $\mathbf{H_2L^{AP(Ph)}}$. The characterisation of ligand $\mathbf{H_2L^{AP(Ph)}}$ by using FT-IR spectroscopy, NMR spectroscopy and mass spectrometry technique has already been discussed in **Chapter IV**.

5.3 Synthesis and Characterization of Copper Complexes (5A and 5B) of Ligand $H_2L^{AP(Ph)}$

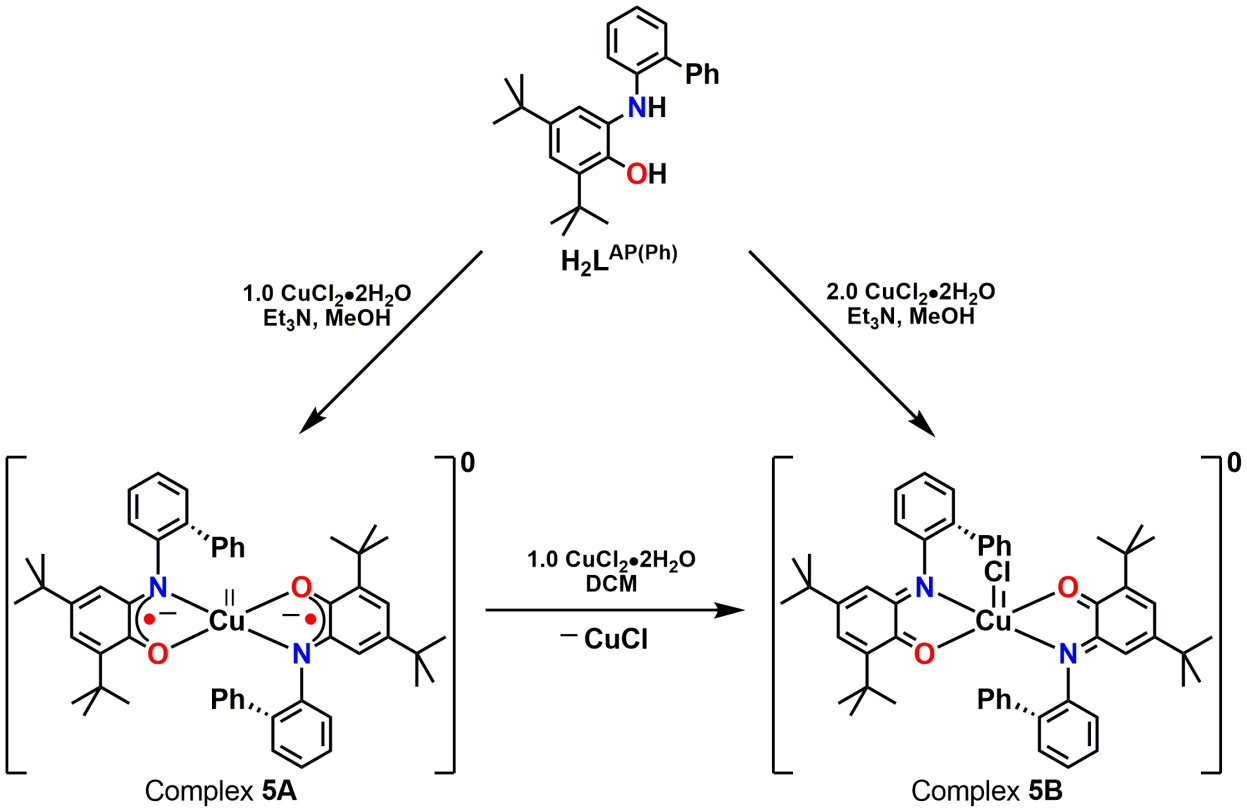

Scheme 5.3: *Synthetic route for the preparation of complex **5A** and complex **5B**.*

Complex **5A** was obtained in 62% yield by reacting the ligand $\mathbf{H_2L^{AP(Ph)}}$ with half equivalent amount of $CuCl_2•2H_2O$ in the presence of triethyl amine (Et_3N) in methanol (MeOH) under air. The reaction of the ligand $\mathbf{H_2L^{AP(Ph)}}$ and $CuCl_2•2H_2O$ in 1:2 molar ratio in MeOH provided complex **5B** in 72% yield. Noteworthy, complex **5B** can also be synthesized by reacting complex **5A** with one equivalent of $CuCl_2•2H_2O$.

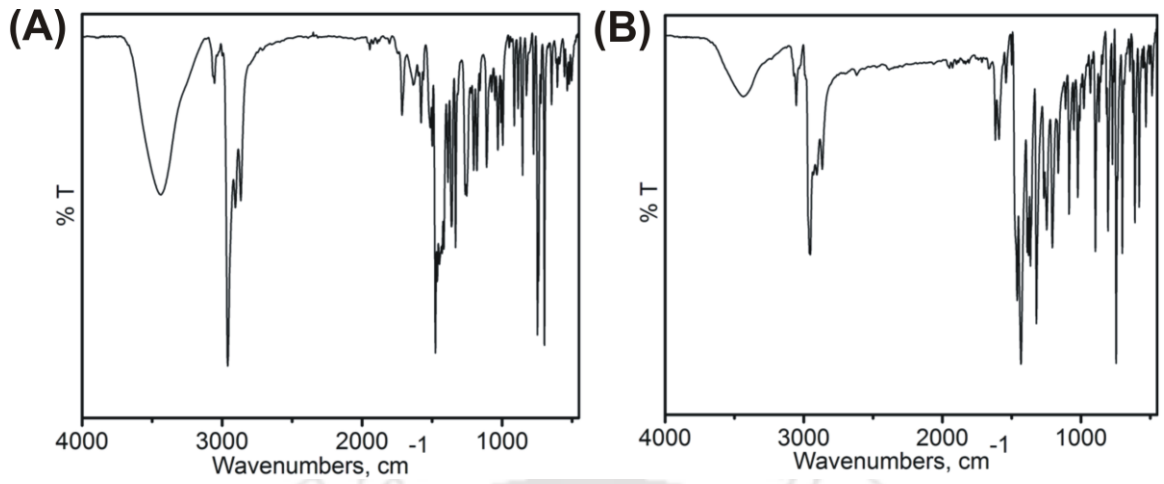

Figure 5.1: ***(A)*** *FT-IR spectrum of complex* ***5A*** ***(B)*** *FT-IR spectrum of complex* ***5B***.

The infrared spectrum of complex **5A** (**Figure 5.1A**) was recorded on KBr pallet at 300 K. The metal coordination with the deprotonated amidophenolate units was confirmed by the disappearance of the ν(O–H) and ν(N–H) stretching bands. A weak band corresponding to $\nu(C_{Ar}–H)$ [Ar stands for aromatic] stretch was observed at 3055 cm^{-1}.[9a] Three bands at 2959, 2905 and 2866 cm^{-1} were attributed for asymmetric, overtone and symmetric bands of ν(C–H) stretches of *tert*–butyl groups, respectively. [9a-d] In addition to this, the ν(C–H) bending vibration of methyl groups appeared at 1475 and 1361 cm^{-1}. On the other hand FT-IR spectrum of the complex **5B** (**Figure 5.1B**) showed no stretching bands for ν(O–H) and ν(N–H) bands, additionally, the presence of the *tert*-butyl stretching frequencies at 2955, 2906 and 2867 cm^{-1} respectively, indicated that the ligand bound with Cu ion where O–H and N–H were deprotonated. The band at 1591 cm^{-1} appeared for the ν(C=N) stretching, in addition ν (C⋯O) stretching frequency appeared at 1432 cm^{-1}.[9f-g]

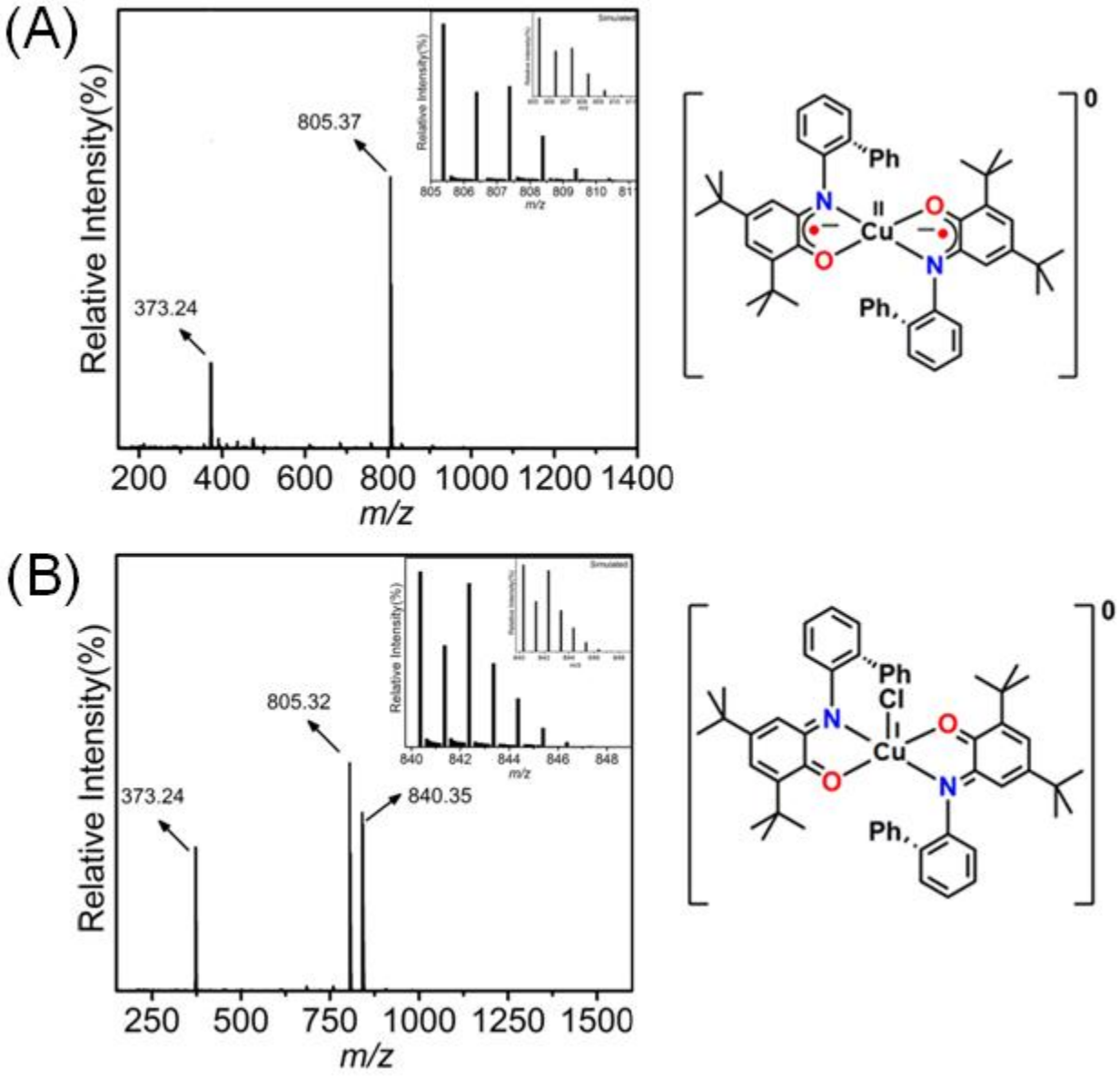

Figure 5.2: *ESI-mass spectra of (A) for **5A**, (B) for **5B**; experimental and simulated isotope distribution pattern (inset).*

Electrospray ionization mass spectra (ESI-MS) were measured in acetonitrile in positive mode. A 100% molecular ion peaks at *m/z* = 805.37 appeared for the complex **5A** (corresponded to $[M]^+$); M = molecular mass (**Figure 5.2A**). On the other hand, a 100% molecular ion peak at *m/z* = 840.35 was found for the complex **5B** (corresponded to $[M]^+$) (**Figure 5.2A**). Isotope distribution pattern examinations of the observed mass peaks revealed the composition of **$C_{52}H_{58}CuN_2O_2$**, for **5A**; **$[C_{52}H_{58}ClCuN_2O_2–Cl]^+$**, for **5B**.

The molecular structure of complex **5A** was clearly established by X-ray diffraction analysis. ORTEP diagram of complex **5A** has been shown in **Figure 5.3** and selected bond distances and bond angles are given in **Table 5.1**. The neutral complex **5A** crystallized in triclinic system, space group '*P*–1'. The geometry around the copper center is a distorted square planar geometry (τ_4 = 0.06) with two oxygen atoms and two nitrogen atoms from the ligands in the basal plane and two –Ph moieties were situated same side from basal plane.

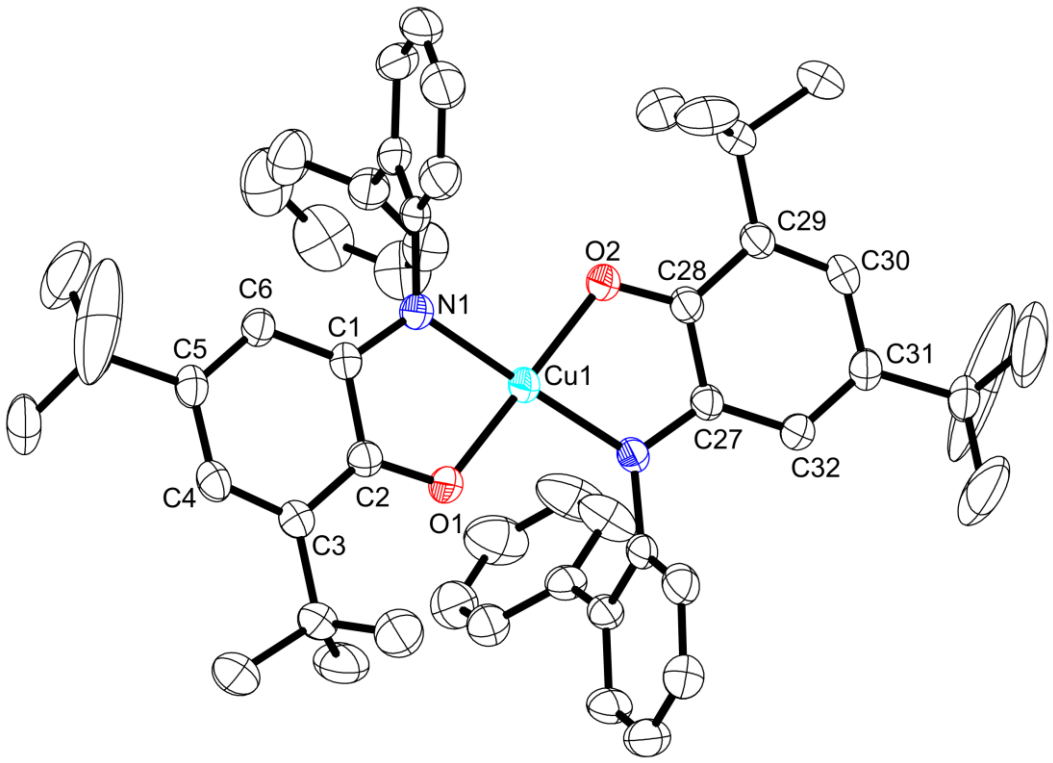

Figure 5.3: *ORTEP diagram of complex **5A**. Thermal ellipsoids were drowning at 40% probability level. Hydrogen atoms were omitted for clarity.*

The N1–Cu1–N2 and O1–Cu1–O2 bond angles were 177.74(11)° and 172.62(11)°, respectively. The average Cu–O and Cu–N bond distances were 1.914±0.002 Å and 1.936±0.001 Å, respectively. These bond distances were in accord with the +II oxidation state of the central Cu1 atom.[7g,10a-b] The average C–N and C–O bond distances for the chelating unit in amidophenolate moiety were 1.338 Å and 1.295 Å, respectively. These bond distances were corroborating neither with their respective single bond nor their respective double bond characters, rather, they existed in between their single bond and double bond characters.

Furthermore, alternating four long bond distances and two short bond distances were observed in the *tert*-butyl groups-containing phenyl rings. The respective C3–C4, C5–C6, C29–C30 and C31–C32 bond distances were 1.376(4), 1.370(4), 1.368(4) and 1.369(4) Å, while, the other two C–C bond distances (**Table 5.1**) in the *tert*-butyl groups attached phenyl rings were in the range of 1.43±0.02 Å. The observed bond distances in the *tert*-butyl attached phenyl rings indicated a quinoid-type distortion and hence, the loss of aromaticity *i.e.* the coordinating ligands exist in their one-electron oxidized form ($ISQ^{\bullet 1-}$) of the ligand was evidenced.[7c,7i,10a-e] Thus, the complex was a neutral diradical-containing square planar one.

Table 5.1: *Selected bond distances (Å) and angels (°) for complex **5A**.*

Cu1–N1	1.935(2)	C6–C1	1.421(4)
Cu1–N2	1.938(2)	N2–C27	1.342(4)
Cu1–O1	1.917(2)	O2–C28	1.295(4)
Cu1–O2	1.911(2)	C27–C28	1.455(4)
N1–C1	1.335(4)	C28–C29	1.423(4)
O1–C2	1.295(4)	C29–C30	1.368(4)
C1–C2	1.454(4)	C30–C31	1.429(5)
C2–C3	1.426(4)	C31–C32	1.369(4)
C3–C4	1.376(4)	C27–C32	1.414(4)
C4–C5	1.425(4)	N1–C15	1.433(4)
C6–C5	1.370(4)	N2–C41	1.425(4)
N1–Cu1–N2	177.74 (11)	C2–O1–Cu1	112.83(19)
O1–Cu1–O2	172.62(11)	C28–O2–Cu1	113.44(19)
O2–Cu1–N1	94.50(9)	C27–N2–Cu1	112.58(19)
N1–Cu1–O1	83.92(9)	C41–N2–Cu1	125.17(19)
O2–Cu1–N2	83.76(9)	C1–N1–Cu1	112.69(19)
O1–Cu1–N2	97.99(10)	C15–N1–Cu1	125.47(18)

Complex **5B** crystallized in the monoclinic space group *C 2/c*. The molecular structure with the selected atom numbering scheme is depicted in **Figure 5.4**. The selected bond distances and bond angles are given in **Table 5.2**.

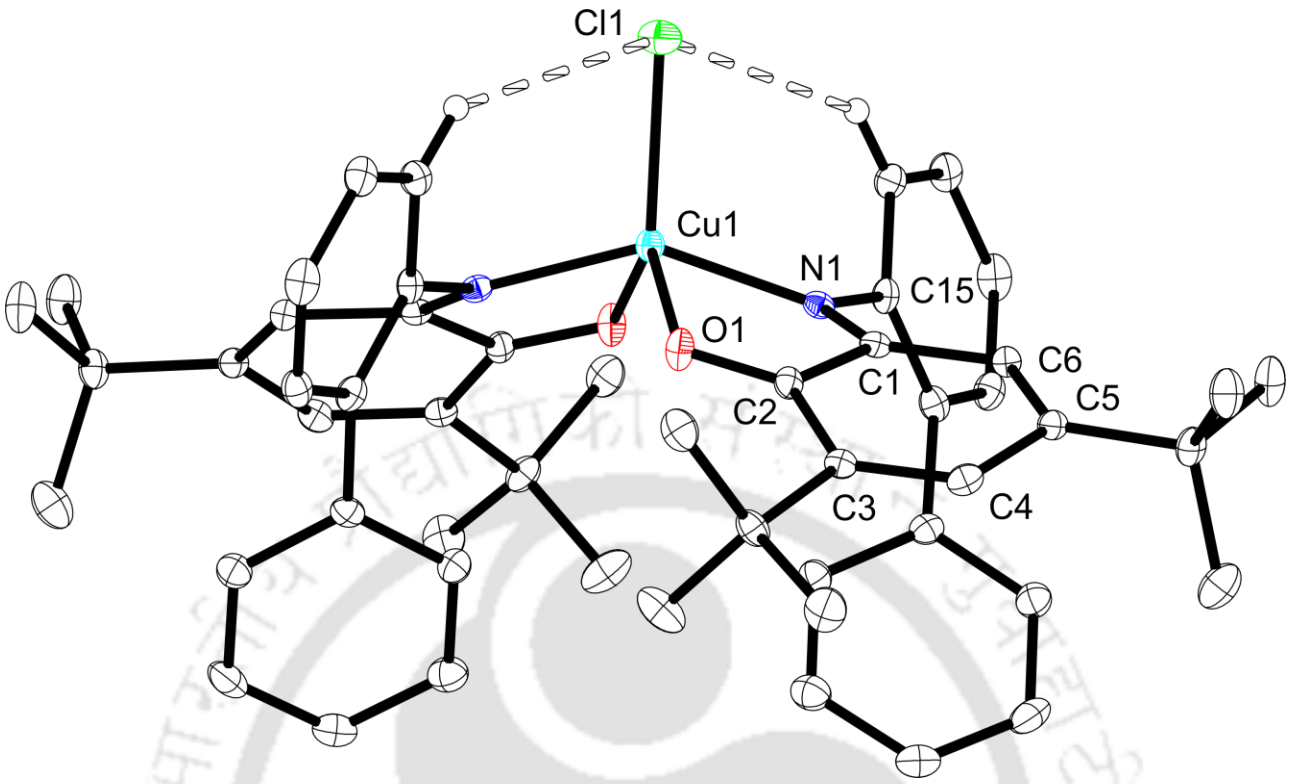

Figure 5.4: *ORTEP diagram of complex **5B**; thermal ellipsoids were drown at 30% probability level. H-atoms, except the H atoms involved in H-bonding with Cl1, are omitted for the sake of clarity.*

The mononuclear, five-coordinate complex **5B** acquired a distorted square pyramidal geometry [τ_5 = 0.25 (τ_5 = 0 for perfect square pyramidal and τ_5 = 1 for perfect trigonal bipyramidal)] where the basal plane was comprised of two NO (N1O1 and N1′O1′) donor sets from two ligand units and the fifth (axial) position was occupied by a chloride atom. The central Cu1 atom was situated ~ 0.77 Å above the basal plane and towards the apical chlorine atom. The apical Cl1 atom experienced two H-bonding interactions (**Figure 5.4**). The Cu1–O1 = 2.3934(17) Å bond (**Table 5.2**) in complex **5B** was much longer compared to the reported Cu–O = 1.906 Å (average) bond in complex **5A** (**Table 5.1**). This feature consolidated the higher oxidation state of the coordinating ligand and lower oxidation state of the central copper ion. Complex **5B** was neutral in charge. Therefore, the possible composition could be either $\{Cu^{II}[L^{ISQ(AP)}][L^{IBQ(AP)}]Cl\}$ or $\{Cu^{I}[L^{IBQ(AP)}]_2Cl\}$ (**Figure 5.5**).

Table 5.2: Selected bond distances (Å) and bond angles (°) for complex **5B** (at 100 K).

Cu1–N1	1.927(2)	C3–C2	1.467(3)
Cu1–O1	2.3934(17)	C3–C4	1.349(3)
Cu1–Cl1	2.2352(10)	C4–C5	1.470(3)
N1–C1	1.302(3)	C6–C5	1.347(3)
O1–C2	1.227(3)	C6–C1	1.432(3)
C1–C2	1.514(3)	N1–C15	1.445(3)
N1–Cu1–N1^{i}	146.44(12)	N1–Cu1–Cl1	106.78(6)
O1–Cu1–O1^{i}	131.14(9)	C1–N1–Cu1	122.32(15)
N1–Cu1–O1	91.44(7)	C15–N1–Cu1	117.68(15)
Cl1–Cu1–O1	114.43(5)	C2–O1–Cu1	107.65(14)

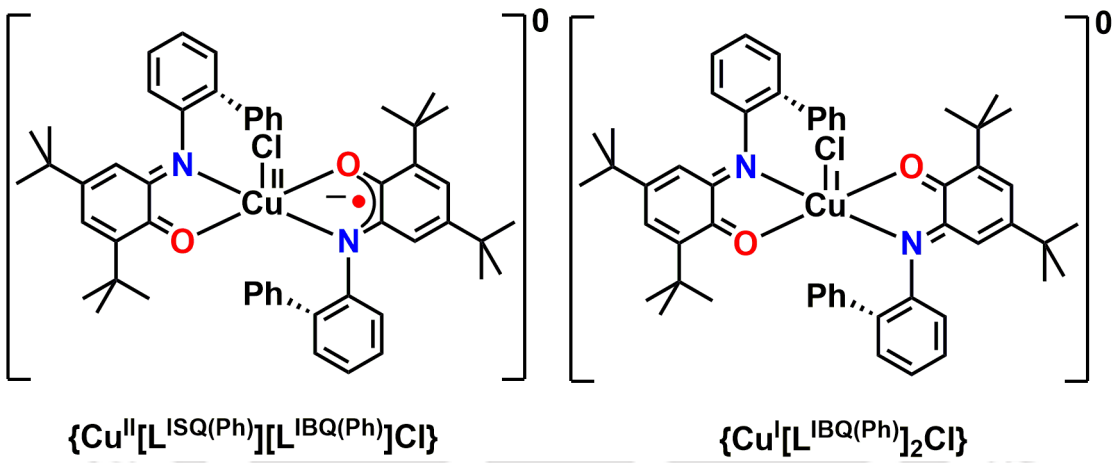

{Cu^{II}[L$^{ISQ(Ph)}$][L$^{IBQ(Ph)}$]Cl} {Cu^{I}[L$^{IBQ(Ph)}$]$_2$Cl}

Figure 5.5: *Two possible structure of complex **5B**.*

The electronic absorption spectra (UV-vis/NIR) for complexes **5A** and **5B** in CH_2Cl_2 solution are illustrated in **Figure 5.6**. The absorption positions and the corresponding extinction coefficient values are summarized in **Table 5.3**.

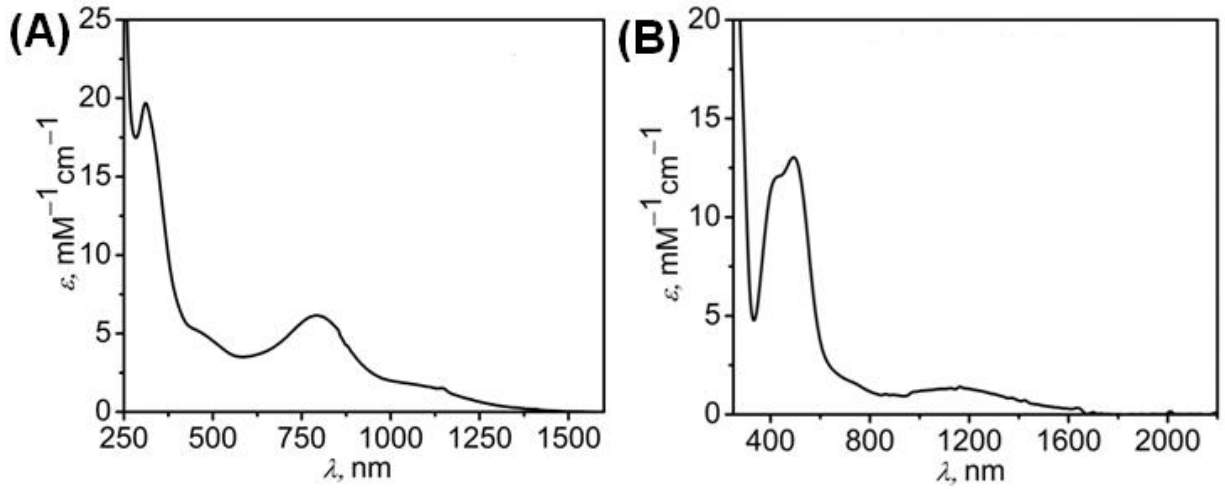

Figure 5.6: *UV-vis/NIR spectrum of (A) complex **5A** and (B) complex **5B** in CH_2Cl_2 at 25 ℃.*

In complex **5A** the bands at 1034 nm (ε = 1850 $M^{-1}cm^{-1}$) and 792 nm (ε = 6200 $M^{-1}cm^{-1}$) were consistent with the previously reported similar Cu(II)-bis(iminosemiquinone) complexes and assigned as combination of MLCT and LLCT transitions.[7c,e-h] The band at λ_{max} = 470 nm (ε = 5000 $M^{-1}cm^{-1}$) appeared due to LMCT transition. In complex **5B**, a broad absorption manifold centered at 1160 nm (ε = 1350 $M^{-1}cm^{-1}$) was present. The low-energy band has been attributed to Cu(I)-to-iminoquinone MLCT transition. The strong bands at λ_{max} = 490 nm (ε = 13050 $M^{-1}cm^{-1}$) and λ_{max} = 420 nm (ε = 11900 $M^{-1}cm^{-1}$) were due to π-to-π* intraligand (ILCT) charge-transfer transitions of iminoquinone moieties.[11]

Table 5.3: *UV-vis/NIR spectral data for **5A**, and **5B**.*

Complex	λ_{max}, nm (ε, $M^{-1}cm^{-1}$)
5A	1034(1850), 792(6200), 470^{sh}(5000), 310(19550)
5B	1160(1350), 725^{sh}(1650), 490(13050), 420(11900)

*sh stand for shoulder

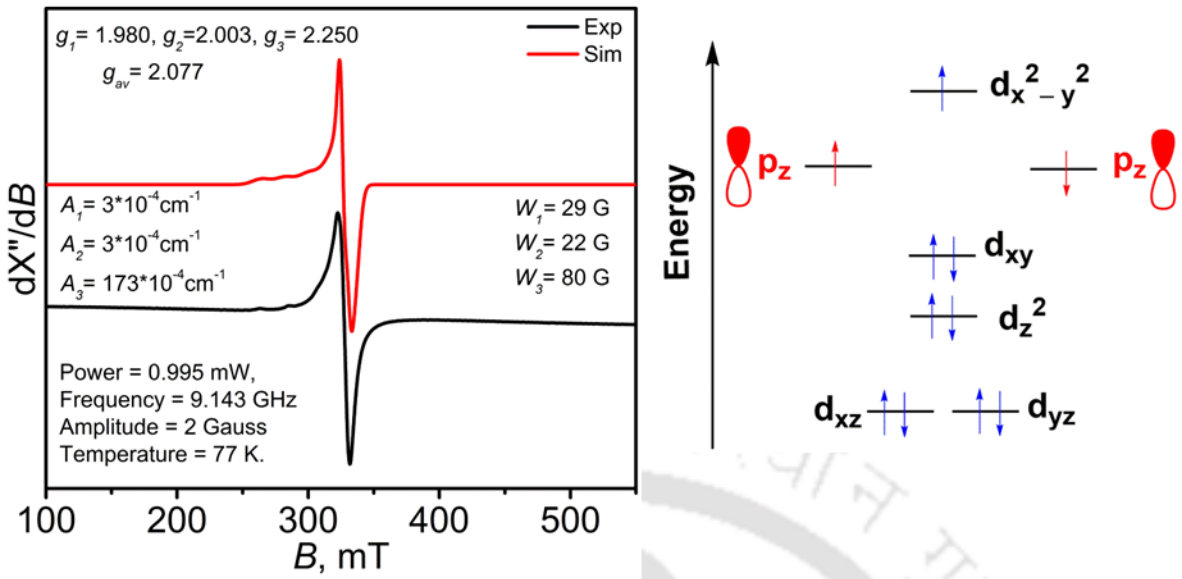

Figure 5.7: *(A) Experimental and simulated X-band EPR spectra of* ***5A*** *in CH_2Cl_2 solution. Conditions: temperature = 77 K, microwave frequency (GHz) = 9.143, modulation frequency (kHz) = 100, modulation amplitude (G) = 2.0 and microwave power (mW) = 0.995.(B) d-orbital splitting of Cu^{2+} ion in square planar geometry and ligand p_z orbital.*

X-band EPR spectrum and simulation spectrum of the experimental results of complex **5A** was shown in **Figure 5.7**. Simulation to the experimental results provided following parameters; g_x = 1.980, g_y = 2.003, g_z = 2.250, W_x = 29 G, W_y = 22 G, W_z = 80 G, $A_x = 3\times10^{-4}$ cm^{-1}, $A_y = 3\times10^{-4}$ cm^{-1}, $A_z = 173\times10^{-4}$ cm^{-1}. From the spectrum pattern and simulation results, it was confirmed that the unpaired electron was residing on the Cu(II) center, and two ligand-center π-radicals were strongly antiferromagnetically coupled and higher in magnitude compared to a radical and Cu(II) ion (S = ½; $dx^2–y^2$).[7c]

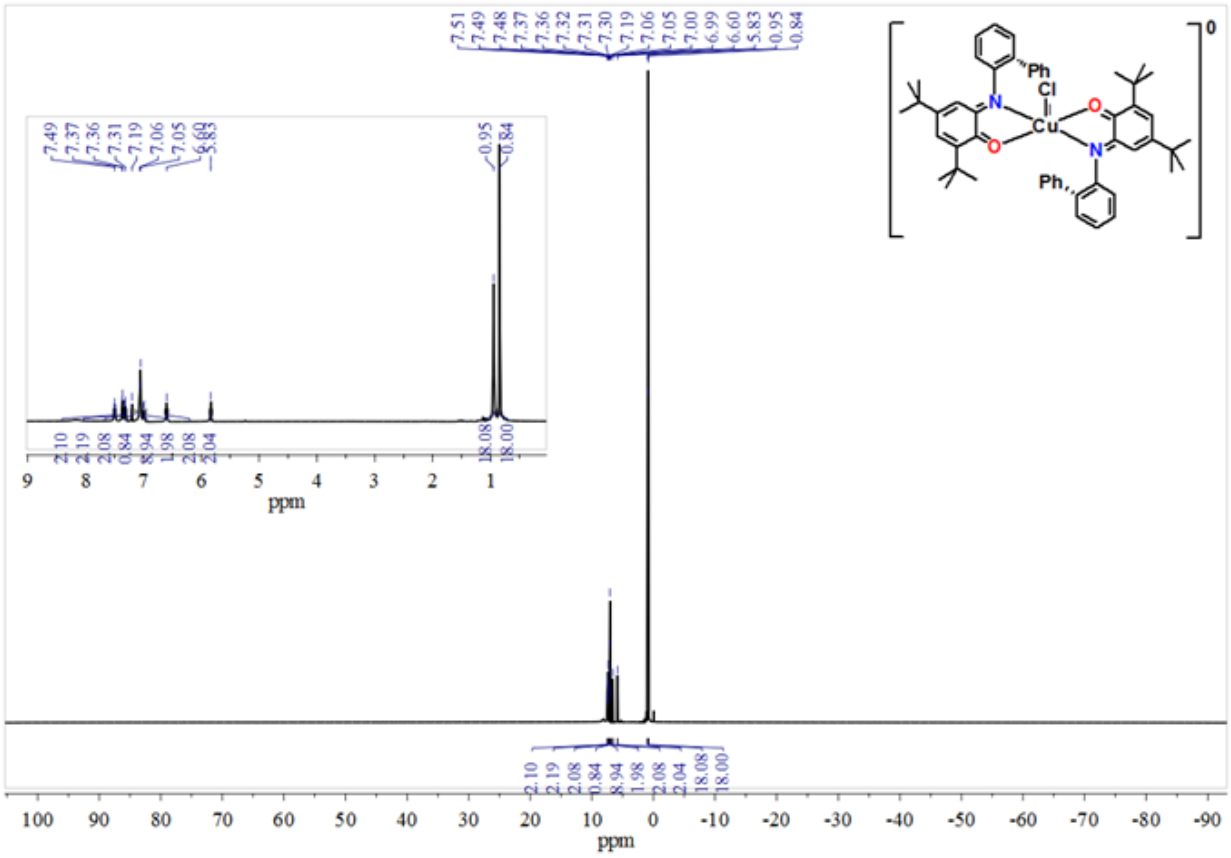

Figure 5.8: *^{1}H-NMR spectrum of complex **5B** in $CDCl_3$.*

Complex **5B**, was diamagnetic in nature with S_t = 0 {Cu(I) = d^{10} and both the coordinating ligand was present in two electron oxidized iminosemiquinone form} ground state which was confirmed by ^{1}H-NMR spectroscopy (**Figure 5.8**). The resonance signals at δ = 0.84 ppm and δ = 0.95 ppm were appeared for each of eighteen hydrogen atoms attached to two *tert*-butyl groups. On the other hand, resonance signals for twenty two aryl protons were appeared in a range of 5.83–7.49 ppm.

The electrochemical behavior of complexes **5A** and **5B** were investigated by cyclic voltametry. Cyclic voltammograms (CVs) of the complexes (1 mM) were being recorded in CH_2Cl_2 solutions containing 0.10 M $[(^{n}Bu)_4N]ClO_4$ as supporting electrolyte at a glassy carbon working electrode, a platinum wire counter electrode, and a Ag/AgCl reference electrode. The experiments were performed at different scan rates. Ferrocene was used as an internal standard, and potentials are referenced *versus* the ferrocenium/ferrocene (Fc^{+}/Fc) couple.

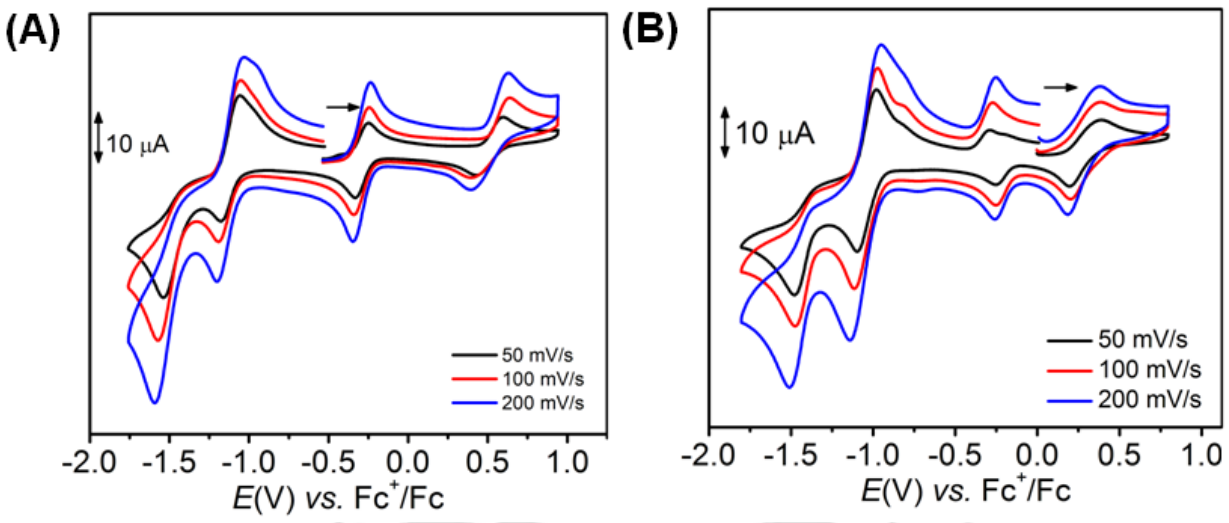

Figure 5.7: *Cyclic voltagrams of (A) complex **5A** and **(B)** complex **5B** measured at 50, 100, and 200 mV/s.*

Complex **5A** underwent two successive one-electron oxidation and two successive one-electron reduction processes in the potential range +1.00 V to -1.80 V *vs.* Fc^{+}/Fc (**Figure 5.7A**). The oxidation and reduction potential values (**Table 5.7**) were in accord with the previously reported Cu(II)-bis(iminosemiquinone) complexes[7c,j-g] and thus, corresponded to the ligand-centered processes, where the oxidation of coordinated $[L^{ISQ(Ph)}]^{1-}$ provided $[L^{IBQ(Ph)}]^{0}$ and reduction of $[L^{ISQ(Ph)}]^{1-}$ generated $[L^{AP(Ph)}]^{2-}$ (**Scheme 5.4**). The potential difference ($\Delta E_{1/2}{}^{ox}$) between the second oxidation ($E_{1/2}{}^{ox2}$) and the first oxidation ($E_{1/2}{}^{ox1}$) processes was ~ 800 mV. This indicated a high electrochemical communication, *i.e.*, delocalization between the two redox-active sites in the complex after the first oxidation, *i.e.*, in $\{Cu^{II}[L^{ISQ(Ph)}][L^{IBQ(Ph)}]\}^{+}$. Conversely, the charge delocalization was less (ΔE = 363 mV) in the one-electron reduced $\{Cu^{II}[L^{ISQ(Ph)}][(L^{Ap(Ph)}]\}^{+}$ species. The CV of complex **5B** showed one one-electron oxidation and three one-electron reduction waves (**Figure 5.7B**). The solo oxidation process occurs at $E_{1/2}{}^{ox}$ = 0.270 V (**Table 5.7**), which was ~ 0.240 V lower compared to the second oxidation process of complex **1**. In complex **2**, the Cu(I) was the only redox-active center, which could be preferably oxidized. Therefore, the oxidation process has been assigned as Cu(I)-to-Cu(II) oxidation and formation of $[Cu^{I}(L^{IBQ(Ph)})_2Cl]^{+}$ species. The second and the third reduction

potential values were closely comparable to that of the reduction potential values observed in complex **5B**. Thus, the reductions corresponded to ligand-based processes.

Table 5.7: Voltammetric redox processes for the complex **5A** and **5B**.

Complex	$E^{0,a}$ V, (ΔEp, mV)			
	$E_{1/2}^{red2}$	$E_{1/2}^{red1}$	$E_{1/2}^{ox1}$	$E_{1/2}^{ox2}$
5A	–1.480 (120)	–1.117 (125)	–0.292 (115)	0.508 (245)
5B	–1.420 (120)	–1.044 (147)	–0.210 (80)	0.270 (160)

[a] E^0 values recorded at scan rates of 100 mV/s and referenced to the Fc^+/Fc couple.

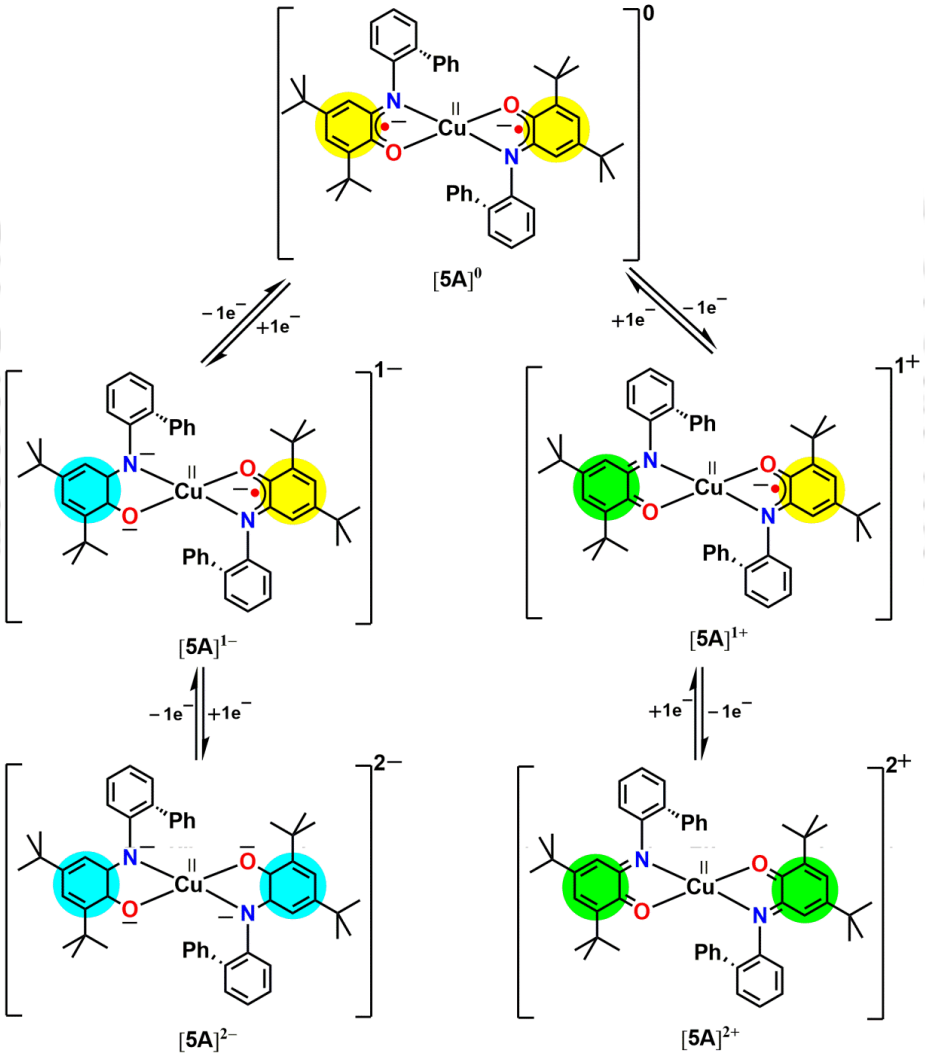

Scheme 5.4: *Species formed by two one-electron oxidation and two one-electron reduction processes.*

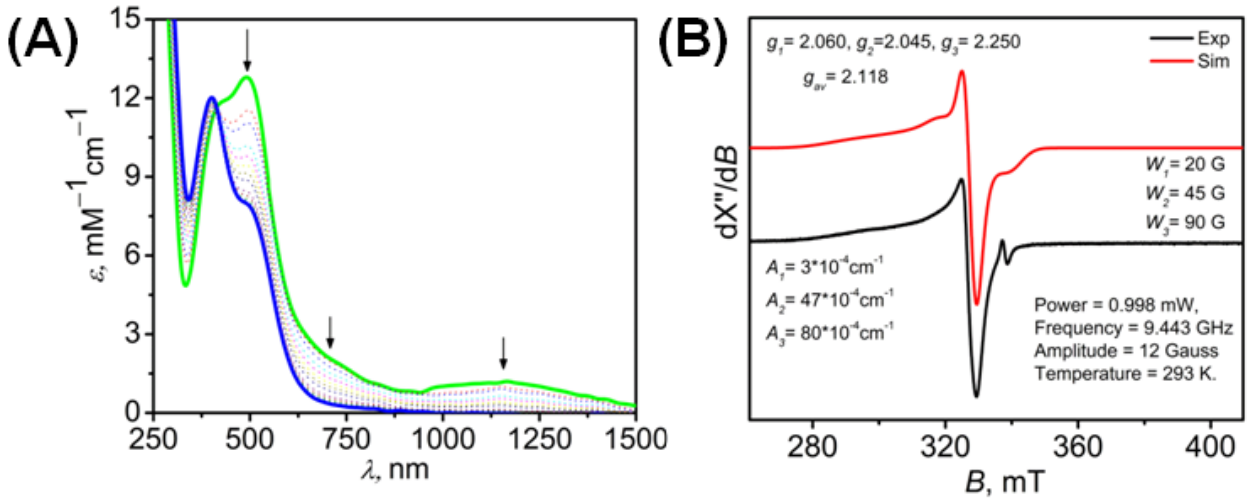

Figure 5.8: *(A) Change in UV-Vis-NIR spectrum of complex **5B** during one-electron fixed potential coulometric oxidation and (B) Experimental and simulated X-band EPR spectra of the oxidized solution. X-band EPR was measured at; frequency = 9.44 GHz, modulation frequency = 100 kHz and amplitude = 12 G, temperature = 298 K.*

The spectroelectrochemical studies for the one-electron oxidation and the first one-electron reduction processes of complex **5B** in order to discern the redox active centers that participate in the processes. In the fixed potential coulometric one-electron oxidation, the intensity of the band at 490 nm diminished, while, the band at 420 nm remained almost unaffected (**Table 5.8A**). The MLCT band at 1160 nm almost vanished (**Figure 5.8A**). This implied the depletion of the Cu(I) species concentration and generation of the corresponding Cu(II) species. To buttress the formation of the Cu(II) species, X-band EPR spectrum of the oxidized solution was measured and shown in **Figure 5.8B**. The EPR spectrum was typical for a Cu(II) species with an unpaired electron residing at $d_x^2-_y^2$ orbital. Simulation to the experimental result provided: g_x = 2.045, g_y = 2.060 and g_z = 2.250; g_{av} = 2.118; ^{Cu}A (3, 47, 80) × 10^{-4} cm^{-1}.

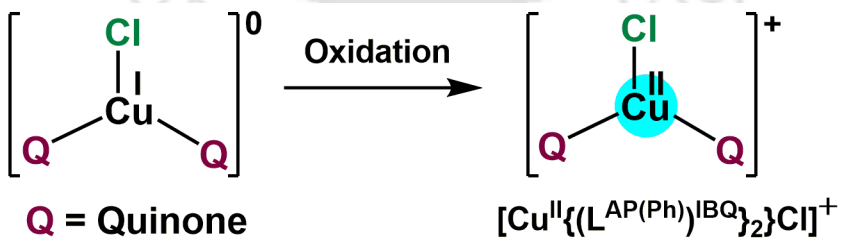

Scheme 5.5: *Formation of complex [**5B**]$^{1+}$ from complex **5B** by coulometric one-electron oxidation.*

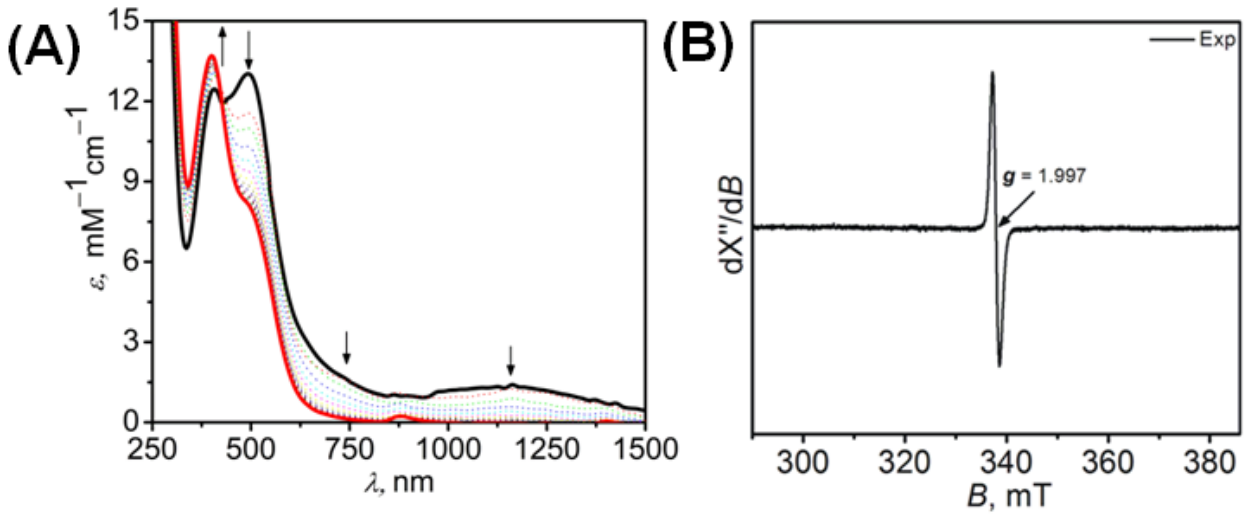

Figure 5.9: *(A) Change in UV-Vis-NIR spectrum of complex **5B** during one-electron fixed potential coulometric reduction and (B) Experimental X-band EPR spectra of the reduced solution. X-band EPR was measured at; frequency = 9.44 GHz, modulation frequency = 100 kHz and amplitude = 50 G, temperature = 298 K.*

During the coulometric one-electron reduction of complex **5B** the ILCT band at 490 nm decreases in intensity gradually, while band at 420 nm increases (**Figure 5.9A**). It has previously been reported that Cu(I)-iminosemiquinone (TPQ-radical) species in AOase absorbs at 463 and 434 nm.[4g-j] Thus, the increase of the band ascribed to the formation of a Cu(I)-iminosemiquinone species by the one-electron reduction of a Cu(I)-coordinated iminoquinone moiety. The depletion of 1160 nm band also supported the reduction of iminoquinone unit to iminosemiquinone unit. X-band EPR spectrum of the solution, obtained after the one-electron reduction, exhibited an isotropic signal at g = 1.997 (**Figure 5.9B**). This supported $\{Cu^{II}[L^{ISQ(Ph)}][L^{Ap(Ph)}]Cl\}^{-}$ composition of complex $[\mathbf{5B}]^{1-}$ (**Scheme 5.6**).

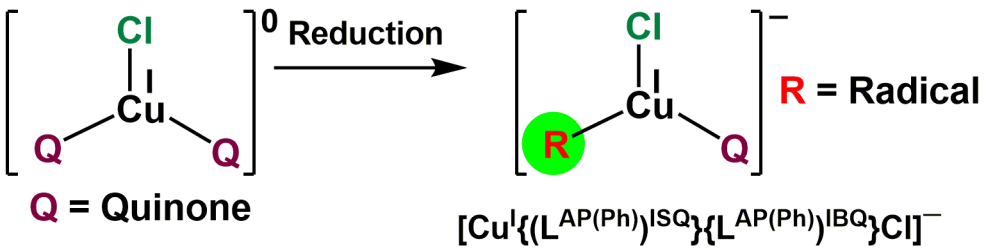

Scheme 5.6: *Formation of complex $[\mathbf{5B}]^{1-}$ from complex **5B** by coulometric one-electron reduction.*

Table 5.8: *Electronic absorption data for species [5A]$^{1+}$ and [5B]$^{1-}$.*

Complex	λ_{max}, nm (ε, $M^{-1}cm^{-1}$)
[5B]$^{1+}$	486(8000), 402(12000)
[5B]$^{1-}$	488(8150), 402(13700)

5.4 Synthesis and Characterization of Complexes 5C and 5D

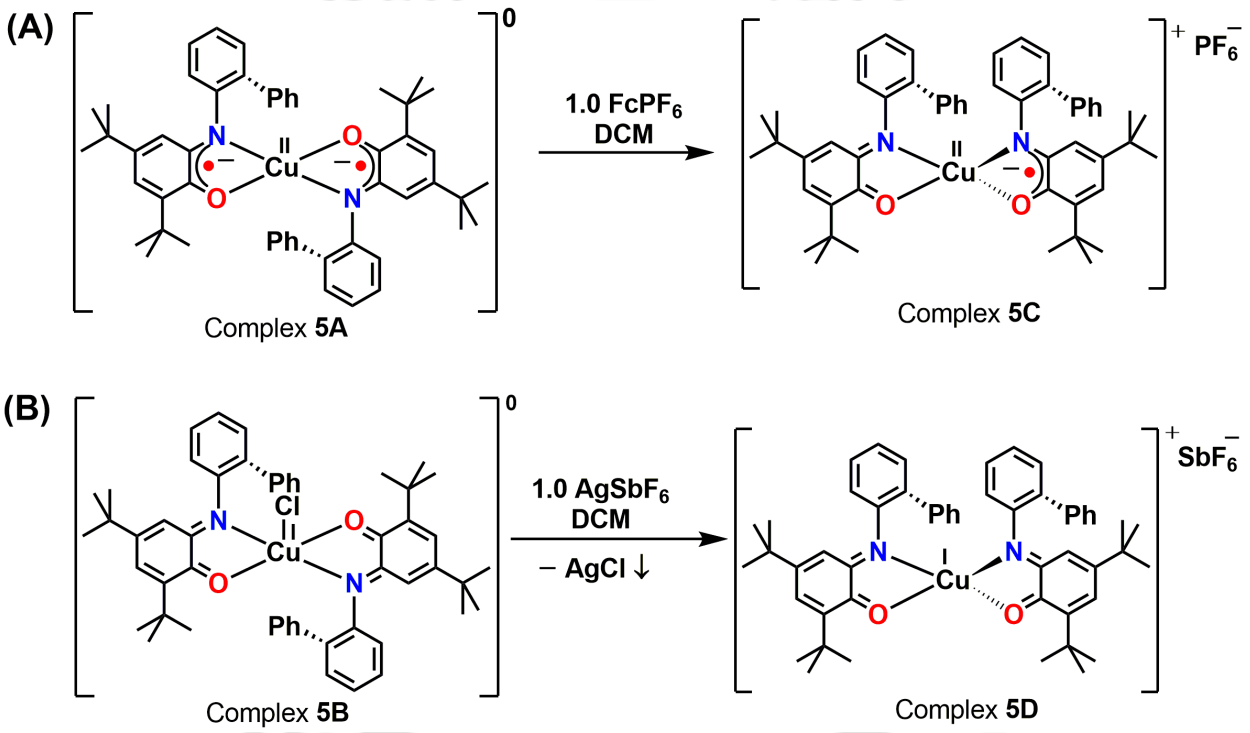

Scheme 5.7: *Synthetic route for the preparation of (A) complex 5C and (B) complex 5D.*

When complex **5A** was treated with an equivalent of ferrocenium hexafluorophosphate ($FcPF_6$) as the oxidant, it provide a four-coordinate Cu(II)-complex [$Cu^{II}(L^{ISQ(Ph)})(L^{IBQ(Ph)})$]$PF_6$ (**5C**) in 45% yield. On the other hand, complex **5D** was synthesized from complex **5B** by employing an equivalent amount of $AgSbF_6$ with subsequent removal of the axial chloride ion as AgCl was precipitate out (**Scheme 5.7**).

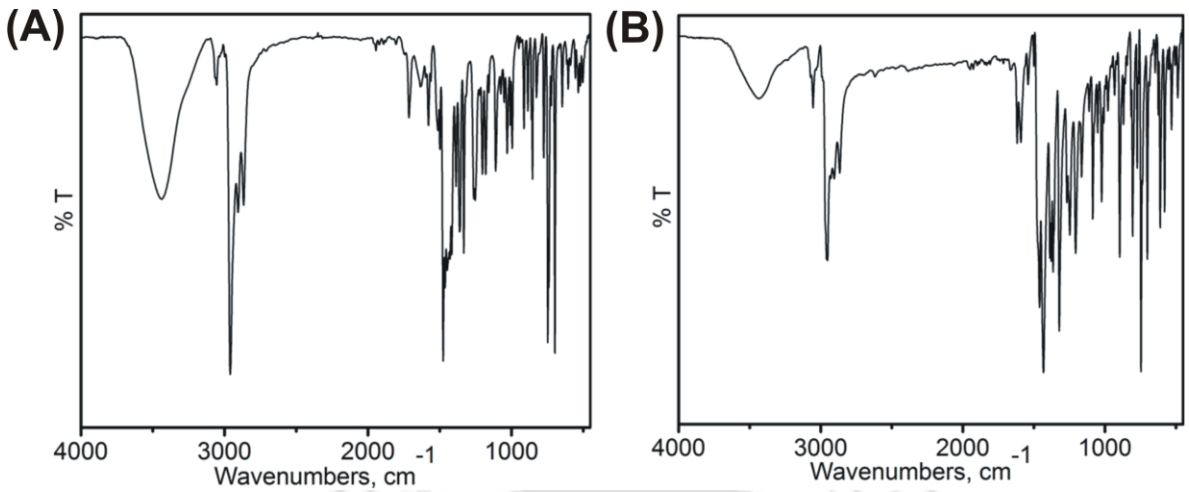

Figure 5.10: ***(A)*** *FT-IR spectrum of complex* ***5C*** ***(B)*** *FT-IR spectrum of complex* ***5D***.

The infrared spectrum of complex **5C** (**Figure 5.10A**) was recorded on KBr pallet at 300 K. A weak band corresponding to $\nu(C_{Ar}–H)$ [Ar stands for aromatic] stretch was observed at 3062 cm^{-1}. Three bands at 2955, 2915 and 2871 cm^{-1} were attributed for asymmetric, overtone and symmetric bands of ν(C–H) stretches of *tert*–butyl groups, respectively.[9a-d] The band at 1635 cm^{-1} appeared for ν(C⋯N) stretching. In addition to this, the ν(C–H) bending vibration of methyl groups appeared at 1469 and 1368 cm^{-1}. On the other hand FT-IR spectrum of the complex **5D** (**Figure 5.10B**) showed no stretching bands for ν(O–H) and ν(N–H) bands, additionally, the presence of the *tert*-butyl containing ν(C–H) stretching frequencies at 2961, 2909 and 2871 cm^{-1} respectively, [9a-d] indicated that the ligand bound with Cu ion where O–H and N–H were deprotonated. The band at 1638 cm^{-1} and 1622 cm^{-1} were attributed for ν(C=O) the ν(C⋯N) stretching. In addition to In addition to that, the ν(C–H) bending vibration of methyl groups appeared at 1473 and 1377 cm^{-1}. [9f-g]

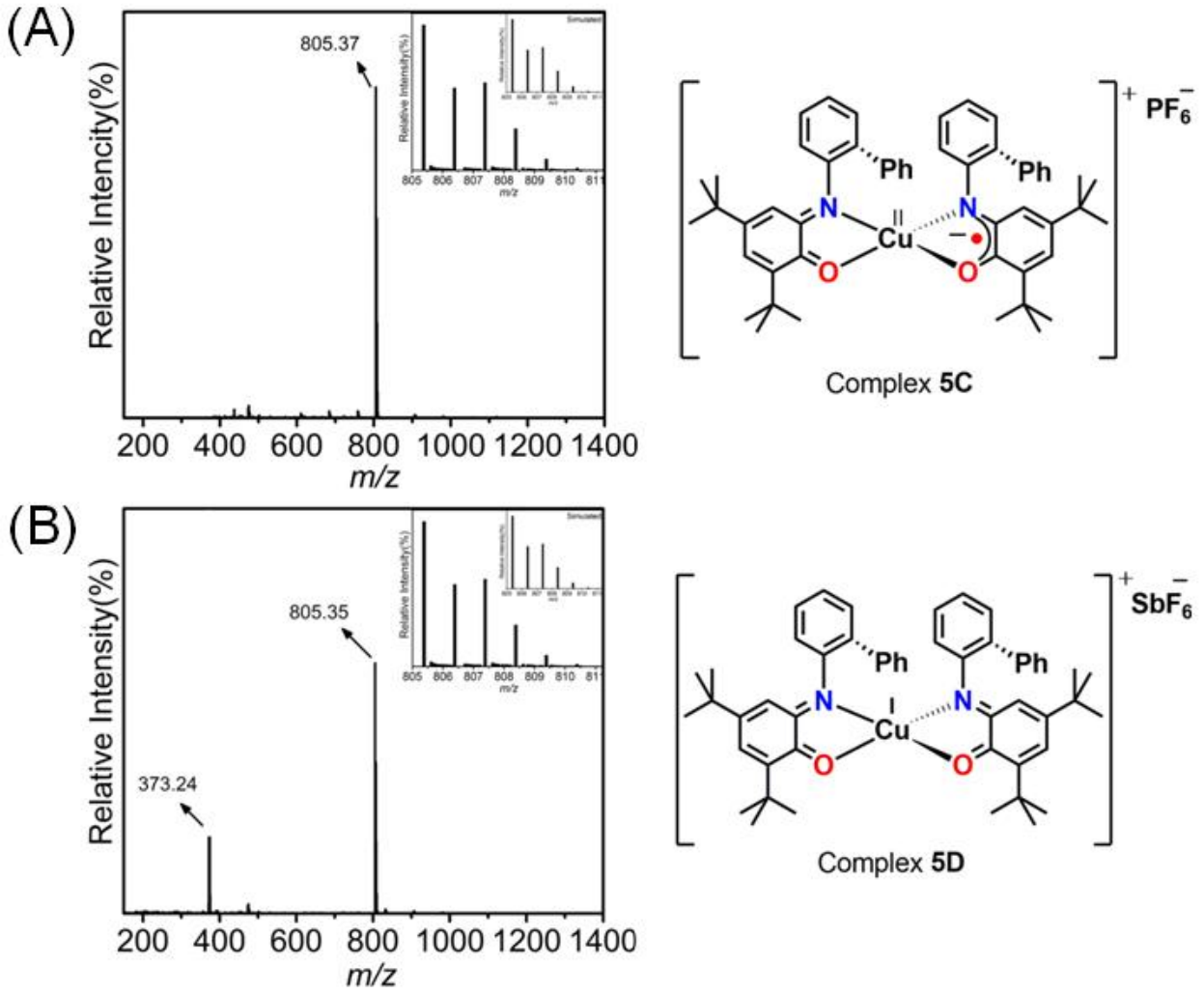

Figure 5.11: *ESI-mass spectra of (A) for **5C**, (B) for **5D**; experimental and simulated isotope distribution pattern (inset).*

Electrospray ionization mass spectra (ESI-MS) were measured in acetonitrile in positive mode. A 100% molecular ion peaks at *m/z* = 805.37 appeared for the complex **5C** (corresponded to $[M]^+$); M = molecular mass (**Figure 5.11A**). On the other hand, a 100% molecular ion peak at *m/z* = 840.35 was found for the complex **5D** (corresponded to $[M]^+$) (**Figure 5.11A**). Isotope distribution pattern examinations of the observed mass peaks revealed the composition of $\mathbf{C_{52}H_{58}CuN_2O_2}$, for **5A**; $\mathbf{[C_{52}H_{58}CuN_2O_2]^+}$, for **5D** (**Figure 5.11**).

The X-ray single crystal measurement of complex **5C** was performed at 293(2) K. The complex crystallizes in the triclinic space group '*P-1*'. The ORTEP molecular structure (cation unit) with atom labeling scheme is presented in **Figure 5.12**. Selected bond distances and bond angles are presented in **Table 5.9**.

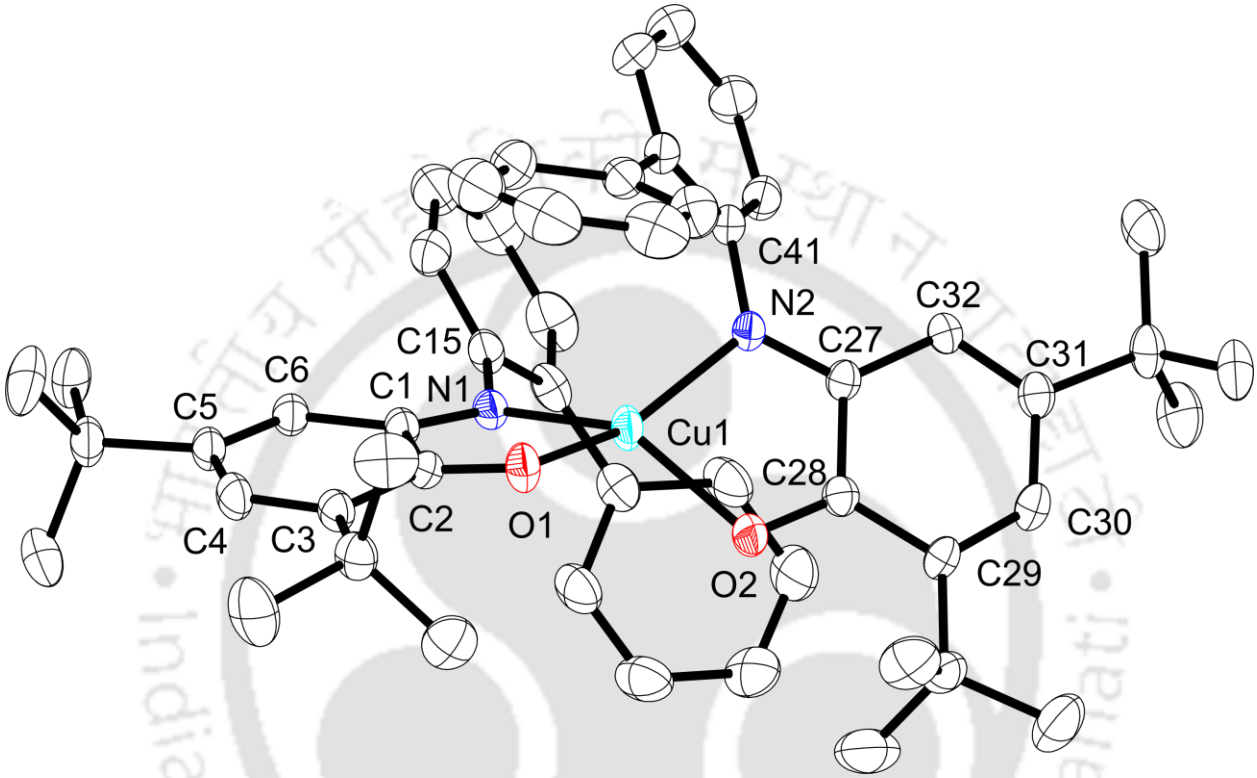

Figure 5.12: *ORTEP diagram of the cation unit of complex* ***5C****; thermal ellipsoids were drown at 30% probability level. Solvent molecules, anion* $[PF_6]^-$ *and H-atoms are omitted for the clarity.*

In the complex **5C**, the central copper atom (Cu1) was four coordinate. The coordination sites were occupied by two N atoms and two O atoms from the two ligand units. Unlike the parent four-coordinate complex **5A**, the two coordinating N and O atoms were adjacent (*cis*-) to each other in complex **5C**. The decrease in ligand field strength upon oxidation of the coordinating ligands (*vide infra*) and steric effect exerted by the two *ortho*- phenyl substituents were attributed to the structural dissimilarity. The geometry around the Cu1 atom was in between of square planar and tetrahedral [τ_4 = 0.54; τ_4 = 0 for square planar and τ_4 = 1.0 for tetrahedral]. The sum of angles (Table 2) around the Cu1 atom ($\sum Cu_\alpha$) was 668. 3° ($\sum Cu_\alpha$ = 720 ° and 657 °

for a perfect square planar and a perfect tetrahedral system, respectively) and further supported the deviation.

Complex **5C** was obtained by one-electron oxidation of complex **5A**. The oxidation could be either metal center or ligand center. The oxidation of Cu(II) to Cu(III) would shorten the Cu–N/O bonds, while an elongation would persist in case of ligand-based oxidation. In complex **5C**, the Cu–N/O = 1.963(3)/2.000(3) bond distances were longer compared to the average Cu–N/O = 1.929(1)/1.906(1) bond distances observed in complex **5A**.[8b] Therefore, ligand-based oxidation was warranted by the structural analysis. The *tert*-butyl groups-containing C_6 rings exhibited quinoid-type distortion as expected for the ligand-based oxidation. In both the ligands C_{Ph}–C_{Ph} bond distances (**Table 5.9**) of the rings were almost same. The C1–N1 = 1.314(4) Å, C27–N2 = 1.312(4) Å, C2–O1 = 1.249(4) Å and C28–O2 = 1.246(4) Å bond distances were longer than previously reported C_{Ph}–N_{Ph}, and C_{Ph}–O_{Ph} bond distances observed in an iminoquinone moiety, and shorter than the bond distances found in a iminosemiquinone moiety. These features emphasized a complete delocalization of the radical over the iminosemiquinone and iminoquinone moieties.

Table 5.9: Selected bond distances (Å) and bond angles (°) for complex **5C** (at 293 K).

Cu1–N1	1.961(3)	C3–C4	1.360(5)
Cu1–N2	1.965(3)	C4–C5	1.437(6)
Cu1–O1	1.999(2)	C5–C6	1.354(5)
Cu1–O2	2.002(3)	C6–C1	1.431(5)
O1–C2	1.249(4)	C27–C28	1.494(5)
O2–C28	1.246(4)	C28–C29	1.454(5)
N2–C27	1.312(4)	C29–C30	1.367(5)
N1–C1	1.314(4)	C30–C31	1.445(5)
C1–C2	1.496(5)	C31–C32	1.352(5)
C2–C3	1.459(5)	C32–C27	1.435(4)
N1–Cu1–N2	116.66(12)	C2–O1–Cu1	112.9(2)
O1–Cu1–O2	104.71(11)	C28–O2–Cu1	113.2(2)
N1–Cu1–O1	81.73(10)	C1–N1–Cu1	114.3(2)
N2–Cu1–O1	144.23(12)	C15–N1–Cu1	122.0(2)
N1–Cu1–O2	139.59(12)	C27–N2–Cu1	114.2(2)
N2–Cu1–O2	81.40(11)	C41–N2–Cu1	120.8(2)

Single crystal of complex **5D** suitable for X-ray diffraction measurement was obtained by the slow evaporation of a CH_2Cl_2/MeOH (3:1) solution of the complex. The diffraction measurement was performed at 100(2) K. The complex crystallized in the trigonal space group '*$P3_121$*'. The molecular structure (cation unit) with atom labelling scheme is depicted in **Figure 5.13**. Selected bond distances and bond angles are given in **Table 5.10**.

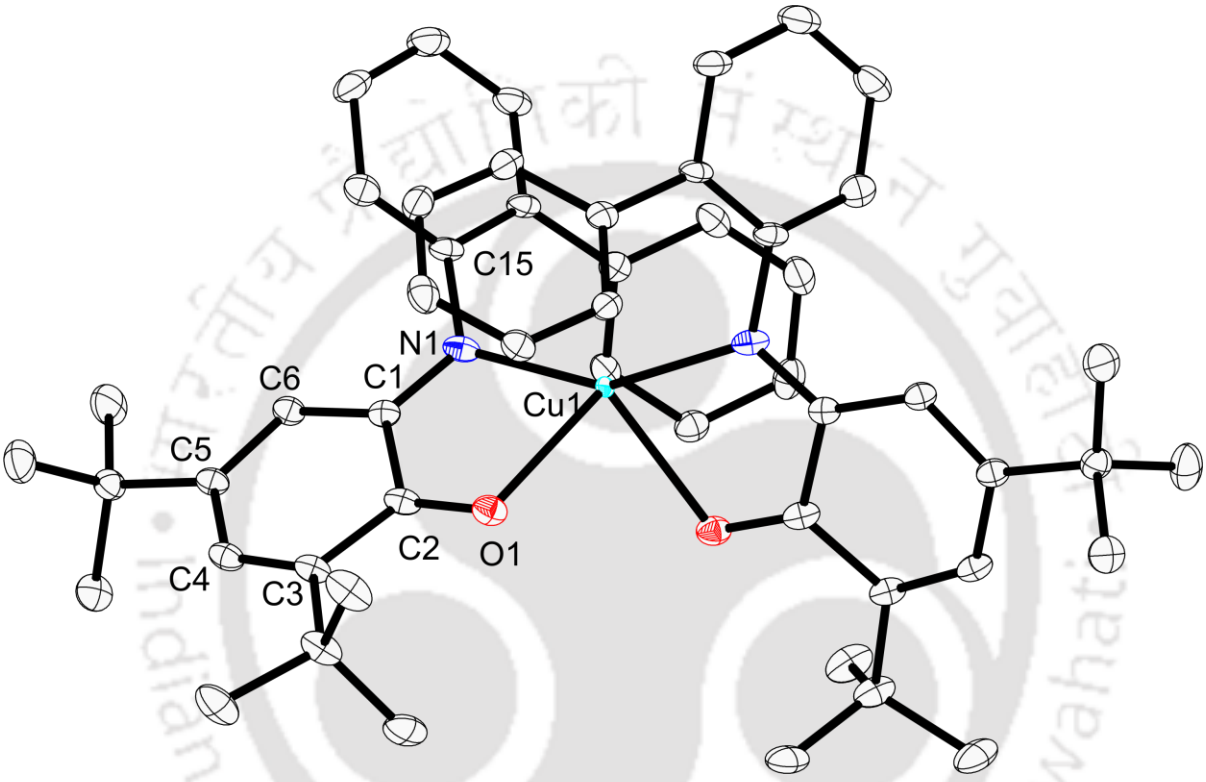

Figure 5.13: *ORTEP diagram of the cation unit of complex **5D**; thermal ellipsoids were drown at 30% probability level. H-atoms and the anion $[SbF_6]^-$ are omitted for the shake of clarity.*

In complex **5D**, the central Cu1 atom was four coordinate (τ_4 = 0.56). The coordination sites were occupied by the two N and two O atoms from the two bidentate ligands. The Cu1–N1 = 2.020(4) Å and Cu1–O1 = 2.352(4) Å bond distances were consistent with the low oxidation state of the central Cu1 atom, *i.e.*, Cu(I), and higher oxidation state of the coordination ligands ($[L^{IBQ(Ph)}]^0$) as observed in complex **5B**. In the complex, the C1–N1 = 1.298(5) Å and C2–O1 = 1.228(4) Å bond distances were almost same as the bond distances found in the five-coordinate congener, complex **5B**. Thus, no change in oxidation state of the central metal ion as well as the coordinating ligands was noticed upon the geometrical change.

Table 5.10: Selected bond distances (Å) and bond angles (°) for complex **5D** (at 100 K).

Cu1–N1	2.020(4)	C3–C4	1.344(6)
Cu1–O1	2.352(3)	C4–C5	1.457(6)
N1–C1	1.298(5)	C5–C6	1.360(6)
O1–C2	1.228(5)	C6–C1	1.441(6)
C1–C2	1.514(6)	N1–C15	1.427(5)
C3–C2	1.478(6)		
N1–Cu1–N1^{i}	149.3(2)	C1–N1–Cu1	120.5(3)
O1–Cu1–O1^{i}	84.90(15)	C15–N1–Cu1	118.9(3)
N1–Cu1–O1^{i}	131.71(13)	C2–O1–Cu1	110.3(3)
N1–Cu1–O1	74.05(12)	C1–N1–C15	120.6(4)

The electronic absorption spectra of complex **5C** and **5D** were recorded in HPLC grade CH_2Cl_2 at room temperature and depicted in **Figure 5.14**. The electronic absorption bands along with corresponding absorption coefficient values were summarized in **Table 5.11**.

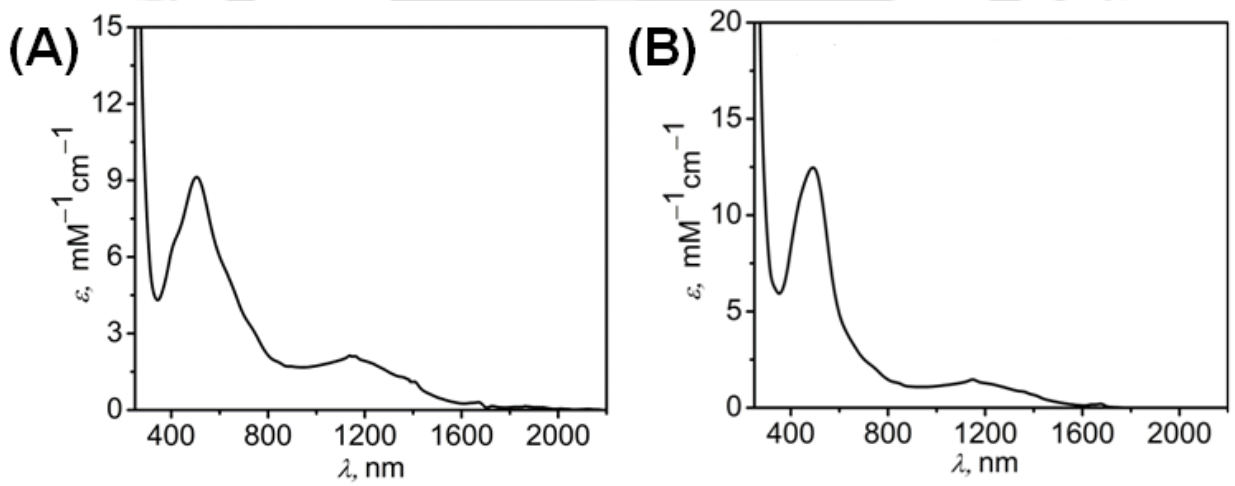

Figure 5.14: *UV-vis/NIR spectrum of (A) complex **5C** and (B) complex **5D** in CH_2Cl_2 at 25 °C.*

A broad band at 1144 nm (ε = 2050 $M^{-1}cm^{-1}$) appeared in the UV-vis/NIR spectrum of complex **5C**. The band arose possibly due to combined ligand-centered intervalence $[L^{ISQ(Ph)}]^{1-}$-to-$[L^{IBQ(Ph)}]^{0}$ charge-transfer (IVLLCT) and metal-to-ligand charge-transfer (MLCT) transitions.[7d] The π-to-π* intraligand (ILCT) charge-transfer transitions of iminoquinone moieties were observed at λ_{max} = 500 nm (ε = 9150 $M^{-1}cm^{-1}$) and 407 nm (shoulder, ε = 6500

$M^{-1}cm^{-1}$). [7i] In complex **5D**, a broad absorption manifold centered at 1160 nm (ε = 1350 $M^{-1}cm^{-1}$) was present. The low-energy band has been attributed to Cu(I)-to-iminoquinone MLCT transition. The strong bands at λ_{max} = 490 nm (ε = 12500 $M^{-1}cm^{-1}$) and λ_{max} = 440 nm (ε = 11200 $M^{-1}cm^{-1}$) were due to π-to-π* intraligand (ILCT) charge-transfer transitions of iminoquinone moieties.[11]

Table 5.11: *UV-vis/NIR spectral data for* ***5C****, and* ***5D****.*

Complex	λ_{max}, nm (ε, $M^{-1}cm^{-1}$)
5C	1144(2050), 500(9150), 407(6500)
5D	1160(1350), 733(2200), 490(12500), 440(11200)

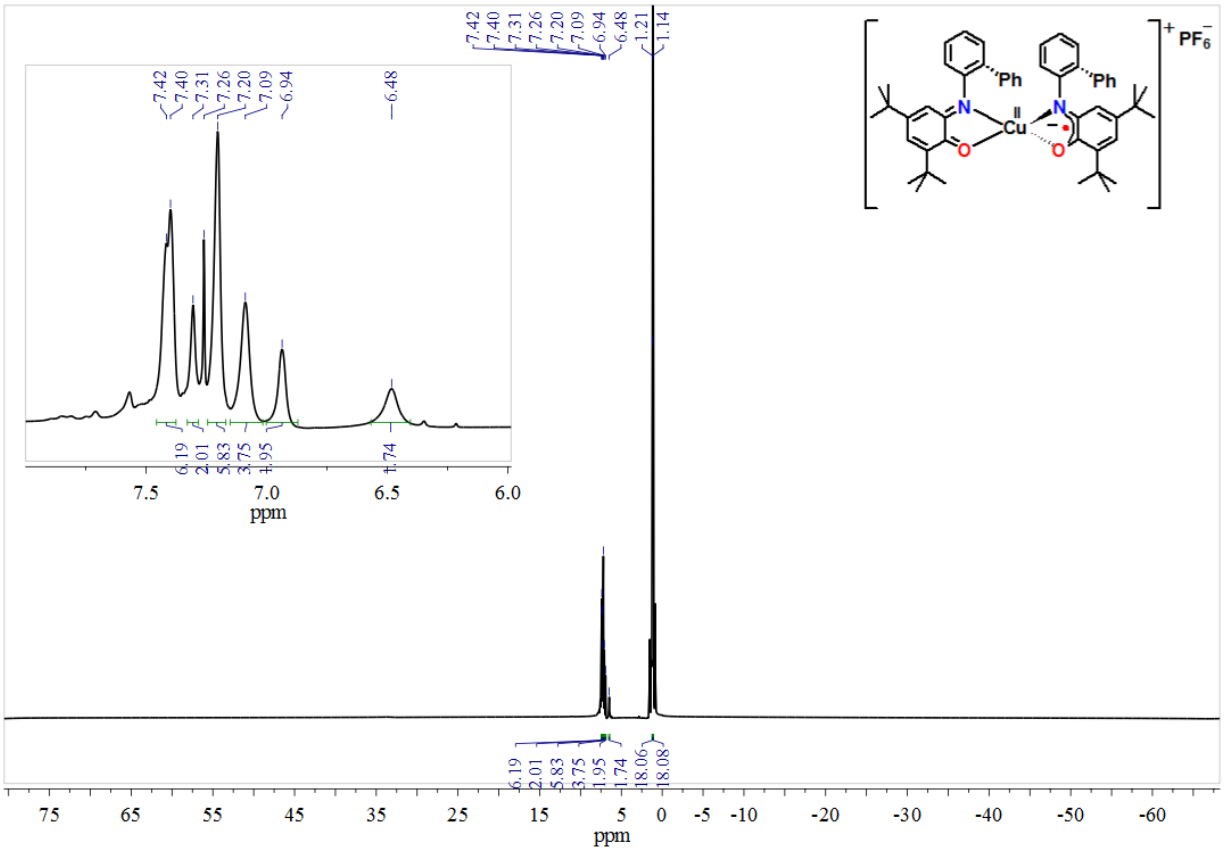

Figure 5.15: *^{1}H-NMR spectrum of complex* ***5C*** *in $CDCl_3$.*

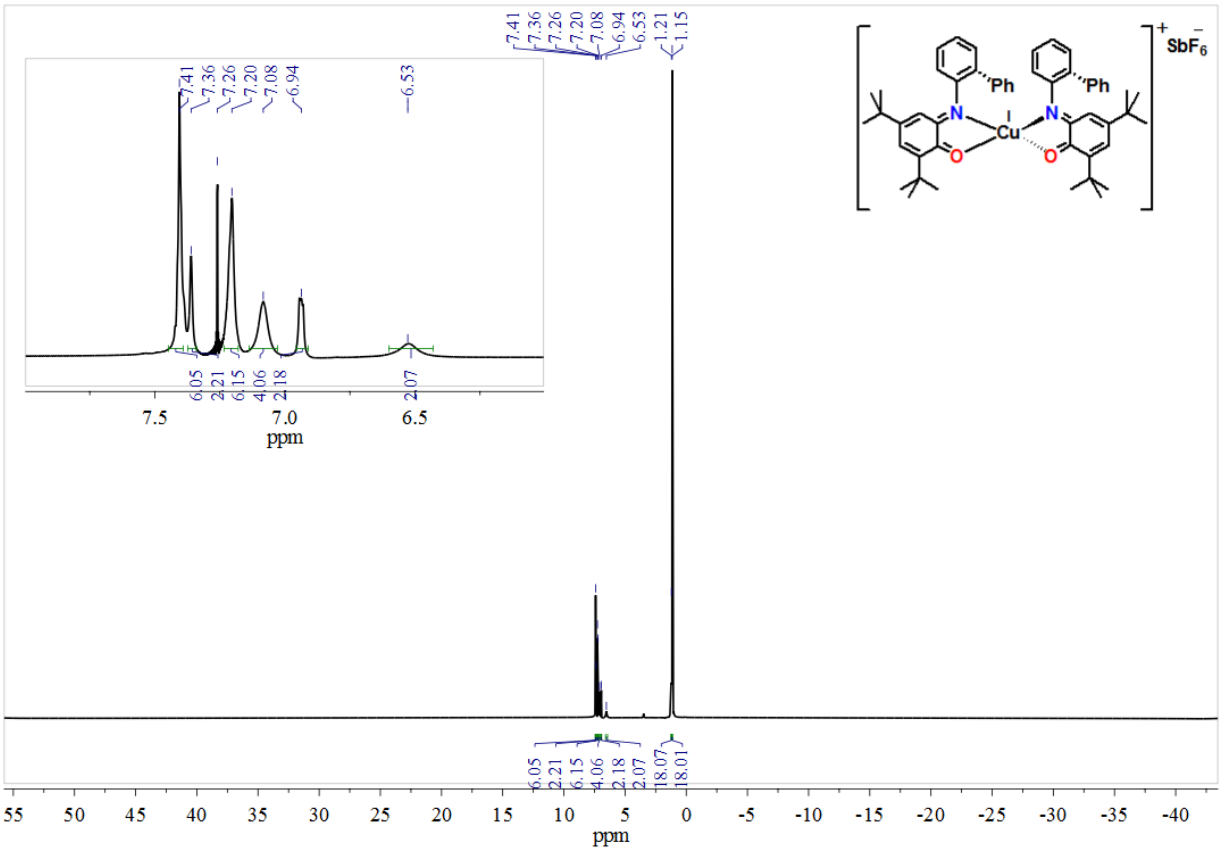

Figure 5.16. *^{1}H-NMR spectrum of complex **5D** in $CDCl_3$.*

No unpaired electron was present in both complex **5C** and complex **5D**. Thus, both of them were diamagnetic. Complex **5C** was consisted of two unpaired electrons: one electron was residing on Cu(II) [S = 1/2, $3d^9$] and the other electron was the ligand-centered radical (S = 1/2). A ferromagnetic coupling between the two S = 1/2 spins would provide S_t = 1 ground state, while a diamagnetic ground state with S_t = 0 would result by an antiferromagnetic coupling between the two paramagnetic centers. Indeed, complex **5C** was diamagnetic owing antiferromagnetic coupling between the spins as evident by ^{1}H-NMR measurements (**Figure 5.15** and **Figure 5.16**)

The electrochemical behavior of complexes **5C** and **5D** were investigated by cyclic voltametry. Cyclic voltammograms (CVs) of the complexes (1 mM) were being recorded in CH_2Cl_2 solutions containing 0.10 M [(^{n}Bu)$_4$N]ClO_4 as supporting electrolyte at a glassy carbon working electrode, a platinum wire counter electrode, and a Ag/AgCl reference electrode. The experiments were performed at different scan rates. Ferrocene was used as an internal standard, and potentials are referenced *versus* the ferrocenium/ferrocene (Fc^+/Fc) couple.

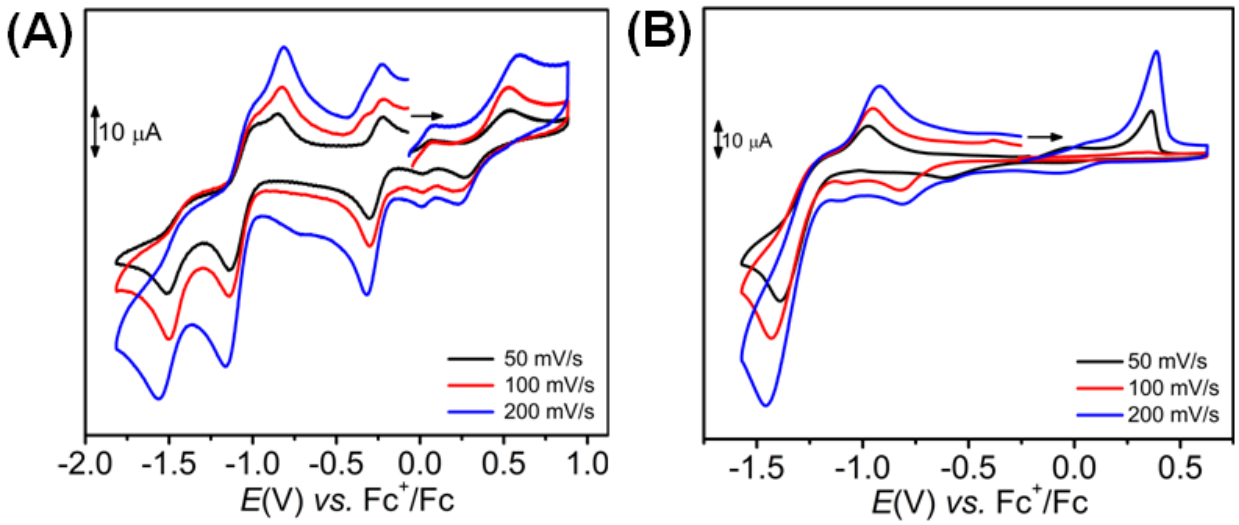

Figure 5.17: *Cyclic voltagrams of (A) complex* ***5C*** *and* ***(B)*** *complex* ***5D*** *measured at 50, 100, and 200 mV/s.*

One one-electron oxidation and three one-electron reduction processes were observed in the CV of complex **5C** (**Figure 5.17A**). The oxidation process occurred at 0.408 mV, which was 0.100 V lower compared to the parent complex **5A**. This difference was attributed to the structural anomaly, *i.e.*, *cis*-(**5C**) *vs. trans*-(**5A**) arrangement of the coordinating sites (parenthesis refers the complex). The reduction potentials were expectedly analogous to complex **5A** (**Table 5.12**). In the CV of complex **5D** (**Figure 5.17B**) irreversible electron transfer processes were noticed. The CV measurement at 100 mv/s scan rate revealed an oxidation at 0.360 V, and two reduction processes at -0.600 V and -1.390 V (**Figure 5.17B**). The peak positions were scan rate dependent.

Table 5.12: Voltammetric redox processes for the complex **5C** and **5D**.

Complex	$E^{0,a}$ V, (ΔEp, mV)			
	$E_{1/2}^{red2}$	$E_{1/2}^{red1}$	$E_{1/2}^{ox1}$	$E_{1/2}^{ox2}$
5C	–1.494 (148)	–1.080 (160)	–0.264 (80)	0.408 (348)
5D	–1.390 (84)	–0.600	0.360	–

[a]E^0 values recorded at scan rates of 100 mV/s and referenced to the Fc^+/Fc couple.

5.5 Reactivity Study of Complex 5B, 5C and 5D with KO_2

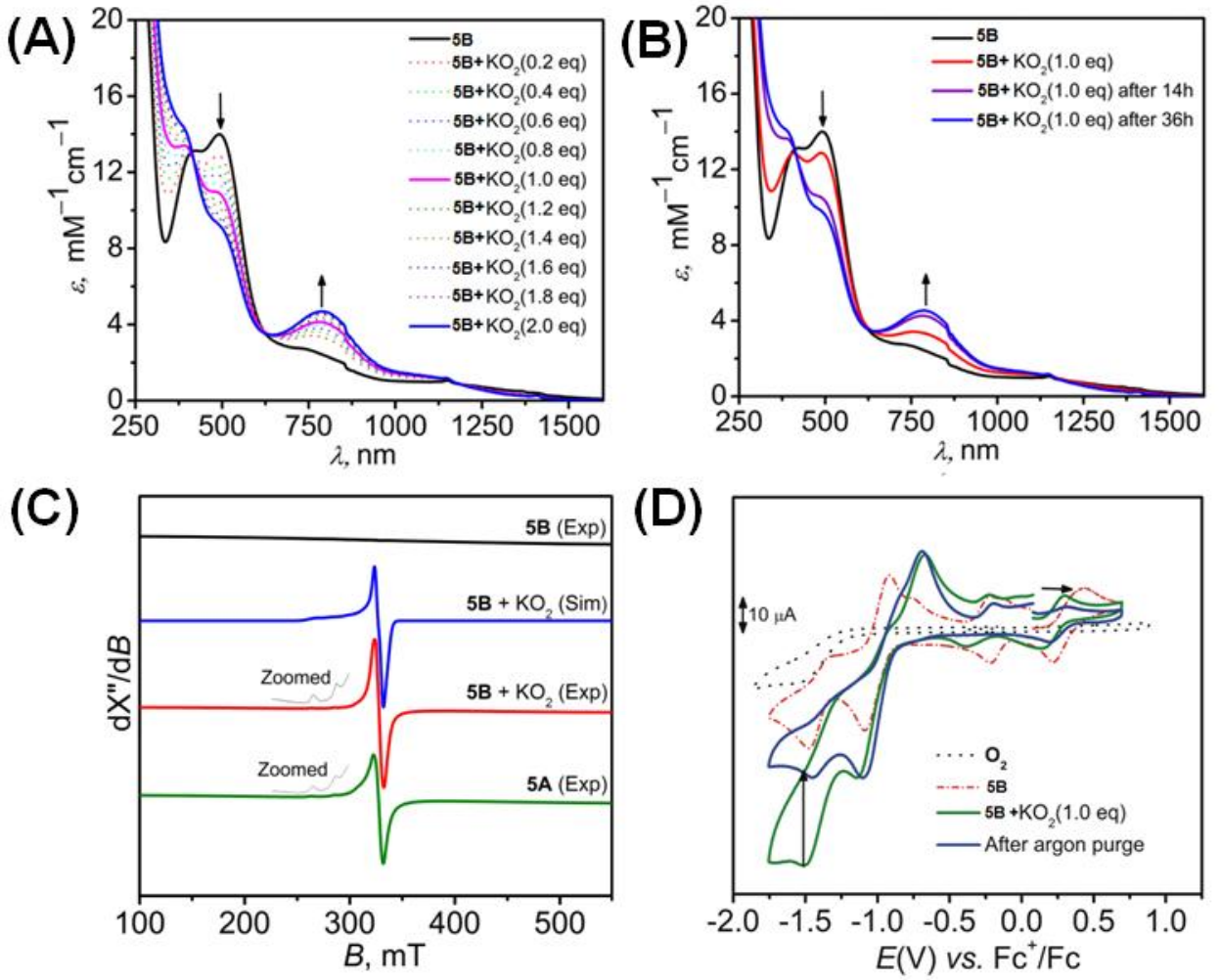

Figure 5.18: *(A) Change in UV-Vis-NIR spectrum of complex 5B during the sequential addition of KO_2, (B) One-step addition of stoichiometric amount of KO_2 and the time-dependent spectral changes; (C) Experimental and simulated X-band EPR spectra of CH_2Cl_2 solutions of 5A, 5B and 5B + KO_2; and (D) detection of O_2 gas by CV measurements. X-band EPR was measured at; frequency = 9.143 (5A), 9.143(5B) GHz, modulation frequency = 100 kHz and amplitude = 2 G, temperature = 298 K (parenthesis indicates the complex).*

Complex **5B** was comprised of a Cu(I) ion and two coordinated-iminoquinone moieties. The synthesis of the complex was carried out under aerial atmosphere. This indicated that the complex is reluctant to aerial oxygen, *i.e.*, no oxidation of Cu(I) occurred. Furthermore, purging of O_2 to the CH_2Cl_2 solution of complex **5B** did not provide any appreciable UV-vis/NIR spectral changes. However, the complex reacted with KO_2, albeit slowly. In the presence of KO_2,

i.e., superoxide radical anion, a new band at 785 nm appeared and 1160 nm band shifted to 1035 nm (**Figure 5.18A**) in due course. These UV-vis/NIR spectral changes corresponded to the generation of complex **5A**. X-band EPR spectrum measurement of the reaction solution provided Cu(II)-centered spectrum that also resembled with the EPR spectrum of complex **5A** (**Figure 5.18C**) and thus, concurred with the formation of complex **5A**. The generation of molecular oxygen during the process was consolidated by CV measurements (**Figure 5.18D**). The reduction peak of the liberated molecular oxygen appeared at –1.482 V. Upon purging of argon gas through the solution, the concentration of oxygen gas diminished as evident by the reduction of current at the potential (**Figure 5.18D**).

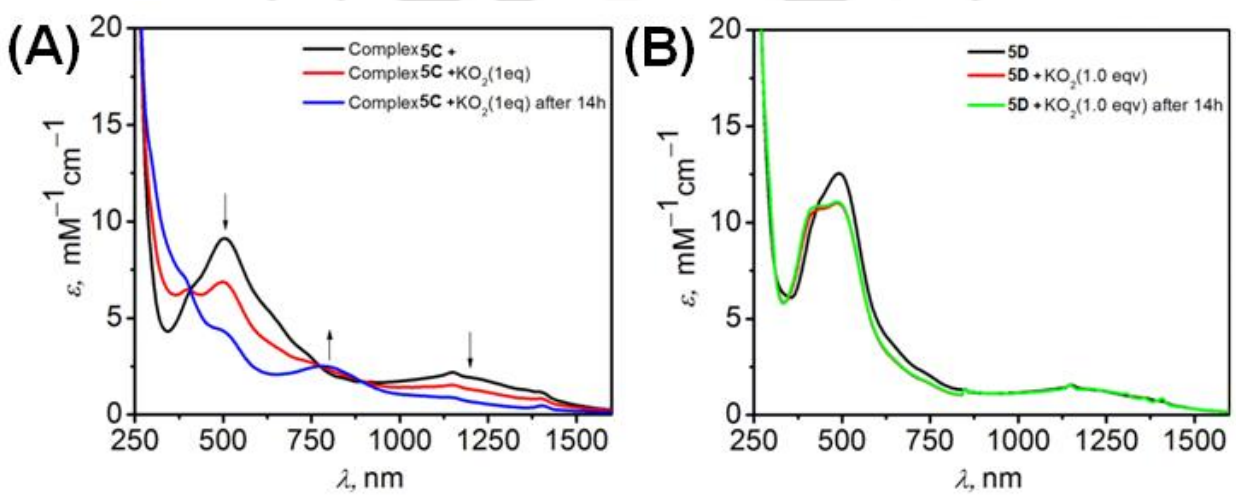

Figure 5.19: *Change in UV-vis/NIR spectrum of CH_2Cl_2 solution of (A) complex **5C** and (B) complex **5D**, in the presence of KO_2.*

Unlike complex **5B**, the congener four-coordinate complex **5D** did not react with KO_2 (**Figure 5.19B**). Interestingly, despite structural similarity with complex **5D** (τ_4 = 0.56, twist angle between two NO coordinating units = 61.4 °), complex **5C** (τ_4 = 0.54, twist angle between two NO coordinating units = 56.4 °) reacted with KO_2 (**Figure 5.19A**) and produced complex **5A** and molecular oxygen. However, the reaction was sluggish. Hence, the geometry as well as oxidation state of copper ion and the coordinated non-innocent ligand units have been found as crucial for the occurrence and the effectiveness of the reaction.

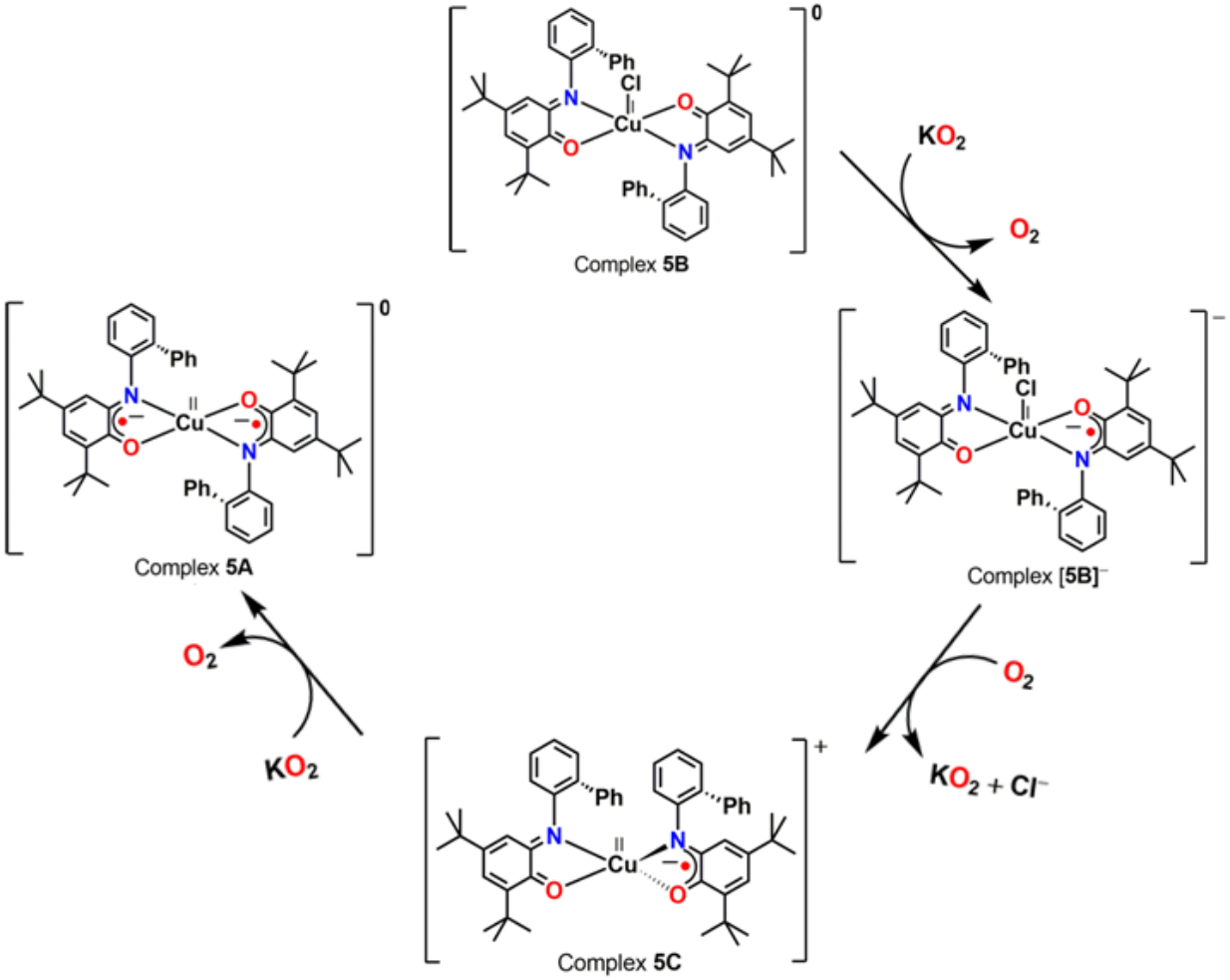

Scheme 5.8: *Proposed mechanism for formation of complex **5A** from reaction of complex **5B** with KO_2.*

Herein, we propose that complex **5B** reacted with KO_2 and produced $[\mathbf{5B}]^{1-}$, which instantaneously underwent metal-centered Cu(I)-to-Cu(II) oxidation in the presence of the generated molecular oxygen and provided complex **5C** with the removal of the axial chloride ion (**Scheme 5.8**). The increase of ligand-based negative character possibly favored the removal of the chloride ion. Finally, KO_2 reduced complex **5C** to complex **5A** with concomitant production of molecular oxygen.

5.6 Conclusions

To conclude, we have successfully synthesis of a five-coordinate mononuclear neutral Cu(I)-bis(iminoquinone)Cl complex (**5B**) by the $CuCl_2 \bullet 2H_2O$ mediated inner sphere one-electron oxidation of Cu(II)-bis(iminosemiquinone) complex (**5A**). In the process, the formed five-coordinate Cu(II)-(iminosemiquinone)(iminoquinone)Cl intermediate underwent an electron transfer from ligand(iminosemiquinone)-to-metal[Cu(II)]. Conversely, the outer sphere one-electron oxidation of complex **5A** did not follow such electron transfer process and provided a four-coordinate Cu(II)-(iminosemiquinone)(iminoquinone) complex (**5C**). No iminosemiquinone-to-Cu(II) electron transfer in complex **5B** was further verified by the synthesis of four-coordinate Cu(I)-bis(iminoquinone) complex (**5D**). Thus, geometry-dependent electron transfer in a copper(II)-monoradical complex, where both the non-innocent ligand units were in different oxidation states, was being documented.

All the complexes were characterized by X-ray single-crystal diffraction measurements. A five-coordinate Cu(I) was previously been stabilized in a rigid macrocyclic glyoxime ligand with a *soft* CO as the axial ligand.[13] To the best of our knowledge, complex **5B** is the first isolated air-stable five-coordinate square pyramidal Cu(I) complex, which is being stabilized in the coordination environment comprising of two bidentate 2-iminobenzoquinone and a chloride ion. Cyclic voltammetry measurement of complex **5B** and **5C** established that the complexes can be the oxidized by an electron and reduced successively by three electrons. Spectro-electrochemical and X-band EPR experiments on complex **5B** emphasized that the solo oxidation wass Cu(I)-centered and the reductions were ligand-based. The oxidation and the reductions potential values found for complex **5C** were comparable to the ligand-based processes as observed in complex **5A**. Thus, the oxidation and the reductions processes occurred in complex **5C** have been assigned as ligand-based.

Finally, the investigation on the reactivity of the complexes on KO_2 revealed that complex **5B** and complex **5C** reacted slowly with KO_2 and oxidized it to molecular oxygen, which was identified by CV measurements. In the processes both the complexes were being reduced to complex **5A**. Complex **5D** was reluctant to KO_2.

References

1. (*a*) J. Stubbe and W.A.V.D. Donk, *Chem. Rev.*, 1998, **98**, 705; (*b*) J. W. Whittaker, *Chem. Rev.*, 2003, **103**, 2347; (*c*) R. H. Holm, P. Kennepohl and E. I. Solomon, *Chem. Rev.*, 1996, **96**, 2239; (*d*) L. Q. Hatcher and K. D. Karlin, *J. Biol. Inorg. Chem.*, 2004, **9**, 669; (*e*) N. Kitajima and Y. Moro-oka, *Chem. Rev.*, 1994, **94**, 737; (*f*) M. A. Kopf and Karlin, K. D. in Biomimetic Oxidations, ed. B. Muenier, Imperial College Press, London, U.K. 2000, *ch. 7*; (*g*) P. Chaudhuri and K. Wieghardt, *Wiley: Hoboken, NJ*, 2001.

2. (*a*) N. Ito, S. E. V. Phillips, C. Stevens, Z. B. Ogel, M. J. McPherson, J. N. Keen, K. D. S. Yadav and P. F. Knowles, *Nature*, 1991, **350**, 87; (*b*) N. Ito, S. E. V. Phillips, K. D. S. Yadav and P. F. Knowles, *J. Mol. Biol.*, 1994, **238**, 794; (*c*) Y. Wang and T. D. P. Stack, *J. Am. Chem. Soc.*, 1996, **118**, 13097; (*d*) Y. Wang, J. L. DuBois, B. Hedman, K.O. Hodgson and T. D. P. Stack, *Science*, 1998, **279**, 537; (*e*) R. Banerjee, *Chem. Rev.*, 2003, **103**, 2081; (*f*) J. W. Whittaker, *Chem. Rev.*, 2003, **103**, 2347; (*g*) L. Benisvy, A. J. Blake, D. Collison, E. S. Davies, C. D. Garner, E. J. L. Mclnnes, J. McMaster, G. Whittaker and C. A. Wilson, *Chem. Commun.*, 2001, 1824; (*h*) A. Sokolowski, H. Leutbecher, T. Weyhermüller, R. Schnepf, E. Bothe, E. Bill, P. Hildebrandt and K. Wieghardt, *J. Biol. Inorg. Chem.*,1997, **2**, 444.

3. (*a*) P. J. Kersten, *Proc. Natl. Acad. Sci.* U S A 1990, **87**, 2936; (*b*) B. Kurek and P. J. Kersten, *Enzyme Microb. Technol.*, 1995, 17,751; (*c*) M. M. Whittaker, P.J. Kersten, N. Nakamura, J. Sanders-Loehr, E. S. Schweizer and J. W. Whittaker, *J. Biol. Chem.*, 1996, **271**, 681; (*d*) M. M. Whittaker, P. J. Kersten, D. Cullen and J. W. Whittaker, *J. Biol. Chem.*, 1999, **274**, 36226; (*e*) D. T. Yin, S. Urresti, M. Lafond, E. M. Johnston, F. Derikvand, L. Ciano, J. G. Berrin, B. Henrissat, P. H. Walton, G. J. Davies and H. Brumer, *Nat. Commun.*, 2015, **6**, 10197.

4. (*a*) D. M. Dooley, *J. Biol. Inorg. Chem.*, 1999, **4**, 1; (*b*) M. Mure, *Acc. Chem. Res.*, 2004, **37**, 131; (*c*) R. Prabhakar and P. E. M. Siegbahn, *J. Am. Chem. Soc.*, 2004, **126**, 3996; (*d*) J. E. Dove and J. P. Klinman, *Adv. Protein Chem.*, 2001, **58**, 141; (*e*) A. C. Rinaldi, C. M. Porcu, S. Oliva, N. Curreli, A. Rescigno, F. Sollai, A. Rinaldi, A. Finazzi-Agro and E. Sanjust, *Eur. J. Biochem.*, 1998, **251**, 91; (*f*) N. Nakamura, R. Matsuzaki, Y. H. Choi, K. Tanizawa and J. S. Loehr, *J. Biol. Chem.*, 1996, **271**, 4718; (*g*) E. M. Shepard, K. M. Okonski and D. M. Dooley, *Biochemistry*, 2008, **47**, 13907; (*h*) B. J. Johnson, E. T. Yukl, V. J. Klema, J.

P. Klinman and C. M. Wilmot, *J. Biol. Chem.*, 2013, **288**, 28409; (*i*) D. M. Dooley, M. A. McGuirl, D. E. Brown, P. N. Turowski, W. S. Mclntire and P. F. Knowles, *Nature*, 1991, **349**, 262; (*j*) R. Medda, A. Mura, S. Longu, R. Anedda, A. Padiglia, M. Casu and G. Floris, *Biochimie*, 2006, **88**, 827.

5. (*a*) R. W. Strange, S. Antonyuk, M. A. Hough, P. A. Doucette, J. S. Valentine, S. S. Hasnain, *J. Mol. Biol.*, 2006, **356**, 1152; (*b*) K. D. Carugo, A. Battistoni, M. T. Carri, F. Polticelli, A. Desideri, G. Rotilio, A. Coda, K. S. Willson and M. Bolognesi, *Acta Crystallogr., Sect. D: Biol. Crystallogr.*, 1996, **52**, 176; (*c*) J. A. Tainer, E. D. Getzoff, K. M. Beem, J. S. Richardson and D. C. Richardson, *J. Mol. Biol.*, 1982, **160**, 181; (*d*) R. M. Ellerby, D. E. Cabelli, J. A. Graden and J. S. Valentine, *J. Am. Chem. Soc.*, 1996, **118**, 6556; (*e*) H. Ohtsu and S. Fukuzumi, *Chem. –Eur. J.*, 2001, **7**, 4947.

6. (*a*) O. R. Luca and R. H. Crabtree, *Chem. Soc. Rev.*, 2013, **42**, 1440; (*b*) C. G. Pierpont and C. W. Lange, *In Progress in Inorganic Chemistry*; K. D. Karlin, Ed.; *Wiley: Hoboken, NJ*, 1994;
(*c*) S. Itoh, M. Taki, S. Takayama, S. Nagatomo, T. Kitagawa, N. Sakurada, R. Arakawa and S. Fukuzumi, *Angew. Chem., Int. Ed.*, 1999, **38**, 2774; (*d*) V. Lyaskovskyy and B. de Bruin, *ACS Catal.*, 2012, **2**, 270; (*e*) W. Kaim, *Eur. J. Inorg. Chem.*, 2012, **2012**, 343; (*f*) R. H. Holm and E. I. Solomon, *Chem. Rev.*, 2004, **104**, 347; (*g*) P. J. Chirik and K. Wieghardt, *Science*, 2010, **327**, 794; (*h*) P. Chaudhuri, K. Wieghardt, T. Weyhermüller, T. K. Paine, S. Mukherjee and C. Mukherjee, *Biol. Chem.*, 2005, **386**, 1023; (*i*) W. Kaim, *Dalton Trans.*, 2003, 761; (*j*) D. L. J. Broere, R. Plessius and J. I. van der Vlugt, *Coord. Soc. Rev.*, 2015, **44**, 6886; (*h*) R. C. Maji, P. P. Das, S. Mishra, A. Bhandari, M. Maji and A. K. Patra, *Dalton Trans.*, 2016, **45**, 11898.

7. (*a*) J. S. Thompson and J. C. Calabrese, *Inorg. Chem.*, 1985, **24**, 3167; (*b*) A. V. Piskunov, K. I. Pashanova, A. S. Bogomyakov, I. V. Smolyaninov, N. T. Berberova, and G. K. Fukin, *Polyhedron*, 2016, **119**, 286; (*c*) C. Mukherjee, U. Pieper, E. Bothe, V. Bachler, E. Bill, T. Weyhermüller and P. Chaudhuri, *Inorg. Chem.*, 2008, **47**, 8943; (*d*) M. K. Mondal, A. K. Biswas, B. Ganguly and C. Mukherjee, *Dalton Trans.*, 2015, **44**, 9375; (*e*) R. Rakshit, S. Ghorai, S. Biswas and C. Mukherjee, *Inorg. Chem.*, 2014, **53**, 3333; (*f*) A. I. Poddel'sky, V. K. Cherkasov and G. A. Abakumov, *Coord. Chem. Rev.*, 2009, **253**, 291; (*g*) S. Ye, B. Sarkar, F. Lissner, T. Schleid, J. van Slageren, J. Fiedler and W. Kaim, *Angew. Chem., Int. Ed.*, 2005, **44**, 2103; (*h*) C. Mukherjee, T. Weyhermüller, E. Bothe and P. Chaudhuri, *Inorg. Chem.*, 2008, **47**,

11620; (*i*) C. Mukherjee, T. Weyhermüller, E. Bothe and P. Chaudhuri, *Inorg. Chem.*, 2008, **47**, 2740.

8. (*a*) J. Jacquet, S. Blanchard, E. Derat, M. Desage-El Murr and L. Fensterbank, *Chem. Sci.*, 2016, **7**, 2030; (*b*) J. Jacquet, E. Salanouve, M. Orio, H. Vezin, S. Blanchard, E. Derat, M. Desage-El Murr, L. Fensterbank, *Chem. Commun.*, 2014, **50**, 10394; (*c*) J. Jacquet, P. Chaumont, G. Gontard, M. Orio, H. Vezin, S. Blanchard, M. Desage-El Murr and L. Fensterbank, *Angew. Chem., Int. Ed.*, 2016, **55**, 10712; (*d*) M. K. Mondal and C. Mukherjee, *Dalton Trans.*, 2016, **45**, 13532.

9. (*a*) G. R. Pandhare, V. M. Shinde and Y. H. Deshpande, *Rasayan J. Chem.*, 2008, **1**, 337; (*b*) J. Coates, *Interpretation of Infrared Spectra: A Practical Approach*, John Wiley & Sons Ltd, Chichester, 2000; (*c*) D. L. Pavia, G. M. Lampman, G. S. Kriz and J. R. Vyvyan, *Introduction to Spectroscopy*, 4th edition, 31; (*d*) P. K. Kipkemboi, P. C. Kiprono and J. J. Sanga, *Bull. Chem. Soc. Ethiop.*, 2003, **17**, 211; (*e*) G. Hastings and V. Sivakumar, *Biochemistry*, 2001, **40**, 3681; (*f*) J. Breton, J. Burie, C. Berthomieu, G. Berger and E. Nabedryk, *Biochemistry*, 1994, **33**, 4953; (*g*) H. Suzuki, M. A. Nagasaka, M. Sugiura and T. Noguchi, *Biochemistry*, 2005, **44**, 11323.

10. (*a*) P. Chaudhuri, C. N. Verani, E. Bill, E. Bothe, T. Weyhermüller and K. Wieghardt, *J. Am. Chem. Soc.*, 2001, **123**, 2213; (*b*) H. Chun, E. Bill, T. Weyhermüller and K. Wieghardt, *Inorg. Chem.*, 2003, **42**, 5612; (*c*) C. Mukherjee, T. Weyhermüller, K. Wieghardt and P. Chaudhuri, *Dalton Trans.*, 2006, 2169; (*d*) C. Mukherjee, T. Weyhermüller, E. Bothe, E. Rentschler and P. Chaudhuri, *Inorg. Chem.*, 2007, **46**, 9895; (*e*) P. Chaudhuri, E. Bill, R. Wagner, U. Pieper, B. Biswas and T. Weyhermüller, *Inorg. Chem.*, 2008, **47**, 5549.

11. (*a*) G. Speier, J. Csihony, A. M. Whalen and C. G. Pierpont, *Inorg. Chim. Acta*, 1996, **245**, 1; (*b*) S. Roy, B. Sarkar, D. Bubrin, M. Niemeyer, S. Zališ, G. K. Lahiri and W. Kaim, *J. Am. Chem. Soc.*, 2008, **130**, 15230.

12. (*a*) X. Sun, H. Chun, K. Hildenbrand, E. Bothe, T. Weyhermüller, F. Neese and K. Wieghardt, *Inorg. Chem.*, 2002, **41**, 4295; (*b*) H. Chun, E. Bill, E. Bothe, T. Weyhermüller and K. Wieghardt, *Inorg. Chem.*, 2002, **41**, 5091; (*c*) H. Chun, P. Chaudhuri, T. Weyhermüller and K. Wieghardt, *Inorg. Chem.*, 2002, **41**, 790; (*d*) K. S. Min, T. Weyhermüller, E. Bothe and K. Wieghardt, *Inorg. Chem.*, 2004, **43**, 2922; (*e*) P. Sarkar, M. K. Mondal, A. Sarmah, S. Maity and C. Mukherjee, *Inorg. Chem.*, 2017, **56**, 8068.

13. (*a*) R. R. Gagne, J. L. Allison, R. S. Gall and C. A. Koval, *J. Am. Chem. Soc.*, 1977, **99**, 7170; (*b*) R. R. Gagne, J. L. Allison and G. C. Lisensky, *Inorg. Chem.*, 1978, **17**, 3563.

Thesis Conclusion and Perspectives

The prime aim of this work is to synthesis and characterization of new aminophenol based non-innocent ligands and their corresponding radical containing first-row transition metal complexes and to examine the catalytic applications of the synthesized complexes.

When the ligand $\mathbf{H_2Gan^{AP}}$ reacted with $Fe(ClO_4)_2 \cdot 6H_2O$ it provided a dinuclear μ_2-oxo-bridge Fe(III) complex **2A**. X-ray crystallographic study of complex **2A** revealed that the presence of a furan derivative, resulting from the oxidative aromatic C–C bond cleavage product of 2-aminophenol unit, in the coordination sphere of each iron center. On the other hand, ligand $\mathbf{H_2Gan^{AP}}$ reacted with $Mn(ClO_4)_2 \cdot 6H_2O$ provided a mono(μ-oxo)-bridged binuclear Mn_2 complex **2C**. X-ray crystal structure analysis of complex **2C** suggested that the oxidation state of each Mn ion was +III and the 2-aminophenol unit of ligand $\mathbf{H_2Gan^{AP}}$ was in its one-electron oxidized iminosemiquinone form.

Piperazine based non-innocent ligand $\mathbf{H_4L^{Piperazine(AP/AP)}}$ reacted with $CoCl_2 \cdot 6H_2O$ provided octahedral Co(III) complex where coordinated piperazine moiety was present in boat form. Ligand $\mathbf{H_4L^{Piperazine(AP/AP)}}$ upon reacting with two equivalent of $CuCl_2 \cdot 2H_2O$ provided a novel binuclear diradical-containing Cu(II) complex (**3B)** where coordinated piperazine moiety was present in chair form. The ligand $\mathbf{H_4L^{Piperazine(AP/AP)}}$ provided a Cu(II) complex(**3C**) where coordination sites occupied by two bidentate acridine unit. Formation of complex **3C** occurred via the C–N bond activation and thereafter homolytic C–H bond breaking and C–C bond formation.

Incorporation of –Ph substituent at –*ortho* position to the N-phenyl ring of $\mathbf{H_2L^{AP}}$ [N(2-hydroxy-3,5-di-*tert*-butyl phenyl) aniline] ligand generate a new ligand $\mathbf{H_2L^{AP(Ph)}}$. Ligand $\mathbf{H_2L^{AP(Ph)}}$ yielded radical-containing square planar Co(III) complex (**4A**) and square pyramidal Co(III) complex (**4B**) by using $Co(ClO)_4 \cdot 6H_2O$ and $CoCl_2 \cdot 6H_2O$ respectively. Complex **4B** reduced diphenyl disulfide (Ph_2S_2) and diphenyl diselenide (Ph_2Se_2) by an electron and provided the corresponding five-coordinate, diradical-containing complexes (**4C** and **4D**) where the axial position was occupied by a –XPh group [X = S (**4C**) and Se (**4D**)]. In addition, catalytic ability of four-coordinate (**4A)**, as well as five-coordinate complexes (**4C** and **4E**) has been investigated for the conversion of RNCO (R = phenyl and naphthyl) to urea derivatives under sunlight.

The ligand $\mathbf{H_2L^{AP(Ph)}}$ reacted with 0.5 equivalent of $CuCl_2 \cdot 2H_2O$ provided a Cu(II)-bis(imonosemiquinone) complex (**5A**). Five-coordinate Cu(I)-bis(iminoquinone)Cl complex

(**5B**) was formed via geometry driven iminosemiquinone radical to Cu(II) electron transfer using excess $CuCl_2$•$2H_2O$ as an oxidant. Oxidation complex **5A** by ferrocenium hexafluorophosphate ($FcPF_6$) yielded four-coordinate Cu(II)-(imonosemiquinone)(iminoquinone) complex (**5C**). Removal of axial Cl^- ion from complex **5B** rendered four-coordinate complex **5D**. No change in the oxidation state of either Cu(I) or iminoquinone moieties was realized on changing the coordination number from five to four. Complex **5B** oxidized KO_2 to oxygen molecule and itself get reduced to complex **5A**.

Future perspective of my thesis work is to design and synthesis of new ligands and their metal complexes for better understanding of their coordination chemistry and gaining an insight into metal-ligand interactions in various metalloenzymes. Since, various metalloenzyme has showed different kinds of multielectron reactivity, usually synthesis of metalloenzyme model complexes and their use as artificial enzyme to perform the enzymatic activity can also be investigate further. In addition to the research in the field of metalloenzyme model systems, high-valent metal-oxo, metal-imido, etc. species can be generate and studied for the understanding of their role in various enzyme-like organic transformation(oxo and imido) transfer reactions. In this regards, the following ligands (**L1**, **L2**) can be utilized for synthesis of new complex.

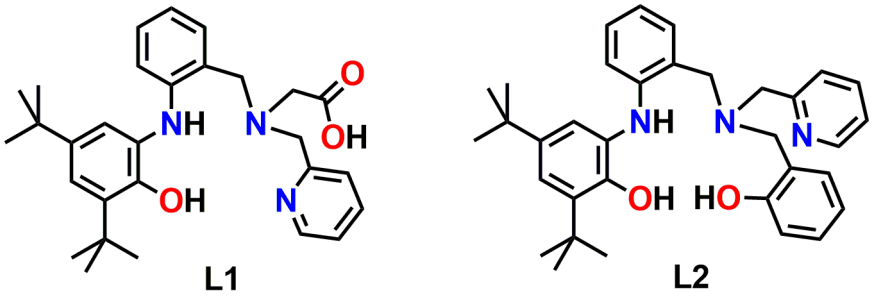

Scheme 1.0: *Proposed ligands (**L1** and **L2**) for synthesizing new complex.*

The mono-radical containing palladium complex of ligand $\mathbf{H_2L^{AP(Ph)}}$ can be utilized as catalyst for C–C cross coupling reaction as well as intramolecular C(sp3)–H amination of aliphatic azide for synthesis of N-heterocyclic compounds.

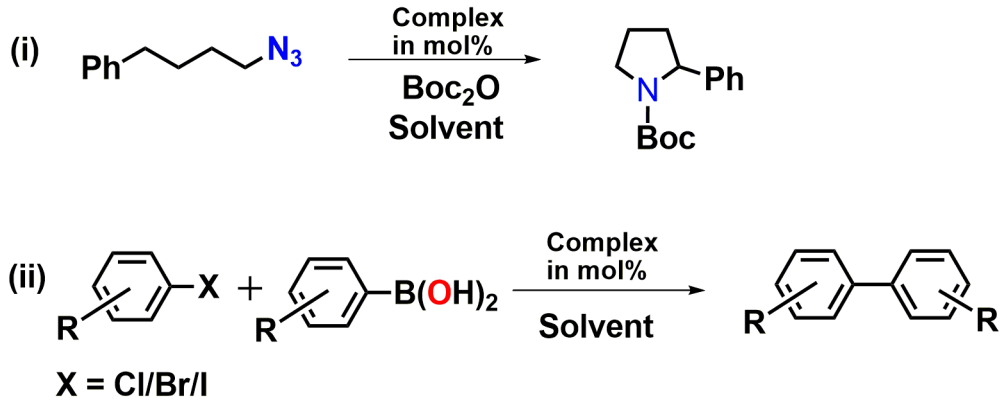

Scheme 2.0: *Proposed scheme for C(sp^3)–H* amination of aliphatic *azide and C–C cross coupling reactions.*

Chapter VI

Equipment and Experimental Section

6.1 Methods and Equipments

All the analyses were performed at 'Instrumental Lab, Department of Chemistry' and 'Central Instrumental Facility' IITG, unless otherwise mentioned.

Chemicals and Solvents

All the chemicals and solvents were obtained from commercial sources and were used as supplied, unless noted otherwise.

Infrared Spectroscopy

Solid state FTIR spectra were recorded (4000–400 cm^{-1}) on 'Perkin Elmer Instrument' at room temperature. The pallet has been made by grinding the sample with IR grade KBr powder.

NMR Spectroscopy

^{1}H, ^{13}C NMR spectra were recorded on 'Varian Mercury plus 400 MHz' and on 'Bruker AscendTm 600 MHz' nuclear magnetic resonance (NMR) spectrometer at 298 K. Chemical shifts,δ (in ppm), are reported relative to TMS [δ (^{1}H) 0.0 ppm, δ (^{13}C) 0.0 ppm] which was used as the inner reference. Otherwise, the solvents ($CHCl_3$) residual proton resonance and carbon resonance appeared at, δ 7.26, 77.2 ppm, respectively. The resultant spectrums were drawn by using 'MestReNova' NMR data processing software.

Mass Spectrometry

Mass spectra were recorded on QTOF–MS Spectrometer ('Waters, Model: Q–Tof Premier') or 'Agilent Accurate–Mass Q–TOF LC/MS 6520' spectrometer and peaks were given in *m*/*z* (% of basis peak). Mass spectra were taken in HPLC grade CH_3CN solvent.

Elemental analysis

The determination of the C, H, N was performed on 'FLASH EA 1112 series' CHN Analyzer at SAIF, Mumbai, on 'Perkin–Elmer 2400 series II' CHN Analyzer at IACS, Kolkata and on 'EuroEA3000' Elemental Analyzer at Guwahati Biotech Park, Guwahati.

UV–Vis/NIR Spectroscopy

The electronic absorption spectrum (UV–Vis/NIR) of the sample(s) was recorded on 'Perkin Elmer, Lamda 750, UV/Vis/NIR spectrometer' in HPLC grade CH_2Cl_2 at room temperature using cuvette of 1 cm width. Thermal electronic absorption spectrum of the complex (**2A**) was recorded on 'Perkin Elmer, Lamda 350, UV/Vis/NIR spectrometer' in HPLC grade toluene at a range of 30–70 ° C.

Electrochemistry

Cyclic voltammetry was performed by using a 'VersaSTAT 3 Potentiostat'. A standard three electrode–cell was employed with a glass-carbon working electrode, a platinum-wire auxiliary electrode and Ag/AgCl (saturated NaCl in water) reference electrode. Measurements were made under an inert atmosphere at room temperature. The potential of the reference electrode was determined using Fc^{+}/Fc as the internal standard.

X–Band EPR Spectroscopy

First derivative X–Band EPR spectra of powdered or frozen solution samples were measured with a 'JEOL JES–FA200 Spectrometer'. The resulting data was simulated by using W95EPR–program written by Frank Neese (MPI for Bioinorganic Chemistry, Mülheim, and University of Bonn).

Single Crystal X-ray Crystallography

Suitable crystal for X–ray diffraction study was obtained from solvent evaporation or solvent diffusion method. X−ray crystallographic data were collected by using either a 'Bruker SMART APEX−II CCD diffractometer', equipped with a fine focus 1.75 kW sealed tube Mo−Kα radiation (λ = 0.71073 Å) at 296(2) or 293(2) K, with increasing w (width of 0.3° per frame) at a scan speed of 3 s/frame or a 'Super Nova, Single source at offset, Eos diffractometer'. Structure was solved with the Superflip, structure solution program using Charge Flipping and refined by direct methods using 'SHELXS–97' and with full–matrix least squares on F2 using 'SHELXL–97', or with the Superflip structure solution program using Charge Flipping and refined with the olex2.refine refinement package using Gauss–Newton minimization. All then non−hydrogen atoms were refined anisotropically.

Theoretical Calculation

All the complexes were optimized at B3LYP/6-31(d,p) level of theory using Gaussian-09 program package and included a dispersion correction using keyword 'empiricaldispersion=gd3bj' where ever applicable. Broken symmetry calculations were done by using 'guess=mix' keyword to understand the coupling pattern between metal ion and the coordinated paramagnetic ligand units in S=0 state. Electronic excitations based on B3LYP optimized geometries were computed using the integral equation formalism polarized continuum model (IEF-PCM) in DCM by using TDDFT formalism. TD-DFT calculations were undertaken on the geometry-optimized structures with the 60 lowest-energy transitions.

6.2 Experimental Section

6.2.1: Synthesis of ligand H_2Gan^{AP}

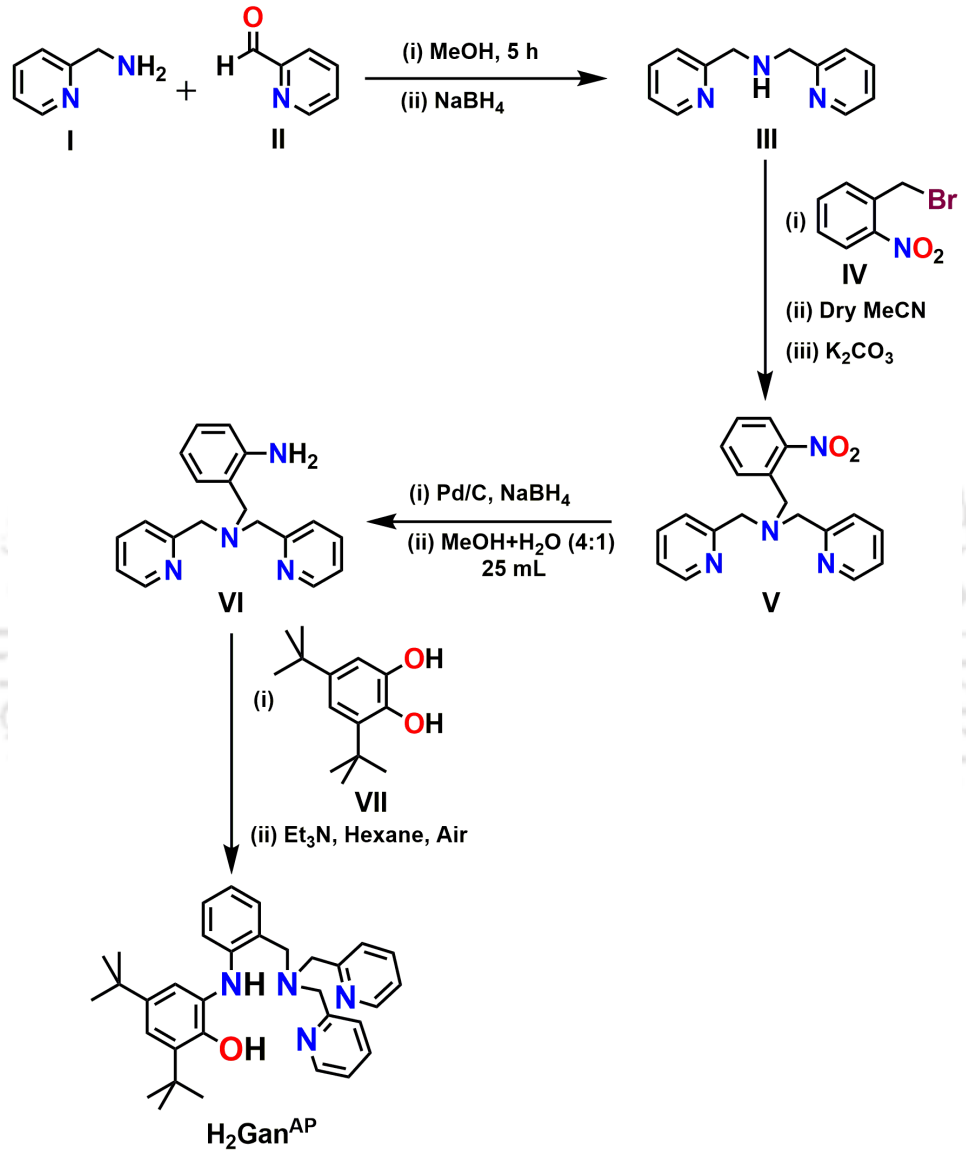

Scheme 6.1: *Synthetic route of ligand* ***H_2Gan^{AP}***.

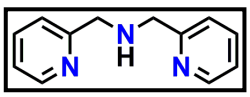

Step 1: Synthesis of N,N-bis(2-picolyl)amine; III: To a solution of 2-pyridinecarboxaldehyde (**II**) (1.073 g, 10 mmol) in dry methanol (15 mL) was added 2-picolyl amine(**I**) (1.082 g, 10 mmol) at room temperature (RT). The resulted brown

solution was stirred for 5 h. Sodium borohydride (0.925 g, 25 mmol) was added to the solution in small portions with stirring at 0 °C. The mixture changed color from brown to yellow and was stirred further for 16 h at room temperature. Conc. HCl was added slowly to adjust the pH to 1, and the solution was stirred for 2 h. Next, a saturated solution of NaOH was added to adjust the pH to 11. The reaction mixture was filtered, and the solvent was removed under vacuum. Water was added to the residue; the aqueous mixture was extracted twice with CH_2Cl_2 (50 mL), and the combined extracts dried over anhydrous sodium sulfate and filtered. The solvent was removed under vacuum. The product was obtained as brown oil.

Yield: 1.720 g, 86%.

FT-IR (KBr pellet, cm^{-1}): 3296, 3055, 2895, 2812, 1590, 1567, 1500, 1471, 1429, 1351, 1138, 1047, 994, 859, 770, 753, 665.

^{1}H-NMR (600.17 MHz, $CDCl_3$): δ 8.55 (d, J = 5.0 Hz, 2H), 7.64 (t, J = 8.4 Hz, 2H), 7.35 (d, J = 7.8 Hz, 2H), 7.17–7.14 (m, 2H), 3.97 (s, 4H), 2.06 (s, 1H) ppm.

ESI-MS (CH_3CN) *m/z* for $[C_{12}H_{13}N_3+H]^+$: Calcd, 200.1188; Found, 200.1186.

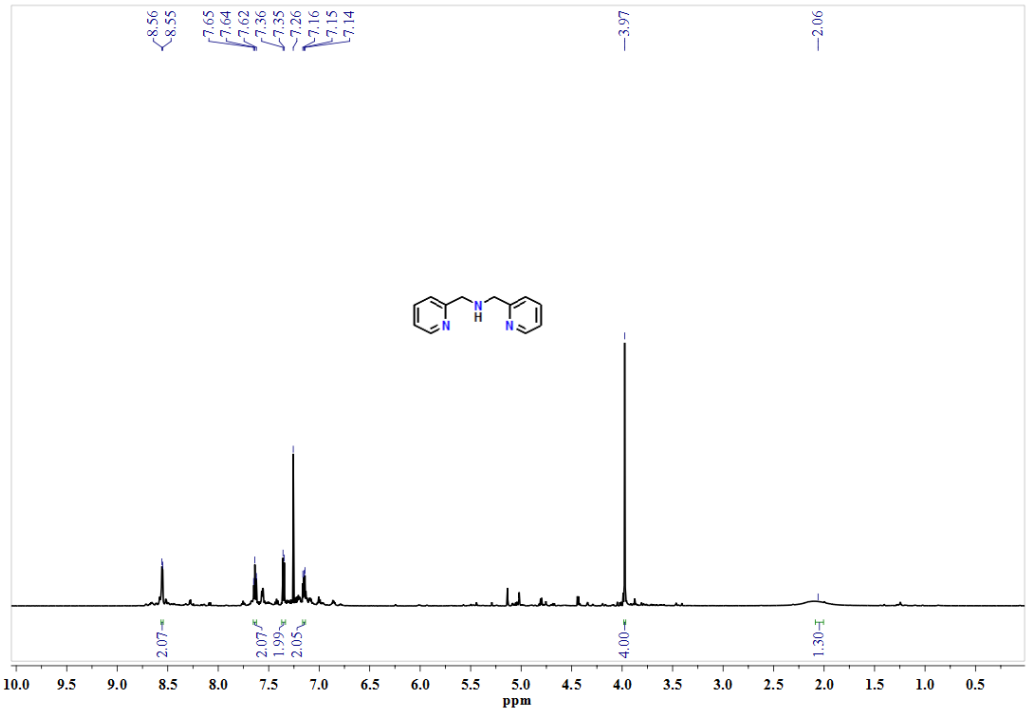

Figure 6.1: *^{1}H-NMR spectrum of 2-[bis(2-pyridylmethyl)aminomethyl]aniline (**III**) in $CDCl_3$.*

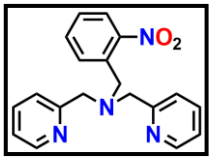

Step 2: Synthesis of 2-[Bis(2-pyridylmethyl)aminomethyl]nitrobenzene; V: 2-Nitrobenzyl bromide (**IV**)(1.42 g, 6.58 mmol) was added to a solution of bis(2-pyridylmethyl)amine (**III**) (1.31 g, 6.58 mmol) in dry CH_3CN (25 mL) with K_2CO_3 (9.01 g, 65.0 mmol). The reaction mixture was heated to reflux with stirring for 2 days. After the solution was cooled and filtered. The solvent was removed by evaporation. Purification of the crude product by column chromatography on silica gel by using CH_2Cl_2/MeOH (40:1 v/v) solvent as an eluent to produced a brown oil of bis(2-pyridylmethyl)aminomethyl)-nitrobenzene (**V**).

Yield: 1.182 g, 54%.

FT-IR (KBr pellet, cm^{-1}): 3062, 3009, 2923, 2851, 1590, 1570, 1524, 1473, 1434, 1346, 1148, 1047, 995, 856, 749, 730.

^{1}H-NMR (600.17 MHz, $CDCl_3$): δ 8.49 (d, J = 5.7 Hz, 2H), 7.75 (d, J = 8.0 Hz, 1H), 7.70 (d, J = 8.1 Hz, 1H), 7.63 (t, J = 7.7 Hz, 2H), 7.48 (t, J = 6.9 Hz, 1H), 7.39 (d, J = 7.8 Hz, 2H), 7.33 (t, J = 7.1 Hz, 1H), 7.14 – 7.10 (m, 2H), 4.06 (s, 2H), 3.77 (s, 4H) ppm.

ESI-MS (CH_3CN) *m/z* for $[C_{19}H_{18}N_4O_2+H]^+$: Calcd, 335.1508; Found, 335.1503.

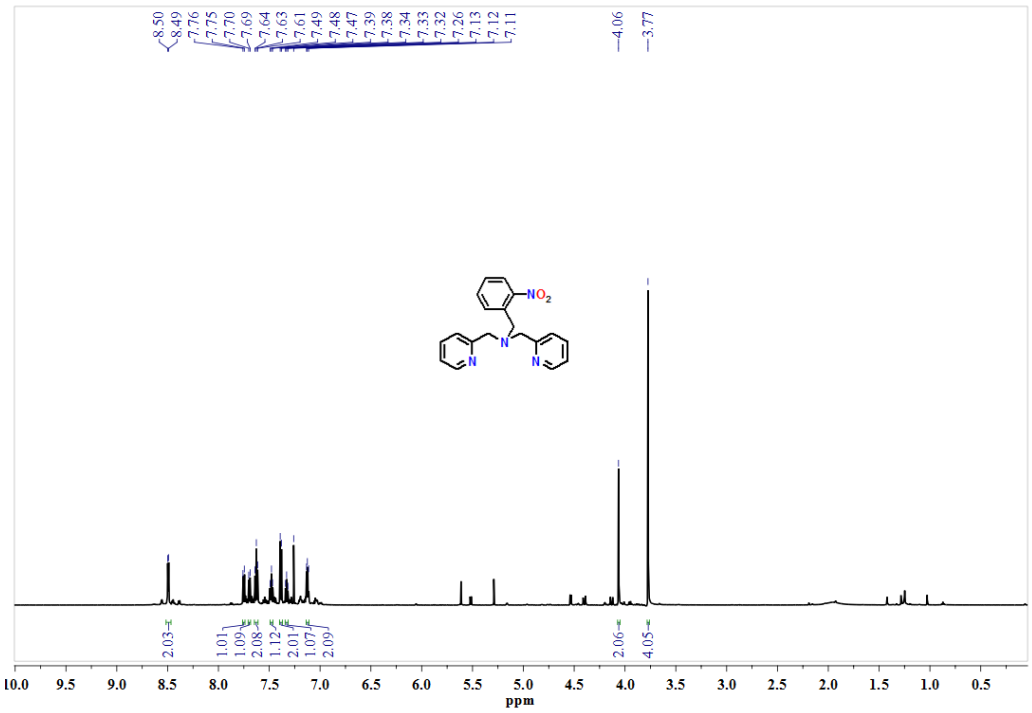

Figure 6.2: *^{1}H-NMR spectrum of 2-[Bis(2-pyridylmethyl)aminomethyl]nitrobenzene(**V**) in $CDCl_3$.*

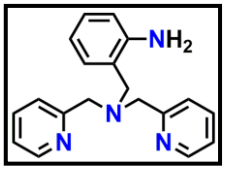

Step 3: Synthesis of 2-[bis(2-pyridylmethyl)aminomethyl]aniline; VI: 10% activated Pd/C (0.035 g) and 2-[bis(2-pyridylmethyl)aminomethyl]-nitrobenzene (**V**), (1.182 g, 3.53 mmol) were combined in a 4:1 MeOH:H_2O solvent mixture (25 mL) and allowed to stirred for 15 min. Then sodium borohydride (1.33 g, 35.3 mmol) was added in small portions with stirring at 0 °C. After that, the reaction mixture was heated to 50 °C with stirring for 12 h. After cooling, the solution was filtered through Celite, and the filtrate was evaporated under reduced pressure. The residue was dissolved in CH_2Cl_2 (40 mL) and dried over Na_2SO_4. After filtration, the solvent was removed in a rotavapour to yield a brown solid of 2-[bis(2-pyridylmethyl)aminomethyl)]aniline (**VI**).

Yield: 0.967 g, 90%.

FT-IR (KBr pellet, cm^{-1}): 3390, 3321, 3211, 3062, 3010, 2920, 2802, 1616, 1590, 1569, 1494, 1474, 1461, 1433, 1370, 1295, 1149, 1119, 1049, 752.

^{1}H-NMR (600.17 MHz, $CDCl_3$): δ 8.53 (d, J = 4.8 Hz, 2H), 7.60 (t, J = 8.5 Hz, 2H), 7.37 (d, J = 7.8 Hz, 2H), 7.17 – 7.10 (m, 2H), 7.04 (dd, J = 7.3, 3.8 Hz, 2H), 6.61 (dd, J = 17.6, 7.3 Hz, 2H), 4.89 (s, 2H), 3.78 (s, 4H), 3.65 (s, 2H) ppm.

^{13}C-NMR (150.93 MHz, $CDCl_3$): δ 159.39, 149.26, 147.17, 136.50, 131.36, 128.63, 123.61, 122.45, 122.16, 117.36, 115.56, 60.32, 58.03.

ESI-MS (CH_3CN) *m/z* for $[C_{19}H_{20}N_4+H]^+$: Calcd, 305.1766; Found, 305.1364.

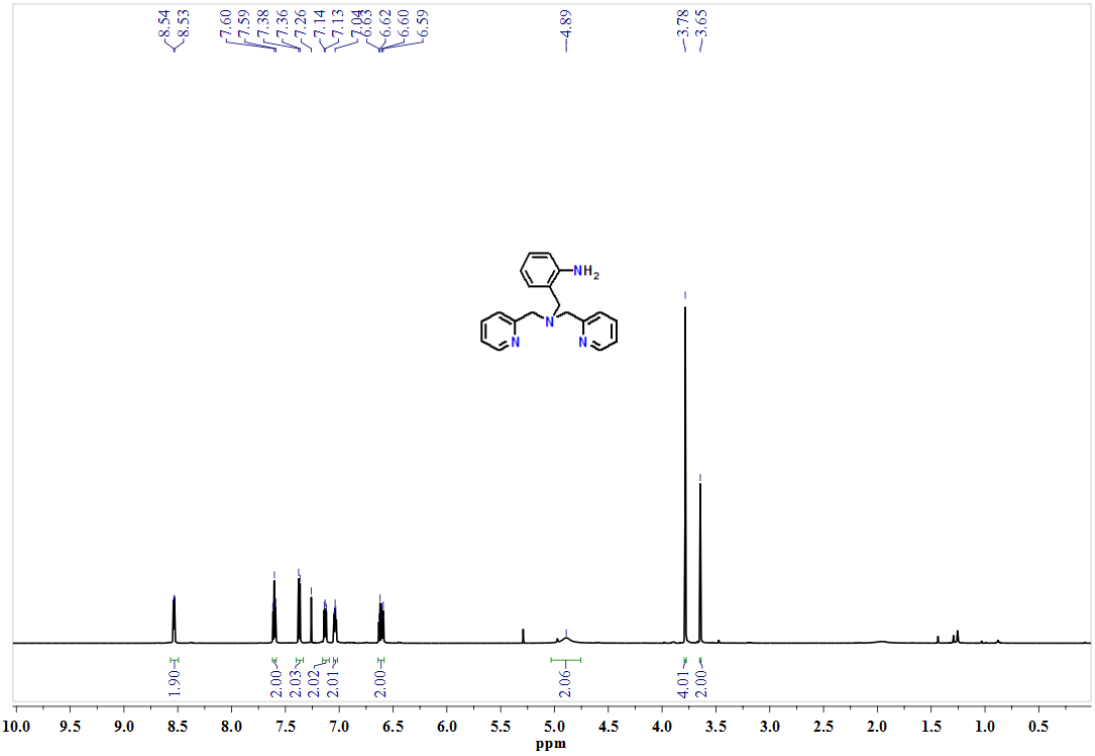

Figure 6.3: *^{1}H-NMR spectrum of 2-[bis(2-pyridylmethyl)aminomethyl]aniline (**VI**) in $CDCl_3$.*

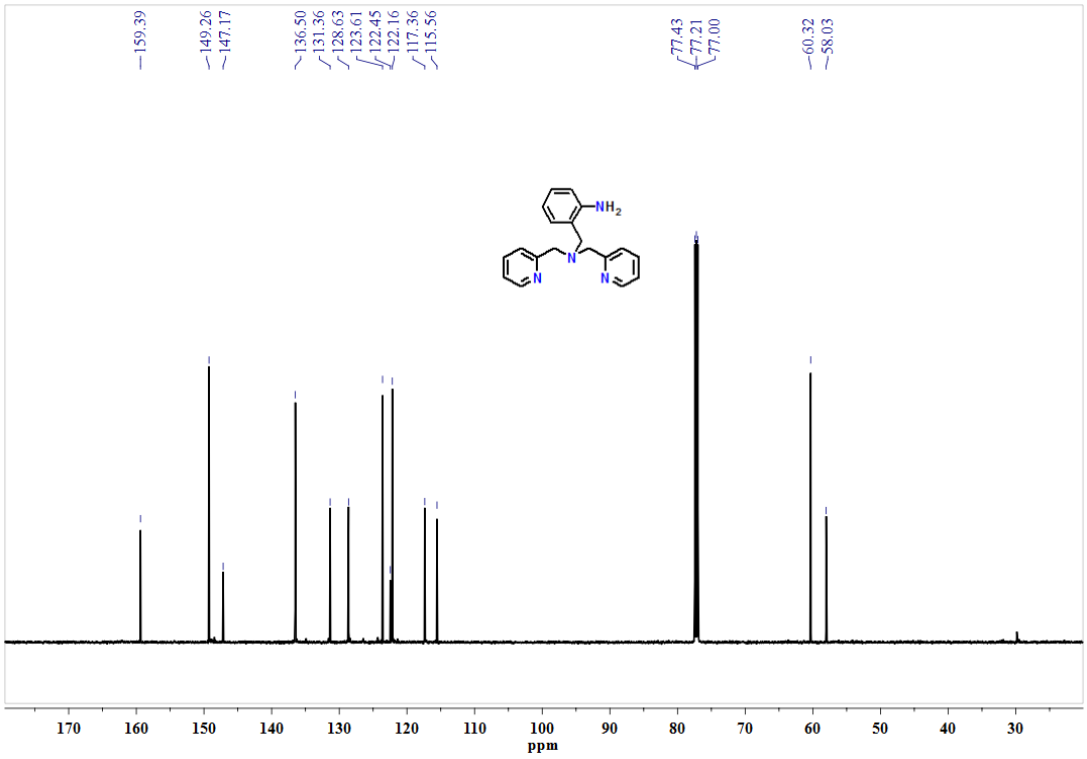

Figure 6.4: *^{13}C-NMR spectrum of 2-[bis(2-pyridylmethyl)aminomethyl]aniline (**VI**) in $CDCl_3$.*

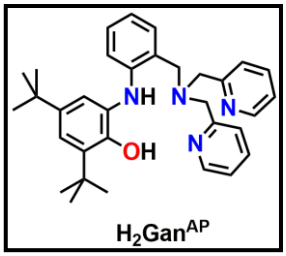

Step 4: Synthesis of $C_{33}H_{40}N_4O$, H_2Gan^{AP}: To a stirred solution of 3,5-di-*tert*-butyl catechol (**VII**) (0.668 g, 3.01 mmol) and 2-[bis(2-pyridylmethyl)aminomethyl]aniline (**VI**) (0.917 g, 3.01 mmol) in hexane (25 mL) triethylamine (0.05 mL) was added and the reaction mixture was refluxed for seven days. The resulted brown color reaction mixture was cooled to room temperature and then, stirred further for two days. After that, the resulted suspension was filtered. The filtrate part was evaporated to afford an amorphous solid. The solid was dissolve in methanol (15 mL) and kept under –20 °C that provided colorless crystal of **H_2Gan^{AP}**.

Yield: 0.760 g, 50%.

FT-IR (KBr pellet, cm^{-1}): 3227, 3181, 3110, 3047, 2955, 2904, 2864, 1592, 1569, 1534, 1479, 1434, 1362, 1337, 1299, 1236, 1148, 983, 744.

^{1}H-NMR (600.17 MHz, $CDCl_3$): δ 9.03 (s, 1H), 8.83 (s, 1H), 8.42 (d, *J* = 4.6 Hz, 2H), 7.53 (td, *J* = 7.4, 1.3 Hz, 2H), 7.42 (d, *J* = 7.8 Hz, 2H), 7.20 (s, 1H), 7.05-7.08 (m, 4H), 7.00 (t, *J* = 7.9 Hz, 1H), 6.94 (d, *J* = 8.1 Hz, 1H), 6.62 (t, *J* = 7.2 Hz, 1H), 3.82 (s, 4H), 3.80 (s, 2H), 1.56 (s, 9H), 1.30 (s, 9H).

^{13}C-NMR (150.93 MHz, $CDCl_3$): δ 158.2, 149.0, 146.4, 145.8, 141.6, 137.1, 136.9, 130.9, 130.2, 128.6, 124.4, 123.0, 122.4, 118.0, 117.6, 117.4, 112.1, 61.0, 60.1, 35.5, 34.6, 31.9, 30.0.

ESI-MS (+) *m/z* for $[C_{33}H_{40}N_4O + H]^+$: Calcd, 509.3274; Found 509.3239.

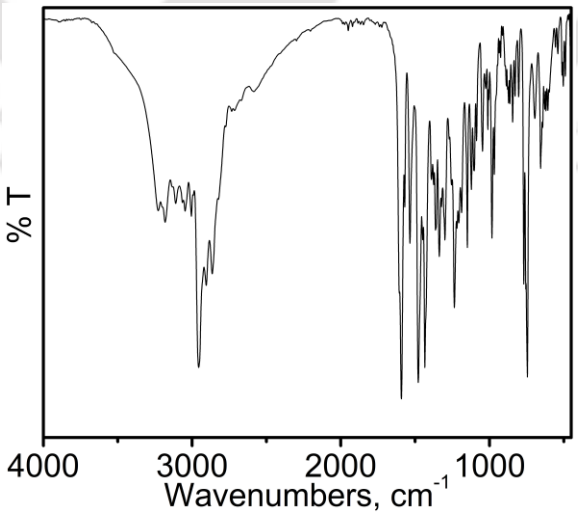

Figure 6.5: *FT-IR spectrum of ligand* ***H_2Gan^{AP}***.

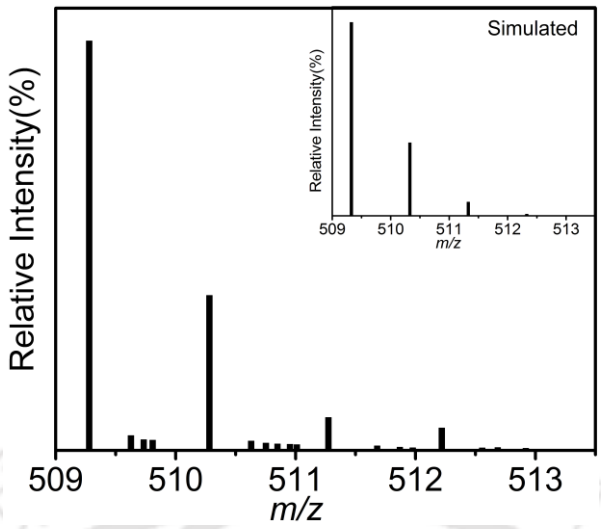

Figure 6.6: *ESI-mass spectra of ligand* ***H_2Gan^{AP}****; experimental and simulated isotope distribution pattern (inset) for* $[C_{33}H_{40}N_4O+H]^+$.

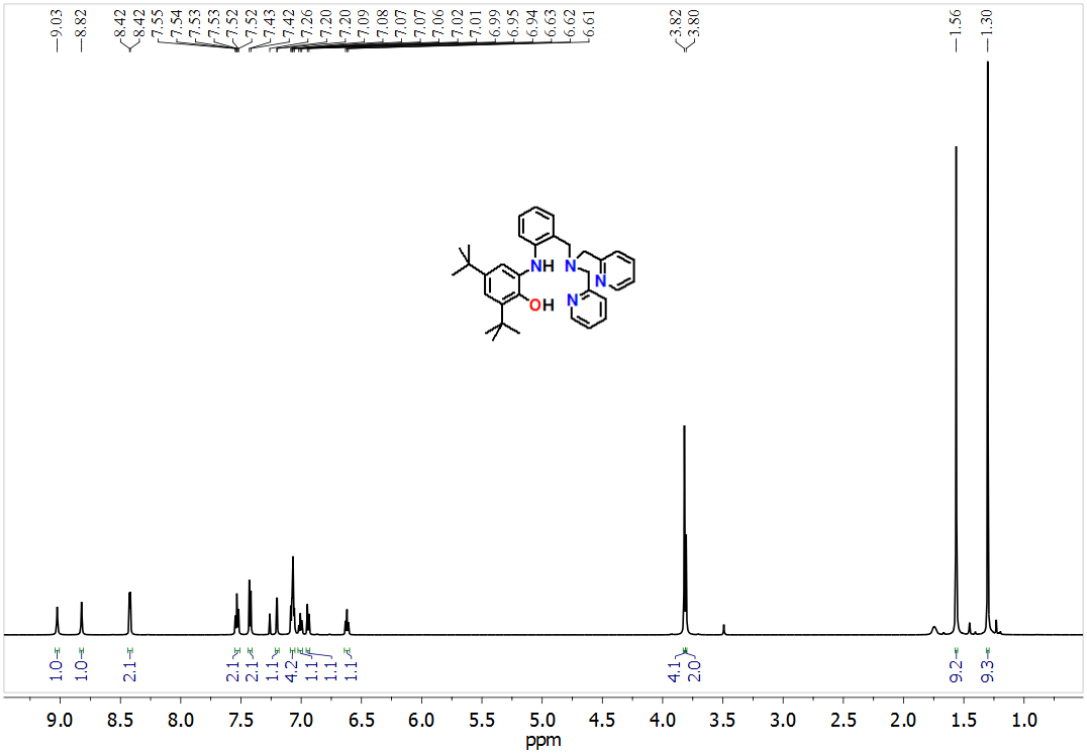

Figure 6.7: *^{1}H-NMR spectrum of* ***H_2Gan^{AP}*** *in* $CDCl_3$.

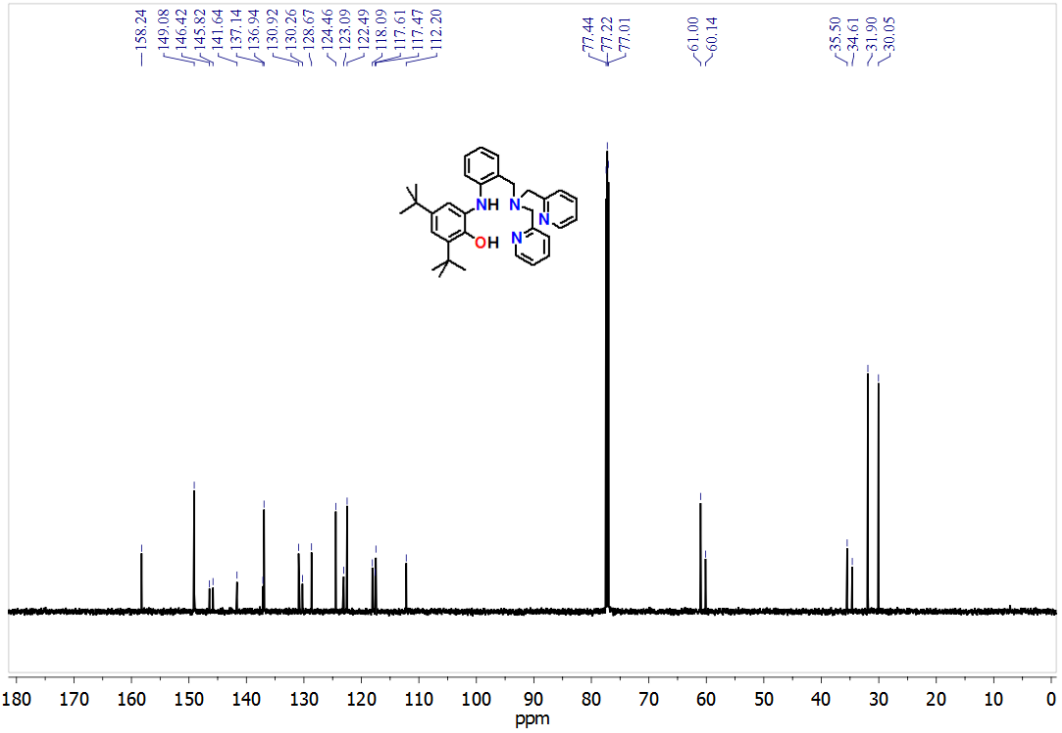

Figure 6.8: *^{13}C-NMR spectrum of* ***H_2Gan^{AP}*** *in $CDCl_3$.*

6.2.2: Synthesis of ligand $H_4L^{Piperazine(AP/AP)}$

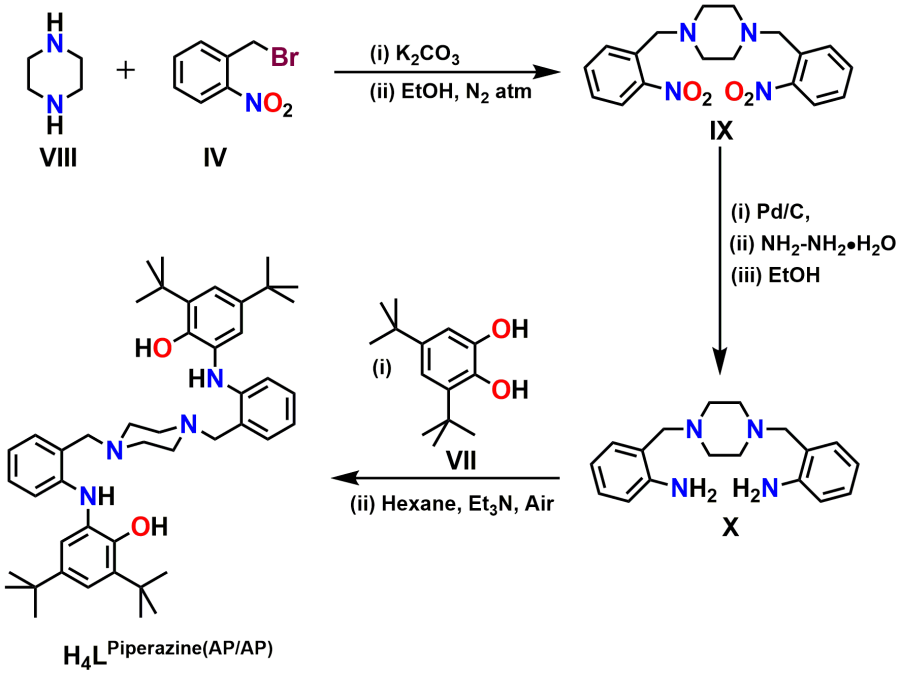

Scheme 6.2: *Synthetic route of ligand* ***$H_4L^{Piperazine(AP/AP)}$***.

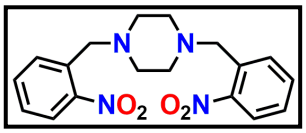

Step 1, Synthesis of 1,4-bis(2-nitrobenzyl) piperazine ; IX: Piperazine (**VIII**) (0.344 g, 4 mmol) was dissolved in ethanol (20 mL) and heated to reflux, then K_2CO_3 (1.380 g, 10.00 mmol) and 2-nitrobenzylbromide (**IV**)(1.728 g, 8.00 mmol) were added to the solution. The mixture was further refluxed for 48 h, and then allowed to cool to room temperature. Solution was dried and water was added to it. The product was extracted with dichloromethane (3 × 25 mL), the product was a yellow powder.

Yield: 1.286 g, 82%.

FT-IR (KBr pellet, cm^{-1}):

^{1}H NMR (399.89 MHz, $CDCl_3$): δ 7.79 (d, J = 8.0 Hz, 1H), 7.59–7.48 (m, 1H), 7.37 (t, J = 7.6 Hz, 1H), 3.76 (s, 1H), 2.40 (s, 1H) ppm.

ESI-MS (+) *m/z* for $[C_{18}H_{20}N_4O_4+H]^+$: Calcd, 356.1485; Found 356.1472.

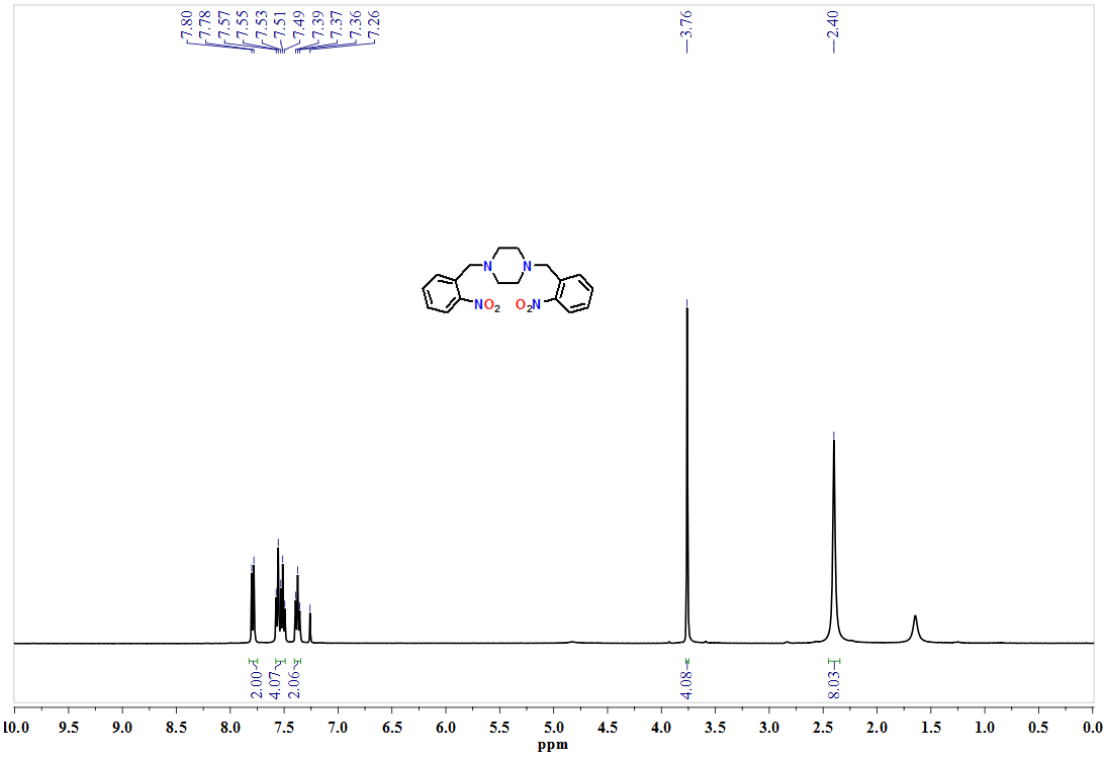

Figure 6.9: *^{1}H-NMR spectrum of 1,4-bis(2-nitrobenzyl) piperazine (**IX**) in $CDCl_3$.*

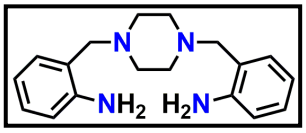

Step 2: Synthesis of 2,2'-[piperazine-1,4-diylbis(methylene)] dianiline; X: 10% activated Pd/C (0.076 g) and 1,4-bis(2-nitrobenzyl) piperazine (**IX**), (1.286 g, 3.61 mmol) were combined in absolute ethanol (15 mL) and stirred for 15 min. Hydrazine hydrate (4.0 mL, 5 mmol) was added in small portions with stirring at 0 °C. The resulted reaction mixture was heated to reflux with stirring under nitrogen atmosphere for 12 h. After cooling, the solution was filtered through celite, and the filtrate was evaporated under reduced pressure. The residue was dissolved in CH_2Cl_2 (40 mL) and dried with Na_2SO_4. After filtration, the solvent was removed to yield a white solid of 2,2'-[piperazine-1,4-diylbis(methylene)] dianiline (**X**).

Yield: 1.286 g, 82%.

FT-IR (KBr pellet, cm^{-1}): 3439, 3264, 3034, 2927, 2812, 2772, 1611, 1587, 1495, 1455, 1347, 1298, 1261, 1154, 1130, 1008, 930, 831, 751, 723, 620.

^{1}H-NMR (600.17 MHz, $CDCl_3$): δ 7.09 (t, J = 8.2 Hz, 2H), 6.97 (d, J = 7.1 Hz, 2H), 6.65 (dd, J = 15.4, 7.7 Hz, 4H), 4.75 (s, 4H), 3.50 (s, 4H), 2.41 (s, 8H) ppm.

^{13}C-NMR (150.93 MHz, $CDCl_3$): δ 147.17, 130.62, 128.56, 122.49, 117.77, 115.67, 62.17, 53.11 ppm.

ESI–MS (+) *m/z* for $[C_{18}H_{20}N_4O_4+H]^+$: Calcd, 356.1485; Found 356.1472.

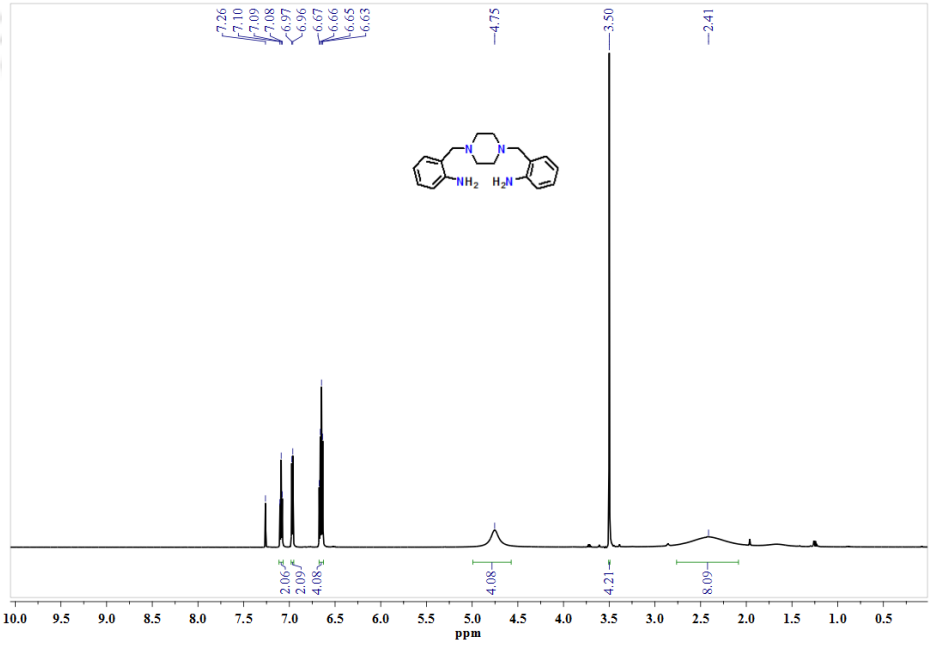

Figure 6.10: *^{1}H-NMR spectrum of 2,2'-[piperazine-1,4-diylbis(methylene)]dianiline(**X**) in $CDCl_3$.*

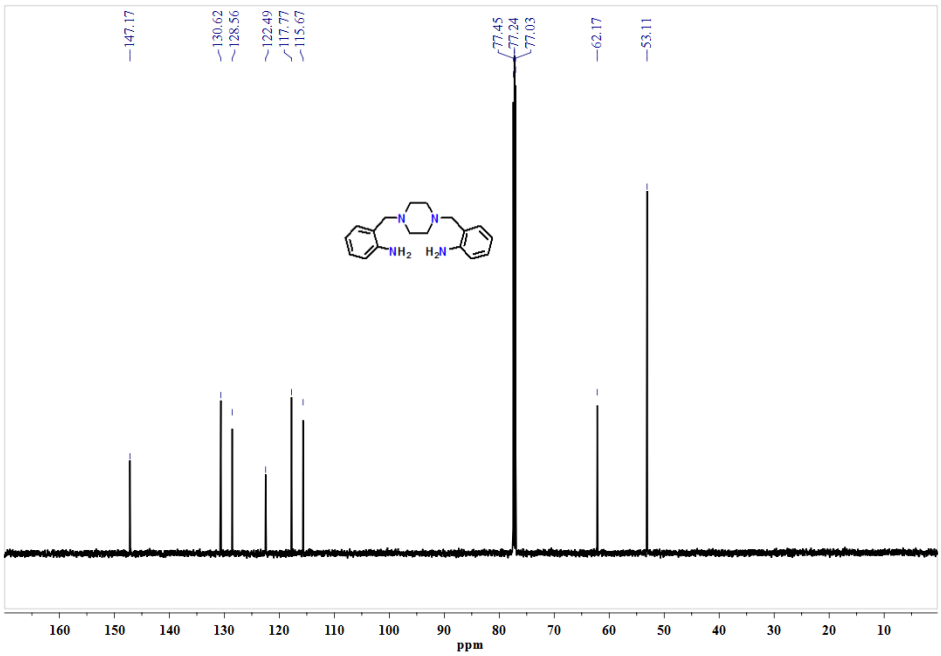

Figure 6.11: *^{13}C-NMR spectrum of 2,2'-[piperazine-1,4-diylbis(methylene)] dianiline (**X**) in $CDCl_3$.*

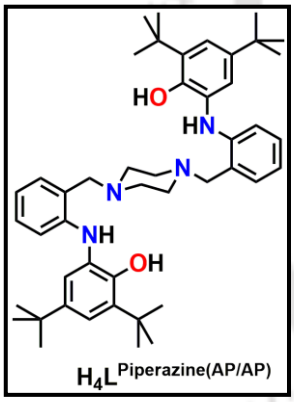

Synthesis of $C_{46}H_{64}N_4O_2$, $H_4L^{Piperazine(AP/AP)}$: To a stirred solution of 3,5-di-*tert*-butylcatechol (**VII**) (1.631 g, 7.35 mmol) and 2,2'-(piperazine-1,4-diylbis(methylene))dianiline (**X**) (1.036 g, 3.50 mmol) in hexane (25 mL), triethylamine (0.05 mL) was added and the reaction mixture was refluxed for four days. The deep brown color reaction mixture was cooled to room temperature and stirred for another two days under air. A white color solid precipitate was formed. It was filtered out, and washed with methanol (15 mL) to obtain an amorphous compound.

Yield: 1.202 g, 49%.

FT-IR (KBr pellet, cm^{-1}): 3494, 3338, 3242, 3157, 3046, 2955, 2905, 2868, 2816, 2772, 1613, 1594, 1495, 1458, 1419, 1376, 1360, 1304, 1248, 1218, 1004, 965, 849, 821, 801, 757.

^{1}H-NMR (600.17 MHz, $CDCl_3$): δ 7.73 (s, 2H), 7.25 (s, 2H), 7.11 (t, J = 7.8 Hz, 2H), 7.06 (d, J = 7.2 Hz, 2H), 7.01 (s, 2H), 6.76 (t, J = 7.2 Hz, 2H), 6.59 (br, 2H), 6.45 (d, J = 8.4 Hz, 2H), 3.69 (s, 4H), 2.92 (br, 4H), 2.30 (br, 4H), 1.48 (s, 18H), 1.34 (s, 18H).

^{13}C-NMR (150.93 MHz, $CDCl_3$): δ 149.46, 147.30, 142.27, 135.53, 130.54, 128.99, 128.51, 122.77, 121.80, 121.73, 118.87, 113.80, 62.28, 52.92, 35.25, 34.58, 31.90, 29.79 ppm.

ESI-MS (+) *m/z* for $[C_{46}H_{64}N_4O_2+H]^+$: Calcd, 705.5108; Found 705.5112.

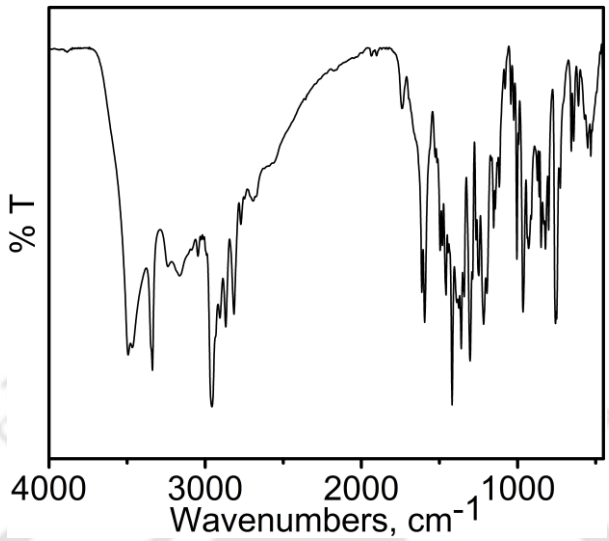

Figure 6.12: *FT-IR spectrum of* $\boldsymbol{H_4L^{Piperazine(AP/AP)}}$.

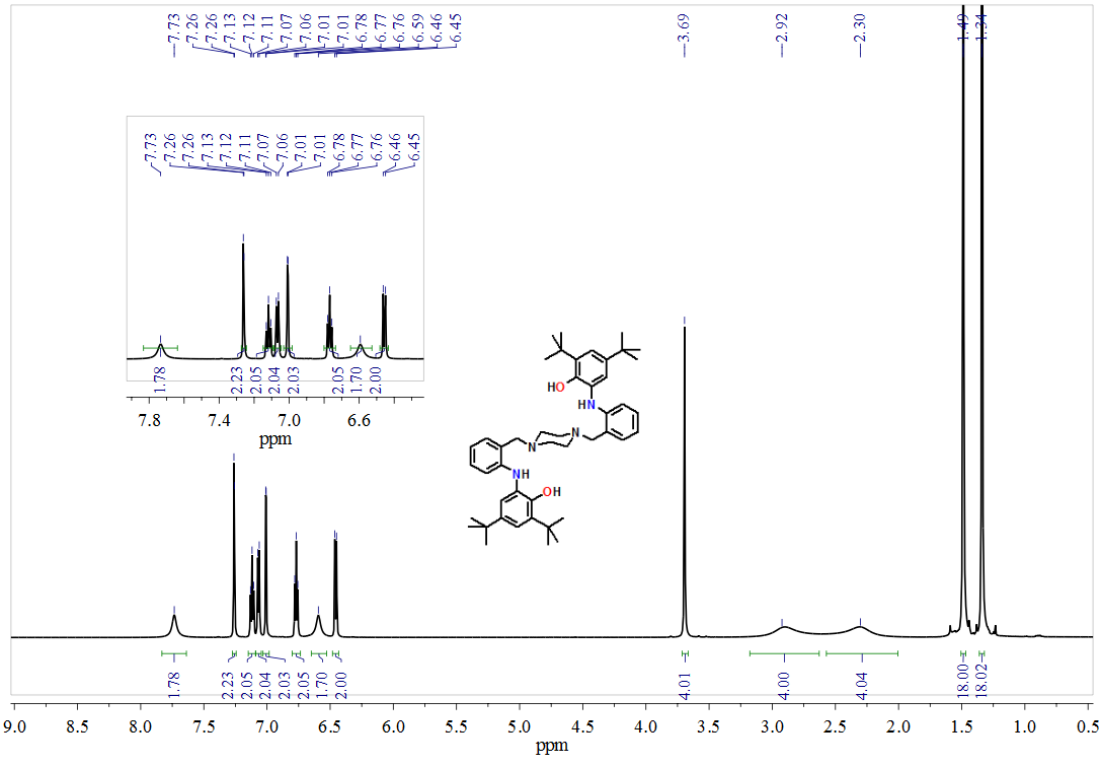

Figure 6.13: *^{1}H-NMR spectrum of* $\boldsymbol{H_4L^{Piperazine(AP/AP)}}$ *in* $CDCl_3$.

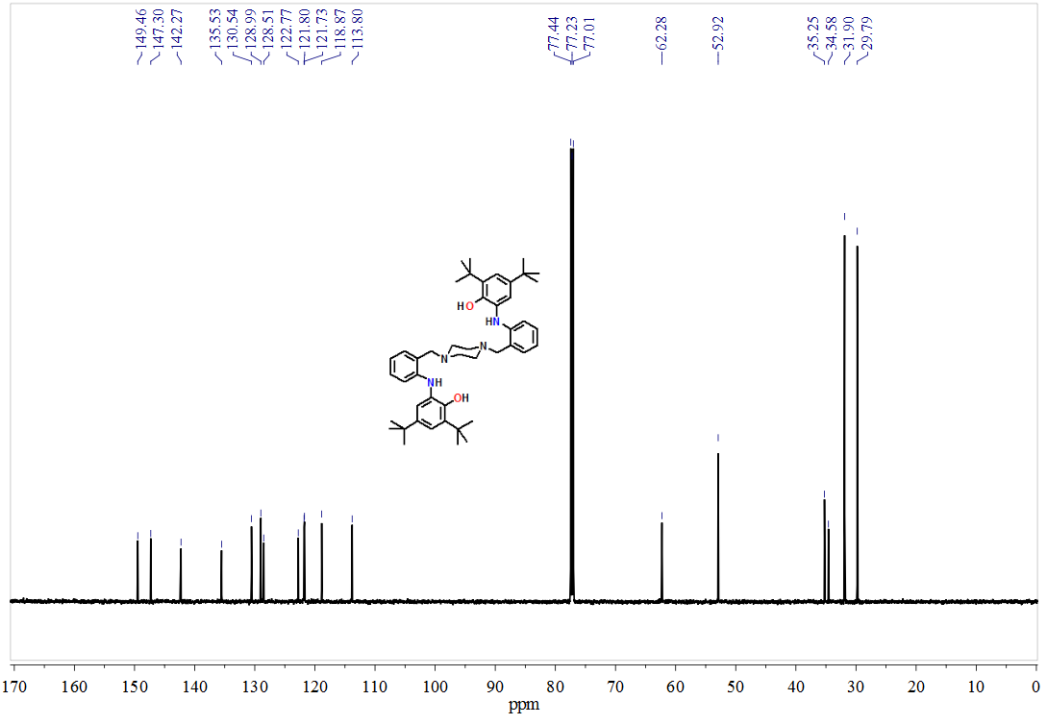

Figure 6.14: *^{13}C-NMR spectrum of $H_4L^{Piperazine(AP/AP)}$ in $CDCl_3$.*

6.2.3: Synthesis of ligand $H_2L^{AP(Ph)}$

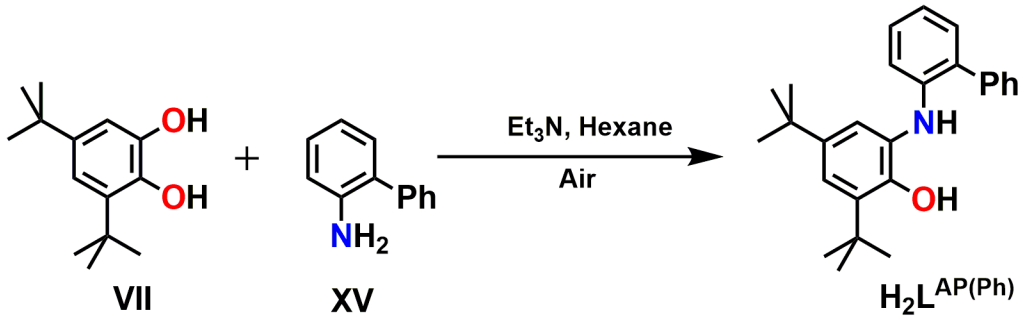

Scheme 6.3: *Synthetic route of ligand $H_2L^{AP(Ph)}$.*

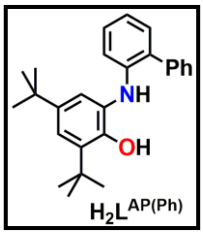

Synthesis of $H_2L^{AP(Ph)}$ [$C_{26}H_{31}NO$]: To a stirred solution of 2-animobiphenyl (**XV**) (0.848 g, 5.01 mmol) in hexane (20 mL), 3,5-di-*tert*-bulyl catechol (**VII**)(1.117 g, 5.02 mmol) and Et_3N (0.05 ml) were added sequentially at room temperature (25 °C) under air. A reddish brown homogeneous solution was obtained on refluxing the reaction mixture for 2 days. Then the solution mixture was cooled in room temperature and stirred for another 2 days. All the solvent was evaporated

under vacuum and product was purified by column chromatography using a hexane:ethyl acetate (98:2) as eluent to give $\mathbf{H_2L^{AP(Ph)}}$.

Yield: 1.65 g (88%).

FT-IR Spectra (KBr pellet cm^{-1}): 3538.85, 3427.06, 3360.01, 3056.49, 2995.96, 2961.22, 2903.57, 2865.07, 1594.53, 1580.22, 1503.89, 1484.58, 1436.16, 1419.48, 1359.73, 1308.55, 1264.53, 1222.24, 1199.47, 1007.96, 764.74, 756.23, 743.09, 700.67, 608.47.

^{1}H-NMR(600.17 MHz, $CDCl_3$): δ 7.55 (d, J = 7.1 Hz, 2H), 7.51 (t, J = 7.0 Hz, 2H), 7.41 (t, J = 6.9 Hz, 1H), 7.23-7.22 (d, 2H), 7.18 (t, J = 7.6 Hz, 1H), 6.98 (s 1H), 6.93 (t, J = 7.2 Hz, 1H), 6.56 (d, J = 8.0 Hz, 1H), 6.40 (s, 1H), 5.22 (s, 1H) ,1.44 (s, 9H), 1.26 (s, 9H) ppm.

^{13}C-NMR (150.93 MHz, $CDCl_3$) δ (ppm): δ 29.7, 31.8, 34.6, 35.2, 114.5, 119.8, 121.8, 122.2, 127.8, 128.0, 128.9, 129.4, 129.6, 130.6, 135.4, 139.1, 142.4, 144.0, 149.7 ppm.

ESI-MS (+) m/z for $[C_{26}H_{31}NO+H]^+$: Calcd, 374.24; found, 374.24.

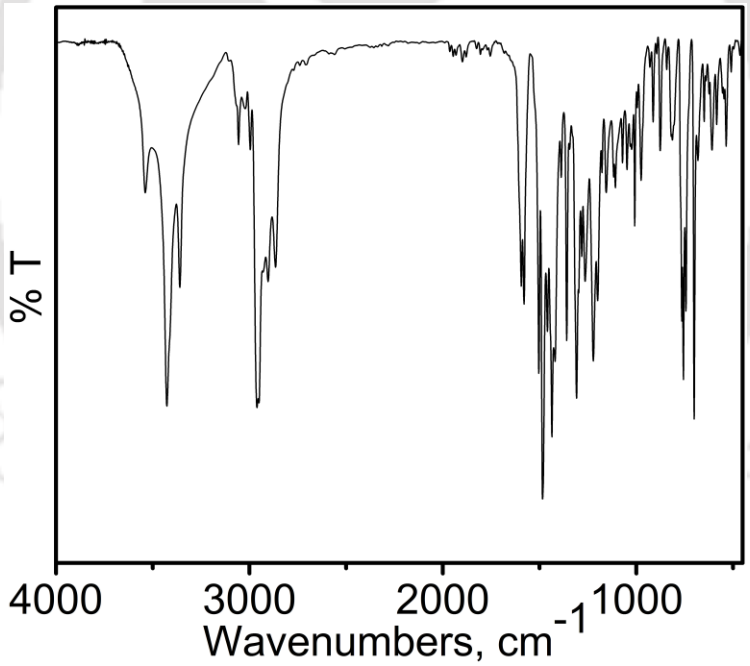

Figure 6.15: *FT-IR spectrum of* $\boldsymbol{H_2L^{AP(Ph)}}$.

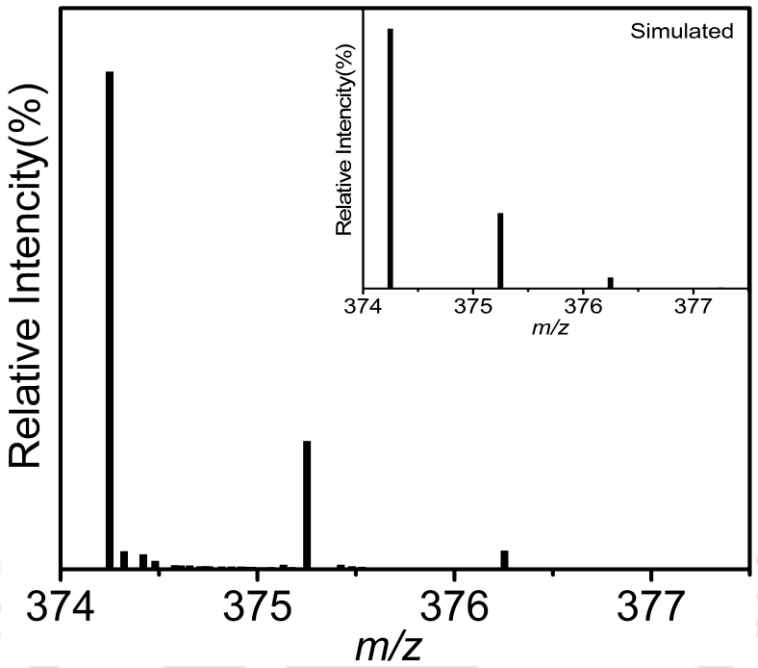

Figure 6.16: *Experimental and simulated mass spectra for* $\boldsymbol{H_2L^{AP(Ph)}}$ $[C_{26}H_{31}NO+H]^+$ *have been shown.*

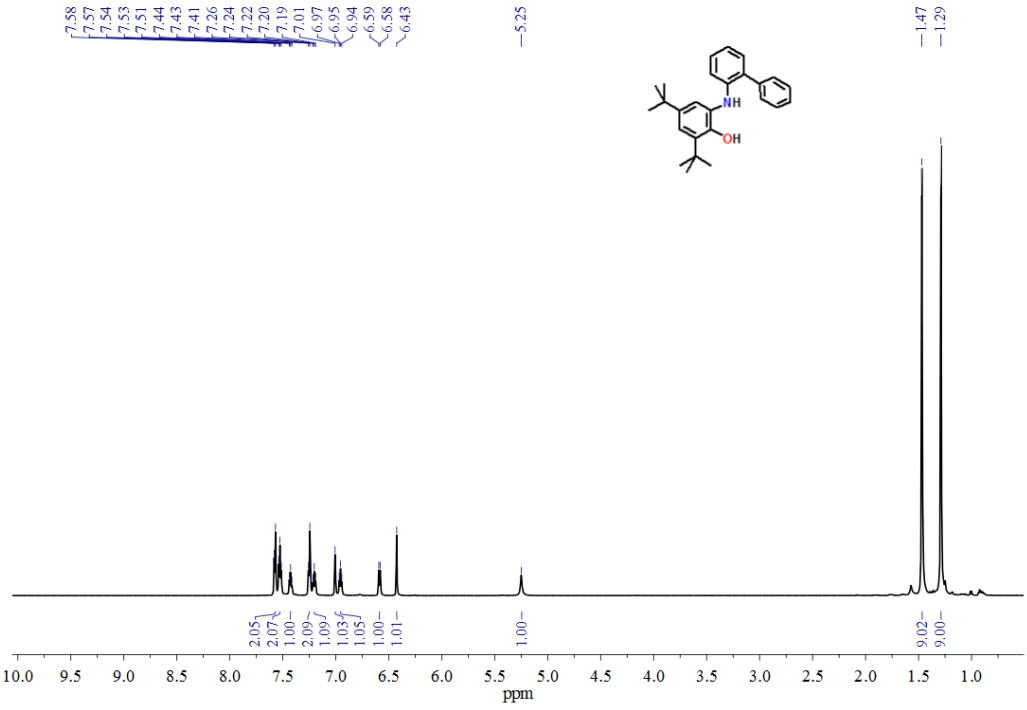

Figure 6.17: ^{1}*H-NMR spectrum of* $\boldsymbol{H_2L^{AP(Ph)}}$ *in* $CDCl_3$.

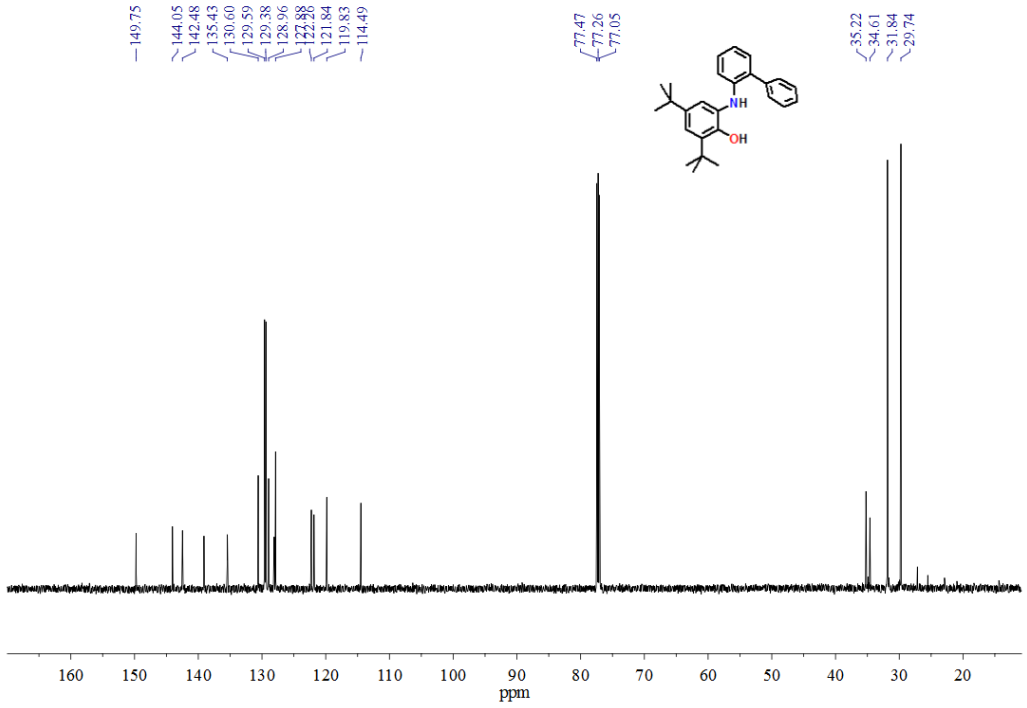

Figure 6.18: *^{13}C-NMR spectrum of* $\boldsymbol{H_2L^{AP(Ph)}}$ *in* $CDCl_3$.

6.2.4: Synthesis of complex 2A, $[C_{66}H_{74}Fe_2Cl_2N_8O_{15}]$:

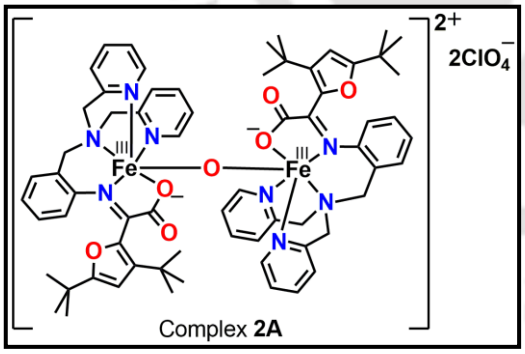

To a stirring solution of ligand $\mathbf{H_2Gan^{AP}}$ (0.206 g, 0.40 mmol) in acetonitrile (15 mL), $Fe(ClO_4)_2 \bullet 6H_2O$ (0.144 g, 0.40 mmol) and Et_3N (0.1 mL) were added sequentially. After stirring for 15 min at room temperature, tetrabutylammonium perchlorate (0.276 g, 0.80 mmol) was added to the solution. The resulting reaction mixture was continued to stir for further 17 h. After that, the reaction mixture was kept for slow evaporation at room temperature for 6 days, during the period needle-shaped crystal appeared.

Yield: 0.145 g, 54 %.

FT-IR (KBr pellet, cm^{-1}): 3070, 2965, 2934, 2872, 2251, 1676, 1607, 1587, 1550, 1485, 1443, 1317, 1278, 1247, 1092, 1002, 869, 850, 760.

ESI-MS (+) *m/z* for $[C_{66}H_{74}Fe_2N_8O_7]^{2+}$: Calcd, 601.2236; Found 601.2298.

UV-vis/NIR (CH_2Cl_2) λ_{max}, nm (ε, $M^{-1}cm^{-1}$): 440(17450), 383(19800), 315(23575), 280(30000).

Anal. Calcd for $C_{66}H_{74}Fe_2Cl_2N_8O_{15}$•1$CH_3CN$: C, 56.61; H, 5.38; N, 8.74. Found: C, 56.30; H, 5.03; N, 8.79 %.

6.2.5: Synthesis of Complex 2B, $[C_{33}H_{38}FeClN_4O_5]$:

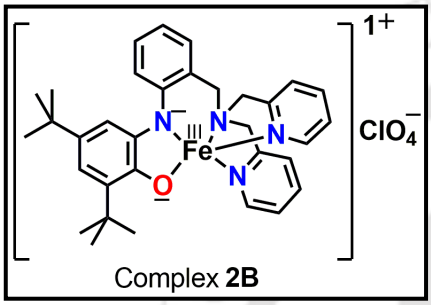

Complex **2B**

Ligand $\mathbf{H_2Gan^{AP}}$ (0.102 g, 0.20 mmol) was dissolved in acetonitrile (10 mL) under nitrogen atmosphere (inside a glove box). To that, Et_3N (0.056 mL) of was added and the solution was allowed to stir for 5 min. After that, $Fe(ClO_4)_2$•$6H_2O$ (0.075 g, 0.21 mmol) of was added and the resulting mixture was allowed to stir for further 10 min. To the solution tetrabutylammonium perchlorate (0.140 g, 0.40 mmol) of was added and the reaction mixture was continued to stir overnight (~10 h). The solvent was removed under vacuum; the residue was dissolved in dichloromethane, and then filtered. The filtrate part was concentrated under vacuum and to the residue hexane was added drop wise until the product precipitated out. The precipitate was filtered and washed with hexane and diethyl ether and then the product was collected as brown solid.

Yield: 0.145 g, 72%.

ESI-MS (+) *m/z* for $[C_{33}H_{38}FeN_4O]^{+}$: Calcd, 562.2441; Found 562.2302.

UV-vis/NIR (CH_2Cl_2) λ_{max}, nm (ε, $M^{-1}cm^{-1}$): 950(800), 578(1350), 376(3200).

Anal. Calcd for $C_{33}H_{38}FeClN_4O_5$•2Et_2O•7H_2O: C, 52.59; H, 7.75; N, 5.98. Found: C, 52.86; H, 8.09; N, 5.93 %.

6.2.6: Synthesis of Complex 2C, $[C_{66}H_{76}Cl_2Mn_2N_8O_{11}]$:

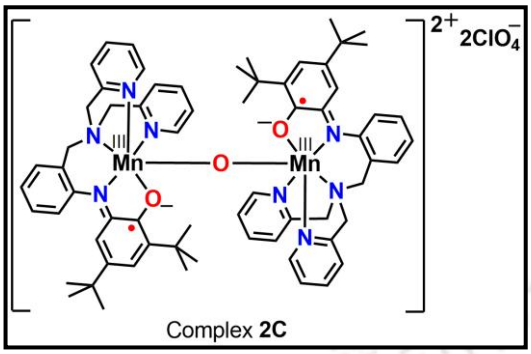

To a stirring methanol (10 mL) solution of ligand $\mathbf{H_2Gan^{AP}}$ (0.150 g, 0.3 mmol), $Mn(ClO_4)_2 \cdot 6H_2O$ (0.108 g, 0.3 mmol) and Et_3N (0.1 mL) were added sequentially. The resulted solution was stirred for 15 min. To the solution tetrabutylammonium perchlorate (0.208 g, 0.60 mmol) was added and the resulting reaction mixture was continued to stir for further 4 h. Then a deep brown colour precipitate was formed. It was filtered and washed with excess methanol (10 mL). Brown colored single crystals were grown by slow evaporation of dichloromethane and methanol (3:1) solvent mixture at room temperature.

Yield: 0.084 g, 42%.

FT-IR (KBr pellet, cm^{-1}): 3070, 2961, 2914, 2871, 1603, 1480, 1443, 1405, 1088, 845, 761, 622.

ESI-MS (+) *m/z* for $[C_{66}H_{76}Mn_2N_8O_3]^{2+}$: Calcd, 569.2400; Found 569.2396.

UV-vis/NIR (CH_2Cl_2) λ_{max}, nm (ε, $M^{-1}cm^{-1}$): 915(2450), 830(2800), 524(5200), 484(5900), 404(15100), 352(19050).

Anal. Calcd for $C_{66}H_{76}Cl_2Mn_2N_8O_{11}$: C, 59.26; H, 5.73; N, 8.38. Found: C, 59.78; H, 5.85; N, 8.46 %.

6.2.7: Synthesis of Complex 3A, $[C_{46}H_{62}N_4O_2CoCl]$:

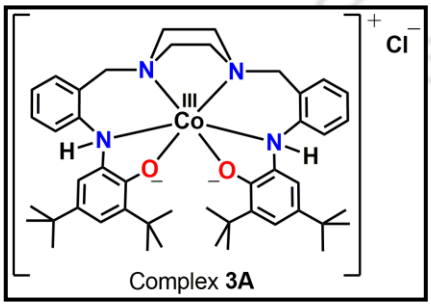

To a stirring solution of ligand $\mathbf{H_4L^{Piperazine(AP/AP)}}$ (0.216 g, 0.30 mmol) in acetonitrile (10 mL), $CoCl_2 \cdot 6H_2O$ (0.074 g, 0.30 mmol) and Et_3N (0.1 mL) were added sequentially. Then it was allowed to stir for 1.5 h, a blue-violet color precipitate was formed, which was filtered out and washed with excess acetonitrile (10 mL). The solid product was recrystallised by using a methanol:chloroform (3:1, v/v) solvent mixture.

Yield: 0.106 g, 46%.

FT-IR (KBr pellet, cm^{-1}): 3601, 3148, 3063, 2951, 2906, 2864, 1602, 1475, 1459, 1408, 1294, 1268, 1261, 766.

ESI-MS (+) *m/z* for $[C_{46}H_{62}CoN_4O_2]^+$: Calcd, 762.4205; Found 762.4214.

UV-vis/NIR (CH_2Cl_2) λ_{max}, nm (ε, $M^{-1}cm^{-1}$): 830(1900), 555(9100).

Anal. Calcd for $C_{46}H_{62}CoN_4O_2$: C, 74.42; H, 8.03; N, 4.13. Found: C, 74.34; H, 7.89; N, 4.51 %.

6.2.8: Synthesis of Complex 3B, $[C_{46}H_{60}Cl_2CuN_4O_2]$:

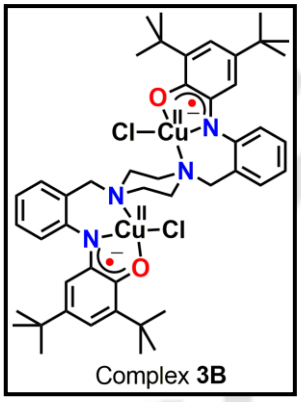

Complex **3B**

$CuCl_2 \cdot 2H_2O$ (0.080 g, 0.45 mmol) was added to a solution of ligand $\mathbf{H_4L^{Piperazine(AP/AP)}}$ (0.152 g, 0.21 mmol) in acetonitrile (10 mL). Upon addition of Et_3N (0.1 mL), the color of the solution changed to deep blue. Then the mixture was stirred for 2.5 h. A dark blue mass formed, which was collected by filtration, washed thoroughly with CH_3CN (10 mL) and dried. The solid was dissolved in a (3:1) dichloromethane/acetonitrile solution. Single crystals suitable for X-ray diffraction analysis were obtained after 4 day by slow evaporation of the solvent at room temperature.

Yield: 0.045 g, 42 %.

FT-IR (KBr pellet, cm^{-1}): 3044, 2954, 2906, 2868, 1625, 1584, 1484, 1458, 1445, 1376, 1360, 1314, 1268, 1234, 1114, 1024, 989, 904, 895, 852, 759, 746, 642.

ESI–MS (+) *m/z* for $[C_{46}H_{60}Cl_2Cu_2N_4O_2]^+$: Calcd, 896.2696; found 896.2659.

UV-vis/NIR (CH_2Cl_2) λ_{max}, nm (ε, $M^{-1}cm^{-1}$): 990(4050), 580(13900), 324(18450).

Anal. Calcd for $C_{46}H_{60}Cl_2Cu_2N_4O_2$: C 61.58, H 6.74, N 6.24; Found C 61.08, H 7.21, N 6.029 %.

6.2.9: Synthesis of Complex 3C, $[C_{42}H_{50}CuN_2O_2]$:

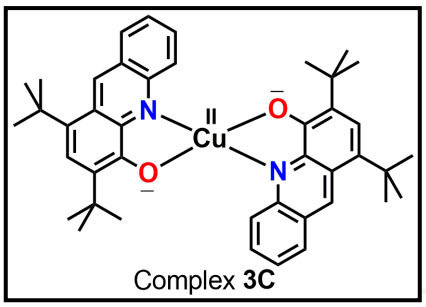

Ligand $\mathbf{H_4L^{Piperazine(AP/AP)}}$ (0.151 g, 0.21 mmol) was treated with an equimolar amount of $Cu(ClO_4)_2 \cdot 6H_2O$ (0.078 g, 0.21 mmol) in acetonitrile (10 mL). After the solution stirred for 5 min at room temperature, 0.06 mL of Et_3N was added. Then the resulting solution was stirred another 35 min to give a green color precipitate, which was collected by filtration and washed with excess acetonitrile (10 mL).

Yield: 0.040 g, 40%.

FT-IR (KBr pellet, cm^{-1}): 3063, 2952, 2919, 2869, 1624, 1578, 1556, 1512, 1440, 1440, 1409, 1351, 1252, 1237, 1150, 1106, 762, 748.

ESI-MS (+) *m/z* for $[C_{46}H_{62}CoN_4O_2]^+$: Calcd, 675.3023; Found 675.3012.

UV-vis/NIR (CH_2Cl_2) λ_{max}, nm (ε, $M^{-1}cm^{-1}$): 545(7950), 668(750)

Anal. Calcd for $C_{42}H_{50}CuN_2O_2$: C, 74.63; H, 7.16; N, 4.14. Found: C, 74.57; H, 7.85; N, 7.38 %.

6.2.10: Synthesis of complex 4A, $[C_{52}H_{58}CoN_2O_2]$:

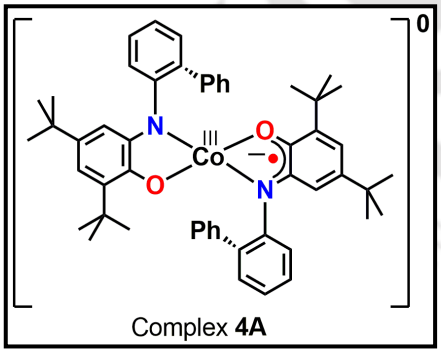

To a stirred solution of ligand $\mathbf{H_2L^{AP(Ph)}}$ (0.189 g, 0.5 mmol) in acetonitrile (10 mL), $Co(ClO_4)_2 \cdot 6H_2O$ (0.187 g, 0.5 mmol) and Et_3N (0.1 mL) were added sequentially at room temperature under air. The solution was then stirred at room temperature for an hour. The resulted precipitate was the filtered and washed with excess acetonitrile (10 mL). Unfortunately, all attempts to grow single crystals of complex **4A** were unsuccessful.

Yield: 0.104 g, 52%.

FT-IR (KBr pellet, cm^{-1}): 3054, 2953, 2902, 2863, 1577, 1536, 1474, 1358, 1302, 1266, 1185, 1140, 1106, 1026, 912, 896, 855, 746, 697, 660, 510.

ESI-MS (+) m/z for $[C_{52}H_{58}N_2O_2Co]^+$: Calcd, 801.3830 ; found, 801.3836.

UV-vis/NIR (CH_2Cl_2) λ_{max}, nm (ε, $M^{-1}cm^{-1}$): 1600(1500), 909(19600), 677(18000).

Anal. Calcd for $C_{52}H_{58}CoN_2O_2$: C, 77.88; H, 7.29; N, 3.49. Found: C, 78.16; H, 7.27; N, 3.16 %.

6.2.11: Synthesis of complex 4B, $[C_{52}H_{58}CoN_2O_2Cl]$:

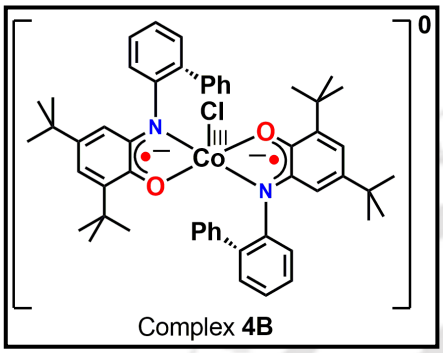

Complex **4B**

$CoCl_2 \cdot 6H_2O$ (0.119 g, 0.5 mmol) was added to a solution of ligand $\mathbf{H_2L^{AP(Ph)}}$ (0.152 g, 0.21 mmol) in acetonitrile (10 mL). Upon addition of Et_3N (0.1 mL), the color of the solution changed to deep blue. Then the mixture was stirred for 2 h 30 min, and a dark blue mass formed, which was collected by filtration, washed thoroughly with CH_3CN (10 mL) and dried. The solid was dissolved in a (3:1) dichloromethane/acetonitrile solution. Single crystals suitable for X-ray diffraction analysis were obtained after 4 day by slow evaporation of the solvent at room temperature.

Yield: 0.104 g, 64%.

FT-IR (KBr pellet, cm^{-1}): 3054, 2953, 2902, 2863, 1577, 1536, 1474, 1358, 1302, 1266, 1185, 1140, 1106, 1026, 912, 896, 855, 746, 697, 660, 510.

ESI-MS (+) m/z for $[C_{52}H_{58}ClN_2O_2Co–Cl]^+$: Calcd, 801.3830 ; found, 801.3839.

UV-vis/NIR (CH_2Cl_2) λ_{max}, nm (ε, $M^{-1}cm^{-1}$): ~865(13800), 675(20350).

Anal. Calcd for $C_{52}H_{58}ClCoN_2O_2$: C, 77.88; H, 7.29; N, 3.49. Found: C, 78.16; H, 7.27; N, 3.16 %.

6.2.12: Synthesis of complex 4C, $[C_{58}H_{63}CoN_2O_2S]$:

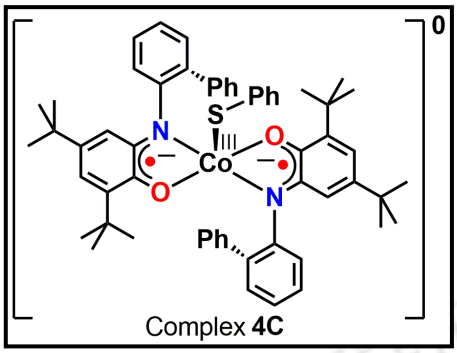

Ligand $\mathbf{H_2L^{AP(Ph)}}$ (0.187 g, 0.50 mmol) was dissolved in acetonitrile (10 mL), $Co(ClO_4)_2 \cdot 6H_2O$ (0.092 g, 0.25 mmol) was added to the solution at room temperature. During stirring the colour of the solution gradually turned to deep blue. The solution was then treated with triethylamine (0.1 mL). After 15 min, diphenyl-disulfide (0.110 g, 0.5 mmol) was added to the blue solution. The solution was further stirred for 2.5 h. A blue colour precipitate was formed, which was isolated by filtration and washed thoroughly with acetonitrile (10 mL). X-ray quality single crystals were grown from a solvent mixture of diethyl ether and acetonitrile (4:1) in a dark place employing solvent evaporation technique.

Yield: 0.107 g, 47%.

FT-IR (KBr pellet, cm^{-1}): 3052, 2956, 2903, 2866, 1591, 1527, 1472, 1432, 1392, 1361, 1331, 1298, 1268, 1243, 1202, 1175, 1104, 1025, 747, 698.

ESI-MS (+) m/z for $[C_{58}H_{63}CoN_2O_2S]^+$: Calcd, 910.3942; Found 910.3946.

UV-vis/NIR (CH_2Cl_2) λ_{max}, nm (ε, $M^{-1}cm^{-1}$): 834(17700), 583(14750).

Anal. Calcd for $C_{58}H_{63}CoN_2O_2S$: C, 76.45; H, 6.97; N, 3.07. Found: C, 77.18; H, 7.121; N, 3.17 %.

6.2.13: Synthesis of complex 4D, $[C_{58}H_{63}CoN_2O_2Se]$:

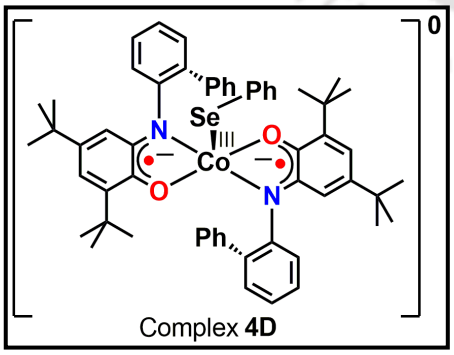

To a stirred solution of ligand $\mathbf{H_2L^{AP(Ph)}}$ (0.187 g, 0.50 mmol)) in acetonitrile (10 mL), $Co(ClO_4)_2 \cdot 6H_2O$ (0.092 g, 0.25 mmol) and triethylamine (0.1 mL) were added, sequentially. The resulted solution was stirred for 15 min and then diphenyl diselenide (0.156 g, 0.5 mmol) was added to the solution. The blue solution was further stirred for 2.5 h. A deep blue colour precipitate was formed during the stirring. The solid was filtered and washed with acetonitrile (15 mL). X-ray quality single

crystals were obtained upon slow evaporation of diethyl ether and acetonitrile (4:1) solvent mixture at room temperature in a dark place.

Yield: 0.080 g, 33%.

FT–IR (KBr pellet, cm^{-1}): 3056, 2961, 2903, 2863, 1525, 1462, 1431, 1361, 1297, 1261, 1202, 1175, 1099, 1026, 802, 784, 735, 696.

ESI–MS (+) m/z for $[C_{58}H_{63}CoN_2O_2Se]^+$: Calcd, 958.3446; Found 958.3398.

UV-vis/NIR (CH_2Cl_2) λ_{max}, nm (ε, $M^{-1}cm^{-1}$): 843(17650), 678(10250), 583(13850).

Anal. Calcd for $C_{58}H_{63}CoN_2O_2Se$: C, 72.62; H, 6.62; N, 2.92. Found: C, 72.86; H, 6.63; N, 2.95 %.

6.2.14: Synthesis of complex 5A, $[C_{52}H_{58}CuN_2O_2]$:

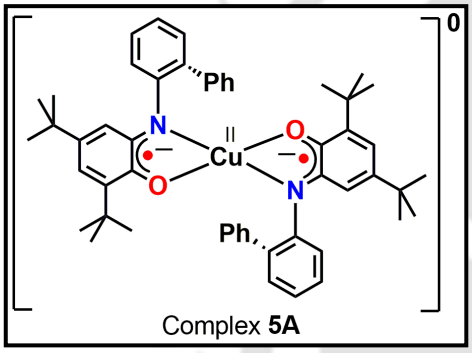

To a stirred solution of ligand $H_2L^{AP(Ph)}$ (0.189 g, 0.5 mmol) in CH_3OH (10 mL), $CuCl_2 \bullet 2H_2O$ (0.860 g, 0.5 mmol) and Et_3N (0.1 mL) were added sequentially at room temperature under air. The resulting solution was stirred at room temperature for 1 hour. The resulted greenish precipitate was filtered and washed with excess CH_3OH (5 mL). Crystals suitable for single crystal X–ray diffraction analysis were grown by slow evaporation of a 3:1 CH_2Cl_2/CH_3OH solvent mixture.

Yield: 0.126 g, 62%.

FT-IR (KBr pellet, cm^{-1}): 3055, 2959, 2905, 2866, 1579, 1475, 1462, 1447, 1386, 1361, 1332, 1253, 1202, 1179, 1110, 1029, 853, 775, 746, 738, 697.

ESI-MS (+) m/z for $[C_{52}H_{58}N_2O_2Cu]^+$: Calcd, 805.3789 ; found, 805.3791.

UV-vis/NIR (CH_2Cl_2) λ_{max}, nm (ε, $M^{-1}cm^{-1}$): 1070(4450), 792(6200), 470(5000), 310(19550).

Anal. Calcd for $C_{52}H_{58}CuN_2O_2$: C, 77.47; H, 7.25; N, 3.47. Found: C, 77.52; H 7.15; N, 3.58.

6.2.15: Synthesis of complex 5B, $[C_{52}H_{58}CuN_2O_2Cl]$:

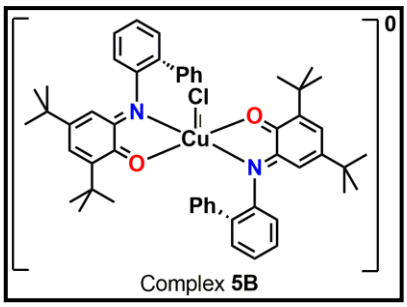

To a stirred solution of ligand $\mathbf{H_2L^{AP(Ph)}}$ (0.188 g, 0.5 mmol) in CH_3OH (10 mL), $CuCl_2 \bullet 2H_2O$ (0.173 g, 1.0 mmol) was added at room temperature under air. Upon addition of Et_3N (0.1 mL), the color of the solution changed to deep blue. After stirring of the solution for 1 hour 5 minutes, a dark blue solid of **2** formed which was collected by filtration. Recrystallization of the solid from a CH_2Cl_2/CH_3OH (4:1) solvent mixture provided blue crystals suitable for single crystal X-ray diffraction analysis.

Yield: 0.152 g, 72%.

FT-IR (KBr pellet, cm^{-1}): 3054, 2952, 2905, 2866, 1617, 1591, 1460, 1432, 1387, 1377, 1364, 1321, 1247, 1206, 1085, 1023, 895, 805, 746, 701, 611, 580, 531.

ESI-MS (+) m/z for $[C_{52}H_{58}N_2O_2CuCl–Cl]^+$: Calcd, 805.3789 ; found, 805.3769.

UV-vis/NIR (CH_2Cl_2) λ_{max}, nm (ε, $M^{-1}cm^{-1}$): 1160(1350), 490(13050), 420(11900).

Anal. Calcd for $C_{52}H_{58}CuN_2O_2Cl$: C, 74.25; H, 6.95; N, 3.33. Found: C 74.47; H, 6.85; N, 3.32.

6.2.16: Synthesis of complex 5C, $[C_{52}H_{58}CuN_2O_2PF_6]$:

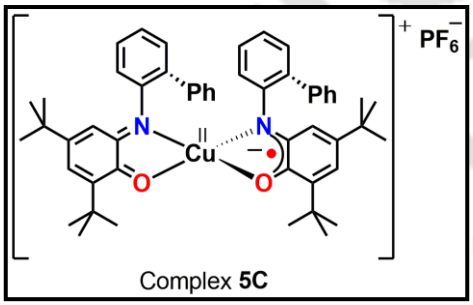

To a stirred solution of the complex **5A** (0.201 g, 0.25 mmol) in CH_2Cl_2 (10 mL), ferrocenium hexafluorophosphate (0.083 g, 0.25 mmol) was added and allowed to stirred for 3 hours. During stirring a deep green color solution was changes to deep blue. Then reaction solution was evaporated to dryness to give amorphous solid. The resulted solid was washed with excess hexane (10 mL). Recrystallization from CH_2Cl_2/hexane (3:1) solution afforded X-ray quality crystals.

Yield: 0.112 g, 45%.

FT-IR (KBr pellet, cm^{-1}): 3062, 2955, 2915, 2871, 1635, 1608, 1563, 1469, 1415, 1387, 1368, 1321, 1270, 1248, 1207, 1173, 1088, 903, 841, 745, 703, 557.

ESI-MS (+) m/z for $[C_{52}H_{58}N_2O_2Cu]^+$: Calcd, 805.3789 ; found, 805.3784.

UV-vis/NIR (CH_2Cl_2) λ_{max}, nm (ε, $M^{-1}cm^{-1}$): 1167(2000), 500(9150).

Anal. Calcd for $C_{52}H_{58}CuN_2O_2PF_6 \bullet 1.5H_2O$: C, 63.85; H, 6.29; N, 2.87. Found: C, 63.91; H, 6.03; N, 2.61.

6.2.17: Synthesis of complex 5D, $[C_{52}H_{58}CuN_2O_2SbF_6]$:

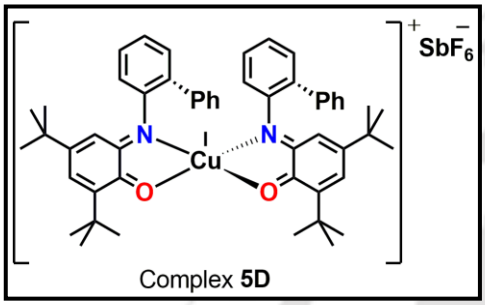

Complex **5D**

To a stirred solution of the complex **5B** (0.210 g, 0.25 mmol) in CH_2Cl_2 (10 mL), silver hexafluoroantimonate (0.085 g, 0.25 mmol) was added and allowed to stirred for 2 hours. During stirring a deep blue color solution changed to reddish–brown. Then reaction solution filtered through celite pad and filtrate part was evaporated to dryness to give amorphous solid of **4**. The solid was recrystallized from a CH_2Cl_2/MeOH (3:1) solvent mixture afforded X–ray quality crystals.

Yield: 0.112 g, 42%.

FT-IR (KBr pellet, cm^{-1}): 3063, 2961, 2909, 2871, 1638, 1622, 1514, 1473, 1377, 1288, 1268, 1251, 1021, 898, 751, 702, 657.

ESI-MS (+) m/z for $[C_{52}H_{58}N_2O_2Cu]^+$: Calcd, 805.3789 ; found, 805.3766.

Anal. Calcd for $C_{52}H_{58}CuN_2O_2SbF_6 \bullet 3H_2O$: C, 57.02; H, 5.89; N, 2.56. Found: C, 56.94; H, 5.63; N, 2.46.

Appendices

7.1 Crystallographic Data and Structure Refinement Parameters

Table 7.1:

	2A	**2C**
Empirical formula	$C_{66}H_{74}Fe_2N_8O_7$,2(CH_3CN), 2(ClO_4)	$C_{66}H_{73}Mn_2N_8O_3$, 2(ClO_4)
Formula weight	1484.04	1335.10
Crystal habit, colour	Needle, Brown	Needle, Brown
Crystal size, mm^3	0.20×0.15×0.05	0.21×0.12×0.08
Temperature, T	296(2)	293(2)
Wavelength, λ (Å)	0.71073	0.71073
Crystal system	monoclinic	monoclinic
Space group	'*P 21/c*'	'*P 21/n*'
Unit cell dimensions	a = 15.2994(3) Å b = 13.1099(3) Å c = 18.3192(4) Å α = 90.00°,β = 93.079(2)°, γ = 90.00°	a = 15.1390(7) Å b = 11.5340(7) Å c = 20.2243(18) Å α = 90.00°, β = 100.575(7)°, γ = 90.00°
Volume, V ($Å^3$)	3669.04(13)	3471.5(4)
Z	2	2
Calculated density, $Mg·m^{-3}$	1.343	1.277
Absorption coefficient, μ (mm^{-1})	0.538	0.502
F(000)	1552	1394
θ range for data collection	2.97° to 25.10°	3.13° to 25.00°
Limiting indices	$-15 \le h \le 18$, $-10 \le k \le 15$ $-15 \le l \le 21$	$-18 \le h \le 14$, $-4 \le k \le 13$, $-20 \le l \le 24$
Reflection collected/unique	17084/6514[R(int) = 0.0269]	14882 / 3987 [R(int) = 0.0350]
Completeness to θ	99.8% (θ = 25.00°)	99.8% (θ = 25.00°)
Max. and min. transmission	0.973/0.908	0.961/ 0.930
Refinement method	'SHELXL–97(Sheldrick, 1997)'	'SHELXL–97(Sheldrick, 1997)'
Data/restraints/parameters	6526/0/464	6109/0/417
Goodness–of–fit on F^2	1.049	1.098
Final R indices [I>2sigma(I)]	R1 = 0.0458, wR2 = 0.1091	R1 = 0.0765, wR2 = 0.1723
R indices (all data)	R1 = 0.0595, wR2 = 0.1178	R1 = 0.1131, wR2 = 0.1929
Largest diff. peak and hole	0.456 and –0.566 $e·Å^{-3}$	0.919 and –0.405$e·Å^{-3}$

Table 7.2:

	3A	**3B**	**3C**
Empirical formula	$C_{46}H_{62}CoN_4O_2$	$C_{46}H_{60}Cl_2Cu_2N_4O_2$	$C_{42}H_{48}CuN_2O_2$
Formula weight	761.93	898.98	676.37
Crystal habit, colour	Needle, Pink	Needle, Blue	Block, Brown
Crystal size, mm^3	0.20×0.15×0.10	0.24×0.12×0.08	0.18×0.15×0.10
Temperature, *T*	293(2)	293(2)	293(2)
Wavelength, λ (Å)	0.71073	0.71073	0.71073
Crystal system	monoclinic	triclinic	triclinic
Space group	'*C 2/c*'	'P –1'	'P –1'
Unit cell dimensions	*a* = 21.1697(8) Å *b* = 10.4712(4) Å *c* = 19.2053(6) Å α = 90.00°, β = 90.924(3)°, γ = 90.00°	*a* = 10.4996(4) Å *b* = 14.3892(9) Å *c* = 16.6632(9) Å α = 105.554(5)°, β = 99.245(4)°, γ = 99.165(4)°	*a* = 11.8586(4) Å *b* = 17.7280(6) Å *c* = 23.0707(6) Å α = 102.249(3)°, β = 100.156(3)°, γ = 103.341(3)°
Volume, *V* ($Å^3$)	4256.7(2)	2339.0(2)	4480.5(3)
Z	4	2	5
Calculated density, $Mg·m^{-3}$	1.189	1.276	1.253
Absorption coefficient, μ (mm^{-1})	0.444	1.063	0.647
F(000)	1636	944	1795
θ range for data collection	3.05 ° to 25.00°	2.89° to 25.00°	2.88° to 25.00°
Limiting indices	$-18 \le h \le 25$, $-12 \le k \le 12$, $-22 \le l \le 22$	$-11 \le h \le 12$, $-17 \le k \le 13$, $-19 \le l \le 19$	$-13 \le h \le 14$, $-20 \le k \le 21$, $-21 \le l \le 27$
Reflection collected/unique	10283 / 3167 [*R*(int) = 0.0235]	17518 / 5422 [*R*(int) = 0.0444]	33418 / 9386 [*R*(int) = 0.0382]
Completeness to θ	99.8% (θ = 25.00°)	99.7% (θ = 25.00°)	99.8% (θ = 25.00°)
Max. and min. transmission	0.957/ 0.923	0.918/ 0.858	0.937/ 0.890
Refinement method	'SHELXL–97(Sheldrick, 1997)'	'SHELXL–97(Sheldrick, 1997)'	'SHELXL–97(Sheldrick, 1997)'
Data/restraints/parameters	3736 /0/250	8229/0/517	15732/0/1090
Goodness–of–fit on F^2	0.991	1.033	1.040
Final *R* indices [*I*>2sigma(*I*)]	*R*1 = 0.0404, *wR*2 = 0.1086	*R*1 = 0.0620, *wR*2 = 0.1069	*R*1 = 0.0638, *wR*2 = 0.1547
R indices (all data)	*R*1 = 0.0476, *wR*2 = 0.1140	*R*1 = 0.1035, *wR*2 = 0.1238	*R*1 = 0.1149, *wR*2 = 0.1866
Largest diff. peak and hole	0.365 and – 0.322 $e·Å^{-3}$	0.489 and –0.332$e·Å^{-3}$	0.606 and –1.043 $e·Å^{-3}$

Table 7.3:

	4B	**4C**	**4D**
Empirical formula	$C_{52}H_{58}ClCoN_2O_2$, CH_3CN	$C_{58}H_{63}CoN_2O_2S$	C_{116} H_{127} Co_2 N_4 O_4 Se_2
Formula weight	878.44	910.39	1917.00
Crystal habit, colour	Needle, Blue	Needle, Dark Blue	Block, Brown
Crystal size, mm^3	0.24×0.18×0.14	0.20×0.15×0.10	0.26×0.17×0.12
Temperature, *T*	293(2)	293(2)	100(2)
Wavelength, λ (Å)	0.71073	0.71073	0.71073
Crystal system	triclinic	monoclinic	monoclinic
Space group	'P –1'	'P 21/n'	'P 21'
Unit cell dimensions	*a* = 12.6286(6) Å *b* = 14.1944(5) Å *c* = 15.1025(5) Å α = 79.358(3) °, β = 78.791(3) °, γ = 68.866(4) °	*a* = 13.2465(3) Å *b* = 16.1975(4) Å *c* = 48.3989(8) Å α = 90.00°, β = 92.1863(17)°, γ = 90.00°	*a* = 10.5924(5) Å *b* = 36.8212(15) Å *c* = 14.0563(6) Å α = 90.00°, β = 96.839(4)°, γ = 90.00°
Volume, *V* ($Å^3$)	2457.45(17)	10376.9(4)	5443.3(4)
Z	2	8	2
Calculated density, $Mg·m^{-3}$	1.187	1.166	1.170
Absorption coefficient, μ (mm^{-1})	0.445	0.413	1.024
F(000)	932	3872	2010
θ range for data collection	3.00° to 25.00°	3.03° to 25.00°	3.13° to 25.00°
Limiting indices	$-14 \le h \le 15$, $-16 \le k \le 14$, $-17 \le l \le 17$	$-15 \le h \le 15$, $-19 \le k \le 15$, $-57 \le l \le 41$	$-12 \le h \le 8$, $-43 \le k \le 41$, $-15 \le l \le 16$
Reflection collected/unique	18632 / 8628 [*R*(int)= 0.0244]	48525/18243 [*R*(int)= 0.0363]	26610/17459 [*R*(int)= 0.0313]
Completeness to θ	99.8% (θ = 25.00°)	99.8% (θ = 25.00°)	99.1% (θ = 25.00°)
Max. and min. transmission	0.940 / 0.908	0.978/0.960	0.884/0.811
Refinement method	'SHELXL–97(Sheldrick, 1997)'	'SHELXL–97(Sheldrick, 1997)'	'SHELXL–97(Sheldrick, 1997)'
Data/restraints/parameters	8628 /0/ 563	18243 /0/1177	17459 /1/1178
Goodness–of–fit on F^2	1.032	1.076	1.076
Final *R* indices [*I*>2sigma(*I*)]	*R*1 = 0.0547, *wR*2 = 0.1385	*R*1 = 0.0581, *wR*2 = 0.1260	*R*1 = 0.0704, *wR*2 = 0.1630
R indices (all data)	*R*1 = 0.0694, *wR*2 = 0.1522	*R*1 = 0.0764, *wR*2 = 0.1358	*R*1 = 0.0910, *wR*2 = 0.1804
Largest diff. peak and hole	0.828and –0.599 $e·Å^{-3}$	0.498 and –0.332$e·Å^{-3}$	0.989 and –0.492 $e·Å^{-3}$

Table 7.4:

	5B	**5C**	**5D**
Empirical formula	C_{52} $H_{58}CuN_2O_2Cl$	$2(C_{52}H_{58}CuN_2O_2)$, $2(PF_6)$, $3(H_2O)$	C_{52} $H_{58}CuN_2O_2SbF_6$
Formula weight	842.00	1957.10	1042.29
Crystal habit, colour	Block, Deep blue	Block, Blue	Needle, Brown
Crystal size, mm^3	0.25×0.20×0.15	0.10×0.08×0.04	0.26×0.12×0.10
Temperature, T	100(2)	293(2)	100(2)
Wavelength, λ (Å)	0.71073	0.71073	0.71073
Crystal system	monoclinic	triclinic	trigonal
Space group	'C 2/c'	'P –1'	'P 31 2 1'
Unit cell dimensions	a = 17.0071(8) Å b = 13.1682(6) Å c = 20.1656(8) Å α = 90.00°, β = 95.639(4)°, γ = 90.00°	a = 11.5692(6) Å b = 12.6901(5) Å c = 17.5488(5) Å α = 94.409(3)°, β = 96.390(3)°, γ = 95.137(4)°	a = 17.2491(4) Å b = 17.2491(4) Å c = 14.2445(5) Å α = 90.00°, β = 90.00°, γ = 120.00°
Volume, V ($Å^3$)	4494.3(3)	2540.29(18)	3670.4(2)
Z	4	1	3
Calculated density, $Mg·m^{-3}$	1.244	1.279	1.415
Absorption coefficient, μ (mm^{-1})	0.587	0.527	1.050
F(000)	1784	1026	1602
θ range for data collection	2.99° to 24.75°	3.11° to 27.50°	3.08° to 27.49°
Limiting indices	$-20 \le h \le 13$, $-15 \le k \le 15$, $-22 \le l \le 23$	$-14 \le h \le 15$, $-16 \le k \le 16$, $-21 \le l \le 22$	$-20 \le h \le 22$, $-6 \le k \le 22$, $-17 \le l \le 18$
Reflection collected/unique	8932/ 3185 [R(int)= 0.0533]	19554 / 8286 [R(int)= 0.0226]	10058/ 4896 [R(int)= 0.0269]
Completeness to θ	96.0% (θ = 24.75°)	96.0% (θ = 27.50°)	97.8% (θ = 27.49°)
Max. and min. transmission	0.916/ 0.869	0.979/ 0.951	0.900/ 0.860
Refinement method	'SHELXL–97(Sheldrick, 1997)'	'SHELXL–97(Sheldrick, 1997)'	'SHELXL–97(Sheldrick, 1997)'
Data/restraints/parameters	3694 /0/ 269	11206 /0/604	5392 /0/ 296
Goodness–of–fit on F^2	1.066	1.014	1.062
Final R indices [I>2sigma(I)]	$R1$ = 0.0424, $wR2$ = 0.1069	$R1$ = 0.0768, $wR2$ = 0.2047	$R1$ = 0.0424, $wR2$ = 0.0959
R indices (all data)	$R1$ = 0.0515, $wR2$ = 0.1160	$R1$ = 0.1008, $wR2$ = 0.2298	$R1$ = 0.0501, $wR2$ = 0.1020
Largest diff. peak and hole	0.368 and –0.392 $e·Å^{-3}$	0.770 and –1.239 $e·Å^{-3}$	0.910 and –0.884 $e·Å^{-3}$

7.2 DFT Optimized Structure and Selected Bond Distances of Complex 2B

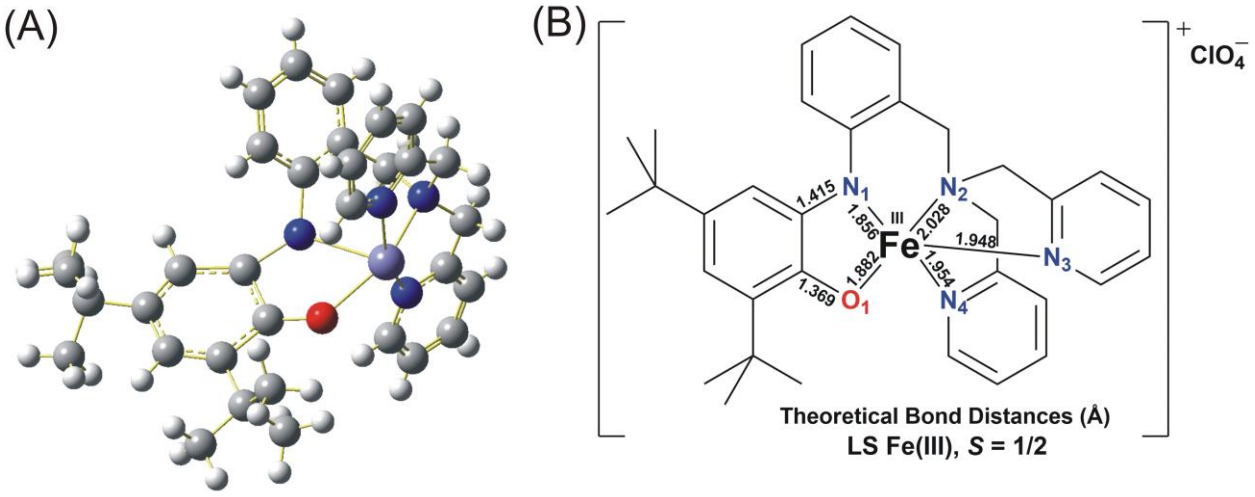

Figure 7.1: *(A) Optimized structure of the complex **2B** obtained from the DFT calculation with an S = 1/2 spin-state. (B) Selected bond distances of complex **2B** obtained from the DFT calculation.*

Table 7.5: Cartesian coordinates for complex **2B**.
LS S = 1/2, Energy = -1780761.941989 Kcal/mol

```
1 2
Fe(PDBName=Fe1,ResName=UNK,ResNum=1) 5.70800000 0.98800000 9.43900000
O(PDBName=O3,ResName=UNK,ResNum=1) 6.35262208 3.04226592 9.95313392
N(PDBName=N1,ResName=UNK,ResNum=1) 3.98795153 2.69397470 9.66374499
N(PDBName=N3,ResName=UNK,ResNum=1) 4.26500000 -0.65100000 9.46300000
N(PDBName=N4,ResName=UNK,ResNum=1) 5.66200000 0.38000000 11.50500000
N(PDBName=N2,ResName=UNK,ResNum=1) 5.11100000 0.89700000 7.38600000
C(PDBName=C16,ResName=UNK,ResNum=1) 2.71400000 2.07700000 8.90400000
C(PDBName=C17,ResName=UNK,ResNum=1) 2.08200000 2.97300000 8.04900000
H(PDBName=H17,ResName=UNK,ResNum=1) 2.43000000 3.82800000 7.93000000
C(PDBName=C23,ResName=UNK,ResNum=1) 4.80600000 1.61000000 10.46300000
H(PDBName=H23A,ResName=UNK,ResNum=1) 5.55000000 2.09600000 10.07700000
H(PDBName=H23B,ResName=UNK,ResNum=1) 4.11800000 2.25200000 10.70100000
C(PDBName=C18,ResName=UNK,ResNum=1) 0.93900000 2.59300000 7.37700000
H(PDBName=H18,ResName=UNK,ResNum=1) 0.51500000 3.19600000 6.80900000
C(PDBName=C21,ResName=UNK,ResNum=1) 2.23000000 0.77700000 9.03900000
C(PDBName=C33,ResName=UNK,ResNum=1) 4.95200000 1.68900000 5.15100000
H(PDBName=H33,ResName=UNK,ResNum=1) 5.15000000 2.34100000 4.52000000
C(PDBName=C34,ResName=UNK,ResNum=1) 5.35600000 1.83300000 6.46200000
H(PDBName=H34,ResName=UNK,ResNum=1) 5.81400000 2.60500000 6.71000000
C(PDBName=C32,ResName=UNK,ResNum=1) 4.26000000 0.57700000 4.79800000
H(PDBName=H32,ResName=UNK,ResNum=1) 3.97700000 0.46500000 3.92000000
C(PDBName=C24,ResName=UNK,ResNum=1) 5.26000000 -0.89000000 11.68800000
C(PDBName=C28,ResName=UNK,ResNum=1) 4.24800000 -1.23600000 8.09500000
H(PDBName=H28A,ResName=UNK,ResNum=1) 3.40300000 -1.69100000 7.95400000
H(PDBName=H28B,ResName=UNK,ResNum=1) 4.95700000 -1.89300000 8.02000000
```

```
C(PDBName=C30,ResName=UNK,ResNum=1) 4.42800000 0.19300000 7.03600000
C(PDBName=C19,ResName=UNK,ResNum=1) 0.42500000 1.34200000 7.54000000
H(PDBName=H19,ResName=UNK,ResNum=1) -0.36200000 1.10400000 7.10700000
C(PDBName=C22,ResName=UNK,ResNum=1) 2.90100000 -0.23200000 9.92900000
H(PDBName=H22A,ResName=UNK,ResNum=1) 2.97800000 0.14300000 10.82000000
H(PDBName=H22B,ResName=UNK,ResNum=1) 2.33800000 -1.01900000 9.98800000
C(PDBName=C20,ResName=UNK,ResNum=1) 1.07000000 0.43100000 8.34400000
H(PDBName=H20,ResName=UNK,ResNum=1) 0.72600000 -0.42900000 8.42600000
C(PDBName=C31,ResName=UNK,ResNum=1) 3.98000000 -0.37600000 5.73300000
H(PDBName=H31,ResName=UNK,ResNum=1) 3.49700000 -1.13700000 5.50200000
C(PDBName=C27,ResName=UNK,ResNum=1) 6.18400000 1.05700000 12.54700000
H(PDBName=H27,ResName=UNK,ResNum=1) 6.46600000 1.93500000 12.42600000
C(PDBName=C25,ResName=UNK,ResNum=1) 5.34200000 1.50500000 12.92400000
H(PDBName=H25,ResName=UNK,ResNum=1) 5.03000000 -2.37300000 13.04100000
C(PDBName=C26,ResName=UNK,ResNum=1) 5.88700000 -0.82200000 13.96500000
H(PDBName=H26,ResName=UNK,ResNum=1) 5.97600000 -1.23200000 14.79500000
C(PDBName=C29,ResName=UNK,ResNum=1) 6.30700000 0.46700000 13.79100000
H(PDBName=H29,ResName=UNK,ResNum=1) 6.67100000 0.94300000 14.50200000
C                                   4.06856454 4.26047016 10.34469543
C                                   5.65405399 4.26517895 10.37430651
C                                   6.17721407 5.77819586 10.47944042
C                                   5.47956007 6.98670486 10.47824142
C                                   4.08473507 6.98662686 10.47776242
C                                   3.38713407 5.77842086 10.47875842
H                                   6.02976007 7.93884786 10.47818242
H                                   2.28753007 5.77860386 10.47857842
C                                   3.10519980 8.79063962 9.02507048
H                                   2.32249429 8.21751251 8.57363122
H                                   2.83665139 9.82638385 9.02111673
H                                   4.01110260 8.65494876 8.47205320
C                                   3.31439689 8.32011001 10.47642793
C                                   1.87800623 8.28681606 11.03075039
H                                   1.87119930 7.78097786 11.97360848
H                                   1.52243376 9.28765017 11.16036255
H                                   1.24237434 7.76868733 10.34342608
C                                   4.18964638 9.21635775 11.37212784
H                                   4.42365526 8.69602941 12.27733404
H                                   5.09502692 9.46020838 10.85664463
H                                   3.65838456 10.11555280 11.60474154
C                                   7.71721381 5.77830790 10.48032828
C                                   8.23029818 7.20828466 10.73234196
H                                   7.93874865 7.84023600 9.91960807
H                                   7.81119640 7.58226969 11.64304986
H                                   9.29744308 7.19590313 10.80946827
C                                   8.23136927 5.28136965 9.11640140
H                                   8.62265747 4.29109518 9.22199507
H                                   7.42528493 5.27321661 8.41279529
H                                   9.00340318 5.93452206 8.76675075
C                                   8.22997308 4.84538148 11.59312936
H                                   7.43652160 4.64156608 12.28145634
H                                   8.57125764 3.92817518 11.16051239
H                                   9.03840768 5.31820137 12.11059901
1 2 1.0 3 1.0 4 1.0 5 1.0 6 1.0
2 45 1.0
3 7 1.0 44 1.0
4 10 1.0 23 1.0 29 1.0
```

```
5 22 1.5 36 1.5
6 18 1.5 26 1.5
7 8 1.5 15 1.5
8 9 1.0 13 2.0
9
10 11 1.0 12 1.0 22 1.0
11
12
13 14 1.0 27 2.0
14
15 29 1.0 32 1.5
16 17 1.0 18 2.0 20 2.0
17
18 19 1.0
19
20 21 1.0 34 2.0
21
22 38 2.0
23 24 1.0 25 1.0 26 1.0
24
25
26 34 1.5
27 28 1.0 32 2.0
28
29 30 1.0 31 1.0
30
31
32 33 1.0 35 1.0
35
36 37 1.0 42 2.0
37
38 39 1.0 40 2.0
39
40 41 1.0 42 2.0
41
42 43 1.0
43
44 45 1.5 49 1.5
45 46 1.5
46 47 1.5 65 1.0
47 48 1.5 50 1.0
48 49 1.5 56 1.0
49 51 1.0
50
51
52 53 1.0 54 1.0 55 1.0 56 1.0
53
54
55
56 57 1.0 61 1.0
57 58 1.0 59 1.0 60 1.0
58
59
60
61 62 1.0 63 1.0 64 1.0
62
```

```
63
64
65 66 1.0 70 1.0 74 1.0
66 67 1.0 68 1.0 69 1.0
67
68
69
70 71 1.0 72 1.0 73 1.0
71
72
73
74 75 1.0 76 1.0 77 1.0
75
76
77
```

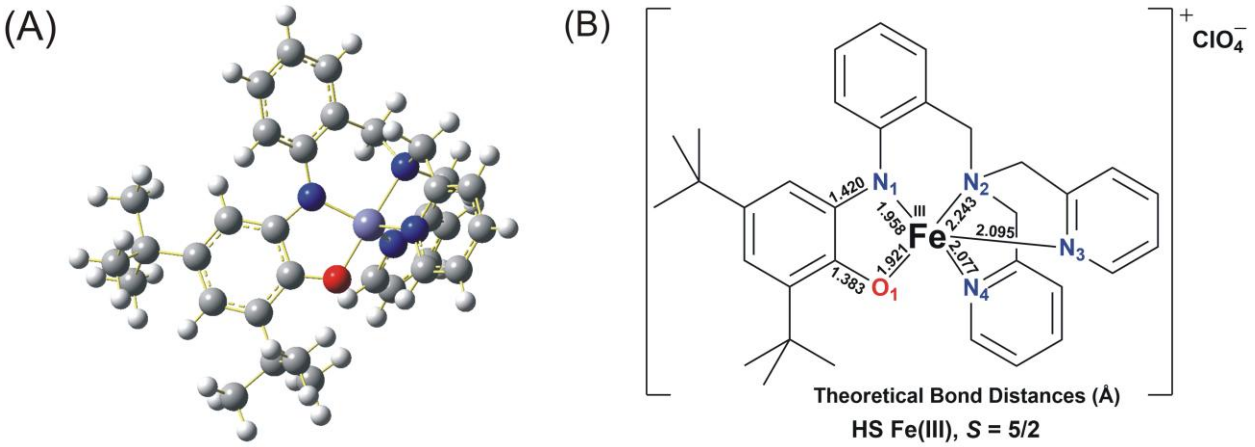

Figure 7.2: *(A) Optimized structure of the complex **2B** obtained from the DFT calculation with an S = 5/2 spin-state. (B) Selected bond distances of complex **2B** obtained from the DFT calculation.*

Table 7.6. Cartesian coordinates for complex **2B**.
HS S = 5/2 Energy = -1780771.054056 Kcal/mol

```
1 6
Fe -1.25285000 0.25847900 -0.01781300
O 0.12712500 1.44379100 0.46576200
N 0.05297000 -1.05601400 0.09574900
N -2.78089300 -0.99473100 -0.47611700
N -1.65998300 0.96632500 -1.78654600
N -2.52592000 0.85846400 1.33804500
C -0.18408100 -2.44961000 0.27876500
C 0.62142700 -3.23323600 1.14317000
H 1.46115500 -2.76608300 1.65513000
C -3.70387900 -0.23023800 -1.41086200
H -4.30927700 0.44643600 -0.78700400
H -4.38943900 -0.91595700 -1.93531900
C 0.32821000 -4.58450100 1.36883700
H 0.96363900 -5.16611900 2.03786900
C -1.33362600 -3.04701400 -0.31378800
C -3.41168600 2.40686200 2.96434000
```

H -3.32601200 3.36180900 3.48063800
C -2.45484600 2.05193600 2.00901200
H -1.60224300 2.67823900 1.75634700
C -4.46732200 1.52351200 3.24829600
H -5.22091400 1.78140900 3.99170800
C -2.85535600 0.57462400 -2.35442600
C -3.48294800 -1.29950400 0.82618500
H -2.86008900 -2.03634700 1.35730000
H -4.47638100 -1.74953700 0.65822800
C -3.56204600 -0.01477100 1.61339000
C -0.78215100 -5.18466500 0.75034200
H -1.00825900 -6.23754100 0.91861800
C -2.25218300 -2.23575200 -1.18593800
H -1.73620500 -1.85847000 -2.08227800
H -3.10353800 -2.85635800 -1.51760000
C -1.61138900 -4.40647400 -0.07231000
H -2.48842000 -4.85916500 -0.54094800
C -4.54103600 0.29725600 2.55937200
H -5.34915300 -0.40685300 2.75832600
C -0.79108000 1.73460800 -2.51930100
H 0.13301000 2.01439300 -2.01948800
C -3.20246600 0.94378500 -3.65531300
H -4.15149900 0.61593300 -4.07986700
C -2.31272800 1.73692900 -4.40472900
H -2.56481300 2.03445600 -5.42201300
C -1.09578500 2.13295600 -3.82406600
H -0.38412400 2.74541200 -4.37558100
C 1.36586500 -0.52672300 0.11576400
C 1.37221500 0.88199400 0.36286200
C 2.59951600 1.59854700 0.49168400
C 3.76875900 0.85231500 0.28274500
C 3.79171600 -0.53817700 -0.04951200
C 2.57528500 -1.22479400 -0.12105400
H 4.72427700 1.36766800 0.36066300
H 2.54499200 -2.27910500 -0.38637000
C 6.04204900 -1.13209700 0.95127000
H 5.56506000 -1.64560400 1.80030800
H 7.01612700 -1.60982600 0.76215100
H 6.23089700 -0.08903200 1.24577200
C 5.15116300 -1.22304600 -0.32320800
C 4.98856800 -2.71754700 -0.69605100
H 4.39125500 -2.84682000 -1.61249100
H 5.97974900 -3.15819500 -0.88086200
H 4.51660300 -3.29308300 0.11605100
C 5.86716100 -0.50287600 -1.50428500
H 5.25659100 -0.55002100 -2.41924800
H 6.06518200 0.55567700 -1.27909000
H 6.83378000 -0.98913300 -1.70968300
C 2.62567300 3.10359700 0.84155700
C 4.06962400 3.66019600 0.91952800
H 4.66586100 3.15058500 1.69231800
H 4.59620200 3.57582800 -0.04422300
H 4.02924500 4.72798500 1.18317700
C 1.94908700 3.31685600 2.22810300
H 0.91495900 2.94737400 2.21777700
H 2.50336200 2.78492000 3.01664400

```
H 1.93985800 4.38938800 2.47949300
C 1.85715700 3.91489800 -0.24276800
H 2.31707500 3.76937400 -1.23365700
H 0.80348300 3.60851400 -0.28434200
H 1.89867500 4.98968300 -0.00499200
1 2 1.0 3 1.0 5 1.0 6 1.0
2 45 1.0
3 7 1.0 44 1.0
4 10 1.0 23 1.0 29 1.0
5 22 1.5 36 1.5
6 18 1.5 26 1.0
7 8 1.5 15 1.5
8 9 1.0 13 1.5
9
10 11 1.0 12 1.0 22 1.0
11
12
13 14 1.0 27 1.5
14
15 29 1.0 32 1.5
16 17 1.0 18 1.5 20 1.5
17
18 19 1.0
19
20 21 1.0 34 1.5
21
22 38 1.5
23 24 1.0 25 1.0 26 1.0
24
25
26 34 1.5
27 28 1.0 32 1.5
28
29 30 1.0 31 1.0
30
31
32 33 1.0
33
34 35 1.0
35
36 37 1.0 42 1.5
37
38 39 1.0 40 1.5
39
40 41 1.0 42 1.5
41
42 43 1.0
43
44 45 1.5 49 1.5
45 46 1.5
46 47 1.5 65 1.0
47 48 1.5 50 1.0
48 49 1.5 56 1.0
49 51 1.0
50
51
```

```
52 53 1.0 54 1.0 55 1.0 56 1.0
53
54
55
56 57 1.0 61 1.0
57 58 1.0 59 1.0 60 1.0
58
59
60
61 62 1.0 63 1.0 64 1.0
62
63
64
65 66 1.0 70 1.0 74 1.0
66 67 1.0 68 1.0 69 1.0
67
68
69
70 71 1.0 72 1.0 73 1.0
71
72
73
74 75 1.0 76 1.0 77 1.0
75
76
77
```

7.3 DFT Optimized Structure and Selected Bond Distances of Complex 2C

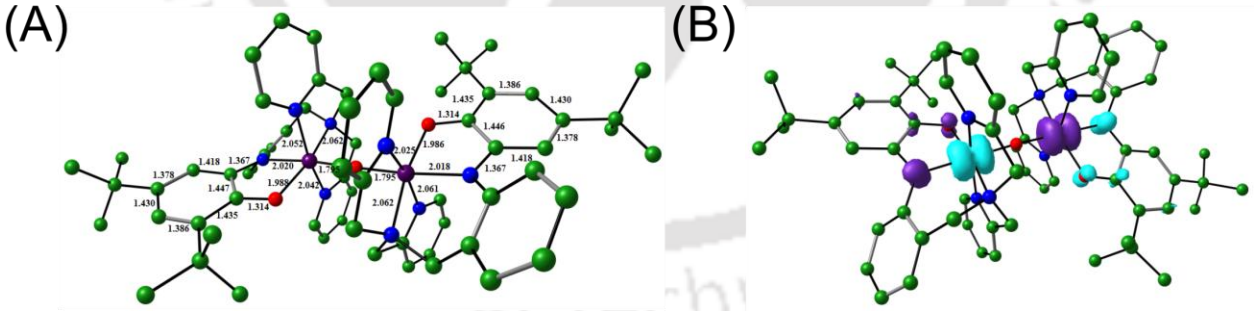

Figure 2.23: *(A) DFT Optimized bond distances parameter of complex* $[\mathbf{2C}]^{2+}$ *(B) Spin density plot of complex* $[\mathbf{2C}]^{2+}$.

Table 7.7. Optimized coordinates for complex $[\mathbf{2C}]^{2+}$.

Charge = 2 Multiplicity = 1

Mn	11.6206	11.6218	10.5438
O	13.2832	11.534	9.9404
O	11.0358	9.842	9.9607
N	9.8243	11.5721	11.3818
N	11.7222	13.7912	10.8251
N	10.8696	12.5444	8.5885
C	11.0721	6.8235	9.7177
H	11.6237	7.5698	9.9662
H	11.5787	6.2203	9.169
H	10.779	6.3656	10.509
N	12.3996	11.7693	12.5647
C	9.77	9.5594	10.1969
C	9.0606	10.5259	10.9961
C	9.1159	8.3864	9.7515
C	9.4623	12.4106	12.4692
C	12.7271	14.0611	11.8569
H	12.531	14.9146	12.2744
H	13.5998	14.1292	11.4394
C	9.7797	13.7635	12.4235
C	8.9072	14.0138	14.6482
H	8.7187	14.5536	15.3818
C	12.7733	13.0057	12.9066
C	7.022	9.2572	10.8549
C	9.8566	7.3241	8.9384
C	9.4942	14.5582	13.5309
H	9.7042	15.4636	13.517
C	11.3288	13.7958	8.3996
C	12.1413	14.3518	9.5209
H	13.0775	14.1488	9.3718
H	12.0437	15.3172	9.5408
C	7.6792	10.3472	11.2923
H	7.2272	10.9896	11.7913
C	8.9895	6.0865	8.6442
H	8.7129	5.6851	9.4692
H	9.5009	5.451	8.1352
H	8.2164	6.3495	8.1392
C	7.7569	8.2583	10.0975
H	7.3048	7.4925	9.8271
C	10.394	14.3748	11.1929
H	9.7838	14.256	10.4474
H	10.5001	15.3275	11.338
C	10.1904	11.9573	7.6044
H	9.8711	11.0934	7.7336
C	8.8875	11.8835	13.6183

H	8.6992	10.9734	13.6621
C	8.5951	12.6793	14.682
H	8.1838	12.3172	15.4335
C	11.117	14.4798	7.2227
H	11.4326	15.3471	7.1134
C	9.9422	12.5894	6.3957
H	9.4576	12.1661	5.7237
C	5.5319	9.0484	11.1332
C	10.4309	13.8546	6.2187
H	10.2955	14.2929	5.4116
C	10.2797	7.9331	7.6044
H	9.4994	8.1822	7.1054
H	10.7877	7.2895	7.1054
H	10.8193	8.7116	7.7635
C	12.5066	10.767	13.4354
H	12.2052	9.9204	13.1929
C	13.2863	13.2583	14.173
H	13.5309	14.1222	14.4195
C	13.0516	10.9527	14.684
H	13.1654	10.2376	15.2665
C	13.4257	12.2272	15.0478
H	13.7744	12.3829	15.8967
C	5.3964	7.7082	11.8589
H	5.8867	7.0346	11.3818
H	4.4697	7.459	11.9006
H	5.7464	7.7901	12.7496
C	4.854	8.7439	9.7774
H	4.538	9.5617	9.3857
H	4.1134	8.1488	9.9165
H	5.4895	8.331	9.1869
Mn	14.9458	11.4462	9.337
O	15.5306	13.226	9.9201
N	16.7421	11.4959	8.499
N	14.8442	9.2768	9.0557
N	15.6968	10.5236	11.2923
C	15.4943	16.2445	10.1631
H	14.9427	15.4982	9.9146
H	14.9877	16.8477	10.7118
H	15.7874	16.7024	9.3718
N	14.1667	11.2987	7.3161
C	16.7964	13.5086	9.6839
C	17.5057	12.5421	8.8847
C	17.4505	14.6816	10.1293
C	17.1041	10.6574	7.4116
C	13.8393	9.0069	8.0239
H	14.0353	8.1534	7.6064
H	12.9666	8.9388	8.4414

C	16.7867	9.3045	7.4573
C	17.6592	9.0542	5.2326
H	17.8476	8.5144	4.499
C	13.7931	10.0623	6.9742
C	19.5443	13.8108	9.0259
C	16.7098	15.7439	10.9424
C	17.0721	8.5098	6.3499
H	16.8621	7.6044	6.3638
C	15.2376	9.2722	11.4812
C	14.4251	8.7162	10.3599
H	13.4889	8.9192	10.509
H	14.5227	7.7508	10.34
C	18.8872	12.7208	8.5885
H	19.3392	12.0784	8.0895
C	17.5768	16.9815	11.2366
H	17.8535	17.3829	10.4116
H	17.0655	17.617	11.7456
H	18.35	16.7185	11.7416
C	18.8095	14.8097	9.7833
H	19.2616	15.5755	10.0537
C	16.1724	8.6932	8.6879
H	16.7826	8.812	9.4334
H	16.0663	7.7405	8.5428
C	16.376	11.1107	12.2764
H	16.6953	11.9746	12.1472
C	17.6789	11.1845	6.2625
H	17.8672	12.0946	6.2187
C	17.9713	10.3887	5.1988
H	18.3826	10.7508	4.4473
C	15.4494	8.5882	12.6581
H	15.1337	7.7209	12.7675
C	16.6242	10.4786	13.4851
H	17.1088	10.9019	14.1571
C	21.0345	14.0196	8.7476
C	16.1354	9.2134	13.6621
H	16.2709	8.7751	14.4692
C	16.2867	15.1349	12.2764
H	17.067	14.8858	12.7754
H	15.7787	15.7785	12.7754
H	15.7471	14.3564	12.1173
C	14.0598	12.301	6.4454
H	14.3612	13.1476	6.6879
C	13.2801	9.8097	5.7078
H	13.0355	8.9458	5.4613
C	13.5148	12.1153	5.1968
H	13.401	12.8304	4.6143
C	13.1406	10.8408	4.833

H	12.792	10.6851	3.9841
C	21.17	15.3598	8.0219
H	20.6797	16.0334	8.499
H	22.0967	15.609	7.9802
H	20.82	15.2779	7.1312
C	21.7124	14.3241	10.1034
H	22.0284	13.5063	10.4951
H	22.453	14.9192	9.9643
H	21.0769	14.737	10.6939
C	21.75711	12.67268	8.55987
H	21.47219	12.00274	9.34403
H	21.48591	12.25115	7.61453
H	22.81528	12.8283	8.59061
C	4.80929	10.39532	11.32093
H	5.0805	10.81685	12.26627
H	5.0942	11.06526	10.53676
H	3.75112	10.2397	11.2902

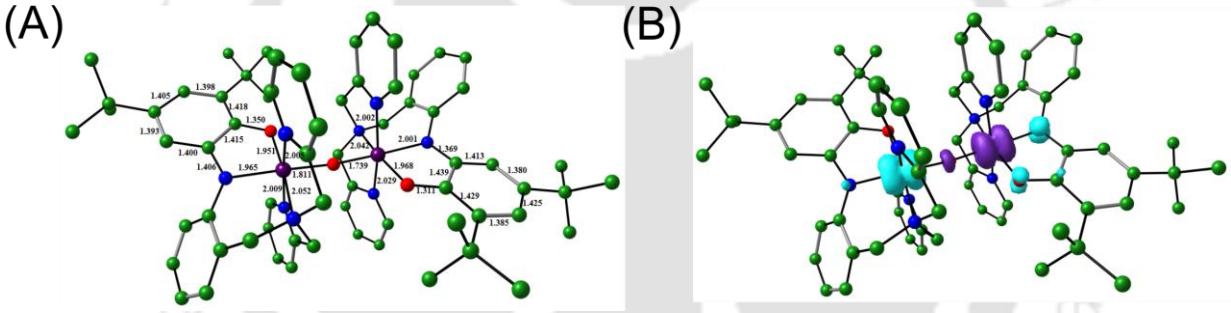

Figure 2.24: *(A) DFT Optimized bond distances parameter of complex [**2C**]$^{1+}$ (B) Spin density plot of complex [**2C**]$^{1+}$.*

Table 7.8. Optimized coordinates for complex [**2C**]$^{1+}$.

Charge = 1 Multiplicity = 2

Mn	1.64215	-0.65596	-0.28275
O	-0.06471	-0.1828	0.09769
O	2.47691	0.95192	0.44359
N	3.50559	-1.2074	-0.57421
N	0.92963	-2.37958	-1.13629
N	1.37654	0.06456	-2.13634
C	3.29704	3.13845	2.36609
H	2.58359	2.32257	2.25931
H	2.77591	4.02623	2.74438
H	4.03994	2.84331	3.11421

N	1.71541	-1.75442	1.39651
C	3.80215	1.02173	0.19448
C	4.39473	-0.1395	-0.35546
C	4.60462	2.16365	0.4433
C	3.90693	-2.51493	-0.34344
C	0.28994	-3.11252	-0.0094
H	0.14022	-4.17166	-0.24691
H	-0.68265	-2.64587	0.15237
C	3.12152	-3.56065	-0.89156
C	4.48283	-5.23846	0.21417
H	4.70873	-6.27876	0.42151
C	1.11121	-2.95404	1.25049
C	6.55944	0.95295	-0.4626
C	3.99708	3.44808	1.02402
C	3.41597	-4.89558	-0.61179
H	2.79874	-5.67344	-1.05529
C	0.53233	-0.69509	-2.86932
C	-0.03093	-1.9111	-2.16997
H	-0.95739	-1.6226	-1.674
H	-0.25441	-2.70518	-2.89289
C	5.7511	-0.1559	-0.70242
H	6.15261	-1.05078	-1.15935
C	5.04898	4.53577	1.30078
H	5.8061	4.19387	2.01264
H	4.55959	5.41536	1.73164
H	5.55736	4.85688	0.38688
C	5.96111	2.08578	0.11328
H	6.58608	2.94805	0.30272
C	1.9993	-3.19239	-1.80339
H	2.37	-2.57196	-2.62531
H	1.53177	-4.08979	-2.22898
C	1.89819	1.18546	-2.65449
H	2.58125	1.72791	-2.01237
C	4.98347	-2.87932	0.49708
H	5.58663	-2.10073	0.94684
C	5.26093	-4.21437	0.76357
H	6.09175	-4.45974	1.41902
C	0.17865	-0.33028	-4.16441
H	-0.49413	-0.9592	-4.73731
C	1.58134	1.61182	-3.94011
H	2.01996	2.52313	-4.32926
C	8.05564	0.9761	-0.80427
C	0.70639	0.84276	-4.70478
H	0.44546	1.14428	-5.714
C	2.99659	4.02232	-0.00335
H	3.53093	4.36093	-0.89686
H	2.45906	4.88372	0.41285

H	2.2736	3.26778	-0.31055
C	2.47813	-1.51216	2.47275
H	2.97034	-0.54588	2.48258
C	1.23106	-3.94134	2.22369
H	0.7537	-4.90363	2.07687
C	2.63846	-2.45085	3.48295
H	3.26847	-2.2268	4.33601
C	2.00278	-3.68683	3.35479
H	2.12548	-4.45087	4.11521
C	8.8699	1.21233	0.48624
H	8.60622	2.16096	0.9624
H	9.94242	1.23484	0.26484
H	8.68667	0.4124	1.21066
C	8.34009	2.11687	-1.80473
H	7.77496	1.96908	-2.73048
H	9.40564	2.15112	-2.05621
H	8.06215	3.09196	-1.39498
Mn	-1.65469	0.43293	0.44008
O	-2.6437	-0.84143	-0.68835
N	-3.50431	1.16628	0.65738
N	-0.88208	1.7707	1.77822
N	-1.70736	-0.75002	2.08861
C	-3.57219	-2.24453	-3.27004
H	-2.77539	-1.57497	-2.94589
H	-3.13522	-3.04026	-3.88349
H	-4.26373	-1.67603	-3.89991
N	-1.37842	1.89753	-0.89878
C	-3.94824	-0.78137	-0.57383
C	-4.47368	0.32407	0.18337
C	-4.84994	-1.70787	-1.18155
C	-3.74108	2.5297	0.84304
C	-0.05999	2.7091	0.96564
H	0.09364	3.65932	1.48657
H	0.91401	2.23258	0.8122
C	-2.91216	3.23533	1.74519
C	-3.96022	5.3274	1.09863
H	-4.04479	6.40368	1.20162
C	-0.66722	2.92844	-0.39704
C	-6.74045	-0.45777	-0.15726
C	-4.32253	-2.84898	-2.06056
C	-3.03535	4.61873	1.86463
H	-2.39819	5.14579	2.56935
C	-0.8222	-0.33561	3.02251
C	-0.06549	0.92798	2.69318
H	0.84958	0.66448	2.1622
H	0.20062	1.47499	3.6057
C	-5.86554	0.45875	0.39018

H	-6.21835	1.27546	1.00467
C	-5.45411	-3.73608	-2.60385
H	-6.1552	-3.17034	-3.22484
H	-5.02636	-4.52747	-3.22632
H	-6.0169	-4.21742	-1.79796
C	-6.20175	-1.51355	-0.94778
H	-6.90152	-2.21201	-1.38633
C	-1.92623	2.47888	2.58169
H	-2.43775	1.71092	3.16915
H	-1.42298	3.15924	3.27944
C	-2.39082	-1.88897	2.27398
H	-3.08768	-2.15823	1.48933
C	-4.66014	3.25603	0.06072
H	-5.26448	2.73111	-0.66894
C	-4.76702	4.63608	0.19285
H	-5.47693	5.17656	-0.42511
C	-0.59329	-1.07645	4.17711
H	0.12324	-0.72431	4.91013
C	-2.20323	-2.68457	3.39838
H	-2.76738	-3.60291	3.51127
C	-8.25625	-0.38713	0.05385
C	-1.28379	-2.27291	4.36203
H	-1.11098	-2.87113	5.2503
C	-3.37459	-3.74656	-1.2357
H	-3.91846	-4.21968	-0.41109
H	-2.96117	-4.54271	-1.86421
H	-2.5513	-3.16745	-0.82057
C	-1.87576	1.95826	-2.14165
H	-2.43909	1.09016	-2.46361
C	-0.44331	4.0767	-1.153
H	0.12232	4.89764	-0.72901
C	-1.67595	3.06449	-2.95576
H	-2.08514	3.08083	-3.95892
C	-0.95177	4.14354	-2.44742
H	-0.78786	5.02962	-3.05176
C	-8.73497	-1.68016	0.75027
H	-8.25479	-1.79608	1.72693
H	-9.81826	-1.64863	0.90435
H	-8.50987	-2.57034	0.15631
C	-8.95513	-0.25078	-1.31698
H	-8.73779	-1.09773	-1.97335
H	-10.04059	-0.20402	-1.18394
H	-8.63405	0.66224	-1.82797
C	-8.6632	0.8123	0.92435
H	-8.22036	0.75786	1.92377
H	-8.36905	1.763	0.46822
H	-9.7499	0.82667	1.04495

C	8.52694	-0.34471	-1.43402
H	8.37491	-1.1925	-0.75844
H	8.00246	-0.55661	-2.37111
H	9.59631	-0.28719	-1.65846

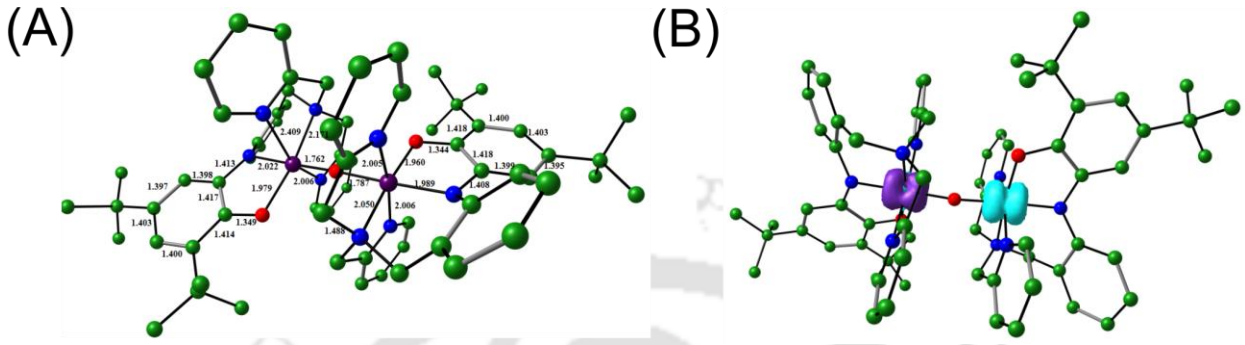

Figure 2.25: *(A) DFT Optimized bond distances parameter of complex [**2C**]^0 (B) Spin density plot of complex [**2C**]^0.*

Table 7.9. Optimized coordinates for complex [**2C**]^0.

Charge = 0 Multiplicity = 1

Mn	1.6425	-0.67018	-0.28816
O	-0.05368	-0.2929	0.21024
O	2.51037	0.93567	0.41386
N	3.51633	-1.21897	-0.66449
N	0.90133	-2.38764	-1.13052
N	1.27154	0.08795	-2.09984
C	3.38318	3.05446	2.37178
H	2.66988	2.23917	2.2611
H	2.86767	3.92773	2.79
H	4.15096	2.74233	3.08794
N	1.78436	-1.78338	1.37573
C	3.82453	1.00118	0.13513
C	4.40772	-0.15213	-0.44649
C	4.6341	2.13838	0.38573
C	3.91683	-2.52335	-0.44404
C	0.29113	-3.11792	0.01479
H	0.12852	-4.17617	-0.22046
H	-0.6703	-2.64037	0.20961
C	3.10249	-3.568	-0.95827
C	4.49099	-5.25709	0.1005
H	4.71325	-6.29931	0.30416
C	1.14502	-2.9657	1.25323
C	6.56872	0.95281	-0.58649
C	4.03818	3.40426	1.01685

C	3.39606	-4.90364	-0.6841
H	2.75176	-5.67588	-1.09913
C	0.41024	-0.67069	-2.81274
C	-0.094	-1.91855	-2.13109
H	-1.02467	-1.65895	-1.62038
H	-0.31274	-2.70099	-2.86825
C	5.75519	-0.15502	-0.82445
H	6.14775	-1.04217	-1.30453
C	5.0935	4.49026	1.2867
H	5.87657	4.13379	1.96307
H	4.61425	5.35554	1.75698
H	5.56962	4.83727	0.36435
C	5.98382	2.07307	0.02209
H	6.61043	2.93446	0.21351
C	1.94917	-3.19614	-1.82948
H	2.29433	-2.56914	-2.65824
H	1.47245	-4.09331	-2.24695
C	1.73479	1.24066	-2.60472
H	2.43232	1.78089	-1.97688
C	5.02387	-2.90068	0.35397
H	5.65031	-2.12734	0.78044
C	5.29839	-4.23716	0.61454
H	6.15095	-4.48712	1.24081
C	-0.02387	-0.26874	-4.07356
H	-0.71961	-0.89191	-4.6245
C	1.33808	1.70258	-3.85404
H	1.7243	2.64307	-4.22908
C	8.0573	0.98293	-0.96079
C	0.44104	0.93633	-4.59692
H	0.11057	1.2695	-5.57561
C	2.99798	4.00009	0.04316
H	3.49348	4.34541	-0.87048
H	2.48567	4.85916	0.49422
H	2.25444	3.25569	-0.23567
C	2.56332	-1.54282	2.43826
H	3.07038	-0.58435	2.43134
C	1.25107	-3.94101	2.24019
H	0.74031	-4.88943	2.11686
C	2.71222	-2.4705	3.46078
H	3.35233	-2.24739	4.3067
C	2.04197	-3.68968	3.35839
H	2.14764	-4.44322	4.13211
C	8.90225	1.19373	0.31429
H	8.64606	2.13127	0.81591
H	9.97081	1.2225	0.07098
H	8.73423	0.37896	1.02585
C	8.3232	2.14215	-1.94492

H	7.7389	2.01084	-2.86122
H	9.38421	2.18422	-2.21736
H	8.04966	3.10798	-1.51107
Mn	-1.66616	0.42605	0.35159
O	-2.63767	-0.74429	-0.90949
N	-3.51513	1.12195	0.6735
N	-0.88894	1.75584	1.87348
N	-1.70151	-0.87355	2.40533
C	-3.54534	-2.15336	-3.42111
H	-2.78618	-1.45558	-3.06787
H	-3.06716	-2.92813	-4.03392
H	-4.24571	-1.60338	-4.05858
N	-1.31593	1.99473	-0.83697
C	-3.97307	-0.73959	-0.73025
C	-4.49439	0.28677	0.09733
C	-4.85033	-1.67371	-1.32709
C	-3.74387	2.47732	0.83021
C	-0.05392	2.71455	1.10519
H	0.12532	3.63771	1.66834
H	0.90627	2.22363	0.92058
C	-2.931	3.19695	1.74943
C	-3.95046	5.30167	1.08366
H	-4.03021	6.37934	1.18115
C	-0.66333	3.02041	-0.2424
C	-6.75309	-0.54803	-0.23008
C	-4.29835	-2.78645	-2.22857
C	-3.04428	4.58351	1.85985
H	-2.40995	5.1034	2.57479
C	-0.78659	-0.34075	3.23229
C	-0.07527	0.92502	2.79096
H	0.81821	0.62745	2.24019
H	0.2322	1.50523	3.67252
C	-5.86731	0.3626	0.35085
H	-6.22184	1.14267	1.01255
C	-5.40118	-3.69156	-2.80045
H	-6.112	-3.12808	-3.41285
H	-4.94966	-4.46132	-3.43561
H	-5.9603	-4.19971	-2.00843
C	-6.21908	-1.54546	-1.05976
H	-6.90106	-2.25475	-1.51165
C	-1.9861	2.43509	2.62605
H	-2.52537	1.64001	3.14949
H	-1.53527	3.10371	3.3734
C	-2.29715	-2.02691	2.71923
H	-3.03571	-2.38509	2.00739
C	-4.66481	3.2217	0.05553
H	-5.28669	2.69731	-0.66018

C	-4.75948	4.6013	0.18244
H	-5.46825	5.1415	-0.43998
C	-0.43961	-0.97639	4.42616
H	0.29919	-0.52924	5.08269
C	-1.99112	-2.73122	3.88158
H	-2.48796	-3.6697	4.10077
C	-8.26768	-0.49839	0.01775
C	-1.04114	-2.19103	4.74692
H	-0.77469	-2.70626	5.66444
C	-3.34233	-3.6747	-1.40178
H	-3.89849	-4.19636	-0.61531
H	-2.86245	-4.43073	-2.03573
H	-2.57283	-3.06495	-0.93044
C	-1.84117	2.14649	-2.06306
H	-2.36841	1.28002	-2.44503
C	-0.51121	4.24101	-0.89448
H	0.00432	5.05303	-0.39569
C	-1.71641	3.33415	-2.76889
H	-2.15077	3.42376	-3.75779
C	-1.04254	4.39962	-2.17092
H	-0.94228	5.3481	-2.68871
C	-8.72581	-1.81447	0.68242
H	-8.21967	-1.95624	1.64277
H	-9.80733	-1.80418	0.86254
H	-8.49738	-2.68042	0.05481
C	-9.00639	-0.32282	-1.32653
H	-8.78927	-1.14419	-2.01488
H	-10.09129	-0.2907	-1.17176
H	-8.70143	0.60895	-1.81347
C	-8.66893	0.66719	0.93654
H	-8.2017	0.58302	1.92256
H	-8.3854	1.63371	0.50818
H	-9.7544	0.67039	1.08032
C	8.51569	-0.32492	-1.6261
H	8.37619	-1.18511	-0.96384
H	7.96848	-0.51902	-2.55389
H	9.5805	-0.26315	-1.87343

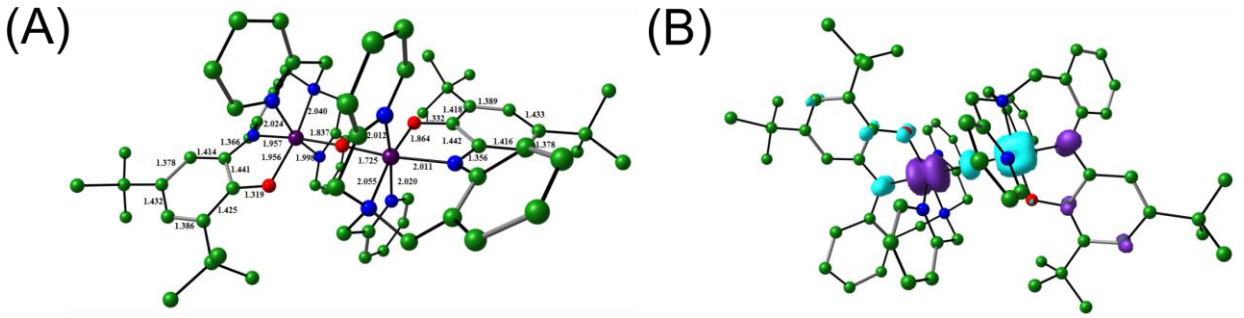

Figure 2.26: *(A) DFT Optimized bond distances parameter of complex [**2C**]$^{3+}$ (B) Spin density plot of complex [**2C**]$^{3+}$.*

Table 7.10. Optimized coordinates for complex [**2C**]$^{3+}$.

Charge = 3 Multiplicity = 2

Mn	1.65268	-0.61989	-0.21015
O	0.062	-0.0999	0.19253
O	2.50257	0.9567	0.29595
N	3.56503	-1.20296	-0.4171
N	0.95885	-2.3905	-0.97328
N	1.37773	-0.06509	-2.13817
C	3.32478	3.29	2.168
H	2.59444	2.47934	2.15029
H	2.82465	4.19981	2.51368
H	4.09462	3.03689	2.90295
N	1.76432	-1.68181	1.49933
C	3.81168	1.04968	0.07433
C	4.44153	-0.17119	-0.36529
C	4.58431	2.22307	0.27631
C	3.98312	-2.5355	-0.25636
C	0.33965	-3.11235	0.17911
H	0.23895	-4.17952	-0.03864
H	-0.65862	-2.6927	0.32014
C	3.18779	-3.56162	-0.80401
C	4.62594	-5.22255	0.22658
H	4.87945	-6.26273	0.39833
C	1.14177	-2.87749	1.43061
C	6.58127	0.9287	-0.51677
C	3.96389	3.53099	0.78132
C	3.52451	-4.89271	-0.5658
H	2.92651	-5.68126	-1.01252
C	0.51388	-0.86416	-2.80843
C	-0.04616	-2.00382	-2.00932
H	-0.96046	-1.67712	-1.5101
H	-0.28863	-2.85926	-2.6467
C	5.82336	-0.21074	-0.67117

H	6.25197	-1.12633	-1.05268
C	5.01225	4.64538	0.93983
H	5.78924	4.37758	1.66153
H	4.52292	5.55027	1.30893
H	5.48952	4.89919	-0.01109
C	5.9354	2.11074	-0.02377
H	6.55592	2.98561	0.1079
C	2.01699	-3.20996	-1.66438
H	2.33599	-2.61949	-2.52711
H	1.53737	-4.11848	-2.04182
C	1.90016	1.01903	-2.74
H	2.58167	1.62072	-2.15463
C	5.06789	-2.87204	0.57461
H	5.63991	-2.08722	1.054
C	5.38846	-4.20595	0.80452
H	6.22999	-4.45177	1.44318
C	0.16321	-0.59566	-4.12678
H	-0.51568	-1.26124	-4.64773
C	1.57511	1.35075	-4.0485
H	2.01548	2.22959	-4.50425
C	8.07005	0.99138	-0.85149
C	0.6968	0.52918	-4.75464
H	0.43908	0.75452	-5.7841
C	2.91356	4.01663	-0.24306
H	3.39614	4.27875	-1.18976
H	2.41496	4.91578	0.13196
H	2.15438	3.26088	-0.44809
C	2.48277	-1.34489	2.58418
H	2.97853	-0.38166	2.55183
C	1.22209	-3.7833	2.48352
H	0.73249	-4.74736	2.40554
C	2.58881	-2.19668	3.67422
H	3.17517	-1.90183	4.53662
C	1.95226	-3.43802	3.61889
H	2.03463	-4.13415	4.44686
C	8.85249	1.37161	0.42837
H	8.55722	2.34732	0.82362
H	9.9204	1.42128	0.20005
H	8.70842	0.62556	1.2156
C	8.29605	2.0687	-1.93848
H	7.75457	1.82108	-2.85636
H	9.36086	2.12697	-2.17861
H	7.97991	3.06324	-1.61153
Mn	-1.66451	0.47973	0.49402
O	-2.54795	-0.8648	-0.63777
N	-3.50507	1.14009	0.61331
N	-1.00323	1.83739	1.84785

N	-1.6964	-0.72451	2.11358
C	-3.39148	-2.28656	-3.28766
H	-2.62611	-1.58678	-2.94707
H	-2.91726	-3.0674	-3.89259
H	-4.08167	-1.73898	-3.93567
N	-1.3495	1.90446	-0.86394
C	-3.86544	-0.83772	-0.59597
C	-4.44055	0.26981	0.12864
C	-4.72267	-1.78075	-1.2327
C	-3.8025	2.50336	0.78884
C	-0.2092	2.82982	1.06677
H	-0.14889	3.79015	1.58629
H	0.79991	2.42954	0.96835
C	-3.07041	3.23288	1.74745
C	-4.17862	5.27542	1.05738
H	-4.33194	6.34272	1.17074
C	-0.77154	3.0016	-0.32669
C	-6.67612	-0.5457	-0.28112
C	-4.15895	-2.91422	-2.10038
C	-3.27028	4.60632	1.87801
H	-2.71765	5.15536	2.63471
C	-0.9176	-0.25005	3.11341
C	-0.18854	1.03799	2.80583
H	0.76241	0.80856	2.32549
H	0.01112	1.60325	3.72231
C	-5.84081	0.38961	0.28898
H	-6.23189	1.20244	0.88475
C	-5.26293	-3.81387	-2.68013
H	-5.94933	-3.25742	-3.32433
H	-4.80757	-4.59896	-3.28988
H	-5.84415	-4.30474	-1.89409
C	-6.08378	-1.5987	-1.04832
H	-6.75728	-2.30786	-1.5088
C	-2.1065	2.5048	2.62691
H	-2.61205	1.71542	3.18914
H	-1.64913	3.19245	3.34702
C	-2.37614	-1.87025	2.28478
H	-2.99616	-2.18601	1.4546
C	-4.69374	3.189	-0.05623
H	-5.21952	2.64669	-0.8325
C	-4.88152	4.56032	0.08548
H	-5.57563	5.07367	-0.57138
C	-0.78524	-0.93447	4.31538
H	-0.16686	-0.52665	5.10726
C	-2.29205	-2.60616	3.46226
H	-2.86317	-3.52094	3.56962
C	-8.19754	-0.50739	-0.12891

C	-1.47983	-2.13268	4.49178
H	-1.40286	-2.67611	5.42763
C	-3.22895	-3.80679	-1.25061
H	-3.79787	-4.29992	-0.45629
H	-2.77979	-4.58948	-1.87098
H	-2.43299	-3.22339	-0.78848
C	-1.81103	1.93173	-2.12409
H	-2.28453	1.02091	-2.47184
C	-0.64439	4.1764	-1.06021
H	-0.19703	5.05278	-0.60617
C	-1.70344	3.06615	-2.91705
H	-2.091	3.06018	-3.92898
C	-1.11671	4.20951	-2.3717
H	-1.03947	5.12039	-2.95584
C	-8.83899	-0.39508	-1.53117
H	-8.58994	-1.24614	-2.17111
H	-9.9279	-0.36504	-1.43639
H	-8.51713	0.51926	-2.03878
C	-8.66832	-1.81182	0.55381
H	-8.22771	-1.91504	1.55009
H	-9.75612	-1.79998	0.66411
H	-8.40753	-2.69993	-0.02882
C	-8.66005	0.68744	0.71885
H	-8.25837	0.64608	1.73633
H	-8.37249	1.64269	0.26765
H	-9.74954	0.67955	0.79822
C	8.59906	-0.35377	-1.37196
H	8.48803	-1.15092	-0.62953
H	8.09766	-0.66008	-2.29554
H	9.66454	-0.26465	-1.59474

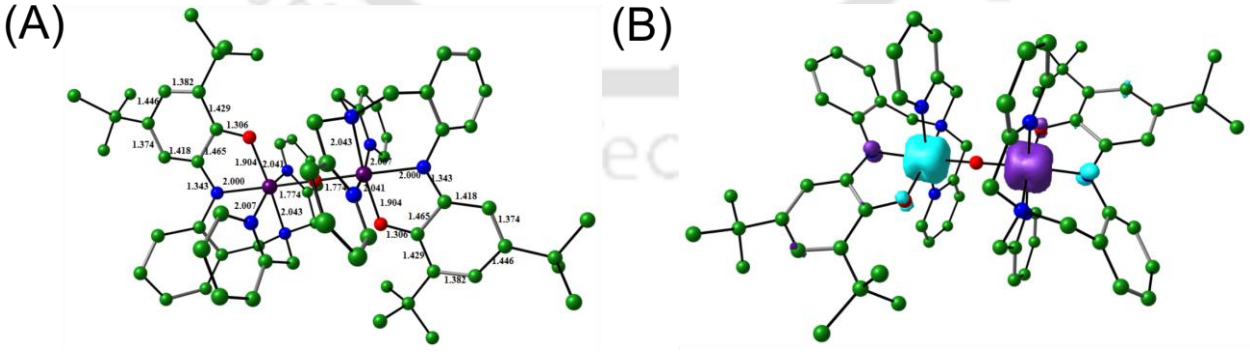

Figure 2.27: *(A) DFT Optimized bond distances parameter of complex [**2C**]$^{4+}$ (B) Spin density plot of complex [**2C**]$^{4+}$.*

Table 7.11. Optimized coordinates for complex [**2C**]$^{4+}$.

Charge = 4 Multiplicity = 1

Mn	1.64241	0.55566	0.34456
O	0.00006	-0.00015	0.00022
O	2.56727	-0.94403	-0.43036
N	3.52053	1.22619	0.40523
N	0.9647	2.08739	1.5077
N	1.64996	-0.37342	2.16578
C	3.29545	-3.11972	-2.52285
H	2.46708	-2.44321	-2.31185
H	2.88803	-4.06891	-2.88299
H	3.8925	-2.6892	-3.33201
N	1.44887	1.87895	-1.14824
C	3.86938	-0.94392	-0.36686
C	4.45715	0.30358	0.1344
C	4.71585	-2.02593	-0.75485
C	3.83542	2.59463	0.45433
C	0.18254	2.9779	0.59761
H	0.10356	3.98601	1.01411
H	-0.82428	2.56131	0.52707
C	3.07242	3.43577	1.29352
C	4.29377	5.35854	0.45603
H	4.47899	6.42703	0.47229
C	0.79185	3.00201	-0.78089
C	6.68025	-0.60341	-0.06024
C	4.16717	-3.36351	-1.2728
C	3.32158	4.80544	1.29563
H	2.76404	5.45031	1.96785
C	0.8574	0.24373	3.07682
C	0.11416	1.43767	2.54828
H	-0.81037	1.1141	2.06913
H	-0.13805	2.14366	3.34531
C	5.86144	0.44115	0.28876
H	6.25997	1.34464	0.72695
C	5.29549	-4.33195	-1.66865
H	5.92584	-3.9242	-2.46417
H	4.8573	-5.2591	-2.04543
H	5.9301	-4.5994	-0.81879
C	6.07045	-1.80045	-0.59904
H	6.74714	-2.59622	-0.87615
C	2.05875	2.84314	2.21982
H	2.52739	2.13703	2.90965
H	1.58692	3.62913	2.81767
C	2.33952	-1.46943	2.53402

H	2.961	-1.92988	1.7798
C	4.78514	3.16151	-0.4191
H	5.31463	2.52925	-1.1213
C	5.01294	4.5329	-0.41137
H	5.74681	4.95921	-1.08667
C	0.74465	-0.21797	4.38147
H	0.1229	0.31502	5.09256
C	2.26353	-1.99324	3.81919
H	2.84172	-2.87358	4.07495
C	8.1924	-0.57637	0.10808
C	1.45744	-1.35631	4.76165
H	1.39628	-1.72794	5.77924
C	3.34443	-4.03623	-0.15044
H	3.98091	-4.26503	0.70975
H	2.92622	-4.98124	-0.50967
H	2.52099	-3.40573	0.19281
C	1.98304	1.77964	-2.37823
H	2.52269	0.86442	-2.5946
C	0.64974	4.06977	-1.66061
H	0.13488	4.96936	-1.342
C	1.86492	2.8017	-3.3094
H	2.31045	2.69427	-4.29156
C	1.1905	3.96821	-2.94227
H	1.10003	4.794	-3.64025
C	8.843	-0.75837	-1.2875
H	8.57584	-1.70914	-1.75703
H	9.93033	-0.74634	-1.17636
H	8.56217	0.0529	-1.96508
C	8.61701	-1.74378	1.03413
H	8.16483	-1.64693	2.02531
H	9.70317	-1.72756	1.15425
H	8.35192	-2.72335	0.62623
Mn	-1.64233	-0.55587	-0.34419
O	-2.5671	0.94393	0.43059
N	-3.52047	-1.22614	-0.40513
N	-0.96465	-2.08781	-1.50709
N	-1.64978	0.37299	-2.16554
C	-3.29543	3.11968	2.52282
H	-2.46706	2.44312	2.312
H	-2.88804	4.0688	2.88316
H	-3.89272	2.68913	3.33179
N	-1.44908	-1.8791	1.14867
C	-3.86919	0.94407	0.36666
C	-4.45702	-0.30333	-0.13473
C	-4.71559	2.02621	0.75443
C	-3.83559	-2.59453	-0.45407
C	-0.18251	-2.97819	-0.59684

H	-0.10338	-3.98632	-1.01327
H	0.82427	-2.5615	-0.5262
C	-3.07254	-3.43598	-1.2929
C	-4.29448	-5.35835	-0.45535
H	-4.47988	-6.42681	-0.47146
C	-0.79205	-3.00223	0.78155
C	-6.68003	0.60403	0.05923
C	-4.16683	3.36367	1.27258
C	-3.32195	-4.8056	-1.29481
H	-2.76436	-5.45071	-1.96675
C	-0.85728	-0.24438	-3.07648
C	-0.11406	-1.43823	-2.54771
H	0.81043	-1.11457	-2.06856
H	0.13822	-2.14433	-3.34463
C	-5.86129	-0.44067	-0.28953
H	-6.25983	-1.34412	-0.7278
C	-5.29509	4.33225	1.66824
H	-5.92576	3.92446	2.46349
H	-4.85686	5.25926	2.0453
H	-5.9294	4.59994	0.81824
C	-6.07019	1.80096	0.59821
H	-6.74682	2.59684	0.87515
C	-2.05862	-2.8437	-2.21916
H	-2.52709	-2.13776	-2.90929
H	-1.58675	-3.62989	-2.81669
C	-2.33929	1.46896	-2.53398
H	-2.96069	1.92964	-1.77984
C	-4.78566	-3.16106	0.41921
H	-5.31522	-2.52857	1.12115
C	-5.01373	-4.53241	0.41168
H	-5.74787	-4.95845	1.08685
C	-0.74456	0.21703	-4.38123
H	-0.12283	-0.31612	-5.09222
C	-2.26335	1.99247	-3.81928
H	-2.84152	2.87278	-4.0752
C	-8.19214	0.57722	-0.10949
C	-1.45734	1.35531	-4.76163
H	-1.39621	1.7267	-5.77932
C	-3.34378	4.03632	0.15041
H	-3.98011	4.26541	-0.70981
H	-2.92534	4.98117	0.5098
H	-2.52048	3.40564	-0.19286
C	-1.98359	-1.77971	2.37851
H	-2.52323	-0.86444	2.5947
C	-0.65024	-4.06995	1.66135
H	-0.13535	-4.9696	1.34292
C	-1.86579	-2.80174	3.30975

H	-2.31159	-2.69425	4.29178
C	-1.19135	-3.9683	2.94286
H	-1.10112	-4.79407	3.64089
C	-8.84303	0.75929	1.28596
H	-8.57587	1.71004	1.75553
H	-9.93034	0.74738	1.17458
H	-8.56244	-0.052	1.96359
C	-8.61637	1.74472	-1.0356
H	-8.164	1.64782	-2.02668
H	-9.70251	1.72866	-1.15596
H	-8.35123	2.72423	-0.62763
C	-8.6788	-0.74555	-0.71971
H	-8.26833	-0.90992	-1.72125
H	-8.42818	-1.60418	-0.08812
H	-9.76615	-0.72281	-0.81574
C	8.67901	0.74649	0.71817
H	8.42814	1.60507	0.08662
H	8.26874	0.91082	1.7198
H	9.76639	0.72388	0.81397

Inorganic Chemistry

Article

pubs.acs.org/IC

Dioxygen Reactivity of an Iron Complex of 2-Aminophenol-Appended Ligand: Crystallographic Evidence of the Aromatic Ring Cleavage Product of the 2-Aminophenol Unit

Ganesh Chandra Paul,[†] Sridhar Banerjee,[‡] and Chandan Mukherjee*[,†]

[†]Department of Chemistry, Indian Institute of Technology Guwahati, Guwahati 781 039, Assam India

[‡]Department of Inorganic Chemistry, Indian Association for the Cultivation of Science, 2A & 2B Raja S. C. Mullick Road, Jadavpur, Kolkata 700 032, India

Supporting Information

ABSTRACT: 2-Aminophenol appended pentadentate ligand H_2Gan^{AP} was synthesized by mixing equimolar amounts of 2-[bis(2-pyridylmethyl)aminomethyl]aniline (A) and 3,5-di-*tert*-butyl catechol in hexane in the presence of Et_3N under air. The ligand reacted with $Fe(ClO_4)_2{\cdot}6H_2O$ or $Fe(ClO_4)_3{\cdot}6H_2O$ in the presence of tetrabutylammonium perchlorate, and Et_3N under air and provided a μ_2 oxo-bridged dinuclear iron complex (**1**). X-ray single-crystal analysis of complex **1** revealed the presence of a furan derivative, resulting from the oxidative aromatic C−C bond cleavage product of 2-aminophenol derivative, in the coordination sphere of each iron center. Mechanistic investigation for the formation of complex **1** established that in the absence of molecular oxygen no oxidation of the appended 2-amidophenolate unit took place. An iron(III)−amidophenolate complex, formed initially, further reacted with molecular oxygen and caused oxidative aromatic C−C bond cleavage via a putative alkylperoxo species.

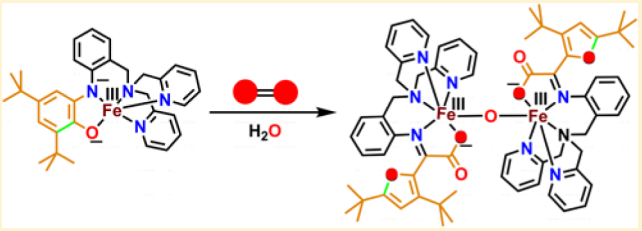

INTRODUCTION

2-Aminophenol-1,6-dioxygenase (APD)[1] belongs to dioxygenase family and catalyzes the biodegradation of 2-aminophenol derivatives via oxidative extradiol-type aromatic C−C bond cleavage at the meta-position (C1−C6) under aerobic atmosphere. In the reaction, fission of a dioxygen bond and incorporation of both the oxygen atoms into aliphatic product 2-aminomuconic acid semialdehyde takes place.[2] The product then undergoes nonenzymatic condensation spontaneously and finally forms 2-picolinic acid (Scheme 1).

Scheme 1. APD-Catalyzed C−C Bond Cleavage of 2-Aminophenol

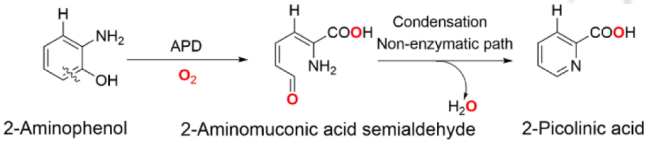

In 2013, Li et al.[3] have reported the crystal structures of APD from *Comamonas sp.* strain CNB-1 as the apoenzyme, the holoenzyme, and as complexes with the lactone intermediate (4*Z*,6*Z*)-3-iminooxepin-2(3*H*)-one, the product 2-aminomuconic-6-semialdehyde, and with the suicide inhibitor 4-nitrocatechol. The active site of APD contains a mononuclear nonheme iron center. The iron is in +II oxidation state,[3] and the "His13-His62-Glu251 facial triad" occupies the coordination sites.[3] During the oxidation catalysis, both N and O atoms from the substrate 2-aminophenol derivative and an oxygen atom from a dioxygen molecule bind to the iron center from the other face. Thus, a six-coordinate intermediate forms. The catalytic path for C−C bond cleavage of 2-aminophenol via the incorporation of two oxygen atoms is being proposed to follow the mechanism similar to that of extradiol cleavage by catechol dioxygenases.[4]

In general, it has been observed that redox-active 2-aminophenol or its derivatives upon coordination to iron center do not undergo aromatic C−C bond cleavage in the presence of dioxygen.[5] Rather, it exists mainly in its one-electron oxidized 2-iminobenzosemiquinonato π-radical state in the coordination complexes.[5] Thus, biomimetic model complexes for APD are very rare.[6] In the model complexes, either tridentate or tetradentate ligand scaffolds along with substrate 2-aminophenol derivatives are being employed to form the corresponding five-coordinate and six-coordinate complexes under inert atmosphere. Dioxygen reactivity of those complexes is then studied for the mechanistic understanding of APD.[6] In all the reports, the aminophenol-derived cleavage products are isolated via acidic workup of the reaction solutions. In the procedure, the possibility of unexpected condensation and/or ring opening of the actual oxidative C−C cleavage species via hydrolysis cannot be revoked. Thus, a direct method for identification of the C−C bond cleavage

Received: June 20, 2016
Published: December 22, 2016

DOI: 10.1021/acs.inorgchem.6b01474
Inorg. Chem. 2017, 56, 729−736

product was necessary. In this endeavor, we incorporated a 3,5-di-*tert*-butyl-2-aminophenol unit at the ortho position of a tripodal *N*,*N*-bis(pyridine-2-ylmethyl)benzylamine ligand scaffold (Scheme 2). Thus, the designed ligand, designated here as

Scheme 2[a]

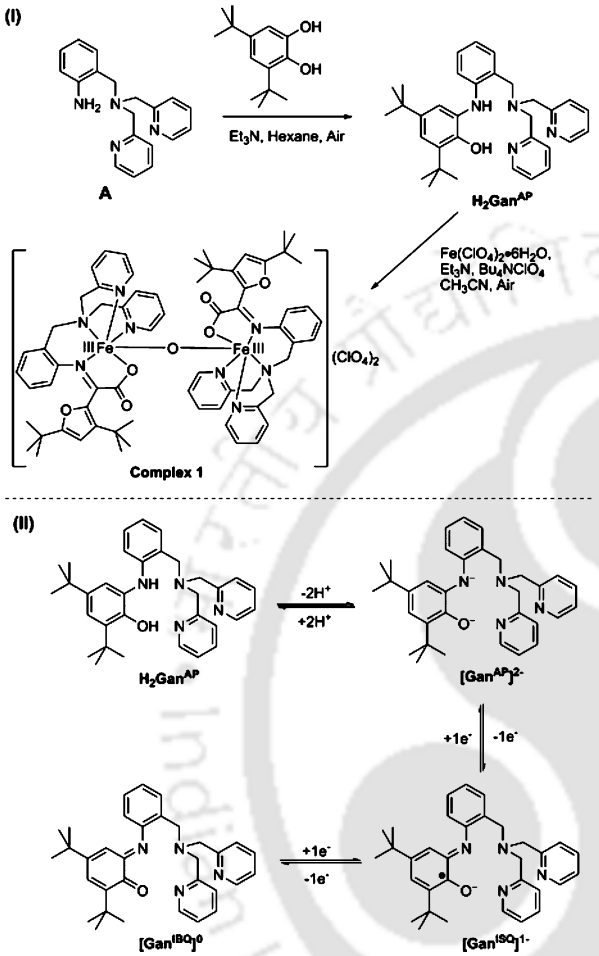

[a](I) A schematic representation for the syntheses of H_2Gan^{AP} and complex **1**. (II) Possible different redox states that can be availed by the ligand H_2Gan^{AP} in its corresponding iron complex.

H_2Gan^{AP}, contains both substrate 2-aminophenol and tripodal N_3 iron coordination site. The ligand would provide a mononuclear five-coordinate iron complex that could allow its reaction toward dioxygen. Thus, complex finally could provide the two oxygen atoms-incorporated C−C cleavage product of 3,5-di-*tert*-butyl-2-aminophenol unit. X-ray crystallographic analysis of the final complex would then provide crystallographic identification of the aromatic oxidative C−C cleavage product.

Ligand H_2Gan^{AP} reacted with stoichiometric amount of $Fe(ClO_4)_2{\cdot}6H_2O$ or $Fe(ClO_4)_3{\cdot}6H_2O$ under air and provided a μ_2 oxo-bridged dinuclear iron complex (**1**) [Scheme 2]. X-ray crystallographic analysis of complex **1** displayed that the complex in its coordination sphere contained a furan derivative that formed via meta C−C cleavage of 2-aminophenol derivative and incorporation of two oxygen atoms into the cleavage product. Thus far, no other existing APD model complex provides direct evidence for the identification of oxidative aromatic C−C cleavage product. The mechanistic study for the formation of complex **1** indicated the generation of a low-spin $[Gan^{AP}Fe^{III}]^+$ species, which reacted with dioxygen through its low-lying excited state, an Fe(II)-ISQ species ($[Gan^{ISQ}Fe^{II}]^+$), causing aromatic C−C bond cleavage. Finally, the labeling experiment employing $^{18}O_2$ confirmed that the two incorporated-oxygen atoms in the cleavage product belonged to dioxygen. Herein, we report the synthesis and characterization of H_2Gan^{AP} and complex **1**. In addition, a mechanistic proposal for the formation of complex **1** is put forward.

RESULTS AND DISCUSSION

The ligand H_2Gan^{AP} was synthesized by mixing equimolar amounts of 2-[bis(2-pyridylmethyl)aminomethyl]aniline (**A**) and 3,5-di-*tert*-butyl catechol in hexane in the presence of Et_3N under air. The reaction of H_2Gan^{AP} and $Fe(ClO_4)_2{\cdot}6H_2O$ or $Fe(ClO_4)_3{\cdot}6H_2O$ (1:1) in the presence of Et_3N and tetrabutylammonium perchlorate in CH_3CN under air yielded complex **1** in 54% yield.

In the electrospray ionization mass spectrum (ESI-MS) of complex **1** in CH_3CN, a 100% molecular ion peak at m/z = 98.94 appeared in the negative mode, while, in the positive mode, a 100% molecular ion peak at m/z = 601.22 was observed. The peak at m/z = 98.94 confirmed the presence of perchlorate anion in the complex. Isotope distribution pattern indicated $[C_{66}H_{74}Fe_2N_8O_7]^{2+}$ composition for the observed positive mode peak at m/z = 601.22 and confirmed the formation of complex **1**. The UV−vis spectrum of complex **1** was predominated by charge transfer transitions (Figure S7). The band at 440 nm (ε = 17 450 M^{-1} cm^{-1}) was attributed to oxo-to-Fe(III) ligand-to-metal charge transfer (LMCT), while 383 nm (ε = 19 800 M^{-1} cm^{-1}) was assigned as $\pi-\pi^*$ transition of the imine (C═N) moiety.

Single crystal suitable for X-ray diffraction measurement was obtained by the slow evaporation of the reaction mixture. The diffraction measurement for complex **1**·1CH_3CN was performed at 296(2) K. The complex crystallized in the monoclinic space group $P21/c$ (No. 14). The molecular structure with atom labeling scheme is presented in Figure 1. Selected bond distances and bond angles are given in Table 1.

Complex **1** was comprised of a dicationic dinuclear oxo-bridged iron coordination unit and two perchlorate ions as

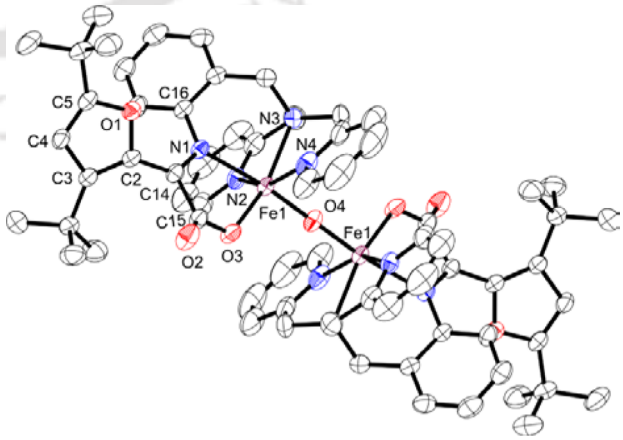

Figure 1. ORTEP diagram of dinuclear dicationic oxo-bridged coordination unit that belongs to complex **1**; thermal ellipsoids were drawn at 40% probability level. Solvent molecule (CH_3CN), anions (perchlorates), and H atoms are omitted.

DOI: 10.1021/acs.inorgchem.6b01474
Inorg. Chem. 2017, 56, 729−736

Table 1. Selected Bond Distances (Å) and Bond Angles (deg) for Complex 1

Fe1−O4	1.7789(3)	C15−O2	1.214(3)
Fe1−O3	1.9739(19)	C14−N1	1.291(3)
Fe1−N2	2.140(2)	C16−N1	1.437(3)
Fe1−N4	2.154(2)	C16−C21	1.393(4)
Fe1−N3	2.183(2)	C21−C22	1.503(4)
Fe1−N1	2.229(2)	C22−N3	1.501(3)
C2−O1	1.386(3)	C23−N3	1.487(4)
C5−O1	1.366(3)	C23−C24	1.492(5)
C2−C3	1.367(4)	C24−N4	1.345(4)
C3−C4	1.435(3)	C28−N3	1.488(4)
C4−C5	1.341(4)	C28−C30	1.497(4)
C14−C15	1.530(4)	C30−N2	1.333(4)
Fe1−O4−Fe1	180.00(2)	C5−O1−C2	107.0(2)
O4 −Fe1−N1	171.54(6)	C4−C5−O1	109.4(2)
O3−Fe1−N1	76.13(7)	C2−C3−C4	104.6(2)
N2−Fe1−N1	81.25(8)	C2−C3−C6	131.2(2)
N4−Fe1−N1	97.00(8)	C4−C3−C6	124.1(2)
N3−Fe1−N1	87.42(8)	C4−C5−C10	134.5(3)
O4−Fe1−N2	92.63(6)	O4−Fe1−O3	100.83(5)
O3−Fe1−N2	110.62(9)	O1−C5−C10	116.0(2)
N2−Fe1−N3	78.12(9)	O1−C2−C14	112.3(2)
N4−Fe1−N3	76.33(10)	C3−C2−C14	137.1(2)
O3−Fe1−N3	159.54(8)	N1−C14−C2	126.3(2)
O4−Fe1−N3	97.08(6)	N1−C14−C15	112.9(2)
N2−Fe1−N4	154.45(10)	C2−C14−C15	120.5(2)
O3−Fe1−N4	93.46(10)	O2−C15−O3	125.7(2)
O4−Fe1−N4	91.04(6)	O2−C15−C14	120.0(2)
C15−O3−Fe1	117.80(17)	O3−C15−C14	114.3(2)

counteranions. In the cationic unit, both the iron centers were six-coordinate and related to each other by means of an inversion center that was located at the bridging μ_2-O4 atom. Thus, one-half of the molecule was reflected by another. The coordination sites of the Fe1 center were occupied by two pyridine-N atoms (N2, and N4), one amine-N atom (N3), one imine-N atom (N1), one carboxylate-O atom (O3), and the bridging-O atom (O4). The Fe1−N1 = 2.229(2), Fe1−N2 = 2.140(2), Fe1−N3 = 2.183(2), Fe1−N4 = 2.154(2), and Fe1−O3 = 1.9739(19) Å bond distances were in accord with the previously reported high-spin Fe(III)−N and Fe(III)−O bond distances.[7] The N1−Fe1−O4 = 171.54(6), N2−Fe1−N4 = 154.45(10), and N3−Fe1−O3 = 159.54(8)° bond angles indicated that Fe1 center acquired distorted octahedral geometry.

In complex **1**, neither 2-amidophenolate unit nor its one-electron oxidized iminobenzosemiquinone (ISQ) unit was found in the coordinated ligand backbone. Instead, a newly formed cyclic C_4O unit was present in the ligand backbone. The N1−C14 = 1.291(3) Å bond distance indicated a double bond (imine) character of the unit. The O1−C2 = 1.386(3), C2−C3 = 1.367(4), C3−C4 = 1.435(3), C4−C5 = 1.341(4), and O1−C5 = 1.366(3) Å bond distances confirmed the furan form of the pendent C_4O unit.[8] The longer O3−C15 = 1.296(3) Å bond distance compared to O2−C15 = 1.214(3) Å confirmed the localization of the carboxylate^{1-} charge on O3 atom. Thus, it was evident from the molecular structure analysis of complex **1** that desired dioxygen incorporation and simultaneous C−C bond cleavage at the meta position of the aromatic 2-aminophenol moiety took place during the complex formation.

The mechanistic investigation on the complex formation was performed to understand the O_2-dependent C−C bond cleavage. All attempts to isolate the iron(II) complex of the ligand failed. However, an iron(III)−amidophenolate complex, $[Gan^{AP}Fe^{III}](ClO_4)$ (**2**), was isolated from the reaction of the ligand and iron(II) perchlorate hydrate in the presence of a trace amount of oxygen. Herein, the presence of small amount of oxygen could oxidize in situ generated Fe(II)-aminiphenolate species to the corresponding Fe(III)-amidophenolate complex. Complex **2** could also be isolated in good yield in the reaction between the liagnd and iron(III) perchlorate hydrate in the presence of Et_3N and tetrabutylammonium perchlorate (Experimental Section). Complex **2** showed a 100% molecular ion peak at m/z = 562.23 in its ESI-positive mode mass spectrum (Figure 2A, inset). Investigation on isotope

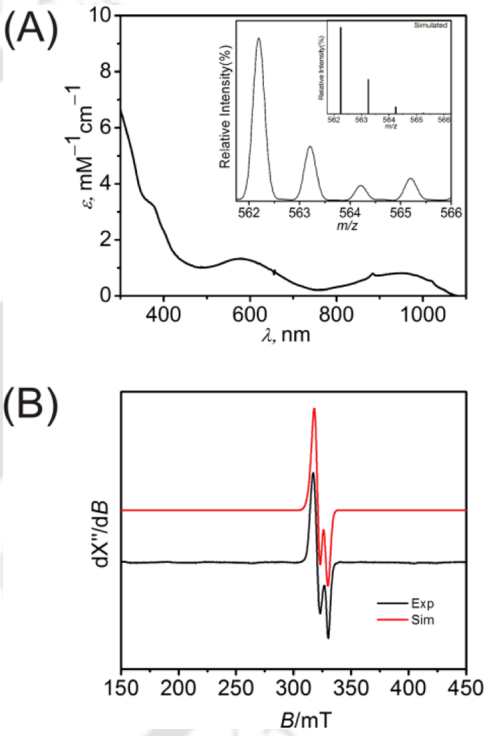

Figure 2. (A) UV−vis/NIR spectrum of complex **2**. (inset) Experimental as well as simulated mass spectra of complex **2**. (B) Experimental and simulated X-band EPR spectrum (9.106 GHz) of complex **2** measured at 77 K, power = 0.998 mW, modulation frequency = 100 kHz, and amplitude = 4 G.

distribution pattern revealed that the peak corresponded to composition $C_{33}H_{38}Fe_1N_4O_1$, which implied the formation of $[Gan^{AP}Fe^{III}]^+$ species. Noteworthy, despite several attempts, X-ray diffraction quality single crystal of $[Gan^{AP}Fe^{III}](ClO_4)$ could not be isolated. Density functional theory (DFT) calculations were performed to optimize the geometry of **2** by considering both high-spin (S = 5/2) and low-spin (S = 1/2) configurations of the central Fe(III) ion (Figure S8; Tables S1 and S2). Indeed, complex **2** with low-spin Fe(III) state was found to be 9.11 kcal/mol more stable compared to high-spin Fe(III) state. Furthermore, X-band EPR spectrum of the species showed a rhombic signal that appeared for an S = 1/2 system (Figure 2B). Simulation to the experimentally obtained spectrum provided the following parameters: g_1 = 1.990, g_2 = 2.035, g_3 = 2.050; g_{av} = 2.025; (W_1, W_2, W_3) = (28, 27, 50) G. From the spectrum nature and the g_{av} value it was evident that the

DOI: 10.1021/acs.inorgchem.6b01474
Inorg. Chem. 2017, 56, 729−736

paramagnetism of species $[Gan^{AP}Fe^{III}]^+$ appeared due to the presence of an unpaired electron that located at the iron center. Thus, the iron center present in the species was low-spin Fe(III) in character,[9] and the 2-amidophenolate unit was in its fully reduced close-shell (S = 0) configuration.

The UV−vis/NIR spectrum of complex **2** in CH_3CN showed two broad absorption bands at 578 nm (ε = 1350 M^{-1} cm^{-1}) and 950 nm (ε = 800 M^{-1} cm^{-1}) [Figure 2A]. Both the bands appeared due to 2-amidophenolate-to-Fe(III) LMCTs.[6b] When an CH_3CN solution of $\{[Gan^{AP}Fe^{III}](ClO_4)\}$ (**2**) was allowed to react with dioxygen, the spectral feature changed instantaneously, and a new absorption manifold centered at ∼800 nm (ε = 750 M^{-1} cm^{-1}) appeared (Figure 3). The band

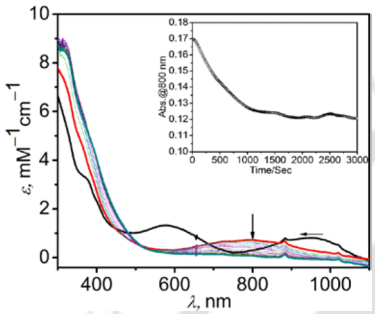

Figure 3. Spectral changes upon purging of molecular dioxygen in the CH_3CN solution of complex **2**. The instant change (black line to red line) occurs upon purging of molecular dioxygen in the solution of complex **2**. (inset) Time-dependent absorption changes at 800 nm.

position as well as the band intensity were comparable to the previously reported five-coordinate Fe(II)−ISQ system.[10] Thus, the formation of a five-coordinate ISQ-containing Fe(II) species ($[Gan^{ISQ}Fe^{II}]^+$) could be attributed during the reaction. The band at 800 nm decreased in intensity with time and finally shifted to lower wavelength (690 nm; ε = 100 $M^{-1}cm^{-1}$) [Figure 3]. This led to the formation of complex **1** as evident by ESI-MS analysis of the final solution (Figure 4A).

To reinforce the incorporation of aerial dioxygen into the meta C−C cleavage product of 2-amidophenolate unit, $[Gan^{AP}Fe^{III}]^+$ was allowed to react with $^{18}O_2$ in CH_3CN. The ESI-MS analysis of the final product confirmed the incorporation of only four ^{18}O atoms in complex **1** (Figure 4B). Therefore, fifth oxygen atom, that is, the bridging oxygen atom, in complex **1** was proposed to come from water molecule instead of aerial dioxygen. To consolidate the proposal, the formation of complex **1** was performed in the presence of H_2O^{18} in CH_3CN, and the positive mode ESI mass spectrum of the solution was recorded (Figure 5A). Interestingly, in addition to the expected molecular ion peak at 602.58 $\{[C_{66}H_{74}Fe_2N_8O_6{}^{18}O_1]^{2+}\}$, two more molecular ion peaks at 603.59 and 604.60 were observed. The respective compositions of the peaks were $[C_{66}H_{74}Fe_2N_8O_5{}^{18}O_2]^{2+}$ and $[C_{66}H_{74}Fe_2N_8O_4{}^{18}O_3]^{2+}$, as confirmed by isotope distribution pattern examinations (Figure S9). Thus, mass spectrum analysis indicated that in addition to the bridging oxygen atom, two more water molecules can participate in the formation of complex **1**. This result implied (i) the generation of a Fe-hydroxyl species as an intermediate in the progress of complex **1** formation and the hydroxyl group can be replaced by a water molecule, and (ii) participation of the hydroxyl group in the formation the furan derivative.

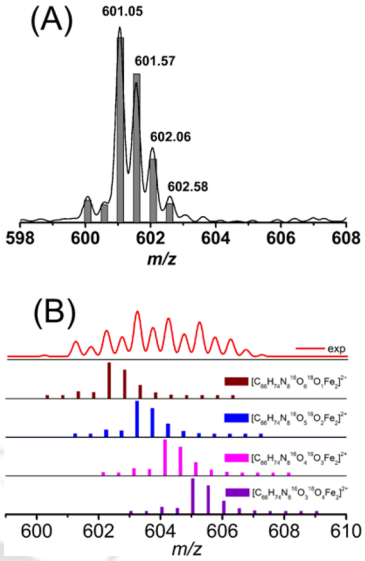

Figure 4. (A) ESI-MS (positive mode) spectrum of the final species that formed by purging of molecular oxygen to CH_3CN solution of complex **2**. (B) Experimental and simulated mass spectra (ESI, positive mode) of the final species upon reacting complex **2** with $^{18}O_2$. All the species were considered as 100% in the plots.

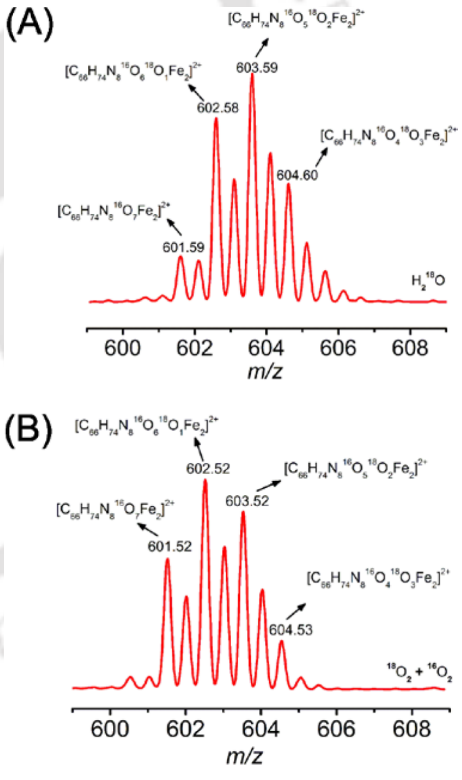

Figure 5. (A) ESI-MS (positive mode) spectrum of the final species that formed by purging of molecular oxygen to CH_3CN solution of complex **2** in the presence of H_2O^{18}. (B) Experimental mass spectra (ESI, positive mode) of the final species upon reacting complex **2** with ∼1:1 $^{16}O_2/^{18}O_2$ gas mixture.

To examine the incorporation of both oxygen atoms of molecular oxygen to form the furan derivative in complex **1**, a ∼1:1 $^{18}O_2/^{16}O_2$ gas mixture was employed in the course of formation of complex **1** in CH_3CN. The positive-mode ESI-MS spectrum of the solution showed molecular ion peaks at 601.52,

DOI: 10.1021/acs.inorgchem.6b01474
Inorg. Chem. 2017, 56, 729−736

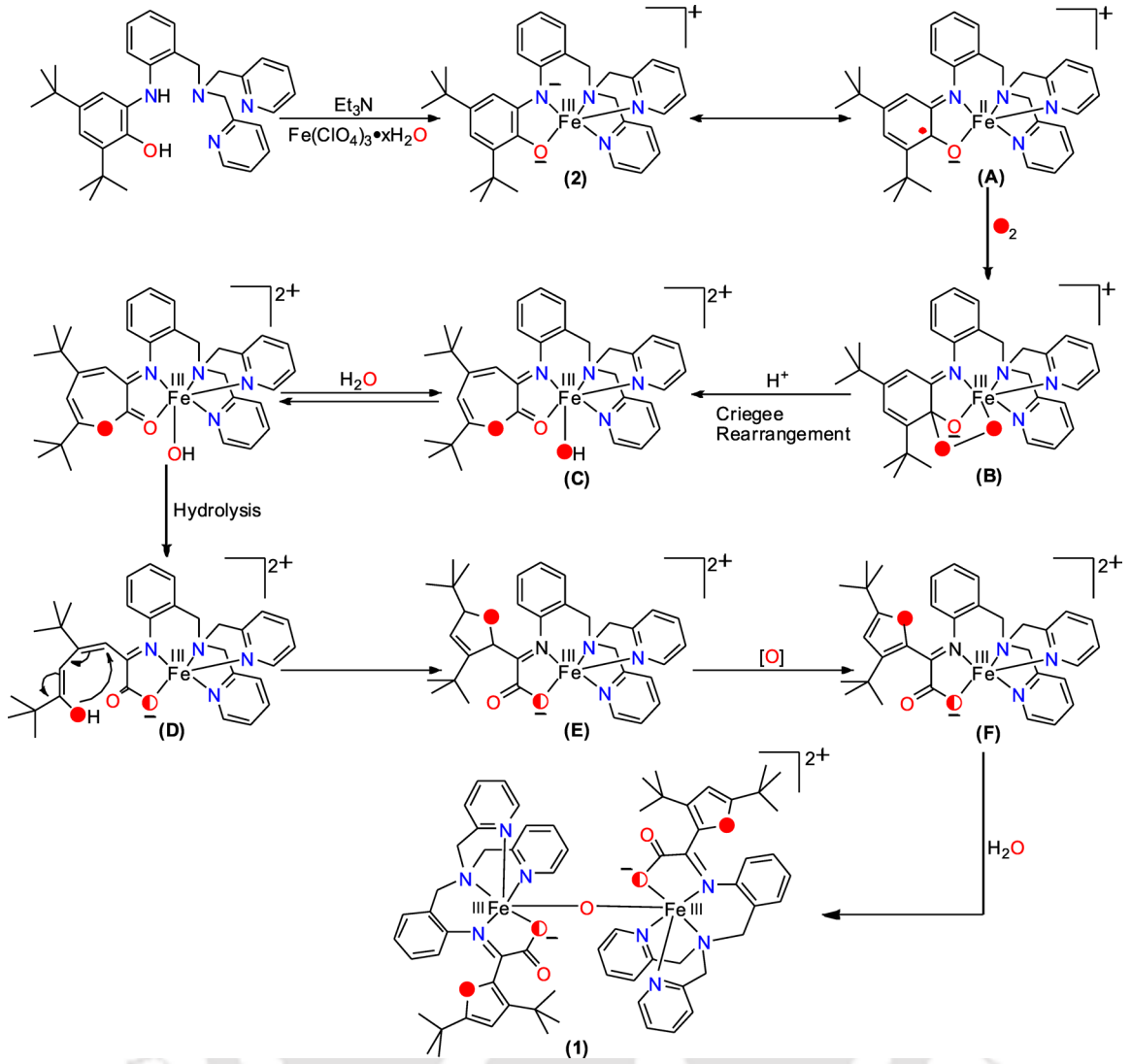

Figure 6. Proposed mechanism for the oxidative meta C−C bond cleavage of 2-aminophenol derivative.

602.52, 603.52, and 604.53 (Figure 5B). The peak at 604.53 corresponded to composition $[C_{66}H_{74}Fe_2N_8O_4{}^{18}O_3]^{2+}$, which indicated the incorporation of three ^{18}O atoms in complex **1**. Thus, it can be argued that both oxygen atoms from an oxygen molecule participated in furan derivative formation. Since the tetra O-18 species was observed in the labeling experiment with $^{18}O_2$ (Figure 4B), the peak was not observed in mixed $^{16}O_2/^{18}O_2$ experiment possibly due to low percentage incorporation and subsequent replacement of an Fe-coordinated $[HO^{18}]^-$ group by a $[H_2O^{16}]^0$ molecule at intermediate **C** stage (Figure 6).

A mechanistic proposal (Figure 6) for the formation of complex **1** by aromatic C−C bond cleavage and incorporation of an oxygen molecule was drawn by summarizing the foregoing experimental results. UV−vis/NIR spectrum along with EPR spectrum revealed that ligand H_2Gan^{AP} upon reacting with Fe(II) perchlorate hydrate and a trace amount of molecular oxygen or iron(III) perchlorate hydrate in the presence of Et_3N and tetrabutylammonium perchlorate provided a five-coordinate $[Gan^{AP}Fe^{III}]^+$ species. Akin to previous reports,[6] it is also postulated that the species remained in equilibrium with its valence tautomeric $[Gan^{ISQ}Fe^{II}]^+$ species, which then reacted with molecular oxygen to generate an Fe(III)-alkylperoxo complex (**B**; Figure 6). Herein, ESI-MS analysis for the formation of complex **1** employing $^{18}O_2$ molecule consolidated the participation of molecular oxygen. The species **B** underwent Criegee rearrangement, and species **C** was formed. In the species, the Fe(III)-coordinated hydroxyl group can be replaced by water molecule as evident by H_2O^{18} experiment. Furthermore, incorporation of three ^{18}O atoms during the reaction consolidated the participation of the hydroxyl group in the formation of the furan derivative. Cyclization of the product from hydrolysis (**D**) resulted in 2,5-dihydrofuran derivative (**E**). Species **E** then underwent oxidation to **F**. Herein, the driving force could be the aromatization via radical pathway, and the process might be facilitated by the presence of Fe-salt and in situ generated superoxide or peroxide species.[11] Finally, two units of **F** combined with a water molecule, as evidenced by H_2O^{18} experiment, and complex **1** was formed (Figure 6). To note, the reactivity observed may in fact be more complicated than the mechanistic scheme proposed.

CONCLUSION

To conclude, we have demonstrated the successful synthesis of 3,5-di-*tert*-butyl-2-aminophenol-appended H_2Gan^{AP} ligand. The

DOI: 10.1021/acs.inorgchem.6b01474
Inorg. Chem. 2017, 56, 729−736

ligand upon reacting with $Fe(ClO_4)_2·6H_2O$ in the presence of air, Et_3N, and tetrabutylammonium perchlorate provides complex **1**. Noteworthy, complex **1** can also be synthesized by using Fe(III) percholorale hydrate as the iron salt. X-ray structural analysis of complex **1** reveals the presence of a furan derivation in the ligand backbone. Thus, the oxidative meta C−C bond scission of 2-aminophenol derivative emulates the function of APD. Noteworthy, the complex provides crystallographic characterization of the cleavage product of 2-aminophenol derivative.

Mechanistic investigation for the scission demonstrates the formation of $[Gan^{AP}Fe^{III}]^+$ species under anaerobic condition. The incorporation of aerial dioxygen to the meta C−C cleavage product is consolidated by mass spectrometric analysis of the final product that is generated by reacting $[Gan^{AP}Fe^{III}]^+$ species with $^{18}O_2$. Finally, the formation of Fe-hydroxy group-coordinated species **C** and the incorporation of the bridging oxygen atom from a water molecule are consolidated by introducing H_2O^{18} during the complex formation reaction.

EXPERIMENTAL SECTION

Materials. All the chemicals and solvents were obtained from commercial sources and were used as supplied, unless noted otherwise. 3,5-Di-*tert*-butylcatechol, 2-pyridinecarboxaldehyde, and 2-picolylamine were purchased from Sigma-Aldrich. Solvents were obtained from Merck (India). Mass spectra were measured in HPLC-grade acetonitrile solution. Labeling experiments were performed using $^{18}O_2$ gas (99 atom %) and H_2O^{18} (98 atom %), which were purchased from Icon Services Inc., USA.

Physical Methods. X-ray crystallographic data were collected using Super Nova, Single source at offset, Eos diffractometer. The data refinement and cell reductions were performed by CrysAlisPro.[11] Structures were solved by direct methods using SHELXS-97 and refined by the full matrix least-squares method using SHELXL-97.[12] All the non-hydrogen atoms were refined anisotropically. IR spectra were recorded on a PerkinElmer Instrument at normal temperature with KBr pellet by grinding the sample with KBr (IR grade). ^{1}H-, and ^{13}C-NMR spectra of the ligand were recorded in Bruker 600 MHz NMR machine. UV−vis/NIR spectra were recorded on a PerkinElmer, Lamda 750, UV/vis/NIR spectrometer by preparing a known concentration of the samples in HPLC-grade CH_2Cl_2 at room temperature (25 °C) using a cuvette of 1 cm width. Solution electronic spectra (single and time-dependent) were measured on an Agilent 8453 diode array spectro-photometer. Mass spectral (MS) data were obtained from quadrupole time-of-flight (QTOF)-MS spectrometer (Waters, model: Q-Tof Premier), and peaks are given in m/z (% of basis peak).

Computational Details. All DFT calculations are performed using Gaussian09 program suite.[13] The geometrical optimization calculations (Table 2) were performed at the level of ubp86/6-311g.

Synthesis of $C_{33}H_{40}N_4O$, H_2Gan^{AP}. To a stirred solution of 3,5-di-*tert*-butyl catechol (0.668 g, 3.01 mmol) and 2-[bis(2-pyridylmethyl)-aminomethyl]aniline (**A**)[14] (0.917 g, 3.01 mmol) in hexane (25 mL) triethylamine (0.05 mL) was added, and the reaction mixture was refluxed for 7 d. The resulting brown color reaction mixture was cooled to room temperature and then stirred further for 2 d. After that, the resulting suspension was filtered. The filtrate part was evaporated to afford an amorphous solid. The solid was dissolved in methanol (15 mL) and kept under −20 °C, which provided colorless crystal. Yield: 0.760 g, 50%. FTIR (KBr pellet, cm^{-1}): 3227, 3181, 3110, 3047, 2955, 2904, 2864, 1592, 1569, 1534, 1479, 1434, 1362, 1337, 1299, 1236, 1148, 983, 744. ^{1}H NMR (600.1737 MHz, $CDCl_3$): δ 9.03 (s, 1H), 8.83 (s, 1H), 8.42 (d, J = 4.6 Hz, 2H), 7.53 (td, J = 7.4, 1.3 Hz, 2H), 7.42 (d, J = 7.8 Hz, 2H), 7.20 (s, 1H), 7.05−7.08 (m, 4H), 7.00 (t, J = 7.9 Hz, 1H), 6.94 (d, J = 8.1 Hz, 1H), 6.62 (t, J = 7.2 Hz, 1H), 3.82 (s, 4H), 3.80 (s, 2H), 1.57 (s, 9H), 1.30 (s, 9H). ^{13}C NMR (150.9279 MHz, $CDCl_3$): δ 158.2, 149.0, 146.4, 145.8, 141.6, 137.1, 136.9, 130.9, 130.2, 128.6, 124.4, 123.0, 122.4, 118.0, 117.6, 117.4, 112.1, 61.0, 60.1, 35.5, 34.6, 31.9, 30.0. ESI-MS (+) m/z for $[C_{33}H_{40}N_4O + H]^+$: Calcd 509.3274; Found 509.3239.

Table 2. Crystallographic Parameters and Refinement Data for 1

empirical formula	$C_{66}H_{74}Fe_2N_8O_7$, 2(CH_3CN), 2(ClO_4)
formula weight	1484.04
CCDC number	1481661
crystal habit, color	needle, brown
crystal size, mm^3	0.20 × 0.15 × 0.05
temperature, T	296(2)
wavelength, λ (Å)	0.710 73
crystal system	monoclinic
space group	$P21/c$
unit cell dimensions	a = 15.2994(3) Å
	b = 13.1099(3) Å
	c = 18.3192(4) Å
	α = 90.00°, β = 93.079(2)°,
	γ = 90.00°
volume, V (Å^3)	3669.04(13)
Z	2
calculated density, Mg·m^{-3}	1.343
absorption coefficient, μ (mm^{-1})	0.538
F(000)	1552
θ range for data collection	2.97° to 25.10°
limiting indices	$-15 \le h \le 18$, $-10 \le k \le 15$, $-15 \le l \le 21$
reflection collected/unique	17 084/6514[R(int) = 0.0269]
completeness to θ	99.8% (θ = 25.00°)
max. and min transmission	0.973/0.908
refinement method	SHELXL-97(Sheldrick, 1997)
data/restraints/parameters	6526/0/464
goodness-of-fit on F^2	1.049
final R indices [$I > 2\sigma(I)$]	$R1$ = 0.0458, $wR2$ = 0.1091
R indices (all data)	$R1$ = 0.0595, $wR2$ = 0.1178
largest diff. peak and hole	0.456 and −0.566 e·Å^{-3}

Synthesis of Complex 1, $C_{66}H_{74}Fe_2Cl_2N_8O_{15}$. To a stirred solution of ligand H_2Gan^{AP} (0.206 g, 0.40 mmol) in acetonitrile (15 mL), $Fe(ClO_4)_2·6H_2O$ (0.144 g, 0.40 mmol) or $Fe(ClO_4)_3·6H_2O$ (0.185 g, 0.40 mmol) and Et_3N (0.1 mL) were added sequentially. After this solution was stirred for 15 min at room temperature, tetrabutylammonium perchlorate (0.276 g, 0.80 mmol) was added to the solution. The resulting reaction mixture was continued to stir for further 17 h. After that, the reaction mixture was kept for slow evaporation at room temperature for 6 d; during this period needle-shaped crystal appeared. Yield: 0.145 g, 54% [using $Fe(ClO_4)_2·6H_2O$]; 0.140 g [using $Fe(ClO_4)_3·6H_2O$]. FTIR (KBr pellet, cm^{-1}): 3070, 2965, 2934, 2872, 2251, 1676, 1607, 1587, 1550, 1485, 1443, 1317, 1278, 1247, 1092, 1002, 869, 850, 760. ESI-MS (+) m/z for $[C_{66}H_{74}Fe_2N_8O_7]^{2+}$: Calcd, 601.2236; Found 601.2298. Anal. Calcd for $C_{66}H_{74}Fe_2Cl_2N_8O_{15}·1CH_3CN$: C, 56.61; H, 5.38; N, 8.74. Found: C, 56.30; H, 5.03; N, 8.79%.

Caution! *Perchlorate salts of metal complexes are potentially explosive and should be handled only in small quantities with sufficient care.*

Synthesis of Complex 2, $C_{33}H_{38}FeClN_4O_5$. Ligand H_2Gan^{AP} (0.102 g, 0.20 mmol) was dissolved in acetonitrile (10 mL) under nitrogen atmosphere (inside a glovebox). To that, Et_3N (0.056 mL) was added, and the solution was allowed to stir for 5 min. After that, $Fe(ClO_4)_3·6H_2O$ (0.100 g, 0.21 mmol) was added, and the resulting mixture was allowed to stir for further 10 min. To the solution tetrabutylammonium perchlorate (0.140 g, 0.40 mmol) was added, and the reaction mixture was continued to stir overnight (∼10 h). The solvent was removed under vacuum; the residue was dissolved in dichloromethane and then filtered. The filtrate part was concentrated under vacuum, and to the residue hexane was added dropwise until the

DOI: 10.1021/acs.inorgchem.6b01474
Inorg. Chem. 2017, 56, 729−736

product precipitated. The precipitate was filtered and washed with hexane and diethyl ether, and then the product was collected as brown solid. Yield: 0.145 g, 72%. ESI-MS (+) m/z for $[C_{33}H_{38}FeN_4O]^+$: Calcd, 562.2441; Found 562.2302. Anal. Calcd for $C_{33}H_{38}FeClN_4O_5 \cdot 2Et_2O \cdot 7H_2O$: C, 52.59; H, 7.75; N, 5.98. Found: C, 52.86; H, 8.09; N, 5.93%.

■ ASSOCIATED CONTENT

Supporting Information

The Supporting Information is available free of charge on the ACS Publications website at DOI: 10.1021/acs.inorgchem.6b01474.

Experimental Section, mass, IR, NMR spectra, UV−vis spectrum of **1**. DFT-based optimized molecular structure of complex **2**. Coordinates for geometrically optimized structure of complex **2** (both low-spin and high-spin states) (PDF)

X-ray crystallographic information (CIF)

■ AUTHOR INFORMATION

Corresponding Author

*E-mail: cmukherjee@iitg.ernet.in.

ORCID

Chandan Mukherjee: 0000-0002-2771-2468

Funding

Science and Engineering Research Board (SERB), India.

Notes

The authors declare no competing financial interest.

■ ACKNOWLEDGMENTS

This project is supported by SERB [EMR/2015/002491], India. G.C.P. thanks Indian Institute of Technology Guwahati (IITG) for his doctoral fellowship, and S.B. thanks CSIR for his doctoral fellowship. C.M. is indebted to Prof. T. K. Paine for scientific discussion and experimental facilities. The Department of Chemistry and CIF, IIT Guwahati are thankfully acknowledged for instrumental facility.

■ REFERENCES

(1) (a) Wu, J.-F.; Sun, C.-W.; Jiang, C.-Y.; Liu, Z.-P.; Liu, S.-J. A novel 2-aminophenol 1,6-dioxygenase involved in the degradation of *p*-chloronitrobenzene by *Comamonas* strain CNB-1: purification, properties, genetic cloning and expression in *Escherichia coli*. *Arch. Microbiol.* **2005**, *183*, 1−8. (b) Takenaka, S.; Murakami, S.; Shinke, R.; Hatakeyama, K.; Yukawa, H.; Aoki, K. Novel Genes Encoding 2-Aminophenol 1,6-Dioxygenase from Pseudomonas Species AP-3 Growing on 2-Aminophenol and Catalytic Properties of the Purified Enzyme. *J. Biol. Chem.* **1997**, *272*, 14727−14732. (c) Lendenmann, U.; Spain, J. C. 2-Aminophenol 1,6-Dioxygenase: a Novel Aromatic Ring Cleavage Enzyme Purified from *Pseudomonas pseudoalcaligenes* JS45. *J. Bacteriol.* **1996**, *178*, 6227−6232.

(2) (a) He, Z.; Spain, J. C. One-step production of picolinic acids from 2-aminophenols catalyzed by 2-aminophenol 1,6-dioxygenase. *J. Ind. Microbiol. Biotechnol.* **2000**, *25*, 25−28. (b) Somerville, C. C.; Nishino, S. F.; Spain, J. C. Purification and Characterization of Nitrobenzene Nitroreductase from *Pseudomonas pseudoalcaligenes* JS45. *J. Bacteriol.* **1995**, *177*, 3837−3842. (c) Zhang, Y.; Colabroy, K. L.; Begley, T. P.; Ealick, S. E. Structural Studies on 3-Hydroxyanthranilate-3,4-dioxygenase: The Catalytic Mechanism of a Complex Oxidation Involved in NAD Biosynthesis. *Biochemistry* **2005**, *44*, 7632−7643. (d) Li, X. W.; Guo, M.; Fan, J.; Tang, W. Y.; Wang, D. Q.; Ge, H. H.; Rong, H.; Teng, M. K.; Niu, L. W.; Liu, Q.; Hao, Q. Crystal structure of 3-hydroxyanthranilic acid 3,4-dioxygenase from *Saccharomyces cerevisiae*: A special subgroup of the type III extradiol dioxygenases. *Protein Sci.* **2006**, *15*, 761−773.

(3) (a) Li, D.-F.; Zhang, J.-Y.; Hou, Y.-J.; Liu, L.; Hu, Y.; Liu, S.-J.; Wang, D.-C.; Liu, W. Structures of aminophenol dioxygenase in complex with intermediate, product and inhibitor. *Acta Crystallogr., Sect. D: Biol. Crystallogr.* **2013**, *69*, 32−43.

(4) (a) Bugg, T. D. H.; Lin, G. Solving the riddle of the intradiol and extradiol catechol dioxygenases: how do enzymes control hydroperoxide rearrangements? *Chem. Commun.* **2001**, *11*, 941−953. (b) Bugg, T. D. H. Dioxygenase enzymes: catalytic mechanisms and chemical models. *Tetrahedron* **2003**, *59*, 7075−7101. (c) Costas, M.; Mehn, M. P.; Jensen, M. P.; Que, L., Jr. Dioxygen Activation at Mononuclear Nonheme Iron Active Sites: Enzymes, Models, and Intermediates. *Chem. Rev.* **2004**, *104*, 939−986. (d) Vaillancourt, F. H.; Bolin, J. T.; Eltis, L. D. The Ins and Outs of Ring-Cleaving Dioxygenases. *Crit. Rev. Biochem. Mol. Biol.* **2006**, *41*, 241−267. (e) Lipscomb, J. D. Mechanism of extradiol aromatic ring-cleaving dioxygenases. *Curr. Opin. Struct. Biol.* **2008**, *18*, 644−649. (f) Siegbahn, P. E. M.; Haeffner, F. Mechanism for Catechol Ring-Cleavage by Non-Heme Iron Extradiol Dioxygenases. *J. Am. Chem. Soc.* **2004**, *126*, 8919−8932. (g) Kovaleva, E. G.; Lipscomb, J. D. Crystal Structures of Fe^{2+} Dioxygenase Superoxo, Alkylperoxo, and Bound Product Intermediates. *Science* **2007**, *316*, 453−457.

(5) (a) Poddel'sky, A. I.; Cherkasov, V. K.; Abakumov, G. A. Transition metal complexes with bulky 4,6-di-*tert*-butyl-*N*-aryl(alkyl)-*o*-iminobenzoquinonato ligands: Structure, EPR and magnetism. *Coord. Chem. Rev.* **2009**, *253*, 291−324. (b) Chun, H.; Bill, E.; Bothe, E.; Weyhermüller, T.; Wieghardt, K. Octahedral (*cis*-Cyclam)-iron(III) Complexes with *O,N*-Coordinated *o*-Iminosemiquinonate(1−) π Radicals and *o*-Imidophenolate(2−) Anions. *Inorg. Chem.* **2002**, *41*, 5091−5099. (c) Chun, H.; Weyhermüller, T.; Bill, E.; Wieghardt, K. Tuning the Electronic Structure of Halidobis(*o*-iminobenzosemiquinonato)-iron(iii) Complexes. *Angew. Chem., Int. Ed.* **2001**, *40*, 2489−2492. (d) Chun, H.; Bill, E.; Weyhermüller, T.; Wieghardt, K. $S = {}^3/_2 \rightleftharpoons S = {}^1/_2$ Spin Crossover Behavior in Five-Coordinate Halido- and Pseudohalido-bis(*o*-iminobenzosemiquinonato)iron(III) Complexes. *Inorg. Chem.* **2003**, *42*, 5612−5620. (e) Bittner, M. M.; Kraus, D.; Lindeman, S. V.; Popescu, C. V.; Fiedler, A. T. Synthetic, Spectroscopic, and DFT Studies of Iron Complexes with Iminobenzo(semi)quinone Ligands: Implications for *o*-Aminophenol Dioxygenases. *Chem. - Eur. J.* **2013**, *19*, 9686−9692. (f) Rajput, A.; Sharma, A. K.; Barman, S. K.; Koley, D.; Steinert, M.; Mukherjee, R. Neutral, Cationic, and Anionic Low-Spin Iron(III) Complexes Stabilized by Amidophenolate and Iminobenzosemiquinonate Radical in *N,N,O* Ligands. *Inorg. Chem.* **2014**, *53*, 36−48.

(6) (a) Chakraborty, B.; Bhunya, S.; Paul, A.; Paine, T. K. Reactivity of Biomimetic Iron(II)-2-aminophenolate Complexes toward Dioxygen: Mechanistic Investigations on the Oxidative C−C Bond Cleavage of Substituted 2-Aminophenols. *Inorg. Chem.* **2014**, *53*, 4899−4912. (b) Chakraborty, B.; Paine, T. K. Aromatic Ring Cleavage of 2-Amino-4-tert-butylphenol by a Nonheme Iron(II) Complex: Functional Model of 2-Aminophenol Dioxygenases. *Angew. Chem., Int. Ed.* **2013**, *52*, 920−924. (c) Chatterjee, S.; Paine, T. K. Oxygenative Aromatic Ring Cleavage of 2-Aminophenol with Dioxygen Catalyzed by a Nonheme Iron Complex: Catalytic Functional Model of 2-Aminophenol Dioxygenases. *Inorg. Chem.* **2015**, *54*, 1720−1727. (d) Lakshman, T. R.; Chatterjee, S.; Chakraborty, B.; Paine, T. K. Substrate-dependent aromatic ring fission of catechol and 2-aminophenol with O_2 catalyzed by a nonheme iron complex of a tripodal N_4 ligand. *Dalton Trans.* **2016**, *45*, 8835−8844.

(7) (a) Jang, H. G.; Cox, D. D.; Que, L., Jr. A Highly Reactive Functional Model for the Catechol Dioxygenases. Structure and Properties of $[Fe(TPA)DBC]BPh_4$. *J. Am. Chem. Soc.* **1991**, *113*, 9200−9204. (b) Zang, Y.; Kim, J.; Dong, Y.; Wilkinson, E. C.; Appelman, E. H.; Que, L., Jr. Models for Nonheme Iron Intermediates: Structural Basis for Tuning the Spin States of Fe(TPA) Complexes. *J. Am. Chem. Soc.* **1997**, *119*, 4197−4205. (c) Roelfes, G.; Lubben, M.; Chen, K.; Ho, R. Y. N.; Meetsma, A.; Genseberger, S.;

Hermant, R. M.; Hage, R.; Mandal, S. K.; Young, V. G., Jr.; Zang, Y.; Kooijman, H.; Spek, A. L.; Que, L., Jr.; Feringa, B. L. Iron Chemistry of a Pentadentate Ligand That Generates a Metastable Fe^{III}−OOH Intermediate. *Inorg. Chem.* **1999**, *38*, 1929−1936.

(8) (a) Zingales, S. K.; Wallace, M. Z.; Padgett, C. W. Crystal structure of (E)-1-(3-chlorophenyl)-3-(furan-2-yl)prop-2-en-1-one. *Acta Crystallogr.* **2015**, *E71*, o707. (b) Martínez de León, C.; Tlahuext, H.; Grévy, J. −M. Crystal structure of 2,5-bis-(diphenylphosphanyl)furan. *Acta Crystallogr.* **2015**, *E71*, o922−o923.

(9) (a) Chun, H.; Verani, C. N.; Chaudhuri, P.; Bothe, E.; Bill, E.; Weyhermüller, T.; Wieghardt, K. Molecular and Electronic Structure of Octahedral *o*-Aminophenolato and *o*-Iminobenzosemiquinonato Complexes of V(V), Cr(III), Fe(III), and Co(III). Experimental Determination of Oxidation Levels of Ligands and Metal Ions. *Inorg. Chem.* **2001**, *40*, 4157−4166. (b) Sik Min, K.; Weyhermüller, T.; Wieghardt, K. *O,N*-Coordinated *o*-iminobenzoquinone and *o*-iminobenzosemiquinonato(1−) ligands in complexes of Ni(II), Co(III) and Fe(III). *Dalton Trans.* **2003**, 1126−1132. (c) Mukherjee, S.; Weyhermüller, T.; Wieghardt, K.; Chaudhuri, P. The molecular and electronic structure of $[Fe^{III}_2(^{t\text{-}bu}L^{ISQ})_4(\mu\text{-}O)]$—a dinuclear ferric complex containing four, *O,N*-coordinated *o*-iminobenzosemiquinonate(1−)π radical anions. *Dalton Trans.* **2003**, 3483−3485. (d) Halder, P.; Paria, S.; Paine, T. K. Dioxygen Reactivity of Biomimetic Iron−Catecholate and Iron−*o*-Aminophenolate Complexes of a Tris(2-pyridylthio)methanido Ligand: Aromatic C−C Bond Cleavage of Catecholate versus *o*-Iminobenzosemiquinonate Radical Formation. *Chem. - Eur. J.* **2012**, *18*, 11778−11787.

(10) (a) Bittner, M. M.; Lindeman, S. V.; Fiedler, A. T. A Synthetic Model of the Putative Fe(II)-Iminobenzosemiquinonate Intermediate in the Catalytic Cycle of *o*-Aminophenol Dioxygenases. *J. Am. Chem. Soc.* **2012**, *134*, 5460−5463. (b) Bittner, M. M.; Lindeman, S. V.; Popescu, C. V.; Fiedler, A. T. Dioxygen Reactivity of Biomimetic Fe(II) Complexes with Noninnocent Catecholate, *o*-Aminophenolate, and *o*-Phenylenediamine Ligands. *Inorg. Chem.* **2014**, *53*, 4047−4061.

(11) (a) Yoo, W.-J.; Li, C.-J. In *C-H Activation;* Yu, J.-Q., Shi, Z., Eds.; Springer: Berlin, Germany, 2010; Vol. *292*. (b) Li, C.-J. Cross-Dehydrogenative Coupling (CDC): Exploring C−C Bond Formations beyond Functional Group Transformations. *Acc. Chem. Res.* **2009**, *42*, 335−344. (c) Liu, D.; Liu, C.; Li, H.; Lei, A. Direct Functionalization of Tetrahydrofuran and 1,4-Dioxane: Nickel-Catalyzed Oxidative $C(sp^3)$−H Arylation. *Angew. Chem., Int. Ed.* **2013**, *52*, 4453−4456.

(12) Sheldrick, G. M. *SHELXL-97,* Program for crystal structure refinement; University of Göttingen: Germany, 1997.

(13) Frisch, M. J.; Trucks, G. W.; Schlegel, H. B.; Scuseria, G. E.; Robb, M. A.; Cheeseman, J. R.; Scalmani, G.; Barone, V.; Mennucci, B.; Petersson, G. A.; Nakatsuji, H.; Caricato, M.; Li, X.; Hratchian, H. P.; Izmaylov, A. F.; Bloino, J.; Zheng, G.; Sonnenberg, J. L.; Hada, M.; Ehara, M.; Toyota, K.; Fukuda, R.; Hasegawa, J.; Ishida, M.; Nakajima, T.; Honda, Y.; Kitao, O.; Nakai, H.; Vreven, T.; Montgomery, J. A., Jr.; Peralta, J. E.; Ogliaro, F.; Bearpark, M.; Heyd, J. J.; Brothers, E.; Kudin, K. N.; Staroverov, V. N.; Kobayashi, R.; Normand, J.; Raghavachari, K.; Rendell, A.; Burant, J. C.; Iyengar, S. S.; Tomasi, J.; Cossi, M.; Rega, N.; Millam, J. M.; Klene, M.; Knox, J. E.; Cross, J. B.; Bakken, V.; Adamo, C.; Jaramillo, J.; Gomperts, R.; Stratmann, R. E.; Yazyev, O.; Austin, A. J.; Cammi, R.; Pomelli, C.; Ochterski, J. W.; Martin, R. L.; Morokuma, K.; Zakrzewski, V. G.; Voth, G. A.; Salvador, P.; Dannenberg, J. J.; Dapprich, S.; Daniels, A. D.; Farkas, O.; Foresman, J. B.; Ortiz, J. V.; Cioslowski, J.; Fox, D. J. *Gaussian 09,* revision C.01; Gaussian, Inc.: Wallingford, CT, 2010.

(14) (a) Raycroft, M. A. R.; Maxwell, C. I.; Oldham, R. A. A.; Andrea, A. S.; Neverov, A. A.; Brown, R. S. Trifunctional Metal Ion-Catalyzed Solvolysis: Cu(II)-Promoted Methanolysis of *N,N*-bis(2-picolyl) Benzamides Involves Unusual Lewis Acid Activation of Substrate, Delivery of Coordinated Nucleophile, Powerful Assistance of the Leaving Group Departure. *Inorg. Chem.* **2012**, *51*, 10325−10333. (b) Burdette, S. C.; Frederickson, C. J.; Bu, W.; Lippard, S. J. ZP4, an Improved Neuronal Zn^{2+} Sensor of the Zinpyr Family. *J. Am. Chem. Soc.* **2003**, *125*, 1778−1787. (c) Miyazato, Y.; Wada, T.; Muckerman, J. T.; Fujita, E.; Tanaka, K. Generation of a Ru^{II}−Semiquinone−Anilino-Radical Complex through the Deprotonation of a Ru^{III}−Semiquinone−Anilido Complex. *Angew. Chem., Int. Ed.* **2007**, *46*, 5728−5730.

DOI: 10.1021/acs.inorgchem.6b01474
Inorg. Chem. 2017, 56, 729−736

ChemComm

COMMUNICATION

View Article Online
View Journal | View Issue

Cite this: *Chem. Commun.*, 2017, 53, 8022

Received 5th May 2017,
Accepted 20th June 2017

DOI: 10.1039/c7cc03486e

rsc.li/chemcomm

Monoradical-containing four-coordinate Co(III) complexes: homolytic S–S and Se–Se bond cleavage and catalytic isocyanate to urea conversion under sunlight†

Ganesh Chandra Paul,‡ Samir Ghorai‡ and Chandan Mukherjee *

Four-coordinate, monoradical-containing Co(III) complexes participated in the non-innocent ligand driven homolytic cleavage of S–S and Se–Se bonds and catalyzed the conversion of RNCO (R = phenyl and naphthyl) to the corresponding urea derivatives (TON 480) in dry CH_2Cl_2 under sunlight stimulus.

Over the last two decades, metal-coordinated redox active organic ligands, known as non-innocent ligands, have been under continuous investigation as electron acceptors and/or electron donors for catalytic oxidation and reduction reactions.[1,2] For instance, Chaudhuri, Wieghardt and coworkers have studied Cu(II)–bis(iminosemiquinone) complexes extensively as functional models of galactose oxidase for the two-electron oxidation of primary alcohols to their corresponding aldehydes.[1f] In addition, a four-coordinate Co(III)–bis(amidophenolate) complex has been successfully employed as a catalyst for C–C bond formation reactions by Soper and coworkers.[1a] Recently, Sarkar and coworkers described an electrocatalytic C–C bond formation reaction employing an electrochemically *in situ*-generated four-coordinate Co(II)–bis(1,2-diamide) complex as the catalyst and benzylbromide as the substrate.[1e] In 2015, van der Vlugt and coworkers utilized the redox active nature of a coordinated 2-amidophenolate derivative in a four-coordinate Pd(II) complex for the one-electron homolytic S–S bond cleavage of diphenyl disulfide.[1i] Recently, we have demonstrated that H_2 gas can be generated by employing the Cu(II)–bis(iminoquinone) complex and $NaBH_4$ in dry acetonitrile.[1g]

To continue our study on the development of ligand radical-containing transition metal complexes for diatomic (homo and/or hetero) bond scission/formation reactions, we investigated a few Co(III) complexes based on the non-innocent ligands, $H_2L^{AP(R)}$ (R = –Me and –Ph), shown in Scheme 1. The ligand scaffolds were primarily based on a bidentate 2-anilino-3,5-di-*tert*-butylphenol (H_2L^{AP}) backbone with methyl and phenyl substituents at the *ortho*-position of the aniline group. We envisaged that the presence of an *ortho*-substituent would exert steric crowding, and consequently it is possible that four-coordinate cobalt complex formation would be favorable over the six-coordinate complex. It is noteworthy that cobalt complexes with unsaturated coordination environments are essential for substrate activation and catalysis.

Herein, we report two four coordinate, monoradical-containing Co(III) complexes (**1** and **2**, $[Co^{III}(L^{AP(R)})(L^{ISQ(R)})]^0$), which were synthesized by reacting the ligands with $Co(ClO_4)_2{\cdot}6H_2O$ under air. The formed complexes reduced diphenyl disulfide and diphenyl diselenide by one electron and provided the corresponding five-coordinate, diradical-containing complexes, where the axial position was occupied by an –XPh group (X = S(**1a**/**2a**) and Se(**2b**); the parentheses indicate the complex, $[Co^{III}(L^{ISQ(R)})_2XPh]^0$). Hence, the lesser-explored one-electron reduction of S–S and Se–Se bonds was investigated. Interestingly, the four- and five-coordinate

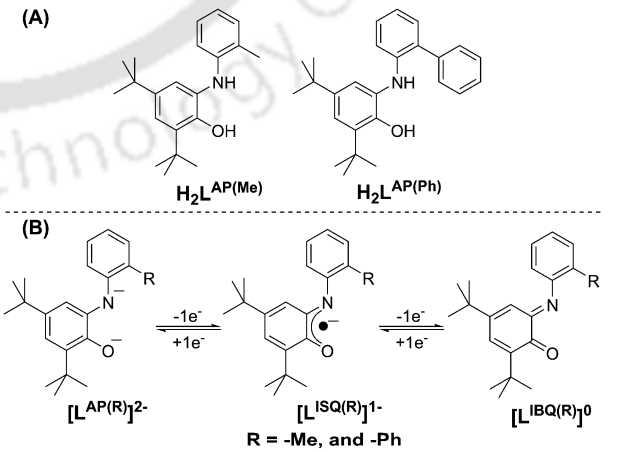

Scheme 1 (A) Structures of the ligands employed in this study. (B) Three possible oxidation states of the ligands. The abbreviations AP, ISQ and IBQ represent the amidophenol, iminosemiquinone and iminobenzoquinone forms of the ligands, respectively.

Department of Chemistry, Indian Institute of Technology Guwahati, Guwahati, 781039, Assam, India

† Electronic supplementary information (ESI) available: Experimental details; IR, NMR, mass and UV-vis-NIR spectra of ligands and complexes; bond distance and bond angle tables for the complexes. CCDC 1454093, 1547976-1547979 and 1555498. For ESI and crystallographic data in CIF or other electronic format see DOI: 10.1039/c7cc03486e

‡ GCP and SG contributed equally.

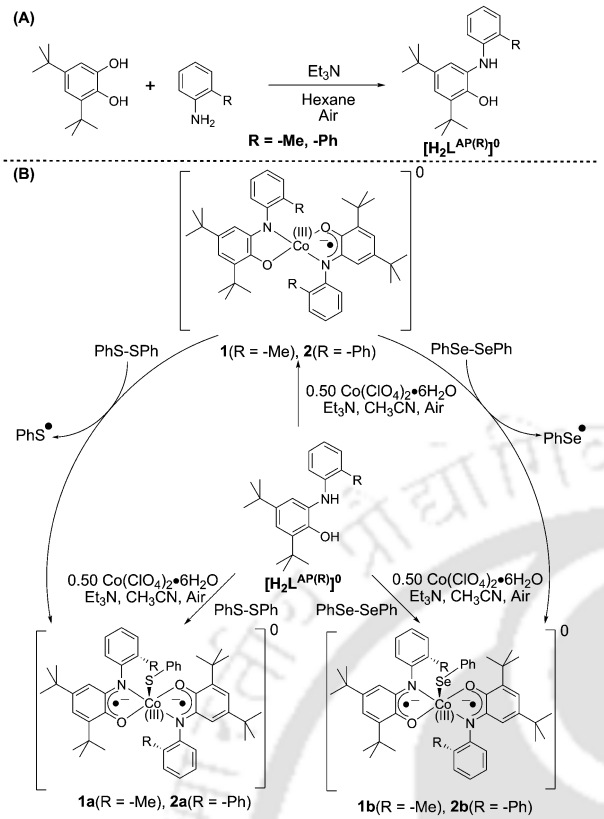

Scheme 2 Schematic representation of the syntheses.

complexes under sunlight in a closed vessel in dry CH_2Cl_2 catalyzed the conversion of phenyl isocyanate and naphthyl isocyanate to the corresponding urea derivatives. A maximum turnover number (TON) of 480 in 6 hours was achieved.

The condensation between a 1 : 1 ratio of 2-*R*-aniline (R = –Me and –Ph) and 3,5-di-*tert*-butylcatechol in the presence of Et_3N and air generated $H_2L^{AP(R)}$ ligands in good yields [Scheme 2(A)]. Under an air atmosphere, the $H_2L^{AP(Me)}$ and $H_2L^{AP(Ph)}$ ligands were reacted individually with 0.5 equivalents of $Co(ClO_4)_2{\cdot}6H_2O$ in acetonitrile in the presence of Et_3N for an hour to synthesize the corresponding four-coordinate, monoradical-containing Co(III) complexes (**1**: 83% yield and **2**: 53% yield). Notably, the use of $CoCl_2{\cdot}6H_2O$ during complex synthesis should be restricted, as the salt assists the formation of five-coordinate diradical-containing Co(III) complexes by the one-electron oxidation of the initially formed four-coordinate, monoradical-containing Co(III) complexes through a putative inner sphere electron transfer mechanism (Scheme S2, ESI†).

The addition of either diphenyl disulfide (Ph_2S_2) or diphenyl diselenide (Ph_2Se_2) during the synthesis of **1** and **2** provided the corresponding five-coordinate diradical-containing complexes **1a**/**2a** and **2b**. The complexes could also be synthesized by reacting Ph_2S_2 or Ph_2Se_2 with the isolated complexes **1** and **2** (Scheme 2B). X-Band EPR measurements during the conversions showed an instantaneous disappearance of the X-band EPR signal of complexes **1** and **2** (*vide infra*), with concomitant generation of an isotropic signal at $g \sim 2.00$ (Fig. S34, ESI†). These features implied the formation of $PhX^{\bullet}$ (X = S and Se) species along with the diamagnetic complexes **1a**/**2a** and **2b**.

A single crystal of complex **1** suitable for X-ray diffraction analysis was obtained by slow evaporation of a 10 : 1 Et_2O : CH_3CN solvent mixture. Notably, complex **2** could not be obtained as a single crystal due to solubility limitations. Furthermore, the complex abstracts chlorine atoms from chlorinated solvents (*e.g.* CH_2Cl_2 and $CHCl_3$) and provided the corresponding five-coordinated, diradical-containing Co(III) complex, **2c** (Fig. S22, ESI†). A similar reaction has also been observed for complex **1**, which provided complex **1b** (Fig. S21, ESI†). Nevertheless, X-band EPR and UV-vis-NIR spectral pattern analysis (*vide infra*) confirmed that **1** and **2** have a similar type of geometry and coordination environment.

Complex **1** had square planar geometry ($\tau_4 = 0.0$).[3] The coordination sphere was composed of two nitrogen atoms and two oxygen atoms from the two ligands (Fig. 1A). The Co–O (1.830(3) Å) and Co–N (1.832(4) Å) bond lengths (Table S2, ESI†) were in accordance with those of the previously reported Co(III) square planar complexes.[4] Hence, the formal oxidation state of the Co atom in the complex was assigned as +III. Notably, complex **1** was neutral in charge. Therefore, in order to maintain the neutrality, the two coordinated non-innocent ligands must be present in the complex in two different oxidation states, *i.e.* one-electron oxidized iminosemiquinone and fully reduced amidophenolate.[4,5] However, the C_{Ph}–O_{Ph} (1.323(5) Å) and C_{Ph}–N_{Ph} (1.371(5) Å) (where C_{Ph}, N_{Ph} and O_{Ph} stand for the C, N, and O atoms attached or belonging to the phenyl ring, respectively) bond distances (Table S2, ESI†) in the two coordinated-ligands were the same, and corresponded to neither the iminosemiquinone (C–N = 1.35 Å, C–O = 1.30 Å) form nor the amidophenolate (C–N = 1.38 Å, C–O = 1.35 Å) form (Scheme 1). These features, as previously reported by Wieghardt, Chaudhuri and coworkers,[4] implied the delocalization of the negative charge and the radical (hole) over the two coordinated-ligand units.

All the five-coordinate neutral complexes were almost square pyramidal ($\tau_5 = 0.05$ [**1a**], 0.08 [**2a**] and 0.0 [**2b**]).[3] In the complexes, the central cobalt atom (Co1) was situated above the N2O2 basal plane, towards the apical –XPh group (Fig. 1). The Co–O (1.858 to 1.881 Å)

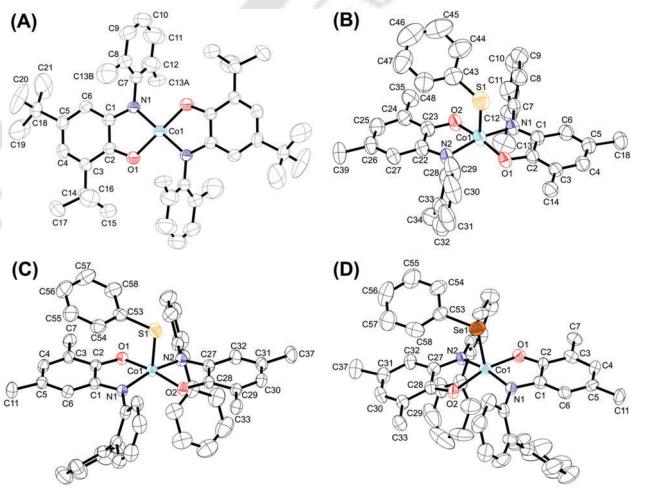

Fig. 1 ORTEP plots of (A) **1**, (B) **1a**, (C) **2a** and (D) **2b**. Thermal ellipsoids were drawn at 50% probability level. The H atoms and methyl groups of the *tert*-butyl groups (of **1a**, **2a** and **2b**) were omitted for clarity. In **1**, the C13 atom is disordered in a 65 : 35 ratio between the C13A and C13B atoms.

TH-2079_136122008

and Co–N (1.845 to 1.871 Å) bond distances (Tables S3 and S5 and S6, ESI†) in the complexes corresponded to the previously reported square pyramidal cobalt complexes having a +III oxidation state.[4] Thus, herein, the oxidation state of the central cobalt atom has been assigned as +III. Not all of the C–C bond lengths of the *tert*-butyl groups containing C_6 phenyl rings were within 1.39 ± 0.01 Å; rather, alternating short–long–short C–C bond lengths were observed, *i.e.* a quinoid-type distortion (Tables S3 and S5 and S6, ESI†). Furthermore, the average C_{Ph}–O_{Ph} (1.311(4) [**1a**], 1.307(3) [**2a**] and 1.298(8) [**2b**] Å) and C_{Ph}–N_{Ph} (1.349(4) [**1a**], 1.351(4) [**2a**] and 1.362(9) [**2b**] Å) bond distances were in between their single bond and double bond values, which emphasized that the one-electron oxidized iminosemiquinone form[4,5] of the coordinated ligands was present in the complexes. Hence, X-ray single crystal analysis suggested that the four-coordinate complex **1** was monoradical-containing, while the five-coordinate complexes (**1a**, **2a** and **2b**) were diradical-containing. Notably, better quality crystal data would have been more convincing, however, diffraction measurements even at 100 K could not improve the structural quality due to the nature of the crystals.

The five-coordinate diradical-containing square pyramidal Co(III) (low-spin, S_{Co} = 0) complexes (**1a**, **2a** and **2b**) were diamagnetic owing to a strong antiferromagnetic coupling between the two ligand-centered π-radicals (S_R = 1/2). The diamagnetic character of the complexes was further supported by ^{1}H NMR analysis (Fig. S18–S20, ESI†). In the monoradical-containing four-coordinate square planar Co(III) complexes (**1** and **2**), the metal center possesses two unpaired electrons residing in the d_{z^2} and d_{xy} magnetic orbitals (S_{Co} = 1.0). An antiferromagnetic coupling between the Co(III) d_{z^2} magnetic orbital and the ligand center p_z orbital led to a S_{total} = 1/2 ground state and paramagnetism in the complexes, where the unpaired electron resided in the d_{xy} magnetic orbital. Hence, cobalt(III)-centered X-band EPR spectra for **1** and **2** were observed. Experimental as well as simulated EPR spectra for **1** and **2** complexes are shown in Fig. S23, ESI.† For both complexes, the signals were anisotropic in nature. Simulation of the experimental spectra provided the following parameters: g_1 = 1.992 [**1**] and 1.980 [**2**]; g_2 = 2.220 [**1**] and 2.020 [**2**]; g_3 = 2.750 [**1**] and 3.215 [**2**]; $^{Co}(A_1, A_2, A_3)$ = (5, 42, 93) × 10^{-4} cm^{-1} for complex **1** and $^{Co}(A_1, A_2, A_3)$ = (2, 1, 110) × 10^{-4} cm^{-1} for complex **2**. The average *g* values for the complexes **1** and **2** were 2.342 and 2.405, respectively, which supported the presence of a metal-centered unpaired electron.

The UV-vis-NIR spectra of **1** and **2** show an absorption manifold centered at around 1600 nm (Fig. S24 and S27, ESI†). It has previously been established that the band appeared due to an intervalence ligand (amidophenolate) to ligand (iminosemiquinone) charge transfer.[4] This experimental fact further confirmed that both complexes have the same electronic structure. In the UV-vis-NIR spectra of the five-coordinate, diradical-containing complexes (**1a**, **2a** and **2b**), the band at around 1600 nm was absent and a ligand (iminosemiquinone) to ligand (iminosemiquinone) charge transfer band was present at around 830 nm (Fig. S25, S28 and S29, ESI†). Thus, the conversion of four-coordinate $[Co^{III}(L^{AP(R)})(L^{ISQ(R)})]^0$ to five-coordinate $[Co^{III}(L^{ISQ(R)})_2XPh]^0$, or *vice versa*, could be monitored by analyzing the band at 1600 nm.

When CH_2Cl_2 solutions of **1a** and **2a** were subjected to sunlight irradiation, the 1600 nm band started to appear, with concomitant shifting of the ∼570 nm band to 660 nm (Fig. S31 and S32, ESI†). This phenomenon indicated homolytic Co–SPh bond cleavage and the consequent generation of **1** and **2**. A similar phenomenon has also been observed for **2b** (Fig. S33A, ESI†), where **2** was generated by the cleavage of the Co–SePh bond. The appearance of a Co-centered EPR signal (Fig. S31–S33, ESI†) in the processes further supported the formation of **1** and **2**. As the five-coordinate, diradical-containing complexes could be converted to the corresponding four-coordinate, monoradical-containing complexes under sunlight stimulus, and the four-coordinate complexes have already been found to be one-electron transferring agents, we investigated the catalytic ability of the four-coordinate as well as the five-coordinate complexes (**1**, **2** and **2a**) for the conversion of RNCO (R = phenyl and naphthyl) to the corresponding C–N coupled urea derivatives. Notably, 1,3-diaryl urea derivatives have agricultural and medicinal uses.[6] Table 1 contains the reaction details. In the catalysed reactions, a maximum TON of 480 was achieved by employing 0.1 mol% of complex **2**. The bulkiness of the substrates and *ortho*-substituents did not have a pronounced effect on the product yield. This emphasized that the substrates approached the Co(III) centre along the axial position. The requirement for both the catalysts as well as sunlight was further established by performing blank reactions (Table 1). No product formation in the absence of a catalyst confirmed that the conversion of the RNCO compounds to their corresponding amines and the photo-driven [2+2] cycloaddition reaction (Table 1, entries 2 and 4)

Table 1 Optimization of urea derivative formation[a]

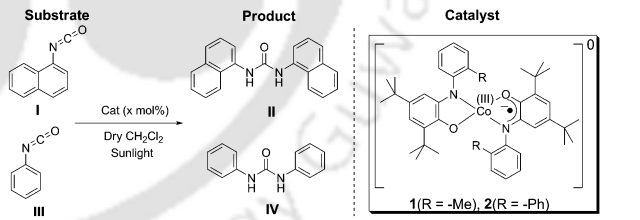

#	Substrate	Product	Cat (mol%) 1	2	2a	Isolated yield (%) 1	2	2a
1	**III**	**IV**	2.5	2.5	2.5	72	78	76
2	**III**	NR	0	0	0	0	0	0
3	**I**	**II**	2.5	2.5	2.5	80	86	82
4	**I**	NR	0	0	0	0	0	0
5	**III** + Ph_2S_2[b]	**IV**	2.5	2.5	—	68	75	—
6	**III**	**IV**	—	1.0	—	—	72	—
7	**III**	**IV**	—	0.1	—	—	48	—
Absence of sunlight								
8	**III**	**IV**	2.5	2.5	2.5	10	12	15
9	**III** + Ph_2S_2[b]	**IV**	2.5	2.5	—	9	12	—
10	**I**	**II**	2.5	2.5	2.5	10	11	10

[a] NR stands for no reaction. The temperature of the reaction bath was 36 °C. All reactions were carried out for 6 hours in a closed tube. [b] 1 : 1 mixture.

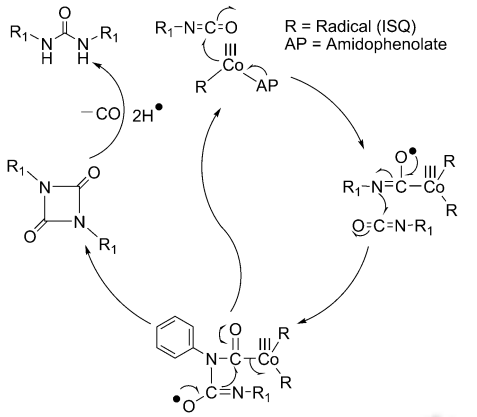

Fig. 2 Proposed mechanism for the formation of a urea derivative from an isocyanate compound.

did not occur. The low TON (4–6) in the absence of sunlight (Table 1, entries 8 and 10) supported the possibility that during catalysis, a substrate-bound five-coordinate intermediate was formed (Fig. 2), and a photo-stimulus was then essential for the regeneration of the four-coordinate catalysts by cleavage of the Co–substrate bond in the intermediate. The formation of 1,1,2,2,-tetrachloroethane was confirmed by GC and GC-MS (Fig. S35, ESI†) analysis during the conversion of **III** to **IV** in the presence of catalyst **2**. The compound was formed by the C–C coupling of two CH_2Cl_2 molecules, and thus implied the abstraction of a hydrogen atom from the solvent molecule during the formation of the urea derivatives. Although further investigation is essential for a better understanding of the catalysis, using the results stated above, a mechanistic proposal for the C–N coupling between two isocyanate molecules to form a urea derivative is given in Fig. 2.

In summary, four-coordinate, monoradical-containing Co(III) complexes have been successfully synthesized and employed for S–S/Se–Se bond activation and scission by electron transfer to the bonds. The only known example in the literature of a ligand-induced S–S bond cleavage reaction is based on an air sensitive Pd(II)–amidophenolate complex. Thus, a lesser-explored phenomenon has been studied by employing air stable Co(III) complexes. The resulting diradical-containing square pyramidal Co(III) complexes, with axial –XPh (X = S and Se) ligands, experienced homolytic Co–XPh bond cleavage under the influence of sunlight and produced the corresponding four-coordinate, monoradical Co(III) complexes (Fig. S31–S33, ESI†). Both four- and five-coordinate Co(III) complexes catalysed the conversion of aromatic isocyanates to the corresponding urea derivatives. Thus, we have presented, to the best of our knowledge, the first examples of the synthesis of urea from the sole use of isocyanate compounds. In our laboratory, sunlight-driven $PhX^{\bullet}$ radical addition reactions to various organic units are currently ongoing.

This project is funded by SERB [EMR/2015/002491], India. GCP and SG thank IITG for their doctoral fellowship and for the instrumental facilities.

Notes and references

1 (*a*) A. L. Smith, K. I. Hardcastle and J. D. Soper, *J. Am. Chem. Soc.*, 2010, **132**, 14358–14360; (*b*) V. Lyaskovskyy and B. de Bruin, *ACS Catal.*, 2012, **2**, 270–279; (*c*) W. I. Dzik, J. I. van der Vlugt, J. N. H. Reek and B. de Bruin, *Angew. Chem., Int. Ed.*, 2011, **50**, 3356–3358; (*d*) O. R. Luca and R. H. Crabtree, *Chem. Soc. Rev.*, 2013, **42**, 1440–1459; (*e*) M. van der Meer, Y. Rechkemmer, I. Peremykin, S. Hohloch, J. van Slageren and B. Sarkar, *Chem. Commun.*, 2014, **50**, 11104–11106; (*f*) P. Chaudhuri, K. Wieghardt, T. Weyhermüller, T. K. Paine, S. Mukherjee and C. Mukherjee, *Biol. Chem.*, 2005, **386**, 1023–1033; (*g*) M. K. Mondal and C. Mukherjee, *Dalton Trans.*, 2016, **45**, 13532–13540; (*h*) D. L. J. Broere, L. L. Metz, B. de Bruin, J. N. H. Reek, M. A. Siegler and J. I. van der Vlugt, *Angew. Chem., Int. Ed.*, 2015, **54**, 1516–1520; (*i*) D. L. J. Broere, R. Plessius and J. I. van der Vlugt, *Chem. Soc. Rev.*, 2015, **44**, 6886–6915.

2 F. Diederich and P. J. Stang, *Metal – Catalyzed Cross – Coupling Reactions*, Wiley-VCH, Weinheim, 1998.

3 L. Yang, D. R. Powell and R. P. Houser, *Dalton Trans.*, 2007, 955–964.

4 (*a*) E. Bill, E. Bothe, P. Chaudhuri, K. Chlopek, D. Herebian, S. Kokatam, K. Ray, T. Weyhermüller, F. Neese and K. Wieghardt, *Chem. – Eur. J.*, 2005, **11**, 204–224; (*b*) A. I. Poddel'sky, V. K. Cherkasov and G. A. Abakumov, *Coord. Chem. Rev.*, 2009, **253**, 291–324; (*c*) S. R. Garaeva, A. A. Medzhidov, O. Beukgunger, A. Aydin, B. Yalcin and M. G. Abbasov, *Russ. J. Coord. Chem.*, 2012, **38**, 140–144; (*d*) D. Herebian, P. Ghosh, H. Chun, E. Bothe, T. Weyhermüller and K. Wieghardt, *Eur. J. Inorg. Chem.*, 2002, 1957–1967; (*e*) A. I. Poddel'sky, V. K. Cherkasov, G. K. Fukin, M. P. Bubnov, L. G. Abakumova and G. A. Abakumov, *Inorg. Chim. Acta*, 2004, **357**, 3632–3640.

5 (*a*) P. Chaudhuri, C. N. Verani, E. Bill, E. Bothe, T. Weyhermüller and K. Wieghardt, *J. Am. Chem. Soc.*, 2001, **123**, 2213–2223; (*b*) S. Ghorai and C. Mukherjee, *Chem. Commun.*, 2012, **48**, 10180–10182; (*c*) S. Ghorai and C. Mukherjee, *Dalton Trans.*, 2014, **43**, 394–397; (*d*) R. Rakshit, S. Ghorai, S. Biswas and C. Mukherjee, *Inorg. Chem.*, 2014, **53**, 3333–3337; (*e*) M. K. Mondal, A. K. Biswas, B. Ganguly and C. Mukherjee, *Dalton Trans.*, 2015, **44**, 9375–9381; (*f*) S. Ye, B. Sarkar, F. Lissner, T. Schleid, J. van Slageren, J. Fiedler and W. Kaim, *Angew. Chem., Int. Ed.*, 2005, **44**, 2103–2106; (*g*) S. Ghorai and C. Mukherjee, *Chem. – Asian J.*, 2014, **9**, 3518–3524; (*h*) S. Ghorai and C. Mukherjee, *RSC Adv.*, 2014, **4**, 24698–24703; (*i*) A. V. Piskunov, K. I. Pashanova, A. S. Bogomyakov, I. V. Smolyaninov, N. T. Berberova and G. K. Fukin, *Polyhedron*, 2016, **119**, 286–292; (*j*) P. Chaudhuri and K. Wieghardt, *Prog. Inorg. Chem.*, 2001, **50**, 151–216; (*k*) L. Que, Jr. and W. B. Tolman, *Nature*, 2008, **455**, 333–340; (*l*) G. A. Abakumov, V. K. Cherkasov, V. I. Nevodchikov, V. A. Kuropatov, G. T. Yee and C. G. Pierpont, *Inorg. Chem.*, 2001, **40**, 2434–2436; (*m*) C. Benelly, A. Dei, D. Gatteschi and L. Pardi, *Inorg. Chem.*, 1990, **29**, 3409–3415; (*n*) C. G. Pierpont, *Coord. Chem. Rev.*, 2001, **216–217**, 99–125; (*o*) A. L. Smith, L. A. Clapp, K. I. Hardcastle and J. D. Soper, *Polyhedron*, 2010, **29**, 164–169; (*p*) C. Mukherjee, U. Pieper, E. Bothe, V. Bachler, E. Bill, T. Weyhermüller and P. Chaudhuri, *Inorg. Chem.*, 2008, **47**, 8943–8956; (*q*) C. Mukherjee, T. Weyhermüller, E. Bothe and P. Chaudhuri, *Inorg. Chem.*, 2008, **47**, 11620–11632; (*r*) S. N. Brown, *Inorg. Chem.*, 2012, **51**, 1251–1260.

6 (*a*) M. C. Mok, S. G. Kim, D. J. Armstrong and D. W. S. Mok, *Proc. Natl. Acad. Sci. U. S. A.*, 1979, **76**, 3880–3884; (*b*) P. Sikka, J. K. Sahu, A. K. Mishra and S. R. Hashim, *J. Med. Chem.*, 2015, **5**, 479–483.

Inorganic Chemistry
Cite This: Inorg. Chem. XXXX, XXX, XXX–XXX
Article
pubs.acs.org/IC

Geometry-Driven Iminosemiquinone Radical to Cu(II) Electron Transfer and Stabilization of an Elusive Five-Coordinate Cu(I) Complex: Synthesis, Characterization, and Reactivity with KO_2

Ganesh Chandra Paul,[†] Kanu Das,[†] Suvendu Maity,[‡] Samiyara Begum,[†] Hemant Kumar Srivastava,[†] and Chandan Mukherjee*[,†]

[†]Department of Chemistry, Indian Institute of Technology Guwahati, Guwahati 781039, Assam, India
[‡]Department of Chemistry, R. K. Mission Residential College, Narendrapur, Kolkata 700103, India

Supporting Information

ABSTRACT: The noninnocent ligand $H_2L^{AP(Ph)}$ contained a bulky phenyl substituent at the *ortho* position to the aniline moiety. The ligand reacted with 0.5 equiv of $CuCl_2·2H_2O$ in the presence of Et_3N under air and provided the corresponding Cu(II)-bis(imonosemiquinone) complex (**1**). The complex upon oxidation by a stoichiometric amount of ferrocenium hexafluorophosphate ($FcPF_6$) yielded the four-coordinate [Cu(II)-(imonosemiquinone)-(iminoquinone)]PF_6 complex (**3**), while the oxidation by an equivalent amount of $CuCl_2·2H_2O$ produced the five-coordinate Cu(I)-bis(iminoquinone)Cl complex (**2**). Thus, a ligand-based oxidation followed by ligand-to-metal electron-transfer was realized for the latter oxidation process. Removal of the Cl^- ion from complex **2** rendered the four-coordinate complex **4**. The oxidation state of both Cu(I) and iminoquinone moieties remained unaltered upon the change in the coordination number. All the complexes were characterized by X-ray crystallography. Complexes **2**, **3**, and **4** were diamagnetic with an $S_t = 0$ ground state as evident by electron paramagnetic resonance (EPR) and ^1H NMR measurements. The UV−vis−NIR spectra of all the complexes were dominated by charge-transfer transitions. Two oxidations and two reductions waves were noticed in the cyclic voltammogram (CV) of complex **1**. Complex **2** and complex **3** underwent one oxidation and three reductions. Unlike complex **3**, which experienced ligand-based oxidation, in complex **2** the oxidation was metal-centered [oxidation of Cu(I)-to-Cu(II)]. UV−vis−NIR spectral changes during the fixed-potential coulometric one-electron oxidation and thereafter EPR analysis consolidated the metal-based oxidation in complex **2**. Complex **2** was air stable; however, it oxidized KO_2 to oxygen molecule, and complex **1** was formed in due course as evident by UV−vis−NIR spectral changes and EPR measurements. Time dependent density functional theory calculations have been incorporated to assign the transitions that appeared in the UV−vis−NIR spectra of the complexes.

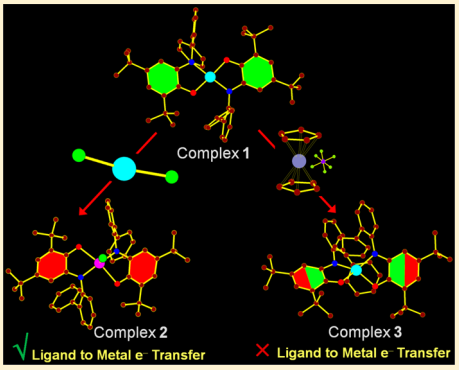

INTRODUCTION

Investigation of radical-containing copper complexes has emerged as a research interest over recent years because of the involvement of copper-radical species in various biological oxidation and oxygenation processes.[1−6] The processes are mainly governed by (I) the geometry of the copper center; and (II) interactions between the redox-active copper (ranging between +I and +II) and the radical centers (phenolate/phenxyl, catecholate/semiquinone/quinine, $O_2^0/O_2^{\bullet-}/O_2^{2-}$).[6] Thus, the understanding of metal−ligand interactions in the geometry-dependent electron transfer processes and the employment of radical-containing copper complexes as biomimetic models and/or catalysts for various organic transformations are the imperative objectives.

In this context, the geometry, electronic structure, and biomimetic reactivity of Cu(II)-bis(radical) and Cu(II)-bis(quinone) complexes have been extensively studied. For example, Cu(II)-bis(radical) complexes have been successfully employed to mimic the function of GOase;[7] Cu(II)-bis(quinone) complexes have been utilized as catalysts for $-CF_3$ transferring reactions, C−N coupling reactions, and H_2 gas production from $NaBH_4$ in dry acetonitrile.[8] While Cu(II)-bis(radical) and Cu(II)-bis(quinone) complexes are familiar in the literature, structurally characterized Cu(II)-monoradical systems with two coordinating noninnocent ligands of two different oxidation states remain elusive[2g,j] and demands special attention for understanding ligand−ligand and metal−ligands interactions, and their possible use as biomimetic catalysts.

Special Issue: Applications of Metal Complexes with Ligand-Centered Radicals

Received: July 11, 2018

DOI: 10.1021/acs.inorgchem.8b01931
Inorg. Chem. XXXX, XXX, XXX–XXX

2-Aminophenol derivatives have been well documented as being stabilized mainly in its one-electron oxidized iminosemiquinone (ISQ^{1-}) radical form in the corresponding Cu(II) complexes.[7] Recently, we have developed a new method where a bis(iminoquinone)-coordinated Cu(II) complex can directly be synthesized in one pot by employing $CuCl_2$ as the oxidant.[8d] The mechanistic investigation (Scheme 1) suggests

Scheme 1. Proposed Mechanism for the $CuCl_2$ Mediated Oxidation of a Cu(II)-bis(radical) Complex to the Corresponding Cu(II)-bis(quinone) Complex[8d]

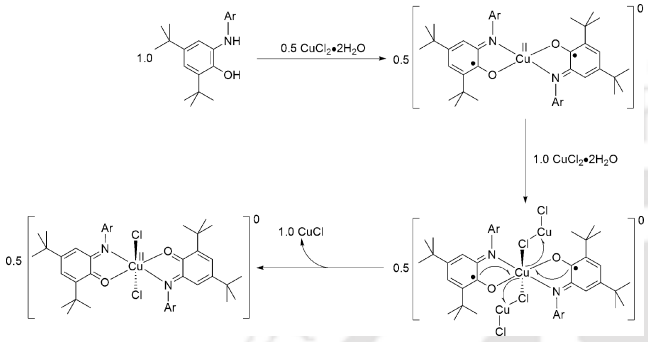

that two chlorine atoms of two individual $CuCl_2$ molecules bind at the axial positions to the Cu(II) center of the initially formed four-coordinate Cu(II)-bis(iminosemiquinone) complex, and subsequent two electrons transfer from two Cu(II)-coordinated iminosemiquinone units to the axially bound two $CuCl_2$ molecules renders a six-coordinate Cu(II)-bis-(iminoquinone) complex with two axial chloride ions. CuCl is the byproduct of the process.

In this study, the aforementioned oxidation method has been examined on the Cu(II)-bis(iminosemiquinone) complex $\{Cu[L^{ISQ(Ph)}]_2\}^0$ (**1**) of ligand $H_2L^{AP(Ph)}$ for the *in situ* synthesis of the corresponding five-coordinate, chloride-bound Cu(II)-(iminosemiquinone)(iminoquinone) complex. In complex **1**, two phenyl rings, which are attached at the *ortho* position to the aniline moiety, are situated *cis* to each other (*vide infra*). The steric hindrance created by the *cis* orientation of the two phenyl rings would block one of the two axial positions and hence would favor the approach of only one $CuCl_2$ molecule along the open axial position to the Cu(II) center of complex **1**. The $CuCl_2$ molecule would then oxidize complex **1** by one electron to provide the expected complex. Interestingly, instead of the expected complex formation, a five-coordinate chloride-bound Cu(I)-bis(iminoquinone) complex $\{Cu^I[L^{IBQ(Ph)}]_2Cl\}^0$ (**2**) was generated via a ligand-[iminosemiquinone]-to-metal[Cu(II)] electron transfer during the $CuCl_2$-promoted oxidation process. To enlighten the geometry dependence on the electron transfer process, outer-sphere, one-electron oxidation of complex **1** has been carried out by employing ferrocenium hexafluorophosphase ($FcPF_6$) as the oxidant. Thus, formed four-coordinate Cu(II)-complex $\{Cu^{II}[L^{ISQ(Ph)}][L^{IBQ(Ph)}]\}PF_6$ (**3**) refrained from such electron transfer phenomenon. Furthermore, a four-coordinate $\{Cu^I[L^{IBQ(Ph)}]_2\}SbF_6$ (**4**) complex was synthesized from complex **2** to extend the investigation on the geometry-dependent metal-to-ligand electron transfer process. All the complexes were subjected to react with KO_2; while complex **2** and complex **3** reacted slowly and provided complex **1** and molecular oxygen as the final products, complex **4** remained indifferent to KO_2. Thus, geometry and oxidation state-dependent reactivity studies are included, herein. Density functional theory (DFT) and time-dependent-DFT (TD-DFT)-based studies have been performed to investigate the geometry and to assign the UV−vis−NIR transitions observed in the complexes.

RESULTS AND DISCUSSION

A schematic diagram for the syntheses of complexes **1**, **2**, **3**, and **4** is presented in Scheme 2A. Ligand $H_2L^{AP(Ph)}$ was

Scheme 2. (A) A Schematic Representation for the Syntheses of Complexes 1, 2, 3, and 4 and (B) Possible Oxidation States of the Ligand

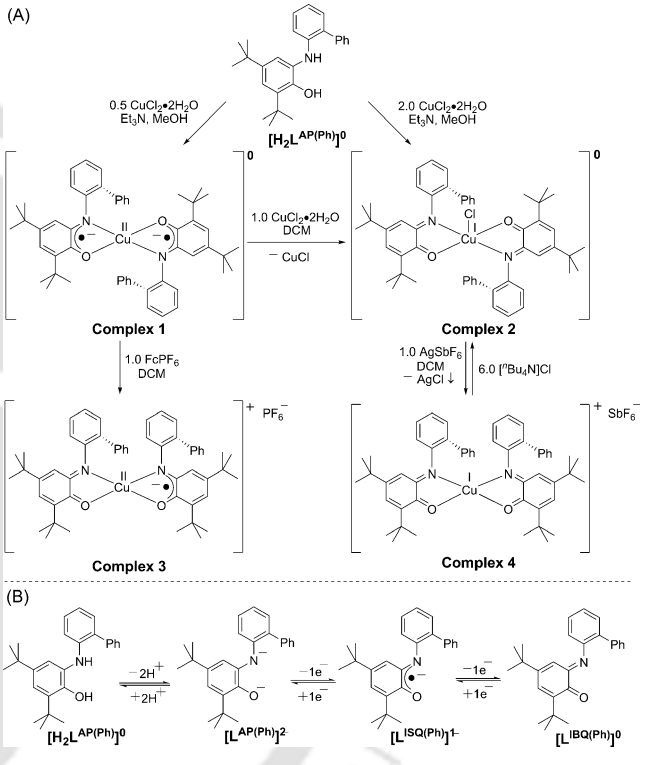

synthesized in 88% yield by the condensation of 1:1 2-phenylaniline and 3,5-di-*tert*-butylcatechol in hexane in the presence of triethyl amine (Et_3N) under air. The three possible oxidation states of the ligands are shown in Scheme 2B. Complex **1** was obtained in 62% yield by reacting the ligand with half equivalent amount of $CuCl_2{\cdot}2H_2O$ in the presence of triethyl amine (Et_3N) in methanol (MeOH) under air. The reaction of the ligand and excess amounts of $CuCl_2{\cdot}2H_2O$ (1:2 molar ratio) in the presence of Et_3N under air in MeOH provided complex **2** ($\{Cu^I[L^{IBQ(Ph)}]_2Cl\}^0$]) in 72% yield. Noteworthy, complex **2** has also been synthesized by reacting complex **1** ($\{Cu^{II}[L^{ISQ(Ph)}]_2\}^0$) with 1 equiv of $CuCl_2{\cdot}2H_2O$. Thus, the formation of complex **1** and thereafter, oxidation of the complex by $CuCl_2$, was established. The removal of the axial chloride ion in complex **2** by employing an equivalent amount of $AgSbF_6$ produced the four-coordinate complex **4** ($\{Cu^I[L^{IBQ(Ph)}]_2\}SbF_6$). The feasibility of the regeneration of complex **2** from complex **4** in the presence of chloride anion was examined. In this regard, 1 equiv of complex **4** was allowed to react with 6 equiv of tetrabutylammonium chloride $[(^nBu)_4NCl$ in dichloromethane (DCM) for 4 h. Recrystallization of the isolated product, obtained by the removal of DCM,

DOI: 10.1021/acs.inorgchem.8b01931
Inorg. Chem. XXXX, XXX, XXX−XXX

from a 3:1 DCM/MeOH solvent mixture provided crystals suitable for X-ray diffraction analysis. The structural analysis of the isolated product confirmed the successful conversion of complex **4** to complex **2**.

The one-electron oxidation of complex **1** by using a stoichiometric amount of oxidant $FcPF_6$ yielded complex **3** ($\{Cu^{II}[L^{ISQ(Ph)}][L^{IBQ(Ph)}]\}PF_6$). The monocationic units in both complex **3** and complex **4** were four-coordinate; however, the electronic structures were different (valence tautomers). A PF_6^{1-} ion was the counteranion in complex **3**, while, in complex **4**, the counteranion was a SbF_6^{1-} ion. To evaluate any possible role of counteranions to the stability of the electronic structures, excess amounts of KPF_6 (6 equiv) were added to a 5:2 DCM/CH_3CN solvent mixture of complex **4**. Single crystal X-ray crystallographic characterization of the isolated product (~80% with respect to the initially used complex **4**) implied no formation to complex **3**. Thus, it could be concluded that the counteranions did not play a significant role in the stabilization of the complexes.

X-ray single crystal diffraction measurements of all the complexes (**1**, **2**, **3**, and **4**) were performed in order to determine the structural features and analyze the oxidation state of the coordinating ligands as well as the central copper ion. The single-crystal structure of complex **1** has previously been reported.[7b] Thus, the structure will not be described further. Nevertheless, the four-coordinate complex **1** consists of a Cu(II) ion, which is coordinated to two units of $L^{ISQ(Ph)}$ form of ligand $H_2L^{AP(Ph)}$. In the complex, the two *ortho* phenyl substituents are situated *cis* to each other (Figure 1) and thus occlude one of the axial positions to external species.

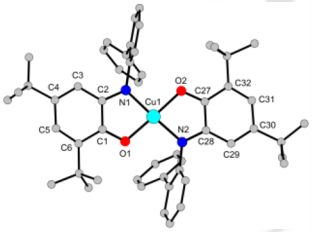

Bond	Distance(Å)	Bond	Distance(Å)
Cu1–N1	1.9267(13)	Cu1–N2	1.9307(13)
Cu1–O1	1.9083(11)	Cu1–O2	1.9046(11)
C1–O1	1.2961(19)	C27–O2	1.2953(19)
C2–N1	1.334(2)	C28–N2	1.336(2)
C1–C2	1.443(2)	C27–C28	1.444(2)

Figure 1. Molecular structure of complex **1** and selected bond distances as reported in ref 7b.

Complex **2** crystallized in the monoclinic space group *C*2/*c*. The molecular structure with the selected atom numbering scheme is depicted in Figure 2. The selected bond distances and bond angles are given in Table 1.

The mononuclear, five-coordinate[9] complex **2** acquired a distorted square pyramidal geometry [τ_5 = 0.25 (τ_5 = 0 for perfect square pyramidal and τ_5 = 1 for perfect trigonal bipyramidal)] where the basal plane was comprised of two NO (N1O1 and N1′O1′) donor sets from two ligand units, and the fifth (axial) position was occupied by a chlorine atom. The central Cu1 atom was situated ~0.77 Å above the basal plane and toward the apical chlorine atom. The apical Cl1 atom experienced two H-bonding interactions (Figure 2). The Cu1–O1 = 2.3934(17) Å bond (Table 1) in complex **2** was much longer compared to the reported Cu–O = 1.906 Å (average) bond in complex **1** (inset Figure 1). This feature consolidated the higher oxidation state of the coordinating ligand and lower oxidation state of the central copper ion. Complex **2** was neutral in charge. Therefore, the possible

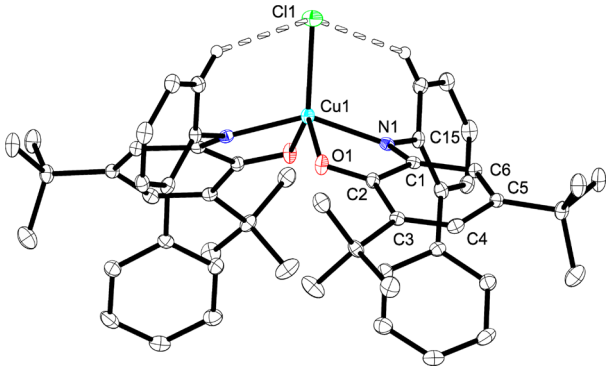

Figure 2. ORTEP diagram of complex **2**; thermal ellipsoids were drawn at the 30% probability level. H-atoms, except the H atoms involved in H-bonding with Cl1, are omitted for the sake of clarity.

Table 1. Selected Bond Distances (Å) and Bond Angles (deg) for Complex 2 (at 100 K), Complex 3 (293 K), and Complex 4 (100 K)

	complex **2**	complex **3**	complex **4**
Cu1–N1	1.927(2)	1.961(3)	2.021(4)
Cu1–N2		1.965(3)	
Cu1–O1	2.3934(17)	1.999(2)	2.352(3)
Cu1–O2		2.002(3)	
Cu1–Cl1	2.2352(10)		
N1–C1	1.302(3)	1.314(4)	1.297(5)
O1–C2	1.227(3)	1.249(4)	1.228(5)
O2–C28		1.246(4)	
N2–C27		1.312(4)	
C1–C2	1.514(3)	1.496(5)	1.514(6)
C2–C3	1.467(3)	1.459(5)	1.478(6)
C3–C4	1.349(3)	1.360(5)	1.344(6)
C4–C5	1.470(3)	1.437(6)	1.457(6)
C5–C6	1.347(3)	1.354(5)	1.360(6)
C6–C1	1.432(3)	1.431(5)	1.441(6)
N1–C15	1.445(3)	1.425(4)	1.427(5)
C27–C28		1.494(5)	
C28–C29		1.454(5)	
C29–C30		1.367(5)	
C30–C31		1.445(5)	
C31–C32		1.352(5)	
C32–C27		1.435(4)	
N1–Cu1–N1^{i}	146.44(12)		149.3(2)
O1–Cu1–O1^{i}	131.14(9)		84.91(15)
N1–Cu1–O1^{i}			131.71(13)
Cl1–Cu1–O1	114.43(5)		
N1–Cu1–Cl1	106.78(6)		
N1–Cu1–N2		116.66(12)	
O1–Cu1–O2		104.71(11)	
N1–Cu1–O1	91.44(7)	81.73(10)	74.04(12)
N2–Cu1–O1		144.23(12)	
N1–Cu1–O2		139.59(12)	
N2–Cu1–O2		81.40(11)	
C2–O1–Cu1	107.65(14)	112.9(2)	110.3(3)
C28–O2–Cu1		113.2(2)	
C1–N1–Cu1	122.32(15)	114.3(2)	120.5(3)
C15–N1–Cu1	117.68(15)	122.0(2)	118.9(3)
C27–N2–Cu1	146.44(12)	114.2(2)	
C41–N2–Cu1	131.14(9)	120.8(2)	

DOI: 10.1021/acs.inorgchem.8b01931
Inorg. Chem. XXXX, XXX, XXX–XXX

composition could be either $\{Cu^{II}[L^{ISQ(Ph)}][L^{IBQ(Ph)}]Cl\}^0$ or $\{Cu^{I}[L^{IBQ(Ph)}]_2Cl\}^0$ (Figure 3).

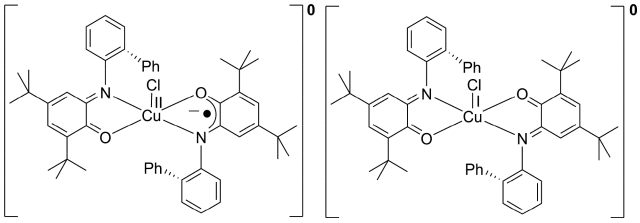

Figure 3. Two possible electronic configurations of complex **2**.

In complex **2** both the coordinating ligands were of same bond distances. Thus, we describe only one ligand unit. The $C_{Ph}-C_{Ph}$ bond distances (Table 1) of the *tert*-butyl groups-containing C_6 ring were not uniform and 1.39 ± 0.01 Å as expected for an aromatic phenyl ring system. Three long bonds followed by an alternate short–long–short bonds sequence were observed. This featured a quinoid-type distortion.[10] The C1–N1 = 1.302(3) Å and C2–O1 = 1.227(3) Å bond distances were unambiguously double bond,[10] and therefore, consolidated the $[L^{IBQ(Ph)}]^0$ form of the coordination ligands in complex **2**. The oxidation state of the central Cu1 atom was thus being assigned as +I, and the neutrality of the complex was maintained by the coordinated-chloride anion [Cu1–Cl1 = 2.2352(10) Å]. Hence, the composition of complex **2** was $\{Cu^{I}[L^{IBQ(Ph)}]_2Cl\}^0$.

Complex **3**·1.5H_2O crystallizes in the triclinic space group $P\bar{1}$. The ORTEP molecular structure (cation unit) with atom labeling scheme is presented in Figure 4. Selected bond distances and bond angles are presented in Table 1.

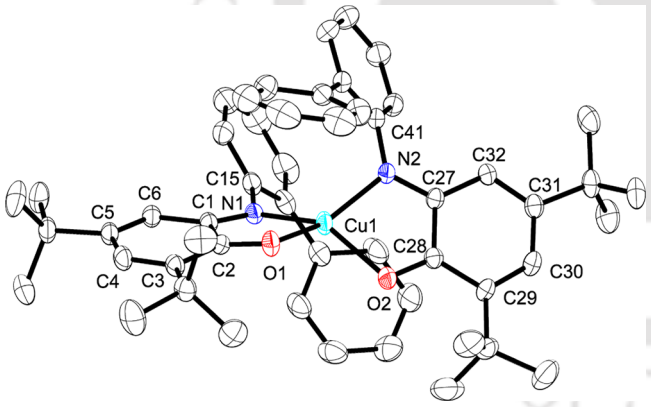

Figure 4. ORTEP diagram of the cation unit of complex **3**·1.5H_2O; thermal ellipsoids were drawn at the 30% probability level. Solvent molecules, anion $[PF_6]^{1-}$, and H-atoms are omitted for the clarity.

In the complex, the central copper atom (Cu1) was four-coordinate. The coordination sites were occupied by two N atoms and two O atoms from the two ligand units. Unlike the parent four-coordinate complex **1**, the two coordinating N and O atoms were adjacent (*cis*) to each other in complex **3**·1.5H_2O. The decrease in ligand field strength upon oxidation of the coordinating ligands (*vide infra*) and steric effect exerted by the two *ortho* phenyl substituents were attributed to the structural dissimilarity. The geometry around the Cu1 atom was in between square planar and tetrahedral [τ_4 = 0.54; τ_4 = 0 for square planar and τ_4 = 1.0 for tetrahedral]. The sum of angles (Table 1 around the Cu1 atom ($\sum Cu_\alpha$) was 668. 3° ($\sum Cu_\alpha$ = 720° and 657° for a perfect square planar and a perfect tetrahedral system, respectively) and further supported the deviation.

Complex **3**·1.5H_2O was obtained by one-electron oxidation of complex **1**. The oxidation could be either metal-centered or ligand-based. The oxidation of Cu(II) to Cu(III) would shorten the Cu–N/O bonds, while an elongation would persist in the case of ligand-based oxidation. In complex **3**·1.5H_2O, the Cu–N/O = 1.963(3)/2.000(3) bond distances were longer compared to the average Cu–N/O = 1.929(1)/1.906(1) bond distances observed in complex **1**.[7b] Therefore, ligand-based oxidation was warranted by the structural analysis.

The *tert*-butyl groups-containing C_6 rings exhibited quinoid-type distortion as expected for the ligand-based oxidation. In both the ligands $C_{Ph}-C_{Ph}$ bond distances (Table 1) of the rings were almost the same. The C1–N1 = 1.314(4) Å, C27–N2 = 1.312(4) Å, C2–O1 = 1.249(4) Å, and C28–O2 = 1.246(4) Å bond distances were longer than previously reported $C_{Ph}-N_{Ph}$ = 1.30 Å, and $C_{Ph}-O_{Ph}$ = 1.24 Å bond distances observed in an iminoquinone moiety, and shorter than the bond distances found in an iminosemiquinone moiety ($C_{Ph}-N_{Ph}$ = 1.35 Å, and $C_{Ph}-O_{Ph}$ = 1.30 Å).[10] These features emphasized a complete delocalization of the radical over the iminosemiquinone and iminoquinone moieties. The delocalization was also supported by the electrochemical behavior of complex **1** (*vide infra*). Hence, according to the structure analysis, the complex can be assigned as [Cu(II)-(iminosemiquinone)(iminoquinone)]PF_6 where the unpaired electron (radical) was completely delocalized over the two coordinating ligand units.

Complex **4** crystallized in the trigonal space group $P3_121$. The molecular structure (monocation unit) with atom labeling scheme is depicted in Figure 5. Selected bond distances and bond angles are given in Table 1.

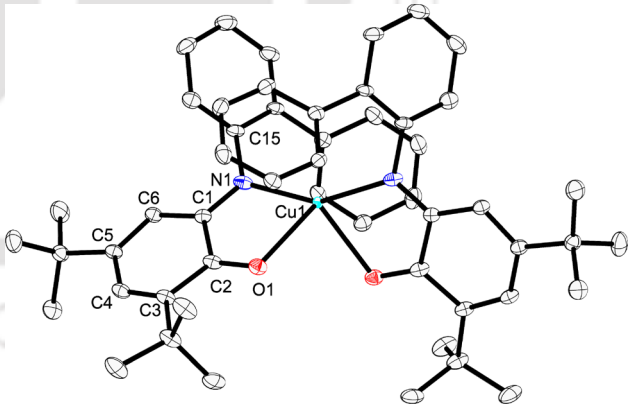

Figure 5. ORTEP diagram of the cation unit of complex **4**; thermal ellipsoids were drown at 30% probability level. H-atoms and the anion $[SbF_6]^{1-}$ are omitted for the shake of clarity.

In four-coordinate complex **4** (τ_4 = 0.56), the Cu1–N1 = 2.021(4) Å and Cu1–O1 = 2.352(4) Å bond distances were consistent with the low oxidation state of the central Cu1 atom, i.e., Cu(I), and higher oxidation state of the coordinating ligands ($[L^{IBQ(Ph)}]^0$) as observed in complex **2**. In the complex, the C1–N1 = 1.297(5) Å and C2–O1 = 1.228(5) Å bond distances were almost same as the bond distances found in the five-coordinate congener, complex **2**. Thus, no change in

DOI: 10.1021/acs.inorgchem.8b01931
Inorg. Chem. XXXX, XXX, XXX–XXX

oxidation state of the central metal ion as well as the coordinating ligands was noticed upon the geometrical change.

No unpaired electron was present in both complex **2** and complex **4**. Thus, both of them were diamagnetic. Complex **3** consisted of two unpaired electrons: one electron was present at Cu(II) [S = 1/2, $3d^9$] ion, and the other electron was the ligand-centered radical (S = 1/2). A ferromagnetic coupling between the two S = 1/2 spins would provide an S_t = 1 ground state, while a diamagnetic ground state with an S_t = 0 would result in an antiferromagnetic coupling between the two paramagnetic centers. Indeed, complex **3** was diamagnetic owing antiferromagnetic coupling between the spins as evident by electron paramagnetic resonance (EPR) and ^{1}H NMR measurements (Figure S10).

The electronic absorption spectra (UV−vis-NIR) for complexes **1**, **2**, **3**, and **4** in CH_2Cl_2 solution are illustrated in Figure 6. Each spectrum was dominated by intense

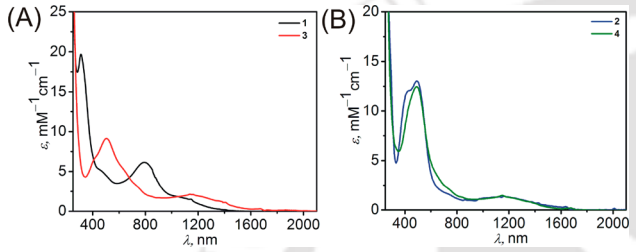

Figure 6. UV−vis-NIR spectra of the complexes recorded at room temperature (25 °C).

absorptions in the visible and near-infrared region. The high intensity of the bands discarded the possibility of Cu(II) d−d transition and implied spin-allowed ligand-to-metal (LMCT), ligand-to-ligand (LLCT), and intraligand (ILCT) charge-transfer transitions. The absorption positions and the corresponding extinction coefficient values are summarized in Table 2.

Table 2. Absorption Data of the Complexes[a]

complex	λ_{max}, nm (ε, M^{-1} cm^{-1})
1	1034 (1850), 792 (6200), 470^{sh} (5000), 310 (19550)
2	1160 (1350), 725sh (1650), 490 (13050), 420 (11900)
$\mathbf{2}^{1+}$	486 (8000), 402 (12000)
$\mathbf{2}^{1-}$	488 (8150), 402 (13700)
3	1144 (2050), 500 (9150), 407^{sh} (6500)
4	1160 (1350), 733 (2200), 490 (12500), 440^{sh} (11200)

[a]sh stands for shoulder.

Complex **1** was comprised of two $[L^{ISQ(Ph)}]^{1-}$ moieties (vide supra), which are coordinated to a Cu(II) ion. The bands at 1034 nm (ε = 1850 M^{-1} cm^{-1}) and 792 nm (ε = 6200 M^{-1} cm^{-1}) were consistent with the previously reported similar Cu(II)-bis(iminosemiquinone) complexes and assigned as the combination of MLCT and LLCT transitions.[7c,e−g] The band at λ_{max} = 470 nm (ε = 5000 M^{-1} cm^{-1}) appeared due to LMCT transition.

In complex **2** ($\{Cu^I[L^{IBQ(Ph)}]_2Cl\}^0$), a broad absorption manifold centered at 1160 nm (ε = 1350 M^{-1} cm^{-1}) was present. The low-energy band has been attributed to Cu(I)-to-iminoquinone MLCT transition. The strong bands at λ_{max} = 490 nm (ε = 13 050 $M^{-1}cm^{-1}$) and λ_{max} = 420 nm (ε = 11 900 M^{-1} cm^{-1}) were due to π-to-π^* intraligand (ILCT) charge-transfer transitions of the Cu(I)-coordinated iminoquinone moieties.[11] The UV−vis-NIR spectrum of complex **4** ($\{Cu^I[L^{IBQ(Ph)}]_2\}SbF_6$) was almost same as that of complex **2** (Figure 6B). This indicated that decreasing the coordination number from five to four and the change in geometry did not influence the charge-transfer transitions appreciably.

A broad band at 1144 nm (ε = 2050 M^{-1} cm^{-1}) appeared in the UV−vis-NIR spectrum of complex **3**. The band arose possibly due to combined ligand-centered intervalence $[L^{ISQ(Ph)}]^{1-}$-to-$[L^{IBQ(Ph)}]^0$ charge-transfer (IVLLCT) and metal-to-ligand charge-transfer (MLCT) transitions.[7d] The π-to-π^* intraligand (ILCT) charge-transfer transitions of the iminoquinone moieties were observed at λ_{max} = 500 nm (ε = 9150 M^{-1} cm^{-1}) and 407 nm (shoulder, ε = 6500 M^{-1} cm^{-1}).[7i]

The electrochemical behavior of complexes **1**, **2**, **3**, and **4** were investigated by cyclic voltammetry. Complex **1** underwent two successive one-electron oxidation and two successive one-electron reduction processes in the potential range +1.00 V to −1.80 V vs Fc^+/Fc (Figure 7A). The oxidation and

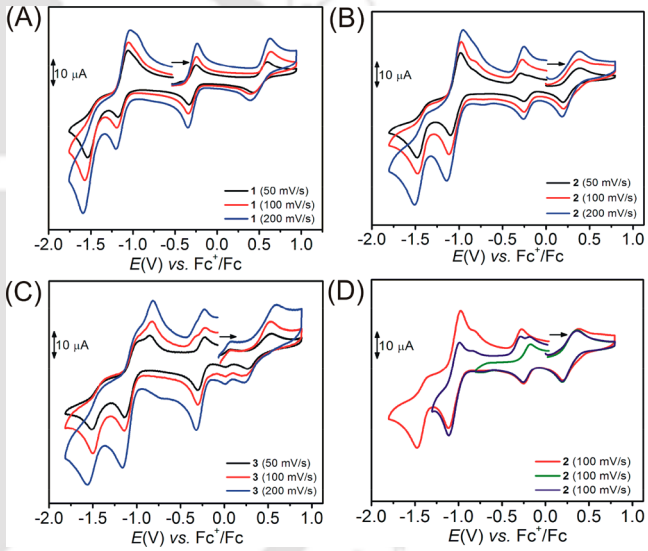

Figure 7. Cyclic voltammograms of complex **1** (A), complex **2** (B and D), and complex **3** (C); measured at 50, 100, and 200 mV/s.

reduction potential values (Table 3) were in accord with the previously reported Cu(II)-bis(iminosemiquinone) complexes[7c,e−g] and thus, corresponded to the ligand-centered processes, where the oxidation of coordinated $[L^{ISQ(Ph)}]^{1-}$ provided $[L^{IBQ(Ph)}]^0$ and reduction of $[L^{ISQ(Ph)}]^{1-}$ generated $[L^{AP(Ph)}]^{2-}$. The potential difference ($\Delta E_{1/2}{}^{ox}$) between the second oxidation ($E_{1/2}{}^{ox2}$) and the first oxidation ($E_{1/2}{}^{ox1}$) processes was ∼800 mV. This indicated a high extent of electronic communication, i.e., delocalization of the radical over the two redox−active coordination sites in the generated complex $\{Cu^{II}[L^{ISQ(Ph)}][L^{IBQ(Ph)}]\}^+$. Conversely, the charge delocalization was less (ΔE = 363 mV) in the one-electron reduced $\{Cu^{II}[L^{ISQ(Ph)}][(L^{AP(Ph)}]\}^{1-}$ species.

The CV of complex **2** showed one one-electron oxidation and three one-electron reduction waves (Figure 7B). The solo oxidation process occurred at $E_{1/2}{}^{ox}$ = 0.270 V (Table 3) was ∼0.240 V lower compared to the second oxidation process of complex **1**. In complex **2**, the Cu(I) was the only redox-active center, which could be preferably oxidized. Therefore, the oxidation process has been assigned as Cu(I)-to-Cu(II)

DOI: 10.1021/acs.inorgchem.8b01931
Inorg. Chem. XXXX, XXX, XXX−XXX

Table 3. Voltammetric Redox Processes for the Complexes

	E^0,[a] V, (ΔEp, mV)			
complex	$E_{1/2}^{red2}$	$E_{1/2}^{red1}$	$E_{1/2}^{ox1}$	$E_{1/2}^{ox2}$
1	−1.480 (120)	−1.117 (125)	−0.292 (115)	0.508 (245)
2	−1.420 (120)	−1.044 (147)	0.270 (160)	
3	−1.494 (148)	−1.080 (160)	−0.264 (80)	0.408 (348)

[a] E^0 values recorded at scan rates of 100 mV/s and referenced to the Fc^+/Fc couple.

oxidation and formation of $\{Cu^{II}[L^{IBQ(Ph)}]_2Cl\}^{1+}$ species. The second and the third reduction potential values were closely comparable to that of the reduction potential values observed in complex **1**. Thus, the reductions corresponded to ligand-based processes.

One one-electron oxidation and three one-electron reduction processes were observed in the CV of complex **3** (Figure 7C). The oxidation process occurred at 0.408 mV, which was 0.100 V lower compared to the parent complex **1**. This difference was attributed to the structural anomaly, i.e., square planar (**1**) vs distorted tetrahedral (**3**) geometry. The reduction potentials were expectedly analogous to complex **1** (Table 3).

In the CV of complex **4** (Figure S12) irreversible electron transfer processes were noticed. The CV measurement at 100 mV/s scan rate revealed an oxidation at 0.360 V and two reduction processes at −0.600 V and −1.390 V (Figure S12). The peak positions were also scan rate dependent.

Herein, we performed spectroelectrochemical studies for the one-electron oxidation and the first one-electron reduction processes of complex **2** in order to discern the redox active centers that participate in the processes. In the fixed potential coulometric one-electron oxidation, the intensity of the band at 490 nm diminished, while the band at 420 nm remained almost unaffected (Table 2). The MLCT band at 1160 nm almost vanished (Figure 8A). This implied the depletion of the

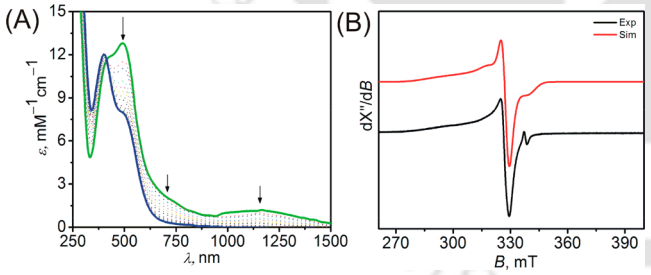

Figure 8. (A) Change in UV−Vis−NIR spectrum of complex **2** during one-electron fixed potential coulometric oxidation and (B) experimental and simulated X-band EPR spectra of the oxidized solution. X-band EPR was measured at frequency = 9.44 GHz, modulation frequency = 100 kHz and amplitude = 12 G, temperature = 298 K.

Cu(I) species-concentration and generation of the corresponding Cu(II) species. To buttress the formation of the Cu(II) species, X-band EPR spectrum of the oxidized solution was measured and is shown in Figure 8B. The EPR spectrum was typical for a Cu(II) species with an unpaired electron residing at $d_{x^2-y^2}$ orbital. Simulation to the experimental result provided: g_x = 2.045, g_y = 2.060 and g_z = 2.250; g_{av} = 2.118; ^{Cu}A (3, 47, 80) × 10^{-4} cm^{-1}.

During the coulometric one-electron reduction of complex **2** the ILCT band at 490 nm decreases in intensity gradually, while band at 420 nm increases (Figure 9A). It has previously been reported that Cu(I)-iminosemiquinone (TPQ-radical)

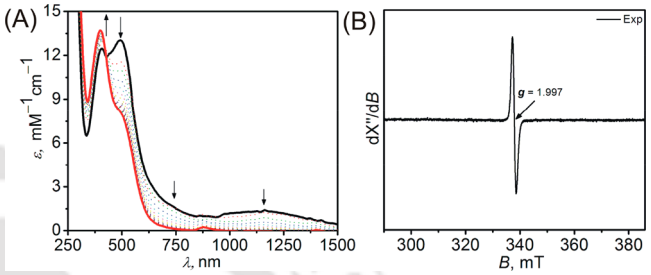

Figure 9. (A) Change in UV−Vis−NIR spectrum of complex **2** during one-electron fixed potential coulometric reduction and (B) experimental X-band EPR spectrum of the reduced solution. X-band EPR was measured at frequency = 9.44 GHz, modulation frequency = 100 kHz and amplitude = 50 G, temperature = 298 K.

species in AOase absorbs at 463 and 434 nm.[4g−j] Thus, the increase of the band ascribed to the formation of a Cu(I)-iminosemiquinone species by the one-electron reduction of a Cu(I)-coordinated iminoquinone moiety. The depletion of 1160 nm band also supported the reduction of iminoquinone unit to iminosemiquinone unit. X-band EPR spectrum of the solution, obtained after the one-electron reduction, exhibited an isotropic signal at g = 1.997 (Figure 9B). The value was very close to the previously reported iminosemiquinone-coordinated Cu(I) complexes ($g \approx 2.005$)[12] and thus supported $\{Cu^{I}[L^{IBQ(Ph)}][L^{ISQ(Ph)}]Cl\}^{-}$ composition of complex $\mathbf{2}^{1-}$.

Reactivity Study. Complex **2** was comprised of a Cu(I) ion and two coordinated-iminoquinone moieties. The synthesis of the complex was carried out under aerial atmosphere. This indicated that the complex was reluctant to aerial oxygen; i.e., no oxidation of Cu(I) occurred. Furthermore, purging of O_2 to the CH_2Cl_2 solution of complex **2** did not provide any appreciable UV−vis−NIR spectral changes. However, the complex reacted with KO_2, albeit slowly (Figure 10B). In the presence of KO_2, i.e., superoxide radical anion, a new band at 785 nm appeared and 1160 nm band shifted to 1035 nm (Figure 10A,B) in due course. These UV−vis−NIR spectral changes corresponded to the generation of complex **1** (Figure 6A). X-band EPR spectrum measurement of the reaction solution provided Cu(II)-centered spectrum [g_x = 1.980, g_y = 2.005, and g_z = 2.250; g_{av} = 2.078; ^{Cu}A (3, 3, 153) × 10^{-4} cm^{-1}], which also resembled with the EPR spectrum of complex **1** (Figure 10C) and thus, concurred with the formation of complex **1**. The generation of molecular oxygen during the process was consolidated by CV measurements (Figure 10D). The reduction peak of the liberated molecular oxygen appeared at −1.482 V. Upon purging of argon gas through the solution, the concentration of oxygen gas diminished as evident by the reduction of current at the potential (Figure 10D).

DOI: 10.1021/acs.inorgchem.8b01931
Inorg. Chem. XXXX, XXX, XXX−XXX

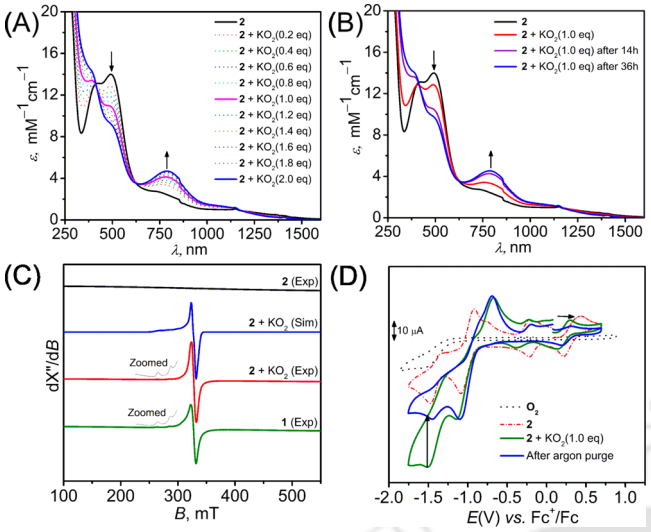

Figure 10. (A) Change in UV−vis−NIR spectrum of complex **2** during the sequential addition of KO_2, (B) one-step addition of stoichiometric amount of KO_2 and the time-dependent spectral changes; (C) experimental and simulated X-band EPR spectra of CH_2Cl_2 solutions of **1**, **2**, and **2** + KO_2; and (D) detection of O_2 gas by CV measurements. X-band EPR was measured at frequency = 9.143 (**1**), 9.143(**2**) GHz, modulation frequency = 100 kHz (**1** and **2**), and amplitude = 2 G (**1** and **2**), temperature = 77 K (parentheses indicates the complex).

Unlike complex **2**, the congener four-coordinate complex **4** did not react with KO_2 (Figure 11B). Interestingly, despite

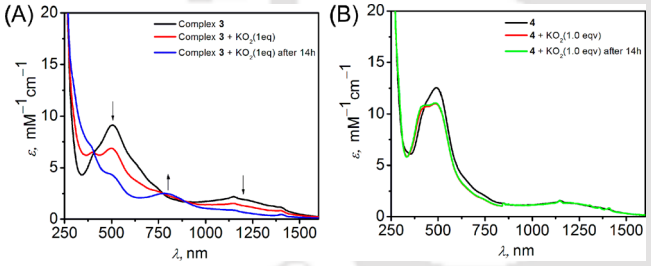

Figure 11. Change in UV−vis−NIR spectrum of CH_2Cl_2 solution of (A) complex **3** and (B) complex **4**, in the presence of KO_2.

structural similarity with complex **4** (τ_4 = 0.56, twist angle between two NO coordinating units = 61.4°), complex **3** (τ_4 = 0.54, twist angle between two NO coordinating units = 56.4°) reacted with KO_2 (Figure 11A) and produced complex **1** and molecular oxygen. However, the reaction was sluggish. Hence, the geometry as well as oxidation state of copper ion and the coordinated noninnocent ligand units have been found as crucial for the occurrence and the effectiveness of the reaction.

Herein, we propose that complex **2** reacted with KO_2 and produced $\mathbf{2}^{1-}$, which instantaneously underwent metal-centered Cu(I)-to-Cu(II) oxidation in the presence of the generated molecular oxygen and provided complex **3** with the removal of the axial chloride ion (Scheme 3). The increase of ligand-based negative character possibly favored the removal of the chloride ion. Finally, KO_2 reduced complex **3** to complex **1** with concomitant production of molecular oxygen.

Theoretical Calculations. The structure of all the complexes and one-electron oxidized and one-electron reduced forms of complex **2** were optimized at B3LYP/6-31G(d) level

Scheme 3. Proposed Mechanism for the Formation of Complex 1 from Complex 2 in the Presence of KO_2

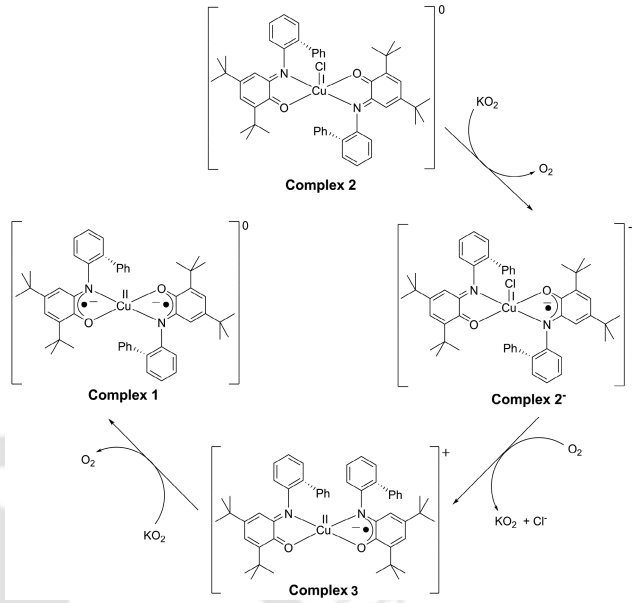

of theory. The details of computational method are given in the Experimental Section. The optimized structures of all the complexes with selected bond distances are presented in Table S1, and respective coordinates are given in Tables S3−S8. Akin to the X-ray crystallographic molecular structures, two O atoms and two N atoms were situated *trans* to each other in both four-coordinate complex **1** and five-coordinate complex **2**. The optimized structure of one-electron oxidized form of complex **2**, i.e., $\mathbf{2}^{1+}$, was five-coordinate. No appreciable change in the $C_{Ph}-O_{Ph}$ and $C_{Ph}-N_{Ph}$ bond distances of the *tert*-butyl groups-containing C_6 rings indicated the retention of the oxidation state of the coordinating units upon the oxidation. The substantial decrease in Cu−O bond [Table S1] confirmed metal-centered Cu(I)-to-Cu(II) oxidation, and the finding was commensurate with the assigned species that was obtained by fixed-potential coulometric, one-electron oxidation of complex **2**. The optimized structure of one-electron reduced species ($\mathbf{2}^{1-}$) of complex **2** showed a large Cu−Cl bond distance (2.716 Å). In addition, the $C_{Ph}-O_{Ph}$ and $C_{Ph}-N_{Ph}$ bond distances indicated one-electron oxidized iminosemiquinone state of the corresponding *tert*-butyl groups-containing two C_6 rings, and Cu−O and Cu−N bond distances indicated +II oxidation state of the copper ion (Table S1). Thus, the formation of stable complex **1** as the final product upon one-electron reduction was implemented. In fact, the reduction of complex **2** by KO_2 showed the formation of complex **1** as the final complex. Noticeable, the UV−vis−NIR spectrum of the optimized $\mathbf{2}^{-}$ was completely different than that of electrochemically generated $\mathbf{2}^{1-}$ species (Figure S13). Hence, the observed structure of $\mathbf{2}^{1-}$ was not supported by DFT calculations. Both complex **3** and complex **4** were four-coordinate. In the optimized structures, the coordinating two N atoms and two O atoms were situated *cis* to each other as found in their X-ray crystallographically characterized molecular structures (*vide supra*). While the $C_{Ph}-O_{Ph}$ and $C_{Ph}-N_{Ph}$ bond distances were similar in both the complexes, the Cu−O bond in complex **3** was much shorter (1.951 Å) compared to the bond (2.280 Å) in complex **4** and indicated a lower oxidation state of copper ion in complex **4** compared to that in

DOI: 10.1021/acs.inorgchem.8b01931
Inorg. Chem. XXXX, XXX, XXX−XXX

complex **3**. The finding was in accord with the crystallographic structural assignment.

The UV−vis−NIR spectra of all the complexes were generated by TD-DFT calculations in DCM solvent and are depicted in Figure S13. The wavelength of absorption maxima, the type of various transitions, and orbital contributions are presented in Table S2a−d. Clearly, the spectral shapes of complex **2**, **3**, and **4** were similar. However, the UV−vis spectra of complex $\mathbf{2}^{1+}$ and $\mathbf{2}^{1-}$ were completely different (Figure S13) than the others.

In the calculated UV−vis-NIR spectrum of complex **1**, the absorption band at 1033 nm appeared due to a combination of MLCT and LLCT transitions. The absorption band involved HOMO−1(α) → LUMO(α) electronic excitation (Figure 12). The calculated band correlated well to 1034 nm transition band observed in the experimental UV−vis-VIR spectrum of the complex. The HOMO−2(α) → LUMO(α) and HOMO−2(β) → LUMO(β) electronic excitations exhibited an LLCT transition at 655 nm in complex **1**. Complex $\mathbf{2}^{1+}$ showed LLCT charge transfer transitions at 529 nm. The band was because of HOMO−8(α) → LUMO+1(α) electronic excitation.

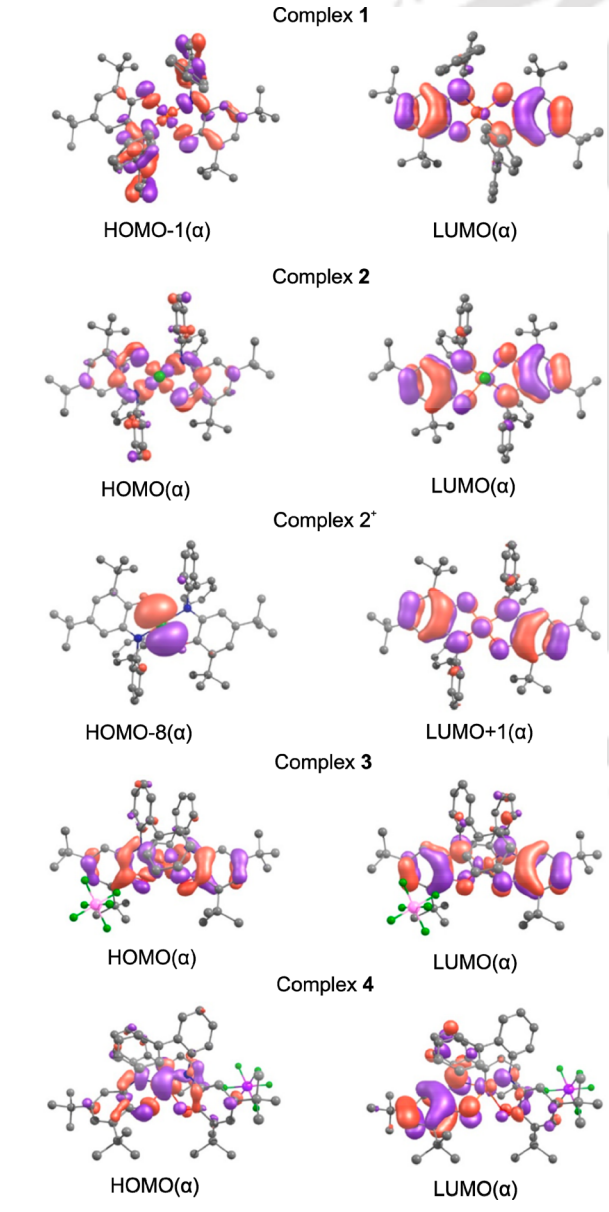

Figure 12. Some FMOs of the complexes that participated in charge transfer transitions. See Table S2 for other FMOs.

CONCLUSION

To conclude, we have presented the successful synthesis of the five-coordinate, mononuclear neutral Cu(I)-bis-(iminoquinone)Cl complex (**2**) by the $CuCl_2{\cdot}2H_2O$ mediated inner sphere one-electron oxidation of the Cu(II)-bis-(iminosemiquinone) complex (**1**). In the process, the initially formed five-coordinate Cu(II)-(iminosemiquinone)-(iminoquinone)Cl intermediate underwent an electron transfer from ligand(iminosemiquinone)-to-metal[Cu(II)]. Conversely, the outer-sphere, one-electron oxidation of complex **1** did not follow such an electron transfer process and provided the four-coordinate Cu(II)-(iminosemiquinone)-(iminoquinone) complex (**3**). Four-coordinate complex **4** was synthesized by the removal of the axial Cl^{1-} ion from complex **2**. No change in the oxidation state of either copper or coordinating ligand was warranted in the complex compared to the parent complex. Thus, it is implied that the formation of initial five-coordinate intermediate $\{Cu^{II}[L^{ISQ(Ph)}][L^{IBQ(Ph)}]Cl\}$ was crucial for the ligand[iminosemiquinone]-to-metal[Cu(II)] electron transfer. Noteworthy, a Cl^{1-} bound pseudo five-coordinate Cu(II)-(iminosemiquinone)(iminoquinone) complex has previously been reported.[7d] No iminosemiquinone-to-Cu(II) electron transfer in the reported complex is noticed. The salient feature of the complex is the almost orthogonal arrangement between two redox-active noninnocent ligand units. Therefore, herein, we propose that a nonorthogonal alignment between two noninnocent ligand units is essential for the electron transfer in the five-coordinate Cu(II)-(iminosemiquinone)(iminoquinone) complex. Thus, the geometry-dependent electron transfer in a copper(II)-monoradical complex, where both the noninnocent ligand units were in different oxidation states and nonorthogonal arrangement, was documented.

All the complexes were characterized by X-ray single-crystal diffraction measurements. A five-coordinate Cu(I) complex has previously been stabilized in a rigid macrocyclic glyoxime ligand with a *soft* CO as the axial ligand.[13] To the best of our knowledge, complex **2** is the first isolated air-stable five-coordinate square pyramidal Cu(I) complex, which was being stabilized in the coordination environment comprising two bidentate 2-iminobenzoquinone and a chloride ion. Cyclic voltammetry measurements on complexes **2** and **3** established that the complexes can be the oxidized by an electron and reduced successively by three electrons. Spectro-electrochemical and X-band EPR experiments on complex **2** emphasized that the solo oxidation was Cu(I)-centered and the reductions were ligand-based. The oxidation and the reductions potential values found for complex **3** were comparable to the ligand-based processes as observed in complex **1**. Thus, the oxidation and the reductions processes that occurred in complex **3** have been assigned as ligand-based.

The investigation on the reactivity of the complexes on KO_2 revealed that complex **2** and complex **3** reacted slowly with KO_2, and oxidized it to molecular oxygen, which was identified by CV measurements. In the processes, both complexes were reduced to complex **1**. Complex **4** remained unreactive to KO_2. Thus, oxidation state and geometry dependent reactivity have been noticed.

DOI: 10.1021/acs.inorgchem.8b01931
Inorg. Chem. XXXX, XXX, XXX−XXX

The geometry of all the complexes, as well as complex 2^{1+} and complex 2^{1-}, were obtained by DFT-based theoretical calculations. TD-DFT calculations showed that absorption bands that appeared in the UV−vis-NIR spectra of the complexes were due to MLCT and LLCT charge transfer transitions.

EXPERIMENTAL SECTION

Materials. All the chemicals and solvents were obtained from commercial sources and were used as supplied, unless noted otherwise. 3,5-Di-*tert*-butylcatechol, ferrocenium hexafluorophosphate, silver hexafluoroantimonate, KO_2, and 2-amino biphenyl were purchased from Sigma-Aldrich. Solvents were obtained from Merck (India). Mass spectra were measured in HPLC grade acetonitrile solution.

Physical Methods. X-ray crystallographic data were collected using Super Nova, Single source at offset, Eos diffractometer. The data refinement and cell reductions were carried out by CrysAlisPro.[14] Structures were solved by direct methods using SHELXS-97 and refined by the full matrix least-squares method using SHELXL-97.[15] All the non-hydrogen atoms were refined anisotropically. Crystallographic parameters and refinement data for 2, 3·1.5H2O and 4 complexes are given in Tables 4, 5, and 6, respectively. IR spectra were recorded on a PerkinElmer Instrument at normal temperature with KBr pellet by grinding the sample with KBr (IR grade). ^{1}H-, and ^{13}C-NMR spectra of the ligand were recorded in BRUKER 600 MHz NMR machine. UV−vis−NIR spectra and spectroelectrochemical data were recorded on a PerkinElmer, Lamda 750, UV/vis/NIR spectrometer by preparing a known concentration of the samples in HPLC grade CH_2Cl_2 at room temperature (25 °C) using a cuvette of 1 cm width. X-band EPR spectra were recorded on JEOL, JES-FA200 machine. Cyclic voltammograms (CVs) of the complexes (1 mM) were being recorded on VersaSTAT 3 instrument in CH_2Cl_2 solutions containing 0.10 M $[(^nBu)_4N]ClO_4$ as supporting electrolyte. A glassy carbon working electrode, a platinum wire counter electrode, and a Ag/AgCl reference electrode were used for the measurements. Ferrocene was used as an internal standard, and herein, all the potentials are referenced versus the ferrocenium/ferrocene (Fc^+/Fc) couple.

Table 4. Crystallographic Parameters and Refinement Data for Complex 2

empirical formula	$C_{52}H_{58}CuN_2O_2Cl$
formula weight	842.00
CCDC no.	1814274
crystal habit, color	block, deep blue
crystal size, mm^3	0.25 × 0.20 × 0.15
temperature, T	100(2)
wavelength, λ (Å)	0.71073
crystal system	monoclinic
space group	$C2/c$
unit cell dimensions	a = 17.0071(8) Å
	b = 13.1682(6) Å
	c = 20.1656(8) Å
	α = 90.00°, β = 95.639(4)°, γ = 90.00°
volume, V (Å^3)	4494.3(3)
Z	4
calculated density, Mg·m^{-3}	1.244
absorption coefficient, μ (mm^{-1})	0.587
F(000)	1784
θ range for data collection	2.99−24.75°
limiting indices	$-20 \le h \le 13$, $-15 \le k \le 15$, $-22 \le l \le 23$
reflection collected/unique	8932/3185 [R(int) = 0.0533]
completeness to θ	96.0% (θ = 24.75°)
max. and min transmission	0.916/0.869
refinement method	SHELXL-97 (Sheldrick, 1997)
data/restraints/parameters	3694/0/269
goodness-of-fit on F^2	1.066
final R indices [$I > 2\sigma(I)$]	R_1 = 0.0424, wR_2 = 0.1069
R indices (all data)	R_1 = 0.0515, wR_2 = 0.1160
largest diff peak and hole	0.368 and −0.392 e·Å^{-3}

Table 5. Crystallographic Parameters and Refinement Data for Complex 3·1.5H$_2$O

empirical formula	$2(C_{52}H_{58}CuN_2O_2)$, $2(PF_6)$, $3(H_2O)$
formula weight	1957.10
CCDC no.	1814276
crystal habit, color	block, blue
crystal size, mm^3	0.10 × 0.08 × 0.04
temperature, T	293(2)
wavelength, λ (Å)	0.71073
crystal system	triclinic
space group	$P\bar{1}$
unit cell dimensions	a = 11.5692(6) Å
	b = 12.6901(5) Å
	c = 17.5488(5) Å
	α = 94.409(3)°, β = 96.390(3)°, γ = 95.137(4)°
volume, V (Å^3)	2540.29(18)
Z	1
calculated density, Mg·m^{-3}	1.279
absorption coefficient, μ (mm^{-1})	0.527
F(000)	1026
θ range for data collection	3.11−27.50°
limiting indices	$-14 \le h \le 15$, $-16 \le k \le 16$, $-21 \le l \le 22$
reflection collected/unique	19554/8286 [R(int) = 0.0226]
completeness to θ	96.0% (θ = 27.50°)
max and min transmission	0.979/0.951
refinement method	SHELXL-97 (Sheldrick, 1997)
data/restraints/parameters	11206/0/604
goodness-of-fit on F^2	1.014
final R indices [$I > 2\sigma(I)$]	R_1 = 0.0768, wR_2 = 0.2047
R indices (all data)	R_1 = 0.1008, wR_2 = 0.2298
largest diff. peak and hole	0.770 and −1.239 e·Å^{-3}

Computational Methodology. The geometries of all the complexes have been fully optimized at B3LYP/6-31G(d) level of theory to have the most favorable structure of the complexes. A double-ζ quality basis set LANL2DZ was used for the atom antimony (Sb) in complex **4**. The vibrational frequency calculations were also performed at the same level of theory to characterize the true minimum structure without any imaginary frequency. TD-DFT[16] calculations at the same methods and basis sets were carried out to generate the UV−vis−NIR spectra. Natural bond orbital (NBO)[17] analysis was carried out to investigate the various charge transfer occur between the interacting orbitals in the complexes. The effect of dichloromethane (DCM) solvent on the electronic structure of the complexes have been included using integral equation formulation of the polarizable continuum model (IEF-PCM)[18] in all the DFT and TD-DFT calculations. All the computations were performed using Gaussian-09 program package,[19] although TD-DFT with standard exchange-correlation functional is believed to yield some errors for the study of charge-transfer excitation energies.[20] In the present computation, it could predict the UV−vis-NIR spectra of all the considered Cu complexes to a certain extent. However, this method should be used with caution, and computational data should be compared with experiments wherever possible.

Synthesis of $C_{26}H_{31}NO$; $H_2L^{AP(Ph)}$. Reported previously.[21]

DOI: 10.1021/acs.inorgchem.8b01931
Inorg. Chem. XXXX, XXX, XXX−XXX

Table 6. Crystallographic Parameters and Refinement Data for Complex 4

empirical formula	$C_{52}H_{58}CuN_2O_2SbF_6$
formula weight	1042.31
CCDC no.	1814278
crystal habit, color	needle, brown
crystal size, mm^3	0.26 × 0.12 × 0.10
temperature, T	100(2)
wavelength, λ (Å)	0.71073
crystal system	trigonal
space group	$P31\ 21$
unit cell dimensions	a = 17.2492(4) Å
	b = 17.2492(4) Å
	c = 14.2445(5) Å
	α = 90.00°, β = 90.00°, γ = 120.00°
volume, V ($Å^3$)	3670.4(2)
Z	3
calculated density, $Mg{\cdot}m^{-3}$	1.415
absorption coefficient, μ (mm^{-1})	1.050
$F(000)$	1602
θ range for data collection	3.08−27.49°
limiting indices	$-20 \le h \le 22, -6 \le k \le 22, -17 \le l \le 18$
reflection collected/unique	10058/4896 [R(int) = 0.0269]
completeness to θ	97.8% (θ = 27.49°)
max and min transmission	0.900/0.860
refinement method	SHELXL-97 (Sheldrick, 1997)
data/restraints/parameters	5392/0/296
goodness-of-fit on F^2	1.080
final R indices [$I > 2\sigma(I)$]	$R1$ = 0.0425, $wR2$ = 0.0965
R indices (all data)	$R1$ = 0.0501, $wR2$ = 0.1025
largest diff. peak and hole	0.911 and −0.886 $e{\cdot}Å^{-3}$

Synthesis of $C_{52}H_{58}CuN_2O_2$; $\{Cu^{II}[L^{ISQ(Ph)}]_2\}^0$ (1). To a stirred solution of ligand $H_2L^{AP(Ph)}$ (0.189 g, 0.5 mmol) in CH_3OH (10 mL), $CuCl_2{\cdot}2H_2O$ (0.086 g, 0.5 mmol) and Et_3N (0.1 mL) were added sequentially at room temperature under air. The resulting solution was stirred at room temperature for 1 h. The resulted greenish precipitate was filtered and washed with excess CH_3OH (5 mL). Crystals suitable for single crystal X-ray diffraction analysis were grown by slow evaporation of a 3:1 CH_2Cl_2/CH_3OH solvent mixture. Yield: 0.126 g, 62%. FT-IR (KBr pellet, cm^{-1}): 3055, 2959, 2905, 2866, 1579, 1475, 1462, 1447, 1386, 1361, 1332, 1253, 1202, 1179, 1110, 1029, 853, 775, 746, 738, 697. ESI−MS (+) m/z for $[C_{52}H_{58}N_2O_2Cu]^+$: Calcd, 805.3789 ; found, 805.3791. Anal. Calcd for $C_{52}H_{58}CuN_2O_2$: C, 77.48; H, 7.26; N, 3.48. Found: C, 77.52; H 7.15; N, 3.58.

Synthesis of $C_{52}H_{58}CuN_2O_2Cl$; $\{Cu^{I}[L^{IBQ(Ph)}]_2Cl\}^0$ (2). To a stirred solution of ligand $H_2L^{AP(Ph)}$ (0.188 g, 0.5 mmol) in CH_3OH (10 mL), $CuCl_2{\cdot}2H_2O$ (0.173 g, 1.0 mmol) was added at room temperature under air. Upon addition of Et_3N (0.1 mL), the color of the solution changed to deep blue. After stirring of the solution for 1 h 15 min, a dark blue solid of **2** formed which was collected by filtration. Recrystallization of the solid from a CH_2Cl_2:CH_3OH (4:1) solvent mixture provided blue crystals suitable for single crystal X−ray diffraction analysis. Yield: 0.152 g, 72%. FT−IR (KBr pellet, cm^{-1}): 3054, 2952, 2905, 2866, 1617, 1591, 1460, 1432, 1387, 1377, 1364, 1321, 1247, 1206, 1085, 1023, 895, 805, 746, 701, 611, 580, 531. ESI−MS (+) m/z for $\{[C_{52}H_{58}ClN_2O_2Cu]\text{-}Cl\}^+$: Calcd, 805.3789 ; found, 805.3769. Anal. Calcd for $C_{52}H_{58}CuN_2O_2Cl$: C, 74.25; H, 6.96; N, 3.33. Found: C 74.47; H, 6.85; N, 3.32.

Synthesis of $C_{52}H_{58}CuN_2O_2PF_6$; $\{Cu^{II}[L^{ISQ(Ph)}][L^{IBQ(Ph)}]\}PF_6$ (3). To a stirred solution of the $\{Cu^{II}[L^{ISQ(Ph)}]_2\}^0$ (**1**) (0.201 g, 0.25 mmol) in CH_2Cl_2 (10 mL), ferrocenium hexafluorophosphate (0.083 g, 0.25 mmol) was added and the resulted solution was allowed to stirred for 3 h. During stirring, the deep green color solution changed to deep blue. Then reaction solution was evaporated to dryness, which provided an amorphous solid of **3**. The solid was washed with excess hexane (10 mL). Recrystallization from CH_2Cl_2/hexane (3:1) solution afforded X-ray quality crystals. Yield: 0.112 g, 45%. FT−IR (KBr pellet, cm^{-1}): 3062, 2955, 2915, 2871, 1635, 1608, 1563, 1469, 1415, 1387, 1368, 1321, 1270, 1248, 1207, 1173, 1088, 903, 841, 745, 703, 557. . ESI−MS (+) m/z for $[C_{52}H_{58}N_2O_2Cu]^+$: Calcd, 805.3789 ; found, 805.3784. Anal. Calcd for $C_{52}H_{58}CuN_2O_2PF_6{\cdot}1.5H_2O$: C, 63.85; H, 6.29; N, 2.87. Found: C, 63.91; H, 6.03; N, 2.61.

Synthesis of $C_{52}H_{58}CuN_2O_2SbF_6$; $\{Cu^{I}(L^{IBQ(Ph)})_2\}SbF_6$ (4). To a stirred solution of the $\{Cu^{I}[L^{IBQ(Ph)}]_2Cl\}^0$ (**2**) (0.210 g, 0.25 mmol) in CH_2Cl_2 (10 mL), silver hexafluoroantimonate (0.086 g, 0.25 mmol) was added and allowed to stirred for 2 h. During stirring, the deep blue color solution of the solution changed to reddish-brown. After that, reaction solution was filtered through a Celite pad, and the filtrate part was evaporated to dryness to give an amorphous solid of **4**. The solid was recrystallized from a CH_2Cl_2/MeOH (3:1) solvent mixture that afforded X-ray quality crystals. Yield: 0.112 g, 42%. FT−IR (KBr pellet, cm^{-1}): 3063, 2961, 2909, 2871, 1638, 1622, 1514, 1473, 1377, 1288, 1268, 1251, 1021, 898, 751, 702, 657. ESI−MS (+) m/z for $[C_{52}H_{58}N_2O_2Cu]^+$: Calcd, 805.3789 ; found, 805.3766. Anal. Calcd for $C_{52}H_{58}CuN_2O_2SbF_6{\cdot}3H_2O$: C, 57.02; H, 5.89; N, 2.56. Found: C, 56.94; H, 5.63; N, 2.46.

■ ASSOCIATED CONTENT

Supporting Information

The Supporting Information is available free of charge on the ACS Publications website at DOI: 10.1021/acs.inorgchem.8b01931.

Infrared, mass, and NMR spectra of the complexes. CV of complex **4**, DFT optimized structures of the complexes, TD-DFT calculated UV−vis-NIR spectra of the complexes, FMOs, coordinates of the optimized structures (PDF)

Accession Codes

CCDC 1814274, 1814276, and 1814278 contain the supplementary crystallographic data for this paper. These data can be obtained free of charge via www.ccdc.cam.ac.uk/data_request/cif, or by emailing data_request@ccdc.cam.ac.uk, or by contacting The Cambridge Crystallographic Data Centre, 12 Union Road, Cambridge CB2 1EZ, UK; fax: +44 1223 336033.

■ AUTHOR INFORMATION

Corresponding Author

*E-mail: cmukherjee@iitg.ernet.in.

ORCID

Hemant Kumar Srivastava: 0000-0001-6589-6854

Chandan Mukherjee: 0000-0002-2771-2468

Funding

Science and Engineering Research Board (SERB), India. Council of Scientific & Industrial Research (CSIR), India.

Notes

The authors declare no competing financial interest.

■ ACKNOWLEDGMENTS

This project is supported by SERB [EMR/2015/002491], and CSIR [01/2817/14/EMR-II], Govt of India. G.C.P. thanks Indian Institute of Technology Guwahati (IITG) for his doctoral fellowship. H.K.S. and S.B. thank DST-SERB for the financial assistance through SB/S2/RJN-004/2015 and PDF/2016/002053 projects, respectively. FIST programme, DST, India, The Department of Chemistry, Param-Ishan Super-

DOI: 10.1021/acs.inorgchem.8b01931
Inorg. Chem. XXXX, XXX, XXX−XXX

computer and CIF, IIT Guwahati, are thankfully acknowledged for instrumental facility.

REFERENCES

(1) (a) Stubbe, J.; van der Donk, W. A. Protein Radicals in Enzyme Catalysis. *Chem. Rev.* **1998**, *98*, 705−762. (b) Whittaker, J. W. Free Radical Catalysis by Galactose Oxidase. *Chem. Rev.* **2003**, *103*, 2347−2364. (c) Holm, R. H.; Kennepohl, P.; Solomon, E. I. Structural and Functional Aspects of Metal Sites in Biology. *Chem. Rev.* **1996**, *96*, 2239−2314. (d) Hatcher, L. Q.; Karlin, K. D. Oxidant types in copper−dioxygen chemistry: the ligand coordination defines the Cu_n-O_2 structure and subsequent reactivity. *JBIC, J. Biol. Inorg. Chem.* **2004**, *9*, 669−683. (e) Kitajima, N.; Moro-oka, Y. Copper-Dioxygen Complexes. Inorganic and Bioinorganic Perspectives. *Chem. Rev.* **1994**, *94*, 737−757. (f) Kopf, M. A.; Karlin, K. D. In *Biomimetic Oxidations*; Muenier, B., Ed.; Imperial College Press: London, U.K., 2000, Chapter 7. (g) Chaudhuri, P.; Wieghardt, K. Phenoxyl Radical Complexes. In *Prog. Inorg. Chem.*; Wiley: Hoboken, NJ, 2001.

(2) (a) Ito, N.; Phillips, S. E. V.; Stevens, C.; Ogel, Z. B.; McPherson, M. J.; Keen, J. N.; Yadav, K. D. S.; Knowles, P. F. Novel thioether bond revealed by a 1.7 Å crystal structure of galactose oxidase. *Nature* **1991**, *350*, 87−90. (b) Ito, N.; Phillips, S. E. V.; Yadav, K. D. S.; Knowles, P. F. Crystal Structure of a Free Radical Enzyme, Galactose Oxidase. *J. Mol. Biol.* **1994**, *238*, 704−814. (c) Wang, Y.; Stack, T. D. P. Galactose Oxidase Model Complexes: Catalytic Reactivities. *J. Am. Chem. Soc.* **1996**, *118*, 13097−13098. (d) Wang, Y.; DuBois, J. L.; Hedman, B.; Hodgson, K. O.; Stack, T. D. P. Catalytic Galactose Oxidase Models: Biomimetic Cu(II)−Phenoxyl−Radical Reactivity. *Science* **1998**, *279*, 537−540. (e) Banerjee, R. Introduction: Radical Enzymology. *Chem. Rev.* **2003**, *103*, 2081−2082. (f) Whittaker, J. W. Free Radical Catalysis by Galactose Oxidase. *Chem. Rev.* **2003**, *103*, 2347−2364. (g) Benisvy, L.; Blake, A. J.; Collison, D.; Davies, E. S.; Garner, C. D.; Mclnnes, E. J. L.; McMaster, J.; Whittaker, G.; Wilson, C. A phenoxyl radical complex of copper(II). *Chem. Commun.* **2001**, 1824−1825. (h) Jazdzewski, B. A.; Tolman, W. B. Understanding the copper−phenoxyl radical array in galactose oxidase: contributions from synthetic modeling studies. *Coord. Chem. Rev.* **2000**, *200−202*, 633−685. (i) Sokolowski, A.; Leutbecher, H.; Weyhermüller, T.; Schnepf, R.; Bothe, E.; Bill, E.; Hildebrandt, P.; Wieghardt, K. Phenoxyl-copper (II) complexes: models for the active site of galactose oxidase. *JBIC, J. Biol. Inorg. Chem.* **1997**, *2*, 444−453. (j) Benisvy, L.; Blake, A. J.; Collison, D.; Davies, E. S.; Garner, C. D.; Mclnnes, E. J. L.; McMaster, J.; Whittaker, G.; Wilson, C. A phenol−imidazole pro-ligand that can exist as a phenoxyl radical, alone and when complexed to copper(II) and zinc(II). *Dalton Trans.* **2003**, 1975−1985.

(3) (a) Kersten, P. J. Glyoxal oxidase of Phanerochaete chrysosporium: its characterization and activation by lignin peroxidase. *Proc. Natl. Acad. Sci. U. S. A.* **1990**, *87*, 2936−2940. (b) Kurek, B.; Kersten, P. J. Physiological regulation of glyoxal oxidase from *Phanerochaete chrysosporium* by peroxidase systems. *Enzyme Microb. Technol.* **1995**, *17*, 751−756. (c) Whittaker, M. M.; Kersten, P. J.; Nakamura, N.; Sanders−Loehr, J.; Schweizer, E. S.; Whittaker, J. W. Glyoxal oxidase from *Phanerochaete chrysosporium* is a new radical−copper oxidase. *J. Biol. Chem.* **1996**, *271*, 681−687. (d) Whittaker, M. M.; Kersten, P. J.; Cullen, D.; Whittaker, J. W. Identification of catalytic residues in glyoxal oxidase by targeted mutagenesis. *J. Biol. Chem.* **1999**, *274*, 36226−36232. (e) Yin, D. T.; Urresti, S.; Lafond, M.; Johnston, E. M.; Derikvand, F.; Ciano, L.; Berrin, J. G.; Henrissat, B.; Walton, P. H.; Davies, G. J.; Brumer, H. Structure−function characterization reveals new catalytic diversity in the galactose oxidase and glyoxal oxidase family. *Nat. Commun.* **2015**, *6*, 10197.

(4) (a) Dooley, D. M. Structure and biogenesis of topaquinone and related cofactors. *JBIC, J. Biol. Inorg. Chem.* **1999**, *4*, 1−11. (b) Mure, M. Tyrosine−Derived Quinone Cofactors. *Acc. Chem. Res.* **2004**, *37*, 131−139. (c) Prabhakar, R.; Siegbahn, P. E. M. A Theoretical Study of the Mechanism for the Biogenesis of Cofactor Topaquinone in Copper Amine Oxidases. *J. Am. Chem. Soc.* **2004**, *126*, 3996−4006. (d) Dove, J. E.; Klinman, J. P. Trihydroxyphenylalanine quinone (TPQ) from copper amine oxidases and lysyl tyrosylquinone (LTQ) from lysyl oxidase. *Adv. Protein Chem.* **2001**, *58*, 141−174. (e) Rinaldi, A. C.; Porcu, C. M.; Oliva, S.; Curreli, N.; Rescigno, A.; Sollai, F.; Rinaldi, A.; Finazzi-Agro, A.; Sanjust, E. Biosynthesis of the topaquinone cofactor in copper amine oxidases. *Eur. J. Biochem.* **1998**, *251*, 91−97. (f) Nakamura, N.; Matsuzaki, R.; Choi, Y. H.; Tanizawa, K.; Loehr, J. S. Biosynthesis of Topa Quinone Cofactor in Bacterial Amine Oxidases: Solvent Origin of C-2 Oxygen Determined by Raman Spectroscopy. *J. Biol. Chem.* **1996**, *271*, 4718−4724. (g) Shepard, E. M.; Okonski, K. M.; Dooley, D. M. Kinetics and Spectroscopic Evidence That the Cu(I)−Semiquinone Intermediate Reduces Molecular Oxygen in the Oxidative Half-Reaction of *Arthrobacter globiformis* Amine Oxidase. *Biochemistry* **2008**, *47*, 13907−13920. (h) Johnson, B. J.; Yukl, E. T.; Klema, V. J.; Klinman, J. P.; Wilmot, C. M. Structural Snapshots from the Oxidative Half-reaction of a Copper Amine Oxidase: IMPLICATIONS FOR O_2 ACTIVATION. *J. Biol. Chem.* **2013**, *288*, 28409−28417. (i) Dooley, D. M.; McGuirl, M. A.; Brown, D. E.; Turowski, P. N.; Mclntire, W. S.; Knowles, P. F. A Cu(I)-semiquinone state in substrate-reduced amine oxidases. *Nature* **1991**, *349*, 262−264. (j) Medda, R.; Mura, A.; Longu, S.; Anedda, R.; Padiglia, A.; Casu, M.; Floris, G. An unexpected formation of the spectroscopic Cu^I-semiquinone radical by xenon-induced self-catalysis of a copper quinoprotein. *Biochimie* **2006**, *88*, 827−835.

(5) (a) Strange, R. W.; Antonyuk, S.; Hough, M. A.; Doucette, P. A.; Valentine, J. S.; Hasnain, S. S. Variable Metallation of Human Superoxide Dismutase: Atomic Resolution Crystal Structures of Cu−Zn, Zn−Zn and As-isolated Wild-type Enzymes. *J. Mol. Biol.* **2006**, *356*, 1152−1162. (b) Carugo, K. D.; Battistoni, A.; Carri, M. T.; Polticelli, F.; Desideri, A.; Rotilio, G.; Coda, A.; Wilson, K. S.; Bolognesi, M. Three-dimensional structure of *Xenopus laevis* Cu,Zn superoxide dismutase *b* determined by X-ray crystallography at 1.5 Å resolution. *Acta Crystallogr., Sect. D: Biol. Crystallogr.* **1996**, *52*, 176−188. (c) Tainer, J. A.; Getzoff, E. D.; Beem, K. M.; Richardson, J. S.; Richardson, D. C. Determination and analysis of the 2 Å structure of copper, zinc superoxide dismutase. *J. Mol. Biol.* **1982**, *160*, 181−217. (d) Ellerby, R. M.; Cabelli, D. E.; Graden, J. A.; Valentine, J. S. Copper−Zinc Superoxide Dismutase: Why Not pH-Dependent? *J. Am. Chem. Soc.* **1996**, *118*, 6556−6561. (e) Ohtsu, H.; Fukuzumi, S. Coordination of Semiquinone and Superoxide Radical Anions to the Zinc Ion in SOD Model Complexes that Act as the Key Step in Disproportionation of the Radical Anions. *Chem. - Eur. J.* **2001**, *7*, 4947−4953.

(6) (a) Luca, O. R.; Crabtree, R. H. Redox-active ligands in catalysis. *Chem. Soc. Rev.* **2013**, *42*, 1440−1459. (b) Pierpont, C. G.; Lange, C. W. The Chemistry of Transition-Metal Complexes Containing Catechol and Semiquinone Ligands. In *Prog. Inorg. Chem.*; Karlin, K. D., Ed.; Wiley: Hoboken, NJ, 1994. (c) Itoh, S.; Taki, M.; Takayama, S.; Nagatomo, S.; Kitagawa, T.; Sakurada, N.; Arakawa, R.; Fukuzumi, S. Oxidation of Benzyl Alcohol with Cu^{II} and Zn^{II} Complexes of the Phenoxyl Radical as a Model of the Reaction of Galactose Oxidase. *Angew. Chem., Int. Ed.* **1999**, *38*, 2774−2776. (d) Lyaskovskyy, V.; de Bruin, B. Redox Non-Innocent Ligands: Versatile New Tools to Control Catalytic Reactions. *ACS Catal.* **2012**, *2*, 270−279. (e) Kaim, W. The Shrinking World of Innocent Ligands: Conventionaland Non-Conventional Redox-Active Ligands. *Eur. J. Inorg. Chem.* **2012**, *2012*, 343−348. (f) Holm, R. H.; Solomon, E. I. Preface: Biomimetic Inorganic Chemistry. *Chem. Rev.* **2004**, *104*, 347−348. Chirik, P. J.; Wieghardt, K. Radical Ligands Confer Nobility on Base-Metal Catalysts. *Science.* **2010**, *327*, 794−795. (g) Chaudhuri, P.; Wieghardt, K.; Weyhermüller, T.; Paine, T. K.; Mukherjee, S.; Mukherjee, C. Biomimetic metal−radical reactivity: aerial oxidation of alcohols, amines, aminophenols and catechols catalyzed by transition metal complexes. *Biol. Chem.* **2005**, *386*, 1023−1033. (h) Kaim, W. The chemistry and biochemistry of the copper-radical interaction. *Dalton Trans.* **2003**, 761−768. (i) Broere, D. L. J.; Plessius, R.; van der Vlugt, J. I. New avenues for ligand-mediated processes − expanding metal reactivity by the use of redox-

DOI: 10.1021/acs.inorgchem.8b01931
Inorg. Chem. XXXX, XXX, XXX−XXX

active catechol, *o*-aminophenol and *o*-phenylenediamine ligands. *Chem. Soc. Rev.* **2015**, *44*, 6886−6915. (j) Maji, R. C.; Das, P. P.; Mishra, S.; Bhandari, A.; Maji, M.; Patra, A. K. Electron transfer mechanism of catalytic superoxide dismutase *via* Cu(II/I) complexes: evidence of cupric-superoxo/-hydroperoxo species. *Dalton. Trans.* **2016**, *45*, 11898−11910.

(7) (a) Thompson, J. S.; Calabrese, J. C. Synthesis, spectroscopy, and structures of copper(II)−3,5−di−*tert*−butyl−o−semiquinone complexes. *Inorg. Chem.* **1985**, *24*, 3167−3171. (b) Piskunov, A. V.; Pashanova, K. I.; Bogomyakov, A. S.; Smolyaninov, I. V.; Berberova, N. T.; Fukin, G. K. Copper(II) complexes bearing *o*-iminosemiquinonate ligands with augmented aromatic substituents. *Polyhedron* **2016**, *119*, 286−292. (c) Mukherjee, C.; Pieper, U.; Bothe, E.; Bachler, V.; Bill, E.; Weyhermüller, T.; Chaudhuri, P. Ligand-Derived Oxidase Activity. Catalytic Aerial Oxidation of Alcohols (Including Methanol) by Cu(II)−Diradical Complexes. *Inorg. Chem.* **2008**, *47*, 8943−8956. (d) Mondal, M. K.; Biswas, A. K.; Ganguly, B.; Mukherjee, C. Unprecedented iminobenzosemiquinone and iminobenzoquinone coordinated mononuclear Cu(II) complex formation under air. *Dalton Trans.* **2015**, *44*, 9375−9381. (e) Rakshit, R.; Ghorai, S.; Biswas, S.; Mukherjee, C. Effect of Ligand Substituent Coordination on the Geometry and the Electronic Structure of Cu(II)−Diradical Complexes. *Inorg. Chem.* **2014**, *53*, 3333−3337. (f) Poddel'sky, A. I.; Cherkasov, V. K.; Abakumov, G. A. Transition metal complexes with bulky 4,6−di−tert−butyl−N−aryl(alkyl)−o−iminobenzoquinonato ligands: Structure, EPR and magnetism. *Coord. Chem. Rev.* **2009**, *253*, 291−324. (g) Ye, S.; Sarkar, B.; Lissner, F.; Schleid, Th.; van Slageren, J.; Fiedler, J.; Kaim, W. Three-Spin System with a Twist: A Bis(semiquinonato)copper Complex with a Nonplanar Configuration at the Copper(II) Center. *Angew. Chem., Int. Ed.* **2005**, *44*, 2103−2106. (h) Mukherjee, C.; Weyhermüller, T.; Bothe, E.; Chaudhuri, P. Targeted Oxidase Reactivity with a New Redox−Active Ligand Incorporating N_2O_2 Donor Atoms. Complexes of Cu(II), Ni(II), Pd(II), Fe(III), and V(V). *Inorg. Chem.* **2008**, *47*, 11620−11632. (i) Mukherjee, C.; Weyhermüller, T.; Bothe, E.; Chaudhuri, P. Oxidation of an *o*-Iminobenzosemiquinone Radical Ligand by Molecular Bromine: Structural, Spectroscopic, and Reactivity Studies of a Copper(II) *o*-Iminobenzoquinone Complex. *Inorg. Chem.* **2008**, *47*, 2740−2746.

(8) (a) Jacquet, J.; Blanchard, S.; Derat, E.; Desage-El Murr, M.; Fensterbank, L. Redox-ligand sustains controlled generation of CF_3 radicals by well-defined copper complex. *Chem. Sci.* **2016**, *7*, 2030−2036. (b) Jacquet, J.; Salanouve, E.; Orio, M.; Vezin, H.; Blanchard, S.; Derat, E.; Desage-El Murr, M.; Fensterbank, L. Iminosemiquinone radical ligands enable access to a well−defined redox-active $Cu^{II}−CF_3$ complex. *Chem. Commun.* **2014**, *50*, 10394−10397. (c) Jacquet, J.; Chaumont, P.; Gontard, G.; Orio, M.; Vezin, H.; Blanchard, S.; Desage-El Murr, M.; Fensterbank, L. C−N Bond Formation from a Masked High-Valent Copper Complex Stabilized by Redox Non-Innocent Ligands. *Angew. Chem., Int. Ed.* **2016**, *55*, 10712−10716. (d) Mondal, M. K.; Mukherjee, C. An unprecedented one-step synthesis of octahedral Cu(II)-bis(iminoquinone) complexes and their reactivity with $NaBH_4$. *Dalton Trans.* **2016**, *45*, 13532−13540.

(9) The sum of van der Waal radii of Cu (1.40 Å) and O (1.52 Å) is 2.92 Å. The observed Cu1−O1 bond distance in complex **2** was 2.3934(17) Å, which is about 0.53 Å shorter and hence, indicated a substantial interaction between Cu1 and O1 atoms in complex **2**.

(10) (a) Sun, X.; Chun, H.; Hildenbrand, K.; Bothe, E.; Weyhermüller, T.; Neese, F.; Wieghardt, K. *o*−Iminobenzosemiquinonato(1−) and *o*−Amidophenolato(2−) Complexes of Palladium(II) and Platinum(II):A Combined Experimental and Density Functional Theoretical Study. *Inorg. Chem.* **2002**, *41*, 4295−4303. (b) Chun, H.; Bill, E.; Bothe, E.; Weyhermüller, T.; Wieghardt, K. Octahedral (*cis*−Cyclam)iron(III) Complexes with *O,N*-Coordinated *o*−Iminosemiquinonate(1−) π Radicals and *o*−Imidophenolate(2−) Anions. *Inorg. Chem.* **2002**, *41*, 5091−5099. (c) Chun, H.; Chaudhuri, P.; Weyhermüller, T.; Wieghardt, K. o−Iminobenzosemiquinonato Complexes of Mn(III) and Mn(IV). Synthesis and Characterization of $[Mn^{III}(L^{ISQ})_2(L^{AP})]$ (S_t = 1) and $[Mn^{IV}(L^{ISQ})_2(L^{AP}\text{-H})]$ (S_t = $^1/_2$). *Inorg. Chem.* **2002**, *41*, 790−795. (d) Min, K. S.; Weyhermüller, T.; Bothe, E.; Wieghardt, K. Tetradentate Bis(*o*−iminobenzosemiquinonate(1−)) π Radical Ligands and Their *o*-Aminophenolate(1−) Derivatives in Complexes of Nickel(II), Palladium(II), and Copper(II). *Inorg. Chem.* **2004**, *43*, 2922−2931. (e) Sarkar, P.; Mondal, M. K.; Sarmah, A.; Maity, S.; Mukherjee, C. An Iminosemiquinone-Coordinated Oxidovanadium-(V) Complex: A Combined Experimental and Computational Study. *Inorg. Chem.* **2017**, *56*, 8068−8077.

(11) (a) Speier, G.; Csihony, J.; Whalen, A. M.; Pierpont, C. G. Iminoquinone coordination to copper(I) in the $[Cu(PhenoxBQ)(\mu\text{-}Cl)]_2$ dimer. *Inorg. Chim. Acta* **1996**, *245*, 1−5. (b) Roy, S.; Sarkar, B.; Bubrin, D.; Niemeyer, M.; Zališ, S.; Lahiri, G. K.; Kaim, W. Stabilizing the Elusive *ortho*-Quinone/Copper(I) Oxidation State Combination through π/π Interaction in an Isolated Complex. *J. Am. Chem. Soc.* **2008**, *130*, 15230−15231.

(12) (a) Abakumov, G. A.; Cherkasov, V. K.; Nevodchikov, V. I.; Kuropatov, V. A.; Yee, G. T.; Pierpont, C. G. Magnetic Properties and Redox Isomerism for 4,4'-Bis(semiquinone) Complexes of Copper. *Inorg. Chem.* **2001**, *40*, 2434−2436. (b) Speier, G.; Tyeklar, Z.; Tóth, P.; Speier, E.; Tisza, S.; Rockenbauer, A.; Whalen, A. M.; Alkire, N.; Pierpont, A. G. Valence Tautomerism and Metal-Mediated Catechol Oxidation for Complexes of Copper Prepared with 9,10-Phenanthrenequinone. *Inorg. Chem.* **2001**, *40*, 5653−5659. (c) Rall, J.; Wanner, M.; Albrecht, M.; Hornung, F. M.; Kaim, W. Sensitive Valence Tautomer Equilibrium of Paramagnetic Complexes $[(L)\text{-}Cu^{n+}(Q^{n-})]$ (n = 1 or 2; Q = Quinones) Related to Amine Oxidase Enzymes. *Chem. - Eur. J.* **1999**, *5*, 2802−2809.

(13) Gagne, R. R.; Allison, J. L.; Gall, R. S.; Koval, C. A. Models for copper-containing proteins: structure and properties of novel five-coordinate copper(I) complexes. *J. Am. Chem. Soc.* **1977**, *99*, 7170−7178.

(14) *CrysAlisPro*, version 1, 171; Oxford Diffraction Ltd., 33.34d [release 27-02-2009 CrysAlis 171. NET].

(15) Sheldrick, G. M. *SHELXL-97, Program for Crystal Structure Refinement*; University of Göttingen: Göttingen, Germany, 1997.

(16) Bauernschmitt, R.; Ahlrichs, R. Treatment of electronic excitations within the adiabatic approximation of time dependent density functional theory. *Chem. Phys. Lett.* **1996**, *256*, 454−464.

(17) Reed, A. E.; Weinhold, F.; Curtiss, L. A.; Pochatko, D. J. Natural bond orbital analysis of molecular interactions: theoretical studies of binary complexes of HF, H_2O, NH_3, N2, O_2, F_2, CO and CO_2 with HF, H2O and NH3. *J. Chem. Phys.* **1986**, *84*, 5687−5705.

(18) Miertuš, S.; Scrocco, E.; Tomasi, J. Electrostatic Interaction of a Solute with a Continuum. A Direct Utilization of ab initio Molecular Potentials for the Prevision of Solvent Effects. *Chem. Phys.* **1981**, *55*, 117−129.

(19) Frisch, M. J.; Trucks, G. W.; Schlegel, H. B.; Scuseria, G. E.; Robb, M. A.; Cheeseman, J. R.; Scalmani, G.; Barone, V.; Mennucci, B.; Petersson, G. A.; Nakatsuji, H.; Caricato, M.; Li, X.; Hratchian, H. P.; Izmaylov, A. F.; Bloino, J.; Zheng, G.; Sonnenberg, J. L.; Hada, M.; Ehara, M.; Toyota, K.; Fukuda, R.; Hasegawa, J.; Ishida, M.; Nakajima, T.; Honda, Y.; Kitao, O.; Nakai, H.; Vreven, T.; Montgomery, J. A., Jr.; Peralta, J. E.; Ogliaro, F.; Bearpark, M.; Heyd, J. J.; Brothers, E.; Kudin, K. N.; Staroverov, V. N.; Kobayashi, R.; Normand, J.; Raghavachari, K.; Rendell, A.; Burant, J. C.; Iyengar, S. S.; Tomasi, J.; Cossi, M.; Rega, N.; Millam, J. M.; Klene, M.; Knox, J. E.; Cross, J. B.; Bakken, V.; Adamo, C.; Jaramillo, J.; Gomperts, R.; Stratmann, R. E.; Yazyev, O.; Austin, A. J.; Cammi, R.; Pomelli, C.; Ochterski, J. W.; Martin, R. L.; Morokuma, K.; Zakrzewski, V. G.; Voth, G. A.; Salvador, P.; Dannenberg, J. J.; Dapprich, S.; Daniels, A. D.; Farkas, O.; Foresman, J. B.; Ortiz, J. V.; Cioslowski, J.; Fox, D. J. *Gaussian 09*, Revision D.01; Gaussian, Inc.: Wallingford, CT, 2013.

(20) Dreuw, A.; Head-Gordon, M. Failure of Time-Dependent Density Functional Theory for Long-Range Charge-Transfer Excited States: The Zincbacteriochlorin−Bacteriochlorin and Bacteriochlorophyll−Spheroidene Complexes. *J. Am. Chem. Soc.* **2004**, *126*, 4007−4016.

DOI: 10.1021/acs.inorgchem.8b01931
Inorg. Chem. XXXX, XXX, XXX−XXX

(21) Paul, G. C.; Ghorai, S.; Mukherjee, C. Monoradical-containing four-coordinate Co(III) complexes: homolytic S−S and Se−Se bond cleavage and catalytic isocyanate to urea conversion under sunlight. *Chem. Commun.* **2017**, *53*, 8022−8025.

DOI: 10.1021/acs.inorgchem.8b01931
Inorg. Chem. XXXX, XXX, XXX−XXX